THE METEOROLOGICAL MAGAZINE

HER MAJESTY'S STATIONERY OFFICE

January 1985

Met.O.967 No. 1350 Vol. 114

METEOROLOGICAL OFFICE Met.O.967

THE METEOROLOGICAL MAGAZINE

No. 1350, January 1985, Vol. 114

551.509.313

The preparation of data for the Meteorological Office operational 15-level forecast model

By Margaret J. Woodage

(Meteorological Office, Bracknell)

Summary

Observational data consist of measured or derived variables at different levels in the atmosphere, and must be converted to the variables required by the model before they can be used in the operational analysis. The preparation of some types of data is very simple, but for others it is much more complicated, and this paper discusses some of the problems involved.

1. Introduction

Coded observational data are received at Bracknell continuously via the Global Telecommunication System (GTS) and are routed by the Telecommunications Branch to the central IBM computer where they are decoded and stored in the Synoptic Data Bank (SDB). The observations are of different variables at various levels in the atmosphere, and must be converted to the appropriate model variables and formed into an ordered data set before they can be used in the analysis. It is also necessary to incorporate the intervention submitted by forecasters in the Central Forecasting Office (CFO) who monitor the data and model products. Erroneous data can be rejected or corrected, and 'bogus' or artificial data inserted in areas where model fields are poor. The preparation of certain types of data is quite straightforward, requiring only a simple change of variable using a standard formula; however, for other types, the conversions could be carried out in a variety of ways involving different approximations and assumptions. It is clearly very important that the methods chosen should provide the analysis with the best possible information, giving a faithful representation of the original data as well as satisfying all the model requirements. This paper outlines the methods used for each type of data, describing in depth some of the more difficult problems encountered, but first, a brief description is given of the operational analysis scheme in which the data are used.

Notation

p	pressure (mb)
p_s	pressure at station level (surface)
p_*	pressure at model surface
T	temperature (K)
t	temperature (° C)
t_d	dew-point temperature (° C)
ω	precipitable water content (mm)
U	relative humidity
q	humidity mixing ratio (g/g)
m	humidity mixing ratio (g/kg)
z	geopotential
u,v	eastward and northward wind components
θ	potential temperature
γ	lapse rate (= $-dT/dz$)
g	9.80665
R	universal gas constant (=287.05 J kg^{-1} K^{-1})
k	= $1-(c_v/c_p)$ = 0.2857143
	c_p = specific heat of gas at constant pressure
	c_v = specific heat of gas at constant volume

2. Operational analysis

The analysis is global with a latitude–longitude grid in the horizontal (with meridional resolution 1½° and zonal resolution 1⅞°) and 15 levels in the vertical (from the surface up to about 25 mb). In the vertical, the terrain-following sigma coordinate system is used, where at any level j,

$$\sigma_j = \frac{p_j}{p_*},$$

p_j being the pressure at level j, and p_* the pressure at the model surface (generally a smoothed version of the real orography). The analysis is performed every six hours using data valid for up to three hours either side of the analysis time. The analysis is a three-dimensional univariate optimal interpolation scheme, which effectively means that prior interpolation of data to special analysis levels is unnecessary, and each variable is analysed independently. The variables required by the analysis are the independent variables of the forecast model, which are θ (potential temperature), q (humidity mixing ratio), u and v (eastward and northward wind components) and p_*. (Full details of the data assimilation scheme can be found in Lyne, Little, Dumelow and Bell 1983.)

3. Data

3.1 *Surface data (surface land stations, surface ships, drifting buoys)*

Typically, surface observations provide values of surface temperature, dew-point, wind and mean sea level (msl) pressure. Exceptions to this are drifting buoys, which report msl pressure and sea surface temperature only, and high-level stations (above 500 m), where reduction of surface pressure to msl

pressure is unreliable. The latter report either station level pressure, or the geopotential of a standard pressure level (see World Meteorological Organization 1982).

Surface temperature data are not used in the analysis, as local anomalies are considered to render them unrepresentative of the atmosphere on the scale of the model grid. For the same reason, surface wind and humidity data are not used over the land, although they are used over the sea after conversion to u and v components, and humidity mixing ratio respectively. The reported pressure must be converted to model surface pressure (p_*). Where the geopotential of the model orography (z_*) is equal to the geopotential of the reported pressure (e.g. over the sea) no work is required as p_* is equal to the reported pressure. However, for most land stations, some extrapolation is required, and assumptions must be made about the temperature structure in the layer between the level of the reported pressure and the model surface in order to calculate p_*. Actual surface temperatures are again considered atypical, especially for thick layers, and therefore no attempt is made to estimate the true vertical temperature structure at the station. The best that can be done is to use model values, and ensure that the method adopted is consistent with the conversion of model p_* values to msl pressure for output.

The calculation is done using the hydrostatic equation integrated assuming a constant lapse rate within the layer. This is derived as follows.

Integrating the hydrostatic equation over any layer bounded by pressures p_1 and p_2 with geopotential heights z_1 and z_2 gives:

$$\int_{p_1}^{p_2} \frac{1}{p}\,\mathrm{d}p = -\frac{g}{R}\int_{z_1}^{z_2} \frac{1}{T}\,\mathrm{d}z,$$

where $g = 9.80665$ and $R = 287.05$ J kg^{-1} K^{-1}.

Assuming $T(z) = T_0 - \gamma(z - z_0)$, where T_0 is a reference temperature at a known height z_0 and γ is the lapse rate (assumed constant), the hydrostatic equation can be integrated to give:

$$\log_e \frac{p_2}{p_1} = \frac{g}{\gamma R} \log_e \left\{ \frac{T_0 - \gamma(z_2 - z_0)}{T_0 - \gamma(z_1 - z_0)} \right\}$$

This can be rewritten as:

$$\frac{p_2}{p_1} = \left\{ \frac{T_0 - \gamma(z_2 - z_0)}{T_0 - \gamma(z_1 - z_0)} \right\}^{\frac{g}{\gamma R}} = \left\{ \frac{T(z_2)}{T(z_1)} \right\}^{\frac{g}{\gamma R}}$$

This equation is used to obtain a reference temperature T_s at the model surface z_* from the temperature at the 5th sigma level of the model, using $\gamma = 6.5$ K km^{-1} which is the value for the ICAO (International Civil Aviation Organization) standard atmosphere up to 11 km. The model temperature at level 5 is used as this is the lowest level outside the model boundary layer.

$$T_s = T_5 \left(\frac{1}{\sigma_5} \right)^{\frac{\gamma R}{g}}$$

Then p_* is obtained from the reported pressure and geopotential:

$$p_* = p_r \left(\frac{T_s}{T_s - \gamma(z_r - z_*)} \right)^{\frac{g}{\gamma R}}$$

This equation is applied whether a pressure, p_r, or the geopotential of a standard pressure level, z_r, is reported. This is illustrated in Fig. 1 which shows schematically three stations, S_1, S_2 and S_3, reporting mean sea level pressure, station level pressure, and the 850 mb geopotential, respectively. The pressure (p_*) at the model surface (z_*) must be calculated in each case from the available pressure (p_r) and geopotential (z_r).

Over many land areas the density of reporting surface stations is too high to be handled by the model. Therefore, during the data extraction program, reference is made to a station list which identifies those stations which are to be passed on to the analysis; stations not appearing in the list are rejected. A similar problem exists with drifting buoys, which report every hour; the difficulty here is one of temporal rather than spatial density. The report closest to the analysis time is selected for each buoy, and the others are rejected.

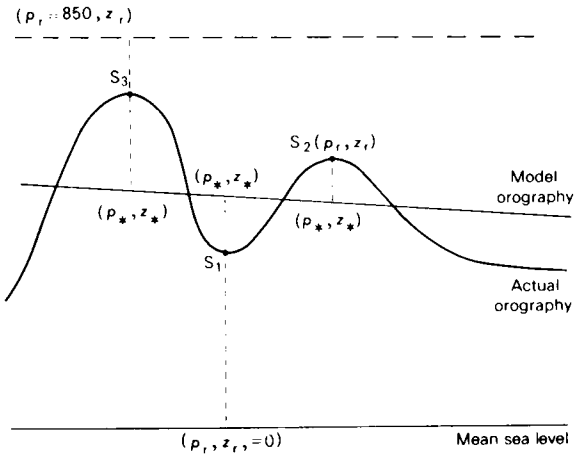

Figure 1. Schematic representation of the derivation of p_* from surface stations with different reporting practices.

3.2 *Upper-air data (radiosondes)*

Radiosonde TEMP messages contain values of geopotential, temperature, dew-point and wind for the standard pressure levels, together with temperatures, dew-points and/or winds at significant levels of the ascent, including the surface. The PILOT messages contain wind data only, at standard and significant pressure levels or at a set of given heights.

The messages generally contain too many levels of data to be handled by the analysis program, and more vertical detail than can be resolved by the model. It is therefore necessary to condense the ascent to a representative set of data at a smaller number of levels. The most convenient levels to choose are model sigma levels, as this reduces the amount of interpolation during the analysis. The simplest method of deriving sigma-level data is to interpolate linearly in $\log_e p$ between neighbouring reported levels. According to the WMO definition of significant levels (World Meteorological Organization 1974), this will give a temperature within 1 °C of the observed value at that level. This was the method originally used. For an ascent with reported levels i, data at sigma levels j, such as illustrated in Fig. 2, can be calculated using the following equation:

$$X_j = X_{i+1} + \left\{ \frac{X_{i+2} - X_{i+1}}{\log_e (p_{i+2}/p_{i+1})} \right\} \log_e (p_j/p_{i+1}),$$

where X is any variable which is being interpolated and $p_{i+2} < p_j < p_{i+1}$. There are 15 sigma levels, distributed so that they are more dense in places where greater resolution is required (i.e. in the boundary layer and near the tropopause). Therefore, the simple method described above of picking 'spot' values from the ascents would generally give a reasonable representation. However, there is a possibility that for some ascents the sigma levels might lie at extreme points, and unrepresentative values be passed to the analysis. Indeed, it was found that using this method, 100 mb height analyses were several decametres too low for ascents where the tropopause was close to a sigma level. For this reason a different method was introduced. This essentially divides the ascent into layers centred on sigma levels and uses all reported values within the layer to produce a mean temperature at the sigma level. This method gives a more accurate representation of heights in the model.

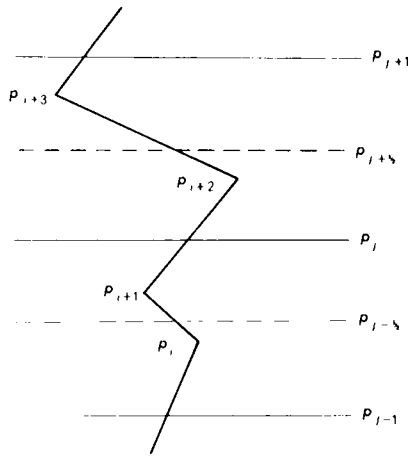

Figure 2. Arrangement of σ-levels, and half-levels $j+\frac{1}{2}$, relative to reported levels i from an ascent.

The half-sigma levels are arranged so that the sigma levels are at the centre of each layer, i.e.:

$$p_j = \sqrt{(p_{j\,\frac{1}{2}} p_{j+\frac{1}{2}})}$$

Referring again to Fig. 2, temperatures at half-sigma levels are derived using simple interpolation:

$$T_{j\,\frac{1}{2}} = T_i + \{ (T_{i+1} - T_i) / \log_e (p_{i+1}/p_i) \} \log_e (p_{j\,\frac{1}{2}}/p_i).$$

Then a weighted mean for the layer is formed:

$$T_j = \{ (T_{j\,\frac{1}{2}} + T_{i+1}) \log_e (p_{i+1}/p_{j\,\frac{1}{2}}) + (T_{i+1} + T_{i+2}) \log_e (p_{i+2}/p_{i+1}) + (T_{i+2} + T_{j+\frac{1}{2}}) \log_e (p_{j+\frac{1}{2}}/p_{i+2}) \} / 2\log_e (p_{j+\frac{1}{2}}/p_{j\,\frac{1}{2}}).$$

This 'layer mean' method is also used to derive sigma-level values of dew-point temperature and wind components.

For PILOT messages with winds at given heights, equivalent pressure levels must be derived. This is done assuming an ICAO standard atmosphere, using the same equations as for converting AIREP flight

levels to pressures (see 3.4). This method is sufficiently accurate, considering the errors involved in determining the heights at the station.

Although reported values of standard-level geopotential are not used directly in the model, they are used to collect statistics on the differences between observed and analysed 100 mb geopotentials. These are used to identify systematic differences between sondes and to derive appropriate corrections, which are given in terms of 100 mb geopotential. These corrections must be incorporated into sigma-level data as an equivalent temperature correction. The temperature correction (ΔT_p) is assumed to vary linearly in $\log_e p$ from zero at the surface up to a constant value (ΔT_T) at the tropopause, i.e.

$$\Delta T_p = \Delta T_T \frac{\log_e \frac{p}{p_s}}{\log_e \frac{p_T}{p_s}} \qquad p > p_T$$

$$\Delta T_p = \Delta T_T \qquad p < p_T$$

where p_s, p_T are the surface and tropopause pressures respectively. Using the integrated hydrostatic equation the 100 mb geopotential correction Δz_{100} can be expressed in terms of the temperature correction at the tropopause as follows:

$$\Delta z_{100} = \frac{R}{g} \frac{\Delta T_T}{2} \log_e \frac{p_s}{p_T} + \frac{R}{g} \Delta T_T \log_e \frac{p_T}{100}$$

This can be inverted to give:

$$\Delta T_T = \frac{g}{R} \frac{\Delta z_{100}}{\log_e \left\{ \frac{\sqrt{(p_s p_T)}}{100} \right\}}$$

Substituting this into the above equations for ΔT_p gives an expression for the temperature correction at any level p, in terms of the 100 mb geopotential correction, the surface pressure and the tropopause pressure. ICAO standard values are used for the surface and tropopause pressures to simplify the calculation. Corrections to the dew-point temperatures are applied in the same way.

Before being passed to the analysis, all sigma-level temperatures are converted to potential temperatures, using $\theta = T(1000/p)^k$, where $k = 0.2857143$. Dew-point temperature is converted to humidity mixing ratio, which is equal to:

$$q = \frac{0.62197e}{p - e}$$

where e is the vapour pressure. From the definition of dew-point temperature t_d (the temperature at which air becomes saturated).

$$e = e_s(t_d)$$

where e_s is the saturated vapour pressure. Now values of e_s are determined by the Goff-Gratch equations (see World Meteorological Organization 1966), which have been calculated and listed in the

Smithsonian Tables. An approximation to the Goff-Gratch equations (Murray 1967) is currently used (with t_d in degrees Celsius):

$$e_s(t_d) = \exp\left(1.80951 + \frac{17.27\, t_d}{237.3+t_d}\right)$$

Thus humidity mixing ratio can be obtained from values of dew-point, temperature and pressure.

3.3 *Satellite data*

Temperature soundings (from the polar orbiting satellites)

The SATEM messages received via the GTS contain thickness values between a given reference level and the standard levels and, for soundings taken in clear conditions, values of precipitable water content (PWC) for standard layers up to 300 mb. The PWC data are not suitable for use as humidity data directly in the model, but are used at source in the conversion of temperatures to thicknesses. Therefore they should be used again when performing the reverse calculation to convert the thickness back to temperatures for the analysis.

The variables initially obtained from the satellite radiances are temperature and humidity mixing ratio. The conversion to thickness and PWC is done using the following equations (from information provided by NOAA in a personal communication):

$$T_{vi} = T_i + \frac{m_i}{6},$$

where T_{vi} is the virtual temperature (K) at level i, T_i is the temperature (K) at level i, and m_i is the humidity mixing ratio (gm/kg) at level i.

Then,
$$z_{i+1} - z_i = -\frac{R}{2g}(T_{vi} + T_{vi+1}) \log_e \frac{p_{i+1}}{p_i},$$

where z_i is height (m) at level i and p_i is pressure (mb) at level i.

Thicknesses are summed to give values over layers between the reference level and standard levels up to 10 mb.

Also,
$$\omega_i^{i+1} = \frac{1}{10}\,\frac{1}{2g}(m_i + m_{i+1})(p_i - p_{i+1}),$$

where ω_i^{i+1} is PWC (mm) of layer $(i, i+1)$, and $p_i > p_{i+1}$.

Values of ω are then summed to obtain data for layers between the reference level and 700 mb, 500 mb and 300 mb.

To recover the original temperature profile as accurately as possible, these equations must be inverted. First, virtual temperatures at mid-points of standard levels are obtained from the thicknesses:

$$T_v(p') = \frac{g}{R}\left(\frac{z_2 - z_1}{\log_e \frac{p_1}{p_2}}\right)$$

where $p_1 > p_2$, $p' = \sqrt{(p_1 p_2)}$

To correct these to true temperatures, humidity mixing ratios must be recovered from the PWC data. The latter must first be split into values for each standard layer, assuming that ω varies linearly with $\log_e p$. For example:

$$\omega_{1000}^{850} = \left(\frac{\log_e \frac{850}{1000}}{\log_e \frac{700}{1000}} \right) \omega_{1000}^{700}$$

Then values of humidity mixing ratio can be found, e.g.

$$m(922) = 10g \left(\frac{\omega_{1000}^{850}}{1000-850} \right)$$

True temperatures are then obtained using:

$$T(p') = T_v(p') - \frac{1}{6} m(p')$$

If PWC data are missing, a relative humidity is assumed in order to calculate a temperature correction. Since this occurs when conditions are cloudy, a high relative humidity is appropriate, and a value of 80% is used. Humidity mixing ratio is related to relative humidity (U) in the following way:

$$U = \frac{m(T)}{m_s(T)} \times 100,$$

where $m_s(T)$ is the saturated humidity mixing ratio at temperature T.

Using the virtual temperature t_v obtained from the thickness data, and the pressures at mid-points of standard levels, values of m_s can be found using the approximate equation:

$$m_s(t_v) = \frac{621.97 e_s(t_v)}{p}$$

where $e_s(t_v)$ is the saturated vapour pressure, and is given by the following approximation to the full Goff–Gratch equations, with t_v in degrees Celsius:

$$e_s(t_v) = \exp\left(1.80951 + \frac{17.27 t_v}{237.3 + t_v}\right)$$

Using these equations, humidity mixing ratio can be found and the temperature correction made as before.

This method gives acceptable results, although it is only approximate. The procedure used at source to convert actual temperatures to virtual temperatures when humidity data are absent is very complex and could not be inverted operationally.

The Satellite Meteorology Branch processes satellite soundings locally to provide data at higher resolution and more quickly than normal. This processing system is known as HERMES (High Resolution Evaluation of Radiances from Meteorological Satellites). Temperatures and dew-points at

standard levels are available, as well as thickness and PWC data. The standard-level temperatures will be used directly when the HERMES data are introduced operationally. The density of data should be acceptable for the fine-mesh model, but would be too high for the coarse-mesh analysis. For this reason, a method of averaging the data has been derived. This involves using the line and element numbers in the original soundings (which locate the data relative to each other) to set up a grid of values (see Fig. 3). The mean of all available data within a given area is then calculated, the size of an area depending on the resolution required. The mean value is simply the sum of all values divided by the number of data points used, and is located at the point obtained by averaging the latitudes and longitudes of the data points used.

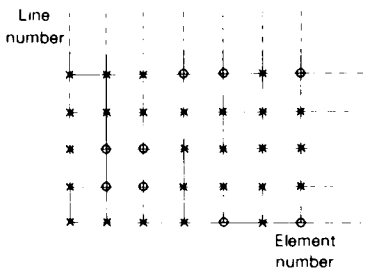

Figure 3. Configuration of HERMES data before averaging.
× data present o data absent

At present the temperatures from all SATEM data are interpolated to sigma levels before being converted to potential temperatures and passed to the analysis. This was originally introduced to give the SATEM data more weight in the model. In addition, SATEMs with reference levels above 1000 mb are rejected, as they were found initially to cause analysis problems over high topography (especially over Greenland). Owing to several changes in the analysis program, it might now be possible to remove the interpolation to sigma levels, and reintroduce SATEMs with reference levels above 1000 mb.

Cloud-track winds (from the geostationary satellites)

SATOB reports contain winds at pressure levels with associated temperatures (the pressure levels being derived at source from the measured temperatures). The winds are simply passed to the analysis at the assigned pressure levels; temperatures are not used, as they are not independent of the pressures.

3.4 *Aircraft data (AIREPs and ASDARS)*

Aircraft reports contain values of wind and temperature together with the flight level, position and time of report. AIREP observations are made by the aircraft every 5° or 10° of longitude along its flight path, and also at certain specified aircraft reporting positions. ASDAR observations are obtained automatically by satellite interrogation of the aircraft at approximately seven-minute intervals while it is in range. Although they provide the same type of data, ASDAR reports occur in strings of close observations whilst AIREPS are more widely spaced. The position, flight level, time and aircraft identifier are checked on all reports; if they are all identical for any two messages, the observed temperatures and winds are examined, and any duplicate or conflicting data are rejected.

The winds and temperatures (after conversion to potential temperatures) can be used directly in the model at the pressure level equivalent to the reported flight level. The conversion of flight level to

pressure is carried out using equations based on the ICAO standard atmosphere, as follows (see World Meteorological Organization 1966):

For flight levels h up to 11000 m, a constant lapse rate $\gamma = 6.5$ K km^{-1}, surface pressure $p_0 = 1013.2$ mb and surface temperature $T_0 = 288$ K are assumed. Then

$$p = p_0 \left(1 - \frac{\gamma h}{T_0}\right)^{\frac{\gamma R}{g}}$$

For flight levels between 11 000 m and 20 000 m an isothermal atmosphere with temperature $T_1 = 216.5$ K, and pressure $p_1 = 226$ mb at height $h_1 = 11\,000$ m is assumed. Then

$$p = \exp\left(\log_e(p_1) - \frac{g(h-h_1)}{RT_1}\right)$$

For flight levels above 20 000 m, a lapse rate $\beta = -1$ K km and pressure $p_2 = 55$ mb at height $h_2 = 20\,000$ m is assumed. Then:

$$p = p_2 \left\{1 - \frac{\beta}{T_1}(h - h_2)\right\}^{\frac{\beta R}{g}}$$

3.5 *Artificial data*

Bogus data

Forecasters in CFO routinely analyse charts of mean sea level pressure, and geopotential at 500 mb, 250 mb and 100 mb over the globe. These are considered to be the best representation available of the atmosphere at the main synoptic hours, and if the corresponding model fields are in major disagreement the forecasters may reject or correct existing data, or insert artificial (bogus) data to correct the model. For example, a feature may be evident from data not available to the model, such as satellite pictures. Mean sea level pressure and standard-level geopotentials are therefore the most natural quantities for the forecasters to insert, although these must then be converted to p_* and potential temperatures for use in the model. The complete set of quantities which may currently be inserted for any latitude and longitude is:

mean sea level pressure and surface wind,
humidity at the surface, 850 mb and 500 mb, and
geopotential and wind at 850 mb, 500 mb†, 250 mb, 100 mb and 50 mb.

Wind and humidity values are simply converted to the appropriate model variables and passed to the analysis at the pressure level specified. Mean sea level pressure values are converted to p_* using the same method as for other surface data (see 3.1); if the geopotential of another level is also entered at the same location, a new 1000 mb geopotential is calculated using the equation:

$$z_{1000} = \frac{R}{g} T_s \log_e \frac{(p_{msl})}{1000},$$

where T_s is the same derived model surface temperature as is used to calculate p_*.

Model values of standard-level geopotential are then used to calculate the increments implied by the bogus data at the intervention levels, as follows:

$$\Delta z = z(\text{bogus}) - z(\text{model}).$$

After calculating the increments for each intervention level, the thickness change implied over each 'intervention layer' is then used to adjust all the temperatures within the layer. The temperature profile is derived at mid-points of standard levels from the model standard-level geopotentials, using the integrated hydrostatic equation. The temperatures thus obtained (from thickness values) are, of course, virtual temperatures and the mid-point pressures are defined by $p' = \sqrt{(p_1 p_2)}$.

These virtual temperatures are then converted to actual temperatures using the model standard-level relative humidities. The method is similar to that used for satellite data without PWC values (see 3.3). Relative humidities are first interpolated linearly in $\log_e p$ to mid-points of standard levels:

$$U(p') = U(p_1) + \left\{ \frac{U(p_2) - U(p_1)}{\log_e(p_2/p_1)} \right\} \log_e(p'/p_1).$$

Then humidity mixing ratios (q) at mid-points of standard levels are obtained by using the virtual temperatures in:

$$q = q_s(T_v) \times \frac{U}{100},$$

where $q_s(T_v) = 0.62197 e_s(T_v)/p$ and $e_s(T_v)$ is the saturated vapour pressure. The virtual temperatures are then converted to actual temperatures using:

$$T = \frac{T_v}{1+0.61q},$$

where T and T_v are in kelvins and q is in g/g.

A full vertical profile of temperatures is thus passed to the analysis for every location at which a bogus geopotential is inserted.

Over the Southern Hemisphere satellite (thickness) data predominate over other types, so charts of 1000–500 mb thickness are analysed instead of 500 mb geopotential. Therefore, bogus data entered at 500 mb are assumed to be thickness and thermal winds. These values are then converted to 500 mb geopotential and wind using either model values of 1000 mb geopotential and wind, or 1000 mb geopotential calculated from the bogus msl pressure, and bogus surface wind, if available.

PAOB data

PAOBS are artificial data generated by Australian forecasters to force their numerical model to fit their manual analyses. Data are specified on a coarse 10° latitude/longitude grid for the whole of the Southern Hemisphere, and also on a finer scale to define important features over the Australian area. They serve a similar purpose to the bogus data inserted into our own analyses, but are generated routinely on a much wider scale as regular input to their numerical model. This is because conventional

†or thickness and thermal wind in the Southern Hemisphere (see end of this section).

data are sparse in the Southern Hemisphere, and heavy reliance is placed on satellite pictures to determine the state of the atmosphere.

The PAOB data received via the GTS are values of msl pressure and 1000–500 mb thickness. They are processed in a similar way to bogus data, but a temperature profile is generated only up to 500 mb, as no data are available for levels above that. PAOBS are received at Bracknell rather late (at approximately $T+10$ hours), and are given a very low weight in the analysis. Those in the area 140° W to 20° E, 30° S to 70° S are permanently rejected as the conventional data available are considered to be superior.

4. Concluding remarks

Data preparation is an essential part of any operational forecasting system, and the formulation of some of the methods used with the Meteorological Office 15-level model have been described here. It is a subject which receives little attention in the scientific literature, not because it lacks importance, but because the problems involved and solutions to them tend to be specific to the model in which the data are to be used, and not generally of relevance to others. However, the objective is always the same, and that is to convert the data into a form which satisfies all the model requirements and also represents the original observations as accurately as possible. In an operational environment, where forecast products are required as soon as possible, there is also a constraint that the pre-processing should be done as quickly as possible. Computational efficiency is an important consideration, and a satisfactory balance must always be found between the cost incurred and the accuracy attained when choosing methods of pre-processing data. Fig. 4 is a flow chart showing all the steps involved in preparing the data for the model.

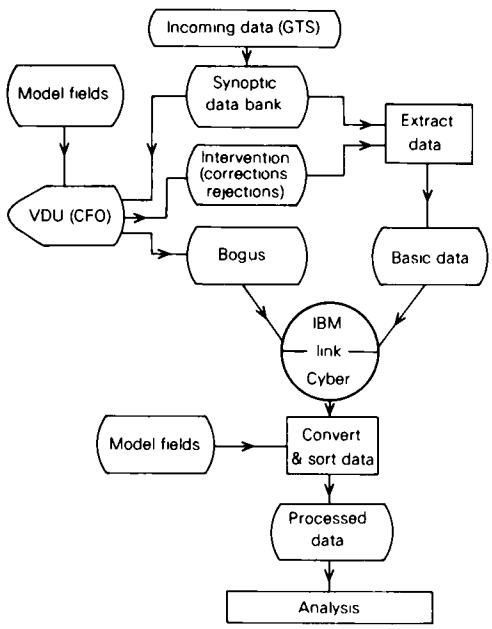

Figure 4. Flow chart showing the different stages of data preparation.

References

Lyne, W. H., Little, C. T., Dumelow, R. K. and Bell, R. S. 1983 The operational data assimilation scheme. (Unpublished, copy available in the National Meteorological Library, Bracknell.)

Murray, F. W. 1967 On the computation of saturation vapour pressure. *J Appl Meteorol*, **6**, 203–204.

World Meteorological Organization 1966 International meteorological tables. Geneva, WMO No. 188, TP94.

1974 Manual on codes. Vol. I. International Codes. Geneva, WMO No. 306.

1982 Manual on codes. Vol. II. Regional codes and national coding practices. Geneva, WMO No. 306.

551.510.42:551.509.325

Forecasting visibility over southern England in polluted easterly airstreams

By R. F. File

(Meteorological Office College, Shinfield Park)

Summary

An analysis of visibilities in easterly airstreams over southern England is presented. The effect of relative humidity is illustrated and graphs enabling visibility to be forecast from surface wind speed and relative humidity are produced for a typically polluted airstream.

1. Introduction

Clean, unsaturated air is virtually transparent. Rayleigh scattering by the molecules themselves is negligible and would still allow a theoretical visibility of several hundred kilometres. However, the air is never clean. Natural airborne particles occur, caused for example by volcanoes, dust-storms, forest fires and the release of salt particles into the atmosphere by the oceans. Over industrialized regions man-made pollution particles are more common than natural particles, and the visibility estimated by any one observation is a snapshot value of a parameter that has a large spatial and temporal spread. There are also problems in the estimation itself. Meteorological visibility is defined as the greatest horizontal distance that a dark object can be seen and recognized with daytime illumination. A suitable reference object should subtend an angle of 0.5 to 5.0 degrees at the observer, but over much of southern England few suitable objects can be seen at distances greater than 10 km. This is particularly true when one remembers that the visibility in the worst direction is reported, and an isolated mast perhaps 15 km away may be the only reference. Thus, even allowing for the high standards of observing in the United Kingdom, daytime estimates will vary somewhat. Night-time visibility should be comparable with daytime but is usually estimated by brightness of lights or their extinction. The further subjects of visual ranges into sun, and slant visibilities are not considered here. The best that meteorologists can offer to users is a forecast of meteorological visibility. It is up to film studios, photographers, pilots and various military users to interpret this forecast in terms of their own requirement. For many purposes including filming or photography the effective limit will be one half of the meteorological visibility. The aim of this study was to assist in the production of a forecast of afternoon visibility (say 1400 GMT) at 0600 and evening visibility (say 2200 GMT) at 1400.

2. Selection of gradient directions

It has been clearly shown by Bonvoisin and McHugh (1983) that easterly surface winds bring the highest frequency of visibilities in the 1–10 km range over southern England. At Gatwick, for example, the greatest frequency of visibilities below 8 km is with surface winds between 060° and 090°.

This is true even in summer when easterlies with their short sea track bring low relative humidity (RH). Thus the major pollutant sources must logically be in the continent. The traditional view of the Ruhr area of West Germany as the industrial heartland of Europe is no longer altogether valid. Aircraft pilots report that Rotterdam is a major source of smoke along with towns in Belgium and north-eastern France. Much of the pollution obviously comes from still further east. Wildenrath and Gütersloh statistics also show a bias towards poor visibilities with easterly airstreams. East Germany, Poland and Czechoslovakia are also sources as shown, for example, by Eliassen and Saltbones (1983). A straight easterly gradient will bring air across successive industrial areas towards southern England. Trajectories are notoriously difficult to establish but the study presented here was done on the basis that at least 24 hours of easterly flow were necessary to bring polluted air to the 'target' stations in southern England. The position of the five stations used in the study is shown in Fig. 1. Four are in rural locations and, since

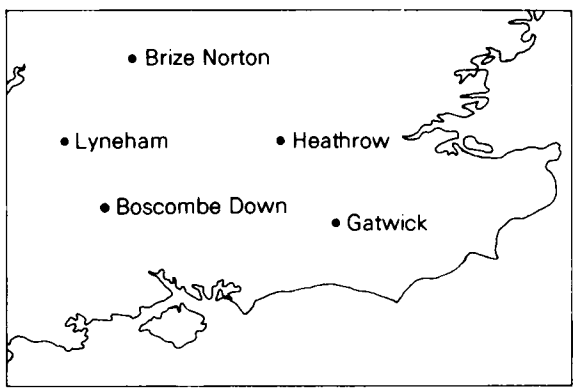

Figure 1. The stations used in the investigation.

the Clean Air Act of 1956 and the subsequent improvement of visibilities over London, Heathrow may be considered as suburban.

The decision to use gradient winds for the selection of dates rather than surface winds was based on a consideration of the likely vertical motion of particles over a 24-hour period. Only with light winds and no convection would surface winds be more relevant. With topography of 500 ft plus and the normal turbulence associated with surface winds greater than 6 knots, gradient direction will be a fair guide to the direction of travel.

The 1200 GMT charts for the years 1979–82 were classified for gradient direction (to the nearest 10 degrees) over central southern England. Out of a total of 1461 days, 137 were classified as 'variable'. These were occasions when no direction could be identified from the chart, and were situations either with very light winds or when a depression was centred over the area.

Gradients of 080° to 130° were considered most likely to be polluted and it was decided that two consecutive days within this 'easterly' arc would normally draw the air from a continental source. An intervening day of 'variable' winds did not necessitate a fresh start. Once the 'easterly' was established

then any succeeding days of 'easterly' or 'variable' gradients also qualified. Thus in the example below those days marked with an asterisk would qualify:

150° 130° *110° 180° 100° Variable *120° *Variable *080° 060°

This selection procedure gave 54 days in the 4-year period, although it was later noted that many near-misses with gradients 140°–170° also had poor visibility. The selection was thus somewhat crude and took no account of the upwind shape of the isobars. A practising forecaster could easily better the selection at 0600 GMT on the day of forecast by considering the likely trajectory from a sequence of synoptic charts. The arc included in the study had boundaries of 075° and 135°, corresponding approximately to surface winds 060° to 120°. However the inclusion of 'variable' days and possible changes in gradient after 1200 GMT on the selected dates means that surface winds during the afternoon and evening could vary quite considerably. On both 'variable' and easterly days some United Kingdom pollution would be added to that already present. The map (Fig. 2) shows the relationship of the main source area to the target area. The southern boundary is marked by the Alps and the northern boundary attempts to exclude clean air which has crossed the Baltic and Scandinavia. Although gradient wind directions were used in the selection of dates, the subsequent analysis dealt with surface wind speeds as these were readily available from the synoptic data.

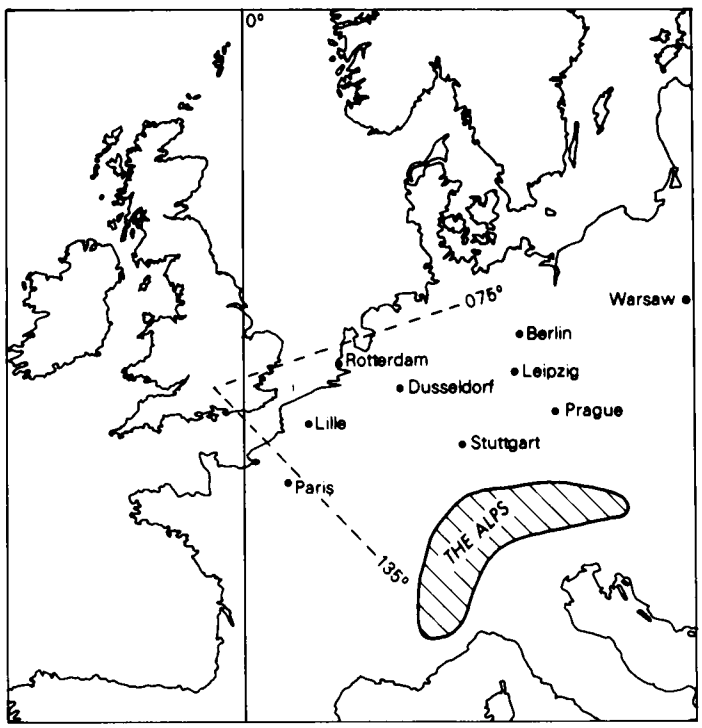

Figure 2. The position of the British Isles in relation to some of the possible sources of continental pollution.

3. Afternoon visibilities on days of persisting easterlies

The visibilities for Brize Norton (03649), Lyneham (03740), Boscombe Down (03746), Heathrow (03772) and Gatwick (03776) were analysed at 1200, 1400 and 1600 GMT on each day of persisting 'easterlies'. They were recorded against relative humidity for three classes of surface wind speed, namely

1-6, 7-11 and over 12 knots. Stronger winds are associated with better visibility, partly because of the greater depth through which the pollution particles are mixed, but also because the air has spent less time over the pollution-producing zone in situations with widespread and persistent strong gradients. Occasions with precipitation falling at the time of observation, precipitation within sight or with blowing snow were discarded (present weather 14, 15, 16, 38, 39, 50–99) as were the very small number of calms. The resulting information for the 7-11 knot wind class is given below (Table I). Note that the items of data are not independent, with 3 values from each of 5 stations giving a possible 15 visibility estimations on any one day.

Table I. *Afternoon visibility (1200, 1400, 1600 GMT) against relative humidity for the 7-11 knot wind class in easterly airstreams*

	Visibility (km)							
Relative humidity (%)	0-0.7	0.8-1.7	1.8-3.6	3.7-4.9	5-7	8-15	16-30	35-60
	Number of occasions							
88-100	4	5	3	7	12	6	5	0
73-87	0	0	7	18	52	63	29	0
58-72	0	0	6	8	26	88	71	8
43-57	0	0	9	3	10	41	81	6
28-42	0	0	0	3	4	24	47	13
13-27	0	0	0	0	0	0	8	2

4. Graph of afternoon visibility against relative humidity

It was decided to draw graphs for each wind class using the median values of visibility for each relative humidity class. Certain assumptions had now to be made. When condensation occurs at 100% RH, it is common experience that a visibility of approximately 0.1 km usually results and the curves were drawn through this point for light and moderate winds, but it was felt unrealistic to extend the strong wind curve above 87%. The drier end of the range provided another problem. The data show that visibility continues to improve with decreasing relative humidity, and in the case of strong winds down to about 40%. This contradicts the widely held view amongst forecasters that hygroscopic nuclei only have a significant effect above 80% or 90%. Evidence from individual days suggested that visibility does vary with RH in the 30–80% range. One late spring example is given in Table II.

Table II. *Variations in visibility on 14 May 1982 at Boscombe Down*

Times GMT	06	07	08	09	10	11	12	13	14	15	16	17	18	19	20	21	22	23
Surface wind speed (kn)	10	8	8	7	8	8	10	15	16	7	8	9	14	10	11	10	12	9
Relative humidity (%)	76	76	70	65	57	53	39	35	34	53	50	49	58	71	75	83	92	96
Visibility (km)	7	7	7	7	8	8	12	15	12	10	11	11	6	7	5	4	3	2

Theoretical work by Hänel (1971) has shown that nuclei are swollen when humidities exceed 30% and for this reason it was decided to draw the curves to an asymptote of this value, as shown in Fig. 3.

5. Graph of evening visibility against relative humidity

The visibility at 2100, 2200 and 2300 GMT was recorded for the same selected days and three further curves were produced (Fig. 4). The evenings provided considerably more high humidity values but these curves must be considered as coming from a different data set from the afternoon visibilities because the

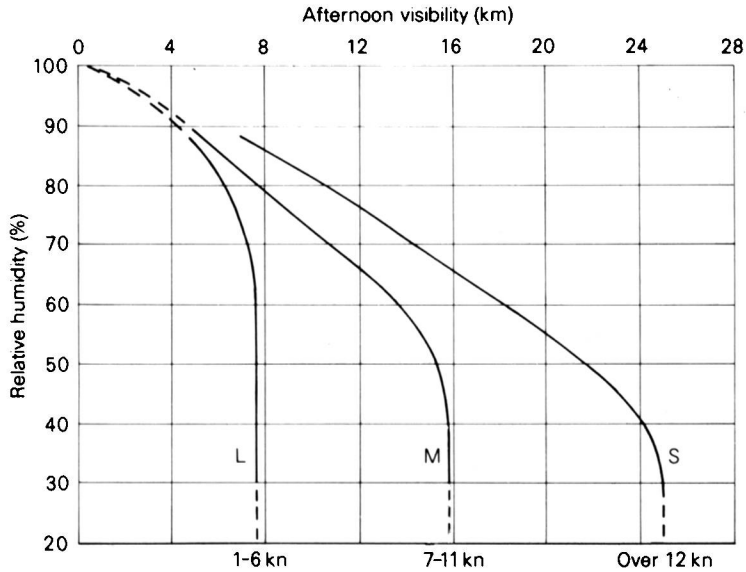

Figure 3. Afternoon visibility against relative humidity for three classes of wind speed in 'easterly' synoptic situations. Median values are represented by L, M and S for light, moderate and strong winds respectively. The curves should be regarded as provisional for relative humidities above 87% and below 30%.

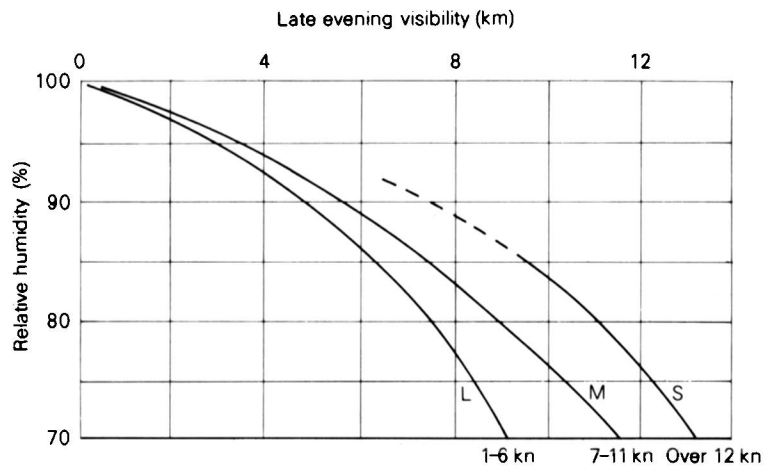

Figure 4. Late evening visibility against relative humidity for three classes of wind speed in 'easterly' synoptic situations. Median values are represented by L, M and S for light, moderate and strong winds respectively. The curve for strong winds should be regarded as provisional for relative humidities above 87% where data were sparse.

surface wind speed will often have halved between 1400 and 2200 GMT as the lower levels of the atmosphere stabilized. The 'over 12 knot' afternoon class should approximate to the evening '7–11 knot' class. The relationship between afternoon and evening visibility could of course be destroyed in a period of 1 to 3 hours if there is a local source of pollution just upwind. There were insufficient data for these curves to be extended below 70%. Both the afternoon and the evening graphs support the view that stagnant conditions and poor visibility go hand-in-hand.

6. Seasonal variations

Although Bonvoisin and McHugh's statistical analysis had shown that winter was markedly the worst season for visibility, this was without reference to moisture content. For the combined 43–72% relative humidity classes in the present study, the values of afternoon visibility were as given in Table III.

Table III. *Seasonal comparison of median values of visibility for humidities in the range 43–72% (wind class 7–11 knots) for easterly airstreams.*

Winter (Dec.–Feb.)	Spring (Mar.–May)	Summer (June–Aug.)	Autumn (Sept.–Nov.)
	kilometres		
12.6	12.2	14.2	15.2

Thus spring emerges as the worst season from this limited selection of dates. The apparent contradiction with Bonvoisin and McHugh is caused by the lower frequency of dry air in winter. So whilst real visibilities are worse in the damp days of winter, the levels of pollution may well be just as great in spring with its high frequency of prolonged blocked situations. Certainly power station and home heating output will be high in winter and early spring, and a marked inversion will often be present in both winter and spring easterlies to form a 'lid' through which pollutants are unable to escape. When little cloud is present (as is often the case in spring with a short sea track) aircraft pilots frequently report a haze top between 2000 feet and 8000 feet.

7. Effects of convection

The popular belief amongst forecasters is that a sudden improvement of visibility occurs when convection develops. This is of course true for most southerly, westerly and northerly airstreams, for with these gradient directions the air aloft is clean and only pollution produced locally in the British Isles is trapped below the early-morning inversion. With the onset of convection the nuclei are spread upwards, and with unstable westerlies and northerlies through such a depth that even with the limited visibility points of southern England an estimated value of 30 or 40 km will be reported. With easterly airstreams the evolution is somewhat different. Local pollution is often trapped below one inversion at say 1000 ft, with continental particles below another inversion at perhaps 5000 ft. In this case the destruction of the low-level inversion by surface-based convection will produce a marked improvement for perhaps 15–30 minutes but soon there will be a partial reversal of the trend as mixing is completed throughout the lowest 5000 ft. Dilution of the pollutant is therefore less effective in easterlies, and such improvement as does take place is partially accounted for by the fall in relative humidity. The surface wind will also usually have increased. A schematic diagram illustrates the point (Fig. 5).

A study of inversion heights in Crawley (03774) radiosonde reports for 1200 GMT reinforced the view that correcting for convection depth is of remarkably little help in forecasting visibilities in easterlies. However, strong surface winds suggest a higher inversion so the depth of mixing is already taken into account by the wind speed categories in Figs. 3 and 4.

8. Sinks for pollution

Much has been written about sources, but what of sinks? The increase in haziness over recent decades has been noted by astronomers at mountain observatories but obviously it is not a one-way traffic. Some dry deposition must occur but the fall speeds of particles of radius 0.2 to 1.0×1.0^{6} m are small in relation

to the normal vertical motions in the atmosphere generated by turbulence or convection. Scorer (1978) has pointed out that deposition can occur where horizontal airflow impinges upon hedges or woodland and this might have a significant effect on visibility in rural locations. Nevertheless, during prolonged easterly or anticyclonic spells a progressive deterioration in visibility usually occurs. Practising forecasters appreciate the considerable benefit of rain in improving the visibility, and occasions were noted during the present study when pollution appeared to be washed out of the atmosphere. Drizzle, on the other hand, may not be as effective as rain because the nuclei possibly avoid collision with small precipitation droplets. Smith (1983) has described lifetimes of particles as 'of the order of a few days' and 'determined by the frequency of interception by rain belts'. Fig. 6 shows the synoptic situation on a day of very poor visibilities over eastern England and Fig. 7 shows the situation as westerlies were re-established, with cleaner air of maritime origin already affecting the British Isles and extending eastwards across Germany. When considering visibilities in polluted airstreams in western Europe, replacement of the air by clean westerlies is the usual mechanism for improvement. As one travels eastwards across Europe wash-out becomes increasingly important because the westerlies themselves are less clean.

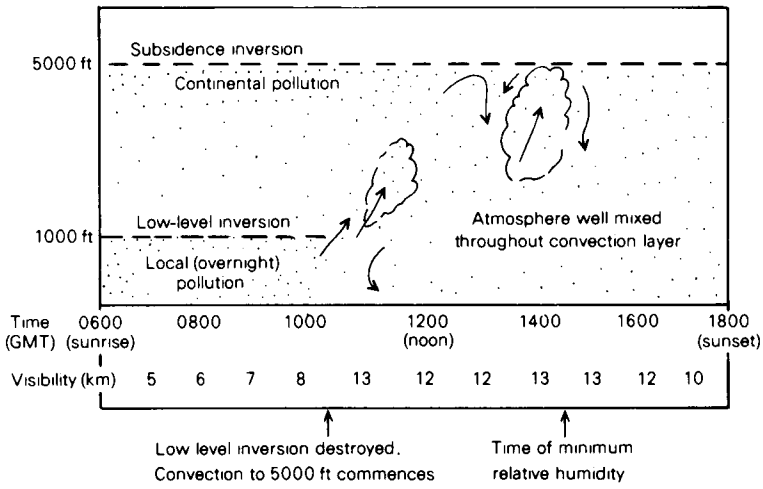

Figure 5. A time cross-section to illustrate typical visibility changes on a day when convection develops in an easterly airstream. In this schematic example two visibility maxima take place. One occurs shortly after the low-level inversion has been destroyed by surface heating and the second occurs around the time of minimum humidity.

9. Practical applications

It is not intended that Figs. 3 and 4 should be used in isolation. A forecast made at 0600 GMT of temperature, dew-point and surface wind speed for 1400 GMT would produce a nominal visibility forecast from the graph. It is far better, however, to look at upwind values of humidity and wind speed to see if they are above or below the median line and then multiply by this 'pollution factor'. For example, if the 1400 GMT visibility were 8 km against a median value of 10 km, then the 2200 GMT forecast should be multiplied by a factor of 0.8, assuming no change of air mass and no special source of local pollution. Yesterday's upwind 1400 GMT observation can be corrected for today's 1400 GMT forecast wind speed and RH.

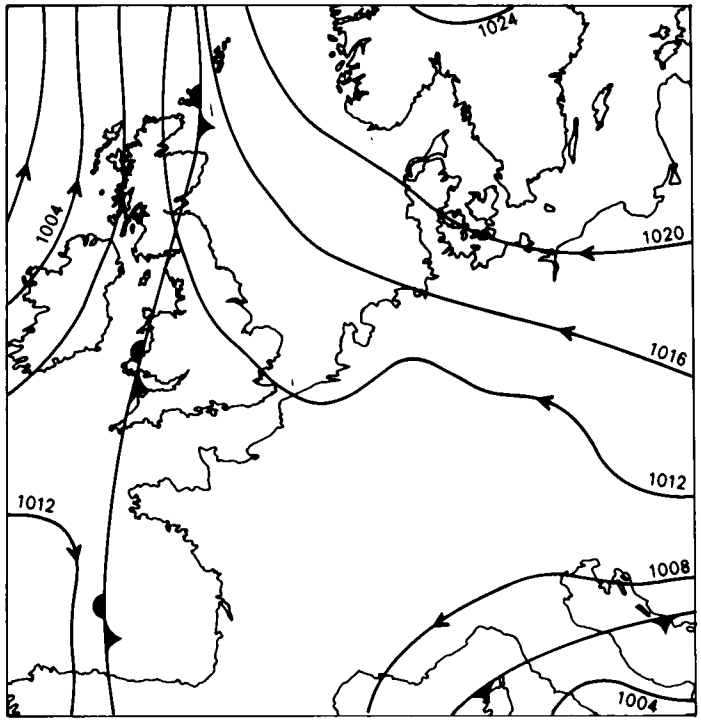

Figure 6. Surface analysis for 1200 GMT on 22 March 1984. Visibilities were poor over Germany, Belgium, Netherlands and the eastern half of England.

The bench forecaster will of course be dealing with temperature and dew-point to produce his forecast humidity and should bear in mind the slight fall of dew-point that usually occurs during the evening, as well as the decrease of surface wind.

On a chart of plotted observations the southern boundary of the polluted arc is far from sharp. There will still be some haze in a 170° gradient. The northern boundary is much more critical and often visible on the working chart. A straight 060° gradient will bring clean air from Scandinavia but a cyclonically curved flow from Germany can approach southern England from 060° loaded with pollutants and a high moisture content to give the worst conditions (see Fig. 8). Some idea of the source regions for this pollution can be gained from Fig. 9 which is taken from the EMEP report by Eliassen and Saltbones (1982). Although this map is of sulphur emissions it gives an indication of the relative degree of industrialization.

In the worst cases, which can occur after a week of light to moderate easterlies, visibilities may get down to half the values indicated by the median line. If winds then increase there will be a time-lag before values reach the 'over 12 knots' category. However, strengthening easterlies often bring only a temporary visibility improvement during a prolonged blocked situation and one still has to wait for an Atlantic front to restore truly clean air.

10. Results from a test of the method

Spot values of visibility at Brize Norton were examined for 'easterly days' in 1983. The dates were chosen by the same method as the original data. Values were recorded for 1400 and 2200 GMT and the

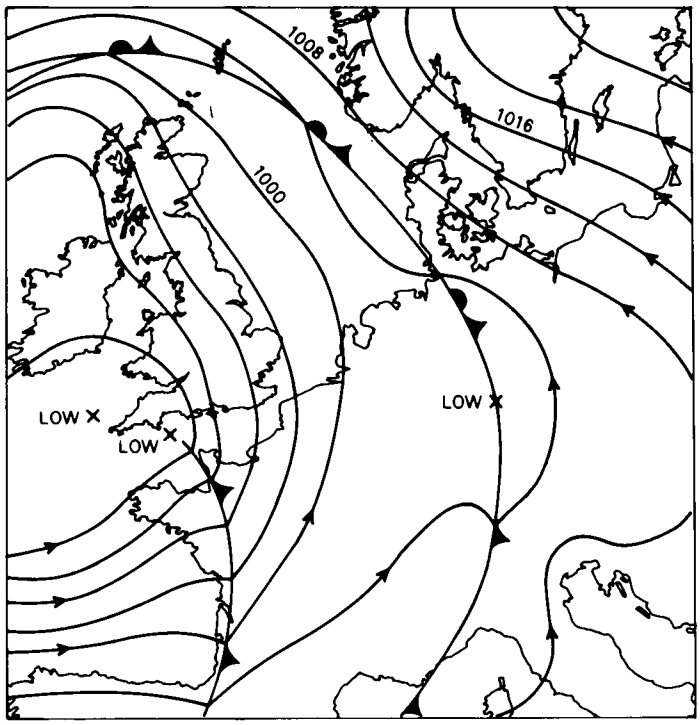

Figure 7. Surface analysis for 1200 GMT on 25 March 1984. The two eastward-moving fronts brought clean air into Europe from the Atlantic.

first 15 results are shown in Table IV. The 'uncorrected forecasts' are those obtained from the graphs, with the admittedly artificial use of the observed values of relative humidity and surface wind speed. 'Actual values' of visibility in the table are those recorded at Brize Norton. The 'corrected forecast' for

Table IV. *Test of method using the correction factor to give a modified forecast for 2200 GMT. Visibilities are in kilometres.*

1400 GMT		2200 GMT		
Uncorrected Forecast	Actual	Uncorrected Forecast	Corrected Forecast	Actual
14.2	20.0	8.9	12.5	18.0
10.7	10.0	10.2	9.5	8.0
12.1	10.0	8.4	6.9	8.0
11.8	15.0	6.2	7.9	8.0
10.5	8.0	7.7	5.9	10.0
7.2	4.0	4.4	2.4	2.0
7.0	4.5	4.0	6.6	4.5
15.3	25.0	14.0	22.9	25.0
20.0	35.0	11.4	20.0	20.0
15.3	10.0	7.5	4.9	4.0
12.5	4.5	7.7	2.8	3.5
15.3	10.0	7.0	4.6	8.0
19.4	25.0	9.0	11.6	8.0
6.7	25.0	4.9	18.3	14.0
13.0	20.0	2.8	4.3	7.0

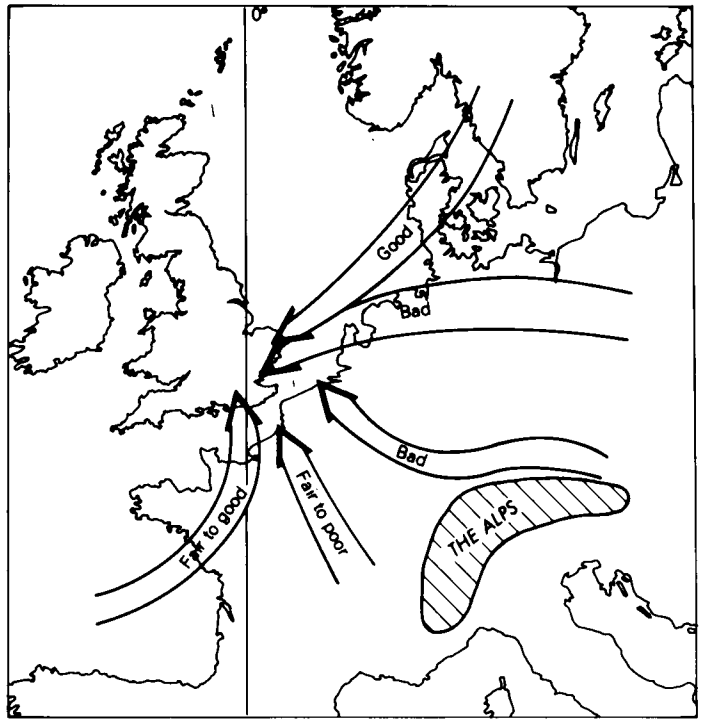

Figure 8. Visibility with various continental airstreams.

2200 GMT is obtained by multiplying the uncorrected graph reading by a 'pollution factor'. This factor corrects for the difference between the particular day of interest and the typical value represented by the median line on the graph. It is the ratio of 1400 GMT actual to the 1400 GMT uncorrected forecast. In practice the forecaster will normally use an upwind observation to obtain the appropriate 'pollution factor'.

A total of 25 days were tested in this way and on 19 occasions the correction based on the 1400 GMT actual was in the 'right' direction.

The artificial use of actual wind speed and humidity will be offset in reality by the ability of the outstation forecaster to look at upwind values of visibility rather than his own station's 1400 GMT values.

Conclusion

No forecasting method for visibility can ever produce accurate answers all the time. A stubble fire at the end of the runway or a fresh burst of activity at a nearby factory will see to that. Equally, though, the forecaster should have some help in establishing a preliminary estimate and the writer hopes that the graphs produced here for easterly airstreams will give him something to set his thought processes in train. The modification of upwind visibilities in terms of changes in relative humidity and surface wind speed plus a small subjective correction for convection depth constitutes a possible way forward.

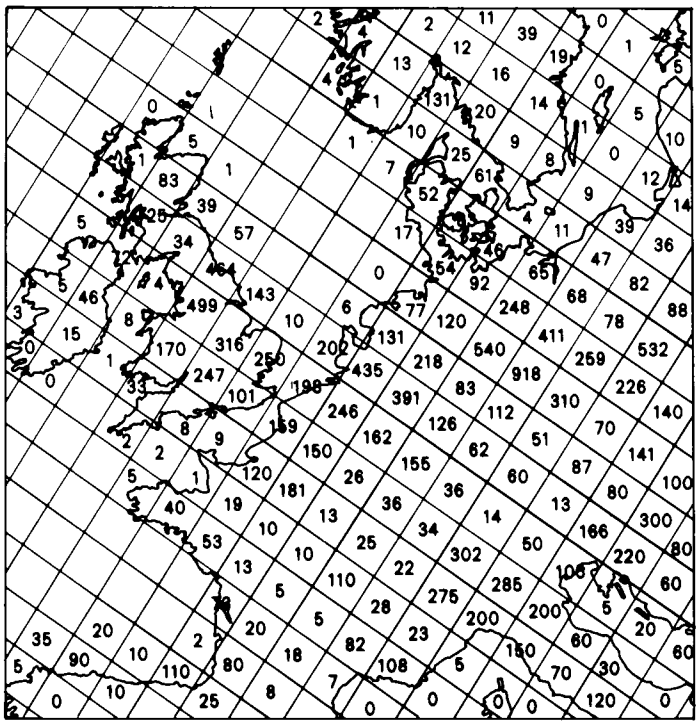

Figure 9. European Monitoring and Evaluation Programme (EMEP) emission data for 1978 in part of the 150 km × 150 km grid network. Units are thousands of tonnes sulphur equivalent per year.

References

Bonvoisin, N. J. and McHugh, B. C. 1983 Statistics of visibility in the 0–10 km range for selected stations. (Unpublished, copy available in the National Meteorological Library, Bracknell.)

Eliassen, A. and Saltbones, J. 1982 Modelling of long-range transport of sulphur over Europe. EMEP/MSC-W Report 1/82, Oslo, Norwegian Meteorological Institute.

1983 Modelling of long-range transport of sulphur over Europe. *Atmos Environ*, **17**, No. 8, 1457–1473.

Hänel, G. 1971 New results concerning the dependence of visibility on relative humidity and their significance in a model for visibility forecast. *Beitr Phys Atmos*, **44**, 137–167.

Scorer, R. S. 1978 Environmental aerodynamics. Chichester, Ellis Horwood Ltd.

Smith, F. B. 1983 Long-range transport of air pollution. *Meteorol Mag*, **112**, 237–244.

551.5(09):551.507.352:92

How the meteorological reconnaissance flights began

By E. B. Kraus

Summary

An account is given, based on personal reminiscence, of how meteorological reconnaissance flights started during the Second World War. Some experiences of the pilots and observers are described.

This is a very personal account of the beginning of the meteorological reconnaissance flights.

In 1939, I was a graduate student of Jack Bjerknes in Bergen, Norway. I also held a Czech private pilot's licence and both British and Czech soaring (C) licences. I had done some soaring on Dunstable Downs during the summer of 1938 and had met, during that visit to England, Professor Lindeman (later Lord Cherwell) and E. Gold (then Deputy Director of the Meteorological Office). I mention these names, because they played a role in the subsequent Meteorological Reconnaissance Flight story.

After the outbreak of the war I volunteered for service in France and finally got there in March 1940. When France collapsed in June 1940, I made my way to England via Algiers and Gibraltar. Things were a bit confused at that time. I arrived in England without any papers and in some trouble after a spat with a senior Czech officer during the passage from Gibraltar to Liverpool. As a result I found myself — with several thousand others — in Pentonville prison while the authorities pondered who we were and what to do with us.

When nothing happened for two weeks or so, I contacted Gold who sent Flt. Lt. Portass, the former Meteorological Liaison officer in France, to Pentonville to identify me. Things developed quickly after that. I was released and asked to join the Czech army in England as a private. At the same time I was offered via Portass a commission as a meteorological officer in the RAF Volunteer Reserve. My experience during the passage from Gibraltar had made me chary of the Czech military. Like other armies-in-exile they were desperately short of enlisted men (officers are much more mobile in defeat). Pilot Officer sounded grander than private 2nd class; it also seemed to offer a chance of flying again. The decision to join the RAF was clinched after a talk with Col. Kalla who was the military attaché at the Czech embassy. He told me not to be a fool and to use my opportunity. (Kalla was executed in Prague after the communist take-over.)

By that time, the Battle of Britain had started. Like all new officers in the RAF I was given 40 guineas to buy myself two uniforms and other paraphernalia. I then reported to Adastral House. The interviewing officer told me that I was posted to familiar grounds in Dunstable and — by the way — here was some secret material which had to be carried by an officer, so would I please take it along. Until then, even after my release from Pentonville, I had to report to the local police once a week as a suspect foreigner. The confidence of this unknown briefing officer had suddenly made me a member of the club. Nothing could have kindled more loyalty to the RAF than this simple and probably unpremeditated casual gesture.

In Dunstable I worked briefly with Douglas* and — I believe — with Durst†. In September or October 1940 I was posted as a Meteorological Officer to No. 4 Group, Bomber Command in York. The Senior Meteorological Officer in York was Richard Veryard‡. We got on particularly well together, but

*C. K. M. Douglas: The Meteorological Office's greatest forecaster. See obituary notice in *Meteorol Mag.* **111**, 1982, 252.
†C. S. Durst: Assistant Director (Special Investigations) 1948–53.
‡R. G. Veryard: Deputy Director (Central Services) 1958–59. President of the Commission for Climatology of WMO 1957–61.

I still wanted to fly. Both Veryard and I felt that meteorological forecasts would be improved if more data were available from oceanic locations. To get these data on a regular basis would require special, long-distance meteorological reconnaissance flights. A letter which rationalized and advocated the institution of such flights was drafted by me and sent — under our joint signature, I believe — to Nelson Johnson who was then Director of the Meteorological Office. This letter is presumably still in the archives. We also discussed the matter with Air Vice Marshal Coningham who was Air Officer Commanding No. 4 Group and who supported the idea through RAF channels.

I do not know whether it was really this initiative which led to the establishment of the meteorological reconnaissance flights. The idea may have been in the air, because I got a very fast response. Within weeks, probably in November 1940, I was summoned to London to see Johnson at the Air Ministry. He referred to Veryard's and my letter and asked me whether I would like to organize and start the flights. The following day in London, I was taken to lunch by Sydney Chapman. We ran accidentally into Lindeman who told me that he had heard about the meteorological flight initiative and that he thought it a good idea. As he was Churchill's adviser, this may have contributed conceivably to the realization of the project.

I was asked to recommend an operational procedure and a data reporting code for Gold's approval. I suggested regular flight tracks over the Atlantic in a north-westerly and south-westerly direction. The North Sea was added to this on Gold's insistence. My suggested plan of operations was to fly out at a low level to a distance to be determined by the range of the aircraft, then make a spiral ascent to the 500-millibar level and then return on a glide path to save fuel and stretch out the aircraft endurance. All this was rather readily accepted, but the proposed code turned out to be much more controversial.

In his time, Gold had devised innumerable codes and standards for the international meteorological community. He considered himself — rightly — an expert in this field. He also was a passionate adherent of the imperial as distinct from the metric system. We fought heatedly over trivia, until I felt that it was unbecoming for a young man to be so dogmatic with this old, experienced gentleman. I then proceeded to accept everything he said, but that too was the wrong policy. Gold loved to argue. From the moment I agreed with him, he turned round and found merit in what he had criticized so bitterly before. In retrospect, I believe Gold to have been probably the brightest and almost certainly the most distinguished scientist in the upper Meteorological Office ranks during the nineteen thirties and forties. It may have been his argumentativeness and his undisguised contempt for anything he considered foolish that kept the directorship of the service out of his grasp.

My first meteorological flight posting was to Aldergrove. When I got there in January 1941, I found three Blenheims and a complement of ground crews at my disposal — but no aircrews. Pilots were at a premium just after the Battle of Britain. For a month or so I moped around in Aldergrove, sending increasingly shrill requests through my direct pipeline to Gold and Johnson for either pilots or for permission to fly myself. In the meantime, I amused myself by flying convoy missions with one of the local Anson squadrons (No. 206) and by borrowing some of their pilots during their spare time for meteorological instrument calibration on the Blenheims.

In due course, I heard from the Air Ministry that there was no time for me to go through pilot school before starting the meteorological flights, but that they would send me to a crash navigators' course instead. As far as I remember, the course was in the Lake District or in Northumberland. It gave me a lifelong interest and facility in reading the lie of the land from the sky; I also learned a lot about celestial navigation but, at the final examination, I failed—in meteorology. One of the questions asked about the weather associated with a lapse rate of 10 °F/1000 feet. The expected answer was that it would be very unstable; instead I pointed out that such a lapse rate is not observed and cannot exist in the free atmosphere. The examiners were not amused and did not pass me, but after some noisy protests to Air Ministry I was told to stick on that badge and for God's sake to stop making such a nuisance of myself. A

long time later, after I left the meteorological flights and after several hundred hours of operational flying during which I had worn my flying badge, I received a totally unexpected letter from HQ. No. 17 (Training) Group, which certified me as a qualified air observer — so I did become legitimate in the end.

While I did my navigation course, two pilots had been posted to 1403 Meteorological Flight in Bircham Newton and I went there to join them at the end of February 1941. The senior of the two, FO Douglas Bisgood (Fig. 1) was a regular fighter pilot, who had somehow been patched together again after being terribly wounded in a head-on air collision during the Battle of Britain. After a few training and calibration flights, as well as a flying visit to Aldergrove to keep up the morale of the still pilotless ground crews of No. 1405 flight there, Douglas Bisgood and I (Fig. 2) carried out the first operational meteorological reconnaissance flight on 14 March 1941.

Figure 1. Douglas Bisgood.

Figure 2. Eric B. Kraus.

Bisgood and I flew together almost every day during the following month (Fig. 3). We tested different psychrometers and experimented with the use of bomb-sights to measure our height above a cloud surface. The Blenheims were not ideally suited for the job we had to do. They barely staggered up to the 500 mb level. We developed a procedure which required straight and level flight or even a shallow dive when the aircraft approached its ceiling. When the speed had become large enough during this phase, the pilot pulled up the nose for a little hop to a higher level where the procedure was repeated again. After a few of these steps we usually managed to get up to 500 mb.

Towards the end of March, Bisgood and I were joined by two other pilots: Flt. Lt. Denis Wykeham-Martin who took over as OC 1403 flight and Flt. Lt. Pat Ritchie (Fig. 4). When I flew with Douglas Bisgood I had to remind him sometimes that his job was no longer that of a fighter pilot. In return he used to tease me mercilessly. One day in April, he came back from a meteorological reconnaissance flight — without me — and saw three Junkers 88s returing from a raid over England to Germany. He stalked them through the summer cumulus clouds, attacked the last of the much bigger aircraft with his single, forward-shooting Blenheim popgun and shot it down. On Wykeham-Martin's recommendation, Bisgood got a DFC for this — I believe it was his second DFC. He died less than a year later.

We split up at the end of April. Bisgood was promoted and became the CO of 1403 flight in Bircham Newton, Ritchie took over as CO in Aldergrove and Wykeham-Martin went to St. Eval to start No. 1404 Meteorological Reconnaissance Flight there. I too had been promoted and was left free to commute between the three flights, though I made my permanent base in St. Eval. Later in the summer of that year, Wykeham-Martin was sent to some course or staff college for three months and I took over as acting CO of 1404 flight during his absence.

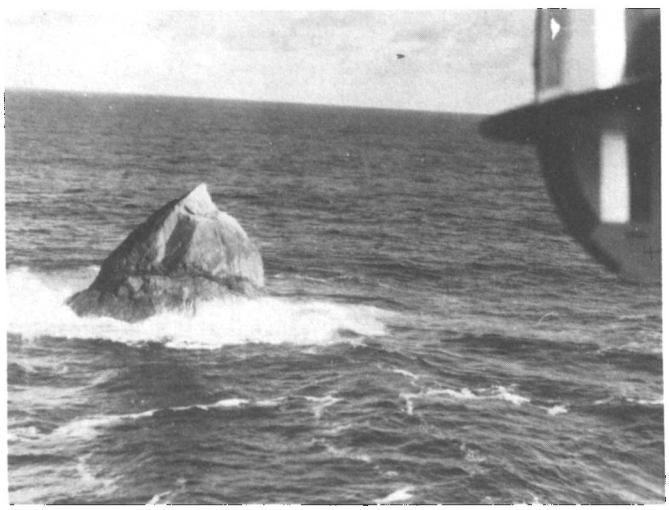

Figure 3. Rockall seen from Blenheim Z7340.

Figure 4. From left to right: Wykeham-Martin, ?, ?, Ritchie, ?

Our flights out of St. Eval over the Bay of Biscay were twice as long as those from Bircham Newton. We saw many U-boats. The fact that our sightings were relatively more frequent than those of the regular anti-U-boat patrols led to a change in official Coastal Command tactics, I believe. Instead of cruising just above the waves the patrols were ordered to fly at the higher level from which the meteorological flight crews had reported most of their first sightings. One day, coming back from the Bay with myself on the controls. I saw a U-boat below. With great excitement I dived down, popgun blazing. It was only when I levelled out above the water that I discovered it had been a poor whale whom I had so mercilessly attacked.

Meteorological flight crews became accustomed to fly in really bad weather when everyone else was grounded. Our unofficial flight badge — umbrella over skull and crossed bones with the motto *Semper in excreta* below — which had been designed by Bisgood and was painted on the side of our Blenheims (Fig. 5) perhaps bears witness to this. The aerodrome at St. Eval was closed officially when the ceiling was down to 400 feet, but we did not like to be diverted and by informal arrangement with the local meteorological officers the indicated ceiling was always at least 400 feet when the meteorological flight came back, whatever the actual cloud-base height. This permitted the returning pilot to make his own decision.

Figure 5. Flight badge of the meteorological flight's Blenheims, designed by Flt. Lt. Bisgood — *not* approved by King George VI.

One of the most experienced pilots in 1404 Flight was Flight Sergeant Portman (Fig. 6). I had recommended him for a commission while I was acting CO. On his first flight as a Pilot Officer, he returned in miserable weather — with the usual indicated ceiling of 400 feet. He broke cloud over what he expected to be the sea, but was in reality the Lizard. The first object he saw was a bush right in front of him. The only thing he could do was to force the aircraft up the slope of a hill which just matched the maximum Blenheim climbing rate. The propellers churned through the heather, a fence was knocked over and an innocent pedestrian only saved himself through violent evasive action. Finally, Portman reached the summit of his hill and then made it safely to St. Eval. His Blenheim, with the leading edge and the landing lights full of gorse which Portman had collected during his climb, is shown in Fig. 6.

Figure 6. Note gorse on Blenheim's leading edge. For left to right: ?, ?, Flt. Sgt. Portman, Flt. Lt. Kraus.

Through most of 1941 I had been able to write my own ticket. I had cut quite a few corners to get the meteorological flights off the ground. In the autumn of 1941, these free-wheeling days came to an end and bureaucracy took over. I was put formally under the command of a Wing Commander Carey at Coastal Command. At the same time, Peter Sheppard was appointed head of a Branch in the Meteorological Office which was to be responsible for meteorological reconnaissance. Carey first kept me in an office next to his at Coastal Command and then ordered me to Iceland to start a reconnaissance flight out of Kaldadharnes. It was the first time I was told by higher authority what to do.

I went by train and ship to Aldergrove and then took one of Ritchie's planes to Iceland. By that time, the Blenheims of 1405 Flight had been replaced by Lockheed Hudsons, which were considered a death-trap in a forced landing on water. I remember that when we landed in Kaldadharnes the wind blew at about the same speed as the landing rate of the Hudson. When Flt. Lt. Eccles put the aircraft down, it rolled to a stop within about ten yards. On the return flight, somewhere between Iceland and Aldergrove, I heard in snatches over the radio about Pearl Harbor and about America's entry into the war. I knew then that the war had entered a new phase.

When I got back to London I had jaundice. I was also tired after some 400 hours of operational flying in eight months. I had to get Carey's permission to get married early in 1942, which was granted rather grudgingly. After a short honeymoon, I was posted as an instructor to a training station in Thornaby. I cannot remember what or whom I taught there — it may have been new meteorological observers. From my log-book I see that I did some flying in Thornaby, participated in two bombing raids and visited Bircham Newton again. In April 1942, I went on four long Meteorological reconnaissance flights out of Wick, Scotland. One of these must have got me over Norway, because I have some photographs of it in my album. Curiously, these days are much less vivid in my mind than the early Meteorological Flight days in Bircham Newton and St. Eval.

After the summer of 1942, when I was posted to Benson, Oxfordshire as the Senior Meteorological Officer with the Photographic Reconnaissance Unit there, I lost contact with the Meteorological reconnaissance flights. Douglas Bisgood, Denis Wykeham-Martin and John Portman were all killed in different places during this year. Ritchie went on after the war to become Master of the Guild of Navigators in Australia and then Managing Director and, I believe, Chairman of Qantas Airways.

Three years after my official departure from the Meteorological Flights, just after the end of the European war, Sqn. Ldr. Saffery and I ferried a long-range photo-reconnaissance Mosquito aircraft from Benson to Calcutta. While we were in India, we were asked to fly to Colombo for a visit to the South East Asia Theatre HQ. I was briefed there about the planned dispatch of several bomber groups from England to China for participation in the war against Japan. In preparation for this effort, I was to explore the Chinese meteorological facilities and also make suggestions for the establishment of a Mosquito meteorological reconnaissance flight over the South China Sea. It was in China — again in the air — between Kunming and Chungking that I heard about the Hiroshima bomb, which made the establishment of a Pacific meteorological flight rather irrelevant.

This article was written in response to a general appeal for such reminiscences; although not originally intended for publication, it will, we think, interest our readers.

Notes and news

MOLARS goes on-line

The Meteorological Office Library Accessions and Retrieval System (MOLARS) contains a bibliography of books, journals and individual articles held by the National Meteorological Library, London Road, Bracknell, Berkshire RG12 2SZ. Since 1972 over 9000 items a year have been catalogued and classified by UDC (Universal Decimal Classification) numbers covering meteorology, climatology and related atmospheric sciences.

On-line access to MOLARS is now available from the European Space Agency Information Retrieval Service (ESA-IRS). Details may be obtained from the United Kingdom agent, DIALTECH (telephone: 01-212 5700). Access to MOLARS from within the Meteorological Office is available on terminals from the main computing complex (COSMOS).

For details of MOLARS, see Harris and McSean (1980).*

Last remaining serving wearer of the 'M' brevet leaves the RAF

Wing Commander B. D. (Brian) Tanner, the last remaining serving wearer of the 'M' brevet, retired from the Royal Air Force last April.

Wg/Cdr. Tanner joined the RAF as a National Serviceman in August 1953 and in March 1957 attended the Aero Met Observers' Course at RAF Aldergrove, and was awarded his now unique 'M' brevet in June 1957. As a Sergeant Meteorological Observer he flew over 1800 hours in Shackleton and Hastings aircraft, deliberately seeking out and flying in the foullest weather to obtain essential weather data. In Septeber 1959 he left the Service but re-entered shortly afterwards and was commissioned in September 1960 into the Air Traffic Control Branch. The Squadron responsible for Meteorological Research, No. 202, was disbanded in 1963 and the majority of the 'M' brevet holders retired soon after. Squardron No. 202 was later re-formed and found further fame in the Search and Rescue role.

As an air traffic controller Wg/Cdr. Tanner has held a wide variety of appointments, including Senior Air Traffic Controller at RAF Leeming and Command Air Traffic Controller at HQ Strike Command; his last was as Officer Commanding Central Air Traffic Control School.

---

*Harris, E. W. C. and McSean, T.; MOLARS — Automating the National Meteorological Library. *Meteorol Mag*, **109**, 1980, 18-21.

Wing Commander Brian Tanner (left) with Squadron Leader Mike Stokes, Officer Commanding, Meteorological Research Flight. The WC130 of the Meteorological Research Flight is in the background.

Reviews

Our threatened climate: ways of averting the CO_2 problem through rational energy use, edited by Wilfred Bach. 182 mm × 248 mm, pp. xxiv + 368, *illus.* D. Reidel Publishing Company, Dordrecht, Boston, Lancaster, 1984. price Dfl 95.00, US $29.00.

Professor Bach is already the author or editor of several books on topics including energy, pollution, food production and climate. Thus, it is not surprising that this book is not just confined to a narrow survey of CO_2 and climate, but delves into wider economic and social issues as well. The book could equally well have been called 'Our threatened world: ways of averting an energy crisis and related problems through rational energy use'. The book, an updated version of the German original, is intended to present the recent state of scientific knowledge in a manner comprehensible to those outside the scientific community and to decision makers in particular. Apart from some reservations listed below, the author has provided a readable text without in general sacrificing scientific accuracy, and his treatment of the climatic aspects of the problem, on which I am best qualified to comment, is for the most part fair and balanced.

The main text is preceded by an executive summary (why 'executive'?) of the chapters to come. Next there is a short introduction, followed by a chapter on climate and climate change, including the history of the earth's climate, a description of the climate system and how it is affected by changes in the concentration of radiatively active gases, and a survey of numerical models of climate. Chapter 3, on

social and political aspects of the problem, discusses population growth, settlement patterns and future energy demands. Chapter 4, on the influence of society on climate, is the heart of the book. It covers not only the carbon cycle, past and future levels of atmospheric CO_2 and their impacts on climate, but also sections of variable quality on the effect of other trace gases, waste heat, and of changes in land use. (The conclusions of the chapter are spelt out in a short question and answer section, just to make sure no-one misses the point!)

Chapter 5, on the impacts of climate changes on society, says much about the impact of climate on society but is necessarily vague and speculative where climate change is mentioned. Consequently, one arrives at Chapter 6 (Strategies for averting a CO_2–climate problem) with little quantitative idea of the problem to be averted. Bach argues that technological fixes to reduce CO_2 emissions are impracticable, hence the only immediate solution is to increase the efficiency of energy use and reduce wastage, allowing time to develop renewable energy sources. The final chapter, on opportunities for the future, develops this theme and suggests how it might be implemented. There are an additional 100 pages which include references, indexes, appendices, a bibliography and a glossary of technical terms.

The style of the presentation is largely descriptive, as befits the intended audience. There is some necessary repetition, as on pages 42 and 104. In places, the author discusses particular examples as if they were generally true, as on page 106 where he does not make it clear that the paragraph on the length of integrations (and initial conditions) refers to a specific study and would be inappropriate, for example, for a model including the oceanic mixed layer. There are also several inaccuracies. For example, the sea temperatures off eastern South America in Figure IV. 13 are overestimated because upwelling is ignored, not just poorly represented in the model; the overlap of CO_2 and H_2O absorption bands does not amplify the CO_2 influence on the radiative flux (page 108) but modifies it, as explained on page 133; and, on page 182, the relationship between sunspot number and climate is at best speculative, and no plausible mechanism such as that suggested in the text has been verified.

Most of the diagrams are clear and well produced, but the text gives an impression of being cramped, and some of the tables are very difficult to read. I noticed few faults, apart from a missing reference (Gornitz *et al.* 1982, on page 188) and one or more missing lines of text on page 174.

Much of the author's argument rests on the premise that the impacts of increased CO_2 are necessarily undesirable and should be avoided. I found the case against CO_2 'not proven', largely because Professor Bach gives inadequate consideration to the possible beneficial effects of increased CO_2, both through direct effects on plant growth and indirectly through changes in climate. However, some of his other arguments for rational energy use are more convincing. To judge for yourself, you will need to read the book.

J. F. B. Mitchell

Carbon dioxide: current views and developments in energy/climate research, edited by W. Bach, A. J. Crane, A. L. Berger and A. Longhetto. 160 mm × 245 mm, pp. xvii + 525, *illus.* D. Reidel Publishing Company, Dordrecht, Boston, Lancaster, 1983. Price Dfl 180, US $72.00.

This book consists of the lectures given at the second course of the International School of Climatology held at Erice from 16 to 26 July 1982. The murky photograph of the participants, a poem on the CO_2 blues (in Italian!) and cartoons (no doubt dreamt up in the evening at the bar) are probably included to remind those who attended what a good time they all had. For other readers, in the foreword it is hoped that the volume will provide a balanced perspective on the CO_2 problem as it currently stands whilst the preface hopes that together the lectures form a coherent text of real educational value. Despite the unfunny cartoons these objectives are largely achieved.

As is customary now for books on CO_2 there are sections on I/the carbon cycle, II/climate effects and III/impacts and strategies with 16 contributions in all. These are mostly of reasonable length and some effort has been made in editing and cross referencing so that themes are developed by different authors without too much repetition.

In part I, Wallen gives an account of the history of monitoring the CO_2 content of the atmosphere from the late 18th century to the present-day measurements made at the Mauna Loa Observatory which show an increase from 315 parts per million by volume (ppmv) in 1958 to 337 ppmv in 1980. The global network of monitoring stations is described with reference to the problems of standardization and the influence of the biosphere on regional and continental stations. Baes then gives a nice introduction to the role of the oceans in taking up the excess CO_2 released into the atmosphere from fossil fuels. The oceanic chemistry is presented clearly and possible changes in the composition of surface waters illustrated by the titration alkalinity/total inorganic carbon diagrams, these are well worth the effort to understand if, like me, you find the numerous possible chemical reactions rather confusing. Attempts to model the carbon cycle are reviewed by Bjorkstrom with particular emphasis on the oceanic uptake which has been modelled using a simple two-box model and more sophisticated models with diffusion and representations of the circulation. Such models have been employed to predict future levels of CO_2 and in the following chapter, Kohlmaier *et al*, discuss the difficult problem of the role of the biosphere in the carbon cycle. The uncertainties in the inventories and fluxes between the various components of an ecosystem are stressed whilst quantifying human impact by changing land use is hampered by lack of data on past changes. They conclude that terrestrial biota may be a net source of atmospheric carbon of from 0 to 5 gigatonnes per 100 years. Also historical changes from forest to agriculture and grasslands in temperate latitudes may have been responsible for some of the observed increase in CO_2 although now such regions may be acting as sinks due to re-growth and are probably balancing the major clearances of tropical rain forest. This is supported by the proxy data on atmospheric CO_2 content from tree rings described here by Lorius and Raynaud. Estimates of the pre-industrial level of 230 to 260 ppmv suggest that late 19th century pioneer agriculture was an important non-fossil fuel source. Ice core studies are also described for longer time-scale variations.

In part II, Kandel describes the basic physics of the greenhouse effect and the likely increase in global mean surface temperature due to increased CO_2 deduced from simple radiative-convective and energy balance models. Some of the arguments on the surface energy balance I found a little difficult to follow and unfortunately the emphasis on global surface temperature changes tends to be a too restrictive view of climate. General circulation models could provide a means of determining possible changes in regional climate such as temperature and changes in the hydrological cycle. The equilibrium response to increased CO_2 is clearly described by Gilchrist with particular reference to experiments performed in the Meteorological Office which are compared and contrasted to those carried out at GFDL. Whilst equilibrium experiments are extremely useful for determining which processes are important it is the transient response that we are likely to experience and Hoffert and Michael consider this in the following chapter, particularly the ocean's role in delaying future warming. This interesting topic is here rather marred by various errors in the equations which although usually obvious are frustrating. In shorter chapters of this section Oerlemans describes models of the reaction of polar ice sheets to CO_2 warming, Flohn speculates on possible major climatic events, and Volz considers the possible impact of aerosols, land-use changes, waste heat release and other trace gases. The last, he concludes, could contribute significantly to the greenhouse effect with the combined effect possibly as large as that of CO_2 alone. Schönwiese deals with statistical techniques that can be used to analyse observed climate variability in the modern instrumental period. Insufficient explanation and detail make this chapter harder to follow than that on the detection of CO_2-induced climate change by Schuurmans.

Part III on impacts and strategies is inevitably more speculative. Kellogg outlines some possible

effects of changes in temperature and rainfall on regional scales to natural vegetation, agriculture, fuel demand, water resources, fisheries, health and human comfort and describes possible strategies to deal with such climate-induced changes. It is emphasized that not everyone will be affected in the same way so impact studies need to treat specific regions and specific economic sectors, and for this the likely climate changes need to be known with more confidence.

Laurmann's chapter on the development of quantitative methods of assessing alternative strategies proposed to reduce or avoid the environmental threat was novel and interesting. However, unfamiliarity with economic jargon and several long-winded and pretentious euphemisms made it difficult to read and grasp the ideas. It is a pity that some basic definitions were not provided to help those not schooled in economics. The obscure language is well illustrated on page 451 '... unless [market penetration time lags] are endogenously put into the model as pre-selected parameters'. I think he means they should be variables of the model.

In the final chapter Bach presents a low CO_2-climate risk policy characterized by using energy more efficiently and requiring less fossil fuel energy than forecast in conventional energy projections based on population and GDP extrapolations. By placing the emphasis on the end-use for which energy is required an analysis of alternative ways of meeting the tasks and substituting fuels reveals the large potential for greater efficiency. From a case study of possible cost-effective improvements towards energy efficiency in West Germany, Bach argues that the world demand for energy could be 37%*lower* in 2030 than in 1975 if such a program were adopted globally.

The book is well produced and the print easy to read apart from a few stray superscripts here and there. The diagrams are mostly clear and uncluttered although some in chapter 1 are rather small and the grey shading, e.g. Figure 1 of Schuurmans, hardly visible. Parts of it could usefully be recommended in advanced courses though, as I have indicated, some chapters are harder to read. On the whole I think a balanced view of the many disciplines involved in the 'CO_2 problem' is provided.

C. A. Wilson

Atmospheric chemistry: Report of the Dahlem Workshop on Atmospheric Chemistry, Berlin 1982, May 2–7, edited by E. D. Goldberg. 150 mm × 210 mm, pp. viii + 385, *illus.* Springer-Verlag, Berlin, Heidelberg, New York, 1982. Price US $19.90.

This book, Volume 4 in a series on Physical and Chemical Sciences Research Reports, arises from a Dahlem Konferenz held in Berlin in May 1982. There are thirteen single-authored papers, one multi-authored, and four group reports.

The thirteen authors are all well known and cover between them most aspects of tropospheric chemistry, albeit with some redundancy. Space does not permit a review of all these chapters, but particular highlights for me included that by Morgan on the pH and oxidation capacity of rain, with its insistence on pointing out the non-linear nature of the system. Jørgensen's review of C, N and S gases from oxygen-deficient environments was very clear, as were the last three chapters, by Niki on homogeneous gas phase oxidation, by Crutzen on the global distribution of hydroxyl and by Penkett on non-methane organics in the remote troposphere.

The volume is slightly marred by Slinn's paper, in which the impact of some well-made points is diluted by being interleaved with musings about the philosophy and politics of pollution which ought to have been filtered out somewhere down the line between the conference bar and the editor's desk.

The four review group reports are well considered, and leave one with a clear impression of the impressive progress made in tropospheric chemistry during the last decade, and also of the scale of

future effort required to endow the subject with predictive power for input to policy decisions on air pollution control strategies. The book should be more useful to those requiring a contemporary survey of the broad state of the field than to those who need an introduction to the basic principles.

A. F. Tuck

Absorption and emission by atmospheric gases: the physical processes, by Earl J. McCartney. 160 mm × 235 mm, pp. xii + 320, *illus.* John Wiley & Sons, New York, Chichester, Brisbane, Toronto, Singapore, 1983. Price £47.50.

This book is aimed at scientists, development engineers, technicians and students in meteorology, atmospheric physics, aerospace surveillance and air pollution control. Such a diverse audience has necessitated a treatment in which topics are developed from the most elementary stages. This can be seen from the Chapter titles: 1, Introductory Ideas and Useful Facts; 2, Gas Properties, Thermodynamics and Molecular Kinetics; 3, Quantized Energy States and Population; 4, Molecular Internal Energies; 5, Spectra of Energy Transitions; 6, Parameters of Line and Band Absorptions; 7, Absorption and Emissions Data. Any reader who has come to atmospheric transmission via an adequate background in spectroscopy, gas kinetics or atmospheric physics is likely to find it a test of his patience in parts, but those who have entered from other traditions may well find it useful. Useful features of the book are the data-laden Appendices and extensive references to the literature.

The book appears in a series in Pure and Applied Optics, and is a companion volume to McCartney's *Optics of the atmosphere: scattering by molecules and particles.* Ever since the appearance in 1964 of Goody's *Atmospheric radiation. I. Theoretical basis* there has been a need for Volume II, on radiative transfer in the real atmosphere. It is an acknowledgement perhaps of the nature and development of the field that it has never appeared. It is badly needed; perhaps the publishers can be persuaded to add such a book to McCartney's pair.

A. F. Tuck

Books received

The listing of books under this heading does not preclude a review in the Meteorological Magazine at a later date.

Weather and climate of the Antarctic, by W. Schwerdtfeger (Amsterdam and New York, Elsevier Science Publishers, 1984. Dfl 120, US $46.25) is No. 15 in the series Developments in atmospheric science. Its purpose is to present an up-to-date description and, as far as possible, an explanation of the meteorological characteristics of the southern continent. Some problems which need further field work and theoretical investigation are outlined in detail. Questions of weather forecasting are discussed only where it appears that new information or understanding of the atmospheric processes involved make it worthwhile. The difficulties of an adequate interpretation of minor regional climate functions are commented on.

World climate change: The role of international law and institutions, edited by Ved P. Nanda (Boulder, Colorado, Westview Press, 1983. £17.25) provides a comprehensive discussion and analysis of the legal and institutional aspects of world climate change and weather-related problems, recognizing that these are no longer isolated issues countries can grapple with individually. The authors appraise several options for atmospheric management and make specific recommendations to reduce and ameliorate the adverse global effects of climate fluctuations and changes.

Climatic changes on a yearly to millennial basis, edited by N.-A. Mörner and W. Karlén (Dordrecht, Boston, Lancaster, D. Reidel Publishing Company, 1984. Dfl 210, US $79.00) is the Proceedings of the Second Nordic Symposium on Climatic Changes and Related Problems held in Stockholm, May 16–20, 1983. It focuses on the processes and data that are typical for the Nordic countries and the papers printed here can be divided into four main groups: paleoclimatological records; historical records; instrumental records; and theories, models and geophysical explanations.

The climate of Europe: Past, present and future, edited by Hermann Flohn and Roberto Fantechi (Dordrecht, Boston, Lancaster, D. Reidel Publishing Company, 1984. Dfl 130, US $49.00) consists of six chapters, prepared by individual specialists, each of which is followed by a summary and/or set of conclusions. It gives a broad view of the complex background to the problem of climatic change and the different factors involved, reviews changes that have taken place in the world's climate over the past thousand years or more, and analyses in greater detail the recent centuries for which instrumental weather data are available. It also discusses the extent to which man himself may affect the climate by his activities, looks into the past to find analogues to what appear to be the more likely lines of climatic development in the future, describes how European agriculture has reacted to climate change and fluctuations over the past 200 years or so, and considers also the effects on future food production.

THE METEOROLOGICAL MAGAZINE

No. 1350 January 1985 Vol. 114

CONTENTS

NOTICE

It is requested that all books for review and communications for the Editor be addressed to the Director-General, Meteorological Office, London Road, Bracknell, Berkshire RG12 2SZ and marked 'For Meteorological Magazine'.

The responsibility for facts and opinions expressed in the signed articles and letters published in this magazine rests with their respective authors.

Applications for postal subscriptions should be made to HMSO, PO Box 276, London SW8 5DT.

Complete volumes of 'Meteorological Magazine' beginning with Volume 54 are now available in microfilm form from University Microfilms International, 18 Bedford Row, London WC1R 4EJ, England.

Full-size reprints of Vols 1–75 (1866–1940) are obtainable from Johnson Reprint Co. Ltd, 24–28 Oval Road, London NW1 7DX, England.

Please write to Kraus Microfiche, Rte 100, Millwood, NY 10546, USA, for information concerning microfiche issues.

HMSO Subscription enquiries 01 211 8667.

Printed in England for HMSO and published by
HER MAJESTY'S STATIONERY OFFICE

£2.30 monthly

Annual subscription £27.00 including postage

Dd. 737126 C14 1/85

ISBN 0 11 727555 7
ISSN 0026–1149

THE METEOROLOGICAL MAGAZINE

HER MAJESTY'S STATIONERY OFFICE

February 1985

Met.O.967 No. 1351 Vol. 114

METEOROLOGICAL OFFICE Met. O.967

THE METEOROLOGICAL MAGAZINE

No. 1351, February 1985, Vol. 114

551.524.2:551.524.4:551.588.2

The variation of surface temperature with altitude

By R. C. Tabony

(Meteorological Office, Bracknell)

Summary

Altitudinal gradients of temperature at screen level are determined by the lapse of temperature in the free atmosphere as modified by the surface. The effects of the surface can be considered in three stages:

(i) The diurnal and seasonal modifications to the lapse rate in the free atmosphere; these depend upon latitude, climate, and state of surface.

(ii) The influence of topography, where it is important to distinguish between local and large-scale effects.

(iii) Changes in climate and state of surface following the ground.

Although explicit consideration of these three factors does not necessarily provide a practical means of estimating surface lapse rates, it does enable the wide variety of observed values to be understood and placed in perspective.

1. Introduction

Altitude is one of the main causes of temperature variations near the surface of the earth. The change in temperature associated with a movement of several hundred kilometres in the horizontal may be accomplished by a change of only a few hundred metres in the vertical. Relatively few meteorological observations are made in mountainous districts and it is often necessary to estimate temperatures at a given location from observations made at a different altitude. As a result, it is important that differences of temperature introduced by altitude be well understood.

The variation of temperature with height in the troposphere is relatively simple. An upper limit to a decrease with altitude of 9.8 °C per km is provided by the dry adiabatic lapse rate resulting from the mixing of air unsaturated with water vapour. The saturated adiabatic lapse rate represents the effect of the mixing of cloudy air and varies with temperature according to the amount of moisture available for latent heat release. Values range from about half the dry adiabatic rate at low levels in the tropics to very close to the dry adiabatic rate near the tropopause, but 6 °C per km is a typical value. Whenever subsidence occurs in the atmosphere, more stable conditions prevail with isothermal and inversion layers being produced.

The final result of these factors is that mean temperatures in the troposphere decrease with altitude in a fashion similar to the saturated adiabatic lapse rate. Exceptions occur near the presence of semi-

permanent subsidence inversions, such as occur over the subtropical oceans. The influence of the surface of the earth also causes modifications to lapse rates in the free atmosphere to occur on diurnal and seasonal time scales. Nevertheless, a lapse rate of 6 °C per km has become accepted as standard, and is commonly used for reducing temperatures to sea level.

The lapse rate of temperature over the ground, that is the variation with altitude of temperature recorded in a screen 1 to 2 metres above the ground, is not the same as that in the free atmosphere. It also depends on the effects of the surface, and these vary with latitude, climate, state of surface, local and large-scale topography. This large number of variables, and the interactions between them, produces a very wide range of lapse rates over the surface. The variations within the United Kingdom are illustrated by Smith (1975), who finds that lapse rates reach a seasonal maximum in spring on the northern Pennines, in summer on the eastern slopes of the Welsh hills, and in autumn on their western slopes.

The variations of surface temperature in mountainous districts have been studied for over a century. Most of the investigations have been local and have taken place in the Alps, where the number of observations available is greater than elsewhere. The reports of these studies are mainly contained in the German literature, but the findings of many of them are reported by Geiger (1965). A very extensive review of the literature is provided by Barry (1981).

Much of the work on the variation of temperature with altitude has been empirical, and the identification of the physical factors responsible for the observed variations in lapse rates has been of secondary importance — in many papers the contributions of the relevant variables have not been recognized explicitly. To the casual reader, therefore, the wide range of lapse rates reported, and the often inadequate physical explanations offered, present a very confusing picture. The main aim of this paper is therefore to present a simple and convincing account of the main factors involved in the determination of surface lapse rates, with special emphasis on the effects of large-scale topography. A general procedure for estimating surface lapse rates is suggested, but this is unlikely to be of direct practical value; it is offered mainly to act as a framework for a general understanding of the subject.

2. Geographical and seasonal variations of lapse rate in the free atmosphere

The continents respond to changes in solar radiation much more readily than the oceans so that winter lapse rates over the land are less than over the sea and decrease with latitude in response to the decreasing elevation of the sun. Over the oceans, however, lapse rates increase with latitude owing to the advection of progressively colder air from the land. In summer, lapse rates over the land are greater than over the sea and again decrease with latitude, but over the ocean latitudinal variations are slight. These changes are illustrated in Fig. 1, which displays profiles of mean temperature determined from radiosonde ascents for three land and three ocean stations. Variations over the sea are small compared to those over the land, where it can be seen that diurnal modifications to the atmosphere commonly extend up to about 1 km, and seasonal effects to 2 km. At Ocean Weather Ship (OWS) 'N', at 31 °N, some evidence of the subtropical subsidence inversion is present between 850mb and 700mb. Geographical and seasonal variations in lapse rate between 850–700 mb and 700–500 mb have been mapped globally by Maejima (1977).

Land temperatures respond fairly rapidly to seasonal variations in solar radiation, but time is required to transmit these changes to the atmosphere and ocean. Thus while the seasonal variations in temperature of the sea surface and atmosphere (as represented by the 1000–500 mb thicknesses) are approximately in phase, they are about a month behind those occurring over the land. This has the effect of making the atmosphere over the land more unstable in the spring than in the autumn. The differences, however, are small compared with those between winter and summer.

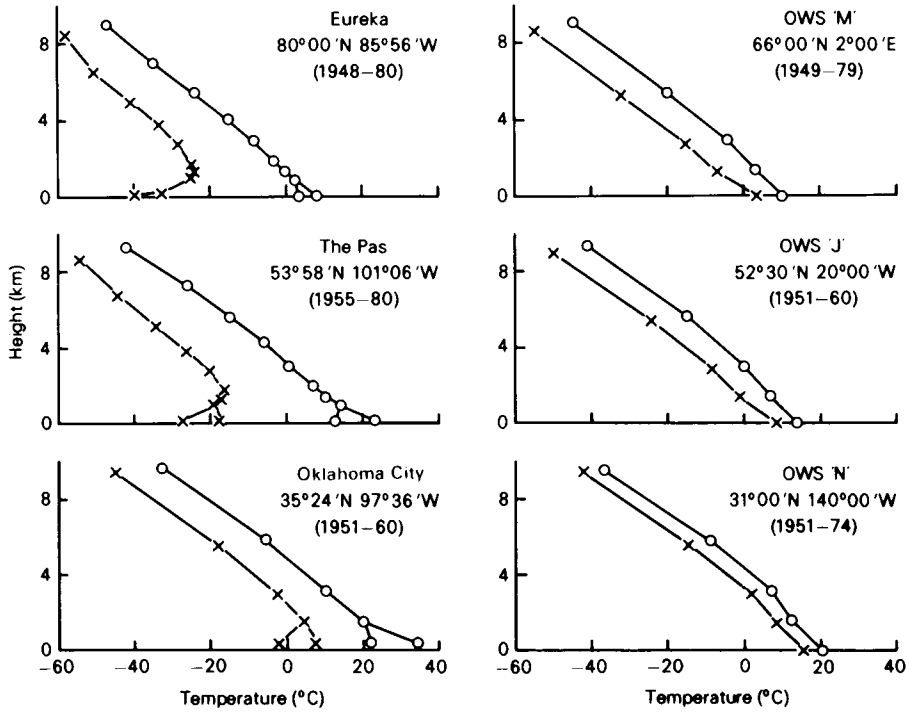

Figure 1. Profiles of mean temperature for stated periods. x—x January c_O-O July.

3. Forced ascent

The lapse rate following the surface of the earth is not the same as that in the free atmosphere; it also depends on the effects of the surface, and the most direct of these is that of forced ascent. When air is forced either up (or down) by the surface, its temperature changes either at the dry or saturated adiabatic rate, irrespective of that in the free atmosphere. The effect can be very important on individual occasions — föhn events, for instance, and when the melting of falling snow has produced an isothermal layer down to the surface. On these occasions, amounts of snow lying on the lowest ground may be small, but forced ascent will produce sub-zero temperatures on relatively high ground, leading to the accumulation of substantial amounts of snow or glaze at modest altitudes (see, for example, Pedgley 1969).

For mean temperatures, however, with which this paper is mainly concerned, forced ascent is not as important as appears at first sight. Surface adiabatic lapse rates caused by forced ascent will differ most from those in the free atmosphere when the latter are stable. Under these conditions, very little forced ascent is likely, either because winds are very light or airflow is occurring around, rather than over, the mountains. Substantial forced ascent is only likely when the lapse rates of temperature in the free atmosphere are close to adiabatic values, and hence when the modifying effects are small. Forced ascent and descent may, however, be responsible for modifying lapse rates by affecting the distribution of cloud and rain, but this is considered later under climatic effects.

4. Local and large-scale topography

Differences between lapse rates following the surface and those in the free atmosphere are mainly due to the effect of radiation at the surface, and this varies on a diurnal and seasonal time scale. The extent to

which surface lapse rates are affected depends on the topography, and in this respect it is important to distinguish between the effects of local and large-scale topography. The term 'local topography' is used to describe the differences between hills and valleys etc. while the term 'large-scale topography' is used to refer to differences in altitude averaged over large areas, e.g. to distinguish between plateaux and plains.

Local topography is responsible for introducing differences in the lapse rate between maximum and minimum temperatures. A low-level station is usually in a valley, while a high-level station is commonly on a summit. The diurnal range in a valley will clearly be greater than that on a summit, and so the lapse of maximum temperatures must be greater than that of minima. Suppose, however, two sites of similar local topography are considered, one on a plain and the other on a plateau. The diurnal range of temperature at the two stations would be similar, and so the lapse rates of maximum and minimum temperatures would be the same.

The effects of local topography are not restricted to those affecting lapses of maximum and minimum temperature. The lapse of mean temperature in the diurnally modified atmosphere is often not the same as that in the seasonally modified atmosphere above it. In daytime in winter, the nocturnal inversion is not properly broken down and the diurnally modified atmosphere is more stable than the overlying layers. The extent of this modification will depend on the local topography and will be greater over a valley than over a plain. The phenomenon may be regarded as the development of a seasonal modification of the 'enclosed' atmospheres in valleys but, because it is a function of local topography, it is for convenience regarded as part of the 'diurnally' modified atmosphere. The seasonally modified atmosphere is intended to refer to the 'free' atmosphere above a level surface rather than the 'enclosed' atmosphere in a valley.

When considering altitudinal gradients of temperature measured along the ground, it is helpful to refer to three topographic models, and these are illustrated in Fig. 2. The first relates to local, and the second and third to large-scale, topography. The differences between the models are illustrated using a schematic temperature profile appropriate to a clear winter's night. Well above the surface a lapse of 6 °C per km is assumed; below this the seasonally and diurnally modified atmospheres are represented by isothermal and inversion layers respectively.

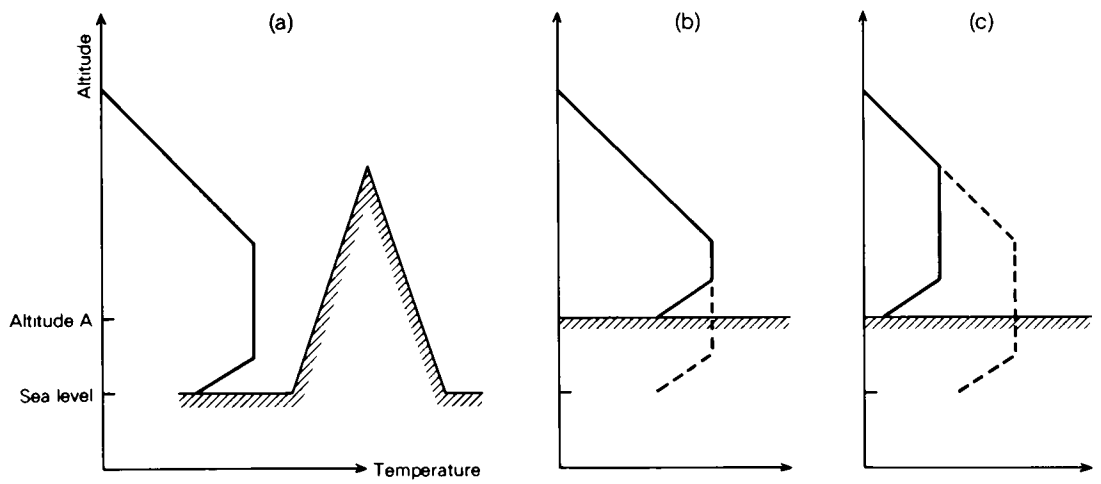

Figure 2. Schematic representation of temperature profiles associated with three models of topography — (a) isolated mountain, (b) limited plateau and (c) extensive plateau. ////// land surface, ——— profile in free atmosphere above land surface, — — — profile if land surface was at sea level.

The first model is of a general lowland with isolated mountains projecting into the free atmosphere. The variations in temperature on the surface will then be similar to those observed in the diurnally and seasonally modified atmosphere. The second model is that of a small-scale plateau which projects into the seasonally modified atmosphere without extending it vertically. Lapse rates across the surface will then be similar to those in the seasonally (but not diurnally) modified free atmosphere. The third model is that of a plateau so extensive that the seasonally modified atmosphere extends as far above the plateau as above the lowlands. Differences in temperature between the plateau and those that would have been observed at sea level are then determined by the lapse in the unmodified atmosphere, i.e. around 6 °C per km. These last two models apply to gently sloping, as well as level, plateaux.

From a comparison of temperatures at sea level with those at an altitude A corresponding to the height of the plateau in models (b) and (c), Fig. 2 shows that for a winter's night:

(i) on an isolated mountain (a), temperature increases with altitude (the diurnally and seasonally modified lapse rates are relevant),

(ii) on a limited plateau (b), temperatures are independent of altitude (the seasonally modified lapse rate is relevant,

(iii) on an extensive plateau (c), temperatures decrease with altitude as the plateau is raised or lowered (the standard lapse rate of 6 °C per km is relevant).

A plateau so extensive as to build a seasonally modified atmosphere of the same depth as that which would occur over a comparable area of lowland (as in model (c)) probably does not exist on earth. The seasonally modified atmosphere, however, will always extend to greater altitudes over high ground than over lowland, so most areas of high ground will have characteristics intermediate between models (b) and (c).

A generalized model of the effects of large-scale and local topography is depicted in Fig. 3. A large

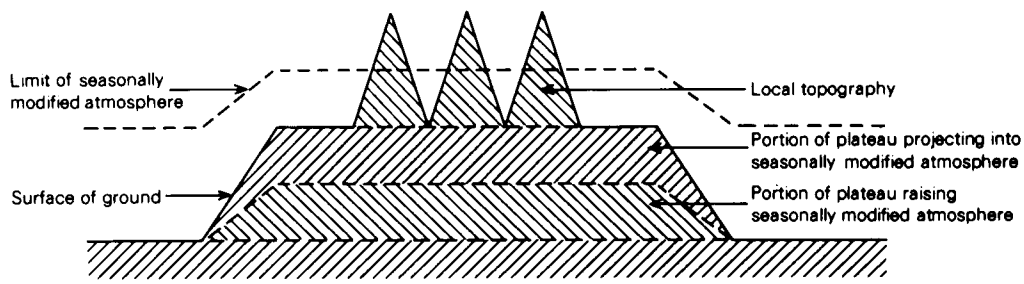

Figure 3. Composite model of topography for estimating surface temperature.

area of high ground will raise the height of the seasonally modified atmosphere, and to this extent may be regarded as belonging to the extensive plateau model of topography. Temperatures will decrease by around 6 °C per km up to the height by which the seasonally modified atmosphere has been raised. The remainder of the high ground may be regarded as projecting into the seasonally modified atmosphere, and lapse rates will be determined by these seasonally modified lapse rates in the free atmosphere. By averaging height over a certain area, a smoothly varying surface can be obtained and used to define the local topography. This is needed to introduce different lapse rates for maximum and minimum temperatures, and also to identify valleys which may contain seasonally modified 'enclosed' atmospheres.

The diurnal and seasonal modifications to lapse rates in the atmosphere are represented in Fig. 2 as being linear. In reality, of course, they will be non-linear, especially in winter, when lapse rates in the free

atmosphere will change gradually from negative (i.e. inversion) near the surface to close to the standard value of 6 °C per km at higher levels. Thus on a gently sloping plateau conforming to model (b), for instance, increasing altitude would be associated with an increase in temperature at the lower levels which would be gradually retarded and eventually reversed at higher elevations.

5. Variation of radiation with altitude

The thinning of the atmosphere with increasing altitude has the effect of increasing both incoming and outgoing radiation. As a consequence, for topographically similar sites, diurnal range will increase slowly with altitude. As temperature decreases, however, outgoing radiation decreases according to Stefan's Law. This causes temperature to decrease slightly less rapidly with altitude over the land than in the atmosphere.

6. Coastal effects

Large changes in the diurnal and seasonal modifications to lapse rates in the free atmosphere occur in the vicinity of coasts. As air passes from sea to land or vice versa, changes in the lapse rate near the surface occur very rapidly (within a few minutes). With the passage of time these changes extend upward so that the diurnal modification is complete within a few hours. The seasonal modification is formed from the accumulated effect, over several days, of the diurnal changes.

Altitudinal gradients of temperature along the ground in coastal districts may be regarded as a combination of a horizontal coastal gradient and the vertical gradient that would have occurred inland. The horizontal coastal gradient will enhance the altitudinal fall in winter, but oppose it in summer. As a result, altitudinal gradients on coastal slopes will be similar to those that occur in the free atmosphere over the sea.

7. Climatic effects

Surface modifications to lapse rates in the free atmosphere are strongly dependent on the radiation received by the surface and this is a function of both climate and latitude. Thus differences in lapse rates of maximum and minimum temperatures induced by local topography will be much greater where the climate is clear and calm than where it is cloudy and windy. The strength of the stable layer which forms over continents in winter will depend on latitude and the frequency of clear, calm conditions. The extent to which these modifications affect lapse rates over the ground depends, as has been shown, on the topography. Thus for the extensive plateau model, differences in temperature from those that would have been observed at sea level depend only on the lapse rate in the unmodified free atmosphere, and are independent of climate. Note, however, that such a model requires the build-up of a large depth of seasonally modified atmosphere above the plateau and this is much more likely to occur if winds are light than if they are strong. Thus the extent to which a given plateau approaches this model may vary seasonally in accordance with variations in the strength of the wind.

Lapse rates following the ground will also depend on changes in climate, whether they be due to changes in the horizontal (e.g. distance from coast) or vertical (e.g. cloud cover). This will induce differences between lapse rates of maximum and minimum temperature, since the diurnal range in one type of climate will usually be different from that in another .Topography itself, of course, has a strong influence on climate. Thus lowlands on opposite sides of a mountain range often have differing degrees of continentality and exposure to given air masses. Isolated mountains and relatively small areas of high

ground often have a cloudier, wetter, and windier climate than the adjacent lowlands. Extensive plateaux, on the other hand, often experience a dry, radiation-dominated climate. Mountain slopes on the windward edge of the plateaux often have a moist, cloudy climate due to the effects of forced ascent, but the air has lost most of its moisture by the time it arrives on the plateau.

Changes in the state of surface (vegetation and soil moisture) will also affect surface lapse rates through the proportion of radiation which is used to provide evaporation rather than surface heating, and there is an interaction with climate here. Thus, in summer, lapse rates in districts where cloud and rain increase with altitude will be greater than those where they decrease. The drier and sunnier location will not only receive more radiation, but the drier soil means that more of that energy will be available for surface heating.

8. Snow cover

The importance of the state of surface is also seen through the effects of snow cover which generally causes a reduction of temperature compared with that observed over exposed ground. Altitudinal gradients of surface temperature will be most affected when snow-free terrain at low levels is replaced by a snow cover at higher altitudes. The effects are likely to be greatest during the period when the snow is melting; some guide to the start of this period is given by the date of maximum snow depth. Using data from Geiger (1965), Table I implies that, in the Austrian Alps, this ranges from January near sea level to June above 3000 metres.

Table I. *Date of maximum snow depth in the Austrian Alps (Geiger 1965)*

Altitude (m)	200	600	1000	1400	1800	2200	2600	3000
Date	18 Jan	28 Jan	11 Feb	21 Feb	14 Mar	8 Apr	3 May	29 May

The evolution of seasonal variations in the depth of snow cover is illustrated by considering two stations whose mean temperatures differ by, say, 4 °C. During the winter, when temperatures at both stations remain below freezing, snow may be accumulating at the same rate at both stations. Suppose that the warmer station reaches its maximum snow depth in March. As spring advances, snow depth at this station decreases while that at the colder station still increases. By the time the snow depth at the colder station has reached its maximum, that at the warmer station may have completely disappeared.

Thus, during the early winter, altitudinal and latitudinal gradients of snow depth are relatively slight. As spring arrives, a steep gradient develops between those regions where the snow has disappeared and those where it has reached its maximum depth. As spring progresses, this boundary advances into regions of greater and greater snow depth, and the gradient of snow depth increases. By June, at high altitudes and high latitudes, snow depth will increase rapidly from zero to very high values. The snow in this transition zone will be melting rapidly and may be expected to exert a considerable influence on temperature. When the highest in a series of stations is located in this zone of melting snow, and a linear relation is fitted to temperature against height, a large value of the lapse rate is likely to result.

9. Case studies

9.1 *The Alps*

Some of the most extensive studies of mountain climate have taken place in the Alps, and some data given by Geiger (1965), and reproduced in Fig. 4, provide a good illustration of the effect of topography

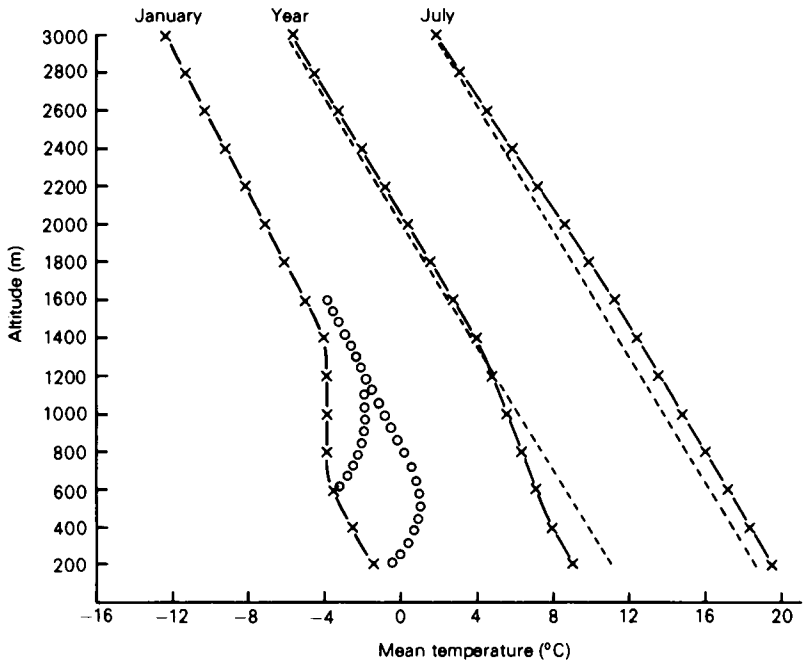

Figure 4. Variation of mean temperature with altitude in the Austrian Alps (Geiger 1965). ×—× temperature, – – – lapse rate of 6 °C per km, ooo estimated temperature in atmosphere above surfaces at 200 m and 600 m.

on the variation of temperature with altitude. Fig. 4 displays the variation of mean temperature in January and July for various altitudes in the Austrian Alps. In summer, there is a reasonably linear relation between temperature and altitude with mean lapse rates close to 6 °C per km. In winter, however, an isothermal layer forms between 700 m and 1400 m. The average height of main Alpine valleys while they are still enclosed by mountains is represented by 700 m. Above 1400 m sites may be regarded as being on the open slopes of mountains projecting into the free atmosphere. Between 700 m and 1400 m sites may be regarded as being enclosed, with the atmosphere 'projecting' into the land. The observed variation of temperature with height is therefore very much a function of the average topographical exposure of a site at a particular altitude. The figures given for 1400 m, for example, would not apply to a valley at that level surrounded by high mountains.

Radiosonde ascents in the vicinity of the Alps show that, in July, temperatures in the free atmosphere are very similar to those displayed in Fig. 4. In January, however, ascents indicate that at the surface, 850 mb and 700 mb, temperatures are about 1 °C higher than those presented. The estimated profiles of mean January temperature in the atmosphere above a surface at 200 m outside the Alps, and above a valley at 600 m in the Alps, have been sketched. It is evident that in the region of the Alps, located towards the western margin of a continent, very little seasonal modification has taken place in the atmosphere, except that the lapse rate above 1400 m is rather less than 6 °C per km. Substantial modifications to mean temperatures extend only to about 500 m above the surface, and do not therefore reach beyond the range of diurnal modifications. The top of this layer, however, has been raised by about 500 m by the Alps, and so for the lowest 500 m temperatures decrease at approximately 6 °C per km in accordance with an extensive plateau model of topography. Thereafter the influence of

local topography is dominant, and the effects of the 'diurnally' modified atmosphere, which includes a lowering of maximum as well as of minimum temperature in winter, represent the typical topographic exposure of a site at a given altitude.

It may be noted in passing that the depression of maximum temperature in Alpine valleys in winter is not solely a product of radiation; the melting of falling snow also makes a contribution. It is well known that when falling snow reaches the melting level, the energy extracted from the atmosphere by the melting can produce an isothermal layer close to 0 °C, and the snow gradually extends to lower and lower altitudes; the process is described by Lumb (1983). What is less widely appreciated is that such a mechanism will operate far more efficiently in light than in strong winds. While the melting of snow alone would produce an isothermal layer, the turbulent mixing caused by strong winds has the effect of producing an adiabatic lapse rate. Thus, in strong winds, the energy extracted from the atmosphere will be the same as in light winds, but the loss of energy will be redistributed vertically. With strong winds, there is also the possibility of warm advection at low levels, either from air that has been over the sea or drawn from outside the precipitation area. Low-level winds in the region of the Alps are often light, and the enclosed nature of Alpine valleys hinders large-scale mixing and encourages the development of an isothermal layer in the valley whenever falling snow reaches the melting level.

9.2 *Eastern slope of the Rockies*

One of the best examples of a gently sloping plateau occurs to the east of the Rocky Mountains in North America. Table II presents mean temperatures in January and July at two sets of stations, the

Table II. *Mean temperature (°C) over the period 1931–60 (with some shorter periods) at various stations on the sloping plateau to the east of the Rocky Mountains*

Station (50°N approx.)	Altitude (m)	Jan	Jul
Calgary	1079	- 10.0	16.7
Swift Current	816	- 13.1	18.9
Regina	574	- 16.5	19.0
Winnipeg	240	- 17.6	20.0
Station (40°N approx.)	Altitude (m)	Jan	Jul
Denver	1613	- 2.0	22.7
Sterling	1201	- 3.9	23.2
McCook	782	- 3.0	25.2
Concordia	448	- 2.6	26.8
Topeka	267	- 1.8	26.6

first, Calgary to Winnipeg, at around 50°N and the other, Denver to Topeka, at around 40°N. Although the precise figures for each station will be influenced by the local topography, the main factor is the large-scale topography. In winter, temperatures increase with altitude at around 9 °C per km at 50°N, while at 40°N they are approximately isothermal. Evidently, the second model of topography, in which the high ground projects into the seasonally modified atmosphere, is appropriate. In Fig. 1, the profile for The Pas, at 54 °N, shows that temperatures increase by around 4 °C in the lowest kilometre of the atmosphere. The seasonally modified atmosphere will be deeper at Winnipeg, near the continental interior, than at Calgary, and this accounts for the additional temperature difference between the two stations. At 40°N, the greater power of the sun prevents the formation of such large temperature inversions near the surface (see Oklahoma City in Fig. 1), and so isothermal conditions prevail. In summer, temperatures decrease with altitude at around 4 °C per km at 50°N and 3 °C per km at 40°N. Both these

figures are less than the 'standard' rate of 6 °C per km. At 40°N, these differences are caused by changes in the climate, which becomes drier and sunnier as one moves west from Topeka towards Denver. The increased radiation and decreased evaporation at Denver permit higher surface temperatures than if the climate were the same as at Topeka, thereby decreasing the lapse rate.

9.3 *The Himalayas and Tibet*

The outstanding example of the effect of climate on lapse rates occurs in the region of the Himalayas. The Tibetan plateau is semi-arid all year, whereas the plains to the south pass dramatically from dry conditions in May to wet in July. Table III compares the lapses of maximum temperature between Leh and Lahore in the west and Lhasa and Patna in the east. The differences in temperature between the high- and low-level stations are almost halved between May and July as maximum temperatures on the lowland are depressed by cloud and rain.

Table III. *Lapse rate of maximum temperature (°C per km) in the Himalayan region (periods vary)*

	Jan	Feb	Mar	Apr	May	Jun	Jul	Aug	Sep	Oct	Nov	Dec
Leh–Lahore	6.6	6.6	6.4	6.6	7.3	6.4	3.9	3.7	4.6	6.1	6.1	6.2
Lhasa–Patna	4.4	4.6	5.7	6.0	5.2	3.4	2.6	2.6	3.1	4.1	4.3	4.1

Lapse rates of mean annual temperatures are considerably less than 6 °C per km, mainly due to the greater radiation and smaller evaporation at high levels in summer. These effects are opposed by the higher latitudes of the elevated stations and, especially in winter at Leh, to greater exposure to cold air masses from the north. The effect of the Tibetan plateau as a high-level heat source in summer is well known, and is discussed by Flohn (1953, 1968, 1974).

The variation of temperature following the ground in the Himalaya region behaves in a non-linear fashion. At low levels, maxima decrease rapidly as the plains are left for the hillsides, and cloud and rain increase. Then, as the Tibetan plateau is approached, temperatures rise as moisture and vegetation decrease. Maximum temperatures at Lhasa are actually higher than at Cherrapungi, 2500 m lower! These changes may be ascribed to horizontal gradients resulting from the change in climate, even though that change is largely caused by the topography in the first instance.

9.4 *The British Isles*

Good accounts of the variations of lapse rates in Britain are given by Manley (1970) and Harding (1978). Harding (1979) also gives a detailed discussion of the factors operating in the northern Pennines while Green and Harding (1980) analyse data in southern Norway to infer probable conditions in Scotland. With the exception of the Aberdeenshire plateau, the relief of Britain approaches that of the isolated mountain model of topography, and this forms the basis of the following description. Over the south-eastern half of England, the variation of solar radiation causes pronounced seasonal and diurnal variations in the lapse rate. Increased cloud and wind cause these variations to diminish towards the north-west. In winter, lapse rates over the seas to the west of Britain increase with latitude, and this, combined with the increased frequency of continental air masses towards the south-east, causes lapse rates over Britain to decrease from north-west to south-east. These differences are illustrated in Fig. 5 using data from Crawley and Stornoway, and OWS 'I' and 'J'. At Crawley, values exceeding 10 °C per km in summer are partly due to the lack of complete radiational screening of thermometers in a thermometer screen.

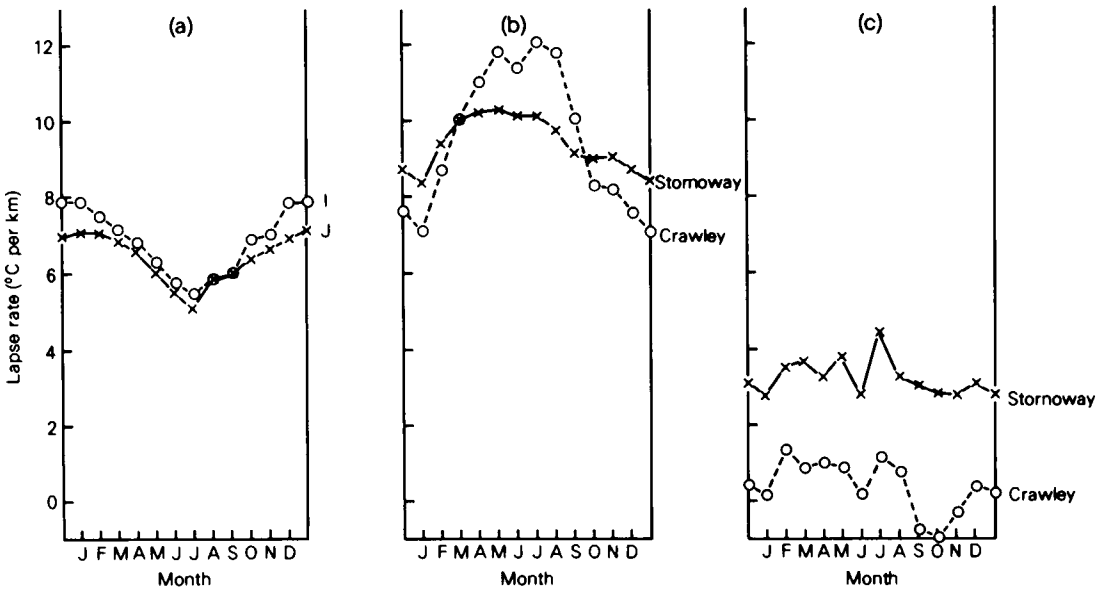

Figure 5. Mean lapse rates in the free atmosphere in the vicinity of the British Isles (1961–70). (a) Surface – 850 mb (b) Maximum temperature, surface – 900 mb. (c) Minimum temperature, surface – 900 mb.

According to Harding (1978) and Green and Harding (1980), the greatest lapse rates on Britain's northern hills are observed in spring. This is partly due to the melting of snow on the summits of these hills. The seasonal variation of lapse rates over the sea is opposite to that over the land, and this causes lapse rates measured along the coastal slopes of hills to reach a minimum in June and a maximum in December. The lapse of minimum temperature is non-linear, and increases gradually from near isothermal conditions in the lowest layers over the south-eastern half of England to close to 6 °C per km above about 1km.

10. Conclusions

Lapse rates of mean temperature in the free atmosphere away from the influence of the surface are generally close to 6 °C per km, although there are exceptions near semi-permanent subsidence inversions such as occur in the zone of trade winds. Diurnal and seasonal modifications to this normal rate are caused by the effect of the surface, and the extent of these modifications depends on the latitude, climate, and state of surface.

Lapse rates of temperature over the ground can be estimated in three main stages:

(i) Take account of the location — the latitude, climate, and state of surface will determine the diurnally and seasonally modified lapse rates in the atmosphere.

(ii) Introduce the topography—part raises the seasonally modified atmosphere, part projects into the seasonally modified atmosphere, and part produces local effects.

(iii) Allow for changes in climate and state of surface following the ground — these are best regarded as being due to changes in the horizontal, even if they were largely caused by orography in the first place.

In more detail the recommended procedure for estimating altitudinal gradients along the ground is as follows:

(a) Obtain the seasonally modified lapse rates at various heights above the surface in the free atmosphere. These can be obtained from radiosonde ascents and, since they vary only on a large scale, can be mapped. For summer, and for the 850–700 mb and 700–500 mb, layers, this has already been done by Maejima (1977). Especially in winter, these lapse rates will be non-linear and will change as the surface is approached. In the zone of diurnal modification, however, lapse rates in the 'seasonally only' modified atmosphere should be regarded as linear extrapolations of those immediately above the zone.

(b) Estimate the height to which the seasonally modified atmosphere extends, and the amount by which it has been raised over areas of high ground. This may vary with season.

(c) Assume a lapse rate of 6 °C per km up to an elevation which equals the amount by which the seasonally modified atmosphere has been raised. Thereafter the lapse of temperature in the seasonally modified atmosphere should be used.

(d) Define a surface (e.g. by averaging height over a large area) which enables variations in height to be shared between a 'sloping plateau' and local topography. This will enable diurnal modifications to the free atmosphere, and seasonal modifications to 'enclosed' atmospheres to be taken into account.

(e) Allow for changes in climate and state of surface. By reducing temperatures to sea level using steps (a) to (d), these changes should be revealed as horizontal gradients, even though they were mainly caused by the orography.

The steps outlined above represent a generalized procedure which can only be implemented after a good deal of local study and empiricism, and are probably impossible to apply in any strictly objective and quantitative fashion. They are offered mainly to act as a framework for a general understanding of the subject and to enable diverse results from different parts of the world to be placed in perspective.

References

Barry, R. G. 1981 Mountain weather and climate. London, Methuen.

Flohn, H. 1953 Hochgebirge und allgemeine Zirkulation. II. Die Gebirge als Wärmequellen. *Arch Meteorol Geophys Bioklimatol*, **A, 5**, 265–79.

1968 Contributions to a meteorology of the Tibetan Highlands. *Atmos Sci Pap* No. 130, Fort Collins, Colorado State University.

1974 Contribution to a comparative meteorology of mountain areas. *In* J. D. Ives and R. G. Barry, (eds), Arctic and Alpine environments. London, Methuen.

Geiger, R. 1965 The climate near the ground. Cambridge, Mass., Harvard University Press.

Green, F. H. W. and Harding, R. J. 1980 The altitudinal gradients of air temperature in southern Norway. *Geogr Ann* **62A**, 29–36.

Harding, R. J. 1978 The variation of altitudinal gradient of temperature within the British Isles. *Geogr Ann* **60A**, 43–49.

1979 Altitudinal gradients of temperature in the northern Pennines. *Weather*, **34**, 190–202.

Lumb, F. E. 1983 Sharp snow/rain contrasts — an explanation. *Weather*, **38**, 71–73.

Maejima, I. 1977 Global pattern of temperature lapse rate in the lower troposphere — with special reference to the altitude of the snow line. Geographical Reports of Tokyo Metropolitan University, **12**, 117–126. Tokyo.

Manley, G. 1970 The climate of the British Isles. *In* C. C. Wallen, (ed), World survey of climatology, **5**, 81–133. Geneva, WMO.

Pedgley, D. E. 1969 Snow and glaze on Christmas Eve 1968. *Weather*, **24**, 480–485.

Smith, L. P. 1975 Change of weather factors with height. (Unpublished, copy available in National Meteorological Library, Bracknell).

551.501.42:551.571

The estimation of humidity parameters

By P. F. Abbott* and R. C. Tabony

(Meteorological Office, Bracknell)

Summary

The calculation of various measures of humidity from wet- and dry-bulb temperatures is made difficult by the need to compute the saturation vapour pressure. Complex semi-empirical equations due to Goff and Gratch are available, but for many applications simpler and less accurate formulations are required. In meteorology, there is a need to calculate the dew-point from the wet-bulb temperature at synoptic observing stations, and this can be conveniently carried out on a programmable calculator. For this purpose an algebraically simple equation due to Magnus is shown to be most suitable, and procedures for its use in calculating humidity parameters at an observing station are described.

1. Introduction

The moisture content of the atmosphere is generally measured cheaply and conveniently by means of a wet- and dry-bulb psychrometer. Unfortunately, however, the calculation of alternative measures of humidity such as the dew-point (T_d), vapour pressure (e) and relative humidity is complex. The calculations are based on the Regnault equation,

$$e = e_s(T_w) - Ap(T - T_w),$$

where T = dry-bulb temperature,
T_w = wet-bulb temperature,
p = atmospheric pressure,
A = a ventilation coefficient, and
$e_s(T_w)$ = saturation vapour pressure at the wet-bulb temperature.†

The source of the computational problems is the saturation vapour pressure (e_s). This is related to temperature by an integration of the Clausius–Clapeyron equation, but this is made difficult by departures from the ideal gas law and the variation of latent heat with temperature. Consequently, semi-empirical formulae were derived by Goff and Gratch (1945) to enable e_s to be calculated to a high degree of accuracy. These equations have been subject to continual refinement and the latest versions are given by Wexler (1976, 1977). The Goff–Gratch equations apply, however, only to the saturation pressure of water vapour in the absence of other gases. When air is added to the water vapour e_s is increased, mainly owing to the extra forces of attraction between the molecules of air and water vapour. The magnitude of the effect at sea level pressures, however, is only about 0.5%. A complete account of humidity and moisture in the atmosphere is given by Wexler and Wildhack (1965), while a useful summary is provided by the World Meteorological Organization (1966).

The Goff–Gratch equations are relatively costly to evaluate on a regular basis and for many purposes they are unnecessarily accurate. Consequently many attempts have been made to devise empirical approximations in which simplicity is traded against accuracy. Some workers, e.g. Richards (1971), Lowe (1977) and Rasmussen (1978) have aimed for relatively high accuracy and developed high-order polynomials. The efforts of Richards and Lowe, together with some unpublished work by Hooper, are

*Now at Royal Air Force High Wycombe.

†Wherever it is important in this paper to distinguish between temperatures in the thermodynamic and Celsius scales, the former is denoted by T and the latter by t.

reviewed by Sargent (1980). Algebraically simpler but less accurate formulae were suggested by Tabata (1973), Revfeim and Jordan (1976), and Blackadar (1983), but the longest established of these simpler approximations is due to Magnus (1844). By incorporating an amendment due to Bogel (1979), Buck (1981) is able to recommend the use of the Magnus formula for a wide variety of uses and provides a choice of coefficients according to the temperature range of interest and the accuracy required. Buck also supplies a choice of equations for taking into account the 'enhancement factor' which represents the difference in saturation pressure between pure water vapour and moist air.

Many of the empirical approximations developed have assumed that the calculations will be performed on a large computer. In this context the simplicity of an equation has been interpreted in terms of its speed of execution. An IBM 3081 computer at the Meteorological Office, for instance, can evaluate a sixth order polynomial in about the same time as a single exponential expression. In operational meteorology, however, calculations have to be made at synoptic observing stations in order to convert from T_w (which is observed) to T_d (which is required by the World Meteorological Organization (WMO) synoptic codes). These calculations have generally been performed with the aid of either tables or slide-rule, but they may be made more conveniently on a microcomputer or programmable calculator. In this context algebraic simplicity is important as it minimizes storage requirements and enables an equation to be reversed in order to calculate temperature from saturation vapour pressure as well as vice versa.

For routine meteorological purposes, the accuracy required of e_s is that equivalent to an error of 0.1 °C in temperature. This is from 0.5% to 1%, and a number of algebraically simple expressions are capable of achieving this accuracy. A number of such formulae are compared, and the brevity, reversibility and accuracy of the Magnus formula are shown to make it ideal for use with a pocket calculator. It is also perfectly suitable for routine climatological applications on a large computer.

The precision to which T and T_d are reported in the WMO synoptic code messages was increased in 1982 from 1 °C to 0.1 °C. This increase in precision made it possible for climatological collecting centres to calculate the other humidity parameters direct from the messages, rather than through internal reporting of T_w. This procedure therefore offers the advantages of increased automation, but requires the recovery of T_w from T and T_d and this is not straightforward. The purpose of this paper is, therefore, threefold:

(i) to compare some of the algebraically simple formulae for calculating e_s,

(ii) to describe and recommend a procedure based on the Magnus formula for calculating humidity parameters from T and T_w,

(iii) to describe a method for recovering T_w from T and T_d.

The recommended procedures can then be implemented either on a large computer at a collecting centre, or on a programmable calculator at the observing site.

2. Integration of the Clausius–Clapeyron equation

The saturation vapour pressure is expressed as a function of absolute temperature by the Clausius-Clapeyron equation

$$\frac{1}{e_s}\frac{de_s}{dT} = \frac{EL}{RT^2}$$

where L = latent heat of vaporization of water = 2.50084×10^{-3} J kg^{-1} at 0 °C,
R = gas constant for dry air = 287.05 J kg^{-1},
and E = ratio of molecular weight of water vapour to that of dry air = 0.62198.

Difficulties in integrating this equation are caused by the fact that L is not constant, but varies with temperature. If this variation is ignored, and L is assumed to be constant then

$$e_s = \exp(21.4 - 5351\,T^{-1}) \quad \ldots\ldots\ldots\ldots\ldots\ldots\ldots\ldots\ldots\ldots \quad (1)$$

where e_s is given in millibars if T is expressed in kelvins. This is the equation used by Blackader (1983) to illustrate the calculation of humidity parameters on a home computer.

A better assumption is clearly to make L a linear function of T,

e.g. $$L = \{\, 2500.84 - 2.34\,(T - 273.15)\,\} \times 10^{-3}\ \mathrm{J\ kg^{-1}}$$

when $$e_s = \exp(55.17 - 6803\,T^{-1} - 5.07\,\ln T) \quad \ldots\ldots\ldots\ldots\ldots\ldots\ldots\ldots\ldots\ldots \quad (2)$$

The performance of equations (1) and (2), when assessed against the solution of the Goff-Gratch equations as given by WMO (1966), is illustrated in Fig. 1. In this diagram, the dotted lines indicate the

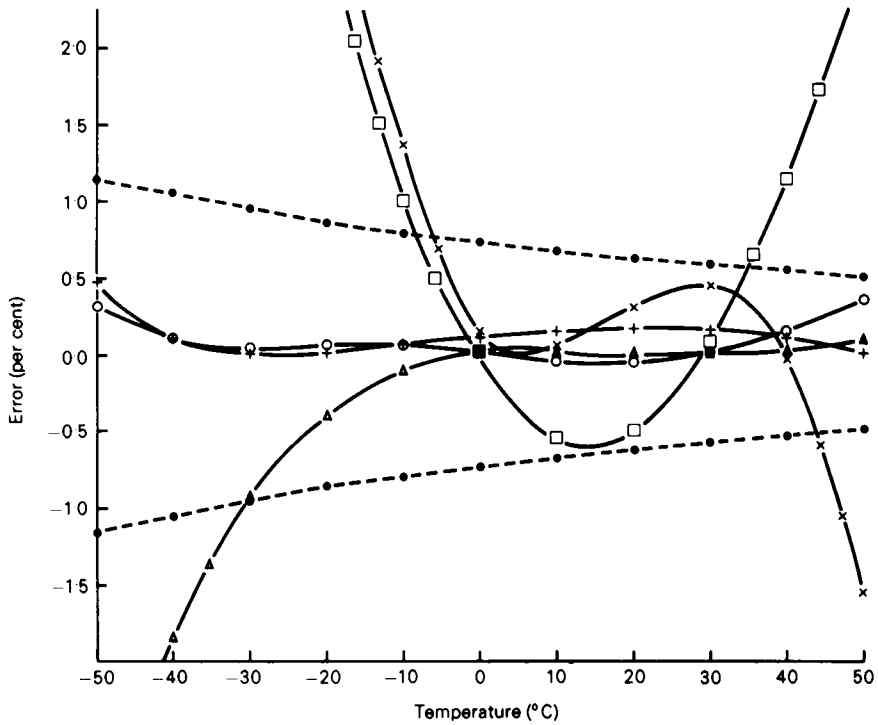

Figure 1. Error in saturation vapour pressure obtained from various formulae. ●- - -● error equivalent to 0.1 °C error in temperature □——□ Blackader, ×——× Revfeim and Jordan, △——△ Magnus, ○——○ Tabata, +——+ Clausius - Clapeyron with L a function of T.

error in e_s which is equivalent to an error in temperature of 0.1 °C. The assumption that L is constant is seen to produce errors within the required limits for temperatures between -10 °C and +35 °C. The

assumption that L is a linear function of temperature, however, results in a considerable improvement and produces errors well within the required limits over the entire range of temperature examined.

3. Empirical expressions for calculating the saturation vapour pressure

The Magnus formula already referred to takes the form

$$e_s = 6.1070 \exp\left(\frac{at}{b+t}\right) \quad \ldots\ldots(3)$$

In this and all subsequent equations, vapour pressure is given in millibars if temperature is expressed in degrees Celsius. The most commonly quoted values of the coefficients for evaporation over water are $a = 17.3$ and $b = 237.3$. Minimum root-mean-square (r.m.s.) errors in millibars with respect to the Goff–Gratch values over the temperature range −40 °C to + 40 °C, however, are obtained by putting $a = 17.38$ and $b = 239.0$ for evaporation over water and $a = 22.44$, $b = 272.4$ for sublimation from ice. With these coefficients, Fig. 1 shows that the Magnus formula produces errors which are within the required range for all temperatures examined above −30 °C.

Revfeim and Jordan (1976) used the relation

$$e_s = \exp\{7.076 - 2.47(1.46 - 0.01t)^2\} \quad \ldots\ldots(4)$$

and Fig. 1 shows that this formulation achieves the required accuracy over a temperature range of −6 °C to +43 °C. Better results may be obtained by using a quadratic in the inverse of absolute temperature, T,

i.e. $$e_s = \exp(19.163 - 4063.2T^{-1} - 184089T^{-2}) \quad \ldots\ldots(5)$$

This form of equation was suggested by Tabata (1973), although the coefficients used are those which minimize r.m.s. errors (in mb) between ±40 °C. The accuracy of this equation is demonstrated in Fig. 1, where the errors produced can be seen to lie within the prescribed limits over the entire temperature range examined.

Of the five equations considered, Fig. 1 shows that those valid over the narrowest range of temperature are those suggested by Blackader (1983) and Revfeim and Jordan (1976). The widest range of applicability is attained by the equation due to Tabata (1973) and that obtained from an integration of the Clausius–Clapeyron equation with L a linear function of T. Unless very low temperatures are to be regularly dealt with, however, it is the Magnus equation which is recommended for use with pocket calculators. It has the advantage of being algebraically very simple and hence reversible, and, for temperatures between 0 °C and 40 °C, is the most accurate of all the equations examined.

The enhancement factor for moist air has not been used in the above calculations since the aim was to reproduce the solutions of the Goff–Gratch equations. It is also ignored in the following sections in order to maintain continuity with past and current Meteorological Office practice. Its omission does not lead to any errors in T_d or the relative humidity, while that in e_s is equivalent to an error in temperature measurement of just less than 0.1 °C. If it is wished to include the effect, however, this can be achieved simply by increasing e_s by 0.46%, i.e. by replacing the constant 6.1070 in the Magnus equation by 6.1351.

4. Recommended procedure for calculating humidity parameters from wet- and dry-bulb temperatures

The starting point is the calculation of e from the Regnault equation, which requires a knowledge not

only of t and t_w but also of $e_s(t_w)$. This can be obtained from the Magnus equation by replacing t by t_w in equation (3) to give

$$e_s(t_w) = 6.1070 \exp\left(\frac{17.38t_w}{239.0+t_w}\right)$$

for $t_w \geq 0\,°C$ and

$$e_s(t_w) = 6.1070 \exp\left(\frac{22.44t_w}{272.4+t_w}\right)$$

for $t_w < 0\,°C$.

Since $e = e_s(t_d)$, the Regnault equation may be written as

$$e_s(t_d) = e_s(t_w) - Ap(t - t_w).$$

For measurements in a screen of the Stevenson type the ventilation coefficient A is 0.000799, except when the wet bulb is frozen when it takes on the value 0.000720. It is important that accurate values of p are used otherwise relatively large errors may ensue. At relative humidities of 10%, for example, the assumption of p=1000 mb when the correct value is 950 mb gives rise to errors of about 20% in e, 2% in relative humidity and 2 °C in t_d.

The second variable to be calculated is t_d, which can be obtained from the calculated value of $e = e_s(t_d)$ by using the transposed Magnus equation for evaporation over water:

$$t_d = \left(\frac{239.0\,K}{17.38-K}\right)$$

where $K = \ln e - \ln 6.1070$.

The next step is the use of the Magnus formula for water to calculate the saturation vapour pressure at the dry-bulb temperature ($e_s(t)$). This enables the relative humidity to be calculated as $e/e_s(t)$.

These steps may be rationalized and summarized as follows:

(i) use the Magnus formula to calculate the saturation vapour pressure at t and t_w,
(ii) use the Regnault equation to calculate $e = e_s(t_d)$,
(iii) use the transposed Magnus equation to calculate t_d and
(iv) calculate the relative humidity as $e/e_s(t)$.

5. Estimation of the wet bulb from the dry bulb and dew-point

The estimation of t_w from t and t_d is a more complex procedure than obtaining t_d from t and t_w. This is essentially because the Regnault equation is expressed in terms of the depression of the wet bulb rather than the dew-point, and so can only be solved for the former by using an iterative procedure.

Less accurate estimates can, however, be obtained using an empirical approach which takes advantage of the fact that t_w lies between t and t_d. At low temperatures, when little water is available for evaporation, t_w is not much less than t, but at high temperatures, t_w is closer to t_d. In other words, the

ratio of the wet-bulb depression to the dew-point depression always lies between zero and unity and increases with temperature. A convenient linear representation of this change is given by

$$\frac{t - t_w}{t - t_d} = 0.34 + 0.006\,(t + t_d).$$

For values of t from − 10 °C to +50 °C and dew-point depressions up to 15 °C, errors in t_w obtained from this equation are always less than 0.3 °C. Improved accuracy could be obtained by introducing a non-linear dependence on $(t + t_d)$ to the right-hand side of the equation — the quoted relation produces a wet-bulb depression which exceeds the dew-point depression at temperatures above about 55 °C and is negative at temperatures below about − 25 °C. It may be more expedient, however, to solve the Regnault equation iteratively.

The Regnault equation may be rearranged as

$$e_s\,(t_w) + Apt_w = e_s\,(t_d) + Apt$$

Using the Magnus equation this becomes

$$6.107 \exp\left(\frac{at_w}{b + t_w}\right) + Apt_w = 6.107 \exp\left(\frac{at_d}{b + t_d}\right) + Apt.$$

All the terms involving t_w are now on the left-hand side. The right-hand side, involving terms in t and t_d, can be evaluated and set equal to a value C. We can then define:

$$F(t_w) = 6.107 \exp\left(\frac{at_w}{b + t_w}\right) + Apt_w - C \quad \ldots\ldots\ldots\ldots\ldots\ldots\ldots\ldots (6)$$

which takes on the value 0 for a correct solution of t_w. This can be obtained using the Newton–Raphson iterative approximation:

$${}_1t_w = {}_0t_w - F({}_0t_w)/F'({}_0t_w)$$

where ${}_0t_w$ and ${}_1t_w$ are the initial and improved estimates of t_w and $F'(t_w)$ is the first derivative of $F(t_w)$,

i.e. $$F'(t_w) = 6.107 \frac{ab}{(b + t_w)^2} \exp\left(\frac{at_w}{b + t_w}\right) + Ap \quad \ldots\ldots\ldots\ldots\ldots (7)$$

The values of a, b, and A to be used in equations (6) and (7) are determined by the value of ${}_0t_w$.

The calculation of t_w from t and t_d may therefore be summarized as follows:

(i) make an initial estimate of ${}_0t_w = 0.5\,(t + t_d)$,

(ii) select the appropriate values of a, b, and A, i.e.

if ${}_0t_w \geqslant 0$ °C	$A = 0.000799$	$a = 17.38$	$b = 239.0$,
if ${}_0t_w < 0$ °C	$A = 0.000720$	$a = 22.44$	$b = 272.4$,

(iii) calculate $C = 6.107 \exp\left(\frac{17.38t_d}{239 + t_d}\right) + Apt$,

(iv) evaluate $F(t_w)$ and $F'(t_w)$ from equations (6) and (7),
(v) obtain an improved estimate ${}_1t_w = {}_0t_w - F({}_0t_w)/F'({}_0t_w)$,
(vi) test for convergence of the procedure, i.e. $({}_1t_w - {}_0t_w) < 0.005$.

If this condition is not met, set ${}_0t_w = {}_1t_w$ and repeat the procedure from step (ii). The criterion is usually satisfied in two or three cycles.

6. Meteorological Office procedures

The introduction of new WMO synoptic codes containing dry-bulb and dew-point temperatures to an accuracy of 0.1 °C created the possibility of increased automation by allowing the calculation of humidity parameters direct from the reported values of t and t_d. This opportunity has been taken by the Meteorological Office whose computer archives of observations from synoptic stations are now based on those contained in the coded messages instead of data keyed from manuscript tabulated returns. The wet-bulb temperatures so archived are no longer those measured, but are now obtained from an iterative solution of the Regnault equation. This peculiar circumstance could only be avoided by the introduction, as a national practice, of the reporting of t_w as well as t_d in the synoptic codes. The vapour pressure and relative humidity are then obtained from a simple application of the Magnus formula. For voluntary climatological stations, for which the wet-bulb temperatures are still received in manuscript form, humidity parameters are calculated using the procedures described in section 4.

The correct pressure to supply to the Regnault equation is that observed at the station, uncorrected for altitude. At voluntary climatological stations the pressure is seldom recorded and so a value of 1000 mb is used. At synoptic stations, users of humidity slide rules are instructed to assume a value of 1000 mb unless the pressure is less than 950 mb. Since the recovery of t_w from t_d is a reversal of a calculation made with a slide rule, the value of the pressure used in this procedure is also set to 1000 mb. For consistency, therefore, all algorithms used to calculate humidity parameters on pocket calculators should use a pressure of 1000 mb. If and when the preparation of synoptic messages is fully automated at all stations, then this could be replaced by the station level pressure.

7. Conclusions

The problems in calculating the various measures of humidity are caused by the difficulty in evaluating the saturation vapour pressure. This is related to departures from the ideal gas law and the variation of latent heat with temperature; these make the Clausius–Clapeyron equation difficult to integrate analytically. Semi-empirical equations due to Goff and Gratch (1945) are available for the accurate computation of saturation vapour pressure, but these are relatively costly to evaluate on a regular basis and for many purposes their accuracy is superfluous. Consequently many attempts have been made to devise simpler approximations providing only the accuracy required. In these attempts, simplicity has been interpreted as the speed and cost of evaluation on a large computer. In operational meteorology, however, there is the need to calculate dew-point from the wet-bulb temperature at synoptic observing stations, and this can be conveniently carried out on a programmable calculator. In this context algebraic simplicity is important and the brevity, reversibility and accuracy of the Magnus formula make it ideal for such a purpose. The Magnus formula is also perfectly suitable for implementation on a large computer and has been used for routine climatological calculations at the Meteorological Office for many years.

References

Blackadar, A. K.	1983	Using home computers to study the weather. *Weatherwise*, **36**, 193–195.
Bogel, W.	1979	New approximate equations for the saturation pressure of water vapour and for humidity parameters used in meteorology. European Space Agency, ESA-TT-509.
Buck, A. L.	1981	New equations for computing vapor pressure and enhancement factor. *J Appl Meteorol*, **20**. 1527–1532.
Goff, J. A. and Gratch, S.	1945	Thermodynamic properties of moist air. *Trans Am Soc Heat Vent Eng*, **51**, 125–157.
Lowe, P. R.	1977	An approximating polynomial for the computation of saturation vapor pressure. *J Appl Meteorol*, **16**, 100–103.
Magnus, G.	1844	Versuche über die Spannkrafte des Wasserdampfes. *Ann Phys Chem, Poggendorff*, **61**, 225.
Rasmussen, L. A.	1978	On the approximation of saturation vapor pressure. *J Appl Meteorol*, **17**, 1564–1565.
Revfeim, K. J. A. and Jordan, R. B.	1976	Precision of evaporation measurements using the Bowen ratio. *Boundary-Layer Meteorol*, **10**, 97–111.
Richards, J. M.	1971	A simple expression for the saturation vapour pressure of water in the range −50 to 140 °C. *J Phys*, D, *Brit J Appl Phys*, Ser. 2, **4**, L15–L18.
Sargent, G. P.	1980	Computation of vapour pressure, dew-point and relative humidity from dry- and wet-bulb temperatures. *Meteorol Mag*, **109**, 238–246.
Tabata, S.	1973	A simple but accurate formula for the saturation vapor pressure over liquid water. *J Appl Meteorol*, **12**, 1410–1411.
Wexler, A.	1976	Vapor pressure formulation for water in range 0 to 100 °C. A revision. Washington, National Bureau of Standards, *J Res*, **80A**, 775.
	1977	Vapor pressure formulation for ice. Washington, National Bureau of Standards, *J Res*, **81A**, 5–20.
Wexler, A. and Wildhack, A.	1965	Humidity and moisture. Measurement and control in science and industry, Vol. 13, Fundamentals and standards. New York, Reinhold.
World Meteorological Organization	1966	International meteorological tables. WMO No. 188, TP 94.

551.501.9

Synoptic observations from Portland Bill

By C. S. Broomfield*

(58 Avebury, Bracknell)

Introduction

Synoptic observations from the keepers of Portland Bill lighthouse recommenced on 18 July 1984 after a break of 15 years, during which period observations were supplied by the Coastguard Service. This article reviews the history of the observing stations at Portland Bill since 1899, and describes some of the problems encountered. Many scores of thousands of useful observations have been made with both forecaster and mariner benefiting from the regular reports, particularly those of fog and wind conditions over the English Channel.

*Formerly of the Meteorological Office, Bracknell.

Station history

Synoptic weather reports made for the Meteorological Office by the lighthouse keepers commenced at Portland Bill lighthouse from an enclosure 54 metres (m) above mean sea level (amsl) on 3 June 1899. The establishment of the weather station was an economy measure which allowed the closure of the stations at Prawle Point and Hurst Castle (Fig. 1).

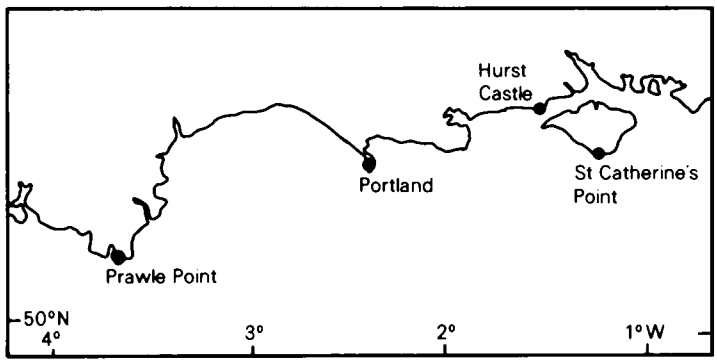

Figure 1. Places mentioned in the text.

In 1906 the meteorological instruments were transferred to the new lighthouse near the Bill (enclosure 6 m amsl — see Figs 2 and 5). No record is available of anything eventful in the very early years, apart from the breakage of both barometers on 1 June 1909 when the wall fitting collapsed.

The thermometer screen was re-sited near the base of the lighthouse in 1913 (Fig. 3). Guy wires were used to brace the screen against strong winds.

The early 1920s saw an increasing number of day trippers, and in the summer of 1923 a motor car ran into the 8-inch rain-gauge. This was no mean feat considering the size of the rain-gauge and the paucity of cars in those days, although the incident was repeated several times the following year. The 1924 inspector reported that holiday makers used the rain-gauge as a foot scraper. Cars and holiday makers were subsequently kept at bay by a 3 ft 6 in paling fence, 15 ft radius from the rain-gauge. However, objections by the Court Leet of the Manor of Portland led to the removal of the fencing in April 1926, followed by car damage to the rain-gauge within three months. A more secure site for the rain-gauge was found in October 1926 on land owned jointly by the Crown and commoners of Portland, for which the Air Ministry paid a yearly rental of 2s.6d. (12½p) to the Crown and 7s.6d. (37½p) to the commoners. The fence was re-erected. The gauge gave low values compared to readings at Portland Royal Naval Air Station (RNAS) and a turf wall was constructed inside the paling fence. This made no noticeable difference and the rain-gauge problems continued throughout the life of the station.

In October 1945 the lighthouse was opened to the public. A car park was provided by the council, and six cafés catered for the visitors. The following summer a harassed inspector, Mr (now Professor) Hubert H. Lamb, found much difficulty in gaining the keepers' attention because of the number of visitors — 1600 to 1800 a day. The magnifying glass provided to assist in the reading of the mercurial barometers soon became a memento for one of them.

In 1947 a shortage of regular light-keepers caused difficulties at the station. Naval ratings were brought in to act as relief light-keepers and, to their astonishment, as auxiliary meteorological observers.

Figure 2. Portland Bill new lighthouse looking east, from an old photograph.

Figure 3. 22 May 1913. Light-keeper Withers (left) and Assistant Light-keeper Ball (right), the observers, by the thermometer screen. Note single-louvered door and mounted thermometers.

The strategic position of the station was given further recognition from 22 April 1956, when Portland Bill's observations were first included in the BBC Shipping Bulletins.

An electrical anemograph system was installed on the lantern roof in March 1963 (Fig. 4). Before this, wind directions had been obtained from the Trinity House vane on top of the lighthouse, and wind speeds estimated.

In 1966 Meteorological Office requirements for hourly full synoptic reports could not be met by the keepers, so the assistance of the nearby coastguards as auxiliary observers was sought. Hourly full

Figure 4. Electrical anemometer head and vane on top of the lighthouse. The exterior ladder allows access for servicing.

synoptic observations by HM Coastguards commenced from an enclosure (53 m amsl) at their look-out (Fig. 5) on 1 January 1967. The thermometer screen and instrumentation were supplied by the Meteorological Office. An anemometer system was erected on a 40 ft lattice tower 150 yards to the east of the meteorological enclosure with an anemograph recorder at the look-out. Overlap observations restricted to 09 and 21 GMT continued at the lighthouse until 31 March 1968, and anemograph records until 31 March 1969 after which the recorder was withdrawn although the rest of the anemometer system remained.

In 1979 it was noticed that the number of breakages of maximum and minimum thermometers was above average. The breakages were attributed to buffeting in strong winds which caused the instruments to move horizontally along their rests until they slipped from the end of the supports and fell through the slatted floor of the thermometer screen to the ground below. Rubber grommets were supplied to slip on to the ends of the thermometers to prevent them from moving along their rests, and these proved successful.

Reorganization of the Coastguard Service meant that from 1 January 1984 the look-out was not manned regularly at night and observations were lost. An appeal for the light-keepers' assistance was readily answered by three of the keepers who agreed to provide three-hourly full synoptic reports when on duty. A thermometer screen has been provided in the lighthouse compound, but there remains no satisfactory exposure for a rain-gauge.

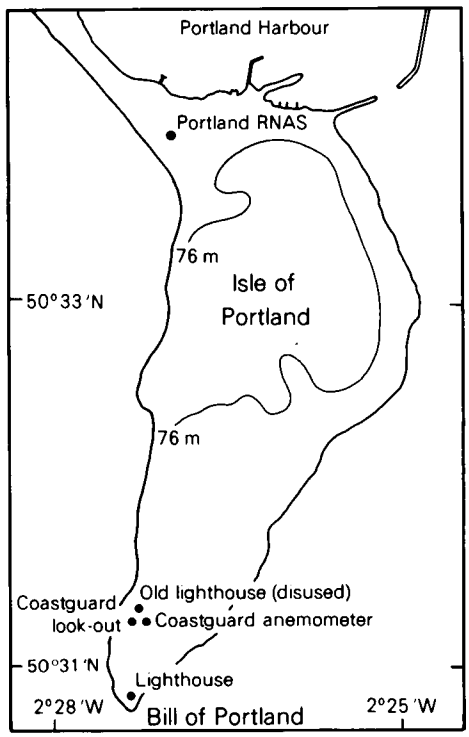

Figure 5. Reporting stations on Portland.

The wheel has thus turned full circle with an Auxiliary Reporting Station re-established at the lighthouse. The original anemometer on the lighthouse lantern is once more used for meteorological observations, although the coastguards still maintain the anemograph record from the anemometer provided for their reports. However, bulletins broadcast for mariners by the BBC now include reports from St Catherine's Point, rather than Portland, in view of their hourly frequency throughout the 24 hours. The Portland reporting program is now:

03855	Portland Bill/Coastguard 53 m amsl	05 (summer), 06 to 17 hourly, 18 (winter) GMT plus other hours when the look-out is manned for coastguard casualty working or bad weather watch. Climatological and anemograph records.
03856	Portland Bill (lighthouse site) 11 m amsl	00, 03, 06, 09, 12, 15, 18, 21 GMT when a co-operating keeper is on duty.

Observations are also made from Portland RNAS (03858) 4 m amsl, when flying is taking place, although the site at this station has a mainly northerly aspect.

Letter to the Editor

Comments on 'Large hail over north-west England, 7 July 1983' (by L. Dent and G. Monk, *Meteorol Mag*, **113**, 1984, 249–263).

(i) You may be interested to know that on 7 June 1983 at 1420 GMT an exceptional thunderstorm occurred here at Chivenor which produced hailstones measuring ½ inch in diameter. The visibility was reduced to 90 metres and a gust of 47 knots was recorded with the temperature falling to 6 °C.

(ii) This storm occurred some 2½ hours earlier than those noted in the above article.

(iii) Cumulonimbus tops were reported to over 40 000 feet.

L. Fraas
(Senior Meteorological Officer)

Meteorological Office
Royal Air Force
Chivenor
Barnstaple
Devon EX31 4AZ

Notes and news

75 years ago

The following extract is taken from *Symons's Meteorological Magazine*, February 1910, **45**, 6–7.

THE GREAT PARIS FLOOD OF 1910

It has been found impossible to obtain data as to the meteorological conditions which led to the widespread floods in France during the last ten days of January in time for a satisfactory account of the disaster in the present issue. We hope to deal with the subject at a later date. It is curious that in the many columns devoted daily by the London press to the spread of the floods, the amount of the rainfall has not been definitely stated, and it remains for the present a matter of speculation. Heavy and continuous rains had fallen for some days before January 21st, and rivers were in flood all over France, but public attention was naturally concentrated on the state of matters in Paris, where damage was done on a scale unequalled in human memory. Indeed, the flood may prove to have been the highest on record. At the Pont Royal the height of floods in the Seine has been recorded for many years, and we quote, on the authority of the Paris correspondent of *The Times*, the following extreme measurements of the height of the river at this point—in 1615 over 32 feet, in 1802 nearly 30 feet, in 1876 about 26 feet, and on January 29th, 1910, over 31 feet. The height of the great flood of 1658 at the Pont de la Tournelle was 29 feet, and that of 1876 was about 21 feet. If we may take 5 feet as the difference in level between the two datum marks it would appear that the present flood fell slightly short of that of 1658.

If data of scientific value have been scanty in the English press, descriptions of the extent of the inundations on both sides of the Seine and of the damage done have been bewilderingly abundant. While the waters were rising traffic was stopped over many of the bridges; but although only a few inches of the central arch of the Pont d'Alma remained above water, none of the bridges collapsed, and traffic was resumed before the flood abated. It is said that 200,000 people were seriously affected by the flood, being either driven from their homes or thrown out of work in consequence of the stoppage of factories or the closing of shops. The low-lying parts of the underground railway system were completely filled with water, and several of the great railway termini were cut off and closed for traffic. This was the case with the Gare de Lyon and the Gare d'Orleans; the traffic to the Mediterranean coast through Paris was suspended, and Mr. Asquith made his way to Nice after the General Election by a roundabout route through Bâle and Genoa. More than 15,000 telephone subscribers in Paris were cut off, and most of the

telegraph wires out of Paris also failed for a time. Water invaded many public buildings, and divers were employed to rescue the archives of the Palais de Justice from under 8 feet of water. The Louvre was seriously threatened, and the spread of the flood was only controlled by the exertions of troops with bags of cement, sand and stones torn from the pavements, which were used to form barricades against the water. Sailors and boats from the Navy were hurried to Paris to save the inhabitants of the inundated streets, and there was practically no loss of life, thanks to the admirable organization shown in dealing with the situation. The extent of the damage is unknown at the time of writing, and must amount to many million pounds. The chief danger is to the stability of buildings by subsidences in the streets as the water goes down, and to health by the accumulation of sewage from the burst sewers. It is probably not too much to say that the flood has been more widespread and productive of distress than any previously known in Europe, though, considering its extent, it has been singularly free from loss of life.

The complete disorganization of the life of a great city in consequence of some unfortunate combination of meteorological conditions is very rarely seen, and it has been pointed out in Paris that the area inundated would have been far less and the resulting suffering not nearly so great if the quay-walls along the river had not been so frequently cut in recent years for facilitating traffic, and if the system of underground railways had not been so greatly developed.

Reviews

Plants and microclimate. A quantitative approach to environmental plant physiology, by Hamlyn G. Jones. 160 mm × 235 mm, pp. xviii + 323, *illus.* Cambridge University Press, Cambridge, London, New York, New Rochelle, Melbourne, Sydney, 1983. Price £27.50, £12.50 (paperback).

The investigation of the relations between plant growth and environment is a topic for both meteorologists and plant physiologists. Most meteorologists who work in this field will probably have made their way by means of books and papers written by physical scientists (e.g. *Principles of environmental physics* by J. Monteith). Plant physiologists, however, working from 'their side' have also made significant progress and here is a book by a plant physiologist which, while firmly rooted in plant physiology, makes a useful contribution to the application of physical principles to the solution of plant growth and ecological problems. The author compiled the book from courses in environmental physiology given to undergraduates, but the treatment is not superficial, with some good discussion of advanced topics.

After an introductory chapter on modelling and experimentation the book is divided into 11 other chapters. Three of these cover the physics of radiation, heat, mass and momentum transfer and also energy balance and evaporation. Much of this material will be familiar to meteorologists, but there is a strong emphasis on molecular transport processes since this is the main agent of diffusion within plants. The chapter on radiation emphasizes the importance of the number of quanta of photosynthetically active radiation rather than total energy in the study of radiation within plant canopies. On page 19 it is unfortunate that the regression coefficients in the relation between global short-wave irradiance and sunshine hours use work done by L. P. Smith nearly 20 years ago and not the more recent appraisal by J. P. Cowley (1978) published in the *Meteorological Magazine* (The distribution over Great Britain of global solar irradiation on a horizontal surface, *Meteorol Mag*, **107**, 357–373).

Similarly, on page 96, L. P. Smith's grassland transpiration model is quoted as still being 'widely used in the UK'. This is not true, and even in 1982 when the book was produced the MORECS system had been in operational use for several years and written up as *Hydrological Memorandum No. 45* in 1981 (The

Meteorological Office rainfall and evaporation calculation system: MORECS (July 1981), by N. Thompson, I. A. Barrie and M. Ayles).

The remaining eight chapters form the bulk of the book and this is where the author takes us right inside plants to explain their growth reactions. There are chapters on the following topics: plant– water relations, stomata, photosynthesis and respiration, plant morphogenesis, temperature, drought, wind altitude and CO_2, and finally a chapter on yield improvement. The water relations of plants are described using water potential, a concept unfamiliar to meteorologists, but here we have a clear account to enable us to read plant physiological literature which uses these ideas. All the factors which could possibly affect stomatal resistance are set out and there is a critical appraisal of the methods currently in use to measure it. The photosynthesis chapter is clearly set out though some of the chemistry is beyond this reviewer. The C_3, C_4, and CAM Photosynthetic pathways are clearly distinguished and there is a detailed discussion of resistances to CO_2 diffusion. Some parts of this chapter would be hard going for most meteorologists. The chapter on plant morphogenesis would also have material unfamiliar to meteorologists, but here the mysteries of phytochrome, photoperiodism and nastic movements are explained. The chapters on temperature and drought discuss how plants react to these environmental factors in terms of photosynthesis, injury and hardening. There is a strong ecological thread to these chapters which tries to explain some of the observed facts of the distribution and natural selection of plants for and within specific environments. There is an interesting section on water use efficiency (i.e. the ratio of net assimilation to water loss) which leads to a section on the modelling of optimum stomatal behaviour. The chapter on wind, altitude and CO_2 is rather more sketchy than the others, but still gives much useful information. A treatment of lodging is given which fails to mention that the main effect of rain on cereals is to increase the weight of the ear and so increase the turning moment about the stem base when the wind blows. The last chapter attempts to conclude what the ideal crop plant ought to be like using some of the ideas from the rest of the book. There are ten appendices giving derivations of some of the formulae used in the text, and then 20 pages of references many of which are from the 1970s and 80s. The index is comprehensive.

For a book of this size and content it is remarkably free from errors. I could find only two: Figure 7.18 where one symbol in the key does not match the diagram and the other in Figure 12.5 where wheat yields of up to 70 t/ha are plotted.

The level of knowledge expected of the reader is variable. Some of the chemistry required has already been mentioned and while torque, for example, is explained on page 242, the Gibb's free energy is mentioned on page 64 without more ado. However, these are minor complaints about an excellent book which all agricultural meteorologists would benefit from using.

M. N. Hough

Milankovitch and climate, edited by A. Berger, J. Imbrie, J. Hays, G. Kukla and B. Saltzman. 2 Vols 155 × 235 mm, pp. Part I xxxiv + 510, Part II ix + 510, *illus.* D. Reidel Publishing Company, Dordrecht, Boston, Lancaster, 1984. Price Dfl 310, US $117.00.

This pair of substantial volumes records most of the papers presented at an international symposium held at the Lamont-Doherty Geological Observatory, Palisades, New York, in December 1982. The aim of the meeting was to consider and refine the theory of Milankovitch (1941) that the Pleistocene ice ages were triggered by variations of the Earth's orbit around the sun.

A systematic account is given of all aspects of current research into the mechanisms underlying the inception, maintenance and termination of the Pleistocene ice ages. Subjects discussed include methods of computing more accurately the orbital variations themselves; geological evidence for Pleistocene and

earlier long-term climatic variations with the periodicities predicted by Milankovitch (approximately 19 000, 23 000, 41 000 and 100 000 years); and modelling long-term climatic variation which may occur in response to orbitally-induced forcing.

All sections of the work convey an atmosphere of new discovery and insight, combined with the realization that many improvements and further discoveries remain to be made. For this reason the papers will rapidly become dated, though they will retain historical interest as examples of scientific methods, co-operation, and progress — V. Milankovitch's memoir of his father is already interesting material for the historian.

A key paper is that of Imbrie *et al.* who use records of the oxygen isotope O^{18} from marine cores to leave little room for doubt that variations in the geometry of the Earth's orbit are the main cause of the succession of late Pleistocene ice ages. The oceans are richer in O^{18} when global ice volume is large, because of preferential evaporation and condensation. Given radiometric and magnetic dating, the cores are found to be consistent with predictions using the 19 000- and 23 000-year precessional cycles and the 41 000-year obliquity cycle, assuming a 17 000-year time-constant for the Earth's response, and allowing phase-tuning to refine the dating. The criticism of possible over-tuning or over-fitting is largely answered by the good fit to the 100 000-year eccentricity cycle which was not included in the phase-tuning of the cores.

By contrast, the uncertainty of many deductions about Pleistocene climate is highlighted by the paper of Janecek and Rea who deduce that glacial periods were moist in middle and low latitudes, in contrast to the aridity claimed by other authors. The analysis of Pacific aeolian sedimentation rates and grain sizes in their paper clearly shows the main Milankovitch cycles, but although the obliquity and precessional cycles in grain size indicate stronger winds during glacials, the eccentricity cycle in grain size indicates the reverse. To explain this the authors had to invoke a change of latitude of the mid-latitude westerlies in association with the eccentricity cycle in glaciation, without invoking a similar change of latitude in response to the obliquity and precessional modulations of glaciation. This is very reasonable, in view of the lesser size of these modulations compared with the apparent imprint of eccentricity on glaciation, but is nevertheless still speculation.

Pestiaux and Berger present a particularly illuminating and useful review of the variety of spectral analysis methods now available. An appreciation of, for example, the somewhat different results which different spectral analysis methods give for the same data will enable the reader to assess more critically the results presented in this (and many other) fields. This paper may not date as rapidly as some of the others.

The paper of Ruddiman and McIntyre is recommended as a thought-provoking review article which considers some possible feedbacks within the atmosphere–ocean–cryosphere system in the context of the precessional and obliquity signals during the Pleistocene. Broecker's invocation of atmospheric carbon dioxide changes as a trigger for rapid deglaciations contrasts markedly with Pollard's ice-calving mechanism and shows that the field in this area remains wide open for debate.

A few of the papers betray hasty proof-reading, and there are some printer's errors. Pages 661 and 666 are interchanged, and the printing reproduction fails to do justice to the diagram on page 66. The authors of the Meteorological Office's contribution on page 721 are omitted from the authors' index. That particular paper is a good example of one which is already out of date (see *Nature* 23 August 1984).

At the end of Volume II there is a summary chapter drawn up at a small subsequent workshop. Although useful it makes less inspiring reading than many of the papers. The recommendations for future work demonstrate how much remains to be done. Simulations of 100 000 years with a realistic fully coupled general circulation model of the atmosphere–ocean–cryosphere system are still a somewhat distant target!

D. E. Parker

THE METEOROLOGICAL MAGAZINE

No. 1351 February 1985 Vol. 114

CONTENTS

NOTICE

It is requested that all books for review and communications for the Editor be addressed to the Director-General, Meteorological Office, London Road, Bracknell, Berkshire RG12 2SZ and marked 'For Meteorological Magazine'.

The responsibility for facts and opinions expressed in the signed articles and letters published in this magazine rests with their respective authors.

Applications for postal subscriptions should be made to HMSO, PO Box 276, London SW8 5DT.

Complete volumes of 'Meteorological Magazine' beginning with Volume 54 are now available in microfilm form from University Microfilms International, 18 Bedford Row, London WC1R 4EJ, England.

Full-size reprints of Vols 1–75 (1866–1940) are obtainable from Johnson Reprint Co. Ltd, 24–28 Oval Road, London NW1 7DX, England.

Please write to Kraus Microfiche, Rte 100, Millwood, NY 10546, USA, for information concerning microfiche issues.

HMSO Subscription enquiries 01 211 8667.

Printed in England for HMSO and published by
HER MAJESTY'S STATIONERY OFFICE

£2.30 monthly

Annual subscription £27.00 including postage

Dd. 737126 C14 2/85

ISBN 0 11 727556 5
ISSN 0026–1149

THE METEOROLOGICAL MAGAZINE

HER MAJESTY'S STATIONERY OFFICE

March 1985

Met.O.967 No. 1352 Vol. 114

METEOROLOGICAL OFFICE Met.O.967

THE METEOROLOGICAL MAGAZINE

No. 1352, March 1985, Vol. 114

The Meteorological Magazine: Editorial Board

It has been decided to set up an Editorial Board for the *Meteorological Magazine*. Members of the Editorial Board will advise the Editor on the content and presentation of articles and encourage the production of scientific papers and other material suitable for publication.

The Board has reached some recommendations on the content of the *Meteorological Magazine*. These may be summarized as follows:

(1) The Editor should continue to seek the submission of articles which describe the results of research in applied meteorology or the development of forecasting techniques. Such articles might be obtained from any source.

(2) Authors should be encouraged to submit papers that are more relaxed and conversational in style than hitherto.

(3) There is a need for review articles which provide up-to-date accounts of different research topics, new operational techniques and procedures, and early informal descriptions of promising new lines of research.

(4) Major research work, the results of which merit publication internationally but is of interest to meteorologists in different specializations, could be made the subject of a simplified article for inclusion in the *Meteorological Magazine*.

(5) Staff at Meteorological Office outstations and observers at co-operating ancillary and climatological stations in the United Kingdom should be encouraged to submit notes or short accounts of interesting or remarkable weather phenomena without necessarily involving profound scientific analysis or explanation.

Our readers may expect therefore some gradual changes in the content and style of writing in future issues of the *Meteorological Magazine*, but not in the quality. The Editorial Board looks forward to receiving an increasing number of interesting contributions from meteorologists and climatologists wherever they may be working.

The Editorial Board at present consists of the following members:

R. P. W. Lewis	(Head of Library and Publications) (Editor and Chairman)
T. Davies	(Central Forecasting Office)
G. J. Jenkins	(c/o Central Directorate of Environmental Protection, Department of the Environment)
P. R. S. Salter	(Headquarters, RAF Strike Command)
P. G. Wickham	(Meteorological Office College).

551.507.352

The use of aircraft to study the atmosphere: the Hercules of the Meteorological Research Flight

By C. J. Readings

(Assistant Director (Professional Training))

Summary

The use of aircraft to study the structure of the atmosphere is illustrated by reference to the Hercules aircraft of the Meteorological Research Flight. In addition to describing the instrumental fittings in some detail the article outlines some of the uses of such a facility.

1. Introduction

It is now well over half a century since meteorologists first started using aircraft to study the structure of the atmosphere. In fact, before the network of balloon observations became established, aircraft were also used to take routine soundings of the atmosphere, recording temperature and humidity as a function of pressure (i.e. height) up to altitudes of around 8 km in unpressurized aircraft. This work is described by Sprigg (1939) and it is interesting to contrast the working conditions of pilots and observers in those early days, operating Bristol Bulldogs and Gloster Gladiators, with those experienced today when enclosed pressurized environments are the norm. In the interim, both aircraft and instruments have advanced considerably and the aim of this article is to give some indication of the facilities now available to atmospheric scientists.

Modern flying laboratories bear little resemblance to the early aircraft used for meteorological research, either in form or in content, being basically contemporary aircraft. Most have been modified so that some of their sensors (notably those used to measure wind and temperature) can be exposed remote from the influence of the airframe. 'Long noses' are common. They are also fitted with complex data recording and 'real time' display systems, enabling scientists not only to check that data are being recorded properly but also to monitor progress during flight, helping to ensure that opportunities are not missed and that the full potential of the facility is realized.

These aircraft are used to study a variety of atmospheric phenomena, ranging from 'classical' studies of phenomena such as fronts or wind structure to topics that have developed more recently (viz. the role of trace gases or the use of satellites). Areas of current interest to the Meteorological Office in which its research aircraft is involved, include:

the structure and dynamics of clouds,
the evolution of fronts and other synoptic and mesoscale phenomena,
the effect of topographic features on wind structure,
the transport of pollutants,
the amounts of trace gases present in the atmosphere,
radiative studies associated with the presence of aerosol,
the effect of clouds on radiative balance, and
the evaluation of proposed satellite remote atmospheric probing systems.

Of course this list only serves to give a general indication of current interests as the area of potential application is much wider.

In some instances a knowledge of basic meteorological variables such as wind, temperature and humidity suffices but in other areas information on cloud structure or chemical composition is required, so that these aircraft have to be equipped with a variety of instruments ranging from the basic (i.e. wind, temperature and humidity) to those designed to reveal details of cloud microstructure, aerosol content or chemical composition. The range has also been extended by current interest in remote sensing so that the generic term 'radiometer' could now be said to cover a wide variety of instruments.

Although on some occasions measurements gathered by flying at a single level along a single flight track are all that is required, in most instances information in three (or four) dimensions is needed. This inevitably leads to a conflict between the time available and the data requirements though normally one aircraft flying a series of different flight tracks does suffice. However, this basic capability occasionally has to be extended either by the use of dropsondes released by the aircraft or else by several aircraft collaborating in a single study. A recent example of the latter was KONTUR, an experimental study of convective activity in the German Bight, in which German and UK aircraft collaborated.

To illustrate the wide range of instruments that have to be carried for this work, one such facility will be described, namely the Hercules aircraft of the Meteorological Research Flight. In so doing, it is logical to group the instruments under general headings, namely basic meteorological variables, aerosol and cloud physics instruments, chemical sampling, radiometers and 'other'. A schematic diagram of the instrumental layout is given in Fig. 1 and Tables I–IV give details of the main experimental equipment carried by the aircraft.

2. The airframe

As can be seen from Fig. 2, the aircraft is a modified Lockheed C-130 'Hercules'. The radar antenna has been moved from its customary forward position just below the flight deck to a pod mounted above the cockpit, permitting a 7-metre 'nose' to be installed at the front of the aircraft. From this nose, meteorological variables such as temperature, pressure and undisturbed airflow, all of which could be adversely affected by the presence of the aircraft, are measured. Other instruments are mounted either on the fuselage or in special pods slung beneath the wings. Data are recorded on magnetic tape.

The aircraft has a ceiling of about 10 km and is capable of operating for some 14 hours, corresponding to a range of about 7500 km, though obviously these figures all depend on factors such as payload, operating altitude, etc. The aircraft is very well suited to studies covering the atmospheric boundary layer, the low stratosphere at high latitudes in winter and the troposphere in general, within clouds and in clear air.

3. Basic meteorological variables (Table I)

These comprise wind, temperature, humidity, position and altitude, and are measured by a combination of slow and fast response sensors. Wind is without doubt the most complex, depending as it does on the accurate determination of the difference between two relatively large vectors (i.e. air flow relative to the aircraft and the movement of the aircraft relative to the ground). The former is determined with the aid of two wind vanes which measure angles of attack and side-slip, coupled with air speed which is derived from a Pitot-static sensor linked to fast response capacitive-type pressure transducers. This probe is aerodynamically compensated to ensure that the static and dynamic pressure measurements are independent of the angle of incidence of the airflow. All these sensors are mounted on the end of the boom (see Fig. 1). Motion of the aircraft itself is measured by an inertial navigation system which gives the three velocity components together with pitch, roll and heading (see Broxmeyer 1964). Inertial

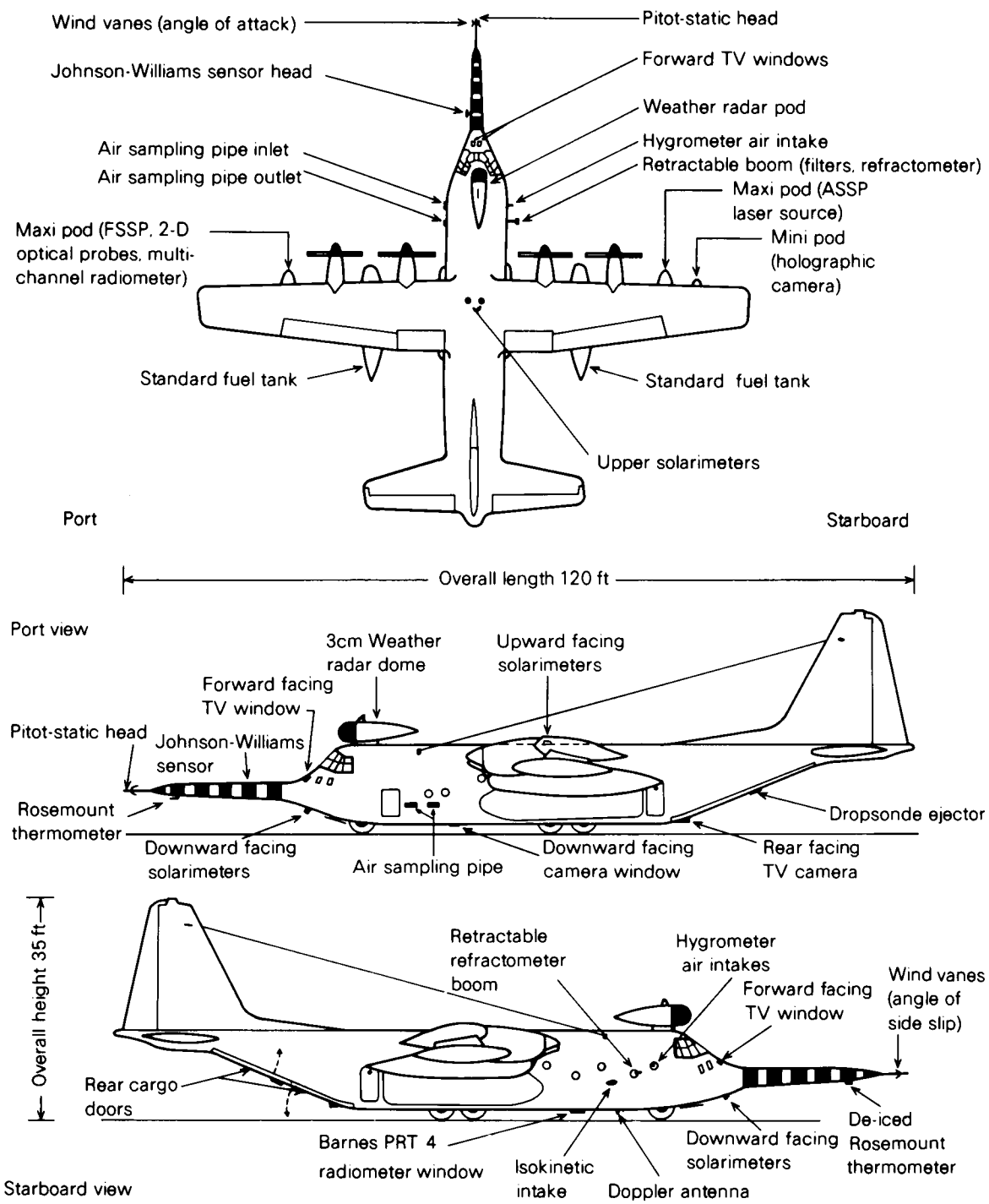

Figure 1. Schematic diagram showing the location of instruments on the Hercules aircraft as seen from above and from the sides.

Figure 2. General view of the Hercules aircraft of the Meteorological Research Flignt.

Table I. *Basic meteorological variables*

Variable	Absolute accuracy	Resolution	Primary instrumental source	Remarks
Horizontal wind component	±0.4 m s^{-1}	±0.06 m s^{-1}	Pitot-static system, inertial platform, Doppler radar, Decca, Omega, Loran, angle of side-slip vane	Assumes full corrections applied including removal of INS drift
Vertical wind component	±0.1 m s^{-1}	±0.09 m s^{-1}	Pitot-static system, inertial platform, angle-of-attack vane	Assumes low-frequency errors removed by reference to changes in static pressure
Temperature	±0.3°C	0.006°C	Platinum-resistance thermometer, Pitot-static system	Corrected for kinetic heating
Humidity mixing ratio	±0.3 g kg^{-1}	±0.02 g kg^{-1}	Refractometer, automatic hygrometer, manual hygrometer, platinum-resistance thermometer, Pitot-static system	Instruments cover different frequency ranges and different ambient conditions. Accuracy and resolution also vary with ambient conditions. Figures quoted refer to the lower levels of the atmosphere.
Geometric altitude	1%	0.8 m	Radar altimeter	
Pressure	±1 mb	0.5 mb	Compensated static ports	

navigation systems (INS) are prone to slow drifts which must be removed if accurate winds are to be derived. For the horizontal components this is done by comparing INS positions with those derived from either a Decca Doppler radar or else a hyperbolic navigation system (i.e. Decca, Loran or Omega — see Meredith 1983). The latter are more accurate as they are not dependent on surface movement (viz. ocean currents). Drift errors in the vertical velocity are removed by reference to pressure changes. Fuller details of the various corrections may be found in Nicholls (1978) and Nicholls *et al.* (1983). Axford (1968) describes the way airflow and INS information are combined to produce wind data. Absolute accuracies of a few tenths of a metre per second are possible. Changes of a tenth of this can be detected up to frequencies of 10 Hz or more.

Temperature is measured by a platinum-resistance thermometer enclosed in a special housing. This is

also mounted on the boom as the aircraft can modify temperatures in its immediate vicinity. Corrections have to be made for both kinetic heating and the de-icing current which is applied to the housing (see Nicholls 1978). For high-frequency data (i.e. above 3 Hz) the variations of the response of the instrument (i.e. platinum element and housing) with frequency must be allowed for. This is done numerically using a technique developed by McCarthy (1973). Within clouds further problems arise as the thermometer becomes wet so that it tends to indicate 'wet-bulb' rather than 'dry-bulb' temperature (see Hess 1959).

Water vapour (i.e. specific humidity— see Hess 1959) is more difficult to measure than temperature as several different instruments are needed to meet all requirements. Two of these depend on the same physical process, namely the condensation of water vapour (as liquid or ice) on a cold surface. The temperature at which this starts to occur is the dew-point (or frost-point). With the manual hygrometer this is detected by an observer monitoring condensation on a metal surface cooled by liquid nitrogen (Cluley and Oliver 1978); with the other instrument it is done automatically using a photoelectric sensor to detect condensation on a mirror which is cooled by the Peltier effect (Nicholls 1978). Both instruments are required as the former can be used at lower temperatures and humidities. For high-frequency data (i.e. above 0.1 Hz) a microwave refractometer mounted on a retractable boom (see Fig. 1), is used. This measures the refractive index of air at centimetre wavelengths where it is dependent on the amount of water vapour present. Refractive index is also a function of temperature and pressure but as both of these parameters are measured it is a relatively simple matter to derive humidity (see McGavin and Vetter 1965). Calibration stability is achieved by matching these values (smoothed to remove high-frequency fluctuations) with those derived from the automatic hygrometer. The refractometer head has to be mounted on a retractable boom because the gold-plated microwave cavity should not be left exposed in all meteorological conditions (i.e. heavy rain, low temperature) though cloud droplets and ice crystals do not usually affect it.

Below 1500 m the height of the aircraft above the ground is measured directly with a radar altimeter; above this level the compensated pressure probe is used. Data from this instrument can be converted to height above the ground, with the aid of temperature and humidity profiles, by applying the hydrostatic equation (Hess 1959).

4. Aerosol and cloud physics instruments (Table II)

The aircraft is also equipped to study the structure of clouds and aerosols, using a variety of optical and other devices. Samples of solid matter present in the atmosphere can be collected on millipore filters (Johnson and Atkins 1975) mounted on the retractable boom (instead of the refractometer). These can subsequently be analysed in the laboratory to determine chemical and physical characteristics. An integrating nephelometer (Ruby and Waggoner 1981) mounted near the retractable boom provides information on the scattering properties of particles (principally in the range $0.1\mu m < r < 1\,\mu m$).

A Pollak counter (Nolan and Pollak 1946) monitors total particle concentrations (in the range $0.005\mu m < r < 0.1\mu m$). This is a derivative of the Wilson cloud chamber in which very high supersaturations ($\approx 300\%$) are applied by rapid decompression causing water to condense on any particles that are present. Reductions in transmission through the condensation chamber can be related to particle concentrations. The Cloud Condensation Nucleus counter (Lala and Jiusto 1977) is similar except that, instead of rapid expansion, a gradient of saturation is maintained. In this instrument, relatively low supersaturations, similar to those occurring in natural clouds, are applied. Thus only those nuclei which influence the microphysical properties of clouds are detected — i.e. generally large ($r > 0.2\mu m$) hygroscopic nuclei. For both of these instruments isokinetic (i.e. independent of particle size) sampling is required, so a specially shaped inlet port has been installed on the starboard side of the aircraft. Air

Table II. *Aerosol and cloud physics instrumentation*

Observable	Device	Size range *micrometres*	Remarks
Aerosol light scattering	Integrating nephelometer	$0.1<r<0.1$	Sampled via alleviator
Particle concentration	Pollak counter	$0.005<r<0.1$	Sampled via alleviator
Condensation nuclei	Cloud condensation nucleus counter	$r>0.2$	Sampled via alleviator
Number densities of cloud particles	ASSP and FSSP	$1<r<15$, $2<r<30$ or $3<r<45$	Choice of ranges. Size correct for water droplets only
	Cloud particle probe	$25<r<800$	
	Precipitation probe	$200<r<6400$	
	Holographic camera	$r>10$	Compact instantaneous 0.5 litre sample
Liquid water concentrations	Johnson–Williams meter	$r<50$	Largest drops shed by wire

flowing through this device is collected in an alleviator (basically a compression chamber) which brings samples up to cabin pressure prior to analysis.

A set of optical probes supply information on the distribution of cloud and precipitation particles (i.e. droplets, ice crystals etc. — see Mason 1962) within clouds. These instruments are mounted in the instrumented pods slung beneath the wings of the aircraft. The Knollenberg FSSP (Forward Scattering Spectrometer Probe) and ASSP (Axially Scattering Spectrometer Probe) measure the numbers of cloud particles lying in various size ranges by detecting the intensity of light scattered by individual particles as they traverse the sampling volume, assuming they are water droplets and that only one lies in the detector chamber at one time. A tape recorder logs the number of 'drops' detected in 15 size categories lying in one of 3 size ranges, namely $1<r<15\,\mu$m, $2<r<30\,\mu$m or $3<r<45\,\mu$m (Ryder 1976, Knollenberg 1976). Concentrations of liquid water within clouds may be obtained either by integrating these 'drop' size distributions or from a device called the Johnson–Williams meter. In this instrument the cooling of a hot wire exposed to the airstream caused by the evaporation of cloud drops colliding with and remaining attached to the wire is related to liquid water content (Strapp and Schemenauer 1982).

Information on the actual shapes of cloud and precipitation particles is provided by two-dimensional optical array probes (Knollenberg 1976) which are also fitted to an instrumented pod. One of these is capable of detecting larger cloud particles (i.e. $25\,\mu\text{m} < r < 800\,\mu$m) while the other covers precipitation elements (i.e. $200\,\mu\text{m} < r < 6.4$ mm). Images of the particles are projected on to 32-element photodiode detectors by laser beams. These arrays are scanned rapidly so that as the particle is advected through the system a two-dimensional image is built up. Further information is obtained with the aid of a holographic camera which records the interference patterns created by particles illuminated by a pulsed laser. The camera and the laser are installed in adjacent instrument pods (Fig. 1). Subsequently, particle images are reconstructed from the hologram in the laboratory using a CW laser which offers several advantages over the pulsed laser including better resolution. Particles larger than $10\,\mu$m in radius can be studied (see Conway *et al.* 1982), the technique having much larger depths of field than is possible with conventional photography. Fig. 3 shows examples of the output from two of these optical devices.

5. Chemical sampling (Table III)

Several different gases may be detected by the equipment on the Hercules, including some of the oxides of nitrogen, sulphur dioxide and ozone. All enter the aircraft via the air-sampling pipe mounted on its port side (Fig. 1). Ozone detection is based on the ethylene–ozone chemiluminescence reaction

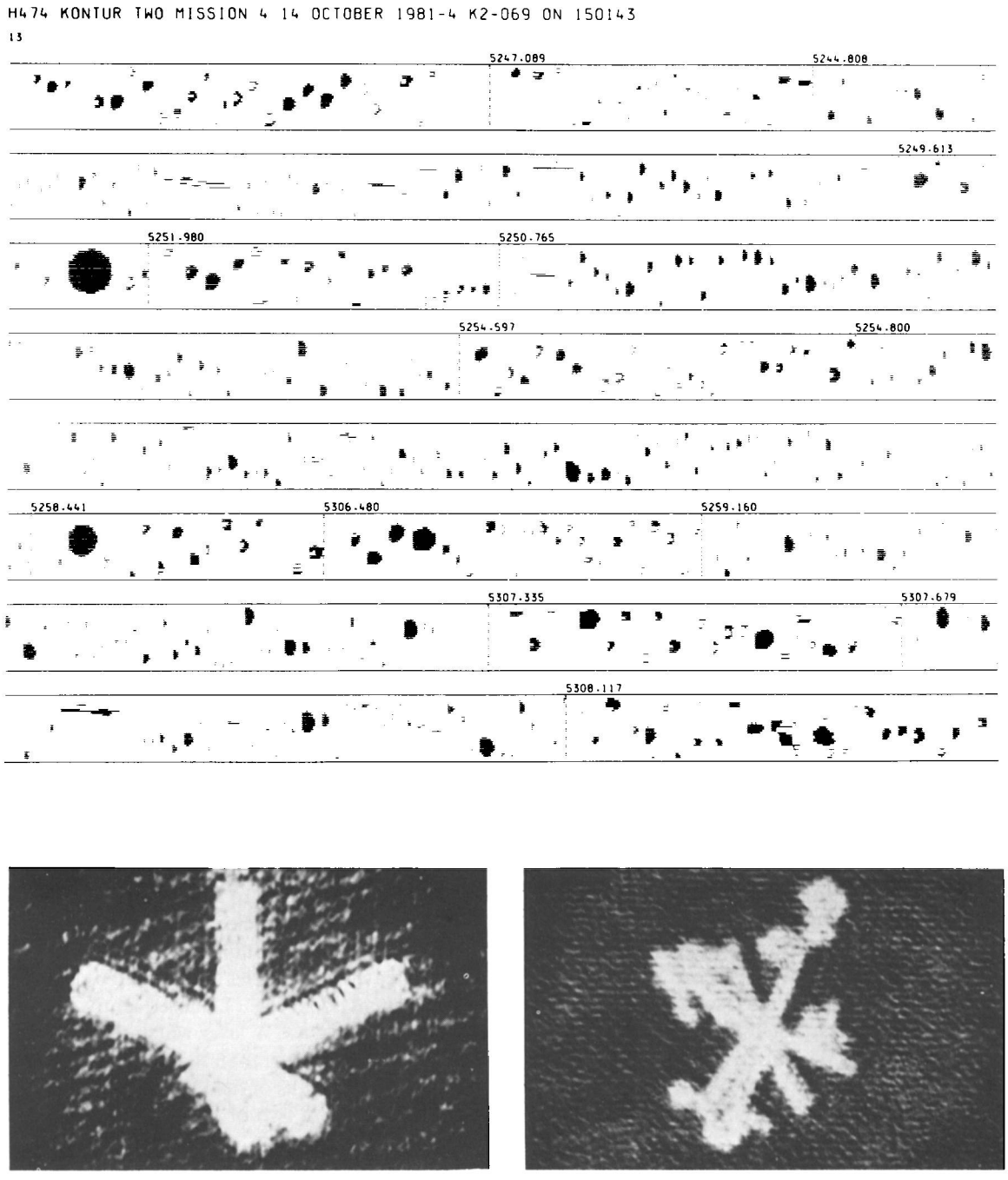

Figure 3. Examples of the output from two of the optical sensors. The top photograph shows reconstructed images of cloud droplets from one of the two-dimensional Knollenberg probes. The bottom two photographs show ice crystal images derived from the holographic equipment.

Table III. *Chemical sampling*

Observable	Device	Remarks
(a) Gases		
Sulphur compounds	Flame photometric analyses	Based on sulphur dimer emission in hydrogen flame
Nitrogen compounds	Chemiluminescent detector	Based on NO/O_3 chemiluminescent reaction: other nitrogen compounds converted to NO
Ozone	Chemiluminescent detector	Based on O_3/C_2H_4 chemiluminescent reaction
Tracers	Electron captive detector	Based on hydrogenations of tracer: two used are SF_6 and C_7F_{14}
General	(a) Gas chromatograph	Three-channel device capable of detecting freons (F-11, F-12), CCl_4, CH_3CCl_3, N_2O and CO_2
	(b) Bag samples	Laboratory analysis
(b) Particulate matter	Millipore filters, laboratory analysis	Possible to detect Ca^{++}, Mg^{++}, Na^+, NH_4^+, K^+, Cl^-, NO_3^-, SO_4^{--}
(c) Cloud liquid water	Samples collected in flight, laboratory analysis	pH can be measured in real time

(McKee 1976), while the detection of nitrogen relies on the nitric oxide-ozone chemiluminescence reaction (Stedman *et al.* 1972). The latter is specific to nitric oxide but the other compounds of nitrogen (i.e. nitrogen dioxide, nitric acid and ammonia) can also be detected by converting them to nitric oxide before mixing the sample with ozone. For all but nitrogen dioxide this is achieved by passing the sample through a steel tube at a temperature lying between 600°C and 800°C. Nitrogen dioxide is reduced to nitric oxide with the aid of a molybdenum catalyst (Winer *et al.* 1974). The detection of sulphur depends on the emission from sulphur dimers when the sample is burnt in a hydrogen flame (Tanner *et al.* 1980). Any sulphur compound (including aerosol sulphuric acid and ammonium sulphate) which is converted to the dimer in the flame is detected — solid matter being removed by filtering (optional) prior to analysis. In all cases (see Table III) commercial instruments are used, modified so that the pressure and temperature of the intake gas can be monitored.

There are in addition to the chemical detectors described above a three-channel gas chromatograph and a tracer detector on board the aircraft. The former can measure a selection of (or all) the following atmospheric trace gases — fluorotrichloromethane (F-11), difluorodichloromethane (F-12), carbon tetrachloride (CCl_4), methyl chloroform (CH_3CCl_3), nitrous oxide (N_2O) and carbon dioxide (CO_2), depending on the choice of column materials and operating conditions (Bamber *et al.* 1984). The tracer detector is a two-channel electron capture device developed specifically to measure concentrations of sulphur hexafluoride and perfluoromethyl-cyclohexane (Blackburn and Dear 1984) which are used to 'label' parcels of air for long-range (i.e. hundreds of kilometres) tracking.

These facilities are backed by a bag sampling facility which enables 'Sarron' bags to be filled with air samples for subsequent analysis in the laboratory. Somewhat more sophisticated are the stainless steel bottles which are also available to take air samples. These have been used to validate the real-time gas chromatograph data and to measure hydrocarbons (Bamber *et al.* 1984). The millipore filters (see above) can be used to collect samples of solid particulate matter. Among the ions that can be measured are:

$$Ca^{++},\ Mg^{++},\ Na^+,\ NH_4^+,\ K^+,\ Cl^-,\ NO_3^-\ \text{and}\ SO_4^{--}.$$

Cloud-water samples may also be taken either in sample bottles for subsequent analysis or else through pipes installed in the aircraft to a pH meter which indicates the sample's acidity in real time. Larger droplets (including actual precipitation) are collected at a bend in the air sampling tube; smaller droplets (i.e. $r<10\mu m$) remaining in the airstream are swirled to the edges of the tube by a fan where they collect in small channels (Walters *et al.* 1983).

6. Dropsonde facility

The Hercules is equipped to release and record data from dropsondes which measure temperature (thermistor), humidity (carbon hygristor) and pressure (solid-state capacitor) during their descent. The dropsondes are ejected from the rear of the aircraft and fall at about 12 m s^{-1} on a parachute designed to follow horizontal airflow. A typical descent takes about 15 minutes. Information from the sonde is relayed back to the aircraft via a UHF radio link. Included in this data stream are Loran C signals (Meredith 1983) detected by the sonde. These give the sonde's position as a function of time, enabling wind profiles to be derived which, averaged vertically over depths of 600 m or so, are accurate to better than 0.4 m s^{-1}. Temperature is measured to within ±0.5 °C, relative humidity to ±5% (over the range 30% to 95%) and pressure to ±0.2 mb. Further details may be found in Ryder *et al.* (1983).

7. Radiometers (Table IV)

Upward and downward facing broad-band radiometers enable fluxes of short-wave (i.e. solar) and long-wave (i.e. terrestrial) radiation to be measured (see Fig. 1). The pyranometers cover the spectral range 0.3 μm to 3 μm while the pyrgeometers cover the range 4 μm to 50 μm. Both types use blackened junctions of thermopiles to detect the radiation. However, in the pyranometer these are covered by two concentric glass domes, while for the pyrgeometer a single-coated silicon dome suffices. Various corrections have to be applied to the instruments to allow for aircraft attitude and ambient conditions. The pyrgeometer in particular is very difficult to operate successfully, the corrections proving quite complex (Albrecht and Cox 1977).

In addition to these broad-band, wide-angle (viz. ±90° subject to cosine response) radiometers, there is also a narrow angle (≈2°) downward-facing long-wave radiometer covering the range from 8 μm to 14 μm. This is intended to measure sea surface temperature. It is calibrated in flight by placing a black body of known temperature in its field of view — this is not practicable with the broad-band, wide-angle radiometers as they are mounted on the outside of the aircraft. To derive sea surface temperature further corrections are required to account for absorption and emission between the aircraft and the surface and the emissivity of the surface (see Nicholls 1978).

Apart from these radiometers there is a multi-channel radiometer mounted in one of the instrumented pods. This is a 16-channel device (i.e. 4 detectors each monitoring 4 separate channels) capable of recording 4 channels simultaneously with a field of view of only 1½°. A mirror provides a scanning capability so that the radiometers can view vertically upwards (i.e. zenith) or between nadir and nadir minus 60°. Triglycine sulphate (TGS) and lead sulphide detectors are used to detect the radiation so

Table IV. *Radiometers*

Device	Nature	Spectral coverage *micrometres*	Remarks
Pyranometer	Broad-band, wide angle, short-wave radiation	0.3–3	Spectral range dependent on choice of domes. Upward and downward facing
Pyrgeometer	Broad-band, wide angle, long-wave radiation	4.0–50	Upward and downward facing
Radiation thermometer	Long-wave, narrow angle (≈2°)	8–14	Downward facing, intended to measure sea surface temperature
Multi-channel	Narrow angle (≈1½°), narrow band, 16 channels (4 × 4)	Narrow band 1–50	Spectral range depends on choice of detectors. Covers zenith and nadir to nadir — 60°

channels can be established in both the infra-red (i.e. 8 μm to 50 μm) and the near infra-red (i.e. 1 μm to 3 μm) regions of the electromagnetic spectrum respectively. The radiometer can be used with very narrow-band filters (viz. $\approx$0.02 μm in the near infra-red). It started life as the prototype of an instrument flown on a Nimbus satellite and has recently been extensively modified after earlier use on the Canberra aircraft of the Meteorological Research Flight (Coffey 1977). In-flight calibration is provided by two black bodies and a solar diffuser.

8. Other facilities including data recording

As well as the instruments described above, the aircraft carries both forward and downward facing cameras. These can take pictures automatically at regular intervals; in fact the forward camera has a cine capability. Information provided by these two devices is supplemented by the use of hand-held cameras and three video cameras, two of which face forwards and one backwards.

A 3 cm weather radar is housed in the pod situated above the flight deck (Fig. 1). This has a forward field of view (i.e. $\pm$90°) and can scan at elevations within $\pm$15°. It has three display ranges (viz. 0–45 km, 0–90 km and 0–280 km) and a rainfall detection threshold of 1 mm h^{-1}. The radar can be programmed to execute a sequence of measurements at different ranges and elevations for later analysis of photographs of the display.

Information from the various instruments is normally recorded in flight on magnetic tape which is later transcribed to a computer-compatible format. Data acquisition is controlled by a Motorola 6809 microprocessor and is capable of handling 33 000 bits of information per second (up to 128 channels, both analogue and digital data). Operators monitor progress via a keyboard and a visual display unit. There is an 'event mark' facility with input buttons sited at locations distributed all over the aircraft. The system is linked to a real-time display unit which enables scientists to carry out preliminary analyses as well as monitoring progress during the flight.

9. Concluding remarks

On an experimental aircraft such as the Hercules, the instrumental fittings are continually evolving. This is, of course, to be expected as new techniques are continually being developed and existing ones improved, making it possible to extend the aircraft's basic capability and to maintain it by replacing items that are worn out or difficult to maintain. Ideally these should all be standard items as these are generally easier to acquire and maintain, but this is not always possible. Other possibilities are: building instruments to designs obtained from other scientists; using equipment supplied by collaborators; or designing, developing and manufacturing in-house. The last is the least attractive as it carries a high element of risk and makes extensive use of scarce resources. Examples of all three types of installation can be found on the Hercules. Of course, what has been presented here represents the current situation. New installations are always in the pipeline and amongst those already well advanced are a new inertial navigation system, a radiometer for measuring temperatures within clouds and a new device for measuring total water content based on the Lyman-alpha hygrometer (Buck 1976).

The particular aircraft considered here, although probably the most extensively equipped for atmospheric research, is not unique and there are similar facilities elsewhere though not many approach the scale of the Hercules. Thus the Natural Environment Research Council has recently acquired a small Cessna aircraft primarily for remote sensing of the surface. However, there are extensive facilities for atmospheric research based on aircraft in several countries including West Germany (e.g. DFVLR, Institut für Physik der Atmosphäre, Oberpfaffenhofen) and the USA (e.g. the National Center for

Atmospheric Research, Boulder, Colorado and the National Oceanic and Atmospheric Administration, Washington D.C.). Some facilities have more than one aircraft available so, although each individually may have a more limited capability than the Hercules, the total capability will be the same or greater. Aircraft are very adaptable, being quite capable of carrying a whole series of different instruments, only a sample of which have been referred to here (the descriptions have, of necessity, had to be brief and are intended to be supplemented by the references). The areas of possible interest are also vast so it is only possible in an article of this nature to give a general indication of the potential of such a facility.

The reader should also bear in mind the man–machine mix. Aircraft are useless unless they are in the right place at the right time. This is very dependent on the skills of the aircrew who operate the aircraft and the scientists who direct its use, often with inadequate information. It takes years of experience to develop the skills necessary to make optimum use of an aircraft by learning, for example, how to interpret instruments such as radars or to recognize what is worth studying and what is not — the eyes of the scientist coupled with his ability to communicate are of crucial importance yet it is all too easy to gloss over this aspect. The photograph of the aviator in Sprigg's (1939) article makes the point better than any text.

Acknowledgements

I wish to express my gratitude to colleagues, both scientists and aircrew, who have provided information and advice during the preparation of this paper.

References

Albrecht, B. and Cox, S. K. 1977 Procedures for improving pyrgeometer performance. *J Appl Meteorol*, **16**, 188–197.

Axford, D. N. 1968 On the accuracy of wind measurements using an inertial platform in an aircraft, and an example of the measurement of the vertical mesostructure of the atmosphere. *J Appl Meteorol*, **7**, 645–666.

Bamber, D. J., Healey, P. G. W., Jones, B. M. R., Penkett, S. A., Tuck, A. F. and Vaughan, G. 1984 Vertical profiles of tropospheric gases: Chemical consequences of stratospheric intrusions. *Atmos Environ*, **18**, 1759–1766.

Blackburn, A. J. and Dear, D. J. A. (1984) A design for an airborne sulphur hexafluoride tracer detector. (Submitted to *Atmos Environ.*)

Broxmeyer, C. 1964 Inertial navigation systems. New York, McGraw-Hill Book Co.

Buck, A. L. 1976 The variable-path Lyman-alpha hygrometer and its operating characteristics. *Bull Am Meteorol Soc*, **57**, 1113–1118.

Cluley, A. P. and Oliver, M. J. 1978 Aircraft measurements of humidity in the low stratosphere over southern England. *Q J R Meteorol Soc*, **104**, 511–526.

Coffey, M. T. 1977 Water vapour absorption in the 10–12μm atmospheric window. *Q J R Meteorol Soc*, **103**, 685–692.

Conway, B. J., Caughey, S. J., Bentley, A. N. and Turton, J. D. 1982 Ground-based and airborne holography of ice and water clouds. *Atmos Environ*, **16**, 1193–1207.

Hess, S. L. 1959 Introduction to theoretical meteorology. New York, Henry Holt and Company.

Johnson, D. A. and Atkins, D. H. F. 1975 An airborne system for the sampling and analysis of sulfur dioxide and atmospheric aerosols. *Atmos Environ*, **9**, 825–829.

Knollenberg, R. G. 1976 Three new instruments for cloud physics measurements: the 2-D spectrometer, the forward scattering spectrometer probe and the active scattering aerosol spectrometer. Boston, Massachusetts, American Meteorological Society. International Cloud Physics Conference, July 26–30, 1976, Boulder, Colorado, USA, 554–561.

Lala, G. G. and Jiusto, J. E. 1977 An automatic light scattering CCN counter. *J Appl Meteorol*, **16**, 413–418.

McCarthy, J. 1973 A method for correcting airborne temperature data for sensor response time. *J Appl Meteorol*, **12**, 211–214.

McGavin, R. E. and Vetter, M. J. 1965 Radio refractometry and its potential for humidity studies. *In* Wexler, A. (ed.). Humidity and moisture. Measurement and control in science and industry. Based on papers presented at the 1963 International Symposium on Humidity and Moisture, Washington, D.C. Vol. 2, Applications (ed. Amdur, E. J.). New York, Reinhold Publishing Corporation, 553–560.

McKee, H. C. 1976 Collaborative testing of methods to measure air pollutants. III, Chemiluminescent method for ozone: determination of precision. *J Air Pollut Control Assoc*, **26**, 124–135.

Mason, B. J. 1962 Clouds, rain and rainmaking. Cambridge, Cambridge University Press.

Meredith, J. S. 1983 Global navigation systems (special issue). *Proc Inst Electr Electron Eng*, **71**, 1123–1227.

Nicholls, S. 1978 Measurements of turbulence by an instrumented aircraft in a convective atmospheric boundary layer over the sea. *Q J R Meteorol Soc*, **104**, 653–676.

Nicholls, S., Brummer, B., Fielder, F., Grant, A., Hauf, T., Jenkins, G., Readings, C. and Shaw, W. 1983 The structure of the turbulent atmospheric boundary layer. *Philos Trans R Soc*, A, **308**, 291–309.

Nolan, P. J. and Pollak, L. W. 1946 The calibration of a photo-electric nucleus counter. *Proc R Ir Acad*, **51A**, 9–31.

Ruby, M. G. and Waggoner, A. P. 1981 Intercomparison of integrating nephelometer measurements. Washington, American Chemical Society, *Environ Sci Technol*, **15**, 109–113.

Ryder, P. 1976 The measurement of cloud droplet spectra. Boston, Massachusetts, American Meteorological Society. International Cloud Physics Conference, July 26–30, 1976, Boulder, Colorado, USA, 576–580.

Ryder, P., Lewis, A. F. and Bennetts, D. A. 1983 The NAVAID dropsonde. *Meteorol Mag*, **112**, 367–380.

Sprigg, T. S. 1939 The flying weather-man, *Flying*, **3**, 7–8, 16–17.

Stedman, D. H., Daby, E. E., Stuhl, F. and Niki, H. 1972 Analysis of ozone and nitric oxide by a chemiluminescent method in laboratory and atmospheric studies of photochemical smog. *J Air Pollut Control Assoc*, **22**, 260–263.

Strapp, J. W. and Schemenauer, R. S. 1982 Calibrations of Johnson–Williams liquid water content meters in a high-speed icing tunnel. *J Appl Meteorol*, **21**, 98–108.

Tanner, R. L., D'Ottavio, T., Garber, R. and Newman, L. 1980 Determination of ambient aerosol sulfur using a continuous flame photometric detection system. I. Sampling system for aerosol sulfate and sulfuric acid. *Atmos Environ*, **14**, 121–127.

Walters, P. T., Moore, M. J. and Webb, A. H. 1983 A separator for obtaining samples of cloud water in aircraft. *Atmos Environ*, **17**, 1083–1091.

Winer, A. M., Peters, J. W., Smith, J. P. and Pitts, J. N. 1974 Response of commercial chemiluminescent NO_x analysers to other nitrogen compounds. *Environ Sci Tech*, **8**, 1118.

551.509.314:551.509.322:624.21/.8

Techniques for forecasting the occurrence of strong winds over the Severn Bridge

By K. C. Wright

(Meteorological Office, Bracknell)

Summary

In an attempt to find useful predictors of the occurrence of strong winds over the Severn Bridge, 503 gusts of 30 kn or more over a 10-year period were analysed. As a result it is suggested that, during periods of cyclonicity, the mean of estimates of the gradient wind and the 900 mb wind provides a better approximation to the actual wind than the gradient wind alone. Furthermore, where adjacent high ground causes severe distortion to the air flow, the lee-wave parameters may be combined to provide an additional predictor.

1. Introduction

The project was started as a result of the introduction (at the meteorological office at Upavon in Wiltshire) of a requirement to issue warnings to the motorway police at Almondsbury whenever frequent gusts of 30 kn or more were expected over the Severn Bridge.

The bridge is situated about 17 km north-north-west of Bristol and is a little over 60 m above the River Severn. The south-west to north-east alignment of the estuary and the distribution of the high ground within 70 km of the bridge leads to four sectors with different topographical features predominating (see Fig. 1). These are:

(1) *North-east.* This contains, on either side of the river, the Cotswold Hills and the Malvern Hills, much of which are above 200 m.

(2) *South-east.* Nearly all this sector is between 100 and 200 m above mean sea level and consists of the south Cotswold Hills, the north-west edge of Salisbury Plain and most of the Mendip Hills.

(3) *South-west.* This is mostly either the river estuary or the adjacent low-lying land.

(4) *North-west.* Much of this sector, which includes the Black Mountains and the Brecon Beacons, is above 400 m.

2. Methodology

2.1 *The data*

The wind speed over the bridge was recorded on a Meteorological Office Mark IV electrical anemograph. The cup sensors are situated on the bridge between the toll booths and the first main tower and are fixed to a post some 4 m above the roadway — a far from ideal exposure! Furthermore, the recording system is sited some 7 km to the south-east at Almondsbury police station. These units are connected by telephone cables whose resistive and capacitive properties are unknown. It is estimated by the Meteorological Office Maintenance Organization that the system may have produced anomalous results, perhaps leading to a reduction of up to 10% in the recorded speed.

Gust data were obtained from anemographs from the period 1973–82 inclusive, but excluding 1980, for which data were not available.

2.2 *The analysis*

The effective predictors of measured gusts from a site near the surface are expected to be those which reflect the large-scale dynamical and thermal structures. Approximations are therefore required to the

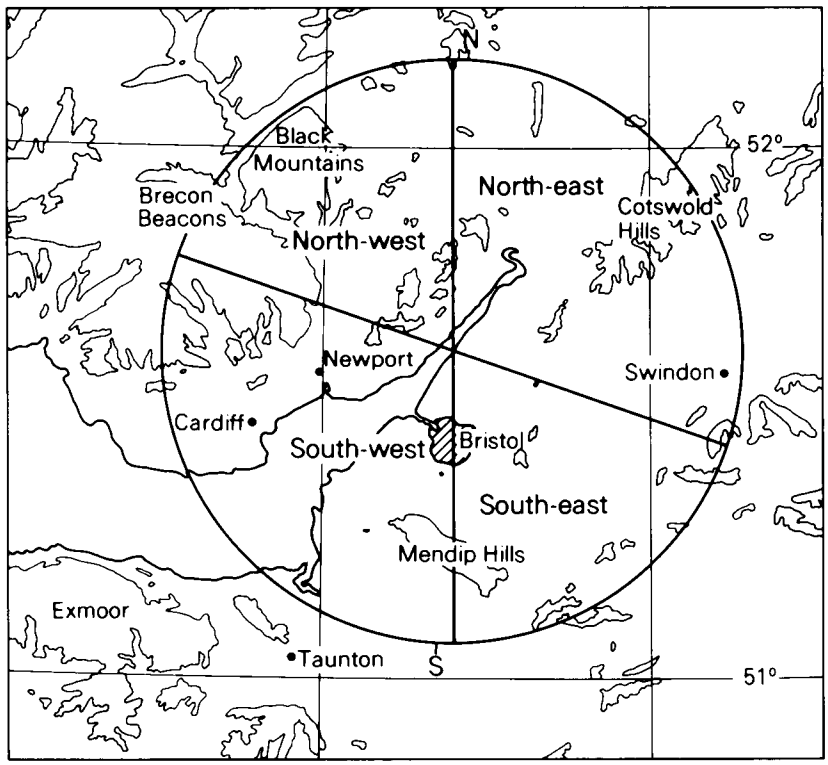

Figure 1. Map of high ground (over 200 m) within 70 km of the Severn Bridge showing sectors used in meteorological analysis.

actual winds and to the low-level temperature lapse rate. In addition, account must be taken of the effects of local topography. The basic method is to stratify the gust data with respect to these variables.

The usual approximation to the actual wind, the gradient wind, was estimated from UK synoptic charts (scale 1:10^6) to the nearest 5 kn, by applying corrections to the isobaric gradient for curvature of the isobars and any isallobaric effect. In view of the requirement for forecasting frequent gusts of over 30 kn, only those occasions when the gradient wind was 35 kn or more were noted so that gusts caused primarily by shower activity were ignored.

The effects of topography were isolated by classifying the gusts into 5° subsets according to the direction of the 900 mb ($\approx$900 m) flow, D_{900}. To this end, interpolations were made for space and time from the six-hourly upper-wind reports (usually Camborne, Crawley and Aughton as, fortuitously, the Severn Bridge lies close to the centroid of the triangle with its vertices at these locations).

Similarly, a representative radiosonde ascent (or the median of several ascents) was used to provide a measure of the low-level instability.

The data were analysed using the forward step-wise linear regression computer program of the biomedical statistical package (University of California 1984) with the objective of reducing the standard error of the residuals, SER, (i.e. actual gust minus expected gust) from the predicting equations to less than 5 kn.

The initial choice of predictors was:

(a) *The low-level temperature lapse over 50 mb (ΔT).* The temperature lapse was calculated by using the difference between the temperature at 50 mb ($\approx$450 m) above the surface from the representative

ascent(s) and the surface temperature recorded at Bristol (i.e. Filton until 1978, then the Weather Centre). This parameter proved more effective, however, if the range was truncated to 1.5–4.5°C inclusive, as neither superadiabatic nor very stable conditions were expected to prevail during strong winds, especially high above a river estuary.

(b) *The gradient wind* (G_r). Analysis of the south-westerly data highlighted the inadequacy of a simple gradient wind approximation as a predictor, particularly in cases of strong cyclonic flow. A comparison of these events with respect to the estimated 900 m wind (U_{900}) showed that, if the gradient wind was greater than U_{900} by 10 kn or more and there was no anticyclonic curvature, then the standard error of the residuals (SER) was much greater at 4.9 kn than at the 3.1 kn for the other occasions.

In order to reduce the SER for the former cases, the curvature rule shown in Table I was adopted to provide a more effective estimate of the actual wind, G_a.

This refinement reduced the SER for cyclonic or straight isobars to 3.7 kn. A plot of all the gust data with respect to G_a and ΔT showed that there was some divergence as G_a increased in value. This effect was negated for the linear regression program by adopting the transform:

$$\Delta T_t = \Delta T \{ 0.5 + (G_a - 15)/40 \}.$$

There also appeared to be some slight curvilinearity as G_a increased, causing the expected gust (E) to be greater than G_a when G_a is less than 40 kn. This effect was corrected by the adoption of:

$$G_t = nG_a + (1 - n)U_{900},$$

where $n = 0.56 - 0.0025\,G_a$. For practical purposes, however, the latter transform may be ignored with no significant loss of accuracy below about 100 kn.

3. Results

As the gusts were grouped into 5° subsets according to D_{900} it was possible to optimize the limits of each of the different geographical sectors. These are shown in Table II.

3.1 *Region 1: south-west and north-east sectors (293 gusts)*

The linear regression program produced the following equation for expected gusts (E):

$$E = 0.63G_a + 2.6\,\Delta T_t \{ 0.5 + (G_a - 15)/40 \} + 1.2,$$

generating the nomogram shown in Fig. 2. This has validity only for values of G_a of 35 kn or more.

The gusts for this sector were regrouped according to the type of terrain within 70 km of the bridge, but the only significant differences occur at high values of G_a; see Table III.

Hence for practical purposes it is sufficient, when $G_a > 70$ kn, to add 4 kn if D_{900} is 210–260° and subtract 4 kn if D_{900} is 180–200° or 270–280°.

3.2 *Region 2: north-west sector (126 gusts)*

The previous methodology used to provide an estimate of the actual wind (i.e. G_a) proved inadequate for this sector owing to the severe distortion to the flow caused by the Welsh mountains. A more

Table I. *Adjustment to the gradient wind, G_r (if $G_r - U_{900} \geqslant 10$ kn) to provide a closer approximation to the actual wind, G_a*

Curvature	Gradient wind, G_r *knots*	Adjustment
Anticyclonic	All	$G_a = G_r$
Cyclonic	>40	$G_a = (G_r + U_{900})/2$
'Straight'	<65	$G_a = G_r - 5$
'Straight'	≥65	$G_a = G_r - 10$

'Straight' isobars have a radius of curvature of more than 1200 nautical miles.

Table II. *Specification of geographical sectors*

Region	Sector	900 mb wind direction, D_{900} *degrees*
1	South-west	180–285
	North-east	360–105
2	North-west	290–355
3	South-east	110–175

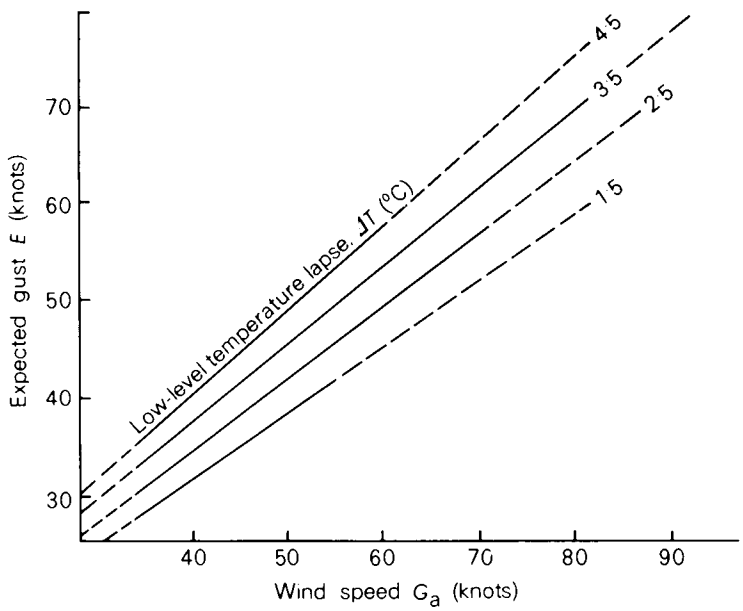

Figure 2. Nomograms for obtaining the maximum gust over the Severn Bridge if the 900 mb wind direction is south-west (180–285°) or north-east (360–105°), where ΔT_l(°C) is the temperature lapse through the lowest 50 mb. The lines are drawn from the equation:

$$E = 0.63G_a + 2.6 \times \Delta T_l \{0.5 + (G_a - 15)/40\} + 1.2.$$

Pecked lines indicate extrapolated data.

Table III. *Variation in expected gust, E (knots) with respect to terrain traversed*

900 mb wind direction, D_{900} *degrees*	Type of terrain	Number of gusts	Standard error of residuals	Expected gust if $\Delta T = 4\frac{1}{2}$ °C $G_a = 40$	$G_a = 80$
210–260	Sea track or little high ground	165	3.4	40	79
360–095	Land track, but little high ground perpendicular to wind flow	48	3.4	39	75
180–200 and 270–285	Land track with significant high ground	80	3.0	39	71
All	—	293	3.3	39	75

objective methodology was adopted in order to minimize the standard error of the residuals. After some experimentation the following algorithm was adopted:

Step 1. Estimate G_1 from the surface pressure difference between Plymouth (Mount Batten) and Birmingham (Elmdon) with corrections for curvature and variation in D_{900}.

Step 2. Estimate G_2 by correcting G_1 for the isallobaric gradient (using the pressure tendencies at Aberporth and Boscombe Down), but only if the isobaric curvature is cyclonic.

Step 3. Let north-west wind be $G_{nw} = (G_2 + U_{900})/2$.

These changes reduced the standard error of the residuals to the values shown in Table IV.

Table IV. *Reduction of the standard error of the residuals (SER) in the calculation of the actual wind for the north-west sector,* G_{nw}

Approximation to actual wind	G_a	G_1	G_2	G_{nw}
SER	7.9	6.7	6.6	5.7

In an attempt to understand the role of atmospheric stability, the residuals (from the results of the linear regression analysis), actual gust minus expected gust, were plotted against the lee-wave parameters of wavelength (λ) and vertical velocity (C_1). These were calculated using Casswell's technique (Casswell 1966). Isotachs were drawn at 5 kn intervals and optimized so that the mean of each group of residuals was as close as possible to its coefficient (see Fig. 3). The introduction of this coefficient, a linear lee-wave index (L), further reduced the SER from 5.7 to 4.0 kn and resulted in the following equation for predicting gusts in north-westerly flow:

$$E = 0.77 G_{nw} + 2.4 \Delta T + 1.0 L - 7.2$$

and the nomograms shown in Fig. 3 were constructed. The technique, therefore, for winds in this sector is to obtain a first estimate of the expected gust using Fig. 3(a) and then apply the lee-wave correction, if any, obtained from Fig. 3(b). It should be noted, however, that the value of L will change along with changes in stability in the lower troposphere, typically by 5 kn every 6 hours. Minimum values (i.e. $\leqslant -10$ kn) occur at about 100 nautical miles behind a cold front as opposed to about 280 nautical miles for maximum values (i.e. $\geqslant 5$ kn). Although this procedure reduced the SER, the variation within each subset of L could still be large.

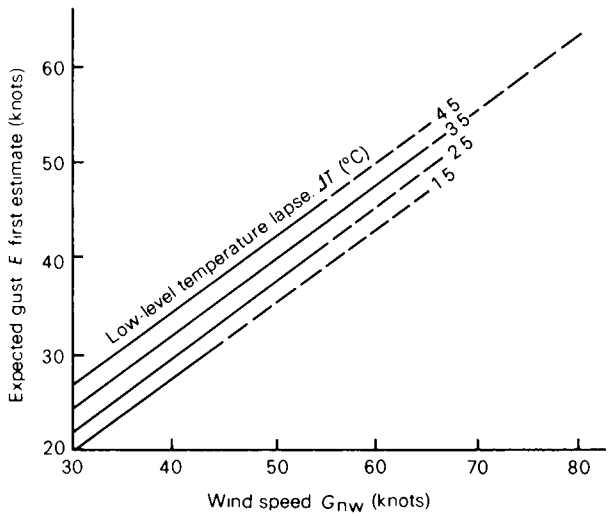

Figure 3(a). Nomograms for obtaining the maximum gust over the Severn Bridge if the 900 mb wind direction is north-west (290–355°), before adding the lee-wave correction, L (see Fig. 3(b)). ΔT(°C) is the temperature lapse through the lowest 50 mb. The lines are drawn from the equation: $E = 0.77G_{nw} + 2.4 \times \Delta T - 7.2$. Pecked lines indicate extrapolated data.

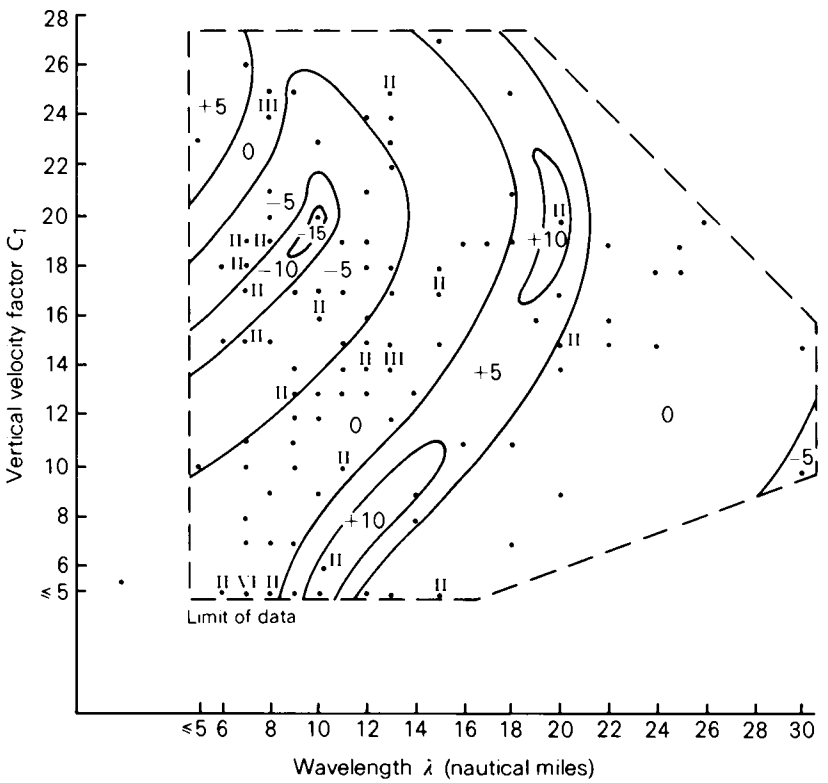

Figure 3(b). Nomogram for obtaining values of the lee-wave correction, L. Each point represents a gust. Roman numerals indicate the number of gusts with the same values of λ and C_1. Values of λ and C_1 are obtained from a representative ascent using the technique devised by Casswell (1966).

The synoptic situations were also checked when the gradient wind was below 30 kn, but the lee-wave effect disappeared completely when G_{nw} was less than 29 kn.

In view of the effectiveness of the above index, the lee-wave parameters were calculated for the other sectors. There was, however, no discernible pattern when they were similarly plotted against the residuals, nor any significant correlation in the linear regression.

3.3 *Region 3: south-east sector (84 gusts)*

Although there is very little ground above 200 m to the south-east, it apparently has the effect of reducing the gusts by at least 15–25 kn compared with similar conditions and terrain in the south-west sector. Furthermore, no dependence on any low-level temperature lapse was detected. Although the quantity of gust data is relatively small, there is some justification for subdividing the sector, for, as is shown in Table V (and the nomogram in Fig. 4), there is a significant variation within the sector.

Table V. *Subdivision of south-east sector*

D_{900}	Number of gusts	SER	Formula for the expected gust, E, if $G_r = 50$	
degrees				
110–115	21	2.9	$E = 0.76G_r - 5.3$	33
120–175	63	3.2	$E = 0.57G_r - 3.5$	25
All	84	4.1	$E = 0.77G_r - 10.4$	28

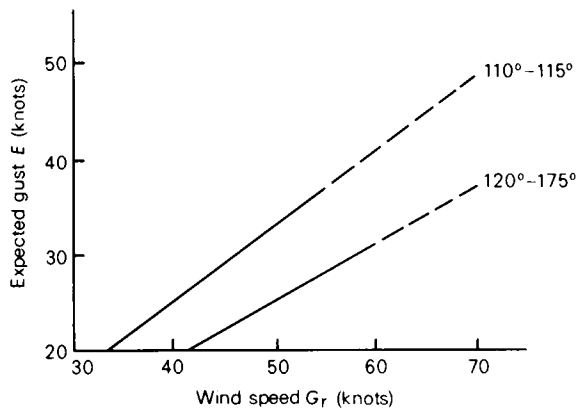

Figure 4. Nomogram for obtaining the maximum gust over the Severn Bridge if the 900 mb wind direction is south-east (110–175°). Lines are drawn from the equations:

$$E = 0.76G_r - 5.3 \text{ for } 110–115°$$
$$\text{and } E = 0.57G_r - 3.5 \text{ for } 120–175°.$$

Pecked lines indicate extrapolated data.

Table VI. *Wind gradient required for an expected gust of 43 kn and* ΔT *or* $\Delta T_t = 3.0°C$

Direction	Lee-wave index, L	Wind *knots*
North-west	10	$G_{nw} = 33$
South-west and north-east	—	$G_a = 50$
North-west	-15	$G_{nw} = 58$
South-east (120-175°)	—	$G_r = 82$

4. Conclusions

To illustrate the wide differences between the sectors Table VI shows the actual wind speed required for an expected gust of 43 kn (i.e. gale force), if the low-level temperature lapse is 3.0°C.

Of the current techniques recommended for the forecasting of maximum gusts, it is believed that none use any parameters other than an approximation (usually an estimate of the geostrophic wind or the gradient wind) and a low-level temperature lapse rate. As has been shown by the analysis of the data, the gradient and geostrophic wind approximations are inadequate during cyclonic synoptic situations (at least in locations such as the Severn Bridge, where there is significant high ground within about 50 km). In such situations a mean of estimates of the gradient wind and the 900 mb wind provides a better approximation to the actual wind. Secondly, where the adjacent high ground causes severe distortion to the air flow (as with the north-west sector for the Severn Bridge) a lee-wave index may provide an additional predictor.

Although the preceding analysis is based on data for 503 gusts, the predicting equations should be verified by a set of independent data. It is hoped that gust data currently being gleaned from the anemograph charts for 1982–83 will be used for this purpose.

5. Acknowledgements

The author would like to thank his many colleagues for their help and advice during the period of this project.

References

Casswell, S. A. 1966 A simplified calculation of maximum vertical velocities in mountain lee waves. *Meteorol Mag*, **95**, 68–80.

University of California 1984 Biomedical computer programs, P-series. Los Angeles, University of California, Health Sciences Computing Facility.

Reviews

Remote sounding of atmospheres, by J. T. Houghton, F. W. Taylor and C. D. Rogers. 155 mm × 230 mm, pp. vii + 343, *illus.* Cambridge University Press, 1984. Price £35.00, US $67.50.

In recent years, satellite observations of the earth's atmosphere have formed a vital part of the data used in the routine production of surface and upper-air analyses, especially over the oceans and in the more remote regions of the world. In addition, data derived from satellites have increasingly proved of value as a research tool for the atmospheric physicist investigating the flow at upper levels, or the distribution of chemical species in the atmosphere. The appearance of this book on atmospheric sounding, which covers the whole field from instrument design to data-retrieval techniques, as well as

dealing with the applications of satellite data, will be welcomed by many operational meteorologists and research physicists alike.

The early sections of the book provide a general discussion of the goals of satellite remote sensing, along with a comprehensive review of the many operational and research spacecraft which have been launched to study the earth's atmosphere since Tiros 1 in 1960. Detailed descriptions of many of the visible and infra-red imaging instruments are given, as well as information on the microwave imagers which have been carried on a number of research satellites. The importance of satellite-borne instruments in providing measurements of elements of the earth's radiation budget is covered in Chapter 4 and results from a number of the experiments are presented, including the Earth Radiation Budget (ERB) experiment mounted on Nimbus 6 and 7.

The theory of remote temperature sounding, both tangentially at the atmosphere's limb and via the more conventional nadir view, is dealt with in considerable detail and the computation of instrument-weighting functions is described. Many of the sounding instruments themselves are illustrated and diagrams of their optical systems are provided along with the details of their weighting functions.

The chapter on retrieval theory deals with the derivation of temperature profiles and other meteorologically useful data from the radiances received at the satellite, and provides a very thorough coverage of the subject. In particular, the questions of uniqueness in the solution of the inversion process and the effects of noise are particularly well described.

The problems of interest to many operational meteorologists, such as the best ways to incorporate satellite data into numerical analysis schemes, are dealt with in Chapter 8, and various analysis schemes in use operationally at the moment are described. Further topics of operational interest that are covered are the problems associated with cloud clearing and the impact of satellite data on the quality of forecasts generated by atmospheric models.

Satellite data have also played a large part in extending our knowledge of the composition and dynamics of the upper atmosphere, and results from many of the experiments designed to explore these regions are presented, including the monitoring of stratospheric warmings via the Nimbus 4 Selective Chopper Radiometer (SCR) and the derivation of ozone profiles using data from the Limb Interferometer Monitor of the Stratosphere (LIMS) on Nimbus 7.

The final chapters of the book deal with the remote sounding of the atmospheres of other planets in the solar system and describe how the basic techniques of remote sounding have been adapted to provide us with new information on the composition and general atmospheric circulation of our neighbouring planets.

With such a rapidly developing subject, this book by three well-known workers in satellite observing provides a much-needed reference work which describes the status of many aspects of the subject and gives a large number of references to further literature. It will certainly find a place on the bookshelves of many researchers in the fields of satellite meteorology and the remote sounding of the atmospheres of other planets, with only the price deterring some people from buying their own copy until a paperback edition becomes available.

J. Turner

The climate of Europe: past, present and future, edited by Hermann Flohn and Roberto Fantechi. 165 mm × 245 mm, pp. x + 356, *illus.* D. Reidel Publishing Company, Dordrecht, 1984. Price Dfl 130, US $49.

The title of this book has a very familiar ring to it and is a little misleading inasmuch as a description of the present climate of Europe is not one of its main aims. The subtitle — Natural and man-induced climatic changes: a European perspective — is a more accurate description of its contents. It was

initiated by the Commission of the European Communities to accompany the European Climatology Research Programme and is a collaborative effort, being based on the contributions of eight specialists.

The book opens with a General Summary which is backed up by further summaries at the end of each chapter. These latter are of variable length and detail, however, and the busy reader is recommended to concentrate on the General Summary, which provides an excellent appraisal of the subject. After a brief introductory chapter, the main narrative begins with a description by Lamb of the changes which have taken place in European climate over the past thousand years. This is followed by a more detailed account by Schuurmans and Flohn of the instrumentally detected changes in the last hundred years or so. Chapter 4 is in many respects the core of the book and discusses Man's impact on climate (Berger). It properly concentrates on the effects of carbon dioxide and is accompanied by a description of the carbon cycle (Duplessy). Chapter 5 (Flohn, Dansgaard) examines some climates from the recent geological past for any clues they may provide to the future behaviour of the climatic system. The section concludes with an examination of the consequences of a glaciated Antarctic continent being accompanied by an ice-free Arctic Ocean. The final chapter (Bourke, Rosini) considers the impact of climatic changes on European agriculture.

Somewhat surprisingly, the weakest part of the book lies in its incomplete account of the physical basis of climate and climatic change. Most of the physical explanations are offered in Chapter 4, but they are all very brief. The account of the greenhouse effect is poor and the role of the oceans is not fully discussed. In the General Summary, for instance, two vulnerable aspects of the climatic system are identified — the extent of polar sea ice and coastal and equatorial upwelling. The possible importance of the latter is emphasized in the discussion of the consequences of one pole being glaciated while the other is ice free. Yet nowhere in the book is there a discussion of the importance of marine life for atmospheric CO_2 levels, or of the Southern Oscillation and El Niño. This contrasts with the very full coverage given to the polar ice, although even here some space could have been devoted to plans for the diversion of Soviet rivers (they are briefly mentioned under the effects of changes in land use). Reasonably enough, minority views are not represented and sunspots are dismissed in a single paragraph in Chapter 1. The uncertainty over the role of volcanic dust, however, is not mentioned; it is presumed to cause surface cooling, and in Chapter 5 is held to be largely responsible for the 'Little Ice Age'.

The discussion of recent climatic changes in Chapter 3 is too long. There is too much presentation of raw data and the reader is showered with statistics and references. It might have been better to have extended Lamb's account of the last thousand years and to have used the extra space for a chapter on the physical basis of climate and climatic change (the present introductory chapter is too short to accomplish this).

There is a fair sprinkling of typographical errors and some of the diagrams lack clarity. There is a good index and many references, although those to papers in journals do not contain the titles of the works.

Despite these criticisms, the book has much to commend it. The main shortcomings mentioned above can probably be ascribed to insufficient collaboration arising out of its combined authorship. Yet it would have been impossible for a single person to have written this book and it is clear that a large amount of editorial and collaborative effort has gone into the work. This has seen its reward in a volume with a well-conceived plan and an impressive unity of style. Each chapter stands on its own and there are extensive cross-references. The scope of the book is especially good. Despite the many publications in this field, it does occupy a niche which is not covered by others, although inevitably it overlaps with many. The General Summary and Chapters 2 and 5 are all excellent and could hardly be improved upon. The volume can certainly be recommended as a readable and well-balanced introduction to the subject of climatic change, even if the reader will need to look elsewhere for further accounts of the greenhouse effect and the roles of the oceans and volcanic dust.

R. C. Tabony

Books received

The listing of books under this heading does not preclude a review in the Meteorological Magazine at a later date.

Atmospheric electrodynamics, by Hans Volland (Berlin, Heidelberg, New York, Tokyo, Springer-Verlag, 1984. DM98, US$35.70) brings together two subjects usually treated separately: low-frequency electromagnetic fields of lower atmospheric origin and those of upper atmospheric origin. The first, known as geoelectricity, deals with thunderstorm phenomena and related problems such as the global electric circuit, lightning and atmospherics. The second subject is associated with ionospheric and magnetospheric electric fields and currents: dynamo currents, Birkeland currents geomagnetic pulsations and the like. Originally considered as part of geomagnetism, this is now a subfield of magnetospheric physics. The book stresses the interconnection between the two and presents to workers in different fields (meteorology, aeronomy, space physics) a unifying view of today's knowledge of lower and upper atmospheric electromagnetic fields and currents at low frequencies (periods larger than 10^{-5} s).

Prophet – or professor? The life and work of Lewis Fry Richardson, by Oliver M. Ashford (Bristol and Boston, Adam Hilger Ltd, 1984. £18.00, US $29.00) is the first full-length biography of Lewis Fry Richardson to be published and contains much material not previously available to the public. It is a timely reappraisal of his life and work, and one that will reach a wide audience. Throughout, no prior familiarity with Richardson's work is assumed, and the more technical aspects of his ideas are kept to a minimum. Nevertheless, for those stimulated by Richardson's ideas, there are extensive references to his published work, as well as to archival material concerning other aspects of his life.

Engineering hydrology (3rd edition) by E. M. Wilson (London and Basingstoke, Macmillan Press Ltd, 1983. £16.00, £7.95 (paperback)) is a new, thoroughly revised and completely reset edition. Some of the findings of the Flood Studies Report (FSR) carried out by the Institute of Hydrology in 1975 have been incorporated. The opportunity has also been taken to expand the sections on flow duration curves and the rainfall data of the British Isles, through use of the Meteorological Office's contribution to the FSR. Finally, the references have been updated and the selection of problems widened.

Honour

We are pleased to record that Mr H. D. Chillingworth, the rainfall observer at Bradwell-on-Sea, Essex was awarded the British Empire Medal in the New Year's Honours List. Mr Chillingworth began making daily observations in 1926, following on from his father whose first observations were made in 1883.

THE METEOROLOGICAL MAGAZINE

No. 1352 March 1985 Vol. 114

CONTENTS

NOTICE

It is requested that all books for review and communications for the Editor be addressed to the Director-General, Meteorological Office, London Road, Bracknell, Berkshire RG12 2SZ and marked 'For Meteorological Magazine'.

The responsibility for facts and opinions expressed in the signed articles and letters published in this magazine rests with their respective authors.

Applications for postal subscriptions should be made to HMSO, PO Box 276, London SW8 5DT.

Complete volumes of 'Meteorological Magazine' beginning with Volume 54 are now available in microfilm form from University Microfilms International, 18 Bedford Row, London WC1R 4EJ, England.

Full-size reprints of Vols 1–75 (1866–1940) are obtainable from Johnson Reprint Co. Ltd, 24–28 Oval Road, London NW1 7DX, England.

Please write to Kraus Microfiche, Rte 100, Millwood, NY 10546, USA, for information concerning microfiche issues.

HMSO Subscription enquiries 01 211 8667.

Printed in England for HMSO and published by
HER MAJESTY'S STATIONERY OFFICE

£2.30 monthly

Annual subscription £27.00 including postage

Dd. 737126 C13 3/85

ISBN 0 11 727557 3
ISSN 0026–1149

THE METEOROLOGICAL MAGAZINE

HER MAJESTY'S
STATIONERY
OFFICE

April 1985

Met.O.967 No. 1353 Vol. 114

METEOROLOGICAL OFFICE Met. O.967

THE METEOROLOGICAL MAGAZINE

No. 1353, April 1985, Vol. 114

551.593.54(41)

Recent measurements of broad-band turbidity in the United Kingdom

By F. Rawlins and R. J. Armstrong

(Meteorological Office, Bracknell)

Summary

The results of recent measurements of turbidity, calculated using pyrheliometer data at 1-minute intervals, are presented. Estimates of turbidity derived from hourly pyranometric observations indicate the annual cycle at different locations within the United Kingdom. The effect of the spread of stratospheric dust from the El Chichon eruption is investigated.

1. Introduction

The attenuation of the direct solar beam under cloudless skies is described by the turbidity of the atmosphere, which is principally determined by the optical depth due to aerosol. The presence of aerosol strongly influences solar radiation received at the earth's surface: both the spectral and the angular character of the radiation field are modified by scattering and by absorption of photons by suspended particles. The turbidity is an important parameter in many short-wave radiative transfer calculations, which are of particular interest for solar energy and agrometeorological studies. Only a limited number of measurements of turbidity in the United Kingdom have been published — Unsworth and Monteith (1972), and an annual series beginning with National Oceanographic and Atmospheric Administration (1973) — so that seasonal and geographical variations are largely unknown.

Owing to the aerosol optical depth being a function of wavelength, turbidity can be described by various coefficients. Here we consider only broad-band coefficients, which depend upon the attenuation over the entire solar spectrum (0.3-3.0 μm), and which can be determined from unfiltered pyrheliometric measurements of normal-incidence direct solar irradiance, as described in Armstrong and Richards (1981). Two coefficients of turbidity are employed: the Unsworth and Monteith (1972) coefficient, τ_a, and the Linke (1922) turbidity factor, T_L. The former is defined by the equation

$$I = I^* \exp(-\tau_a m) \quad .. \quad .. \quad .. \quad .. \quad .. \quad .. \quad .. \quad .. \quad .. \quad .. \quad (1)$$

where I^* is the normal incidence irradiance at the bottom of a dust-free atmosphere with a specified water vapour content, I is the normal incidence direct irradiance at the same level, and m is the air mass

number. The Linke factor is defined by

$$I = I_0 \exp(-T_L \tau_s m) \quad \ldots\ldots\ldots\ldots\ldots\ldots\ldots\ldots\ldots\ldots (2)$$

where I_0 is the extraterrestrial direct irradiance and τ_s is the broad-band Rayleigh scattering optical depth. A convenient approximation for inverting equation (2) and obtaining T_L is supplied by Kasten (1980),

$$(\tau_s m)^{-1} = 0.9 + 9.4m^{-1} \quad \ldots\ldots\ldots\ldots\ldots\ldots\ldots\ldots\ldots\ldots (3)$$

which is sufficiently accurate for the calculations described. The Linke factor (for a constant aerosol content) is dependent upon the water vapour optical path and hence upon the air mass number, m. When the water vapour content is known, the Unsworth–Monteith coefficient can be used to study changes in aerosol. However, the Linke factor is useful for applications when the water vapour content of the atmosphere is not available.

Three sources of turbidity data are considered: from occasional, manual pyrheliometric measurements, starting in 1968; from more recent pyrheliometric data recorded at a resolution of 1 minute; and from hourly pyranometric observations. Data have been recorded from pyrheliometers at three sites in the United Kingdom with a resolution of 1 minute, which facilitates identifying cloud-free conditions and allows the broad-band turbidity to be found whenever the vicinity of the sun's disc is unobscured by clouds; these results are presented in terms of the Unsworth–Monteith coefficient of turbidity.

Less precise estimates of average turbidity are obtained from hourly direct solar irradiation, calculated from pyranometric measurements of hourly global and diffuse irradiation, using the method of Page (1978), in which the problem of cloud contamination is circumvented — this method is described in a later section. Although several sources of error are introduced in this procedure, it has the considerable merit of providing an estimate of average turbidity, here labelled a 'derived turbidity', from routine solar radiation measurements, allowing values to be calculated from a larger number of stations over a longer period. These results are presented in terms of the Linke factor, partly because the atmospheric water vapour content is not required for this coefficient (which, by the method of Page, is based on a set of measurements on different days) and partly to distinguish between these pyranometric estimates of average turbidity and individual pyrheliometric observations.

Aerosol in the atmosphere arises from many sources, including the emission of pollutants, wind-blown dust and the chemical reaction of trace gases — the turbidity is largely determined by aerosol loading within the boundary layer, where the nature and concentration of particles exhibit great variability. However, a major perturbation in the aerosol optical depth at stratospheric heights occurred after the El Chichon eruptions in Mexico during April 1982 (Pollack *et al.* 1983). Large amounts of volcanic debris were injected into the stratosphere and gradually extended a veil of dust into northern latitudes during the following months. A stratospheric aerosol optical depth exceeding 0.1 (at 0.5 μm) was found from aircraft measurements by Dutton and DeLuisi (1983) at 50° N during December 1982; the background value is about 0.005 (at 0.55 μm) (Toon and Pollack 1976). This raises the possibility of detecting the spread of stratospheric dust to United Kingdom latitudes through turbidity measurements, although these include the effect of aerosol within the entire depth of the atmosphere.

2. Measurements

The United Kingdom network for measuring solar radiation is co-ordinated by the National Radiation Centre at Beaufort Park, near Bracknell, which maintains standard instruments with calibrations traceable to the World Radiation Reference. A list of stations within the network and their

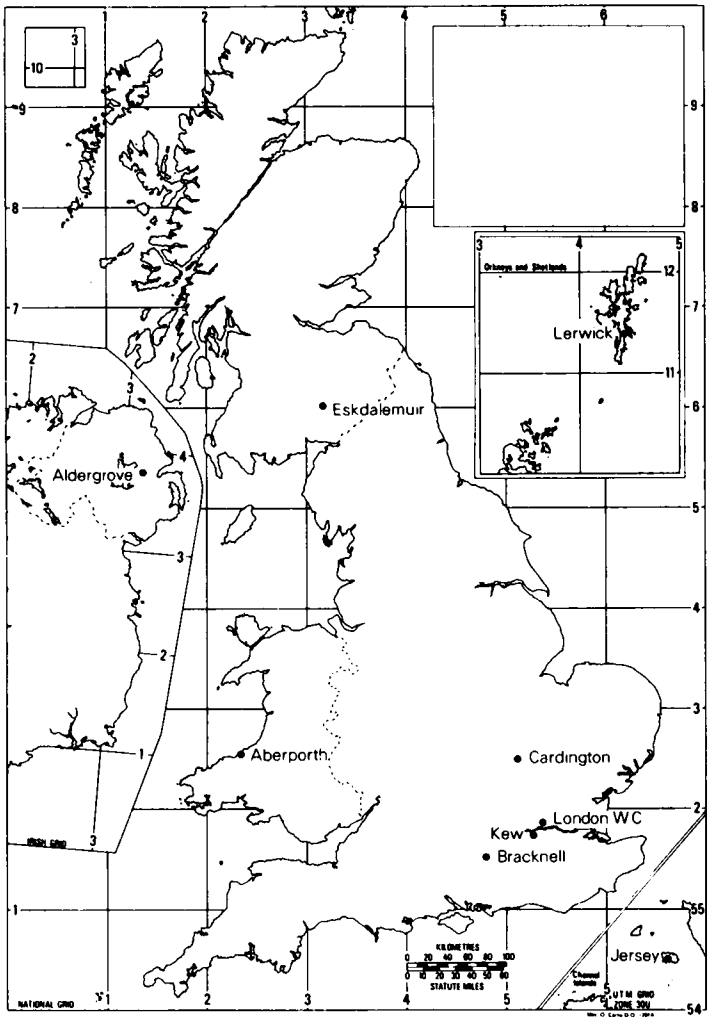

Figure 1. The geographical location of stations in the United Kingdom solar radiation network for which estimates of turbidity have been made.

periods of observation can be obtained from the Meteorological Office; calibration techniques are described in Budgen and Price (1981).

Currently, three stations measure normal incidence direct irradiance using Eppley NIP sun-tracking pyrheliometers — observations began in 1974 at Bracknell, and in 1981 at Lerwick and Eskdalemuir. From 1979 onwards, these measurements have been recorded at a resolution of 1 minute. Hourly global irradiation, G, and diffuse irradiation, D, have been obtained for at least 10 years since 1970 at nine sites using Kipp and Zonen thermopile pyranometers; the geographical locations are shown in Fig. 1. Diffuse irradiation is measured by obscuring the pyranometer with a shade ring — routine corrections are normally applied for the obscured regions of sky, assuming a uniform radiance distribution. This correction is too small under most conditions, and especially for clear skies, owing to the anisotropy of

the sky radiance. Hence in this paper, measured values, D_m, are corrected by an empirical expression in the form suggested by Kasten *et al.* (1983),

$$D/D_m = 1.148 - 0.142\,(D_m/G)^3 - 0.0012\delta \quad \ldots\ldots\ldots\ldots\ldots\ldots \quad (4)$$

where δ is the solar declination (in degrees), and the coefficients were calculated from a comparison of diffuse irradiation measured by pyranometer with that obtained from pyrheliometric observations, for all available hourly data within the United Kingdom.

Occasional measurements of turbidity have been performed at Kew during 1968-73, and Bracknell during 1974-78, using Ångström compensation pyrheliometers (Armstrong and Richards 1981). Data were obtained on about 150 days — a minor drawback of these measurements is that a majority were taken on days chosen for the calibration of pyrheliometers, which biases the data towards settled, cloudless conditions.

In 1982, Eko sun photometers were introduced at Bracknell and at Eskdalemuir. These are manually aligned to measure the solar irradiance in small spectral intervals at four wavelengths and, potentially, can reveal more information concerning the character of atmospheric aerosol than can be obtained from a single broad-band measurement (Volz 1974). Unfortunately, the stability of calibration was poor and these measurements have not been used.

3. Turbidity from pyrheliometric measurements (1-minute resolution)

When the sun is unobscured by cloud, values of the Unsworth-Monteith coefficient, τ_a, can be found for each minute from the record of normal incidence direct irradiance, using equation (1). I^* was calculated from tables, supplied by Unsworth (1975), as a function of the precipitable water vapour content of the atmosphere, which was estimated from synoptic observations of the surface vapour pressure, e (mb). The precipitable water vapour content (in millimetres) was approximated by $1.7e$ (Dogniaux and Lemoine 1982). This empirical estimate is sufficiently accurate for calculations of τ_a. In this procedure the effect of attenuation due to water vapour absorption is removed, and τ_a represents a broad-band aerosol optical depth. Fig. 2(a) shows an example of the turbidity found on a mostly cloudless day.

An obstacle to obtaining reliable values of turbidity is the passage of cloud, particularly cirrus, in front of the sun, which leads to a spuriously high estimate of turbidity. Fig. 2(b) indicates the turbidity calculated from the 1-minute record on a day of intermittent sunshine. This problem was overcome by dividing the measurement period into running 11-minute intervals: any single value of τ_a larger than 0.5 was considered to be due to cloud, not aerosol, and the entire interval was rejected. Also, if the range of values of τ_a within the 11 minutes exceeded 0.1 it was assumed that cloud was present and the record was eliminated. After these checks an average of the remaining 11-minute segments was taken and these averages constitute the basis of the turbidity record described subsequently.

Clearly, some difficulty remains in distinguishing between the incursion of a thin, uniform cloud layer and a heavily polluted air mass: it is likely that some days of high, variable turbidity will be rejected accidentally. Other problems, such as a marginal misalignment of the sun-tracking pyrheliometer, will also tend to lead to an overestimate of τ_a. Hence the minimum turbidity recorded during the day is a more reliable indicator of changes in aerosol than an average value, particularly because of the ambiguity in defining an upper limit for τ_a. Fig. 3 indicates the variation of the daily minimum turbidity for each month of the year, with total samples of 410, 400 and 780 days at Lerwick, Eskdalemuir and Bracknell respectively. The averages of the daily minima are shown, and the vertical bars mark the extent of the 30% and 70% levels of the frequency distribution of daily minimum τ_a (i.e. if the

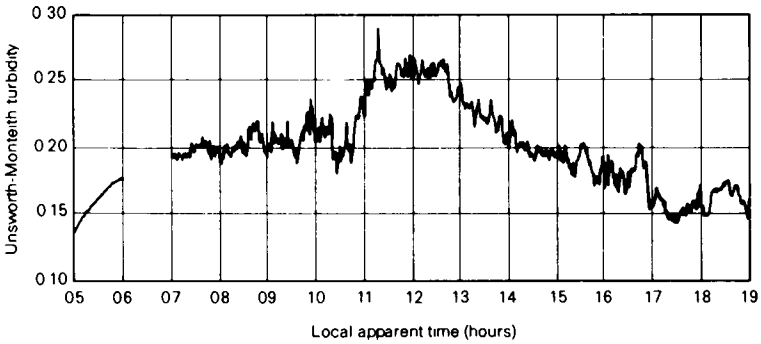

Figure 2(a). An example of the variation of Unsworth–Monteith turbidity at 1-minute resolution, measured by a sun-tracking pyrheliometer, for a day with little cloud (Bracknell, 13 May 1980).

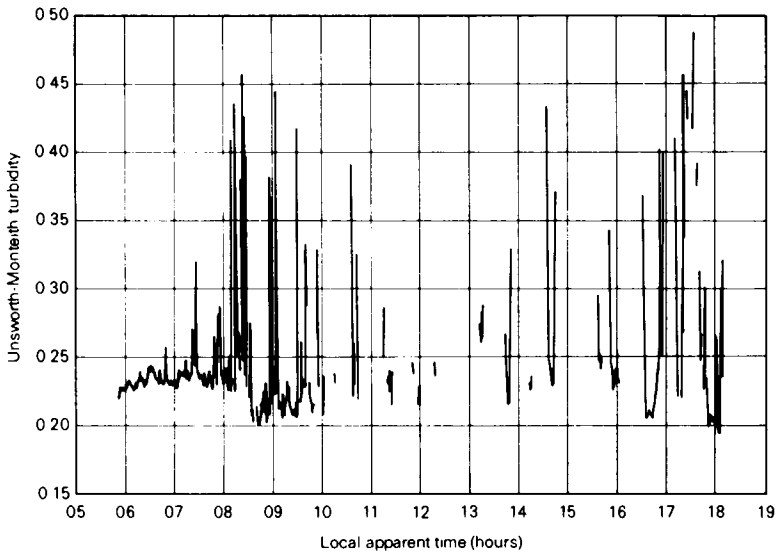

Figure 2(b). As fig. 2(a), for a day with intermittent cloud (Bracknell, 12 April 1983).

distribution was Gaussian, this would approximate to plus or minus one standard deviation). An annual cycle is obviously present, with the least turbid conditions occurring in winter months; the intra-month variation is shown to be large, and a significant difference between Bracknell (southern England suburban location) and the two sites in less-populated areas is evident.

Minimum turbidity 1981–83

The minimum values of τ_a in each month from 1981 until 1983 are shown in Fig. 4 — only those months with four or more days of reliable turbidity measurements were included. In the period of interest, all three sites indicate an increase in the monthly turbidity. Fig. 5 shows the minima averaged over the three stations, as well as an annual cycle based on all pre-July 1982 data. An increase in the minimum turbidity, compared to earlier values, is seen to extend from October 1982 until the end of the record.

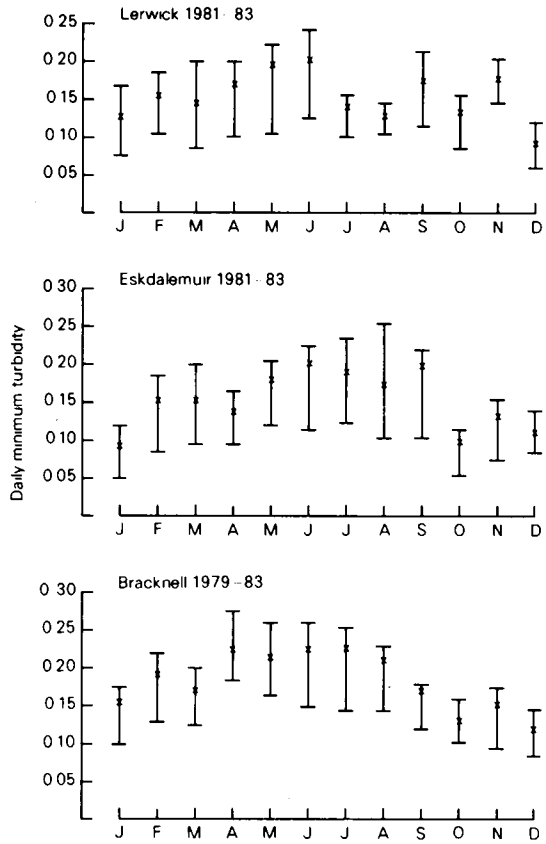

Figure 3. The distribution of daily minima of Unsworth–Monteith coefficients of turbidity in each month of the year at Lerwick, Eskdalemuir and Bracknell. The turbidity value at the upper end of the error bar is exceeded on 30% of occasions and that at the lower end on 70% of occasions. Averages of the daily minima are denoted by ×.

Owing to the brevity of the measurement period and to gaps in the data record, the duration and significance of the perturbation in turbidity is difficult to quantify. However, it is notable that at all sites and in every month, from October 1982 to May 1983, the minimum value of τ_a was higher than in any corresponding month outside that period. The average increase in minimum turbidity from October 1982 to May 1983 was about 0.06. Although it cannot be conclusively demonstrated that this change was due to the evolving El Chichon dust veil, the results are consistent with an enhancement of the aerosol optical depth over a large geographical area, partially masked by local variations in boundary-layer aerosol.

4. Turbidity from pyranometric measurements

(i) *Preliminary work*

When pyrheliometric measurements are not available, the normal incidence direct irradiance, I, can be found from pyranometric measurements of global and diffuse irradiance, from the relationship

$$I = (G - D)/\cos z \qquad (5)$$

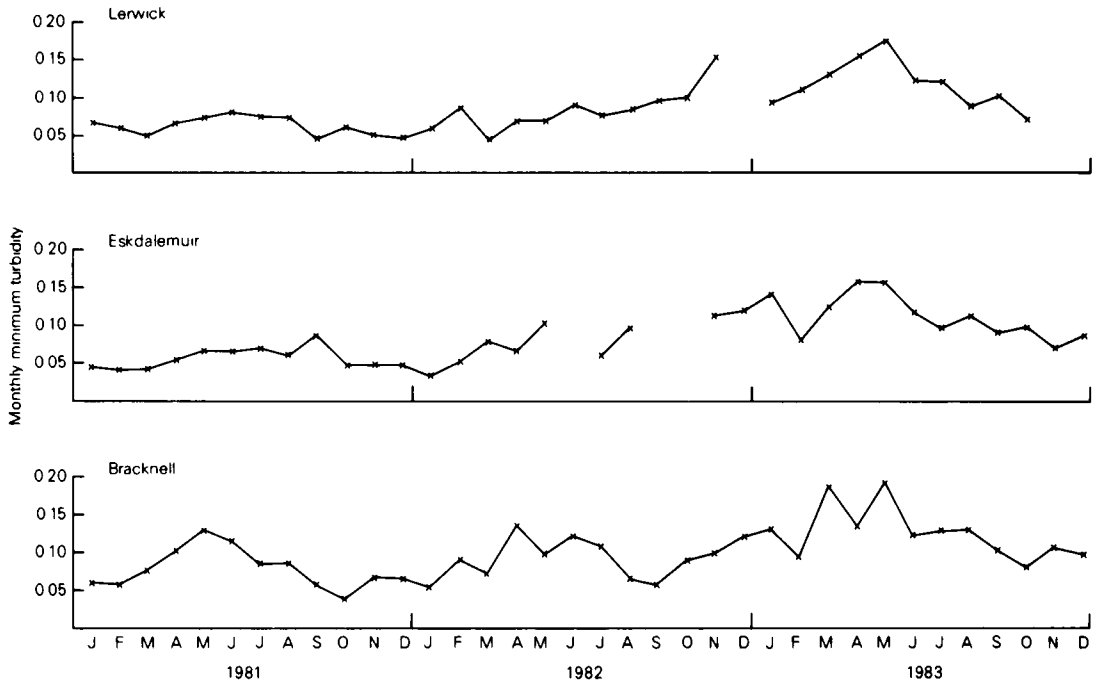

Figure 4. The variation of monthly minima of Unsworth–Monteith coefficients of turbidity during 1981–83, measured by pyrheliometers at Lerwick, Eskdalemuir and Bracknell.

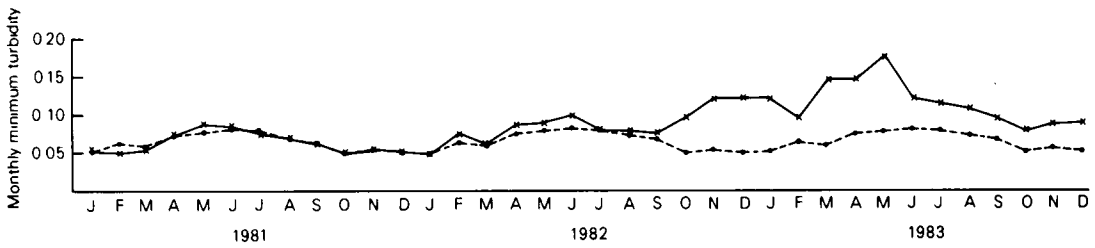

Figure 5. The mean over three stations of the monthly minimum Unsworth–Monteith turbidity during 1981–83. The dotted line represents the mean over three stations of the average monthly minimum turbidity computed from pre-July 1982 values, with the cycle repeated annually.

where z is the solar zenith angle. Equation (5) can also be applied to routinely performed hourly integrated measurements, with an averaged cos z term. For an hour of uninterrupted sunshine, a mean Linke turbidity, T_L, is found from equations (2) and (3). Page (1978) suggested this method for deriving turbidity, using mean values of G and D.

For most hours the sun is partially or completely obscured by cloud for some of the time, leading to a spuriously high value of turbidity from equation (2) and the problem of determining a realistic T_L reduces to finding cloud-free hourly measurements. This can be circumvented by selecting a representative value of I/I_0 from a large ensemble of hourly measurements. In this work the hourly value

of I/I_0 which is exceeded on only 5% of occasions in each month of the year is selected to represent the average clear sky irradiance; only hourly measurements between 0900 and 1500 local apparent time for each day are used in a sample of over 10 years. The sample excludes hours for which the average solar altitude is less than 10°, when equation (5) yields only very poor estimates. A 'derived Linke turbidity' is obtained from equation (2) and this can be regarded as an average turbidity for the month.

Fig. 6 compares the monthly Linke turbidity derived by this method from the sample 1968–73 for Kew, and 1974–78 for Bracknell, with the mean turbidity found from the series of occasional, manual observations by pyrheliometers during the same periods — the vertical bar denotes the standard error of the mean of the latter. Although complete agreement between measured and derived turbidity is not

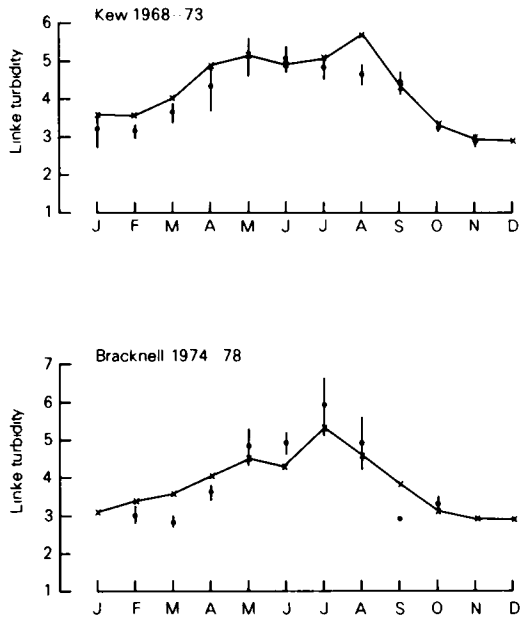

Figure 6. Comparison of monthly averages of Linke coefficients of turbidity at Bracknell and Kew, between measurements from Ångström pyrheliometers (with the standard error of the mean) and values derived from hourly pyranometer data (the continuous trace). The periods of the respective types of measurement are chosen to correspond to each other.

seen, the seasonal variation is successfully reproduced. Taking the deficiencies of the measurements into account, the agreement was deemed to be sufficiently good to treat the derived turbidity as a useful supplement to conventional measurements and justifies the choice of the 95% level a posteriori. The inclusion of latter values of T_L obtained from 1-minute resolution data (not shown) does not significantly affect these results.

Sources of error in the derived turbidity include: differences in the cosine response of the pyranometers which measure global and diffuse irradiation; averaging the cos z term in equation (5) over an hour; the shade-ring correction for diffuse irradiation; and the choice of a representative value of I/I_0 for clear conditions. Clearly, quantitative results should be treated with caution, especially for northern sites in winter, when relatively few uninterrupted hours of sunshine occur. This topic is discussed in Rawlins (1983).

(ii) *Average turbidity within the United Kingdom*

The Linke turbidity was derived from hourly global and diffuse irradiation for the period 1970-83 at nine sites: the monthly figures are given in Table I. It should be noted that the results are in accord with a subjective assessment of the relative aerosol concentration at each location, particularly for summer months, with the lowest turbidity found in coastal or rural areas and the highest turbidity recorded inland, at urban sites — this encourages confidence in the method employed. Data from some months are missing, owing to the infrequency of cloud-free hours in winter — at these times turbidity values found from 1-minute resolution pyrheliometric measurements are also scarce, for the same reason. The seasonal variation of T_L is shown in Fig. 7, with all stations combined.

Table I. *Monthly averages of Linke turbidity factor derived from hourly pyranometric data for different sites within the United Kingdom*

Station	Period	Jan.	Feb.	Mar.	Apr.	May	June	July	Aug.	Sept.	Oct.	Nov.	Dec.
Lerwick	1970-83	-	2.9	3.4	3.6	3.5	3.5	4.3	3.8	3.7	3.3	3.3	-
Eskdalemuir	1970-83	2.1	2.4	3.6	3.6	3.8	4.0	4.2	4.3	4.1	3.0	2.2	2.2
Aldergrove	1970-83	2.4	2.8	3.2	3.7	4.0	4.4	4.7	4.2	3.6	3.1	2.5	2.6
Aberporth	1970-83	2.8	3.2	3.2	3.5	3.6	3.6	3.9	3.8	3.6	3.3	3.0	2.8
Cardington	1970-79	2.7	3.2	3.7	4.4	3.9	4.8	5.0	4.7	3.8	3.3	2.8	2.6
London W.C.	1970-83	3.3	3.9	4.1	4.9	5.1	5.0	5.4	5.1	4.3	3.6	3.3	3.3
Kew	1970-80	2.9	3.6	3.9	4.7	4.7	4.7	5.2	5.0	3.9	3.3	2.8	2.9
Bracknell	1970-83	2.8	3.4	3.7	4.3	4.6	4.7	5.1	4.7	3.9	3.1	2.8	2.8
Jersey	1970-83	2.7	3.0	3.2	3.5	3.8	3.9	3.9	3.8	3.4	3.0	3.0	2.8

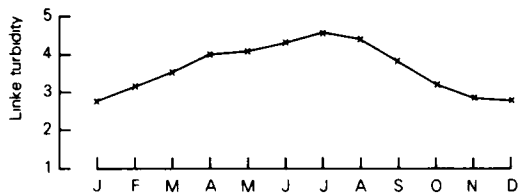

Figure 7. Annual variation of average Linke turbidity derived from hourly pyranometric measurements, averaged over nine stations around the United Kingdom for the period 1970–83.

5. Discussion

Three types of turbidity measurement have been described: manual observations using Ångström pyrheliometers, values found from the 1-minute resolution data record of sun-tracking pyrheliometers and estimates derived from routine hourly pyranometric measurements of global and diffuse irradiation. These constitute a longer period of measurement, for more areas, than previously available in the United Kingdom. The current series of 1-minute resolution normal incidence direct irradiance measurements can lead to a climatology of broad-band turbidity at three sites; this method uses existing routine observations with no need for extra manual intervention and is efficient in exploiting any cloud-free intervals.

There is some uncertainty concerning the relative importance of aerosol sources. Some aerosol arises from local natural or man-made sources, and some by transport from more distant regions. The dependence of turbidity on the prevailing air mass has been described by a number of workers, including Kondratyev (1969), Ball and Robinson (1982) and is assumed by Unsworth and Monteith (1972) to be

largely responsible for the variability shown in any month of the year (cf. Fig. 3). Regional differences in turbidity are also present, which are not due simply to a different prevalence of air mass types and some authors, for example in International Energy Agency (1980), have proposed estimating the turbidity of a location from the nature of its surroundings. Fig. 3 indicates relatively small differences in the daily minimum turbidity between the three sites of different character, compared to the variation between days within the same month of the year, as indicated by the frequency distribution.

Regional differences are more obvious in the Linke turbidity derived from long-term pyranometric measurements (Table I). Owing to several sources of error inherent in its determination, the derived turbidity should be considered only as a supplement to conventional measurements. However, in the absence of other measurements, values of derived turbidity provide useful estimates. There have been other attempts to estimate turbidity — e.g. from the maximum duration of bright sunshine (Unsworth and Monteith 1972); their results produced slightly larger values of turbidity than presented here, probably owing to the influence of thin cloud. Also, Dogniaux and Lemoine (1983), estimated mean annual turbidity from the 'Ångström' regression coefficients of global irradiation against bright sunshine duration — the extension of this work to allow rough estimates of monthly values of turbidity in the United Kingdom is described in Rawlins (1983).

Turbidity is dominated by the loading of aerosol in the troposphere, particularly within the boundary layer, and the contribution of dust at stratospheric heights to the attenuation of the direct solar beam is usually negligible. A number of workers at different locations (e.g. Spinhirne 1983, Swissler *et al.* 1983) have established that a major perturbation in the stratospheric aerosol optical depth followed the eruption of El Chichon in 1982. Our results for the United Kingdom do not reveal a large jump in turbidity at every location, when compared with normal variations within the data record. However, a coherent picture emerges from different stations: all sites recorded an increase in turbidity from about October 1982 until March 1983, of the order of $\Delta \tau_a \approx 0.06$, with a less widespread enhancement continuing throughout 1983. The limited scope of the measurements precludes a conclusive demonstration of detecting a progressive incursion of stratospheric aerosol above the United Kingdom but the results are consistent with a gradual northwards spreading of volcanic debris, which affects the minimum turbidity measured at widely separated stations.

References

Armstrong, R. J. and Richards, C. J. 1981 The measurement of atmospheric turbidity. *Meteorol Mag.* **110**, 303–312.

Ball, R. J. and Robinson, G. D. 1982 The origin of haze in the central United States and its effect on solar irradiation. *J Appl Meteorol.* **21**, 171–188.

Budgen, P. and Price, N. M. 1981 Routine calibration of solar radiation instruments. *Meteorol Mag.* **110**, 253–259.

Dogniaux, R. and Lemoine, M. 1982 Méthode approché d'estimation de l'irradiation solaire journalière de surfaces réceptrices orientées et inclinées. *Int J Sol Energy.* **1**, 71–84.

1983 Classification of radiation sites in terms of different indices of atmospheric transparency. Dordrecht, Commission of the European Communities, EUR 8333, 94–107.

Dutton, E. and DeLuisi, J. 1983 Spectral extinction of direct solar radiation by the El Chichon cloud during December 1982. *Geophys Res Lett.* **10**, 1013–1016.

International Energy Agency 1980 An introduction to meteorological measurements and data handling for solar energy applications. Washington, US Department of Energy.

Kasten, F. 1980 A simple parametrization of the pyrheliometric formula for determining the Linke turbidity factor. *Meteorol Rundsch.* **33**, 124–127.

Kasten, F., Dehne, K. and Brettschneider, W.	1983	Improvement of measurement of diffuse solar radiation. Dordrecht, Commission of the European Communities, EUR 8333, 221–225.
Kondratyev, K. Ya.	1969	Radiation in the atmosphere. London, Academic Press.
Linke, F.	1922	Transmissionkoeffizient und Trubungsfaktor. *Beitr Phys Freien Atmos*, **10**, 91.
National Oceanographic and Atmospheric Administration	1973	Atmospheric turbidity and precipitation chemistry data for the world. Washington, NOAA, Environmental Data Service.
Page, J. K.	1978	Methods for the estimation of solar energy on vertical and inclined surfaces. University of Sheffield, BS 46.
Pollack, J. B., Toon, O. B. and Danielsen, E. F.	1983	The El Chichon volcanic cloud: an introduction. *Geophys Res Lett*, **10**, 989–992.
Rawlins, F.	1983	Estimation of hourly solar irradiation over the UK. Dordrecht, Commission of the European Communities, EUR 8333, 151–155.
Spinhirne, J. D.	1983	El Chichon eruption cloud: latitudinal variation of the spectral optical thickness for October 1982. *Geophys Res Lett*, **10**, 881–884.
Swissler, T. J., McCormick, M. P. and Spinhirne, J. D.	1983	El Chichon eruption cloud: comparison of lidar and optical thickness measurements for October 1982. *Geophys Res Lett*, **10**, 885–888.
Toon, A. B. and Pollack, J. B.	1976	A global average model of atmospheric aerosols for radiation transfer calculations. *J Appl Meteorol*, **15**, 225–246.
Unsworth, M. H.	1975	Variations in the short wave radiation climate of the UK. International Solar Energy Society, UK Section. Conference on UK Meteorological Data and Solar Energy Applications at the Royal Institution, London, February 1975, 18–36.
Unsworth, M. H. and Monteith, J. F.	1972	Aerosol and solar radiation in Britain. *Q J R Meteorol Soc*, **98**, 778–797.
Voltz, F. E.	1974	Economical multispectral sun photometer for measurements of aerosol extinction from 0.44 μm to 1.6μm and precipitable water. *Appl Optics*, **13**, 1732–1733.

551.501.45:551.553.6

Investigation of the effect of length of record upon extreme values

By Catherine F. Boyack

(Meteorological Office, Bracknell)

Summary

The variability of extreme wind speed estimates using short-period data has been investigated using wind-speed data from Prestwick, Gorleston and Point of Ayre.

Introduction

The long-accepted method of obtaining environmental extreme data for design or planning purposes is to apply the statistical theory of extremes as developed by Fisher and Tippett. This requires long periods of data (Tabony 1983) from which annual extremes can be extracted. In the case of structures offshore, designers require data on waves but there are few locations with instrumental wave data for more than a few years. Such runs of data provide only a small number of data points, so the Fisher–Tippett type of distribution cannot be used. Instead it is normal practice to fit a frequency distribution to the complete data set and then extrapolate to obtain values corresponding to the required return period. Inevitably, the value of this technique can be questioned since it implies that extremes will lie on the same frequency distribution as the main body of the data. Tabony has shown that even extreme values do not necessarily belong to one distribution.

In order to examine the accuracy of extremes derived from short data runs Painting (1980) applied the Weibull (1951) distribution to observations of wind and waves at Ocean Weather Station 'I'. He compared the results of using overlapping 3-year runs of data with those obtained using the whole (18 years) data set. He showed that the once-in-50-year values based on 3 years of data could differ by up to 7% for wind and 16% for waves from those obtained using all the data. Painting's results could be queried because the wave data used were visual estimates and, therefore, not very reliable. Also, wind observations from weather ships are averaged by eye from an anemometer dial, with reference to the state of sea, rather than being a true 10-minute instrumental reading as should be the case for a land-based observer having an anemograph. His figures for winds may have been affected as a result.

This paper describes the results of an investigation repeating Painting's work for a land station using both the 10-minute 'synoptic' winds and the hourly mean winds obtained from anemograph traces.

Choice of site

Prestwick was chosen for the study because it has one of the longest records of wind data in the computer archive and had no major site or instrument changes during the period of record used (1959–82 inclusive). The Prestwick anemometer has an effective height of 10 metres and is situated on an unobstructed site in the centre of the airfield, although wind speeds from the south-west may be affected by the close proximity of Prestwick town. A change from pressure-tube anemograph to electrical recording anemograph occurred in 1958 but since then the site and instrument type have remained substantially unchanged.

Method

Estimates of once-in-50-year and once-in-5-year 10-minute mean wind speeds were calculated from all the data (1959–82 inclusive) and from data for overlapping 3-year periods (i.e. 1959–61, 1960–62, etc.) using the Weibull distribution. All Weibull analyses were carried out entirely by computer to ensure objectivity in the results. A once-in-50-year Gumbel* extreme 10-minute wind speed was also calculated using the Lieblein technique (Lieblein 1974). The overlapping short-period once-in-50-year extremes were then plotted as percentages of the once-in-50-year Weibull estimate based on all the data and as percentages of the once-in-50-year Gumbel estimate based on all the data (see Fig. 1). The estimate plotted for 1960 uses data from 1959–61, that for 1961 uses data from 1960–62, etc.

The above work repeats that undertaken by Painting although, in practice, the Meteorological Office Marine Enquiry Bureau does not use the Weibull distribution extrapolated to long return periods unless there are other corroborating values available, such as a Gumbel extreme value from a nearby station. This is because there is evidence (Graham 1983) that the Weibull distribution underestimates values at long return periods. What constitutes a long return period depends on the site and location but, in general, a return period greater than 5–10 years would be described as long. Jenkinson (1977) and Graham (1982) have used long periods of wind data from coastal stations to obtain average slopes of the Gumbel distribution. Values at 16 stations quoted by Graham gave an average value of 0.82 for the ratio of the once-in-5-year extreme to the once-in-50-year extreme (with a standard deviation of 0.02). Using more stations, Jenkinson quotes a value of 0.83. For enquiry purposes this value is used to estimate once-in-50-year Gumbel extremes from once-in-5-year values obtained using the Weibull distribution. The ratio for Prestwick is 0.82.

For each 3-year period once-in-50-year extremes were recomputed by first calculating the 5-year value using the Weibull distribution, and then applying the 0.83 standard ratio. These values were plotted as percentages of the once-in-50-year Gumbel extreme based on all the data (see Fig. 1). Using the complete data the once-in-5-year, 10-minute mean value derived using the Gumbel distribution and that derived using the Weibull distribution were virtually identical (43.0 and 43.2 knots). This justifies the use of this scaling technique to obtain 50-year Gumbel extremes from 5-year Weibull extremes.

The graphs shown in Fig. 1 were replotted using extremes estimated from hourly mean wind-speed data (see Fig. 2).

It can, of course, be argued that meteorological events are subject to physical limits and that the extreme-value distribution used to represent wind should be the Fisher–Tippett type 3 (bounded) and not the Type 1 (straight line, unbounded). Values derived from the latter distribution may, themselves, be overestimates as a consequence. However, Figs 3(a) and 3(b) show that there is no evidence of any significant curvature in the distribution of extremes and that, at least for a return period of 50 years, it is satisfactory to use the straight-line, unbounded form. For practical applications it is probably safer to use the straight-line distribution to guard against the kind of effect noted by Tabony who showed that there could be discontinuities in extreme-value distributions which might not be well represented even with quite long periods of data.

Results

Figs 1 and 2 show that even if the once-in-50-year Weibull estimate based on all the data is capable of giving an accurate extreme value, the extremes based on only 3 years of data vary by as much as 14% from this value. In practice, the Weibull distribution applied to winds apparently gives an overestimate

* The Fisher–Tippett Type 1 (straight line) extreme value distribution was popularized by Gumbel (1958) and, for the sake of brevity, will be referred to as the Gumbel distribution.

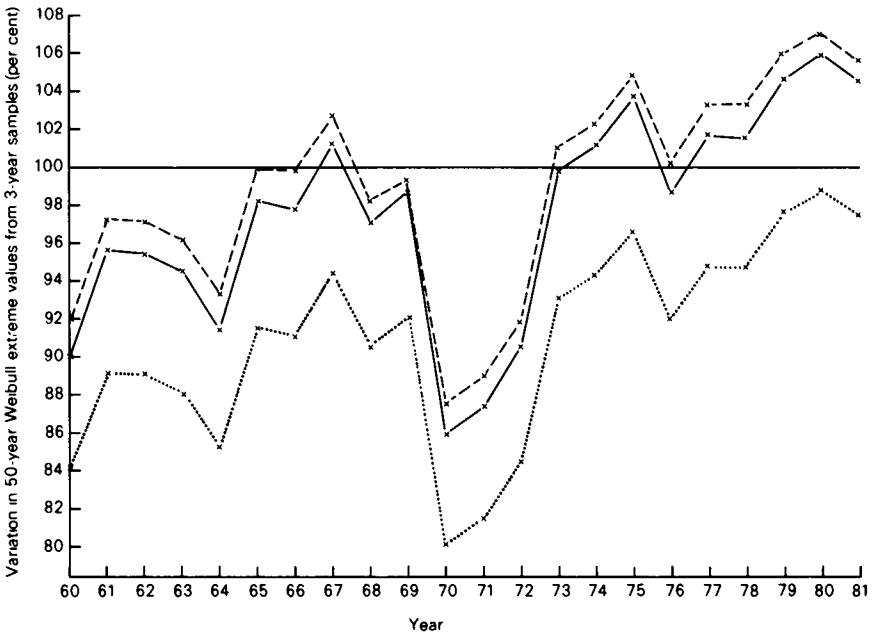

Figure 1. Weibull estimates of extreme 10-minute mean wind speeds based on 3-year running data samples from Prestwick compared with extreme values based on all the data (1959–82).
× ———— × All-data Weibull estimate × ····· × All-data Gumbel estimate
× — — — — × All-data Gumbel estimate where Weibull estimates are derived from once-in-5-year winds and the standard ratio.

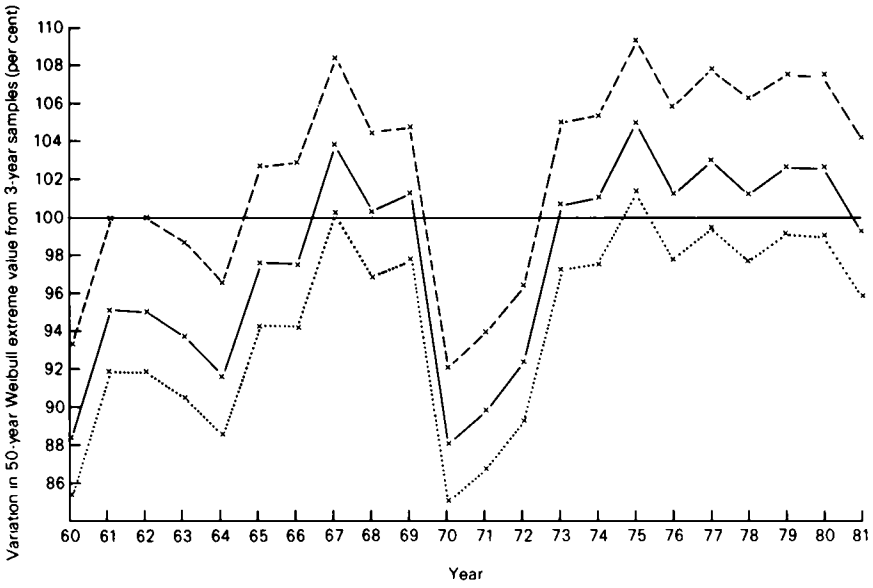

Figure 2. Weibull estimates of extreme hourly mean wind speeds based on 3-year running data samples from Prestwick compared with extreme values based on all the data (1959–82).
× ———— × All-data Weibull estimate × ····· × All-data Gumbel estimate
× — — — — × All-data Gumbel estimate where Weibull estimates are derived from once-in-5-year winds and the standard ratio.

of extreme values at short return periods and an underestimate at long return periods, so the variation from the 'true' extreme may be even greater than shown in the graphs.

The once-in-50-year Gumbel estimate based on all the data is generally thought to be close to the 'true' extreme value. Figs 1 and 2 show that the once-in-50-year Weibull extremes based on only 3 years of data varied by as much as 20% from this 'true' value. Similarly, Figs 1 and 2 show that the once-in-50-year extremes calculated from only 3 years of data using the once-in-5-year Weibull estimate and the standard return period conversion factor (0.83) varied by nearly 13% from the 50-year Gumbel estimate.

The standard error (SE) associated with fitting a Gumbel distribution by the Maximum Likelihood method can be calculated as

$$SE(\chi) = \alpha\,(1.11 + 0.52Y + 0.61Y^2)^{1/2}/M^{1/2}$$

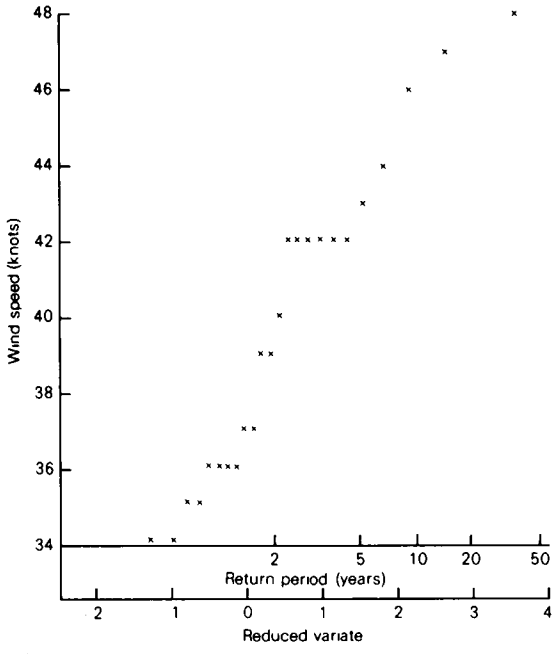

Figure 3(a). Annual maximum 10-minute mean wind speeds at Prestwick, 1959–82.

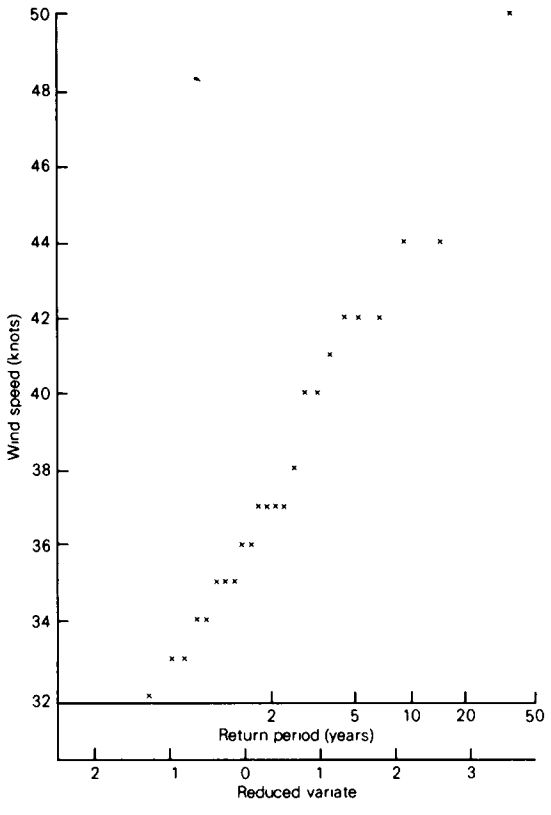

Figure 3(b). Annual maximum hourly mean wind speeds at Prestwick, 1959–82.

The annual maximum mean wind speed values shown in Figs 3(a), 3(b) and 6 were plotted according to the relation $p = (m - 0.31)/(M + 0.38)$, which gives a cumulative probability p to the mth ranking of a series of M observations and has often been used in the Meteorological Office since it was adopted by Jenkinson (1969).

Comparison of Figs 3(a) and 3(b) casts some doubt on the maximum observed 10-minute wind at Prestwick shown, unusually, to be slightly less than the maximum hourly mean wind. Careful examination of the original wind trace suggests that the highest 10-minute wind (0400 GMT on 15 January 1968) might have been slightly higher, but not sufficiently so to affect in any significant quantitative sense the results of this paper. A 2-knot increase in the maximum 10-minute wind leads to an increase from 51.4 to 51.7 knots in the once-in-50-year Gumbel value.

where α is the slope, M is the number of extremes and Y is the value of the reduced variate corresponding to an estimate χ of the variable under analysis (Natural Environment Research Council 1975). This expression gives standard errors of 2.5 knots for both the once-in-50-year, 10-minute mean and hourly mean wind-speed estimates produced using the Gumbel technique (51.4 knots and 49.5 knots respectively) and although, strictly, it applies to Maximum Likelihood estimates, the standard error associated with fitting a Gumbel distribution by the Lieblein technique is not likely to be significantly different from this figure. This means that the percentage variation of extremes using short periods of data from the 'true' extreme value may be even greater than that shown in the graphs.

Comparison with other sites

Although Prestwick was chosen for the study because it has one of the longest records of wind data in the computer archive with no major site or instrument changes, the once-in-50-year Gumbel estimate was an extrapolation based on only 24 annual maximum wind-speed values (i.e. values for the years 1959–82 inclusive). A number of stations with longer periods of record were not considered suitable for the original study owing to site changes, instrument changes or relatively short records of wind data in the computer archive. Two stations, Gorleston and Point of Ayre, were chosen as examples of stations having longer records of annual maximum wind speeds and the work carried out using Prestwick data was repeated for comparison purposes.

Once-in-50-year hourly mean Gumbel estimates for Gorleston and Point of Ayre were multiplied by 1.06 (Hardman *et al.* 1973) to obtain 10-minute mean extreme values. The Gorleston value was based on 57 annual maxima, recorded over the period 1913–81, and that for Point of Ayre on 46 annual maxima, recorded over the period 1936–81. Weibull estimates were calculated from Gorleston and Point of Ayre 10-minute mean wind data for the years 1957–74 and 1957–82 respectively. The extreme-value distributions (Fig. 4(a) and (b)) both show little evidence of any curvature and the 50-year Gumbel values can be regarded as definitive values rather than estimates.

Although the Gorleston and Point of Ayre Gumbel estimates are applicable to heights of 10 metres and 11 metres respectively and there were site changes during the record of 10-minute mean wind speeds, the once-in-50-year Gumbel estimates and Weibull 10-minute mean estimates were plotted with no correction for height as it appears that the effective heights of the anemometers were always between 8 and 13 metres at both stations. Figs 5 and 6 show values of once-in-50-year 10-minute winds for Gorleston and Point of Ayre using the same representation as Figs 1 and 2 for Prestwick.

Comparisons of the results obtained using 10-minute mean wind data from Prestwick with those obtained using Gorleston and Point of Ayre 10-minute mean wind data are shown in Fig. 7 and Table I and it is clear that the extremes based on only 3 years of data from Gorleston and Point of Ayre vary from the all-data extremes by a smaller amount than the corresponding values from Prestwick. The use of only 16 three-year data sample extremes (compared to 22 for Prestwick and 24 for Point of Ayre) may explain some of the reduction in variation for Gorleston. However, the Weibull extremes for Gorleston and Point of Ayre based on only 3 years of data still vary by as much as 10% (Gorleston) or 11% (Point of Ayre) from the Weibull extremes based on all the data and by as much as 13% (Gorleston) or 19% (Point of Ayre) from the Gumbel extremes based on all the data. Similarly, Figs 5 and 6 show that the once-in-50-year extremes calculated from only 3 years of data using the once-in-5-year Weibull estimate and the standard return period conversion factor (0.83) varied by as much as 9% from the 50-year Gumbel estimate at both Gorleston and Point of Ayre.

Conclusion

The variability of extreme wind speeds derived from short periods of data has been studied using homogeneous wind records from Prestwick. The study has shown that extremes estimated from a period

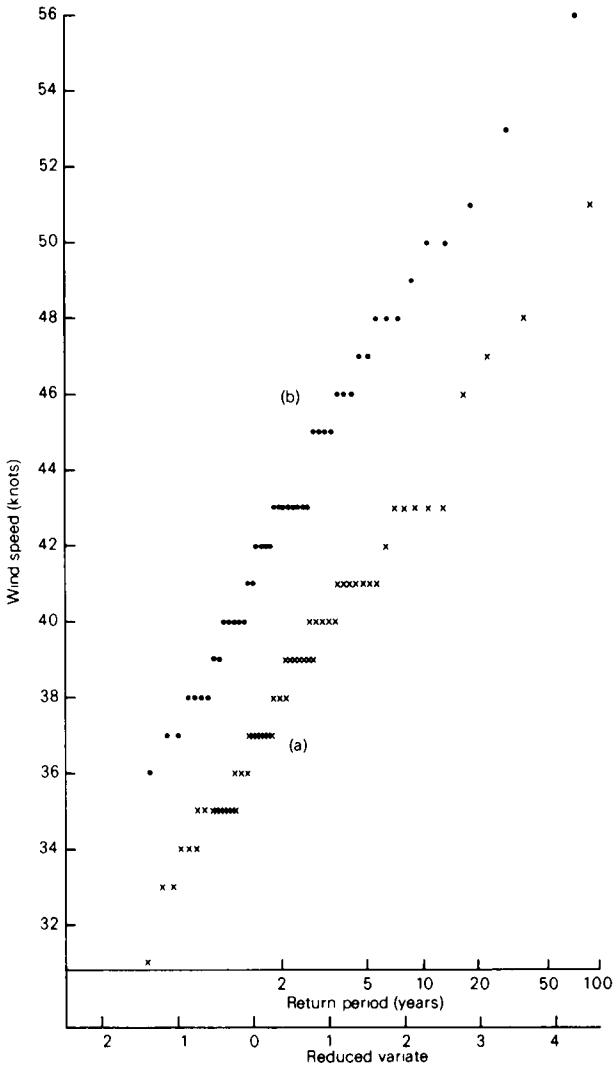

Figure 4. Annual maximum hourly mean wind speeds at (a) Gorleston, 1913–81, and (b) Point of Ayre, 1936–81.

as short as 3 years may be in error by an unknown amount, which could be as large as 20% and therefore cannot be used with confidence for design purposes. A comparison study using less reliable wind data indicated that errors may not always be as large as this although the 3-year data sample extremes from Gorleston and Point of Ayre did differ from the well-defined Gumbel estimates by up to 19% and could not be used with confidence.

Whether these results can or should be applied to wave data is uncertain. Painting showed that for Ocean Weather Station 'I' the variability of the 50-year estimates for wave data was about twice that for wind. However, wave heights are subject to more easily definable physical limits than are wind, so a long

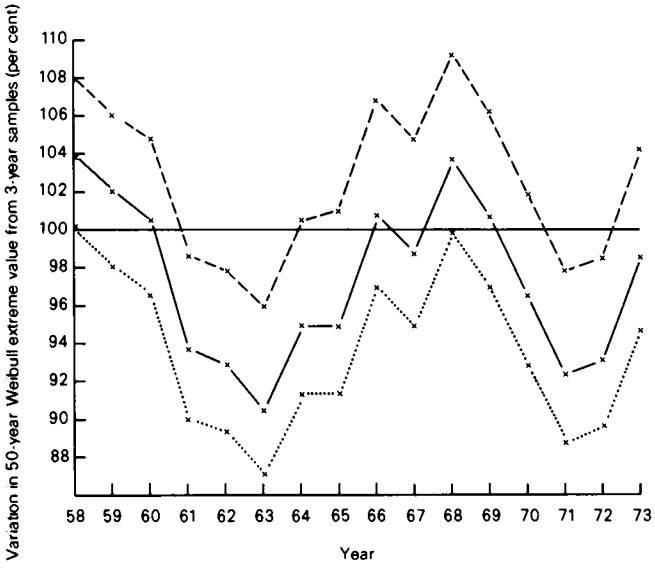

Figure 5. Weibull estimates of extreme 10-minute wind speeds based on 3-year running data samples from Gorleston compared with extreme values based on all the data.
×————× All-data Weibull estimate, 1957–74 × ····· × All-data Gumbel estimate, 1913–81
× — — — — × All-data Gumbel estimate where Weibull estimates are derived from once-in-5-year winds and the standard ratio.

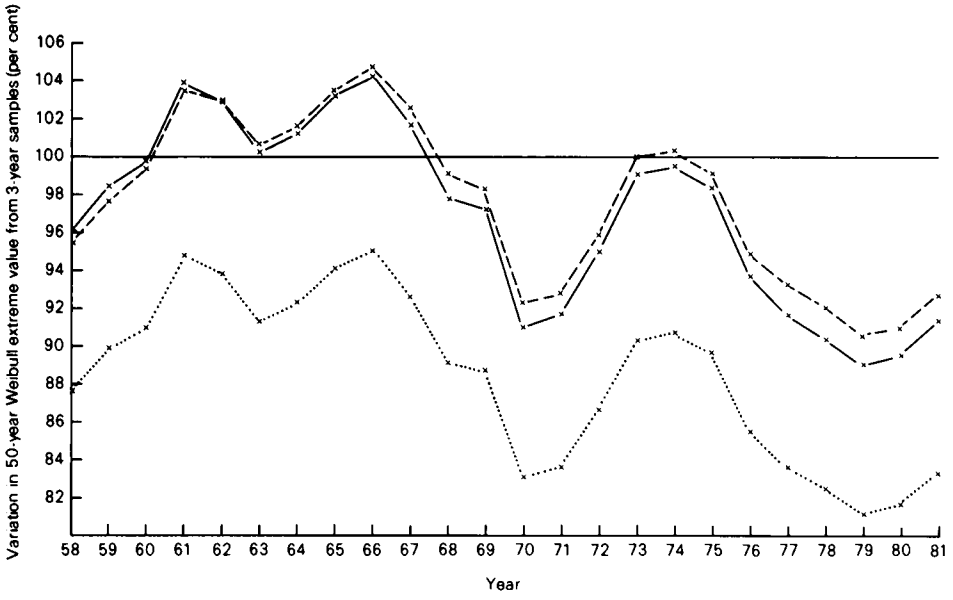

Figure 6. Weibull estimates of extreme 10-minute wind speeds based on 3-year running data samples from Point of Ayre compared with extreme values based on all the data.
×————× All-data Weibull estimate, 1957–82 × ····· × All-data Gumbel estimate, 1936–81
× — — — — × All-data Gumbel estimate where Weibull estimates are derived from once-in-5-year winds and the standard ratio.

Table I. *Comparison of results obtained using 10-minute mean wind data from Prestwick, Gorleston and Point of Ayre*

	Prestwick	Gorleston	Point of Ayre
	Range of variation of Weibull estimates (based on 3-year data samples)		
	per cent		
From all-data Weibull estimate	20	14	15
From all-data Gumbel estimate	19	13	14
(where Weibull estimates were derived from once-in-5-year winds and standard ratio)	20	13	14

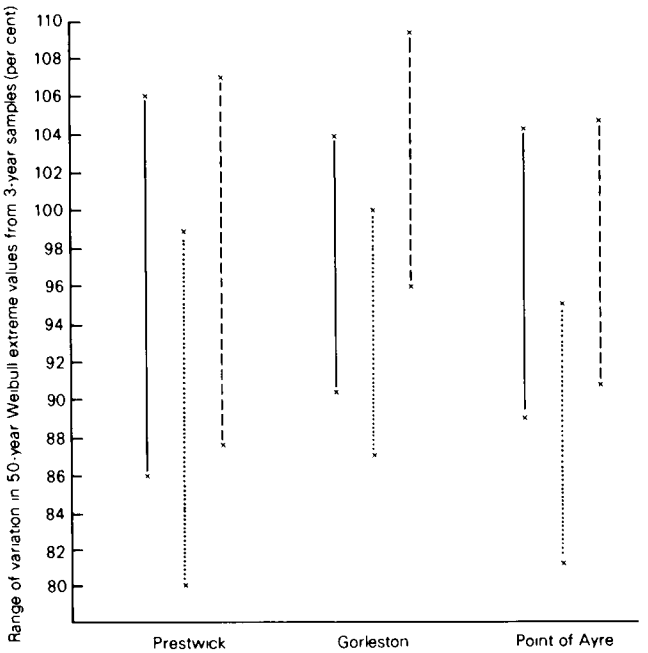

Figure 7. Comparison of the range of variation in Weibull estimates of extreme 10-minute mean wind speed based on 3-year running data samples from extremes based on all data, for Prestwick, Gorleston and Point of Ayre.
×————× All-data Weibull estimate ×·····× All-data Gumbel estimate
×— — — — —× All-data Gumbel estimate where Weibull estimates are derived from once-in-5-year winds and the standard ratio.

period of maximum values might well show a clear trend to a bounded (Fisher–Tippett Type 3) distribution. There are, however, no records of instrumental wave data of sufficient length in the region of the United Kingdom to obtain a reasonably definitive 50-year extreme. The question cannot, therefore, be put to the test.

References

Graham, Anne E.	1982	Comments on some assumptions made in extreme value analysis. (Unpublished, copy available in the National Meteorological Library, Bracknell.)
	1983	A study of the Gumbel and Weibull methods of extreme-value analysis using air temperature data for six Ocean Weather Stations. *Meteorol Mag*, **112**, 303–317.
Gumbel, E. J.	1958	Statistics of extremes. New York, Columbia University Press.
Hardman, Carol E., Helliwell, N. C. and Hopkins, J. S.	1973	Extreme wind speeds over the United Kingdom for periods ending 1971. *Climatol Mem. Meteorol Off.* No. 50A.
Jenkinson, A. F.	1969	Statistics of extremes. *In* Estimation of maximum floods. Geneva, WMO, *Tech Note* No. 98, 183–257.
	1977	Analysis of maximum significant wave height data for selected North Sea storms. (Unpublished, copy available in the National Meteorological Library, Bracknell.)
Lieblein, J.	1974	Efficient methods of extreme-value methodology. Washington, National Bureau of Standards. Final Report NIBSIR 74-602.
Natural Environment Research Council	1975	Flood studies report, Vol. I. London.
Painting, D. J.	1980	The variability of wind and wave statistics as observed at OWS 'I'. Reuil-Malmaison, Institut Français du Pétrole, Association de Recherche Action des Eléments. Collection Colloques et Séminaires 34, Climatologie de la Mer (Sea Climatology), Conférence Internationale, Paris 3–4 Octobre 1979, 257–269.
Tabony, R. C.	1983	Extreme value analysis in meteorology. *Meteorol Mag*, **112**, 77–98.
Weibull, W.	1951	A statistical distribution function of wide applicability. *J Appl Mech*, **18**, 293–297.

551.5(09):551.507.352:358.4

Meteorological reconnaissance flights

By R. J. Ogden

Summary

An informal account, based largely on pilot reminiscences, is given of meteorological reconnaissance flights from the United Kingdom during and shortly after the Second World War.

Introduction

This note is an attempt to set down some recollections of meteorological reconnaissance flights (which used to be referred to colloquially as 'Met Recce' flights) from the point of view of a pilot. It is based primarily on conversations during May 1984 with Captain D. H. ('Bill') Mackie, formerly of British Airways, but also includes some material culled from other sources. The routes followed by the various reconnaissance flights were given code-names, and these are illustrated in Fig. 1.

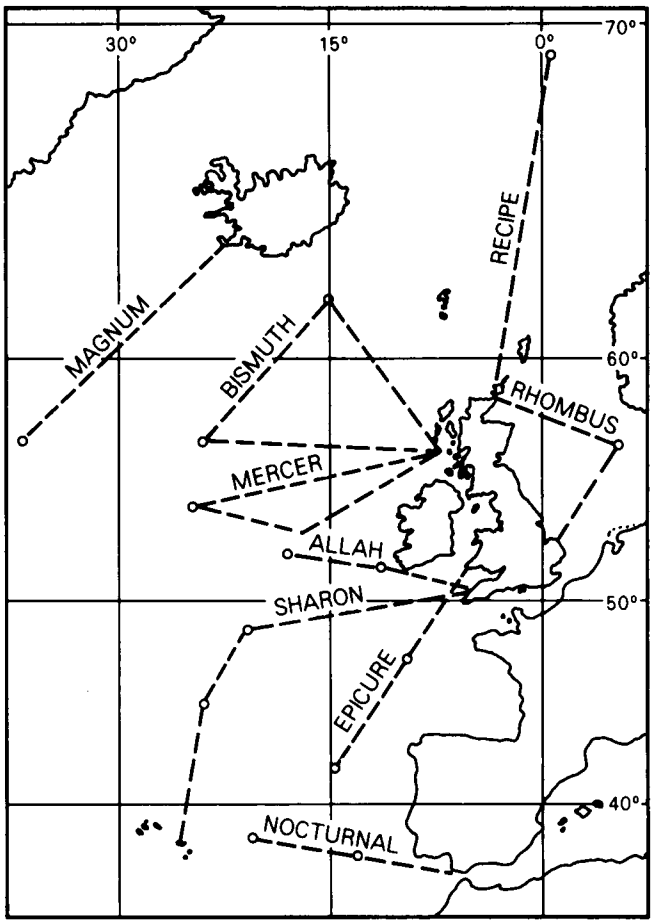

Figure 1. Tracks of meteorological reconnaissance flights in September 1944.

Bill Mackie joined 518 Squadron at Tiree in August 1944, serving as a co-pilot for three months, but thereafter as captain on the BISMUTH and MERCER meteorological reconnaissance flights. Apart from a short detachment to Wick, flying RECIPE flights whilst the squadron there converted from Fortress to Halifax aircraft, he remained at Tiree until August 1945 when the squadron there was moved to Aldergrove to continue the BISMUTH flights from there. In March 1946 he left 518 Squadron, at first remaining at Aldergrove as Commander of the Communications Flight, then moving to St. Eval for a spell as Adjutant of 210 Squadron which was based there for general reconnaissance and air-sea rescue duties. In November 1948 he agreed to return to Aldergrove as Flight Commander of B Flight, 202 Squadron. By this time, 202 Squadron had taken over the BISMUTH flights as its major responsibility, although it also had a subsidiary role in air-sea rescue, when necessary dropping Lindholme gear — self-inflating rubber dinghies equipped with rations, wireless, and so on. Bill Mackie continued with the BISMUTH flights until March 1951, by then having completed some four years and over 1700 hours flying on these duties — probably more than any other RAF pilot. He was awarded the AFC for this work.

On leaving the RAF, Bill Mackie joined BEA (later British Airways), flying several different types of aircraft until his retirement as Captain in 1977. Throughout this time he maintained his interest in aviation meteorology, and in 1976 received an award from the Director-General for long and meritorious service in providing meteorological reports from civil aircraft (see *Meteorol Mag*, **107**, 1978, 97–98).

Aircraft and crews

During 1944, 518 Squadron was equipped with Halifax V aircraft, fitted with Merlin engines; these were gradually replaced by the Halifax III, fitted with Hercules engines. In late 1950, these in turn were replaced by Hastings.

The Halifax bomber was designed to be operated by a crew of seven, namely: captain, navigator, flight engineer, wireless operator, bomb aimer and two air gunners. For meteorological reconnaissance flights the aircraft were unarmed, so the gunners and bomb aimer were not needed. It was decided that, instead, a second pilot and second wireless operator should be added to the crew, plus the meteorological observer. The second pilot occupied a collapsible seat from which he could assist the captain, for example with control of the throttles during take-off, but the aircraft could not be flown independently from his position. The second wireless operator was used only as a relief and no second working position was provided. The meteorological observer occupied the front turret, which offered a wide view for observing purposes.

The Halifax was not pressurized, so the use of oxygen was essential during high-level flight. Normal climb speed was 140 kn and the cruising speed was 165 kn. Cabin heating arrangements were very primitive. There was no de-icing equipment; a paste was applied to the leading edges of the wings before take-off, but in practice this was far from effective. Modifications to the aircraft to fit them for meteorological reconnaissance work included changes to the turret canopies (in the absence of guns), the installation of the co-pilot's seat and the provision of a radio altimeter for use by the captain in addition to his normal pressure altimeter. Appropriate meteorological instruments (e.g. external thermometers, aneroid barometer connected to a static vent) were fitted for use by the meteorological observer, who was also provided with a radar altimeter for accurate height determination at standard and other pressure levels.

From the pilot's point of view, the Hastings was in several ways an improvement on the Halifax. Although a civil version of the Hastings (known as the Hermes and flown by BOAC during the 1950s) had a tricycle undercarriage and was fully pressurized, the meteorological reconnaissance squadron Hastings still had the traditional tail wheel and were not pressurized. However, they did have de-icing equipment, a higher cruising speed of 185 kn, somewhat better cabin heating and much-improved seating arrangements. The co-pilot had a proper seat alongside the captain and, although the instrument panel was not duplicated, the aircraft could be flown from that position. The modifications to the Hastings aircraft for meteorological reconnaissance work were carried out at Radlett.

Flight procedures

The flights from Tiree and, later, Aldergrove took anything from a minimum of seven hours to nine hours or more, and required prolonged concentration on the part of the captain. By late 1944, both BISMUTH and MERCER flights were on triangular tracks, each leg being some 400 to 500 nautical miles. Routine meteorological observations (cloud, temperature, weather, icing, height of pressure surface, etc.) were made every 50 nautical miles (i.e. at about 20-minute intervals); winds were computed by the navigator.

After take-off the aircraft climbed to 950 mb. The meteorological observer advised the captain when this pressure level was reached; thereafter the captain maintained flight at this pressure level by flying at a constant indicated altitude on his pressure altimeter, the sub-scale being left unchanged. Every 150 nautical miles (i.e. roughly every hour), with the aid of the radio altimeter, the aircraft was brought down to 50 ft above the sea to enable a reliable estimate of mean-sea-level pressure to be made.

At the end of the first leg (i.e. some 500 nautical miles from base), after descending to 50 ft for a mean-sea-level pressure check, the aircraft climbed, using a series of short legs on alternating reciprocal headings; at appropriate standard pressure levels the aircraft was levelled out for a minute or so to allow time for the thermometer to stabilize and so permit determination of an accurate vertical temperature profile. The climb continued in this way to the 500 mb level, oxygen masks being put on at 10 000 ft.

The second leg was flown at 500 mb and at the end of this the aircraft descended to 50 ft above the sea, using short reciprocal-heading legs as on the climb. The final leg home was similar to the first leg, i.e. at 950 mb, but with descents to 50 ft above the sea every 150 nautical miles.

The navigator maintained an air plot throughout the trip. GEE fixes could be obtained only near base and the main navigational aid was loran. However, the wireless operator was able from time to time to obtain bearings by W/T from certain land stations in the United Kingdom and thus provide some additional fixes to help the navigator, who computed winds and passed them to the meteorological observer. On the low-level runs, smoke floats were sometimes dropped to enable winds to be derived by observing drift.

In addition to obtaining W/T fixes, the wireless operator transmitted the meteorological information in the form of coded messages after every third routine meteorological observation, i.e. at roughly hourly intervals; during the War years the messages had to be encyphered before transmission. A continuous listening watch was maintained throughout the rest of the time.

From August 1944 until after VE Day, two BISMUTH and two MERCER flights were operated each day from Tiree, one flight on each track being made at night. Subsequently the night flights were dropped, and with the move to Aldergrove the MERCER flights ceased altogether; from then on, at least until 1951, the commitment at Aldergrove was for one daylight BISMUTH flight each day.

General recollections

It was a point of honour that flights would take off if humanly possible, no matter how bad the weather was, and the regularity of the operational sorties was outstanding. For example, during the period from August 1944 to June 1945 at Tiree, only one or two of the scheduled four flights per day were cancelled for weather reasons (personal communication from Fred Gee who was a meteorological air observer with 518 Squadron during this time).

By definition the flights were sent out to enable weather to be observed, and it was not infrequently far from clear in advance exactly what weather would be experienced; some of this proved to be very bad, indeed hazardous, especially during night flights. Because of the lack of de-icing equipment, airframe icing was a particular problem with the Halifax aircraft. On occasions (e.g. 10 February 1945) aircraft were struck by lightning. Turbulence was also a notable and unwelcome feature of the 950 mb legs during the winter because, all too frequently, cumulus and cumulonimbus clouds seemed to have their bases at or near this level, so the aircraft was constantly being bounced up and down.

The sorties had to be flown on standard tracks, using standard flight procedures which had been designed to enable as much useful meteorological information as possible to be obtained from each flight. This program called for a high degree of flying discipline and, inevitably, the constant repetition of routine manoeuvres during long flights, day after day, led to more than a little boredom on the part of the pilot.

Clearly the captain had overriding responsibility for the safety of the aircraft and its crew, and in the event of trouble he had to decide if and when it became essential to modify the standard flight procedures or even to abort the flight. Enemy action was not a problem to meteorological reconnaissance aircraft operating from Tiree. But the flight tracks went far out over the Atlantic where there was no possibility of making an emergency landing, and the chances of successful air-sea rescue if forced to ditch far from home were slender.

The most worrying part of the flight from the captain's point of view was the climb from 50 ft to 500 mb at the end of the first leg. The aircraft was then at its maximum distance from base (about 500 nautical miles) and, after three hours or so flying at low level, the engines were called upon to produce more or less sustained full power for the climb. The likelihood of engine failure was at a maximum at this stage of the flight and there were often the added problems of airframe and engine icing. For example, on one occasion, after the aircraft had managed to reach 10 000 ft, airframe icing became so severe that even the relatively unladen aircraft was brought down to 4000 ft before level flight could be maintained. A different type of icing was responsible for serious trouble on the first operational sortie using the Hastings aircraft (see below).

Two especially hazardous flights

In retrospect after more than 35 years, two flights in particular stand out as examples of the sort of extreme difficulties that could occur.

During the climb at the end of the first leg in a Halifax aircraft, at about 10 000 ft there was a muffled bang followed by an immediate yaw to starboard. The same thing happened again two minutes later. By then oil pressure on the starboard outer engine had fallen to zero and use of the feathering button had no effect at all. Increased drag was apparent and, although the aircraft continued to fly, it was immediately decided that the sortie would have to be aborted. After what must have seemed a very long leg, the aircraft was landed successfully at Aldergrove, and it was then found that a large part of the engine nacelle and fairings was completely missing. Subsequent investigation by AIB established the cause of the accident as the explosion of two fire bottles set off by displacement of part of the primitive cabin heating system so that certain pipes became red hot in the engine exhaust. Although it could not be proved, this incident suggested a possible cause for the unexplained disappearance of a Halifax on a previous operational mission.

The other especially memorable flight, on 14 December 1950, was the first operational sortie using a Hastings aircraft; as flight commander, Bill Mackie acted as captain on this flight. From earlier RAF flying with this aircraft, there had been a suggestion that difficulties might sometimes arise due to what was known as 'oil coring', i.e. the freezing of oil in the engine oil cooler, but before this incident there was nothing concrete to go on. Although in 1950 flights were scheduled as daylight trips, for various reasons take-off on this occasion was delayed so that the climb at the end of the first leg was made in darkness. During the ascent, first one, then two, three and finally all four engines developed dangerous drops in oil pressure due to coring. One of the few advantages of the North Atlantic in winter from the flying point of view is that the sea temperature never falls to freezing point, so there is at least a possibility of coping with serious icing if the aircraft can successfully be brought down to near the sea surface. On this occasion, using the radio altimeter, the aircraft was levelled off at a height of 100 ft above the sea and the sortie was aborted. Fortunately, despite the very low oil pressures on all four engines they continued to function, and after a long period at this low level the frozen ice cores gradually melted and the oil pressures recovered so that on approaching landfall at Tory Island it was safe to climb again for the final leg over land to Aldergrove. Needless to say, this incident led to the introduction of a modification to the engine lubrication system to prevent recurrence.

Postscript

As a practising forecaster during the period of operation of the meteorological reconnaissance flights, I should like to record the gratitude of all forecasters for the fact that these invaluable observations appeared so regularly on our charts; without them, the charts would have been bare indeed to the west of the British Isles. Although at the time the aircrew must sometimes have wondered why they were given these rigid schedules, tracks and flight procedures, there is no doubt whatever about the value of their contribution. I should also like to thank Captain Mackie for the care and patience with which he recalled for me his experiences with the meteorological reconnaissance flights.

551.5:06:551.509.1:35:519.7

The use by the Meteorological Office of decyphered German meteorological data during the Second World War

By R. P. W. Lewis

(Meteorological Office, Bracknell)

Summary

An account is given of some aspects of the interception and decypherment of broadcast meteorological data from Axis-occupied Europe during the Second World War and how these data were used by the Central Forecasting Office of the Meteorological Office.

The fall of France in June 1940, following the occupation of Denmark and Norway, meant that the supply of meteorological information from most of the continent of Europe to the United Kingdom was cut off, and thus the means were no longer available of constructing the actual and forecast weather charts that were of vital importance for prosecuting aerial warfare. It is a remarkable fact, therefore, that within a year or two British Intelligence was able to supply the Central Forecasting Office at Dunstable with information of such good quality, so fast, that surface and upper-air charts could be plotted, covering the whole of Axis-occupied Europe, that for something like two-thirds of the time were nearly as good as if there had not been a war on at all.

This was principally due to two facts. The first was that German military installations were spread so widely that communications had largely to be conducted by radio transmission and could thus be intercepted, and the second was the skill and devoted hard work of the meteorological section of the Government Code and Cypher School (GC and CS) at Bletchley Park. The work at Bletchley Park has received considerable publicity in recent years, particularly in connection with the decyphering of the German 'Enigma' messages. Many other codes and cyphers were, however, tackled at Bletchley Park, among them the meteorological ones, and success in this latter field had, indeed, important repercussions on the Enigma work.

The precise methods by which the German cyphers were broken have not been explained. One may be certain, however, that laborious persistence in collating days and weeks of broadcast messages known or suspected to be meteorological, and the exploitation of minor weaknesses and blunders on the part of the Germans must all have played a part. It is clear from works such as that by Kahn (1966) that success in code and cypher breaking in real life is very much in line with Edison's description of genius as one per cent inspiration and ninety-nine per cent perspiration.

The principal German meteorological cyphers were based on trigraph substitution tables (Benkendorff 1946) such that all possible three-digit groups from 000 to 999 were replaced by alternative arbitrary groups. For most of the war, a five-digit group in the ordinary international (Copenhagen) meteorological code would first be replaced by a six-digit group such that the sum of the third and fourth digits, modulo 10, was equal to the third digit of the original group. For example, 12345 could be written as 127645, or 128545, or 121245. The six-digit group would then be encyphered by splitting it into two three-digit groups and applying the substitution tables. Different tables were used at different hours of the day, and from time to time new sets were introduced.

In addition to encyphering conventional surface observations set out in the well-known international code, the Germans also found it necessary, owing to rapid technological advances, to devise new types of code for upper-air information obtained from balloons, sondes, and aircraft reconnaissance flights (the 'Zenith' code); messages in the form of these new codes would then be themselves encyphered. The decyphering of intercepted messages whose basic structure is not understood is clearly a much more difficult problem, and success here may well have depended to some extent on the adventitious capture of coding-sheets and log-books from shot-down aircraft or pilots.

In addition to the purely meteorological value of the work of the Meteorological Unit at Bletchley Park, it was also of great importance in helping to crack the German naval Enigma as is explained by Hinsley (1979):

> From the same date, the spring of 1941, a similar bonus was derived from GC and CS's work on the systems which most countries had introduced at the outbreak of war for encoding the reports transmitted by their meteorological stations. As the reading of these cyphers was in any case of operational importance, and indispensable for the weather forecasting of the Meteorological Office, it required careful organisation and absorbed an increasing amount of labour; although the cyphers were relatively simple, large numbers of them existed and they had to be read with next to no delay. But one of them, the German naval meteorological cypher, turned out to be of especial importance. It was first broken in February 1941 and in May of that year the Meteorological Section at GC and CS discovered that it carried weather reports from U-boats in the Atlantic which had originally been transmitted in the naval Enigma. Thereafter its decrypts were no less useful than those of the dockyard cypher in helping to break the Enigma keys. As we shall see, they were also to be valuable by providing direct statements of the positions of U-boats when the U-boat Command decided that the U-boats must disguise the positions they announced in their Enigma signals.

Examples of the success of GC and CS during periods when the cypher tables had been largely solved, and of their comparative failure immediately after the introduction by the Germans of a new set of tables, are shown in Figs 1–4. Only surface charts are shown, because the presence or absence of decyphered data show up more dramatically than on the upper-air charts, but this should not be taken to mean that upper-air data were unimportant; they were, indeed, extremely important for the conduct of Bomber Command's operations. Ratcliffe (1984) has explained how surface and upper-air observations were used during the War to forecast winds and temperatures to as high as 200 mb; the application of the techniques developed by Swinbank, Petterssen and others would have been impossible had not GC and CS supplied Dunstable with most of the data from occupied Europe. The forecasts for D-day, too, would have been far inferior in the absence of this information (Stagg 1971).

References

Benkendorff, R.	1946	The German Meteorological Service in War. (Unpublished, copy available in the National Meteorological Library, Bracknell.)
Hinsley, F. H.	1979	British Intelligence in the Second World War, Volume One. London, HMSO.
Kahn, D.	1966	The Codebreakers. London, Weidenfeld & Nicholson.
Ratcliffe, R. A. S.	1984	Some aspects of weather forecasting for the RAF during the Second World War. *Weather*, **39**, 219–221.
Stagg, J. M.	1971	Forecast for Overlord. London, Ian Allen.

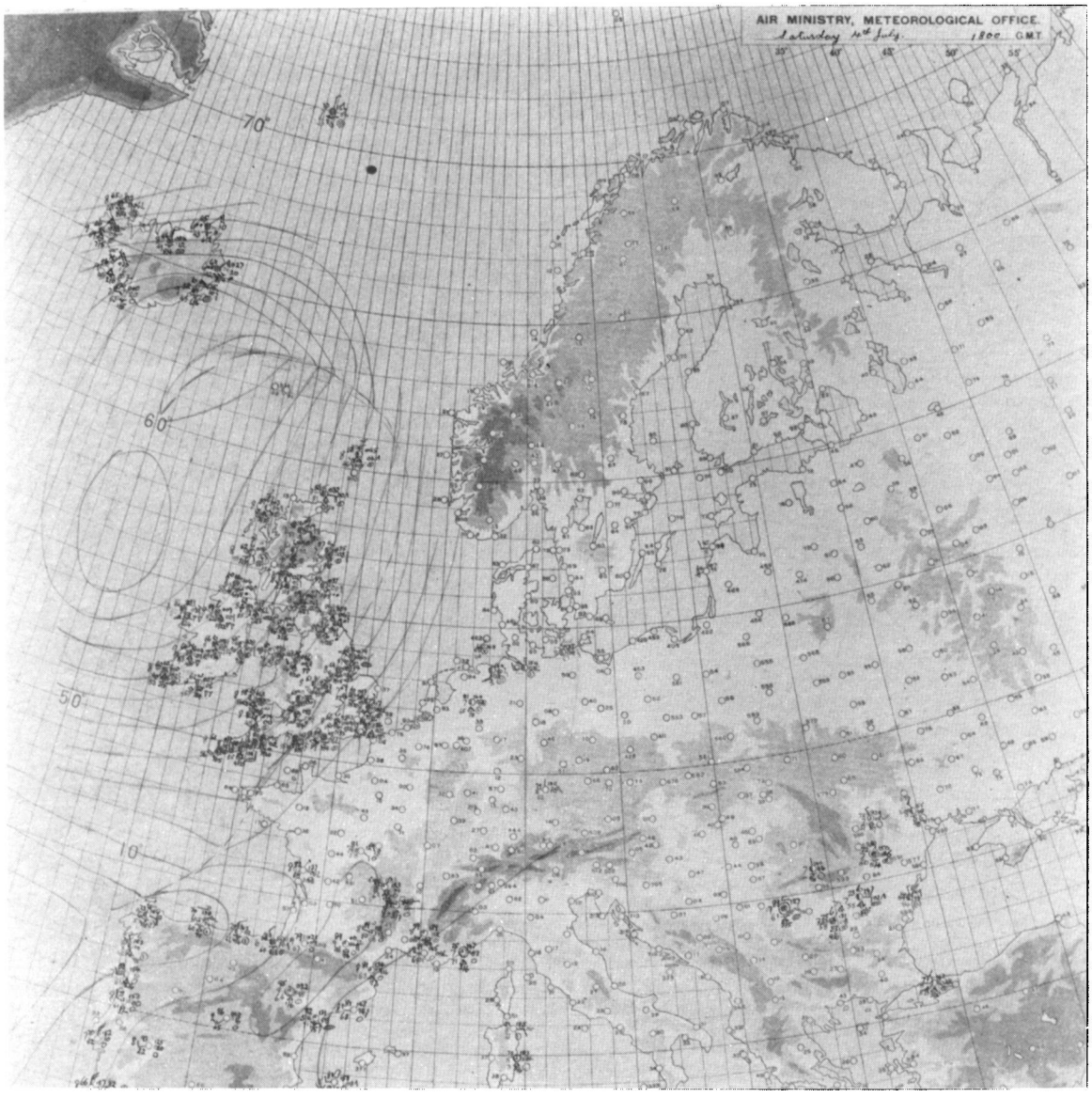

Figure 1. Surface chart as plotted and analysed in the Central Forecasting Office, Dunstable showing decyphered observations from German and other sources over enemy-occupied Europe 4 July 1942 at 1800 GMT.

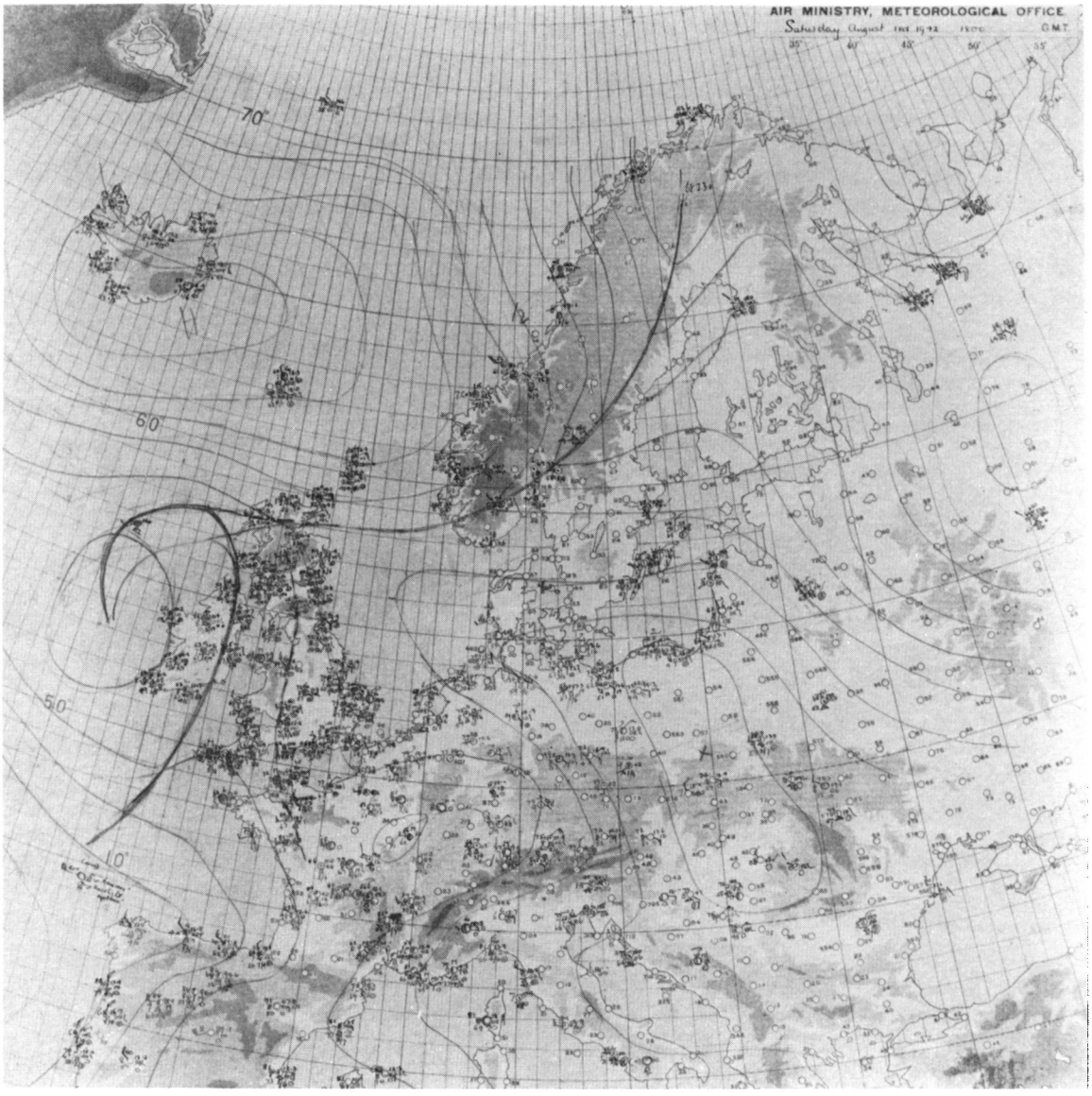

Figure 2. As Fig. 1 for 1 August 1942 at 1800 GMT.

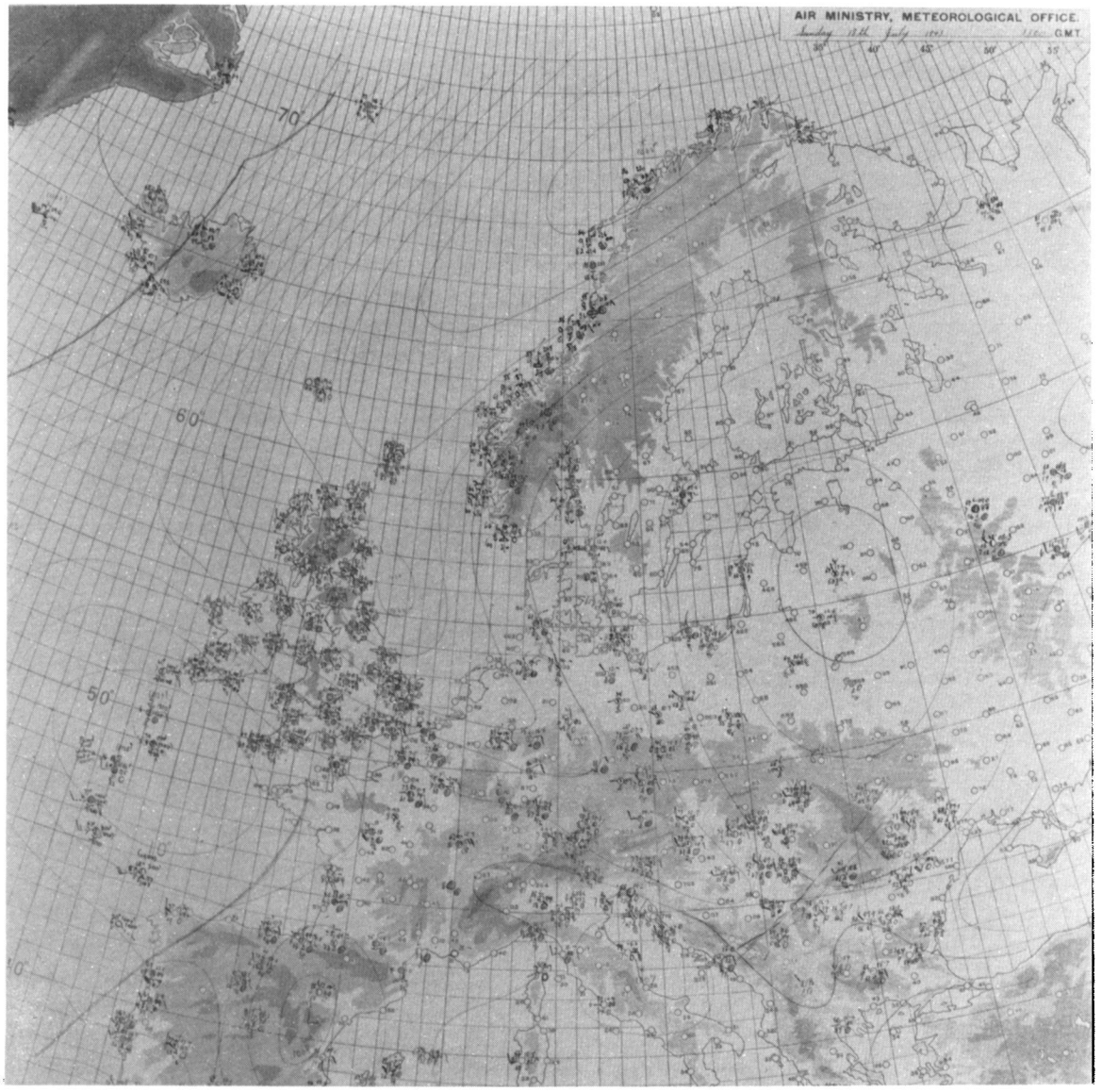

Figure 3. As Fig. 1 for 18 July 1943 at 1300 GMT.

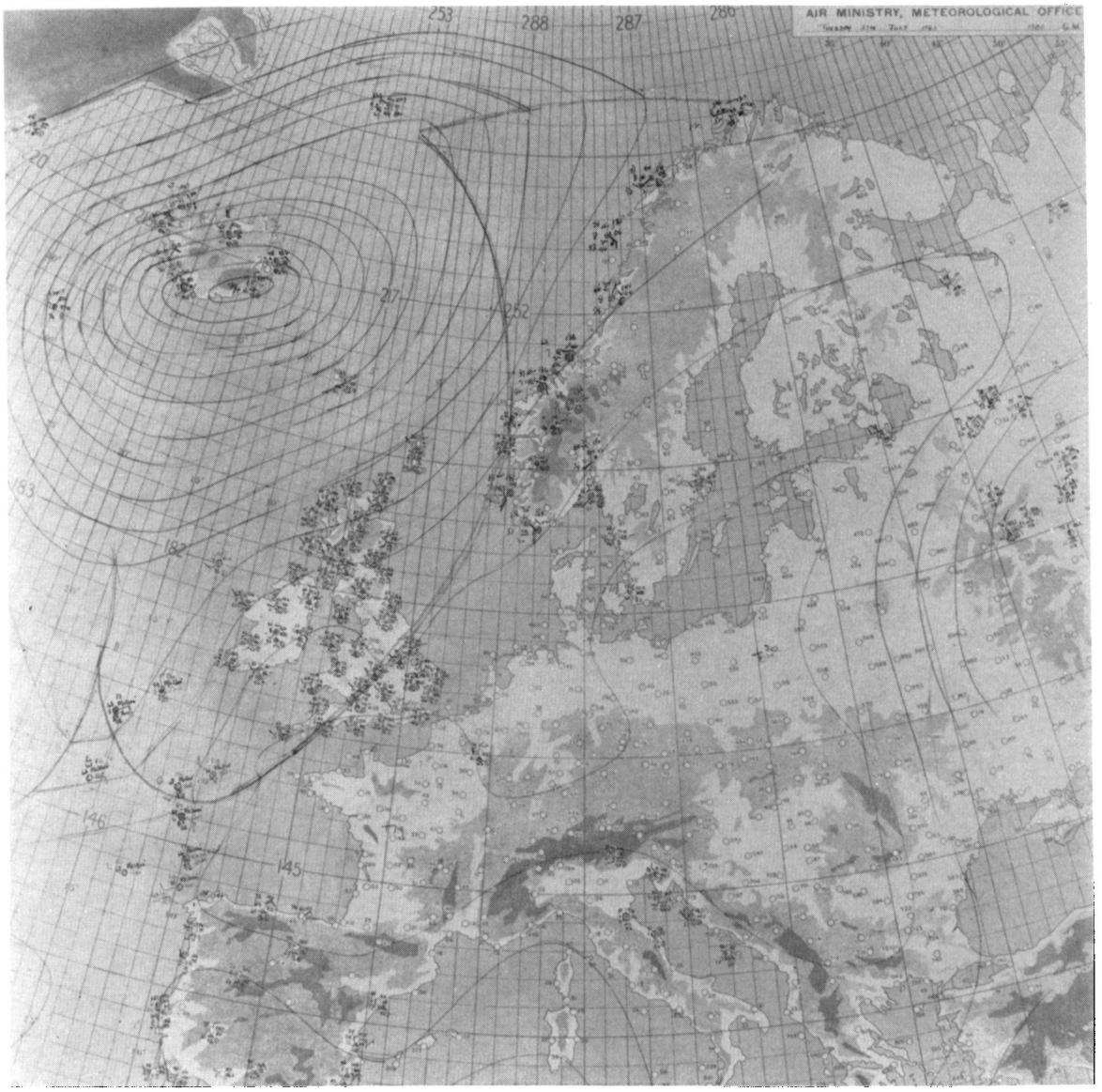

Figure 4. As Fig. 1 for 27 July 1943 at 1300 GMT.

551.5:06(a):556.02

World Meteorological Organization Commission for Hydrology (CHy) Seventh Session, Geneva, 27 August–7 September 1984

By B. R. May

(Meteorological Office, Bracknell)

Every day we are reminded of the importance of water in our lives. The present drought in Ethiopia with its attendant human misery demonstrates how dependent are many developing countries on the efficient use of much-needed water supplies. In contrast, many countries are still ravaged periodically by floods, bringing danger to lives, health and property. It is fitting, then, that one of the WMO's five major programs should be the Hydrology and Water Resources Programme (HWRP), regarded as a means of encouraging activities both within and between countries in tackling these and other problems. The co-operation with water-related programmes of other international organizations.

Operational Hydrology Programme (OHP), particularly the Hydrological Operational Multipurpose Sub-programme (HOMS),

Applications and Services to Water Resources, and

co-operation with water-related programmes of other international organizations.

Much of this session of the Commission was devoted to reviewing progress in these areas and planning future activities.

OHP/HOMS was recognized as a successful means of transferring hydrological 'know-how', particularly from developed to developing countries. With its distribution of National Reference Centres, a manual of over three hundred information components contributed by twenty-six countries and subject to more than six hundred requests, HOMS has already demonstrated its worth. It was agreed, though, that more feedback on the value and applicability to the user of the transferred information was required to increase its effectiveness.

The Applications and Services to Water Resources Programme is intended to bring together hydrological and meteorological activities in support of water resource development. The collection and processing of the data needed for these developments and for the protection of the environment are seen as important factors here.

Many other international organizations have activities in the field of hydrology, particularly UNESCO with its International Hydrological Programme. The need for inter-organization collaboration to increase the effectiveness of WMO activities in operational hydrology was stressed.

Within the two weeks of formal meetings of the session, a two-day technical conference on the use of microprocessors and microcomputers, along with an exhibition of equipment, was organized.

The UK delegation consisted of Mr C. V. Smith and Mr B. R. May of the Meteorological Office and Dr J. C. Rodda and Mr M. A. Beran of the Institute of Hydrology; Dr Rodda also attended in his capacity as Secretary of the International Association of Hydrological Sciences. Over one hundred delegates from fifty-one countries attending the session unanimously approved Dr O. Starosolszky of Hungary and Mr A. J. Hall of Australia as President and Vice-President respectively for the next four-year intersessional period. Three working groups, on instruments, data collection and hydrological models were formed and twenty-eight rapporteurs appointed; Mr M. A. Beran was appointed as rapporteur on the World Climate Programme, Water Component. The appointment of the Advisory Working Group completed the list of members who are to carry out the vigorous programme of work of the Commission during the next four years.

Review

Climatic changes on a yearly to millennial basis, edited by N. A. Mörner and W. Karlen. 155 mm × 240 mm, pp. xviii + 667, *illus.* D. Reidel Publishing Company, Dordrecht, Boston, Lancaster, 1984. Price Dfl 210.00, US$79.00.

This book contains the Proceedings of the Second Nordic Symposium on Climatic Changes and Related Problems held in Stockholm in May 1983. This international symposium was particularly concerned with Nordic records and their relation to global climatic changes. Of the more than 60 papers presented, 52 are included in this volume together with 3 invited contributions. The contents have been divided into four sections — the Deglaciation period, the Holocene, the last 1500 years and finally a discussion of models and mechanisms. Case studies of the Deglaciation period concentrate on southern Scandinavia, the French Alps and Mexico, while vegetation and sedimentary studies from the Holocene include areas as far apart as west Greenland and Lake Chad. The largest number of papers is in the section on the last 1500 years and among the subjects considered in detail are the dendrochronology records in Sweden and in Washington State, USA, and the evidence for links between settlement, agricultural changes and climate. Models and mechanisms are considered in a rather more perfunctory way although there are interesting papers on the effect of solar activity on the earth's atmosphere and on atmosphere–cryosphere interactions.

Scandinavia is a classical area for the study of climatic fluctuations during the last 20 000 years, and the symposium has concentrated on regional processes and data, taking care to distinguish between local, hemispherical and global climatic changes. Indeed one of the major conclusions of the conference was that none of the sometimes rapid climatic changes and shifts during the last 20 000 years has been of global extent and therefore it is redistribution of heat over the globe, regionally and hemispherically, that is of prime importance. One of the editors (N. A. Mörner) in an epilogue suggests that storage and transformation of heat due to oceanographic processes and particularly as a result of differential rotational changes, closely linked to gravitational changes, may represent the primary driving mechanism of climatic change.

This is a stimulating collection of papers, and of particular interest are the many contributions from Scandinavian scientists who are not so well known outside their own countries. This is not to decry the famous names who are well represented and lend the volume authority. Too many of the diagrams are unfortunately difficult to interpret because of their small size and it is a pity that the paper quality of the book is so poor.

Climatic changes at high latitudes of the northern hemisphere have for long been regarded as of great importance, since general trends appear to be magnified in such areas. Scandinavia is an ideal 'laboratory' not only for studying climatic changes but also for measuring the effects of climate on society. The Stockholm symposium brought forward a wealth of new observational data and theories about its interpretation, and the appearance of this collection of papers will be widely welcomed.

A. H. Perry

THE METEOROLOGICAL MAGAZINE

No. 1353 April 1985 Vol. 114

CONTENTS

NOTICE

It is requested that all books for review and communications for the Editor be addressed to the Director-General, Meteorological Office, London Road, Bracknell, Berkshire RG12 2SZ and marked 'For Meteorological Magazine'.

The responsibility for facts and opinions expressed in the signed articles and letters published in this magazine rests with their respective authors.

Applications for postal subscriptions should be made to HMSO, PO Box 276, London SW8 5DT.

Complete volumes of 'Meteorological Magazine' beginning with Volume 54 are now available in microfilm form from University Microfilms International, 18 Bedford Row, London WC1R 4EJ, England.

Full-size reprints of Vols 1–75 (1866–1940) are obtainable from Johnson Reprint Co. Ltd, 24–28 Oval Road, London NW1 7DX, England.

Please write to Kraus Microfiche, Rte 100, Millwood, NY 10546, USA, for information concerning microfiche issues.

HMSO Subscription enquiries 01 211 8667.

Printed in England for HMSO and published by
HER MAJESTY'S STATIONERY OFFICE

£2.30 monthly

Dd. 737126 C13 4/85

Annual subscription £27.00 including postage

ISBN 0 11 727558 1
ISSN 0026–1149

THE METEOROLOGICAL MAGAZINE

HER MAJESTY'S STATIONERY OFFICE

May 1985

Met.O. 967 No. 1354 Vol. 114

METEOROLOGICAL OFFICE Met.O.967

THE METEOROLOGICAL MAGAZINE

No. 1354, May 1985, Vol. 114

551.513.1:551.521.1

Simulation of the earth's radiation budget with the 11-layer general circulation model

By A. Slingo

(Meteorological Office, Bracknell)

Summary

This article examines the components of the earth's radiation budget as simulated by the first integration of the Meteorological Office 11-layer atmospheric general circulation model through a complete annual cycle. Comparisons with two independent satellite data sets are used to assess the quality of the simulation and also to highlight disagreements between the satellite data themselves. The model employed cloud amounts and heights taken from climatological data, thus providing a useful reference against which results from subsequent integrations with model-predicted cloudiness may be compared.

1. Introduction

1.1 *The earth's radiation budget*

It is well known that the ultimate energy source which drives the general circulations of the earth's atmosphere and oceans is the absorption and emission of electromagnetic radiation (Gill 1982, Houghton 1984). Short-wave radiation from the sun at wavelengths between about 0.2 and 5 μm is absorbed mainly at the surface, but also to a lesser degree by clouds and by minor atmospheric constituents such as water vapour, ozone and carbon dioxide. About 30% of the incident radiation is reflected back to space by clouds, the surface, and by Rayleigh scattering from the atmosphere itself. The largest contribution to the reflected flux comes from clouds, because of their high reflectivity and extensive coverage (on average about half the globe is covered by clouds at any instant). By reducing the short-wave radiation available for absorption, clouds act so as to cool the earth–atmosphere system. This is often referred to as the 'albedo effect'. The contribution from the surface is generally smaller than that from clouds, but is enhanced considerably over snow- and ice-covered surfaces.

The earth's radiation budget is balanced by the emission of long-wave (heat) radiation back to space, at wavelengths between about 4 and 100 μm. The important difference compared with the short-wave spectral region is that the atmosphere is a strong absorber, and hence also a strong emitter, of long-wave radiation in a series of spectral bands. This is because the minor constituents have many vibrational and rotational energy transitions which may be excited by radiation at these wavelengths. The absorption by

water vapour is especially important, because it is considerable across the entire long-wave spectrum apart from the 8–13 μm region, which is commonly known as the 'atmospheric window'. Water droplets are even more efficient absorbers at all wavelengths beyond about 2 μm, so that most clouds absorb essentially all the long-wave radiation incident on them and emit radiation similar to that of a black body at the temperature of the cloud boundary. The absorption by the minor constituents and by clouds has a profound influence on the earth's climate through the so-called 'greenhouse effect'. The net long-wave cooling of the surface is reduced considerably by the downward long-wave flux from the atmosphere. The long-wave energy radiated back to space is also reduced because the radiation from the surface is absorbed and replaced by that from higher, and hence colder, levels. The system is, therefore, much warmer than if the clouds and the atmosphere were transparent to long-wave radiation.

1.2 *Representation of clouds in numerical models*

It will be clear from the above that numerical models of the atmospheric general circulation need to include schemes for calculating both the short-wave and long-wave radiative fluxes, not only within the atmosphere but also at the surface. There are many problems associated with the design of radiation schemes, for example in the choice of spectral resolution and the treatment of the minor constituents. However, the fundamental problem is in the representation of clouds, because of their significant effect on the fluxes. In most synoptic situations the cloud field has a complex structure, with different cloud types at several levels and of various horizontal and vertical extents. The radiation scheme must be designed so that it can cope with such a configuration, within the constraints of the limited vertical and horizontal resolution of the model. The effect of clouds must be modelled carefully in both spectral regions, because the net radiative effect of clouds on climate is a subtle balance between their contributions to the albedo and greenhouse effects. This means that care must be taken firstly to use realistic cloud amounts at each model level and secondly to choose radiative properties which are appropriate for each cloud type.

There are two distinct approaches to determining the cloud amounts to be used in an integration. Firstly, one can attempt to predict the cloud amounts explicitly for each grid point at each level from the other model variables. Unfortunately, there is no general theory of cloud formation which can be used to guide the modeller in this area. It is therefore common practice to use simple parametrizations based on the concept that the cloud amount in a model layer must be related in some general way to a parameter such as the mean relative humidity, which can be calculated easily from the model variables (Slingo 1980). The coefficients of such a parametrization may then be tuned so that the mean cloudiness produced by the model agrees with climatological estimates. This approach allows the model to reproduce some of the complex feedbacks associated with changes in cloud cover, but there is of course no guarantee that these feedbacks will be properly represented. It is quite possible that the increased degrees of freedom in a model with interactive cloud will lead to less realistic simulations than for a more highly constrained model. In the second approach, cloud amounts are therefore fixed at climatological values throughout an integration, which for many applications is an acceptable compromise. Unfortunately, reliable information on the vertical distribution of cloudiness is at present available only as zonal averages. Many integrations have therefore been performed with fixed cloud amounts which are a function of latitude and height only.

Whatever approach is chosen for the cloud amounts, it is also necessary to decide how to model the cloud optical properties, i.e. the long-wave emissivity and the short-wave reflectivity (albedo), transmissivity and absorptivity. For most water clouds the emissivity is essentially unity but this is not the case for cirrus, for which it is a strong function of the ice crystal content. Observational and theoretical studies have also shown that the short-wave properties are strong functions of microphysical

parameters such as the number and size distribution of the water drops and macrophysical parameters such as the cloud thickness and shape. Detailed radiation schemes are now available which can predict the optical properties from these parameters. Good agreement has been obtained between the fluxes from such schemes and aircraft measurements (e.g. Stephens *et al.* 1978, Slingo *et al.* 1982). Such schemes can, in principle, be used directly in a model and many interesting developments are taking place in this area. However, it is impossible to predict all the required input parameters from the model variables, so that most have to be prescribed. The alternative approach used until recently in most models is to prescribe the optical properties themselves for each cloud type at the values most commonly observed. This allows a less elaborate but faster radiation scheme to be used.

1.3 *Model verification*

With so many approximations, it is important to verify that the radiation scheme used in a numerical model is producing realistic fluxes within an integration. It is difficult to make global comparisons for the surface fluxes because of the sporadic distribution of surface radiation stations. However, satellite measurements of the earth's radiation budget afford an excellent opportunity to compare the model fluxes at the top of the atmosphere with observations at similar resolution, obtained over several years. In this article, radiation budget quantities from the first annual-cycle integration of the Meteorological Office 11-layer atmospheric general circulation model (GCM) are compared with two independent satellite data sets. The 11-layer model is under development in the Dynamical Climatology Branch as part of an integrated model for studying climate, which will also include an ocean GCM and a sea-ice model.

2. The 11-layer model

2.1 *Background and basic structure*

Numerical modelling of the atmospheric general circulation in the Dynamical Climatology Branch began with the development of the 5-layer model (Corby *et al.* 1972, Corby *et al.* 1977) which was integrated on the Science Research Council's 'Atlas' computer and subsequently on the Meteorological Office's IBM 360/195 computer (Hinds 1981). This model has been used in several studies, notably of the atmospheric response to sea surface temperature anomalies (Rowntree 1976), of the effect of soil moisture anomalies on the summer circulation (Rowntree and Bolton 1983), of the factors which control the earth's radiation budget (J. M. Slingo 1982) and of the effect of increases in carbon dioxide concentrations on climate (Mitchell 1983). In many respects the 11-layer model is very similar, with the obvious difference of enhanced vertical resolution. The model is a primitive equation global GCM with 11 unevenly spaced layers and sigma (pressure divided by its surface value) as the vertical coordinate (Fig. 1). The horizontal grid in the version used here is 2° in latitude, with the number of points in each row progressively reduced towards the poles, so as to maintain a roughly uniform resolution of about 220 km. A leap-frog integration scheme with time smoothing and non-linear horizontal diffusion is employed. A limited-area version of this model was used in the GARP Atlantic Tropical Experiment (Lyne *et al.* 1976) and for experiments with a cloud parametrization scheme (Slingo 1980). Global integrations on the 360/195 were mostly of 50 days duration with fixed external forcing conditions for either January or July.

Physical processes are modelled in four subroutines, which deal with boundary-layer and surface exchanges, convection, large-scale precipitation and finally radiation and clouds. The boundary layer is assumed to occupy the lowest three model layers in all conditions, and transfers of heat, moisture and momentum between the layers are modelled by an eddy diffusivity approach (Carson 1982a, b). A more

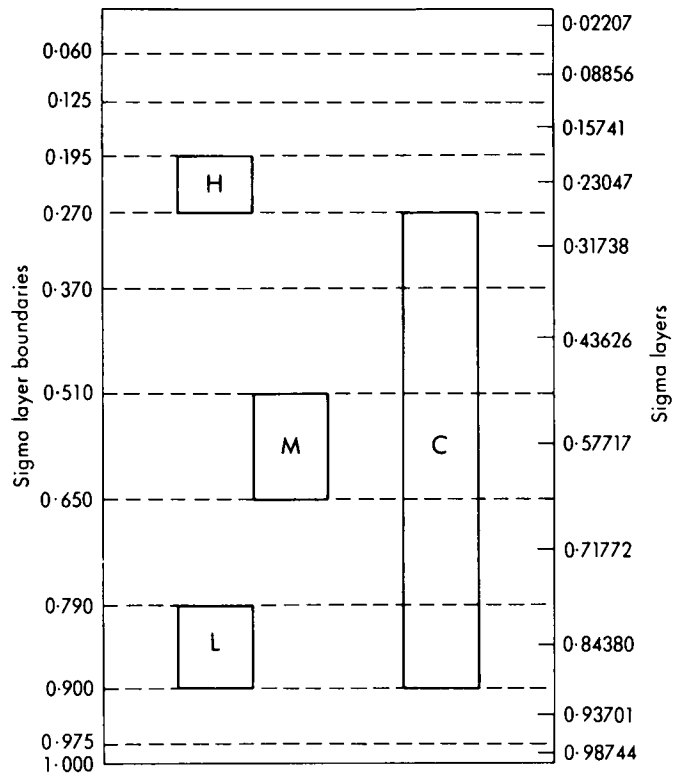

Figure 1. Vertical resolution of the 11-layer model and a possible configuration of the high (H), medium (M) and low (L) layer clouds and a convective tower (C).

general scheme in which the number of model layers within the boundary layer is allowed to vary has also been developed (e.g. Heasman 1983) and has been adapted for the Meteorological Office operational numerical weather prediction model (Gilchrist and White 1982, Dickinson and Temperton 1984). Both schemes have the same treatment of the surface with interactive soil moisture and snow depth, similar to that used in the 5-layer model (J. M. Slingo 1982). Evaporation is limited for soil moisture less than 5 cm of water and runoff occurs to prevent the soil moisture from exceeding 15 cm. The convection scheme treats both unsaturated and saturated convection as it penetrates the vertical grid of the model (Lyne and Rowntree 1976) and this has also been incorporated into the operational model. Large-scale precipitation, in the form of rain or snow, is formed whenever the relative humidity exceeds 100%.

2.2 *Treatment of radiation and clouds*

The logical structure of the radiation scheme (Walker 1977) is determined by the cloud configuration (Fig. 1). It is assumed that layer cloud may exist at any one of three levels (high, medium and low) and that convective cloud may also be present. The layer cloud is assumed to be one sigma layer in thickness, but the convective cloud may occupy more than one sigma layer. The clouds overlap randomly in the vertical, except that where layer and convective clouds are present at the same level then the overlap of the layer clouds occurs only in the clear air, after allowance has been made for the convective cloud.

In the short-wave spectral region the absorption by the minor constituents and the absorption and reflection by clouds and the surface are treated in a single spectral band. The absorptivity curves for

water vapour, carbon dioxide and ozone were taken from Manabe and Möller (1961). Pressure scaling is applied only to the water vapour absorber amounts. In reality the absorptions take place in different spectral regions so that the total absorption in such a scheme is simply the sum of that from each gas. As it traverses the atmosphere the incident solar radiation splits into a maximum of five components (direct beam and diffuse beam from each cloud layer). The absorption by the minor constituents is applied to each component and also to the diffusely reflected beams, which for simplicity are assumed to pass out to space without interacting further with the other cloud layers. However, a simple treatment of the enhanced surface absorption due to multiple reflections between cloud and ground is included. For the diffuse beams the gaseous path lengths are multiplied by the usual diffusivity factor, whose value is taken to be 1.67 (Paltridge and Platt 1976). Rayleigh scattering from the air molecules is parametrized very simply by reducing the incident solar radiation by 3%. It is important to note that as a consequence this contributes about 10% to the globally averaged flux reflected back to space by the model. The cloud optical properties are prescribed for each cloud type with the values given in Table I and no account is

Table I. *Cloud short-wave properties assumed in the radiation scheme*

	Cloud type			
	High	Medium	Low	Convective
Reflectivity	0.2	0.6	0.7	0.7
Transmissivity	0.75	0.3	0.2	0.2
Absorptivity	0.05	0.1	0.1	0.1

taken of the dependence of these properties on the solar zenith angle or cloud thickness. The surface albedos are 0.06 (sea), 0.2 (land), 0.5 (snow-covered land) and 0.8 (sea-ice and land-ice; e.g. Antarctica and Greenland). A more realistic geographical distribution of the snow-free land surface albedo for the model has recently been incorporated as part of a joint project with Liverpool University.

In the long-wave region, seven spectral divisions are used to represent the complex wavelength dependence of atmospheric absorption and emission. These divisions are grouped into five distinct intervals as shown in Table II. The first interval treats both the 6.3 μm vibration/rotation band and the

Table II. *Division of the long-wave spectrum*

	Spectral interval						
	1	2	3	5	4	5	1
Wavenumber limits (cm^{-1})	0–500	500–700	700–800	800–900	900–1100	1100–1200	1200–2850
Wavelength limits (μm)	∞–20	20–14.3	14.3–12.5	12.5–11.1	11.1–9.1	9.1–8.3	8.3–3.5
Water vapour	✓	✓	✓	✓	✓	✓	✓
Carbon dioxide		✓	✓				
Water vapour continuum			✓	✓	✓	✓	
Ozone					✓		

far infra-red rotation band of water vapour. The second and third intervals deal with the overlap between water vapour and the well-known 15 μm band of carbon dioxide. The final two intervals cover the contributions in the atmospheric window from weak water vapour bands, the 9.6 μm band of ozone (which is important in the stratosphere) and the water vapour continuum. The continuum is so called because the absorption coefficient varies only slowly with wavelength, as opposed to the rapid fluctuations for band absorption (Bignell 1970). A component of the continuum absorption has been found to be dependent on the partial pressure of water vapour, which in moist profiles leads to a

significant increase in the atmospheric radiative cooling near the surface. The mathematical method used to calculate the long-wave fluxes in the scheme is known as the emissivity approximation (e.g. Liou 1980). Emissivities and transmissivities for each gas in each interval at a temperature of 263 K are stored in the program as look-up tables and were calculated by applying the random-band model of Hunt and Mattingly (1976) to the spectroscopic data of McClatchey *et al.* (1973). The gaseous absorber amounts are scaled to take account of the pressure dependence of the absorption, but the temperature dependence is ignored. Clouds and the surface are assumed to absorb and emit as if they were black bodies, but the amounts of high cloud used in the long-wave calculations are halved as a simple representation of the lower emissivities which have been observed for cirrus. More recently, the long-wave part of the scheme has been revised following detailed comparisons with other schemes (Slingo and Wilderspin 1984).

2.3 *The first annual-cycle integration*

The first integration of the 11-layer model through a complete annual cycle was carried out on the Cray-1 computer at the European Centre for Medium Range Weather Forecasts, using some of the time allocated to the United Kingdom as a member state (Cunnington 1983). The integration was run for just over 500 model days, starting from an analysis for 25 July 1979 produced by the assimilation version of the model during the First GARP Global Experiment (Lyne *et al.* 1982). The sea surface temperatures, sea-ice limits and cloud amounts were prescribed and updated in the same way as for the annual-cycle integrations of the 5-layer model (J. M. Slingo 1982). The zonally averaged cloud amounts were taken from surface-based climatologies as described by Bolton (1981). Ozone concentrations were also prescribed and updated monthly. Apart from other applications, such an integration is useful in assessing runs with the cloud-prediction scheme, because with prescribed climatological cloud amounts one has a right to expect that the model should produce a realistic radiation budget, at least in the zonal mean. One can therefore hope to separate errors due to the radiation scheme and the rest of the model from those due solely to the prediction of unrealistic cloud amounts. The results presented in this article were taken from the last year of this integration.

3. Satellite data

The use of satellite measurements for studying the earth's radiation budget and the data currently available have been discussed, for example, by Stephens *et al.* (1981), J. M. Slingo (1982) and Ohring and Gruber (1983). Further information on the satellites themselves has been given by the Satellite Meteorology Branch (1982). Two independent compilations are used here:

(i) Data from the series of operational meteorological satellites launched by the US National Oceanic and Atmospheric Administration (NOAA) are described by Gruber and Winston (1978). A 45-month climatology from 1974 to 1978 has been compiled by Winston *et al.* (1979). These data have good spatial resolution (2.5° latitude), but in both the short-wave and long-wave spectral regions they are derived from measurements in narrow spectral intervals (approximately 0.5–0.7 μm and 10.5–12.5 μm respectively) and regression techniques are used to produce the broad-band fluxes. This introduces uncertainties which are especially serious in the short-wave region, as it is known that the radiative properties of clouds, land surfaces, snow and ice are all strong, and different, functions of wavelength.

(ii) Data from various research satellites, such as Nimbus 6, were collected by Stephens *et al.* (1981) and presented in diagrammatic and tabular form. The measurements are of low spatial resolution but they are for broad spectral bands.

Both these compilations are from measurements by polar-orbiting satellites and it is important to appreciate the limitations of such data. The height of a polar-orbiting satellite (roughly 1000 km) and the inclination of its orbit to the earth's equator (about 99°) are normally chosen so that the orbit precesses

around the earth's axis once per year. As a result, the satellite is 'sun-synchronous' and each equator crossing takes place at the same local (solar) time. Each point near the equator is thus sampled only twice per day, typically once in daylight and once at night (giving one short-wave and two long-wave measurements), whereas at higher latitudes the increasing overlap of the areas covered by each overpass leads to more frequent sampling. Sun-synchronous satellites therefore give only limited information on the diurnal variation of the radiation budget or of cloudiness, which is especially pronounced in the tropics.

It is interesting to note that the first satellite to be designed primarily for radiation budget measurements (launched by the National Aeronautics and Space Administration, USA in October 1984 and called ERBS — Earth Radiation Budget Satellite) is in an asynchronous orbit to provide data at different solar times. The advanced sensors used by ERBS are also mounted on two NOAA operational satellites (NOAA F, launched in December 1984 and NOAA G, to be launched in August 1985) so that comprehensive measurements will be available throughout the duration of the Earth Radiation Budget Experiment (Barkstrom 1984).

4. Results

The components of the earth's radiation budget as modelled and observed are presented here as global and zonal averages through the annual cycle. The geographical distributions from the model will not be shown, as the use of zonally averaged clouds means that these are not directly comparable with the observed distributions. The global averages are also compared with those from a 3-year integration of the 5-layer model, which was studied by J. M. Slingo (1982) and used as a control for experiments with increased carbon dioxide concentrations and sea surface temperatures (Mitchell 1983). The results shown here are from the mean of two years of that run, the differences from the single year studied by Slingo being minimal.

4.1 *Global averages*

The annual means of the global averages from the model integrations and the satellite data sets are given in Table III. Various values for the solar constant have been assumed, that used by Stephens *et al.*

Table III. *Global annual averages of earth radiation budget quantities in model integrations and satellite data sets*

Source	Solar constant ($W m^{-2}$)	Planetary albedo (per cent)	Absorbed short-wave ($W m^{-2}$)	Outgoing long-wave ($W m^{-2}$)	Net radiation ($W m^{-2}$)
11-layer model	1395	32.2	236.3	239.1	-2.8
5-layer model	1395	33.2	233.0	239.2	-6.2
NOAA satellites	1353	31.4	232.0	244.9	-12.9
Research satellites	1376	30.0	240.8	231.9	8.9

(1981) being closest to the value of 1373 $W m^{-2}$ suggested by Neckel and Labs (1981). The annual mean incoming short-wave radiation per unit area at the top of the atmosphere may be found by simply multiplying the value of the solar constant by one quarter. Note that the modelled planetary albedos are slightly higher than the observed values. The 5-layer model albedo is higher than that for the 11-layer model, mainly because of the neglect of the additional absorption by the minor constituents of the short-wave radiation reflected back to space by clouds and the surface. The modelled values of the absorbed short-wave and outgoing long-wave radiation are similar to those observed, although the disparity

between the satellite data sets is quite marked. This disparity is also evident in the values of net radiation, which is the difference between the absorbed short-wave and the outgoing long-wave radiation, and illustrates one of the difficulties in comparing the modelled and observed radiation budgets. In the model integrations the external forcing repeats exactly every year, so that variations in the inter-annual heat storage are negligible. This does not necessarily imply that the annual mean net radiation will be zero, because in integrations with fixed sea surface temperatures the oceans effectively provide an infinite store of heat which can balance any radiative deficit. It is clearly desirable that the modelled annual mean net radiation should be as close to zero as possible, although the magnitude of the deficits shown here is not serious. In the real world the net radiation may well be non-zero, but the large and contradictory values from the satellite data merely reflect the difficulty in estimating the small difference between two large fluxes, which are measured independently with absolute errors as high as 10 W m^{-2} (Stephens *et al.* 1981). This is too large to enable the absolute values of the globally averaged fluxes from the model to be checked rigorously. However, the zonally averaged fluxes show a much larger range with latitude and time of year than 10 W m^{-2}. The satellite data, therefore, do allow a reasonably accurate assessment of whether the pole to equator gradient in radiative heating is being modelled correctly, as will be seen later.

The factors which control the variation of the global means through the year (Fig. 2) have been

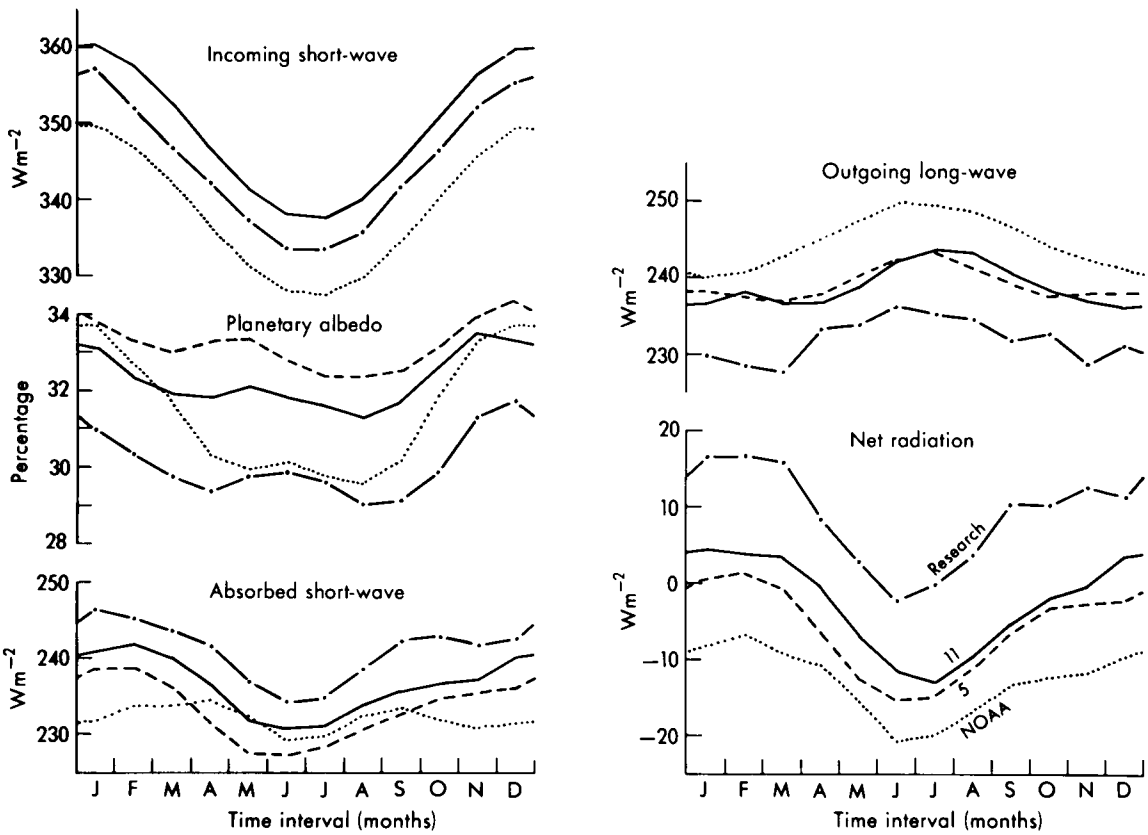

Figure 2. Monthly means through the year of various globally averaged earth radiation budget quantities from the 11-layer and 5-layer model annual-cycle integrations and from NOAA and research satellites. (The solid line in the 'Incoming short-wave' diagram represents both the 11- and 5-layer models.)

discussed by J. M. Slingo (1982) and are worth summarizing briefly. The earth's elliptical orbit produces a roughly sinusoidal variation in the incoming short-wave radiation with an amplitude of about 7%, the flux being greatest in January when the earth is closest to the sun. The planetary albedo shows a maximum at this time of year owing to the illumination of Antarctica and a weaker maximum in northern spring from the illumination of the northern hemisphere sea-ice and continental snow cover. In all but the NOAA data set the variations in the planetary albedo only partly offset those in the incoming short-wave, so that the forcing from the latter is clearly visible in the absorbed short-wave radiation. The seasonal variation in surface temperature is much greater in the northern than in the southern hemisphere due to the larger land area, so the globally averaged outgoing long-wave radiation is a maximum in northern summer, despite the fact that the incoming radiation is a minimum at this time. The outgoing long-wave is in anti-phase with the absorbed short-wave, so the net radiation shows a strong seasonal variation with a maximum in northern winter. In general the modelled changes agree well with the satellite data, apart from the systematic differences discussed earlier. However, the amplitude of the planetary albedo variations is less than in the satellite data, due to a much weaker maximum in the southern summer, which will be discussed later.

4.2 *Zonal averages*

4.2.1 *Incoming short-wave radiation*. The zonal averages are shown in the form of time–latitude diagrams of the monthly meaned data. These are a convenient way of demonstrating the response of the model to the seasonal changes in the applied forcing. On such a diagram the mean incoming short-wave radiation (Fig. 3(a)) has a characteristic pattern which follows the changing declination of the sun, shown as the dotted line. The shape of the pattern is strongly influenced by the changes in the length of day, especially at high latitudes. For example, at the solstice the permanent daylight over the summer pole leads to a larger mean value than over the tropics. The magnitude of the peak over the South Pole in December is slightly larger than that over the North Pole in June because the earth is closer to the sun. Averaged over the year, however, the two hemispheres should receive identical solar radiation totals. This is not the case in the model integrations, in which various simplifying assumptions were made (J. M. Slingo 1982). As a result, the southern hemisphere received 1.3% more radiation than the northern hemisphere through the year, although this does not affect the results shown here significantly. For a more complete discussion see A. Slingo (1982).

4.2.2 *Albedo*. The two main factors which determine the global albedo (Fig. 3(b)) are the cloud cover and the state of the surface. The albedo is a minimum in the subtropics where the cloud amounts are smallest and there is a weak maximum near the equator from the cloud associated with the Inter-Tropical Convergence Zone (ITCZ). In the southern hemisphere the albedo increases towards about 60°S owing to the extensive cloudiness in the circumpolar depression belt. A marked jump is apparent at 60°S as the edge of the Antarctic sea-ice is reached, the variations at this latitude through the year being due to changes in the imposed sea-ice distribution, which reaches its maximum extent in the southern spring. Further south the albedo is high throughout the year because of the permanent snow and ice cover of Antarctica. In the northern hemisphere the effects of the cloud in the depression tracks and of the imposed sea-ice distribution are also important, but there is an additional contribution from the changes in the continental snow cover, which is not imposed but is predicted by the model. This is largely responsible for the significant seasonal variation in the global albedo between about 30°N and 70°N.

The behaviour of the modelled albedo is in broad agreement with that in the two satellite data sets. However, it is instructive to make the comparison more rigorous by calculating the differences between the modelled and observed albedos, which can be plotted in time–latitude form. This emphasizes the

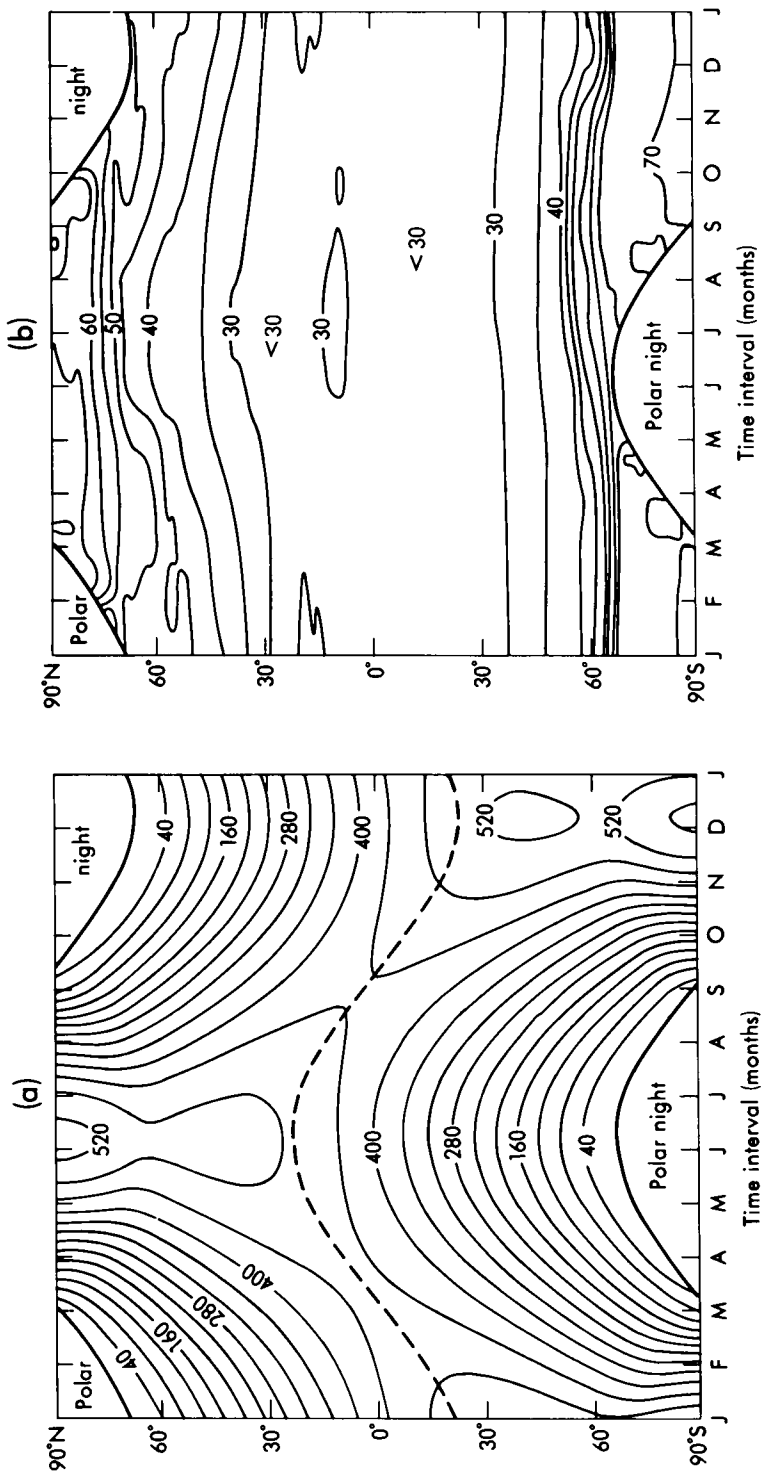

Figure 3. Time–latitude diagrams of the zonal averages of the monthly meaned (a) incoming short-wave radiation (W m^{-2}) and (b) global albedo (per cent) from the 11-layer model.

areas of disagreement between the model and the satellite data sets and also between the satellite data sets themselves. The results are shown in Fig. 4, where the clear areas indicate that the modelled albedo is higher than that from the satellites, the reverse being true in the shaded areas. Over most of these figures there is good agreement between the satellites, so that the errors in the modelled albedos are well defined. An obvious exception is the ITCZ. In the model this feature is artificially broadened because the cloud climatology is specified at 10° latitude intervals. However, the good spatial resolution of the NOAA satellites leads to a realistic representation of the narrowness of the albedo maximum, so that in Fig. 4(a) there is a thin shaded band near the equator where the modelled albedo is too low. There is some suggestion of this feature in Fig. 4(b) but it is much weaker than in the comparison with the NOAA data. Over the rest of the tropics and in the northern hemisphere in summer the albedo from the model is clearly too high, in some places by over 5%, representing a 20% overestimate of the observed value. The importance of clouds in determining the planetary albedo in these areas suggests that either the cloud albedos or the cloud amounts used in the model are too high. Certainly the albedos for low and convective cloud which are assumed (Table I) are at the upper limits of values which have been observed for such cloud.

In the southern hemisphere between about 35°S and 60°S there is a large underestimate of the global albedo, by up to about 10%. A similar underestimate was also noted in the 5-layer model integration (J. M. Slingo 1982) and was attributed to the neglect of the increase of ocean albedo with solar zenith angle. However, the magnitude of the error shown in Fig. 4 and the fact that it occurs over the southern hemisphere depression belt strongly suggests that it is caused by problems with the treatment of clouds. In the southern hemisphere the cloud climatology was taken from Sasamori *et al.* (1972), who took the total cloud cover data compiled by van Loon (1972) and with various assumptions derived a breakdown into the component cloud amounts. However, the combination of these amounts and the assumption in the model of random overlap leads to a significant underestimate of the total cloud cover compared with van Loon's original data. In more recent integrations the component amounts have therefore all been increased so that van Loon's total cloud cover amounts are reproduced. These amounts are also in good agreement with the climatology of Berlyand *et al.* (1980). The use of the revised cloud climatology leads to a marked improvement in the modelled planetary albedo in this region. It also increases the amplitude of the annual variation of the globally averaged planetary albedo to a value much closer to that observed (Fig. 2). This suggests that the marked maximum in the observed globally averaged albedo in the southern summer is caused by the illumination not only of Antarctica but also of the clouds in the circumpolar depression belt, the amounts of which are more realistic in these later integrations.

At the southern edge of the depression belt the modelled albedo is too high, most noticeably from August to November but also to a lesser degree through to March. This suggests that either the sea-ice limits are too far north or the surface albedo for sea-ice is too high. Comparison of the sea-ice distribution with the data of Lemke *et al.* (1980) showed that the sea-ice was much too extensive, owing to a logical error in creating the pentad sea surface temperature data sets. This has been corrected in more recent versions of the model. The surface albedo used (0.8) may also be too high, especially in marginal ice regions where the effect of reduced areal coverage of ice and the presence of melt-water pools would lead to a much lower areal average albedo in reality.

Over Antarctica there are significant differences between the albedos from the two satellite data sets, the NOAA satellites giving much higher values (80–90% as opposed to 70–80%). At about 70% the model values appear to be too low. Over the northern high latitudes the patterns in the difference plots are similar, but the feature at 70°N in April/May is much more marked in the comparison with the NOAA data. Both data sets suggest that over the North Pole in June the modelled albedo at 65% is about 10% too low. This is not due to the state of the surface, as the Arctic is assumed to be covered in sea-ice throughout the year. It has been found that the cloud amounts used over the Arctic at this time of year

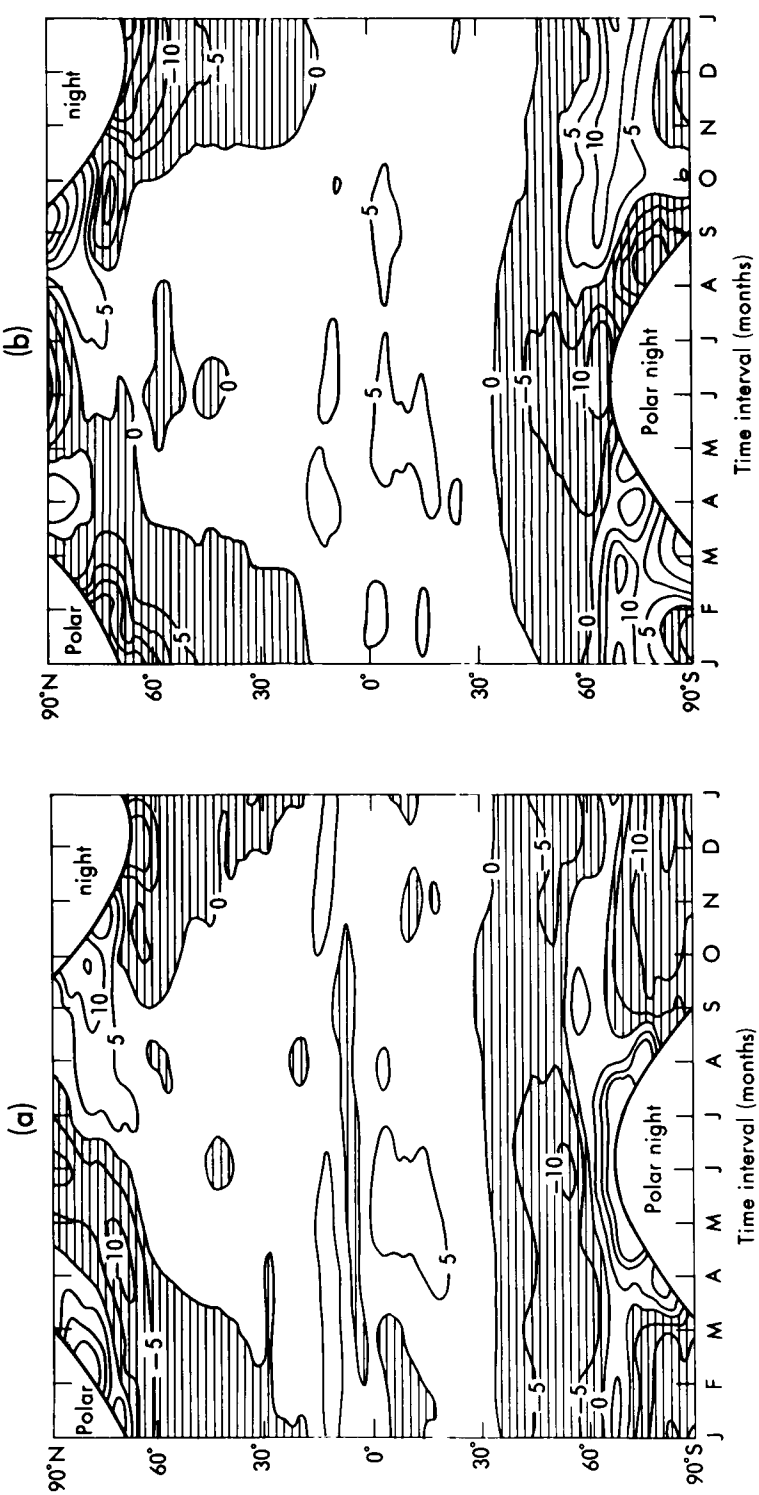

Figure 4. Time-latitude diagrams of the differences (per cent) between the global albedo from the model and from (a) the NOAA and (b) the research satellites.

are too low. Low-cloud amounts were 41%, whereas Huschke (1969) gives values of about 70% for the central Arctic. However, increasing the low-cloud amounts produces virtually no change in the planetary albedo, because of enhanced absorption from the increased multiple reflections between cloud and surface. Reducing the low-cloud absorptivity, which at 10% is probably too high to represent Arctic stratus, would remove the insensitivity to the cloud amounts. Detailed aircraft measurements of the radiative properties of cloud layers in the Arctic (e.g. Herman and Curry 1984) are thus most useful in helping to resolve these uncertainties.

Disagreements between the observed and modelled planetary albedos cannot be due entirely to errors in the model. An overestimate by the NOAA satellites of the planetary albedo at high latitudes has been known about for some time (e.g. Ohring and Gruber 1983). It is often attributed to the fact that the NOAA sensors work in the 0.5–0.7 μm band where the albedos of snow and ice are much higher than at longer wavelengths (Shine *et al.* 1984). Nevertheless, there are also large disagreements between data sets from broad-band measurements. For example, Jacobowitz *et al.* (1979) show results from the first 18 months of the Nimbus 6 Earth Radiation Budget Experiment. Albedos over Antarctica were in the range 70–75% and over the Arctic were 65–70%, which is closer to the model values than the satellite data used here. Stephens *et al.* (1981) include the same Nimbus 6 data, but as processed by Campbell and Vonder Haar (1980). In this data set the planetary albedo exceeds 80% over both poles. It is clearly difficult to make definitive statements about the modelled albedos at high latitudes when there are such wide variations in the measurements.

4.2.3 *Reflected and absorbed short-wave radiation*. The importance of the polar regions in influencing the globally averaged planetary albedo is emphasized by Fig. 5(a), which shows the reflected short-wave energy from the model. At the solstices there are large peaks over the summer pole due to the constant illumination of the ice and snow. In northern winter the maximum in the globally averaged albedo (Fig. 2) is clearly not due to the northern hemisphere cloud and snow cover, as suggested by Ohring and Gruber (1983) but to the illumination of Antarctica (J. M. Slingo 1982) and its surrounding sea-ice and cloudiness. The entire northern hemisphere contributes only about one quarter of the total reflected short-wave radiation in December, despite the underestimate of the southern hemisphere cloud amounts discussed earlier.

The high albedo of the polar regions in summer significantly reduces the amount of absorbed short-wave energy compared with lower latitudes. The positions of the maxima in the time–latitude diagram of absorbed short-wave radiation (Fig. 5(b)) are thus much closer to the equator than for the incoming radiation, the pattern showing strong symmetry about the latitude corresponding to the sun's declination. Comparison with Fig. 3(b) shows that the seasonal changes in the planetary albedo produce relatively minor variations in the shape of the diagram. Time–latitude diagrams of the differences between the modelled and observed reflected and absorbed short-wave radiation are not shown as these are of the same basic shape as Fig. 4.

4.2.4 *Outgoing long-wave radiation*. The model successfully reproduces the main features of the variations in the outgoing long-wave radiation (Fig. 6(a)). The high cloudiness of the ITCZ leads to a weak minimum in outgoing long-wave radiation over the equator and there are maxima in the subtropics associated with relatively clear skies. The strong latitudinal gradient in tropospheric and surface temperatures leads to a corresponding drop in the long-wave flux towards the polar regions, the lowest values of about 100 W m^{-2} being found over the central Antarctic plateau in the southern winter. Apart from over Antarctica itself, the seasonal variation in outgoing long-wave radiation is small in the southern hemisphere owing to the moderating influence on temperatures of the extensive oceans. In

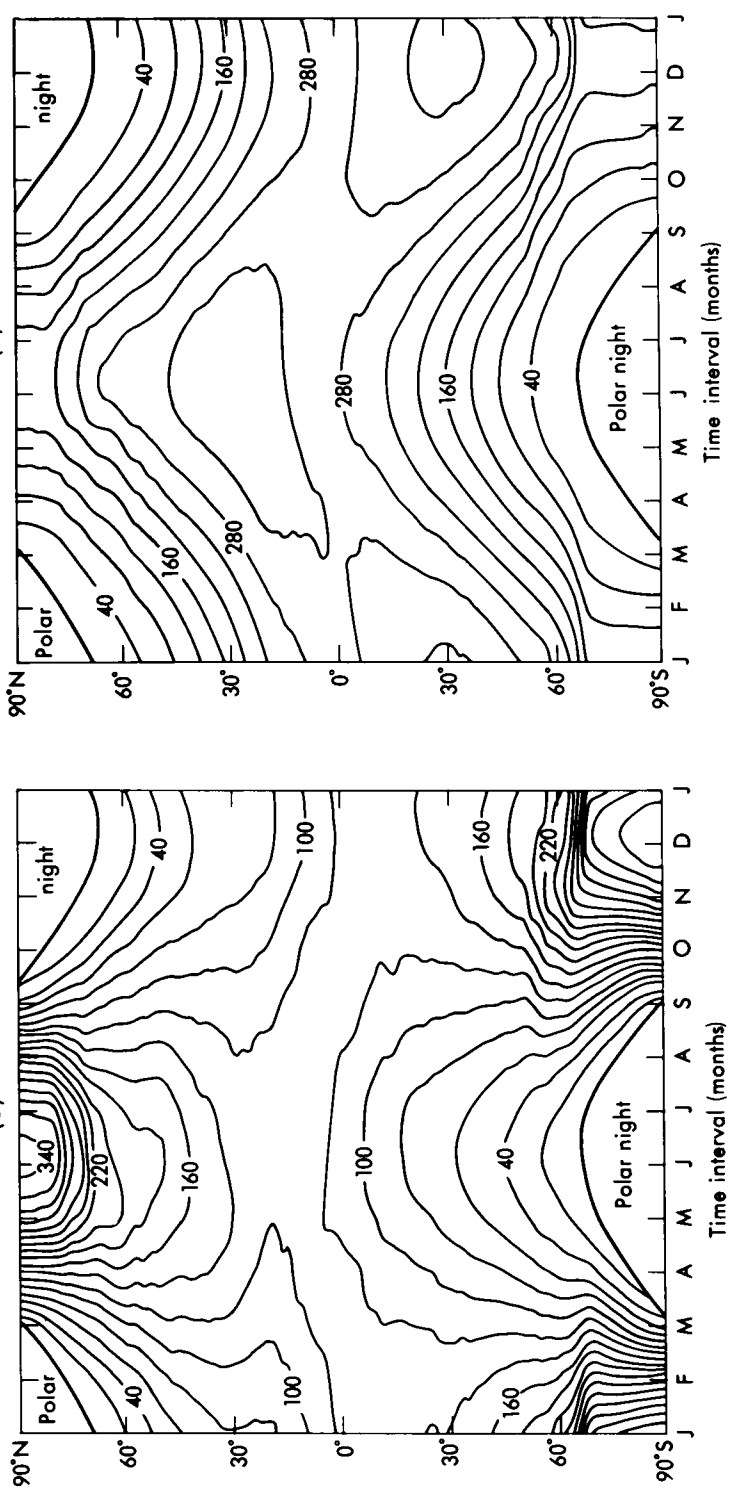

Figure 5. Time–latitude diagrams of the (a) reflected short-wave radiation (W m^{-2}) and (b) absorbed short-wave radiation (W m^{-2}) from the model.

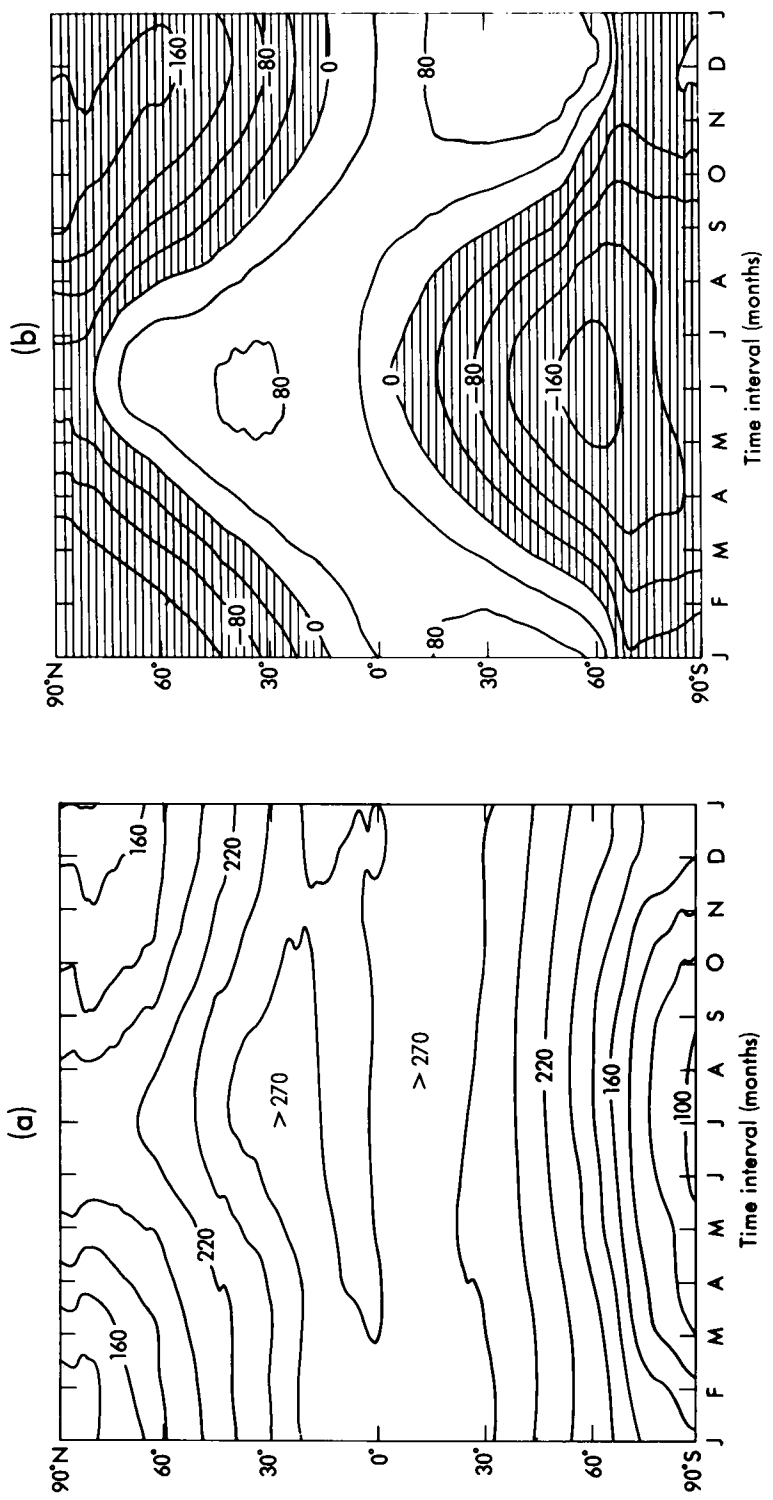

Figure 6. Time–latitude diagrams of the (a) outgoing long-wave radiation (W m^{-2}) and (b) net radiation (W m^{-2}) from the model.

contrast, the land masses of the northern hemisphere produce a much stronger variation between about 30°N and 70°N. Over the Arctic the seasonal variation is similar to that over Antarctica, although values are generally about 40 W m^{-2} higher.

Comparison with the satellite values (Fig. 7) shows that the minimum in outgoing long-wave radiation over the ITCZ is too weak in the model. This could be due to the artificial broadening of the ITCZ by the cloud climatology, as mentioned earlier. It may also be that the very simple treatment of the reduced emissivity of high cloud compared with lower (and hence optically thicker) cloud, namely the halving of the amounts in the long-wave part of the radiation scheme, is too crude. This is an area of the model where a sounder physical basis for the parametrization is under consideration. Over the rest of the tropics and the high latitudes there are substantial areas of disagreement between the satellite data sets over the sign of any model error, reflecting the large differences in the global averages shown in Fig. 2. NOAA have recently revised their algorithms for deriving the outgoing long-wave radiation, leading to a better agreement with other data (Gruber and Krueger 1984). Nevertheless, the general impression is that the modelled values are too low towards the polar regions. This is probably due to the tendency for the model to be too cold in these areas compared with climatological data (Cunnington 1983). Northward of about 70°N, for example, tropospheric temperatures are 5–10 °C lower than in the data of Newell *et al.* (1972). The reason for the cooling has not yet been isolated and is the subject of current research.

4.2.5 *Net radiation.* The balance between the heating of the system by the absorption of short-wave radiation and the cooling from the emission of long-wave radiation to space is shown in the time–latitude diagram of net radiation (Fig. 6(b)). Areas of positive net radiation, indicating a net warming by radiative processes, are shown unshaded. Over most of the globe the seasonal changes in outgoing long-wave radiation are much smaller than those in the short-wave absorption, so the latter dominates the shape of the net radiation diagram and the latitude of the maximum follows the sun's declination. It is interesting that the large seasonal variation in southern mid-latitudes is almost entirely due to the changes in the illumination (i.e. Fig. 3(a)), as the changes in the albedo (Fig. 3(b)) and the outgoing long-wave radiation (Fig. 6(a)) are much weaker. In the polar regions the signal from the outgoing long-wave radiation is more important and of course during polar night is the only term in the net radiation.

In calculating the differences between the modelled and observed net radiation (Fig. 8) two corrections were made to remove the systematic biases between the data sets which are evident in Fig. 2. The satellite values of absorbed short-wave radiation were first corrected for the different values assumed for the solar constant. The differences between the modelled and observed net radiation were then adjusted by a single value at each point to ensure that the global annual mean was zero. Following these corrections, the two comparisons are in good agreement in most areas. Both satellite data sets indicate that the latitudinal gradient of system radiative heating is too weak in the model integration. In the tropics, the net radiation is about 20 W m^{-2} too low. This is a result of the overestimates of both the planetary albedo and the outgoing long-wave radiation, due to the assumed cloud radiative properties and the cloud climatology, as discussed earlier. In the polar regions the net radiation is generally too high and the apparent albedo underestimate in certain regions leads to large differences, e.g. about 100 W m^{-2} compared with the NOAA data over the South Pole in December.

5. Discussion

The comparisons presented in this article demonstrate the importance of satellite earth radiation budget measurements in validating the radiation and cloud schemes employed in climate models. The

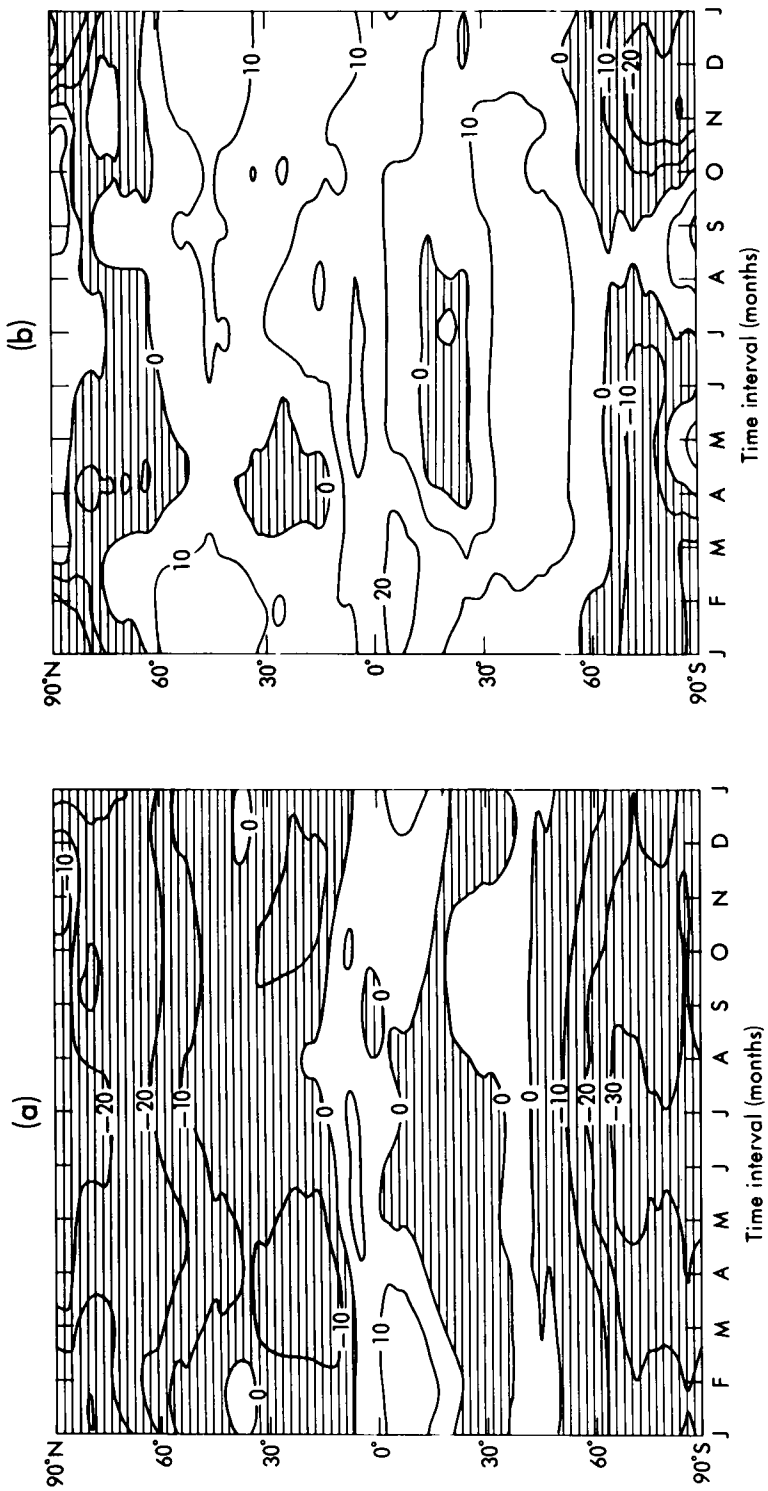

Figure 7. Time–latitude diagrams of the differences (W m^{-2}) between the outgoing long-wave radiation from the model and from (a) the NOAA and (b) the research satellites.

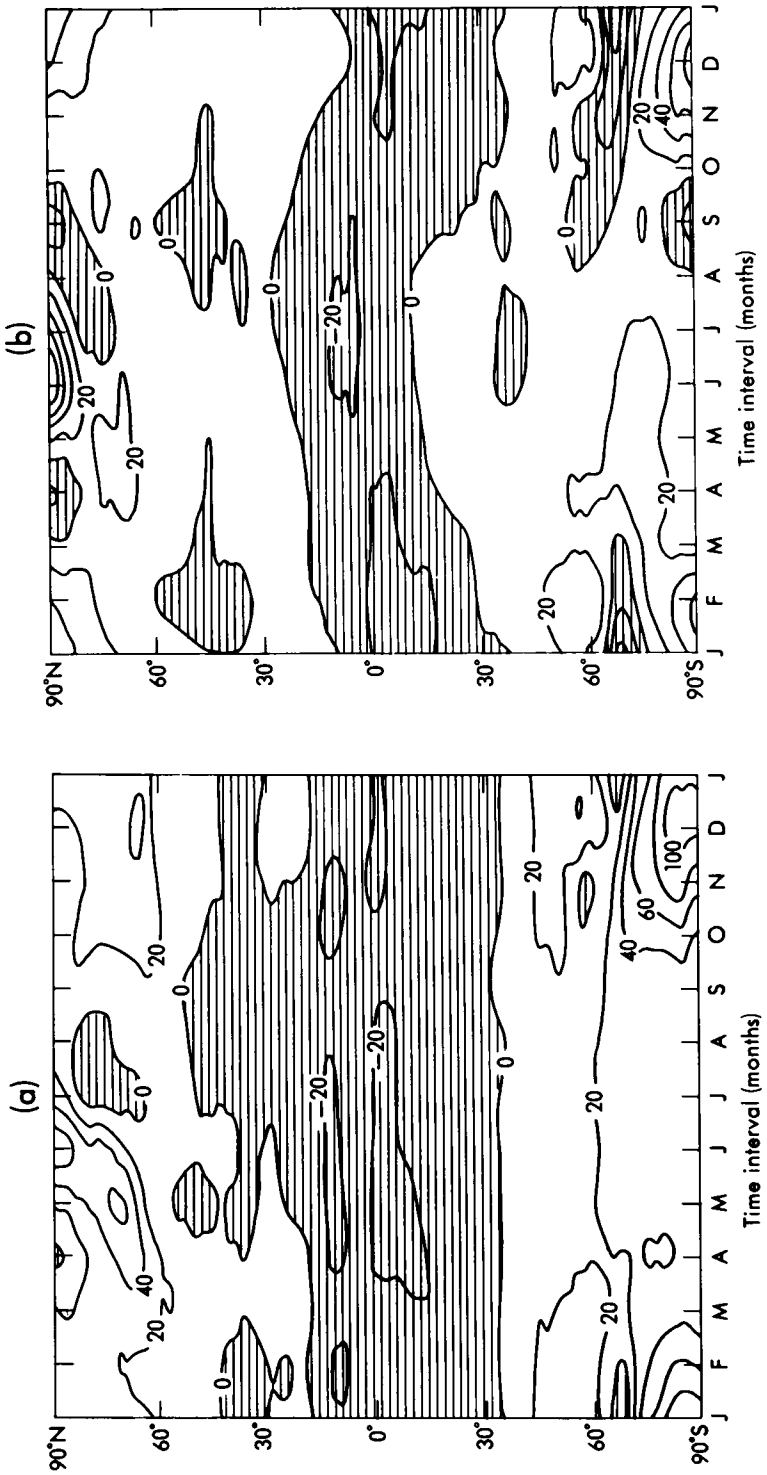

Figure 8. Time–latitude diagrams of the differences (W m^{-2}) between the net radiation from the model and from (a) the NOAA and (b) the research satellites. The differences have been corrected to remove biases from the data sets, as described in the text.

main features of the seasonal variations in the radiation budget have been reproduced in the first annual-cycle integration of the 11-layer GCM. The use of two independent satellite data sets has allowed the model's deficiencies to be determined with some confidence. However, it has also emphasized the significant disagreements between those data sets. Some of the model's deficiencies may be attributed simply to errors in its formulation, such as the excessive areas of sea-ice around Antarctica, which stand out in the albedo comparisons. Several others have been shown to be due to the cloud climatology and cloud radiative properties which were assumed. Relatively small adjustments to either of these would remove many of the more obvious errors and for some applications such 'tuning' would be perfectly acceptable. However, the use of fixed zonally averaged cloud amounts deprives the model of the ability to represent some important feedback mechanisms which should operate when a perturbation is applied.

The development of a method for predicting realistic cloud distributions in long integrations of the model therefore has a high priority in current research. Several experiments have been made with versions of the cloud prediction scheme proposed by Slingo (1980). Forecast experiments with this scheme show that it can represent quite well the major synoptic features in the global cloud distribution; but in longer integrations the cloud amounts become unrealistic because of interactions with model systematic errors (Slingo 1983). Useful progress has been made in understanding and rectifying some of these errors. Satellite observations of the earth's radiation budget will continue to play an important part in model development, but the model itself should provide an ideal tool for studying interesting features in the observations, such as inter-annual variations caused by anomalies in the cloud cover or surface state. This symbiotic relationship between climate models and satellite data should provide much stimulating research in the next few years.

References

Barkstrom, B. R. 1984 The Earth Radiation Budget Experiment (ERBE). *Bull Am Meteorol Soc*, **65**, 1170–1185.

Berlyand, T. G., Strokina, L. A. and Greshnikova, L. E. 1980 Zonal cloud distribution on the earth. *Soviet Meteorol and Hydrol* No. 3, 9–15.

Bignell, K. J. 1970 The water-vapour infra-red continuum. *Q J R Meteorol Soc*, **96**, 390–403.

Bolton, J. A. 1981 The estimation of zonally averaged climatological cloud data for use in the 5 level model radiation scheme. (Unpublished, copy available in National Meteorological Library, Bracknell.)

Campbell, G. G. and Vonder Haar, T. H. 1980 An analysis of two years of Nimbus 6 earth radiation budget observations: July 1975 to June 1977. Colorado State University, *Atmos Sci Pap* No. 320.

Carson, D. J. 1982a Comments on the sensitivity of numerical simulations to different parameterizations of the boundary-layer properties and processes. ECMWF Workshop on planetary boundary layer parameterization, 25–27 November 1981.

1982b Current parametrizations of land-surface processes in atmospheric general circulation models. *In* Eagleson, P. S. (ed.), Land surface processes in atmospheric general circulation models. Cambridge University Press.

Corby, G. A., Gilchrist, A. and Newson, R. L. 1972 A general circulation model of the atmosphere suitable for long period integrations. *Q J R Meteorol Soc*, **98**, 809–832.

Corby, G. A., Gilchrist, A. and Rowntree, P. R. 1977 United Kingdom Meteorological Office five-level general circulation model. Methods in computational physics Volume 17, 67–110. New York, Academic Press.

Cunnington, W. M.	1983	An annual-cycle integration of the 11-layer model. (Unpublished, copy available in National Meteorological Library, Bracknell.)
Dickinson, A. and Temperton, C.	1984	The operational numerical weather prediction model. (Unpublished, copy available in National Meteorological Library, Bracknell.)
Gilchrist, A. and White, P. W.	1982	The development of the Meteorological Office new operational forecasting system. *Meteorol Mag*, **111**, 161–179.
Gill, A. E.	1982	Atmosphere-ocean dynamics. International Geophysics Series Volume 30. New York, Academic Press.
Gruber, A. and Krueger, A. F.	1984	The status of the NOAA outgoing longwave radiation data set. *Bull Am Meteorol Soc*, **65**, 958–962.
Gruber, A. and Winston, J. S.	1978	Earth-atmosphere radiative heating based on NOAA scanning radiometer measurements. *Bull Am Meteorol Soc*, **59**, 1570–1573.
Heasman, C. C.	1983	Boundary layer schemes used in the 11-layer model. (Unpublished, copy available in National Meteorological Library, Bracknell.)
Herman, G. F. and Curry, J. A.	1984	Observational and theoretical studies of solar radiation in Arctic stratus clouds. *J Climatol Appl Meteorol*, **23**, 5–24.
Hinds, Mavis K.	1981	Computer story. *Meteorol Mag*, **110**, 69–81.
Houghton, J. T.	1984	The global climate. Cambridge University Press.
Hunt, G. E. and Mattingly, S. R.	1976	Infrared radiative transfer in planetary atmospheres—I. Effects of computational and spectroscopic economies on thermal heating/cooling rates. *J Quant Spectrosc Radiat Transfer*, **16**, 505–520.
Huschke, R. E.	1969	Arctic cloud statistics from 'air calibrated' surface weather observations. *RAND Corp Memo* RM-6173-PR.
Jacobowitz, H., Smith, W. L., Howell, H. B., Nagle, F. W. and Hickey, J. R.	1979	The first 18 months of planetary radiation budget measurements from the Nimbus 6 ERB experiment. *J Atmos Sci*, **36**, 501–507.
Lemke, P., Trinkl, E. W. and Hasselmann, K.	1980	Stochastic dynamic analysis of polar sea ice variability. *J Phys Oceanogr*, **10**, 2100–2120.
Liou, K.-N.	1980	An introduction to atmospheric radiation. International Geophysics Series Volume 26. New York, Academic Press.
Lyne, W. H. and Rowntree, P. R.	1976	Development of a convective parameterisation using GATE data. (Unpublished, copy available in National Meteorological Library, Bracknell.)
Lyne, W. H., Rowntree, P. R., Temperton, C. and Walker, Julia M.	1976	Numerical modelling using GATE data. *Meteorol Mag*, **105**, 261–271.
Lyne, W. H., Swinbank, R. and Birch, N. T.	1982	A data assimilation experiment and the global circulation during the FGGE special observing periods. *Q J R Meteorol Soc*, **108**, 575–594.
McClatchey, R. A., Benedict, W. S., Clough, S. A., Burch, D. E., Calfee, R. F., Fox, K., Rothman, L. S. and Garing, J. S.	1973	AFCRL Atmospheric absorption line parameters compilation. Environmental research papers No. 434. Bedford, Mass., Air Force Cambridge Research Laboratories.
Manabe, S. and Möller, F.	1961	On the radiative equilibrium and heat balance of the atmosphere. *Mon Weather Rev*, **89**, 503–532.
Mitchell, J. F. B.	1983	The seasonal response of a general circulation model to changes in CO_2 and sea temperatures. *Q J R Meteorol Soc*, **109**, 113–152.
Neckel, H. and Labs, D.	1981	Improved data of solar spectrum irradiance from 0.33 to 1.25 micron. *Solar Phys*, **74**, 231–249.
Newell, R. E., Kidson, J. W., Vincent, D. G. and Boer, G. J.	1972	The general circulation of the tropical atmosphere and interactions with extratropical latitudes. Vol I. Cambridge, Mass., MIT Press.
Ohring, G. and Gruber, A.	1983	Satellite radiation observations and climate theory. Advances in geophysics Volume 25, 237–304. New York, Academic Press.
Paltridge, G. W. and Platt, C. M. R.	1976	Radiative processes in meteorology and climatology. Developments in atmospheric science, **5**. Elsevier.

Rowntree, P. R.	1976	Response of the atmosphere to a tropical Atlantic Ocean temperature anomaly. *Q J R Meteorol Soc*, **102**, 607–625.
Rowntree, P. R. and Bolton, J. A.	1983	Simulation of the atmospheric response to soil moisture anomalies over Europe. *Q J R Meteorol Soc*, **109**, 501–526.
Sasamori, T., London, J. and Hoyt, D. V.	1972	Radiation budget of the southern hemisphere. Meteorology of the southern hemisphere. *Meteorol Monogr*, **13**, No. 35.
Satellite Meteorology Branch (Meteorological Office)	1982	Meteorological satellites: a current survey. *Meteorol Mag*, **111**, 126–133.
Shine, K. P., Henderson-Sellers, Ann and Slingo, A.	1984	The influence of the spectral response of satellite sensors on estimates of broadband albedo. *Q J R Meteorol Soc*, **110**, 1170–1179.
Slingo, A.	1982	Insolation calculations for a 360-day year. (Unpublished, copy available in National Meteorological Library, Bracknell.)
	1983	Clouds and radiation in the Meteorological Office 11-layer general circulation model. (Unpublished, copy available in National Meteorological Library, Bracknell.)
Slingo, A. and Wilderspin, R. C.	1984	Development of a revised longwave radiation scheme for an atmospheric general circulation model. (Unpublished, copy available in National Meteorological Library, Bracknell.)
Slingo, A., Nicholls, S. and Schmetz, J.	1982	Aircraft observations of marine stratocumulus during JASIN. *Q J R Meteorol Soc*, **108**, 833–856.
Slingo, Julia M.	1980	A cloud parametrization scheme derived from GATE data for use with a numerical model. *Q J R Meteorol Soc*, **106**, 747–770.
	1982	A study of the earth's radiation budget using a general circulation model. *Q J R Meteorol Soc*, **108**, 379–405
Stephens, G. L., Paltridge, G. W. and Platt, C. M. R.	1978	Radiation profiles in extended water clouds, III. Observations. *J Atmos Sci*, **35**, 2133–2141.
Stephens, G. L., Campbell, G. G. and Vonder Haar, T. H.	1981	Earth radiation budgets. *J Geophys Res*, **86**, 9739–9760.
van Loon, H.	1972	Cloudiness and precipitation in the southern hemisphere. Meteorology of the southern hemisphere. *Meteorol Monogr*, **13**, No. 35.
Walker, Julia M.	1977	Interactive cloud and radiation in the 11-layer model. Part I: Radiation scheme. (Unpublished, copy available in National Meteorological Library, Bracknell.)
Winston, J. S. Gruber, A., Gray, T. I., Varnadore, Marylin S., Earnest, C. L. and Mannello, L. P.	1979	Earth–atmosphere radiation budget analyses derived from NOAA satellite data June 1974–February 1978, Volumes 1 and 2. NOAA S/T 79–187.

Notes and news

100 years ago

The Minutes of the Proceedings of the Meteorological Council used to carry regular monthly reports of the work of the Office which then had between 30 and 40 staff.

That for May 1885, submitted on 3 June 1885, is as follows:

MARINE ROOM.

Examined 19 new logs. June 3, 1885.

North Atlantic Weather Charts.

Making additions to isobars for November and December 1882.

Preparing weather areas and generalized winds for December 1882, and for part of January 1883.

Drawing of air and sea isotherms for May completed.

Making 'tracings' of all data for June also drawing air and sea isotherms.

Testing glass pens for use with eidographs.

Various work in connexion with land isobars, isotherms, and winds.

The female clerks steaming June charts, plotting the observations for July and August, assisting in the copying of land isobars, isotherms and winds, and preparing 'tracings' of data. Three members of the staff practising the working of the eidographs.

General.

Indexing data in ocean 10-degree squares, and obtaining amount and distribution of data in the Office to the end of 1884.

(Signed) CHAS. HARDING.

The Marine Superintendent.

Forwarded for the information of the Council.

(Signed) HENRY TOYNBEE,
Marine Superintendent.

TELEGRAPHIC (FOREST AND STORM WARNING) BRANCH.

Monthly Weather Reports. — 1885, *February*. — Expected from printer daily (complete). 1885, *March*. — In printer's hands. 1885, *April*.—Half done. There has been some little delay with these just lately on account of holidays, and sickness of various clerks.

Checking Daily Forecasts. — Complete up to date.

Checking Storm Warnings, 1884. — Completed.

Weekly Weather Report.

1884, Appendix II. — Sheets 3 and 4 of proof have been received, corrected, and returned for press, and the printer has been requested to deliver remainder of proof at once.

1885. — All numbers have appeared promptly.

Comparing the Records of Mr. Galton's ('trigger') Anemometer, with Estimations of Wind Force on board the Newarp Light Vessel. — Computations all finished. Inquiry is now being made as to method of observing, &c., as the results appear somewhat peculiar.

(Signed) FREDC. GASTER.
3/6/85.

PANTAGRAPH ROOM.

June 1, 1885.

Quarterly Weather Report, Part IV., 1877. — Chart plate XVI. partly drawn.

Observatory Returns. — The Hourly Readings for May 1883 sent to printer. Proof read and revised to end of March, and Part I. signed for press.

The calculation of vapour tension values, and of daily, five-daily, and monthly means for May completed.

Harmonic Analyser. — A correction for non-periodicity has been applied to the coefficients for the 12 years 1871–1882. The examination of the readings of the machine (Minutes, April 29, 1885) is now in hand. Several plates of curves have been drawn with General Strachey's instrument.

Krakatoa Air Waves. — My own time has been chiefly occupied in discussing, under the Chairman's instructions, the observations relating to these phenomena; Mr. Thompson has also been partly engaged on diagrams for the work.

Miscellaneous. — Bunhill Row sunshine cards for the first three months of the year tabulated for the Royal Meteorological Society.

Some assistance has been given to the Examination Room by myself and others during the month.

R. H. Scott, Esq., F.R.S. (Signed) R. H. CURTIS.

Reported — That the cash accounts for the six months ended the 31st March 1885 had been audited this day by the Chairman and Professor Darwin, and would be sent forthwith to the Treasury for the Audit Office. The receipts for the six months, exclusive of a balance of 1,123*l*. 2*s*. 11*d*. on the 1st October 1884, amounted to 9,199*l*. 12*s*. 6*d*. The payments amounted to 8,579*l*. 10*s*. 7*d*., leaving a balance of 1,743*l*. 4*s*. 10*d*. in hand and at the Bank on 1st April 1885.

[There followed a list of cheques drawn during the month.]

Submitted at the same meeting was a report on the forecasts for May 1885, district by district (11 in all), classified by the letters a to d, where a stood for 'complete success', b 'partial (i.e. more than half) success', c 'partial failure', and d 'total failure'. There was also a summary table as follows:

SUMMARY

	3.30 P.M.					8.30 P.M.			
	Percentages.			Percentage of Success a + b.		Percentages.			Percentage of Success a + b.
	Wind.	Weather.	Average Forecast.			Wind.	Weather.	Average Forecast.	
BRITISH ISLES a	51	69	60	86	BRITISH ISLES a	52	64	58	88
,, ,, b	33	19	26		,, ,, b	33	26	30	
,, ,, c	12	6	9		,, ,, c	12	5	8	
,, ,, d	4	6	5		,, ,, d	3	5	4	

These figures seem to compare very favourably with those for the present day!

Weather information in the Shetland Isles

One of the problems in providing accurate weather forecasts for oil industry operations in and out of the bleak, remote oil terminal at Sullom Voe in the Shetland Isles has been the shortage of accurate and detailed weather observations from the local area. Five years ago the Meteorological Office put an automatic weather station on Muckle Holm, an island in Yell Sound, to provide information from this vital channel for large tankers entering Sullom Voe. Last year the gap in observations from the direction of the prevailing south-westerly winds was filled, thanks not only to the latest in automatic weather stations but also the co-operation of two crofters, Mr and Mrs Holbourn on the island of Foula.

This small, remote but inhabited island 40 miles west of Lerwick and about the same distance south-west of Sullom Voe is a key site for meteorological observations. The nearest land to the west is the southern tip of Greenland, 1500 miles away. An automatic weather station on Foula was installed last June by the Meteorological Office with the co-operation of the Shetland Islands Council. It is battery powered and has a 20-foot lattice mast on which the meteorological instruments and a VHF aerial are mounted. It became fully operational on 1 August and now every hour measurements of wind speed and direction, barometric pressure, relative humidity and air temperature are sent out automatically to Shurton Hill near Lerwick and then by microwave link through Bressay to Sella Ness. If measurements are needed between times the station can be interrogated by telephone by any meteorological office which has the right equipment.

Automatic weather stations like the one on Foula cannot yet provide adequate information about clouds, visibility or other weather phenomena — however, Mr and Mrs Holbourn have agreed to be local meteorological observers. Every 3 hours during the day they send reports to Lerwick Observatory to complete the picture of the weather on Foula; their reports include details of the cloud over the island, its amount, height and type, also visibility, whether it is raining or snowing and so on. Mr and Mrs Holbourn require great dedication to fit weather observing duties into their busy and demanding life on a croft, but they know that their reports are a vital link in the chain that provides essential meteorological information and forecasts.

Reviews

Land surface processes in atmospheric general circulation models, edited by P. S. Eagleson. 180 mm × 250 mm, pp. ix + 560, *illus*. Cambridge University Press, 1982. Price £30.00.

This is a large book with 14 main contributions prepared specially for the World Meteorological Organization/International Council of Scientific Unions Joint Scientific Committee Study Conference held at Greenbelt, Maryland in January 1981. The conference was carefully planned to help bridge a gap in communication between general circulation modellers, wishing to represent the large-scale effects of the micro-scale land surface processes (i.e. 'parametrize' them), and hydrologists and soil scientists with an understanding of these smaller scales. The book's structure reflects these different scales, the first three sections, constituting nearly two-thirds of the book, covering (I) general circulation models, (II) microphysical processes of momentum, heat and water transfers and (III) mesoscale parametrizations of those transfer processes. Most of the rest of the book is entitled 'Land surface global data sets' with a final one-chapter section on remote sensing.

J. Smagorinsky introduces the first section with an instructive and readable discussion of climate models and the need for parametrization of small-scale processes. This is followed by S. Manabe's more detailed description of the structure of atmosphere and coupled (atmosphere–ocean) general circulation models (GCMs) with good illustrations of the simulations they give. D J. Carson provides an admirably comprehensive review of the treatment of land surface processes in 13 different models, with detailed

discussions of the theory behind the parametrizations. What should have been the final contribution on the sensitivity of the models to albedo and soil moisture by Y. Mintz was regrettably not available in time.

The section describing microphysical processes contains three chapters on the vertical fluxes of heat and moisture for a bare soil surface (W. H. Brutsaert), a vegetated surface (L. J. Fritschen) and snow and ice (M. Kuhn). Brutsaert provides a thorough exposition of the mathematical treatments of the flow of water in soil and of surface evaporation. Heat transfer is dealt with similarly, with a discussion of methods of determining the soil heat flux. Both this and Kuhn's briefer chapter on snow and ice make a real attempt to provide a practical basis for parametrization. Fritschen's topic is much more complex so he presents a model for its solution together with an extensive collection of estimates of evaporation for various crops etc. which occupy half this long chapter. It is difficult to see that they are very useful except as references to the original papers. It would have been more helpful and appropriate here to introduce important concepts such as stomatal and root resistances; the reader will find a more useful discussion of the topic in R. E. Dickinson (1984). (Modelling evapotranspiration for three-dimensional global climate models. Climate processes and climate sensitivity. *Geophys Monogr*, **29**, 58–72.) In this volume, Perrier's chapter in the 'data sets' section is more informative while Fritschen's evaporation data might have been better placed in that section.

The third section on mesoscale parametrizations focuses on hydrology. J. C. I. Dooge points out that hydrologists have mainly emphasized flood hydrology and ground-water systems, with least progress where climate modellers need help — the accounting and transfer of soil moisture. The heterogeneity at field scale, evident in studies reviewed here, explains much of the pessimism of hydrologists about the GCM parametrization problem. P. S. Eagleson provides a systematic introduction to mesoscale hydrology, reviewing the state of art of parametrization for each of the main terms (evapotranspiration, runoff etc.).

In the fourth section on global data sets, M. J. Gardiner provides a history of soil classification and mapping with some informative (though globally incomplete) maps of soil types. The latest series of maps go part of the way towards providing the data on soil moisture capacity and permeability and albedo needed for climate models. A. Perrier contributes a useful review of vegetation types and the dependence on them of albedo, roughness length and, especially, stomatal resistance including the large seasonal variations of some crops. V. M. Kotliakov and A. N. Krenke briefly review available data on snow and ice. A valuable collection of data on surface solar albedo and long-wave emissivity is provided by K. Ya Kondratyev, V. D. Korzov, V. V. Mukhenberg and L. N. Dyachenko. Zenith angle and spectral and seasonal dependences are well covered with global albedo maps for four months. These maps have some incomplete contours and tropical forests are given an albedo of 0.18, well above the 0.12–0.13 favoured in the text. A. Baumgartner discusses water balance equations at some length, quotes a set of parametrizations for evaporation and run off having little in common with those given by Carson or Eagleson and notes the large discrepancies between two recent calculations of the global water balance with mean precipitations differing by 15%.

Finally, K. Itten contributes a clear statement of the basic principles of remote sensing of albedo, cloud cover and several land surface quantities with an assessment of the current (1981) status.

In summary, this volume contains a wealth of information, much of it of value to anyone concerned with the physics of the land surface. Of the 560 pages, 74 are occupied by reference lists — these are separate for each chapter so there will be overlaps. The book stands between a conference proceedings and a textbook. The topics have been selected in a coherent, well-directed manner as with a textbook, though there are omissions — frozen soil is explicitly omitted by Kuhn — and some subjects are not where one might expect to find them — momentum flux is only covered under GCMs (Carson) and

global data sets (Perrier). The book draws on the expertise of several writers, who have on the whole done a sound job and so should achieve more than a textbook with one author. However, there is little apparent attempt at editorial control after the original planning so that there are overlaps (e.g. Bouchet's advection–aridity approach to evaporation is discussed by Dooge, Eagleson and Perrier); there is no index, no common use of symbols, and several typefaces are used. It is perhaps more a reference book than a textbook, but here of course the lack of an index is a significant drawback. Nevertheless, for the modeller who needs to know about land surface processes and parametrizations, it is a unique collection of papers to which he will make frequent reference.

P. R. Rowntree

Dynamics of the middle atmosphere, edited by J. R. Holton and T. Matsuno. 150 mm × 240 mm, pp. viii + 543, *illus*. Terra Scientific Publishing Company (TERRAPUB), Tokyo and D. Reidel Publishing Company, Dordrecht, Boston, Lancaster, 1984. Price Dfl 220, US $ 89.50.

Most dynamical meteorologists are concerned with winds in the troposphere, which contains about 90% of the mass of the atmosphere and extends from the earth's surface to a height of about 10 km. For many years, studies pertaining to higher levels in the earth's atmosphere (stratosphere, mesosphere, ionosphere, etc.) and to the atmospheres of the other planets were often regarded as whimsical and possibly even suspect 'fringe' activities of a few people who might, one day, see the light and join the mainstream of tropospheric dynamics. But many able young scientists who entered meteorology in the past two decades were attracted to the problems concerning the dynamics of the stratosphere and mesosphere, and their impact on the subject is evident in this book, edited by two of their number, as a record of the proceedings of a USA–Japan seminar held in Honolulu in November 1982.

Recent work on the middle atmosphere has been stimulated by questions concerning possible anthropogenic perturbations of the stratospheric ozone layer, posed at a time when techniques of observation, particularly those involving the use of satellite-borne instruments, were being improved, and advances in basic theory, particularly of wave mean flow interactions, were being made. Studies of dynamical phenomena were central to the seminar, with radiation and chemistry entering only in the context of dynamical problems.

The book comprises six main sections, starting with one on gravity waves, the importance of which in upper-atmospheric studies was first appreciated by Hines 25 years ago. This is the largest section in the book and includes contributions by Lindzen, Walterscheid, Schoerberl, Strobel, Horota, Balsley, Eckland, Fritts, Yamanaka, Tanaka, Hayashi and Matsuno. Next comes a short section comprising four articles on tides and free oscillations by Kato, Aso, Vincent, Miyahara, Hirota and Hirooka. Large-scale waves and wave mean flow interactions are treated in the third section, with contributions by Plumb, Takahashi, Miyahara, Gille, Lyjak, Kanzawa and Matsuno. The shortest section is headed 'Radiation' and consists of a single article by Leovy on infra-red radiation exchange. Fifth come four articles by Holton, Mahlman, Andrews, Hartmann, Matsuno, Murgatroyd, Tung and Hasebe, on the transport of tracers, and the book ends with three articles on modelling, by Geller, Mahlman, Umschied, Tokioka and Yagai, an author index, and a subject index.

As one would expect of the proceedings of a meeting of active workers in an important and challenging comparatively new field of atmospheric science, this book contains a great deal of interesting material on observations and on attempts to make sense of them in terms of basic dynamical processes. Aimed at research workers, the book makes few concessions to the general reader, so that experts in the field will buy it and others will skim through it in their libraries.

R. Hide

Books received

The listing of books under this heading does not preclude a review in the Meteorological Magazine at a later date.

Atmospheric thermodynamics, by J. V. Iribarne and W. L. Godson (Dordrecht, Boston, London, D. Reidel Publishing Company, 1981) is the second edition of a textbook originally published in 1973. It contains a review of general thermodynamics and includes the basic formulas for open and heterogeneous systems. One chapter introduces new material while more than half the book deals with problems of direct application to meteorology: aerological diagrams, basic processes occurring in the atmosphere, atmospheric statics, integration of the hydrostatic equation and a rather extensive consideration of the vertical stability, including the different methods for analysing it, rate of precipitation, and energy relations and conversions in the atmosphere.

Problems and prospects in long and medium range weather forecasting, edited by D. M. Burridge and E. Källén (Berlin, Heidelberg, New York, Tokyo, Springer-Verlag, 1984. DM 45, US$ 17.50) surveys some aspects of the problem of atmospheric predictability and provides elements of the theoretical background, examples of operational forecasting systems and predictability experiments with general circulation models. Basic theoretical concepts and ideas are covered in the introductory chapter. Other theoretical topics include solitons, modons and bifurcation mechanisms — relatively novel concepts in the field of atmospheric predictability. The chapters on numerical prediction discuss the scientific and practical problems of making ten-day forecasts and the possibilities of using deterministic general circulation models to predict, beyond the theoretical limit of predictability, the largest scales and long-term averages.

Weathering, by Cliff Ollier (London and New York, Longman, 1984. £11.50) is a second edition which has been published to take account of the recent developments in the subject and to provide the most up-to-date text available. It considers the breakdown and alteration of material near the earth's surface into products that are more in equilibrium with the newly imposed physico-chemical conditions. The processes at work, the material operated upon (rocks, minerals and clay minerals) and the products of weathering, including soil profiles, weathering profiles and some landforms are all considered in this account together with the time factor which is treated on the geological scale.

Eddies in marine science, edited by Allan R. Robinson (Berlin, Heidelberg, New York, Tokyo, Springer-Verlag, 1983. DM 120, US$ 49.60) surveys the results of recent research in eddy science and explores its implications for ocean science and technology. It attempts a comprehensive review suitable for a wide audience of marine scientists. The investigation of eddy-current phenomena is rapidly advancing; however, many of the most fundamental dynamical questions of eddy dynamics are still not understood. The book therefore intends to contribute to a global synthesis, to facilitate further research into eddy dynamics, and to encourage practical application. The knowledge of the physical science of eddies has important implications for biological, chemical and geological oceanography, for modern ocean science and for practical activities in the sea including exploitation and management of the marine environment and its resources.

Atlantic hydrophysical polygon-70, edited by V. G. Kort and V. S. Samoilenko (Rotterdam, A. A. Balkema Publishers, 1984. £15.50) includes the main results of hydrophysical and aerometeorological research on the Atlantic hydrophysical polygon. Projects and studies on the following subjects were carried out: space-time variability of oceanological fields under conditions of the open ocean; thermohaline structure of water masses; dynamic and thermal interaction between ocean and atmosphere; and meteorological phenomena in the tropical zone of the ocean. Also investigated were acoustic, geophysical, hydrochemical and biological matters and the radioactivity of the air environment.

Nuclear winter, by Mark A. Harwell (Berlin, Heidelberg, New York, Tokyo, Springer-Verlag, 1984. DM 54) is an authoritative account of the consequences of nuclear war for humans and the environment.

It is the first comprehensive analysis of the world after nuclear war that includes both effects on humans and the phenomenon of nuclear winter. Basing his work on realistic scenarios, the author presents new quantification of the direct effects of such a war, its impact on society and agriculture, and detailed analyses of the major effects of temperature and light reductions, radiation, ultraviolet light increases, and numerous other environmental stresses. This unique book draws on virtually all the sciences in giving the reader a description of life on earth in the days, years and decades after a nuclear war.

Awards

We are pleased to record that:

Dr K. A. Browning, FRS, Head of the Meteorological Office Radar Research Laboratory at Malvern, has been awarded the Jule G. Charney Award by the American Meteorological Society for fundamental contributions to our understanding of severe convective storms, the kinematics of fronts and cyclonic storms, and the methodology of Doppler radar observations.

Dr A. E. Gill of the Dynamical Climatology Branch has been awarded the Charles Chree Medal by the Institute of Physics. This award is made every two years.

Obituary

We regret to record the death of Eric Stirland, TTO II of the Operational Instrumentation Branch (Met O 16), on 7 December 1984.

Eric Stirland joined the Office as a Radio Technician in 1956 having spent some time in the electronics industry. After several years servicing a range of meteorological equipment on bases in the United Kingdom and abroad he was posted to the newly formed Cloud Physics Branch as a TTO III in 1967. He remained in that Branch for 17 years, during which time he was promoted to TTO II. During this period the emphasis of cloud physics research changed from laboratory-based studies to field experiments and Eric was involved in a wide range of practical tasks culminating in the development of a dropsonde for deployment from the C130 aircraft of the Meteorological Research Flight. He will be remembered for the patience and thoroughness with which he carried out his duties, often under arduous conditions, and for his willingness to carry out duties which involved many different skills. Eric returned to Met O 16, in order that he would become familiar with the developments in the operational instrumentation area, only a few months before his death.

Eric Stirland was popular among his colleagues and his advice and help were frequently sought. He had a keen interest in the well-being of his fellow technicians, was an active member of AGSRO and has served on Branch Council.

When not working Eric's main interests were his garden and his car, both of which were maintained with care and attention. His car, bought on return to Bracknell from Aden in 1967, and still in regular use after nearly 18 years, is a witness to his patience and skill.

Correction

Meteorological Magazine, January 1985, p. 32, 16th line from top of page, first word. For 'necessary' read 'unnecessary'.

THE METEOROLOGICAL MAGAZINE

No. 1354 May 1985 Vol. 114

CONTENTS

NOTICE

It is requested that all books for review and communications for the Editor be addressed to the Director-General, Meteorological Office, London Road, Bracknell, Berkshire RG12 2SZ and marked 'For Meteorological Magazine'.

The responsibility for facts and opinions expressed in the signed articles and letters published in this magazine rests with their respective authors.

Applications for postal subscriptions should be made to HMSO, PO Box 276, London SW8 5DT.

Complete volumes of 'Meteorological Magazine' beginning with Volume 54 are now available in microfilm form from University Microfilms International, 18 Bedford Row, London WC1R 4EJ, England.

Full-size reprints of Vols 1–75 (1866–1940) are obtainable from Johnson Reprint Co. Ltd, 24–28 Oval Road, London NW1 7DX, England.

Please write to Kraus Microfiche, Rte 100, Millwood, NY 10546, USA, for information concerning microfiche issues.

HMSO Subscription enquiries 01 211 8667.

Printed in England for HMSO and published by
HER MAJESTY'S STATIONERY OFFICE

£2.30 monthly

Dd. 738362 C13 5/85

Annual subscription £27.00 including postage

ISBN 0 11 727559 X
ISSN 0026–1149

THE METEOROLOGICAL MAGAZINE

HER MAJESTY'S STATIONERY OFFICE

June 1985

Met.O.967 No. 1355 Vol. 114

METEOROLOGICAL OFFICE Met.O.967

THE METEOROLOGICAL MAGAZINE

No. 1355, June 1985, Vol. 114

551.590.3

Climatic impact of explosive volcanic eruptions

By D. E. Parker

(Meteorological Office, Bracknell)

Summary

An analysis of sea surface temperatures for the northern hemisphere around the times of major volcanic eruptions in the past 100 years does not reveal any consistent tendency to significant post-eruption coolness. Air temperature anomaly maps suggest that volcanic eruptions do not predispose the atmospheric circulation to particular patterns. A report of overall coolness over land culminating a few months after northern hemisphere eruptions appears to be essentially correct, but such results may suffer from slight systematic bias induced by the Southern Oscillation.

1. Introduction

Kelly and Sear (1984) reported a marked air temperature decrease over land in the northern hemisphere in the 2 months following major northern hemispheric eruptions, and a lesser decrease in the 18 months following major southern hemispheric eruptions. The present paper extends the analysis of Kelly and Sear, using marine temperatures together with a land air-temperature data set based on Russian analyses and documented by Robock (1982).

The volcanic eruptions selected were the same as those used in the superposed epoch analysis of Kelly and Sear — see Table I. In this table the Volcanic Explosivity Index (VEI) is as defined by Simkin *et al.* (1981) and by Newhall and Self (1982); and the Dust Veil Index (DVI) (not weighted by the extent of the veil) is as defined by Lamb (1970). Following Kelly and Sear, the October 1902 eruption of Santa Maria (14.8°N, 91.6°W: VEI=6, DVI=600) was omitted from the superposed epoch analysis, because it followed Pelée and Soufrière by only 5 months. The effect of this choice is discussed later in the paper.

Monthly sea surface temperature anomalies (relative to 1951–60) from the Meteorological Office Historical Sea Surface Temperature data set (MOHSST3) were corrected for instrumental factors as in Folland *et al.* (1984), and then areally averaged over the northern hemisphere, before being combined into superposed epoch time series extending from 1 year before to 4 years after the eruption date. As done by Kelly and Sear, the northern and southern hemispheric eruptions were treated as separate sets. Individual eruptions were also considered separately. Fig. 1 shows the results of the superposed epoch analyses, and corresponds to Fig. 1 of Kelly and Sear. One difference from Kelly and Sear's procedure is that the sea surface temperature anomalies were not normalized, because the inter-annual standard deviation of monthly northern hemisphere sea surface temperatures has no discernible annual cycle,

Table I. *Volcanic events selected for superposed epoch analysis*

Date	Eruptions	Latitude	Longitude	VEI	DVI
		Northern hemisphere			
May 1902	Pelée	14.8°N	61.2°W	4 (twice)	100
	Soufrière	13.4°N	61.2°W	4	300
Mar. 1907	Ksudach	51.8°N	157.5°E	5	500
June 1912	Novarupta (Katmai)	58.3°N	155.2°W	6	500
Mar. 1956	Bezymyannaya	57.1°N	160.7° E	5	30
		Southern hemisphere			
Aug. 1883	Krakatau	6.1°S	105.4°E	6	1000
June 1886	Tarawera	38.2°S	176.5°E	5	800
Apr. 1932	Azul (Quizopu)	35.7°S	70.8°W	5	70
Mar. 1963	Agung	8.3°S	115.5°E	4	800

being (on the basis of data for 1951–80) between 0.13 °C and 0.17 °C for all months. Fig. 1 does follow Kelly and Sear, however, in referring the sea surface temperatures to the average level in the pre-eruption year.

Fields of air temperatures over land and sea were also subjected to limited superposed epoch analysis, in a search for systematic geographical, circulation-related changes.

Finally, the effects of altering the choice of eruptions have been assessed, and the uncertain effect of the 1982 eruption of El Chichon is noted.

2. Results

(a) *Superposed epoch analysis*

Fig. 1(a) is unlike the corresponding sequence obtained by Kelly and Sear, in that there is not a sharp minimum 2 months after the eruption, but a broad trough from 6 months to nearly 2 years after it. There is evidence, however, in both cases that cooling began before the eruption, suggesting that the shape of Fig. 1(a) may be a fortuitous result of the effects of fluctuations on 2–5 year time-scales, such as the Southern Oscillation. The dashed lines in Fig. 1 represent the 95% significance levels $\pm 2\sigma N^{-\frac{1}{2}}$ where σ is assumed to be 0.15 °C and $N = 4$ eruptions. The number of excursions beyond these lines does not exceed random expectation (5% of 60 months, i.e. 3 months). This statistical test is probably too lax because the data are serially correlated, and Kelly and Sear's Monte Carlo test is to be preferred: but the lack of significance found by the lax test emphasizes the nullity of the results. It can of course be expected that the ocean, owing to its thermal capacity, responds more slowly and to a lesser degree to short-term thermal forcing than does the land. However, Fig. 1 does not show that there is any clear-cut response whatsoever. Fig. 1(b) presents a particularly unsystematic picture.

The possible influence of the Southern Oscillation on Fig. 1(a) was investigated by combining into a superposed epoch time series the Southern Oscillation Index of Wright (1977) for the periods around the relevant four northern hemispheric eruptions (Fig. 2). Analysis of MOHSST3 data has revealed that, in general, maximum (minimum) northern hemisphere sea surface temperature lags behind minimum (maximum) Southern Oscillation Index by about 9 months. Although the trends in Fig. 2 are not

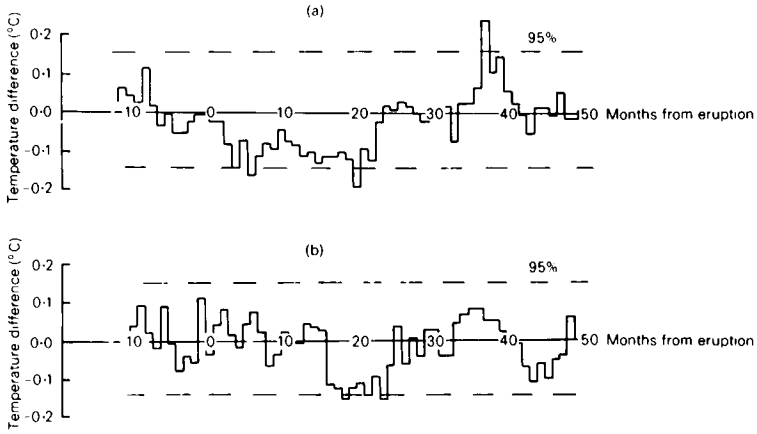

Figure 1. Sequences of northern hemisphere sea surface temperature difference around the time of major volcanic eruptions in (a) the northern hemisphere and (b) the southern hemisphere. The reference level is the mean of months -12 to -1, and the dashed lines represent the 95% significance levels.

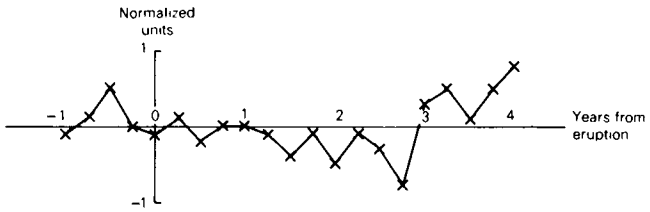

Figure 2. Sequences of Southern Oscillation Index around the time of major volcanic eruptions in the northern hemisphere.

marked, they would indicate a weak fortuitous minimum of sea surface temperature about one season (3 months) after the eruption. The maximum atmospheric (as opposed to oceanic) warmth occurs 6 months after minimum Southern Oscillation Index or maximum eastern tropical Pacific sea surface temperature (Pan and Oort 1983), but this includes the tropics where the lag is reduced: over the generally higher latitude northern hemisphere land area studied by Kelly and Sear the lag is likely to be nearer 9 months, as for the ocean, again giving minimum warmth about one season after the eruption. Thus sampling bias with respect to the Southern Oscillation may have slightly affected the results of Kelly and Sear.

The land air-temperature data from the Russian source, documented by Robock (1982), were used to repeat the computations made by Kelly and Sear including the normalization process. The results were very similar to those of Kelly and Sear, with peak coolness 2 months after eruptions, as expected in view of the high correlation (>0.9) between data sets (Jones *et al.* 1982).

(b) *Sequels to individual eruptions*

Fig. 3 (northern hemispheric eruptions) and Fig. 4 (southern hemispheric eruptions) demonstrate the diversity of the sequels to the eruptions. Soufrière and Pelée were followed by a brief warming of the northern hemisphere sea surface, and Ksudach by little change despite its DVI of 500 (Table I). The prolonged minimum in Fig. 1(a) appears to have resulted largely from one eruption, Katmai, with small or shorter contributions from the other three, weighing against the statistical significance of the composite. The shape of Fig. 1(b) derives to a considerable extent from the sequel to Agung (Fig. 4(d)).

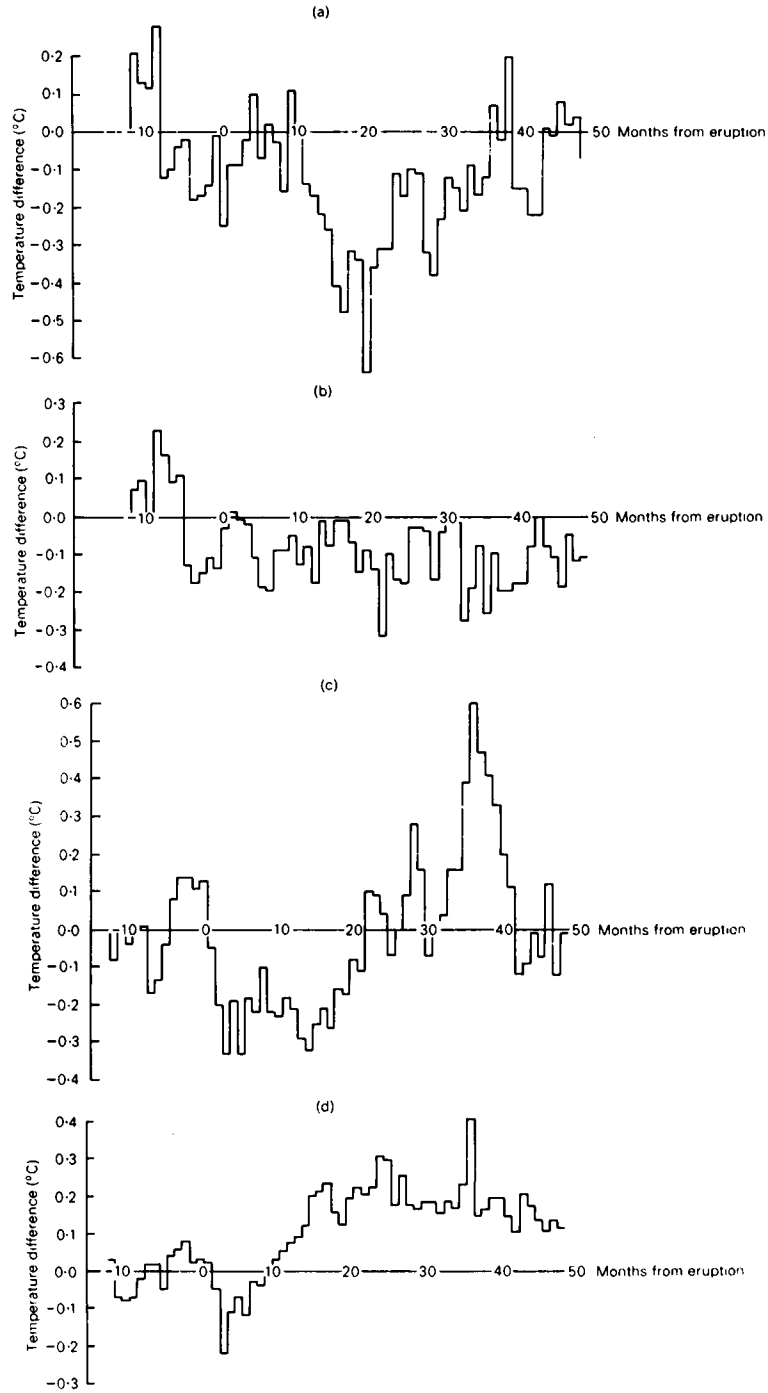

Figure 3. Sequences of northern hemisphere sea surface temperature difference around the time of major volcanic eruptions in the northern hemisphere, (a) Soufrière and Pelée (May 1902), (b) Ksudach (March 1907), (c) Novarupta (Katmai) (June 1912) and (d) Bezymyannaya (March 1956). The reference level is the mean of months -12 to -1.

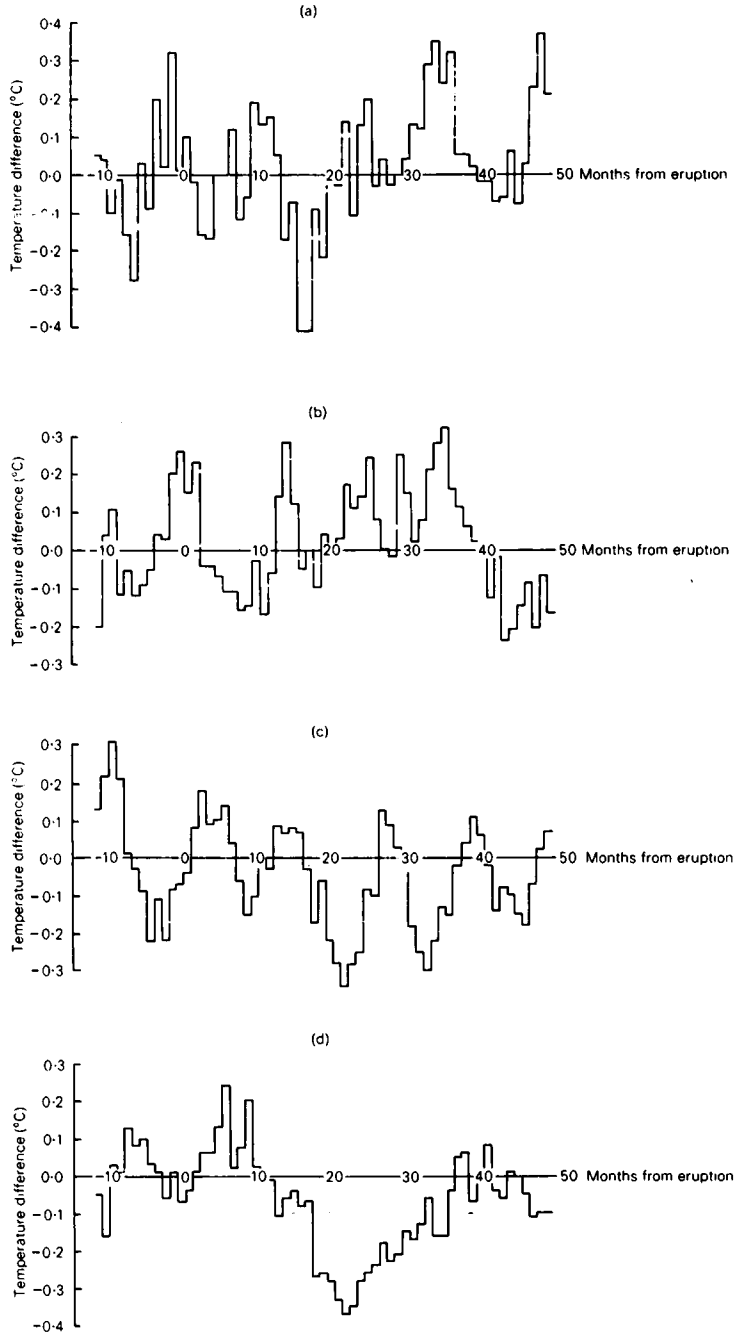

Figure 4. Sequences of northern hemisphere sea surface temperature difference around the time of major volcanic eruptions in the southern hemisphere, (a) Krakatau (August 1883), (b) Tarawera (June 1886), (c) Azul (April 1932) and (d) Agung (March 1963). The reference level is the mean of months -12 to -1.

Note an apparent annual cycle in some of the sequences in Figs 3 and 4. This is likely to be partly the result of a need to apply seasonally varying corrections to sea surface temperatures as measured from uninsulated buckets; but the sequel to Azul (Fig. 4(c)) also appears to reflect a real enhancement of the annual cycle in the 1930s in the Gulf Stream region, affecting marine air temperatures also and probably resulting from enhanced summer anticyclonicity and enhanced winter north-westerly flow in the atmosphere.

Fig. 3 of Kelly and Sear shows rather diverse sequels to southern hemispheric eruptions, but their Fig. 2 consistently indicates relatively cold conditions about 2 months after each northern hemispheric eruption. The present paper therefore now examines fields of air temperatures world-wide 2 months after the northern hemispheric eruptions, in order to discover geographical patterns of, and possible reasons for, the consistent results obtained by Kelly and Sear. Fig. 5(a) shows a composite field which refers to 2 months later than each of the four eruptions. The land air temperatures are from the Russian source documented by Robock (1982), and the marine air temperatures are from the Meteorological Office Historical Marine Air Temperature (MOHMAT2) night-time data set. These times of observation were used to avoid spurious heating on deck. The data are not normalized: this would have been necessary over land if the months combined had ranged throughout the calendar, but in fact they only ranged from May to August. The data are anomalies with respect to 1951–80. There are no land data for the southern hemisphere. It is immediately clear that the composite cooling of Kelly and Sear derived from a marked effect over Canada, changes elsewhere being weak, though detailed interpretation of Fig. 5(a) is inappropriate because the reference is 1951–80 and not the pre-eruption years. Fig. 5(b) presents the same anomalies relative to those prevailing in the eruption months: the coldness over North America is again evident, but is greater in the southern USA and in northern Siberia than in Fig. 5(a), because the eruption months happened, on average, to be warm in these regions. The reverse applies to south-eastern Europe. Figs 6 to 9 display air temperatures (relative to 1951–80) 2 months after the individual eruptions, and show that the Canadian coldness resulted from the sequels to Ksudach and Bezymyannaya (Figs 7 and 9) and not the other two eruptions, which, however,

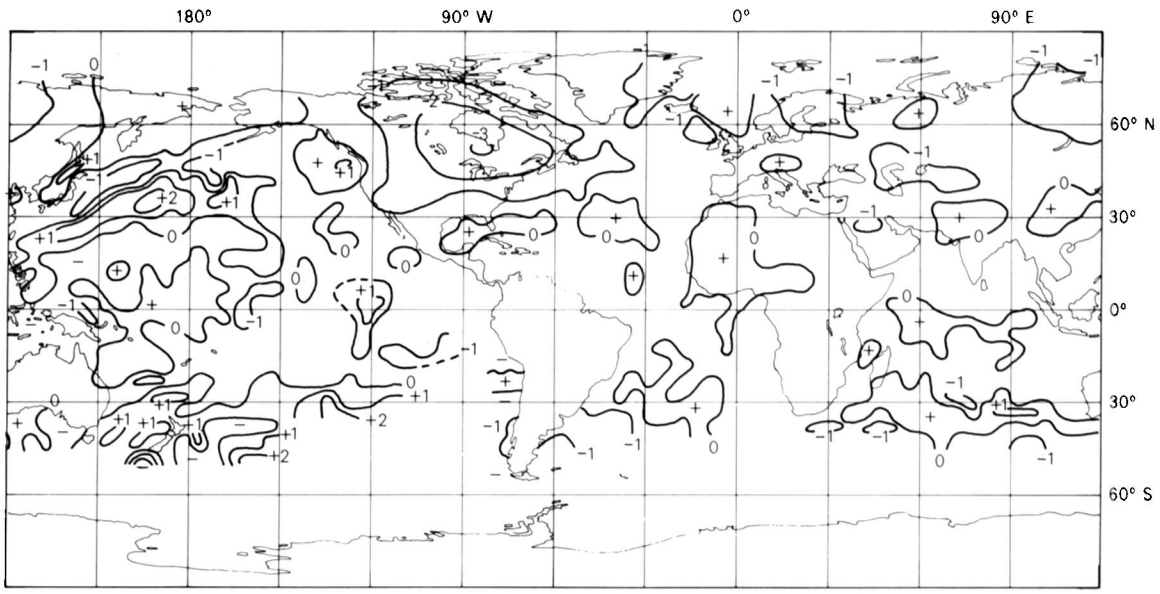

Figure 5(a). Land air temperature and night-time marine air temperature anomalies (°C), with respect to 1951–80, composited from data for July 1902, May 1907, August 1912 and May 1956 (2 months after each northern hemispheric eruption).

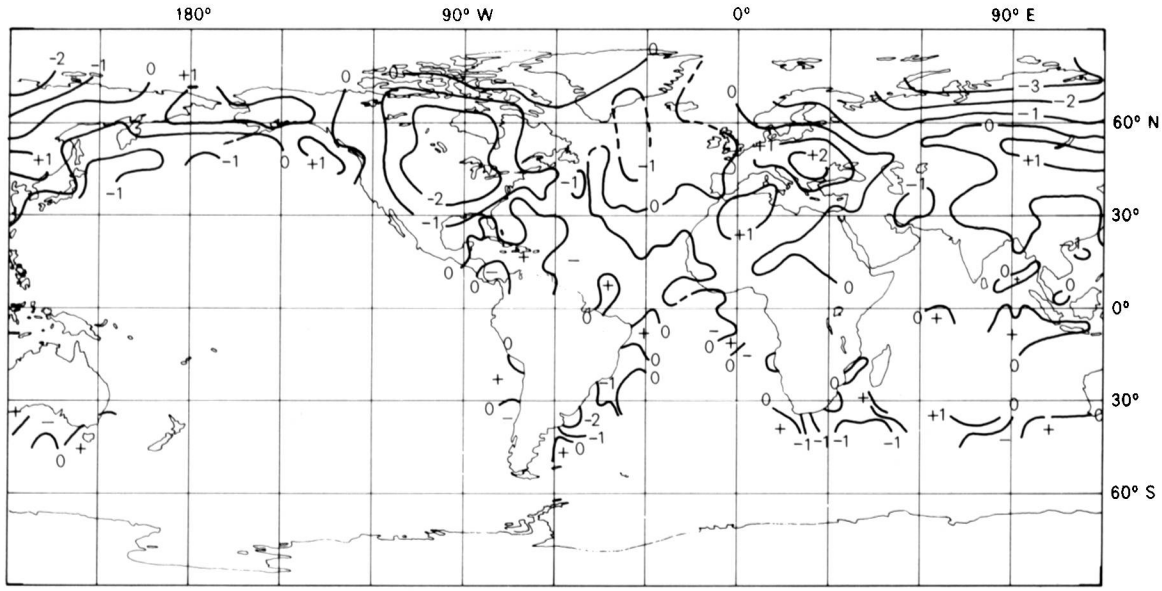

Figure 5(b). Land air temperature and night-time marine air temperature composited anomalies (°C) for July 1902, May 1907, August 1912 and May 1956 with respect to composited anomalies for May 1902, March 1907, June 1912 and March 1956.

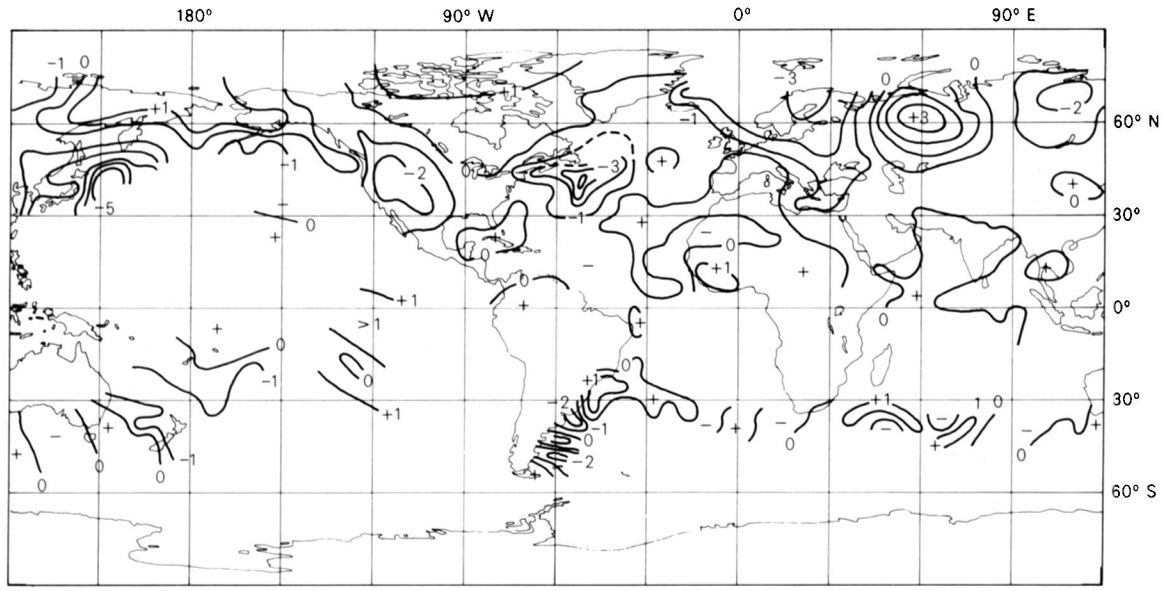

Figure 6. Land air temperature and night-time marine air temperature anomalies (°C), with respect to 1951–80, for July 1902 (2 months after Soufrière and Pelée).

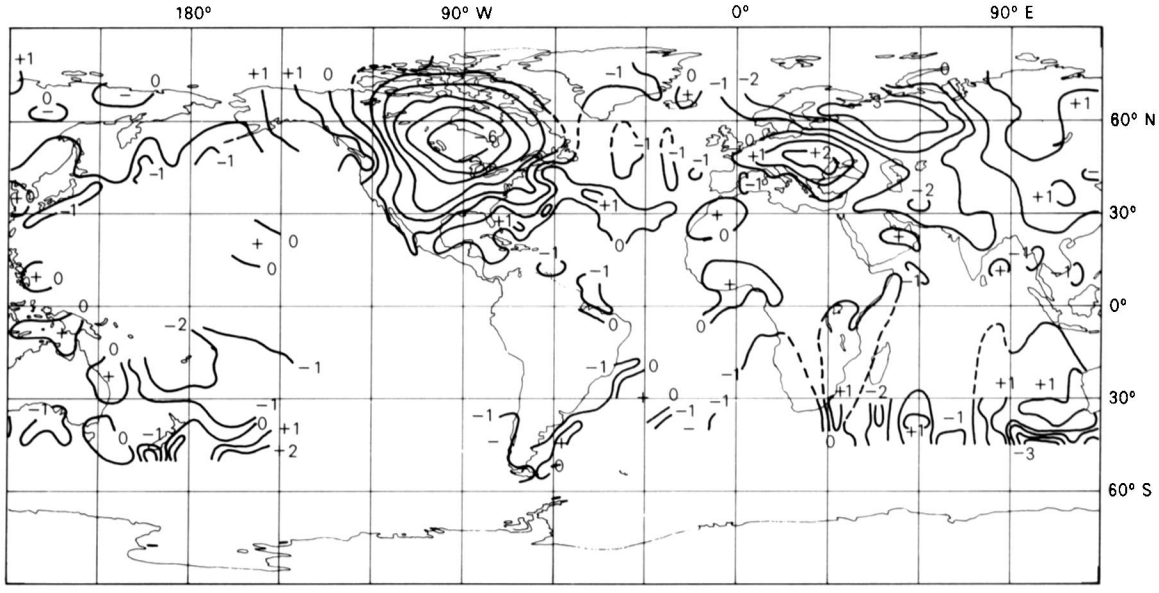

Figure 7. Land air temperature and night-time marine air temperature anomalies (°C), with respect to 1951–80, for May 1907 (2 months after Ksudach).

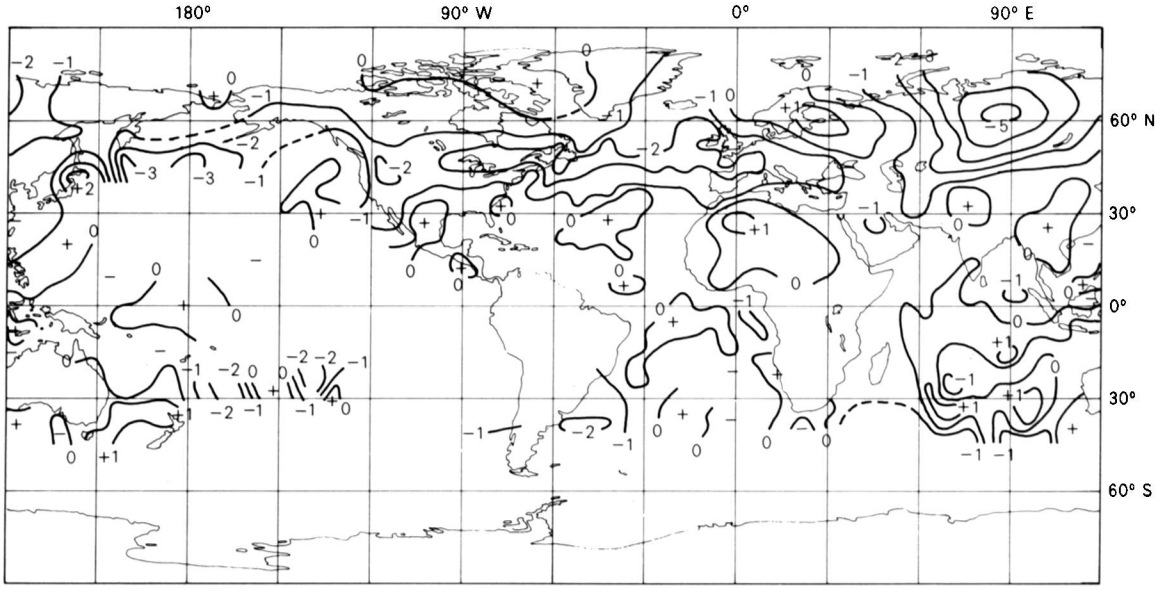

Figure 8. Land air temperature and night-time marine air temperature anomalies (°C), with respect to 1951–80, for August 1912 (2 months after Katmai).

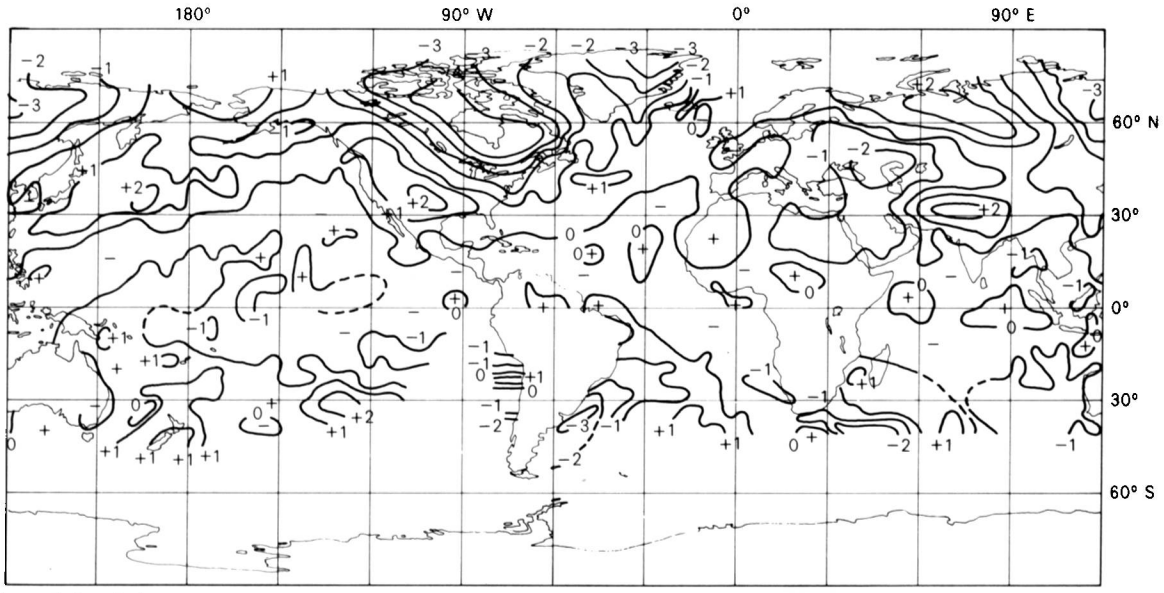

Figure 9. Land air temperature and night-time marine air temperature anomalies (°C), with respect to 1951–80, for May 1956 (2 months after Bezymyannaya).

happened to have predominantly cold sequels over the northern hemisphere land masses (Figs 6 and 8) in agreement with Fig. 2 of Kelly and Sear. The extreme cold of August 1912 (Fig. 8), 2 months after Katmai, stands out even against the average conditions for 1911–20 which were colder than the 1951–80 normal (Fig. 10: see also Folland *et al.* (1984)). The diversity of the results in Figs 6 to 9 weighs against the hypothesis, discussed by LaMarche and Hirschboeck (1984), that volcanic eruptions predispose the atmospheric circulation to particular anomalous patterns. Although the general coldness in Figs 6 to 9 supports Kelly and Sear, the caveat concerning sampling with respect to the Southern Oscillation still stands. A further problem, the small sample size, cannot yet be overcome because of the brevity of reliable observational records.

(c) *Santa Maria*

The eruption of Santa Maria was larger than that of Pelée or Soufrière (Table I), and there is therefore a strong case for using its date (October 1902) as the zero-time for the 1902 eruptions. Examination of Kelly and Sear's Fig. 2 shows that this will slightly weaken the immediate post-eruption cooling, as the standardized temperature remained constant for 2 months after Santa Maria, before a sharp temporary rise. Their essential result would, however, be unchanged. A similar amendment to the present work for sea surface temperature would move the bottom of the trough in Fig. 2(a) to 10–15 instead of 15–20 months, without drastically altering the general conclusions.

It is relevant to note that there was a sharp global marine cooling around 1903, introducing the coldest period of the 1856–1984 record (Folland *et al.* 1984). The spatial distribution of this cooling is shown for summer in Fig. 11 which also shows that the land did not, on average, cool significantly at this time. There was a major cooling of the mid-latitude North Atlantic. This cooling is consistent with changes of Ekman drift and evaporation caused by the distribution of mean-sea-level pressure change shown in Fig. 12: in other words, the 1903 cooling appears, on cursory examination, to be an ocean–atmosphere interactive phenomenon which may not have any connection with the volcanic eruptions of 1902. It has already been stressed that in the light of Figs 6 to 9, volcanic eruptions do not seem to encourage particular atmospheric circulation patterns.

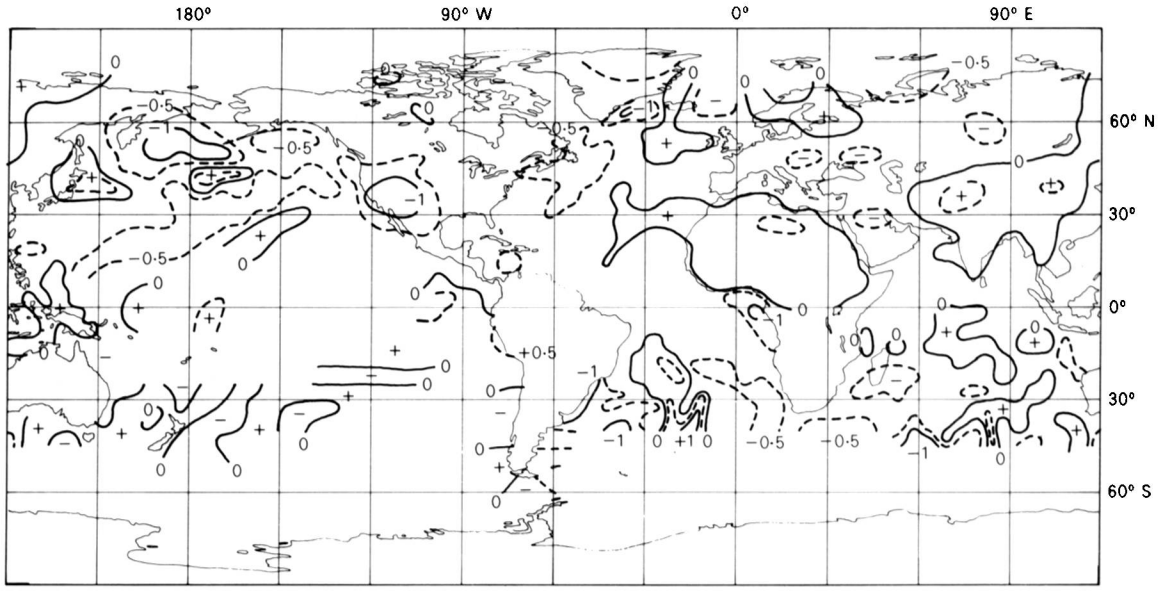

Figure 10. Average land and night marine air temperatures for July–September 1911–20 relative to 1951–80. Contours every °C (solid lines) and at ½°C (dashed lines).

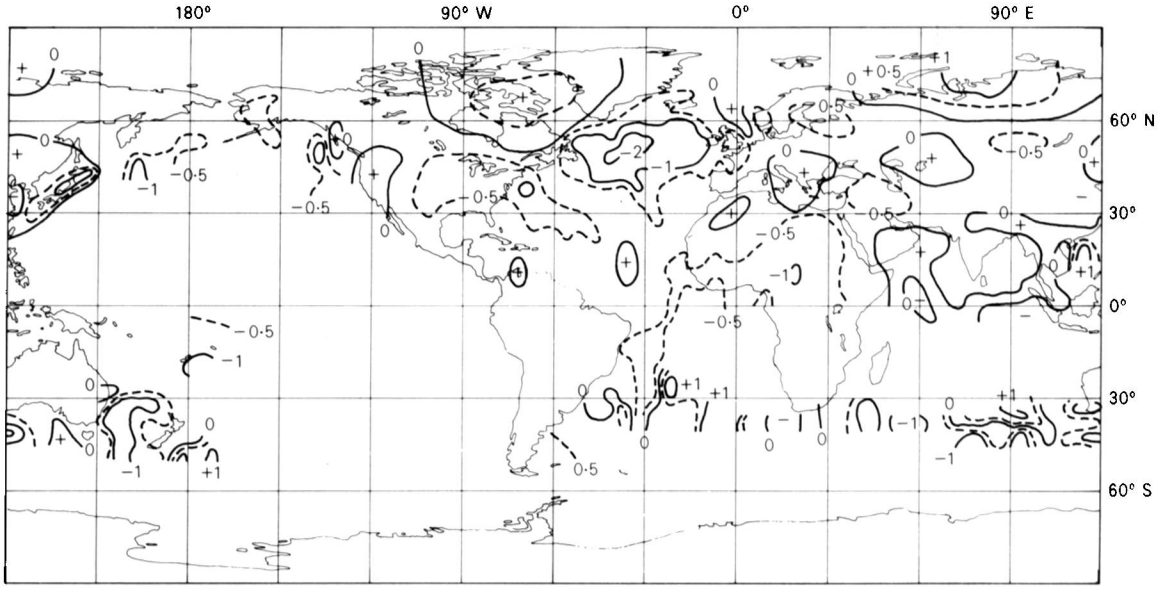

Figure 11. Average land and night marine air temperatures for July–September 1903–7 relative to those for 1898–1902. Contours every °C (solid lines) and at ½°C (dashed lines).

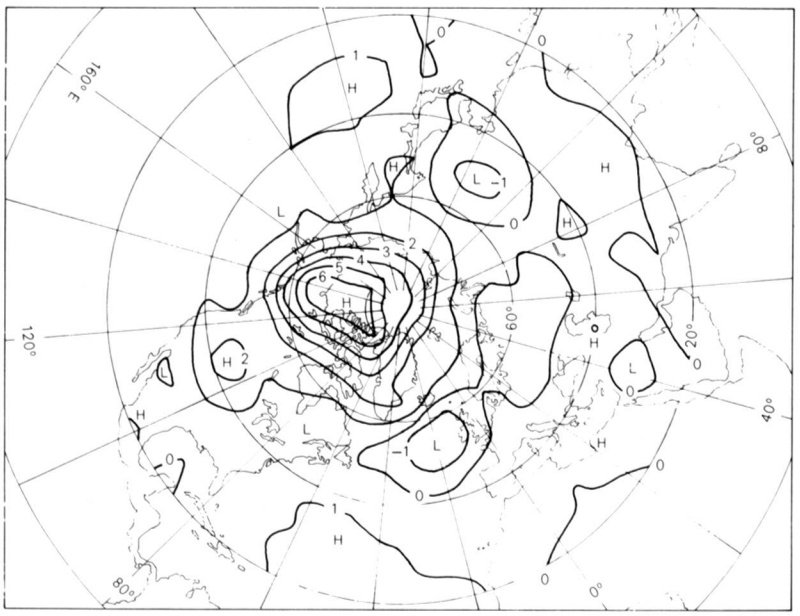

Figure 12. Mean-sea-level pressure for June–September 1903–7 relative to that for 1898–1902. Contours every mb.

(d) *Bezymyannaya (The Russian word means 'nameless')*

This eruption may have been feebler than the others in Table I, and its omission must therefore be considered. This would make the results obtained by Kelly and Sear more marked, because Bezymyannaya was followed by the weakest cooling (their Fig. 2). Omission of Bezymyannaya would also strengthen the present results (Fig. 3(d)).

(e) *El Chichon*

The temperature anomaly field in June 1982, 2 months after the major eruption of El Chichon (Mexico), is shown in Fig. 13 and adds further variety to the sequels already shown in Figs 6 to 9. Kelly and Sear point out that study of the effects of El Chichon is likely to be very difficult because of the exceptional warmth of 1981 and the onset of cooling before the eruption. The sea surface temperature sequence for the northern hemisphere (Fig. 14) appears to show a discontinuity between December 1981 and January 1982, when the operational data set succeeds the historical data set. The historical data set is probably unreliable for late 1981 because the data are sparse: the operational data are more plentiful but have been subjected to less stringent quality control. Thus, firm conclusions cannot be drawn, but there appears to be only gradual cooling during 1982–4, and the maximum coolness 5 months after the eruption is not marked in view of the 0.15 °C inter-annual standard deviation of northern hemisphere monthly sea surface temperature.

4. Conclusion

The present study does not reveal any consistent tendency to significantly low northern hemisphere sea surface temperatures after the eruptions. Air temperature anomaly maps suggest that volcanic eruptions do not predispose the atmospheric circulation to particular patterns.

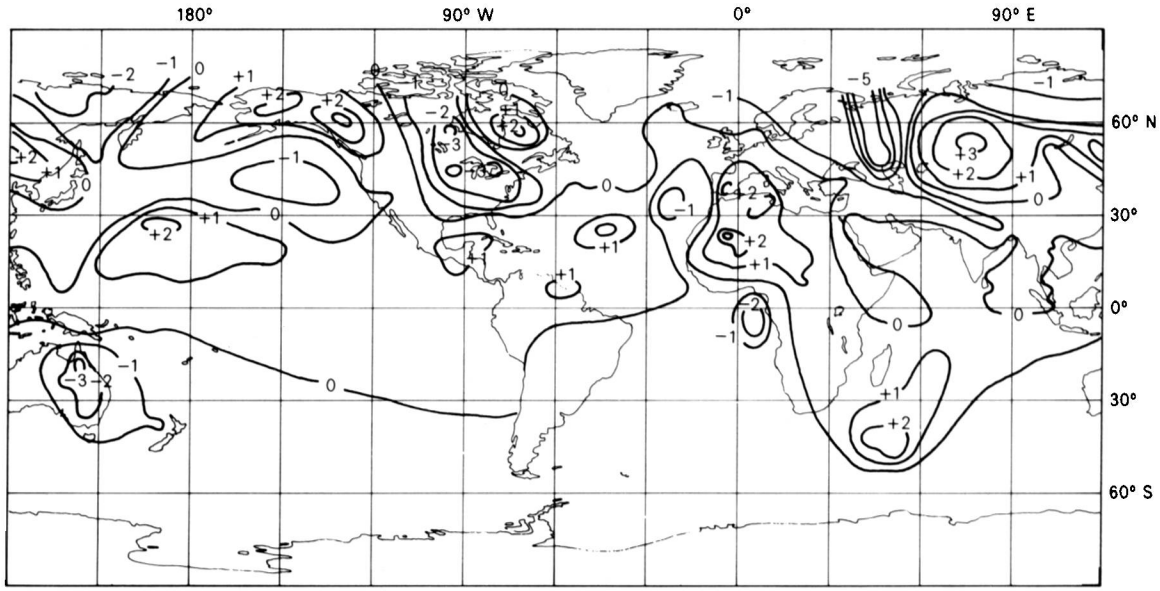

Figure 13. Land air and sea surface temperature anomalies (°C) for June 1982 (2 months after El Chichon). A variety of periods was used for 'normals'.

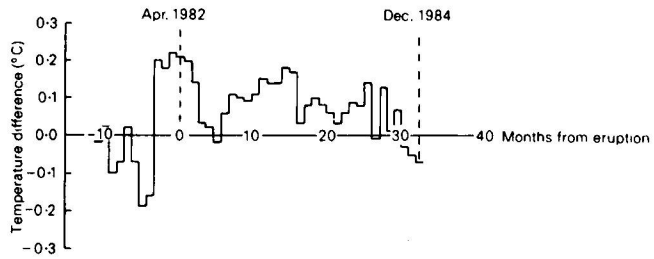

Figure 14. Sequence of northern hemisphere sea surface temperature difference around the time of the eruption of El Chichon. The reference level is the mean of months -12 to -1.

The result obtained by Kelly and Sear, of coolness over northern hemisphere land peaking 2 months after northern hemispheric volcanic eruptions, is as valid as can be obtained in the present situation, but the following factors weigh against the statistical significance of the results:

(a) slight systematic bias in the superposed epoch analyses, resulting from the Southern Oscillation and

(b) the unavoidably small sample size.

The selection of volcanic events used by Kelly and Sear is sound in view of the known volcanic record (e.g. Lamb 1970). The results are not sensitive to slight changes in the selection criteria.

References

Folland, C. K., Parker, D. E. and Kates, F. E. 1984 Worldwide marine temperature fluctuations 1856–1981. *Nature*, **310**, 670–673.

Jones, P. D., Wigley, T. M. L. and Kelly, P. M. 1982 Variations in surface air temperatures: Part 1. Northern Hemisphere, 1881–1980. *Mon Weather Rev*, **110**, 59–70.

Kelly, P. M. and Sear, C. B.	1984	Climatic impact of explosive volcanic eruptions. *Nature*, **311**, 740–743.
LaMarche, V. C. and Hirschboeck, Katherine K.	1984	Frost rings in trees as records of major volcanic eruptions. *Nature*, **307**, 121–126.
Lamb, H. H.	1970	Volcanic dust in the atmosphere; with a chronology and assessment of its meteorological significance. *Philos Trans R Soc*, **266**, 425–533.
Newhall, C. G. and Self, S.	1982	The Volcanic Explosivity Index (VEI): an estimate of explosive magnitude for historical volcanism. *J Geophys Res*, **87**, 1231–1238.
Pan, Y. H. and Oort, A. H.	1983	Global climate variations connected with sea surface temperature anomalies in the eastern equatorial Pacific Ocean for 1958–73 period. *Mon Weather Rev*, **111**, 1244–1258.
Robock, A.	1982	The Russian surface temperature data set. *J Appl Meteorol*, **21**, 1781–1785.
Simkin, T., Siebert, L., McClelland, Lindsay, Bridge, D., Newhall, C. and Latter, J. H.	1981	Volcanoes of the world. Washington Smithsonian Inst., Stroudsberg, Penn., Hutchinson Ross.
Wright, P. B.	1977	The Southern Oscillation — patterns and mechanisms of the teleconnections and the persistence. Hawaii Institute of Geophysics HIG-77-13.

551.501.7:551.507.362.2:681.3

The HERMES system

By J. Turner, J. R. Eyre, D. Jerrett and E. McCallum

(Meteorological Office, Bracknell)

Summary

A description is given of the mini-computer-based system which has recently been installed in the Satellite Meteorology Branch of the Meteorological Office to aid research into the uses of high-resolution satellite data. Examples of images processed on the system are illustrated, as well as results from the Local Area Sounding System.

1. Introduction

The HERMES (High-resolution Evaluation of Radiances from MEteorological Satellites) system is a minicomputer-based data-processing facility which was installed in the Satellite Meteorology Branch of the Meteorological Office during 1983. The aim is to assist research and development into the applications of high-resolution digital satellite data which are broadcast by the polar-orbiting and geostationary satellites. So far, this work has mainly concentrated on two specific topics: firstly the development of a Local Area Sounding System (LASS) which can routinely generate temperature and humidity profiles for the North Atlantic and western European area from the raw sounding-instrument data broadcast by the USA's TIROS-N series satellites; secondly, the investigation of ways that the full-resolution, multi-spectral, digital-imagery data can best be exploited to provide forecasters with useful satellite products.

This paper has been prepared to give an account of the development of the system and a status report on both these projects, but with particular emphasis on the LASS development work since soundings generated by the system are now being used operationally within the Meteorological Office.

2. Hardware

The HERMES system is based on a Digital Equipment Corporation (DEC) VAX 11/750 minicomputer with 2 megabytes of memory and three Winchester hard discs capable of storing over 500 megabytes of data. Fig. 1 shows the major hardware components of the VAX computer and the system console. Access to the system is via eight visual display units (VDUs) in the Satellite Meteorology Branch, and development work can take place in parallel with the semi-operational tasks connected with LASS operations.

Figure 1. The DEC VAX 11/750 computer of the HERMES system.

A Sigmex Electronics Advanced Raster Graphics System (ARGS) 7000 (shown in Fig. 2) is available for the display of satellite imagery or graphical output from LASS in a number of forms including fields of data, tephigrams and cross-sections. The ARGS contains its own 16-bit microprocessor along with 3 megabytes of image memory which can be configured in a number of ways depending on the application. The monitor has a resolution of 1024 by 1024 picture elements (pixels) with a palette of 16 million colours available for use in image displays!

There are currently three main external communications links from the HERMES system:

(a) A Remote Job Entry link to the Meteorological Office's COSMOS computing facility, running at 9.6 kilobits per second.

(b) A link, operating at 9.6 kilobits per second, to the satellite receiving station at Lasham in Hampshire, along which the sounding data from the polar-orbiting satellites are transmitted.

(c) A DECnet link to 'HOMER', the twin computer system of HERMES, at the Meteorological Office Unit at Oxford University where part of the Satellite Meteorology Branch is now located. This operates at 48 kilobits per second over a British Telecom KILOSTREAM link.
A schematic diagram of the HERMES system is shown in Fig. 3.

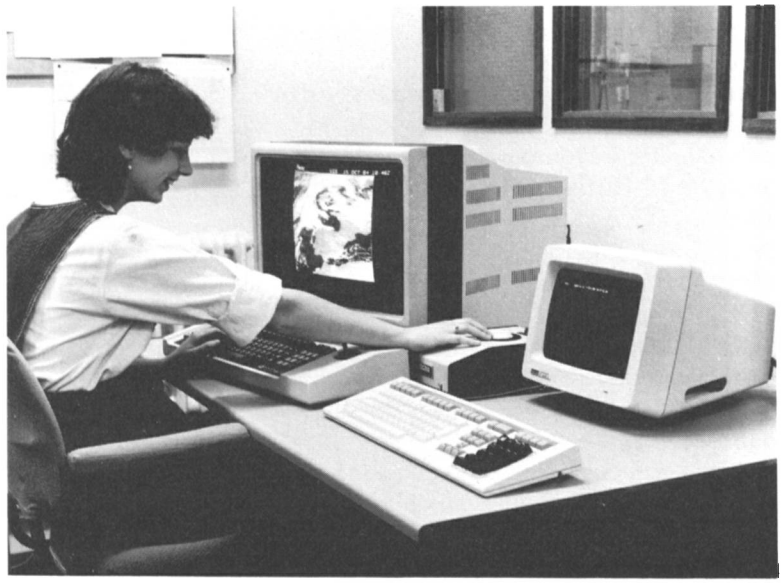

Figure 2. The Sigmex ARGS 7000 used on the HERMES system.

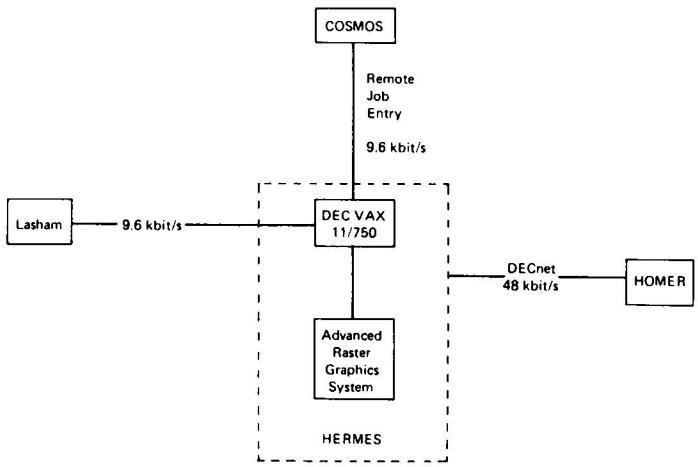

Figure 3. The HERMES system and its data links.

3. Image processing

The computing facilities of the HERMES system offer great scope for investigations into the uses of satellite imagery, both for specific research tasks and also for developing new products for future operational dissemination.

The operational satellite imagery dissemination system currently used within the Office (AUTOSAT and SATFAX) is largely based on data broadcast by the satellites in analogue format. These data are primarily intended for output on facsimile recorders and provide data with a coarser horizontal resolution, a lower number of grey levels, and with fewer spectral channels than can be obtained if the full digital data stream from the satellite is used.

Research is therefore under way into applications of the full-resolution data which will shortly be available at Bracknell in near-real time via the METSATNET link from Lasham. METSATNET will use a British Telecom MEGASTREAM link operating at 2 megabits per second to send Meteosat PDUS (Primary Data Users' Station) and TIROS-N series AVHRR (Advanced Very High Resolution Radiometer) data from Lasham to the Meteorological Office Headquarters.

Until METSATNET is operational, selected images in digital format are obtained on computer compatible tapes (CCTs) for use in research projects on the HERMES system. Five-channel AVHRR images, at the full horizontal resolution of 1 kilometre, are obtained from the University of Dundee, who store all AVHRR data for passes over the United Kingdom, or from the Royal Aircraft Establishment at Farnborough who maintain a 1-week rolling archive of the data received at Lasham. Occasional CCTs of Meteosat PDUS images are also obtained from Lasham.

Fig. 4 is a typical example of a full-resolution, single-channel AVHRR image displayed on the ARGS, and shows the channel 2 (0.9 μm) image from NOAA-6 at 1819 GMT on 5 June 1980. At this time there

Figure 4. A NOAA-6 AVHRR channel 2 image at 1819 GMT on 5 June 1980.

was intense convective activity in the Midlands, and the deep vertical extent of the cumulonimbus clouds can be seen from the shadows cast by the early evening sunlight. Fig. 5 shows a section from a Meteosat visible image for 1000 GMT on 15 October 1984. At the latitude of the United Kingdom the horizontal resolution is approximately 3 km in the east–west and 5 km in the north–south direction.

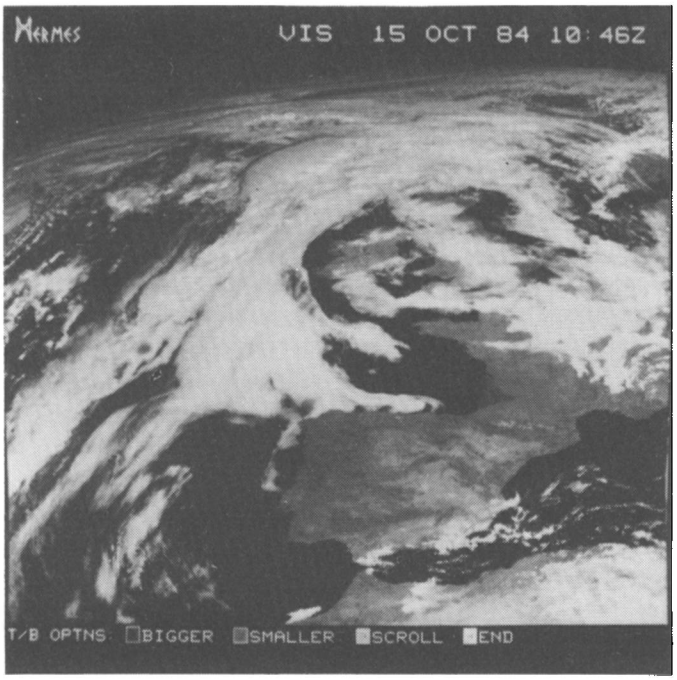

Figure 5. A Meteosat visible image at 1000 GMT on 15 October 1984.

One of the earliest studies with these data has been in the detection of fog or low stratus at night using data from the 3.7 and 11 μm channels of AVHRR. This technique is now being evaluated for possible operational use in the future and has been described by Eyre *et al.* (1984).

Currently, imagery research is taking place on a number of specific topics, with one of the most important being the derivation of surface temperatures from the 'split-window' 11 and 12 μm channels of the AVHRR/2 on NOAA-7 and NOAA-9. The basic technique used has been described by Llewellyn-Jones *et al.* (1984) and the possible applications of these data for use by forecasters and as input to the mesoscale model are under investigation. See Golding (1984) for the current status of the mesoscale model.

These high-resolution digital data offer tremendous possibilities for assisting operational forecasters in many areas of their work, and imagery research on the HERMES system is being directed towards preparing for its operational utilization in the future.

4. The Local Area Sounding System (LASS)

4.1 *Why a local area sounding system?*

Until recently the only atmospheric sounding data available routinely within the Office were the SATEM messages derived in the USA and received over the Global Telecommunication System (GTS),

in the form of thicknesses between standard levels. These are produced by the National Environmental Satellite Data and Information Service of the National Oceanic and Atmospheric Administration (NOAA/NESDIS) in Washington from the global raw satellite-instrument data which are recorded on the satellites and replayed to one of three reception stations. The problem with these data is that the time between the satellite making an observation and the resulting sounding being received at Bracknell is at least 3 hours and can be much longer. Consequently many of the observations fail to arrive early enough to be included in the main numerical analyses which are produced at $T+2$ hours and $T+(3$ hours 20 minutes) for the fine-mesh, limited-area and coarse-mesh, global analyses respectively. This delay results in the forecasts being run when only about 25% of the potentially available SATEMs have been received.

The other disadvantage of the SATEMs is that the data are horizontally averaged to a resolution of around 400 km and, while this may be adequate to describe the broad-scale thermal structure, it is not possible to resolve sub-synoptic-scale features.

The LASS was therefore established with the aim of exploiting the full potential of the sounding data, by deriving atmospheric profiles with a much higher horizontal resolution (currently 80 km) and delivering the data to the operational users within a very short period of the satellite overpass. (See Table I.)

Table I. *Comparison of SATEM data and LASS soundings*

	SATEMs	LASS
Coverage	Global	3000 km radius of Lasham
Horizontal resolution	400 km	80 km
Time lag (reaching COSMOS)	At least 3 hours	40 minutes
Data available	Thickness values and precipitable water content for standard layers	Standard-level temperatures, dew-points, plus derived thermal winds, thicknesses and precipitable water content

4.2 *The satellite instruments*

The TIROS-N series of polar-orbiting satellites contain a number of instruments for monitoring the atmosphere and the underlying surface. The best known are the imaging radiometers which produce high-resolution images for use in synoptic analysis, and also allow the computation of surface and cloud-top temperatures. These instruments measure radiation at wavelengths in the visible and infra-red regions of the spectrum where the atmospheric absorption is low, and consequently depict the surface or cloud tops with only minimal atmospheric attenuation.

However, the TIROS-N satellites also carry radiometers which detect radiation at wavelengths where most of the radiation has been emitted by the atmosphere itself, and from which information on the temperature and humidity structure of the atmosphere can be derived. This group of sounding instruments is collectively known as the TIROS Operational Vertical Sounder (TOVS) and is made up of the three following components:

(a) The High-resolution Infra-Red Sounder (HIRS/2), which has 19 infra-red channels (and 1 visible) for sounding in the troposphere and the lower stratosphere.

(b) The Microwave Sounder Unit (MSU) which has four channels at frequencies at around 55 GHz, also for sounding in the tropopause.

(c) The Stratospheric Sounder Unit (SSU) which has three channels in the infra-red at around 15 μm and uses a pressure modulation technique to detect radiation from the middle and upper stratosphere.

Further information on the design and operation of the TOVS can be obtained from Schwalb (1978), while the SSU (which is provided by the Meteorological Office) has been described in detail by Miller *et al.* (1980).

Each of the instruments scans the earth from left to right, covering a swath below the satellite track which is over 2000 km wide for the HIRS and MSU, and 1500 km for the SSU.

At wavelengths for which atmospheric absorption is high, most of the radiation measured at the satellite has been emitted by the atmosphere itself. It is possible to isolate radiation emitted by particular layers of the atmosphere by careful selection of the wavelengths sensed by the instrument. (See Eyre and Jerrett (1982) for a fuller discussion of the selection of wavelengths.) The 20 channels of the HIRS have been chosen so that information is available for a number of different sounding tasks. The temperature sounding data are available from seven channels in the 15 μm carbon dioxide band and five channels in the 4.3 μm carbon dioxide/nitrous oxide band, while water vapour sounding can be performed using the three channels in the 6–8 μm water vapour band.

The four MSU channels are all located around 55 GHz with three channels in a region of strong oxygen absorption to provide temperature sounding data which are little affected by cloud contamination.

The SSU is designed to produce data from which stratospheric (25–50 km) temperature profiles can be determined. In conjunction with HIRS and MSU data it is therefore possible to generate temperature profiles from the surface to 50 km. At the moment SSU data are not processed on HERMES, although the system could be modified to do so.

4.3 *The LASS processing system*

As described earlier the global TOVS data are recorded on the spacecraft and transmitted to the ground stations for the generation of the SATEMs. However, the full TOVS data for the area currently viewed by the satellite are also broadcast in real time, and can be acquired by any receiving station in the satellite's direct line of sight. Since September 1983 the HERMES system has been receiving the TOVS data in real time from the ground station at Lasham, which can receive data from the TIROS-N series spacecraft when they are within about 3000 km.

The processing of the raw TOVS data into temperature and humidity mixing ratio profiles takes place automatically on the HERMES system which, when there are two satellites operating, can process up to 16 passes per day.

The suite of programs which generate the meteorologically useful products was originally obtained from the NOAA/NESDIS Development Laboratory at Madison, Wisconsin, and modified to allow it to be run on the hardware configuration of the HERMES system. The technique used to perform the 'retrieval' (i.e. to obtain temperature and humidity profiles from the radiances received at the satellite) is very similar to that used to derive the SATEMs and has been described by Smith *et al.* (1979). The scheme is based on the use of multiple linear regression to obtain the standard-level temperatures and humidity mixing ratios from the HIRS and MSU radiances, with the regression coefficients currently being received every week from the USA. The coefficients are derived from collocations of satellite soundings and radiosondes over the previous 2 weeks, and separate coefficients are provided for each 30° latitude band. Interpolation is used to prevent steps at zone boundaries.

The actual processing of the satellite data involves many stages. However, the major components of the system are illustrated in Fig. 6 and can be summarized as follows:

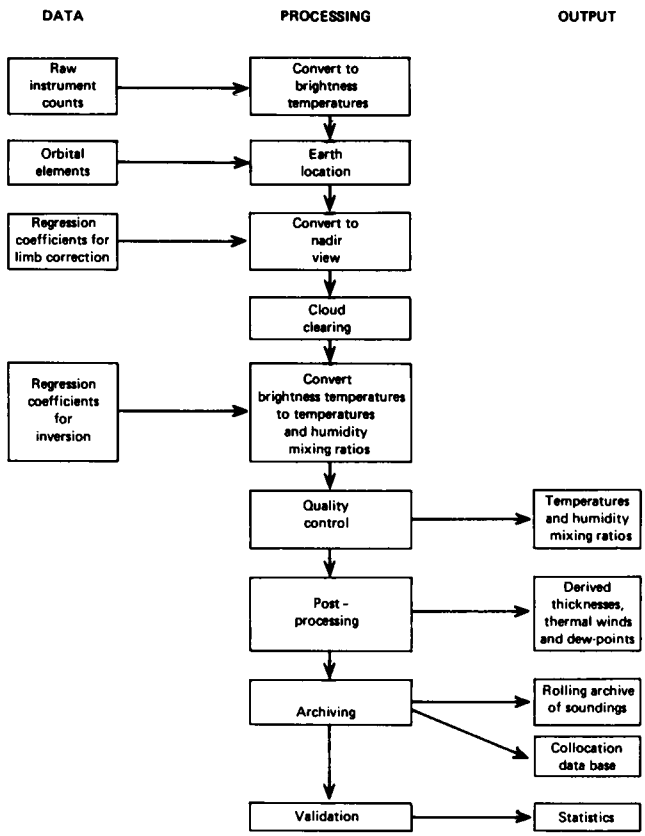

Figure 6. The LASS processing system.

(a) Unpacking the raw satellite data and converting the instrument counts into radiances by using the calibration information in the data stream and then deriving an equivalent black-body temperature (brightness temperature).

(b) Computing the latitude and longitude of each sounding using orbital information received over the GTS.

(c) Converting the measured brightness temperatures to those which would have been obtained if the instruments had been looking vertically at the same atmospheric profile. (This is necessary since the instruments are looking at an angle of over 50° from the sub-satellite track at the edges of the swath.)

(d) Detecting cloud-free soundings, and attempting to remove the effects of the cloud from other soundings so that the 'cloud-free' radiances can be obtained. In very cloudy conditions the cloud-clearing process may not work, in which case the MSU-only retrieval can be supplied.

(e) Using multiple linear regression to obtain standard-level temperatures and humidity mixing ratios from the calculated brightness temperatures.

(f) Quality control of the resulting soundings by comparing the HIRS+MSU soundings with MSU-only soundings.

(g) Derivation of additional products such as the dew-points from the humidity mixing ratios, thicknesses from the standard-level temperatures and thermal winds from the local thickness gradients.

(h) Sending the LASS products to the main COSMOS computing system where the data are used in the numerical analyses and charts of 1000–500 mb thickness are produced for use in the Central Forecasting Office (CFO).

(i) Archiving all LASS products on CCTs and inclusion of the last 16 passes of data in a rolling archive of results which can be displayed on the ARGS.

(j) Collocating the LASS soundings with radiosonde ascents for validation of the retrievals.

Further details of the LASS can be found in Eyre and Jerrett (1982) and Jerrett *et al.* (1982), while the whole question of satellite remote sounding is dealt with by Houghton *et al.* (1984).

4.4 *An example of the LASS products*

The LASS products used most frequently in CFO are the charts of 1000–500 mb thicknesses and derived thermal winds, and a typical example is shown in Fig. 7 for 12 November 1984. On this occasion it was possible to receive four consecutive passes beginning at 0220 GMT over eastern Europe and finishing south of Cape Farewell at 0720 GMT. Fig. 8 shows the CFO 1000–500 mb thickness analysis for 0000 GMT on the 12th and it can be seen that the analysis of the LASS soundings gives very much the same pattern, although the absolute values differ in places. There is, however, much more detail

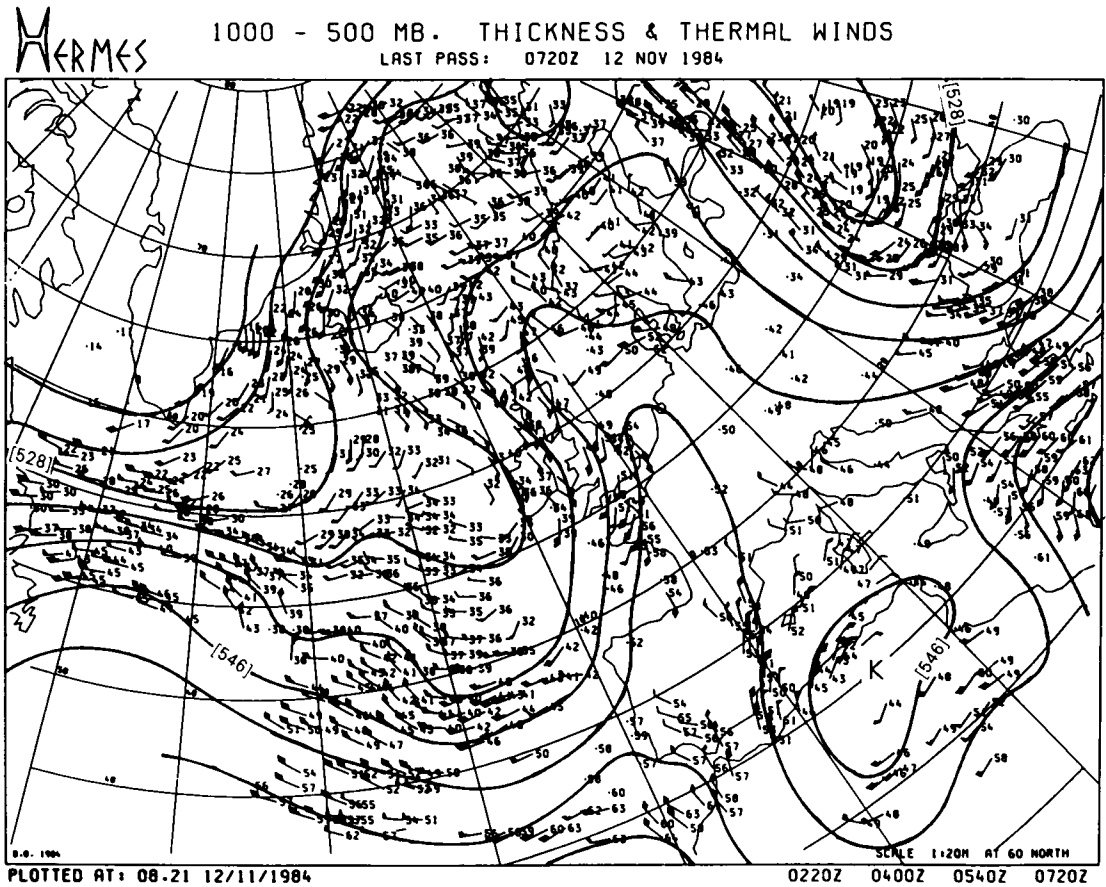

Figure 7. LASS thicknesses and thermal winds together with analysis for 12 November 1984.

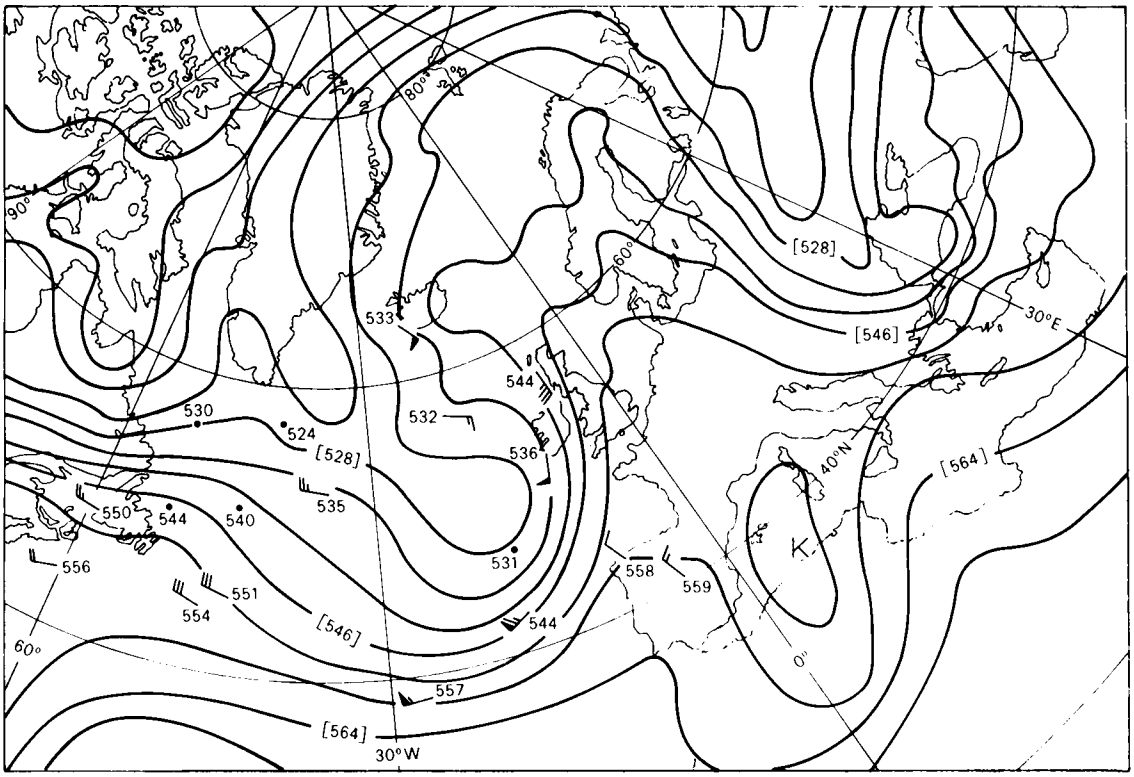

Figure 8. CFO 1000–500 mb thickness analysis for 0000 GMT on 12 November 1984.

apparent with the LASS data, especially over the Atlantic where there are few conventional soundings. In particular the LASS soundings were able to provide useful guidance in the area of the push of cold air south-eastwards around 50°N, 20°W and where, with hindsight, it is possible to suggest that the thicknesses within the elongated trough were greater than those of the CFO analysis, which had little data in this area.

4.5 *How accurate are the LASS soundings?*

As part of the routine validation of the LASS products, all soundings which are found to collocate with radiosonde ascents are stored with the corresponding radiosonde profile to allow a comparison to be made of the soundings from these two very different observing systems.

The statistics generated from the collocation data base consist of mean bias differences and standard deviations (SDs) for temperatures and dew-points at standard levels, and thicknesses of various atmospheric layers. These statistics are calculated each day as means for all collocations within the LASS area, and monthly mean figures are also computed.

Fig. 9 shows the monthly mean bias and SD collocation figures for October 1984 and illustrates some of the problems associated with satellite-derived temperature soundings. The features of most interest in Fig. 9 are:

(a) The larger SDs at low levels and around the tropopause.
(b) The cold bias at 1000 mb.
(c) The warm bias at the tropopause.

The problems at low levels are thought to be mainly due to the inability of the present LASS processing scheme always to detect and correct for the effects of cloud. Because of the broad weighting functions of the instruments the LASS soundings will always tend to be slightly bland and lacking in definition in the vertical. Fig. 10 gives an example of a collocated radiosonde and LASS retrieval and illustrates many of the strengths and weaknesses of satellite-derived temperature soundings. In particular the soundings are able to describe the mean features well, but do not show the fine structure obtainable with a balloon-borne sensor. It is also clear that the satellite sounding is unable to resolve fully the sharpness of the tropopause and for this reason the monthly mean statistics at the level of the tropopause invariably have a larger SD than at other levels.

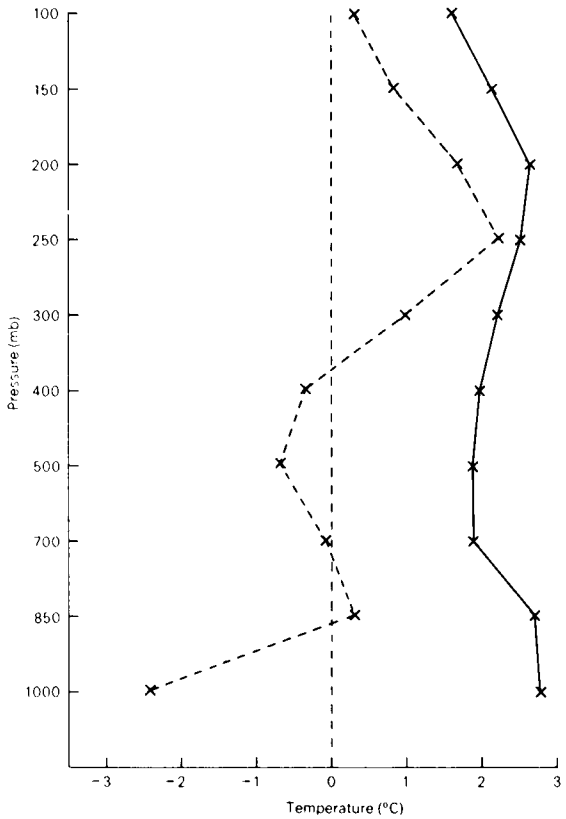

Figure 9. Monthly mean bias (pecked lines) and standard deviation (solid lines), for October 1984, for collocated LASS and radiosonde data.

However, the LASS soundings are able to provide useful information on the overall horizontal structure of the atmosphere which is especially valuable in data-sparse areas such as the Atlantic Ocean. The lack of vertical resolution is also less of a problem when the data are included in the numerical analysis system, as the model used in the operational assimilation cycle has relatively coarse vertical resolution. Thus the LASS soundings should be able to add information to the analyses in the data-sparse areas provided that any biases in the soundings can be handled.

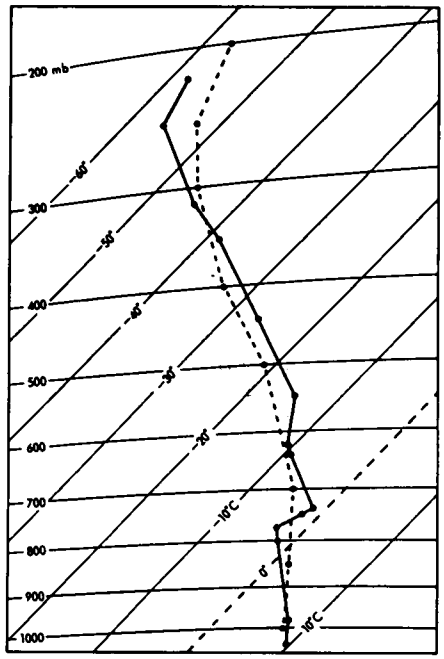

Figure 10. Radiosonde profile for Lerwick (solid lines) at 1200 GMT on 14 May 1984 with collocated LASS retrieval profile (pecked lines) at 0907 GMT on the same day.

4.6 *Future developments*

During the last 2 years the LASS system has been developed to a point where data from all the passes of TIROS-N series satellites over the United Kingdom are processed automatically and temperature and dew-point profiles supplied to the forecaster in CFO and to the fine- and coarse-mesh numerical analyses. During this period it has been established that the quality and characteristics of the LASS soundings are almost identical to those of the SATEMs.

Work is now taking place to assess fully the accuracy of the soundings, both by comparing the retrievals against radiosondes, and by examining the data in conjunction with the numerical analyses and CFO subjective analyses. Several significant problems have been identified and a number of these have been outlined above. At the moment the major areas of development are:

(a) The generation of our own regression coefficients from a carefully compiled set of historical radiosonde profiles and corresponding calculated brightness temperatures for the North Atlantic/European area. For a number of reasons these coefficients are expected to give better local results than the global NESDIS coefficients.

(b) The development of improved cloud detection and cloud-clearing techniques.

(c) Reassessing the limb corrections applied at the edges of the swaths where larger errors are found.

(d) Examining the possibility of using retrieval techniques which make more use of the radiative transfer equations and which use model forecast information as a background field.

5. Conclusion

This paper has outlined the main components and functions of the HERMES system. Using this system with the full range of digital data broadcast by the satellites, it is possible to explore a large range

of imagery and sounding products which have useful research and operational applications. The sounding data are now used operationally in the numerical analyses and will play an increasing role as retrieval techniques improve. It is also hoped that the high-resolution imagery data will, over the next few years, come into operational use both at the Meteorological Office Headquarters and at outstations and have a significant impact on the Office's operations. The computing facilities available within the HERMES system will make it possible to take full advantage of these potentially very valuable data.

References

Eyre, J. R., Brownscombe, J. L. and Allam, R. J. 1984 Detection of fog at night using Advanced Very High Resolution Radiometer (AVHRR) imagery. *Meteorol Mag*, **113**, 266–271.

Eyre, J. R. and Jerrett, D. 1982 Local-area atmospheric sounding from satellites. *Weather*, **37**, 314–322.

Golding, B. W. 1984 The Meteorological Office mesoscale model: its current status. *Meteorol Mag*, **113**, 288–302.

Houghton, J. T., Taylor, F. W. and Rogers, C. D. 1984 Remote sounding of atmospheres. Cambridge University Press.

Jerrett, D., Eyre, J. R. and McCallum, E. 1982 High resolution soundings of temperature in the European/North Atlantic Area. Proceedings of the Remote Sensing Society, Liverpool, 15–17 December 1982.

Llewellyn-Jones, D. T., Minnett, P. J., Saunders, R. W. and Zavody, A. M. 1984 Satellite multichannel infrared measurements of sea surface temperature of the N.E. Atlantic Ocean using AVHRR/2. *Q J R Meteorol Soc*, **110**, 613–631.

Miller, D. E., Brownscombe, J. L., Carruthers, G. P., Pick, D. R. and Stewart, K. H. 1980 Operational temperature sounding of the stratosphere. *Philos Trans R Soc* A, **296**, 65–71.

Schwalb, A. 1978 The TIROS-N/NOAA satellite series. NOAA *Tech Memo* NESS 95, Washington.

Smith, W. L., Woolf, H. M., Hayden, C. M., Wark, D. Q. and McMillin, L. M. 1979 The TIROS-N operational vertical sounder. *Bull Am Meteorol Soc*, **60**, 1177–1187.

551.5(09):551.501.1:35:662.1

Smoke-screens — the early years

By R. J. Ogden

Summary

A reminiscent account is given of work carried out in the United Kingdom during the Second World War on the meteorological conditions necessary for the successful laying of smoke-screens as a protection against enemy air raids.

During the War years, urgent posting notices for Meteorological Office staff were sometimes issued on the meteorological broadcast channel during the hourly break for collection of observations. Not surprisingly, with the teleprinter in local circuit, local jokers could all too easily prepare a spurious message posting a colleague to some outlandish location. In July 1940, when stationed at Croydon

Airport, I was presented one day with a teleprinter signal ordering me to report as soon as possible to 71 Ewell Road, Surbiton. My first reaction was to ignore this as a typical bogus message; but checks revealed that the instruction was quite genuine, although no-one at Headquarters was prepared to say what I was supposed to do at such an off-beat location.

On arrival next day at the given address, I became even more suspicious about a possible hoax, because 71 Ewell Road proved to be a large three-storeyed house on a busy main road, with a notice board in the front garden informing the public that this was the local Food Control Office, where one could obtain ration books. Enquiries inside at first drew a complete blank and I was on the point of returning on my bicycle to Croydon when someone suggested that perhaps I was connected with 'that odd man in the attic'. So I climbed the stairs and found that I had indeed come to the right place. The man in the attic was a forecaster who had arrived a few days previously and was struggling to create, out of virtually nothing, a completely new kind of meteorological advisory unit in support of a smoke-screen.

The concept of industrial smoke-screens

Many years later I discovered that, on 29 May 1940, the Prime Minister had directed that a committee should be set up to review the possibility of using smoke-screens to hide factories from aerial attack at night (see Air Ministry (Air Historical Branch) 1954). In those days, shortly after Dunkirk, and under threat of German bombing and indeed invasion, decisions could be acted upon remarkably quickly. Admittedly there had been some earlier studies at Porton about the use of smoke-screens, but even so it is astonishing that within a month from the date of Churchill's minute, the committee had considered the matter and reported favourably, the Ministry of Home Security had set up an appropriate organization, and a full operational trial had been mounted at Stewartby, near Bedford. This was made under full-moon conditions on 20 June 1940, and although aircraft observations of the effectiveness of the screen were inconclusive, there was enough positive evidence to encourage a Cabinet decision to go ahead, as quickly as possible. The following month, in July 1940, smoke-screens were set up to protect ten key factories, including the one at Tolworth with which I was then concerned, Incidentally, the small meteorological unit at Ministry of Home Security Headquarters set up to oversee the scheme was headed by P. A. Sheppard, later Professor of Meteorology at Imperial College. Also working in Sheppard's team was A. W. Brewer, later to become Reader in Meteorology at Oxford University and then Professor of Meteorology at Toronto University.

It was initially assumed that pin-point visual identification of a target from the air at night would be possible only in bright moonlight; this implied that screens were needed only during a period of about a fortnight each month when the moon — at least half full — was above the horizon for some part of the night. Within this potential risk period, a screen had to be laid whenever there was expected to be less than full cover of cloud (or thick fog) below 5000 feet, unless the wind exceeded about 20 knots in which case it was recognized that any screen would be ineffective. The required meteorological input was therefore firstly for a general forecast of the occurrence or otherwise of the limiting cloud and strong-wind conditions, and secondly, on operating nights, for a detailed local wind forecast so that generators could be positioned to give the necessary smoke cover over the target.

The smoke generators used during the early years were mostly of the orchard heater type. Each consisted of a cylindrical 'pot' containing 20 gallons or so of diesel oil, and surmounted by a tall chimney so that the whole assembly was about 4 feet high. Pots were positioned about 10 yards apart, ideally in a semi-circle about 2000–3000 yards upwind of the target. An alternative array for use in flat calm or very light and variable winds was that of a cross centred near the target and extending outwards to the circuit used when the wind was determinate. In practice, however, for obvious logistic reasons, the ideal layout

could rarely be achieved because generators had to be located on roads, or at least on tracks which could be used by lorries. The generators burnt about 2 gallons of diesel oil per hour and produced thick, black, oily smoke.

The July 1940 operation

The first (and only) operational period of the Tolworth screen can only be described as a total shambles. Not surprisingly, in view of the extremely short period between the decision to go ahead with industrial smoke-screens and this first operation, generators were in very short supply and there were barely enough for a modest arc upwind of the target. Thus, not only had they to be positioned afresh each night according to the predicted wind directions and then be returned to the depot after close down, but also if the wind direction changed during the night, generators had to be extinguished, moved, and re-lit in new positions. With 10 gallons of diesel inside the pot it must have weighed the best part of a hundredweight, so all this moving about was no easy task.

The Ministry of Home Security District Officer at each screen was responsible for obtaining locally both transport and the necessary staff. Finding suitable lorries was difficult enough, but recruiting a labour force was a nightmare. His first approach was naturally to the local Labour Exchange, but most of the registered unemployed proved to be quite useless for heavy work of this kind; far from being able to hump fuel oil in bulk, some of the men who turned up had themselves to be lifted up onto the lorries. In the 1980s it may sound hard to believe, but the temporary solution was to obtain volunteers from the staff of a large department store in Kingston, who agreed to turn out at night after a day's work to help us out.

Meteorologists also had their share of problems. The direction of a wind of 1 knot is of no consequence at an airfield, but for an effective smoke-screen it is absolutely vital to understand, and to be able to predict the almost imperceptible but sometimes quite steady drifts of air that occur on a good radiation night. Similar problems, logistic and meteorological, were found at all other screens during this first moonlight period of operations, and it was wisely decided to have a breathing space before the next operation.

Meteorological field-work

In August 1940, all the meteorological staff working on smoke-screens were brought together in two groups; those from screens in hilly areas went to Rogerstone, near Newport (Gwent) and the remaining dozen of us went to Slough (Bucks). We were given 4 weeks in which to discover as much as possible about airflow at night across mixed urban–suburban–rural areas, especially under clear sky, light gradient conditions. This was indeed a fascinating challenge, and despite the obvious difficulties of working out of doors nearly every night for a month in the black-out and sometimes during air raids, we learnt many lessons that were subsequently put to very good use in helping to achieve more effective screens.

It was clear that for reference purposes, a good observer would have to make full and more or less continuous observations at a representative and well-exposed site in the area. Remaining members of the team were then positioned to give detailed coverage of the study area for the night, for example in and around a wood, a housing estate, farm land, the town centre and so on. We investigated the extent to which streets of houses, trees, large buildings and hedges affected the local airflow in stable inversion conditions and up to roughly what height. We were also very much concerned to discover the detailed effects of local orography on katabatic drainage. It emerged from this latter study that when one is

interested in the extremely light drifts that will move smoke, quite modest areas of higher ground can initiate katabatic flow. At Slough we expected a katabatic wind from the Chilterns to the north (indeed under ideal conditions it can reach 5 knots), but we were surprised to find also a perceptible southerly drift across the Thames into the outskirts of the town from Windsor Great Park, the highest parts of which are only some 150 feet above the valley floor.

I can recall solitary nights during this field-work period spent sitting on a kerbstone in a housing estate with a smoke generator for company, in a field of cows (who seemed to make noises of one sort or another throughout the night), on a sewage farm, wandering along hedged country lanes north of the town, and in the middle of a field of cabbages. It was in this last location, having just released a pilot balloon with lantern, that I was shot at by a Home Guard who fortunately missed. I must confess that the call of self-preservation was then louder than the call of duty, and abandoning the rest of my observing program for the night I crawled out of the field and returned to base. Working as we were in an area which by virtue of the target was extremely sensitive from a security point of view, we naturally maintained very close liaison with the RAF, Army, Police and Home Guard, so that everyone concerned should have known in advance exactly what we were doing, where, and at what times. In addition to the normal RAF passes we all carried special Ministry of Home Security identity cards authorizing us to enter and work in security areas, and for the most part these kept us out of serious trouble. But none of these measures gave complete protection from Home Guards who were, very properly, highly suspicious of odd behaviour. Their internal dissemination of information was at times virtually non-existent, and individuals on patrol seemed often to be genuinely unaware of our activities, despite thorough briefing of Home Guard Duty Officers at the local Headquarters. One of my colleagues, then based at a screen in the Midlands, was arrested by the Home Guard and kept in solitary confinement for 48 hours before he was allowed to see an officer who ordered his release after checking his credentials.

There is no doubt at all that our activities and indeed our appearance were somewhat bizarre. On setting forth for a night's work, for obvious reasons in old clothes, one was equipped with: a sensitive cup anemometer, a ribbon on a pole for wind direction plus a tin of swansdown for very light winds, a whirling psychrometer, three or four filled balloons on strings (these had to be filled in the yard behind the office), lanterns and candles, stop-watch, clipboard and data sheet, torch, matches, gas mask, tin hat, sandwiches and perhaps a flask of coffee. The observer at the reference site also had a theodolite, tripod and pilot balloon slide-rule. Balloons released at other locations were only partially filled to give either no lift (a not very successful method of tracking light surface airflows) or ascent at a gentle rate; these were observed, qualitatively, by eye alone. With hindsight it is surprising that we did not land in deeper trouble. One can hardly blame an ill-briefed Home Guard for suspecting the worst when he encounters, at 3.00 a.m., a rather scruffy figure standing on a bridge over the main railway lines to the West Country holding a cup anemometer at arm's length, or wandering along a quiet country lane in pursuit of a balloon at the end of a long thread, not to mention sending up a candle-lit lantern during the black-out from a cabbage field adjacent to a vital factory.

Subsequent operations

At the end of the month of field-work, it was decided not to continue with the Tolworth screen, and I remained at Slough where our first task was to reorganize the generator layout in the light of our findings. By this time, there were sufficient pots to permit a permanent array approximating to the ideal circle and cross; this was divided into 30 or more numbered sections, and on any particular night only those sections needed to provide an effective screen were lit. The idea of using local labour was abandoned; responsibility for fuelling, lighting, looking after and extinguishing the generators was taken over by a company of the Army Pioneer Corps, and this arrangement worked quite smoothly.

During each moonlight period, our daily cycle of work started with a visit in late afternoon or early evening to Headquarters 11 Group at Uxbridge to look at the charts in the meteorological office there and to discuss the situation with the local staff on duty. If a screen seemed likely to be needed, on return to Slough we advised which sections of the array should be lit. We then spent most of the night driving round the area in the smoke monitoring the effectiveness of the screen. If the wind was not exactly as predicted and the smoke was going in the wrong direction, some sections might have to be closed down and others lit. After close down, and in a filthy condition after some hours spent in the smoke, we went back to our digs for some sleep; but no matter how late one got to bed, attendance at a morning conference at 10.00 a.m. was obligatory. At this there was a general discussion about the previous night's operation with Ministry of Home Security and Army staff, and a daily meteorological report had to be written and sent to Headquarters.

By mid-autumn when the operation had settled down, although we worked very long hours, mostly at night, during the moonlight periods, we had time to spare during the rest of the month; I was then normally detached to an RAF station for a short spell of normal meteorological duties on day shift. But in December 1940 it was decided that in suitable weather two of the screens should be run on non-moonlight nights also, and early in 1941 I had a busman's holiday as leave relief on the Nottingham screen whilst the Slough screen was not working. Later, after I had been posted back to mainstream duties at RAF stations, this practice was extended to other screens. Shortly before I left Slough, I spent one non-moonlight period surveying the ground and advising on the circuit for a new screen being planned at Langley, some miles east of the Slough screen. From the total of 9 screens in operation during late 1940, numbers grew steadily to reach a peak of over 30 in 1942; thereafter a few were closed each year and the final operations took place in September 1944.

One of the minor irritations of the job was the fact that our offices were not equipped with secure telephones. Conversations on the public network with Uxbridge had to be conducted in a form of verbal code in which names of animals were substituted for each of the necessary words in a forecast. Of the hundreds of words in the code-book I recall that octopus, ocelot, barracuda and basking-shark cropped up regularly in place of the familiar phrases like surface wind, gradient wind, visibility, locally, and so on. We also had to invent a similar code of our own to use when informing the Army, police, etc. about each night's operation. With what I felt to be a misguided sense of humour, the forecaster at Slough in July 1940 had elected to use the name of a drink for each of the different sections of the circuit. There was no problem with words like tea, coffee, beer or milk, but dictating phrases like 'Chateau d'Yquem' to a corporal in an Army orderly room did present problems.

Needless to say, the operation of smoke-screens in residential areas was not welcomed with open arms by the local population. Those who understood roughly what it was all about reluctantly accepted the need for screens, but nobody wanted a generator belching smoke and half-burnt diesel oil outside his front door. Keeping curtains or anything else clean must have been well nigh impossible, and we received many vociferous protests. I recall one winter evening when we had to light the cross part of the array which ran along two major roads through the town. The smell penetrated into a large cinema where the manager misguidedly switched on his full ventilation system; within minutes, the screen was invisible from the balcony and the box office was beseiged by patrons demanding their money back. There was nothing we could offer the manager but sympathy. In general, no compensation whatsoever was paid to anyone for dirt and inconvenience, so I counted it as a minor triumph that after several months of argument I eventually succeeded in persuading the Ministry of Home Security to pay a few shillings for the cleaning of a raincoat that had inevitably become impregnated with soot and oil.

Perhaps the most difficult problem faced by meteorologists was the situation when radiation fog was expected to form during the burn period. Timing such events to the nearest 10 minutes was difficult if not impossible, despite almost continuous monitoring of visibility and humidity in the area. Usually, when

fog was clearly imminent, we took a chance and gave orders for the pots to be extinguished, but if the fog beat us to it because we had allowed insufficient time for an officer to get round the circuit telling the Army 'minders' to stop making smoke, the results could be quite catastrophic. I can remember very vividly one occasion when the fog formed quite suddenly and became so thick that it was impossible to get round the circuit giving instructions to douse. Within an alarmingly short time, the mixture of fog and smoke reduced visibility in the town centre to literally no more than 2 yards; it took me about an hour to walk barely half a mile along a main road from where I had abandoned my car to our office in the High Street.

Reference

Air Ministry (Air Historical Branch) 1954 The Second World War 1939–1945: Meteorology, 215–219. (Unpublished, copy available in the National Meteorological Library, Bracknell.)

Notes and news

Retirement of Mr C. V. Smith

Mr C. V. Smith, B.Sc., MA, Assistant Director (Agriculture and Hydrometeorology) retired from the Meteorological Office on 29 March after a career of almost thirty-seven years. During the early years he saw service as a forecaster at home and overseas but latterly will be remembered for his pioneering, far-sighted and productive application of meteorology to the needs of agriculture in the United Kingdom.

Cliff Smith was born in 1925 and was educated at the Coopers' Company School, Bow. During the war he was evacuated to a farm in Kent, an event which was to excite an interest in agriculture which found fulfilment many years later. He went on to gain a B.Sc. in Physics and Mathematics at Birkbeck College, and an MA in Physics and Chemistry at Cambridge. He joined the Office as a Scientific Officer in September 1948. After the customary spell at the Training School he was posted to the 'deep end' of a busy London Airport. This began his association with the synoptic forecasting for aviation which characterized the first half of his career.

In 1951 he started a three-year posting to the long-range forecasting team in M.O.22 under the guidance first of Sutcliffe and then of Sawyer; there he published useful papers with Forsdyke and Sumner on the properties of the long waves and use of Rossby theory. In 1954 he carried this experience back to operational forecasting in M.O.2. at Dunstable and was promoted to Senior Scientific Officer in 1955, whereupon he became a Senior Forecaster on the upper-air bench. He demonstrated a flair for forecasting synoptic development and continued to write and have published papers on techniques for medium-range forecasting based on the 500 mb flow.

In 1958 he began an overseas tour at RAF Luqa, Malta, where he rapidly made an impression as an above-average forecaster who demonstrated originality and initiative.

January 1962 represented an important watershed; Cliff returned to the United Kingdom and took up a post in M.O.7 which required him to study and advise on the ventilation of animal houses and grain stores. Although nothing in his previous professional career had prepared him for such work he made an immediate and impressive impact. Despite this the posting system did not quite have the courage of its convictions — in September 1963 he was moved on promotion to the Central Forecasting Office! However, even as a Senior Forecaster he continued to write up and publish the results of his research work in agrometeorology and two years later he became the Senior Meteorological Officer at Cambridge alongside the other specialists in the Eastern and East Midland Regions of the then National Agricultural Advisory Service.

During the next twelve years he transformed agrometeorology in the United Kingdom and, as an active and forthright member of the Commission on Agrometeorology of the World Meteorological Organization, extended his influence and reputation even more widely. There was almost no aspect of modern agrometeorology which did not receive his attention during this period. His earlier work on ventilation was extended to the problems of grain and potato storage, to the conditions favouring the outbreak of cereal mildew and to the environmental factors which influence animal growth and well-being. He made significant contributions in advising on the design and siting of glasshouses and on the calculation and practical use of concepts of 'degree days', 'machinery work days' and 'soil moisture deficit'. Throughout he was guided by the need to provide practical solutions to problems. He was ahead of his time in extolling the role of meteorology as a management aid in the agricultural industry and of the business approach to meteorology. His pioneering work on the potential benefits of meteorology to agriculture continues to be worthy of study.

In the summer of 1975, Cliff was posted to Met O 1 at Bracknell to gain some experience of Headquarters before the promotion to Assistant Director which was then foreseen. He settled down quickly, making well-received proposals for reorganization of the North Sea observing networks and of radiation work in the Office, which he subsequently helped to implement.

He was promoted and took up his appointment as Assistant Director, Agriculture and Hydrometeorology, in the spring of 1977. Since then Cliff has continued to apply himself and his staff very effectively to the practical exploitation of meteorological data and knowledge for the benefit of hydrology and agriculture. It is his avowed intention to seek new opportunities for such application in retirement. We therefore expect to see a lot of him in future. We look forward to that, whilst wishing good health and happiness to him and his wife Sylvia during his retirement.

P. Ryder

50 years ago

The following extract, including the editorial note, is taken from the *Meteorological Magazine*, June 1935, **70**, 118.

Blue Snow and Inky Rain in the Shetlands

Rain which fell on the forenoon of March 16th was quite dark-coloured. My attention was called to the colour of the water in the pools and when I got home I at once examined the water in the rain-gauge and found it too was tinted; looked as if it had been slightly diluted with black ink. The sky looked thundery, but I did not hear any thunder, though a thunderstorm was reported from Lerwick about 40 miles distant.

T. EDMONSTON SAXBY

Halligarth, Baltasound, Shetland, April 2nd, 1935.

[According to the *Shetland Times* of March 23rd, following a spell of very fine bright weather, the sky was overcast after daylight on Saturday, March 16th, and there were showers of wet snow. Thunder was heard shortly after 9h. and by 10h. the morning was becoming darker, with an ominous looking sky and a peculiar greenish light. Heavy thunder and several bright flashes of lightning followed between 10h. and 11h. and about 10h. 30m. exceptional darkness was experienced. In some districts heavy rain fell and in Lerwick the thunderstorm was followed by a heavy shower of wet snow and later rain. By noon weather conditions were normal and afternoon and evening were fine. A peculiar feature in several districts during the thunderstorm was that the snow which fell was of a dirty bluish colour and rain water which was collected in tanks and barrels was something of the colour of ink. Dr. Harrison, of Lerwick Observatory, states that black rain was reported from Bressay, 'but we saw nothing of this or of blue snow here'. The pressure gradient on March 15th and 16th was such that air from industrial districts might have reached Shetland. — ED., *M.M.*]

A summer school on mesoscale meteorology

A week-long, residential summer school is being organized jointly by the Meteorological Office and Reading University, on the general topic of mesoscale meteorology. It will be held at the Meteorological Office College, Shinfield Park, near Reading from 8 to 12 July 1985.

The program will consist of a series of lectures covering different aspects of mesoscale meteorology, supplemented by case-studies of specific situations carried out in working groups. The case-studies have been chosen to illustrate mesoscale features of fronts and of convective phenomena. The coupling of the case-studies with the lectures is intended to ensure that participants acquire a good understanding of the theoretical concepts introduced by speakers as well as giving some practical knowledge of their application and relevance to atmospheric phenomena.

The speakers will be mainly from the Meteorological Office and Reading University. Contributions will also come from the European Centre for Medium Range Weather Forecasts, Imperial College and the mesoscale research group at the Centre National de la Recherche Météorologique, Toulouse, who are working with the Meteorological Office on a joint venture — the Mesoscale Frontal Dynamics Project.

The participants, about 50 in number, will be drawn from both the Research and Forecasting Branches of the Meteorological Office, together with representatives from the universities and two French research groups. The steering group for the summer school consists of Dr K. A. Browning, Professor B. J. Hoskins, Dr B. Golding and Dr C. J. Readings.

Review

Prophet — or professor? The life and work of Lewis Fry Richardson, by Oliver M. Ashford. 160 mm × 240 mm, pp. xiv + 304, *illus*. Adam Higler Ltd., Bristol and Bolton, 1984. Price £18.00.

The title of Oliver Ashford's biography of Lewis Fry Richardson (1885–1953), *Prophet — or professor?* implies that the author had it in mind to leave the reader with the responsibility for assessing L. F. Richardson's life and works on the evidence he presents. Was L. F. Richardson a prophet or a professor? There is much about his life which was enigmatic, even to his contemporaries. His preference for solitude and an apparently less than easy relationship with his various employers in his early professional career probably stemmed from his unwillingness to become part of any organization or bureaucracy which threatened to inhibit the free exercise of his intellectual curiosity or force him to compromise on the truth as he saw it. For L. F. Richardson truth lay in the mathematical expression of phenomena as diverse as the flow of drainage water in peat, numerical forecasting and the foreign policies of nations.

The author describes how L. F. Richardson's published contributions to meteorology began in 1915 with a paper on thunderstorm detection by clicks on telephone lines. His subsequent published meteorological output ranged widely over many subjects including the physics and dynamics of precipitation, the use of balloons for recording upper-air temperatures and his classic book *Weather prediction by numerical processes* which was published in 1922. His final paper in meteorology was on 'The reflectivity of woodland, fields and suburbs between London and St Albans', published in 1930, although he published a brief note in the *Quarterly Journal of the Royal Meteorological Society* in 1952 replying to criticism of his 1920 paper on atmospheric turbulence. It is a measure of his productivity as a mathematician that his biographer cites 57 references to his published work after 1930, when his scientific output was almost entirely concerned with his search for the quantification, and the possible predictability, of conflict between nations.

L. F. Richardson has become a legendary figure to subsequent generations of meteorologists, largely because of his 1922 book of numerical forecasting in which he worked his way through a series of separate statements about the dimensions of atmospheric disturbances, the required accuracy, a discussion of the use of mathematical equations in the numerical prediction of the behaviour of the atmosphere and the variables which needed to be considered such as soil moisture transfer rates, evaporation and turbulence. A whole chapter is devoted to radiation processes, parcel theory and the definition of sea temperature. He then dealt with vertical velocity, the stratosphere and the observed data available to initialize his fields. L. F. Richardson was always open in his work and made available, separately from his book and financed out of his own pocket, a set of 23 computing forms . . . 'to assist anyone who wishes to make partial experimental forecasts from such observational data as are now available'. The core of his book lay in a worked example of a numerical weather forecast starting with the observed state of the atmosphere at 0700 GMT on 20 May 1910. The results were a disaster. An anonymous 'meteorological correspondent' in the *Manchester Guardian*, probably Sir Napier Shaw, noted that L. F. Richardson's fantasy of an orchestrated computing operation involving 64 000 human computers in a room the size of the Albert Hall 'sounds like the rhapsodies of an irresponsible visionary but, actually, it is an attempt to picture a "forecast-factory" of the future in which the weather of the whole globe will be predicted on highly rational and scientific lines'. L. F. Richardson was fallible, as his biographer points out elsewhere. His figure of 64 000 human computers was based on an error in his calculation — it should have been 256 000 — and Hyde Park rather than the Albert Hall would have been a more appropriate venue!

It is a remarkable commentary on subsequent developments in numerical forecasting that its foundations were relaid by a later generation of meteorologists working in the Napier Shaw Research Laboratory at Dunstable 30 years on and that L. F. Richardson's 'forecast-factory' is now well established as an operational national global forecasting centre, with an international role as one of the two World Area Forecast Centres for civil aviation with the National Meteorological Centre in Washington, in the Richardson Wing of the Headquarters building of the Meteorological Office at Bracknell.

By the summer of 1920 L. F. Richardson had come to a personally distressing decision to leave the Meteorological Office. He had been Superintendent of Eskdalemuir Observatory from 1913 to 1916, working in geomagnetism, atmospheric electricity and seismology, until he resigned to serve with the Friends Ambulance Unit in France from 1916 to January 1919 when he returned to the Meteorological Office, joining W. H. Dines in developing methods of upper-air measurement at Benson Observatory. The move of the Office into the newly created Air Ministry meant that he would have had to compromise his strongly felt Quaker beliefs. But his resignation was, as it proved, for the best. Basic meteorological research was not encouraged in the pre-war Meteorological Office. Others were to gain. L. F. Richardson's devotion to the cause of peace and to the service of others, which is the hallmark of the Quaker tradition and conscience, prompted him to look to the quantification of conflict within and between nations as an outlet for his scientific talent and energy. He left the Meteorological Office to lecture at Westminster Training College and, later, to become the Principal of Paisley Technical College. His interest in psychology led him to work in such diverse areas as colour perception, the quantification of pain and the analysis of mental processes before concentrating almost exclusively on the mathematics of the psychology of war, leading to his work on generalized foreign politics which he published as a monograph in the *British Journal of Psychology* in 1939. By 1950 he had privately produced two books on microfilm — *Arms and insecurity* and *Statistics and deadly quarrels*. In 1951 he published a note in *Nature* with the title 'Could an arms race end without fighting?'.

Oliver Ashford is careful not to interpose his views between the reader and his subject more than is absolutely necessary but his detailed and objective account of the life of L. F. Richardson suggests that perhaps the greater value of his life will come to be recognized in his analytical studies of war. In that field he was a true pioneer whose contribution is only just beginning to be recognized. In meteorology there were others — and not the least was Vilhelm Bjerknes who predated L. F. Richardson by nearly 20 years in looking to an adequate representation of the observed state of the atmosphere as the first and essential diagnostic step in the integration of the fundamental hydrodynamic and thermodynamic equations, leading on to prognosis. The development of numerical forecasting from Bjerknes' original work was not an evolutionary process through L. F. Richardson. The present-day operational 15-level primitive-equation global model has its foundations in research which began in the early 1950s when sufficient computing power became available to test newly-developed and relatively simple numerical models. As numerical forecasting developed it moved rather more closely to L. F. Richardson's original ideas but numerical forecasting would have taken off in the 1950s even if L. F. Richardson had not published his classic book. It was his vision which remained the inspiration to a later generation.

Thirteen years after the death of L. F. Richardson in 1953, Sir Graham Sutton, in correspondence with G. W. Platzman which was published in the *Bulletin of the American Meteorological Society*, summarized much about L. F. Richardson which is confirmed by the detailed evidence in Oliver Ashford's biography: 'This gentle man was unshakeable in his decision to conduct his life in accordance with the principles of his creed. It may be, of course, that he would not have fitted easily into any team, for it is clear that he was very much the individual worker. But what an inspiration he would have been as a consultant!'

The author poses a question, presents all the available evidence and leaves the reader to decide the answer for himself. Was L. F. Richardson a prophet or a professor or is the author's question unfair to his subject? There is evidence enough in his biography to justify both descriptions as appropriate. There are two quotations on the flyleaf. The first is from Samuel Johnson, of Oliver Goldsmith — 'He touched nothing that he did not adorn.'. The second is from William Wordsworth, of Isaac Newton — '. . . a mind for every voyaging through strange seas of thought, alone.'. The first quotation has an element of the sycophantic which is totally absent from Oliver Ashford's text. The second quotation summarizes, at least for the reviewer on the evidence presented and I suspect for most of the readers of this biography, the personality of L. F. Richardson.

Oliver Ashford's last three words — '. . . searcher after truth' — conclude this admirable biography with a fitting epitaph for its subject.

I. J. W. Pothecary

Books received

The listing of books under this heading does not preclude a review in the Meteorological Magazine at a later date.

Wind as a geological process on Earth, Mars, Venus and Titan, by Ronald Greeley and James D. Iversen (Cambridge University Press, 1985. £35.00, US $59.50) deals with the geological aspects of windblown material. Aeolian processes play an important role in the modification of the Earth's surface and are known to be active on Mars. The book begins with an introduction to aeolian processes and a general overview of aeolian activity on the planets, then goes on to discuss the physics of particle motion and the effects of windblown sand and dust on the topography of the Earth and Mars, together with some speculations about Venus and Titan. The book is written for readers with a fundamental science background and should be of particular interest to students and professionals in the fields of planetary science and earth science.

Weather (second edition), by Louis J. Battan (Englewood Cliffs, New Jersey, USA, Prentice-Hall, Inc., 1985. £17.15) is a basic textbook on general meteorology, which includes a chapter on forecasting techniques. It is well illustrated and written in an easily readable style, which should make it comprehensible to anyone with a rudimentary knowledge of physics.

Principles of remote sensing, by Paul J. Curran (London and New York, Longman, 1985. £11.95) is a textbook intended for graduate and undergraduate students. It discusses the basic theory concerning the interactions between electromagnetic radiation and the earth's surface and goes on to describe the equipment used, and the processing and interpretation of the images which are obtained. The book is profusely illustrated with diagrams and photographs and there is an extensive bibliography.

Looking at weather, by Ingrid Holford (Brockenhurst, Weather Publications, 1985. £1.95) is aimed at anyone who is interested in weather, but particularly teachers and instructors at sports establishments who have to introduce the subject but are not themselves meteorologists. It includes some basic physics with few words but many easily understood diagrams.

Obituary

We regret to report the death, on 29 December 1984, of Thelma Patricia Powell, Scientific Officer in the Observational Requirements and Practices Branch (Met O 1). Miss Powell, educated at Willesden County School, joined the wartime Air Ministry as a Clerical Assistant in 1945, but transferred to become a Meteorological Assistant the following year. Her career was spent within the climatology branches of the Office, initially in M.O.3 as a data quality-control assistant in the manual and early punched-card eras. With the move of the Harrow headquarters she came to Bracknell in 1961. After hydrometeorology was transferred to Met O 8 (Agriculture and Hydrometeorology Branch) she was part of the archival data-processing team for the United Kingdom Flood Studies project, and over the past decade she established a close working relationship with the Water Authorities of England and Wales whilst engaged on technical administration liaison duties in Met O 1.

Throughout her career in the Office she was involved in a variety of social and club activities, ranging from the organization of children's Christmas parties at Harrow, a long association with the Horticultural Society, through to committee membership of the Gramophone and Music Society, of the Camera Club, and from time to time of the main Social and Sports Association.

THE METEOROLOGICAL MAGAZINE

No. 1355 June 1985 Vol. 114

CONTENTS

NOTICE

It is requested that all books for review and communications for the Editor be addressed to the Director-General, Meteorological Office, London Road, Bracknell, Berkshire RG12 2SZ and marked 'For Meteorological Magazine'.

The responsibility for facts and opinions expressed in the signed articles and letters published in this magazine rests with their respective authors.

Authors wishing to retain copyright for themselves or for their sponsors should inform the Editor when they submit contributions which will otherwise become UK Crown copyright by right of first publication.

Applications for postal subscriptions should be made to HMSO, PO Box 276, London SW8 5DT.

Complete volumes of 'Meteorological Magazine' beginning with Volume 54 are now available in microfilm form from University Microfilms International, 18 Bedford Row, London WC1R 4EJ, England.

Full-size reprints of Vols 1–75 (1866–1940) are obtainable from Johnson Reprint Co. Ltd, 24–28 Oval Road, London NW1 7DX, England.

Please write to Kraus Microfiche, Rte 100, Millwood, NY 10546, USA, for information concerning microfiche issues.

HMSO Subscription enquiries 01 211 8667.

Printed in England for HMSO and published by
HER MAJESTY'S STATIONERY OFFICE

£2.30 monthly

Dd. 736047 C13 6/85

Annual subscription £27.00 including postage

ISBN 0 11 727560 3
ISSN 0026–1149

THE METEOROLOGICAL MAGAZINE

HER MAJESTY'S
STATIONERY
OFFICE

July 1985

Met.O.967 No. 1356 Vol. 114

METEOROLOGICAL OFFICE Met.O.967

THE METEOROLOGICAL MAGAZINE

No. 1356, July 1985, Vol. 114

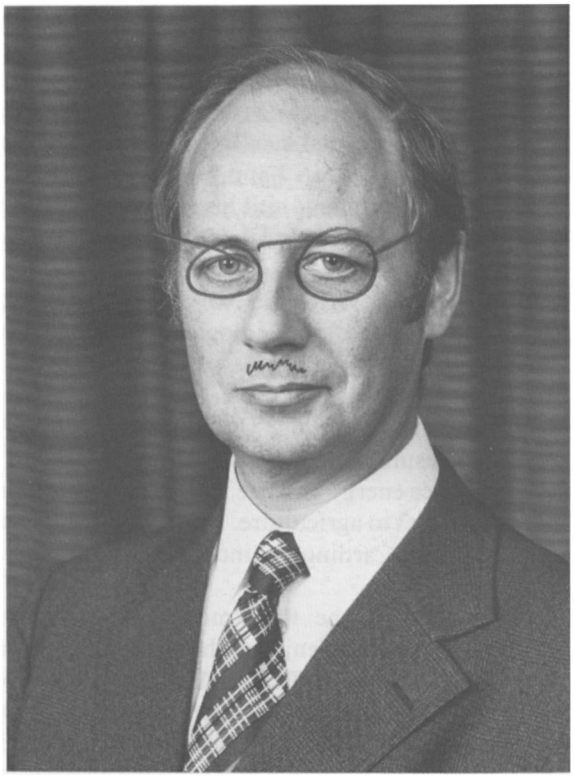

Retirement of Mr M. J. Blackwell

Mr Michael Blackwell, Deputy Director (Communications and Computing), retired from the Meteorological Office on 28 June 1985 after a career of almost thirty-five years in the Office during which time he was active in a wide range of tasks both in Research and in the more operational activities of the Services side of the Office.

Mr Blackwell was educated at University College School, Hampstead and St Albans School before

joining the RAFVR as a Sergeant Compass Adjuster in 1943. In 1945, however, he moved to the Meteorological Branch of the RAFVR and was trained as a 'dependant forecaster'. By 1947 he had become a Flying Officer forecasting at RAF Finningley and, although he was offered the chance to join the Meteorological Office as an Assistant Experimental Officer, he decided instead to take his chances at St John's College, Cambridge. Graduating with an Honours Degree in Physics in 1950, he accepted the offer of a post as a Scientific Officer in the Meteorological Office in August 1950.

After the usual training at Alexandra House, and a short spell of forecasting at ATCC Gloucester, he was posted into research in 1951 at Kew Observatory under Dr G. D. Robinson. There he quickly settled down to work on solar and terrestrial radiation, and papers on the automatic integration of solar radiation and 'Five years of continuous recording of daylight illumination at Kew Observatory' showed his keen interest in all aspects of the observational side of meteorology.

In April 1955 he married and, on promotion to Senior Scientific Officer, was posted to become Superintendent of Eskdalemuir Observatory. His responsibilities there included observations of geomagnetism, atmospheric electricity, ozone, atmospheric chemistry and pollution, evaporation, and snow gauging, and during the following three years he significantly improved the standard of the instrumentation at Eskdalemuir, bringing it fully up to date.

The year of International Geophysical Co-operation in 1959 — in effect an extension of the immediately preceding International Geophysical Year — led to Mr Blackwell's secondment from November 1958 to June 1960 to the Falkland Islands Dependencies Service as Chief Scientist, Halley Bay, at the British Antarctic Survey Base Z, Coats Land. He was in charge of a wide range of geological, oceanographic and meteorological measurements and his work during 1959, and the resulting papers, were later recognized by the award of the Polar Medal. He returned from the snow and ice in 1960 to a short period of forecasting on the upper-air bench at Bomber Command, High Wycombe, but, following promotion to Principal Scientific Officer in November 1960, he soon moved to take over the post of Senior Meteorological Officer of the Meteorological Research Unit attached to the School of Agriculture, Cambridge University.

There followed a most productive period during which Mr Blackwell forged a new, close relationship with the Plant Breeding Institute and the Cambridge University Schools of Agriculture and Botany. He wrote a number of papers on the measurement of natural evaporation, the turbulent transfer of water vapour near the ground and the surface energy balance, and became well known as an expert in the field of micrometeorology and its applications to agriculture. In 1964 he also became responsible for the work at the Meteorological Research Unit, Cardington including the use of constant density balloons (tetroons) as Lagrangian tracers.

In early 1967 Mr Blackwell attended the three-month General Management Course at the Administrative Staff College, Henley where he enjoyed the syndicate work and the 'despecialization of the specialist'. This was followed by a move to Bracknell where he took over as Head of the Surface Instrument Development Section in the Operational Instrumentation Branch. The work involved the introduction of synoptic and marine automatic weather stations and the development of new instrumentation to measure winds, temperature, humidity and rain. He also became the UK representative at international meetings of WMO Working Groups of the Commission for Instruments and Methods of Observation.

In 1970 he was promoted to Senior Principal Scientific Officer and took over as the Assistant Director (Operational Instrumentation). With the rapid evolution of technology these were exciting times, and Mr Blackwell was a pioneer in encouraging the early stages of two important COST projects (COST — Co-operation in Science and Technology — is an organization working under the aegis of the Commission of the European Communities). The COST-43 project buoy program (which is now successfully operating both fixed and drifting buoys in the North Atlantic and the North Sea) had its

origins in his work in the early 1970s, and the COST-72 project on meteorological instrumentation dealt with balloons, radiosondes and automatic weather stations in the 1970s before taking on its new role in the 1980s of encouraging the development of a European weather radar network. During this period Mr Blackwell was also actively encouraging co-operation on many international committees, and his long experience and broad viewpoint were sought widely. He also found time to be Chairman of the Staff General Purposes Committee, and a member of the Institution of Professional Civil Servants Higher Grades Committee as well as acting on the Royal Meteorological Society's *Weather* Board as the News Editor.

In April 1976 came well-deserved promotion to Deputy Chief Scientific Officer as Deputy Director (Communications and Computing). It must have come as quite a surprise to enter this completely new field at this level, but within a year he was firmly in the saddle applying an even temper, sound judgement and common sense to the rapidly evolving 'high technology' world of super-computers and information technology. The period 1976–85 has seen a revolution in these areas. The computer complex known as COSMOS has been enhanced by the introduction of the Cyber 205 and the IBM 3081D, which has allowed new, advanced numerical weather prediction models to be run. The telecommunications centre (AUTOCOM) has changed from teleprinter operation and 50-baud line to high-speed message switching using the Ferranti Main Enhancement, and now the Phase IV Tandem system; and a forward-looking strategy and implementation plan for the future requirements of the Office for outstation communications and automation has been developed. New forms of digital facsimile and graphical display systems have also come into operation. All this has required careful technical planning and close liaison between diverse groups of users, operators and manufacturers. Mr Blackwell has directed these developments with quiet authority and confidence.

Mr Blackwell's first wife died in 1978, and he remarried late in 1981. I shall miss his wise and helpful counsel and I am sure that all his colleagues will want to join me in wishing Michael and his wife, Joy, a long and happy retirement in their new home in Henley.

D. N. Axford

551.509.325:551.575.1

Field investigations of radiation fog formation at outstations

By J. Findlater

(Meteorological Office, Bracknell)

Summary

Special instrumentation placed at selected outstations for evaluation of its potential usefulness to local forecasters has been utilized to provide detailed information on the development of radiation fog. Relationships between the height of the fog top and the base of the capping inversion have been derived.

It is demonstrated that the cessation of turbulence, which is often coincident with the formation of radiation fog *in situ*, can be detected by a low-speed anemometer mounted at a height of 2 m.

Data from a mini-radiosonde system have indicated that the surface temperature at the time the sky becomes obscured by fog is preserved at the base of the capping inversion as it rises aloft. A possible technique for estimating the height of the top of the developing fog is suggested.

1. Introduction

During the winters of 1981/82, 1982/83 and 1983/84 some investigations into the formation and persistence of radiation fog were carried out at Bedford. The investigations had two main aims. Firstly, using the results from earlier field studies at Cardington by the Meteorological Office Cloud Physics Branch, to examine the usefulness to local forecasters of:

(i) a low-speed anemometer mounted at a height of 2 m capable of measuring speeds down to 0.2 m s^{-1};
(ii) a commercially-available monostatic acoustic sounder;
(iii) a mini-radiosonde system for local soundings of the boundary layer.

Secondly, to acquire data for further studies of the structure and development of radiation fog directed towards improving local forecasting. It is the latter aspect to which this report refers. Some data are also included from Lossiemouth where the mini-sonde was sited in summer 1983 to gather data in sea fogs. Examples from that station where radiation fog formed in the slab of moist air advected inland are presented.

2. Historical

Taylor (1917) noted that conditions favourable for the formation of radiation fog were moist air at the surface, mainly clear skies, and generally light winds. Deposition of dew took place when the surface cooled below the dew-point of the air in the lowest metre or so. Stewart (1955) drew attention to the fact that the air at screen level may itself be saturated for a few hours before fog formation and that the direct cooling of the lowest 1 km of air by radiation and by turbulent diffusion were comparable. Monteith (1957) pointed out that dew deposition decreased abruptly when the wind speed at 2 m fell to less than 0.5 m s^{-1} and Kraus (1958) found that radiation fog began to form when the wind at 1 m fell to less than 0.5 m s^{-1} and the initial shallow fog was often detached from the surface by a few tens of centimetres.

Detailed studies by Roach *et al.* (1976), Brown and Roach (1976) and Roach (1976), using data from balloon-borne probes at Cardington, indicated that significant fog development occurred when low-level winds (at about 2 m) decreased from a mean speed of 1–2 m s^{-1} to 0.5 m s^{-1} or less. As the fog thickened the soil heat flux overcame radiative cooling and the surface temperature rose slightly. Simultaneously, the inversion base rose aloft from the surface as the sky became obscured, with a slightly superadiabatic lapse rate developing in the fog layer. It was concluded by these authors that radiational cooling favours fog formation whilst turbulence inhibits fog formation by mixing warmer air downwards. Turbulence also allows moist air to be brought down to the surface where its moisture is condensed out as dew, but when turbulence is suppressed, as in very light winds with a strong stable lapse rate, continued cooling leads to formation of fog droplets in the lower layers. Other important factors which emerged from the Cardington studies were the roles of soil heat flux and the removal of water by gravitational settling, perhaps aided by some scavenging of fog droplets by vegetation.

Further studies of the Cardington data by Caughey *et al.* (1978) related the fog-top height deduced from temperature profiles to the echo layer from an acoustic sounder and the fog-top height indicated by a balloon-borne droplet spectrometer to the base of the capping inversion.

The Cardington data from 26 cases of radiation fog were also used by Findlater (1981) to indicate the relative constancy of the temperature at the base of the inversion during the nocturnal formation and persistence phases of radiation fog, and to demonstrate an average height difference of about 50 m between the base of the inversion and the fog top, i.e. the inversion base lay below the fog top.

A schematic representation of the development of radiation fog *in situ* is shown in Fig. 1 and emphasizes the importance of very light winds at a height of 1–2 m above the ground. However, most radiation fogs are complicated to a greater or lesser degree by advective effects.

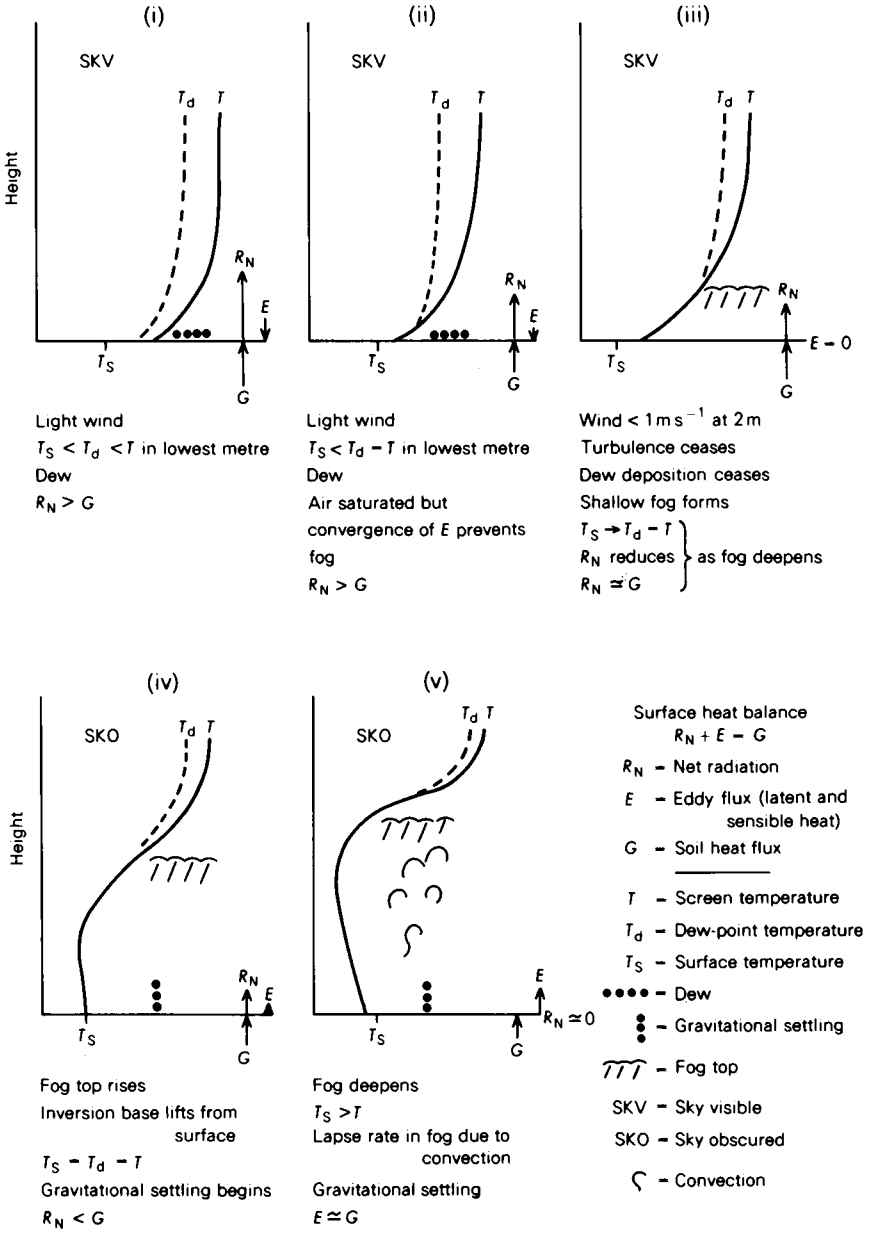

Figure 1. Schematic diagram of the development of radiation fog *in situ*.

Fig. 2 shows one example of a radiation fog at Cardington based on data from instrumented captive balloons. Features of interest are:

(i) The lifting of the inversion base from the surface at about the time that the fog becomes deep enough for the sky to become obscured.

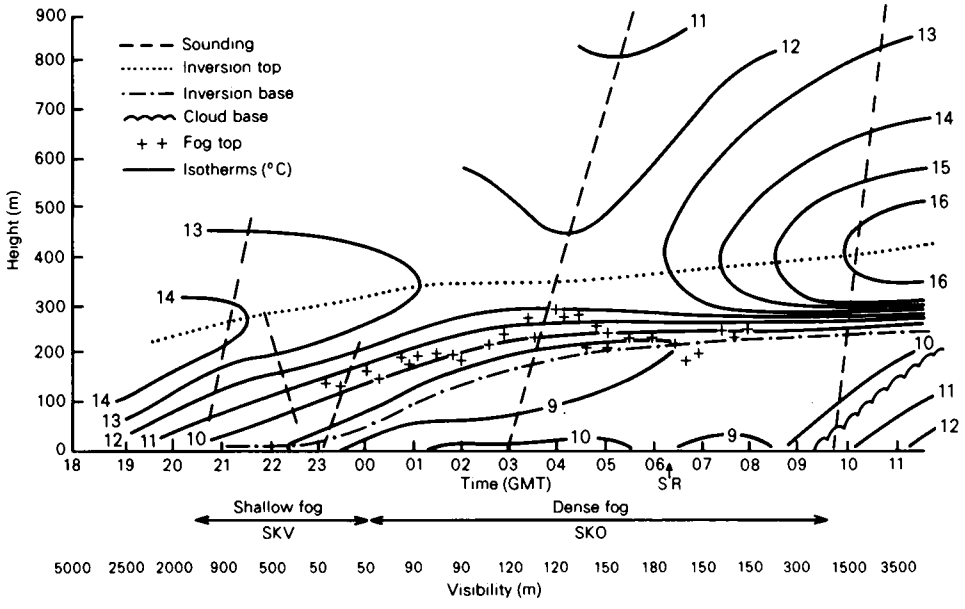

Figure 2. Time cross-section of the development of a radiation fog at Cardington, 17–18 October 1977. SR — sunrise, SKV — sky visible, SKO — sky obscured.

(ii) The rise of surface temperature when the sky becomes obscured and the establishment of a lapse rate up to the inversion base.

(iii) The relative constancy of the temperature of the inversion base as it rises from the surface to a height of about 230 m.

(iv) Small-scale fluctuations of fog-top height, indicated by a droplet spectrometer and a point visibility meter supplemented by data from an acoustic sounder. The balloon soundings of temperature did not have the time resolution to reveal any concomitant small-scale fluctuations in the level of the inversion base.

Data from the droplet spectrometer and point visibility meter have been used to indicate, as in Fig. 3, that the fog top often lies about 50 m (± 20 m) above the base of the inversion.

3. The experimental equipment

Synoptic reporting stations are equipped with standard anemometers mounted at a height of 10 m above the ground and these have stopping speeds of about 3 or 4 knots (1.5–2.0 m s^{-1}). These instruments are not suitable for monitoring the important changes in very light wind speeds at 1 or 2 m to which the earlier studies had drawn attention. The Working Group on the Acquisition and Operational Use of Boundary Layer Measurements recognized this deficiency and recommended that a Porton low-speed anemometer be placed at an airfield for use in local fog studies. The Royal Aircraft Establishment at Bedford was chosen as the site because of a fog-flying program at that station.

Also, a Sensitron monostatic acoustic sounder acquired for evaluation as a local forecasting aid was later installed at Bedford. A report on the operation of this instrument and the potential usefulness of the data to forecasters has been prepared by Findlater and Cole (1983).

Early in 1983 a Kaymont mini-sonde system was sited temporarily at Bedford. The sondes were

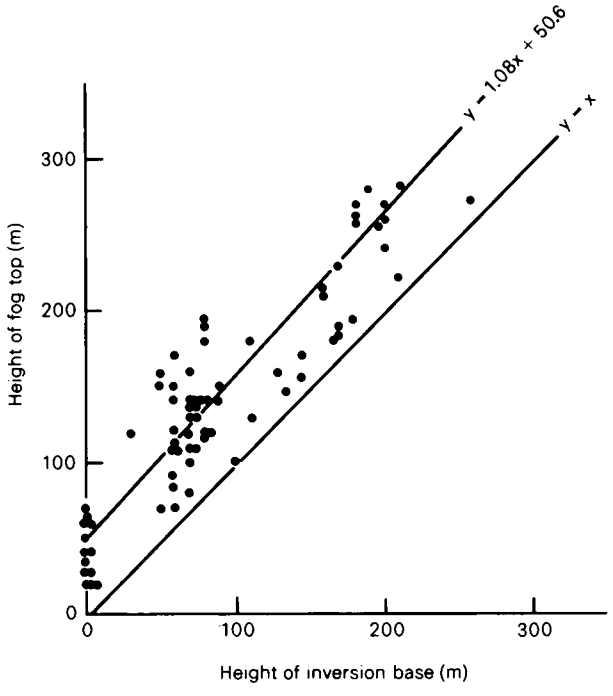

Figure 3. Relation between height of inversion base and height of radiation fog top, based on data from Cardington.

released from the meteorological office whilst the 2 m anemometer was 110 m to the north-east, near the acoustic sounder, on an open grass area. The standard 10 m anemometer is 450 m east-north-east of the meteorological office. In the summer of 1983 the mini-sonde system was transferred to Lossiemouth for studies of sea fog.

Reports on the actual usefulness of the acoustic sounder and the mini-sonde system to local forecasters have been prepared for consideration by the Working Group and what follows are a few examples of how the data have been used for subsequent studies.

4. Case studies at Bedford

(a) *18–19 January 1982*

Fog formed in patches at 1925 GMT with visibility ranging from 800 to 1500 m. At the time of patchy fog formation the 2 m wind dropped to 1.5 m s^{-1} for a few minutes with lulls to 1.2 m s^{-1} and was non-turbulent during this short period. Thereafter the speed and the turbulence increased. The profiles of wind speed and direction at 2 m and 10 m, and of visibility and temperature, are shown in Fig. 4. All values are reduced to 5-minute mean values from the original records.

From 2120 to 2125 GMT wind speeds at both levels fell until 2145 GMT. At this time the 10 m speed increased slightly whilst the speed at 2 m continued to fall to a minimum value of 0.5 m s^{-1} at 2200 GMT with a marked reduction in turbulence characteristics of both speed and direction — coincident with the fog thickening and becoming more widespread. Indeed, at the time of fog formation a decreasing speed at 2 m appeared to be related to an increase at 10 m, and vice versa, (as in Fig. 4) from 2145 to 2230 GMT. However, no firm conclusions can be drawn owing to the horizontal separation of the two anemometers.

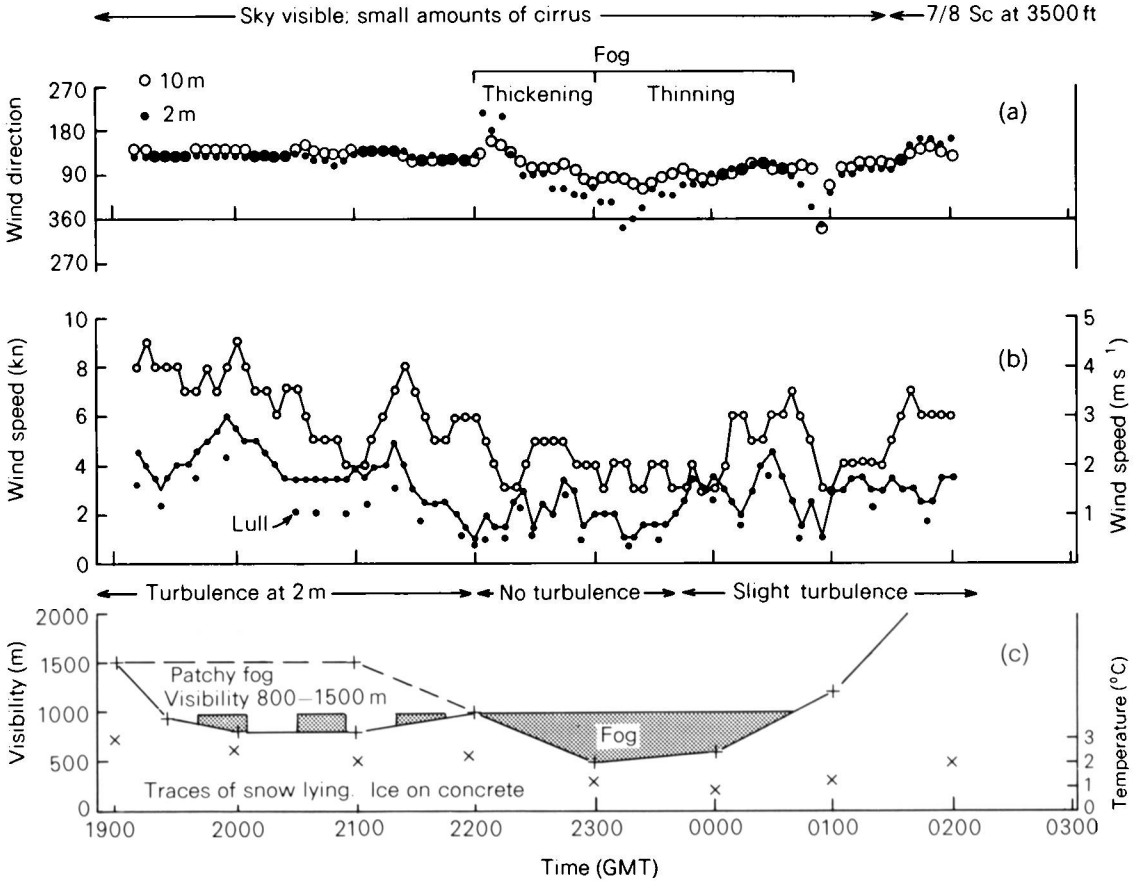

Figure 4. Wind direction (a) and speed (b) at 2 m and 10 m, and visibility and temperature (c) at Bedford, 18–19 January 1982 (x indicates temperature).

The wind speed at 10 m fell from 2200 GMT to reach its minimum at 2210–2215 GMT, i.e. 10–15 minutes after the minimum at 2 m, with a temporary change of direction similar to that at 2 m. The 2 m wind direction swung from the general south-easterly to a south-westerly of short duration (10 minutes) and the air could then have moved towards the 10 m anemometer, 380 m distant, at about 0.75 m s^{-1} to reach the 10 m instrument 8 or 9 minutes later. The reasonable correspondence of the actual time of arrival of this fickle wind suggests that this change was indeed advective.

Whether the extensive fog which formed at eye-level at 2200 GMT deepened significantly is not known. The acoustic sounder, which does not record information below about 45 m, showed a stable layer up to between 200 and 300 m, but because the sky remained visible throughout the period, the inversion was almost certainly ground-based and the fog shallow.

The record of the 2 m anemometer shown in Fig. 5 indicates the striking change in the character of turbulence at 2200 GMT when fog formed. Wind speed continued to vary after fog formation but the difference between gusts and lulls over short periods (say 5 minutes) was markedly reduced. No such detailed change of turbulence can be detected in the record of the 10 m anemometer (Fig. 6).

It may be concluded that, in this case, the sensitive anemometer at 2 m provided more information relevant to the local development of fog than the standard anemometer at 10 m. The former showed clearly the suppression of low-level turbulence at the time of fog formation and thickening, with speeds

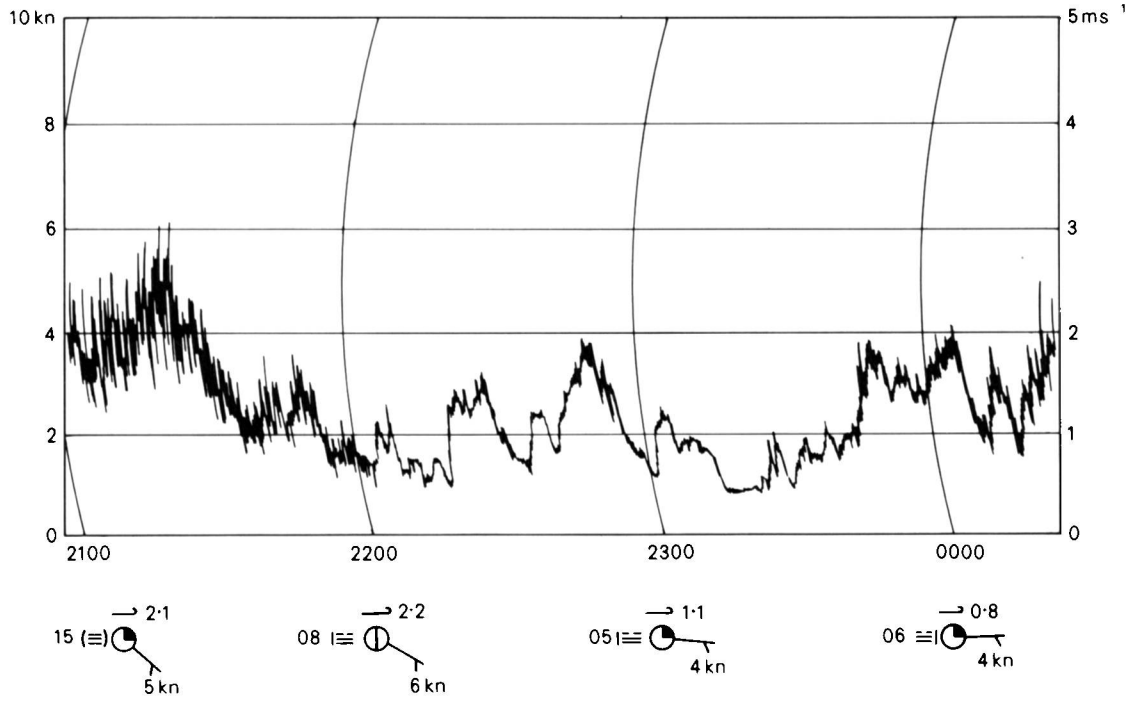

Figure 5. Record of 2 m wind speed and hourly observations at Bedford, 18–19 January 1982.

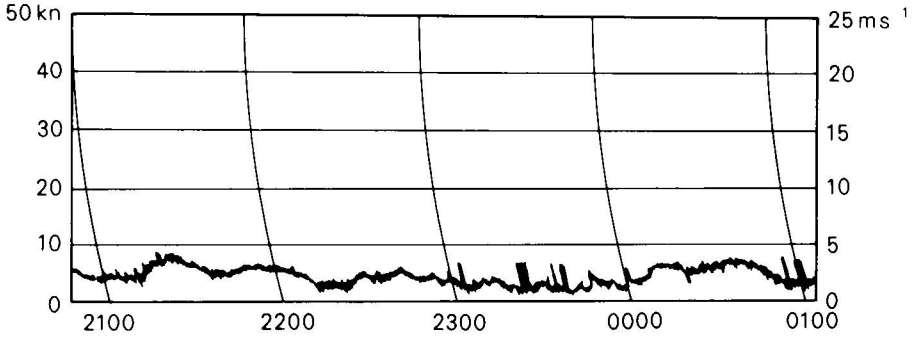

Figure 6. Record of 10 m wind speed at Bedford, 18–19 January 1982.

lulling to 1 m s^{-1} at the time of patchy fog formation and to 0.5 m s^{-1} or less during the thickening phase. Advective effects are considered to have been absent.

(b) *8–9 November 1983*

Another example of the change in turbulence characteristics at the time of significant fog development is shown in Fig. 7 by the open-scale record of the 2 m sensitive anemometer. The gust–lull difference steadily decreased after 2300 GMT to become small from 2320 GMT when visibility fell from 2500 to 600 m and then to 200 m by 0000 GMT. Subsequently the difference became smaller and the visibility fell to 100 m in dense fog at 0015 GMT. Again, these changes cannot be detected in the coarse-scale record of the 10 m anemometer shown in Fig. 8. Though the fog was dense the sky remained visible and

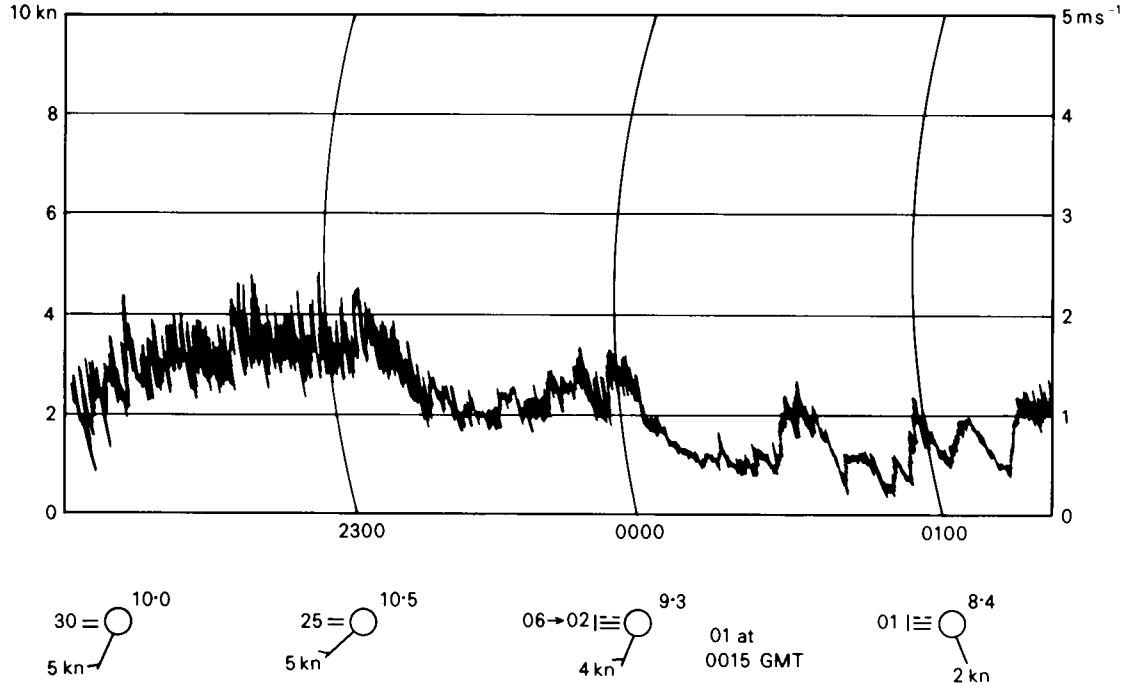

Figure 7. Record of 2 m wind speed and hourly observations at Bedford, 8–9 November 1983.

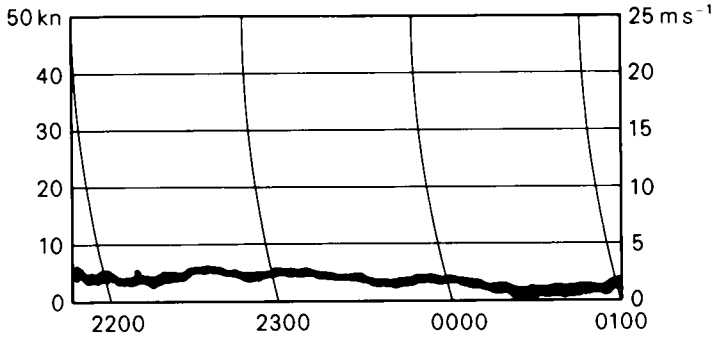

Figure 8. Record of 10 m wind speed at Bedford, 8–9 November 1983.

it may be deduced that the inversion remained based on the surface. In this case, as in the former, the acoustic sounder could not be used to determine the fog top since the inversion base was below 45 m.

Several other cases examined show the same 2 m low-speed anemograph trace characteristics whilst others do not. Those which do not are associated with the higher wind speeds at both 2 and 10 m levels where the fogs, whilst developing, had a marked advective component and *in situ* developments could not be detected. Other cases were upslope fogs from the south-east.

(c) *9–10 November 1983*

This example was the only case where significant amounts of data were available simultaneously from

the mini-sonde, the low-speed anemometer at 2 m, the acoustic sounder and from aircraft operating in the fog.

A sequence of mini-sondes was flown from the afternoon of the 9th, before fog formation, until late morning on the 10th when the fog had deepened to about 140 m. A time cross-section of this period is shown in Fig. 9. During the afternoon and evening, under clear skies, the screen temperature fell steadily and visibility was reduced to below 1000 m at 1830 GMT. With sky visible and outgoing long-wave radiation the screen temperature continued to fall and the fog became dense. Fog tops of 10 and 15 m were measured by the duty observer who climbed the control tower staircase at 2110 and 2230 GMT whilst the horizontal visibility was about 100 m. The screen temperature reached its minimum value of 7.3 ° C at 0100 GMT when the sky had become obscured and, owing to reduced outgoing long-wave radiation and the soil heat flux, it subsequently rose to over 8 °C by 0400 GMT as a lapse rate became established in the deepening fog. Visibilities of 50 m or less occurred during this phase. The inversion base rose steadily (but see later) from the surface to reach 100 m by 0900 GMT. Aircraft reports of fog top near this time confirmed the top of the fog to be about 25 m above the inversion base. The three measurements of inversion base temperature of 7.3 °C at the surface, 7.8 °C at 45 m, and 7.2 °C at 100 m over a period of 8–9 hours confirm the earlier finding from the Cardington data of the conservative nature of this parameter. This fog was in association with 2 m winds of 2–3 m s^{-1} from the east-north-

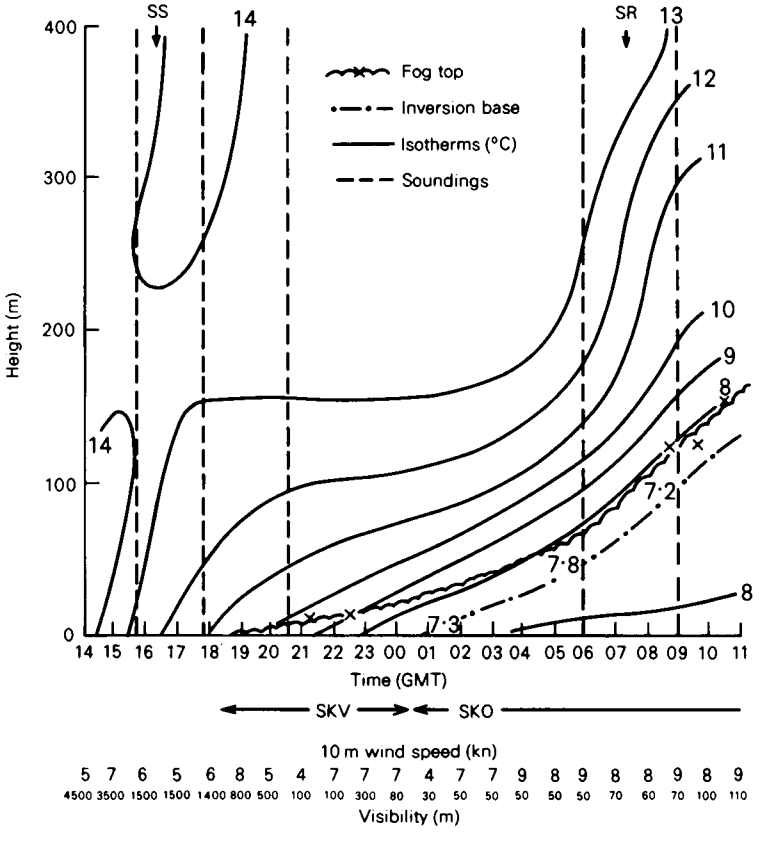

Figure 9. Time cross-section of fog development at Bedford, 9–10 November 1983. SS — sunset, SR — sunrise, SKV — sky visible, SKO — sky obscured.

east and the advective contribution masked any changes in turbulence at 2 m similar to those of the earlier analyses.

The time cross-section shown in Fig. 9 may be used to reconstruct soundings at 2-hour intervals as in Fig. 10(d) (Figs 10(a), (b) and (c) will be discussed later) and from this several points of interest emerge. These apply only to the formation and deepening phase of fog formation, and are as follows:

(i) The marked fall of screen temperature between 1900 and 0100 GMT whilst the fog thickened but the sky remained visible.

(ii) The rise of screen temperature from 0100 to 0500 GMT after the sky became obscured in the deepening fog.

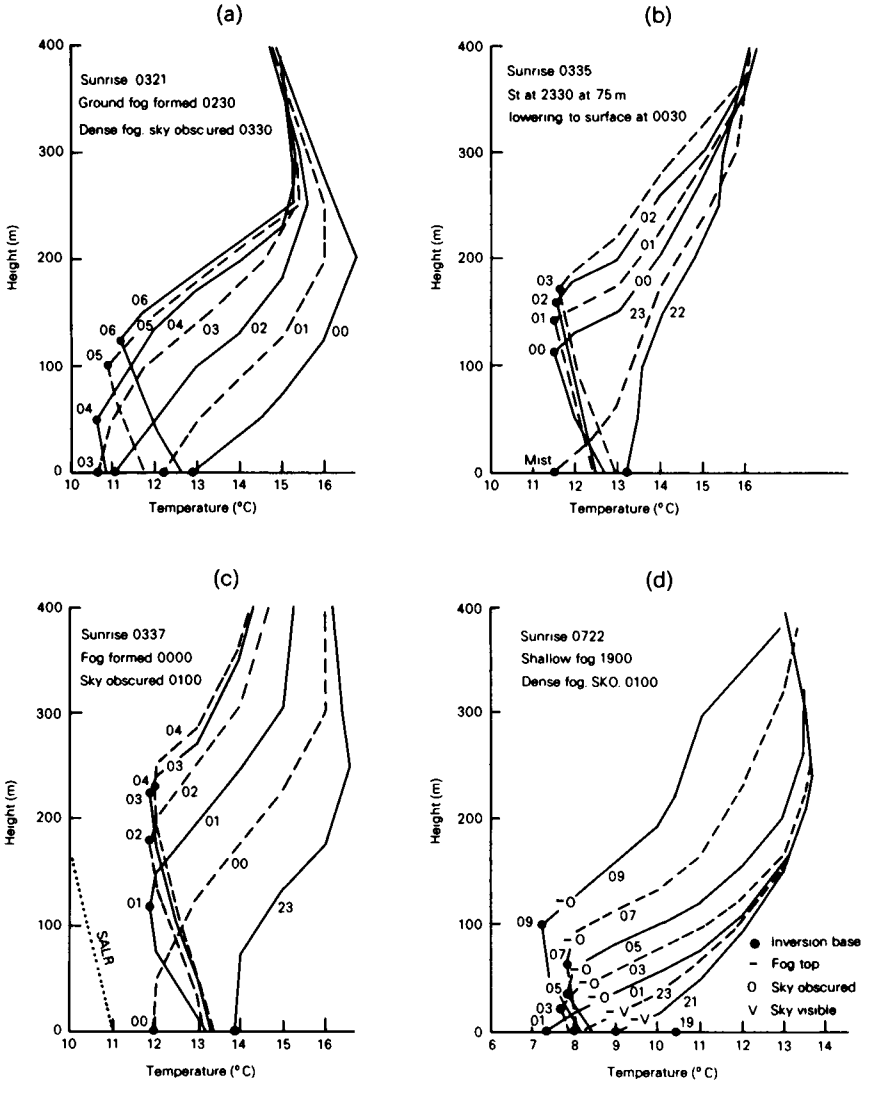

Figure 10. Reconstructed soundings in radiation fog at (a) Lossiemouth, 20 June 1983, (b) Lossiemouth, 7–8 July 1983, (c) Lossiemouth, 10–11 July 1983 and (d) Bedford, 9–10 November 1983. Figures 23, 00, 01, etc. indicate times of the soundings. All times are GMT. SALR — saturated adiabatic lapse rate.

(iii) The warming of the bottom of the fog layer between 0100 and 0500 GMT.

(iv) The cooling of the fog top until shortly after the sky became obscured, when the fog-top temperature remained sensibly constant as it rose aloft.

(v) The relative constancy of the inversion-base temperature (within 1 °C) after the sky became obscured.

(vi) The steady cooling of the air up to about 100 m above the fog top until 0500 GMT. Changes in the upper temperature profile after 0500 GMT, e.g. a cooling of 3 °C at 200 m between 0500 and 0900 GMT, may reflect advective rather than developmental changes.

The acoustic sounder record from Bedford for the period 0600 to 1100 GMT on 10 November 1983 is reproduced in Fig. 11(a), where the dark vertical lines extending downwards from the top of the record after 0730 GMT are due to background noise from road traffic and aircraft. The quasi-horizontal dark echo is that generated by the scattering of sound from temperature inhomogeneities on a scale of about half the wavelength of the transmitted sound, and indicates the lower part of the inversion layer. Below the inversion layer, which is mainly from 100 to 200 m, are the convective plume echoes in the fog layer. The transition from convective plumes to the dark layer echo marks the base of the inversion at about 100 m in this case. For a fuller explanation of the interpretation of acoustic records in fog situations the reader should refer to Caughey *et al.* (1978). Earlier work at Cardington indicated that the fog top often lay about 50 m (± 20 m) above the base of the inversion.

The dark vertical line at 0850 GMT indicates the noise made by an aircraft taking off in fog, when the visibility was 70 m. The aircraft reported the fog top at a height of 120 m. Later flights measured fog tops at 125 m at 0930 GMT and 150 m at 1035 GMT as the fog deepened. These fog tops are shown in Fig. 11(a) and are approximately 50 m above the indicated inversion base.

A sounding made by the mini-sonde at Bedford at 0611 GMT is included in Fig. 11(b) for comparison of the inversion layer with the echo layer. In this case the dark echo layer corresponds well with the

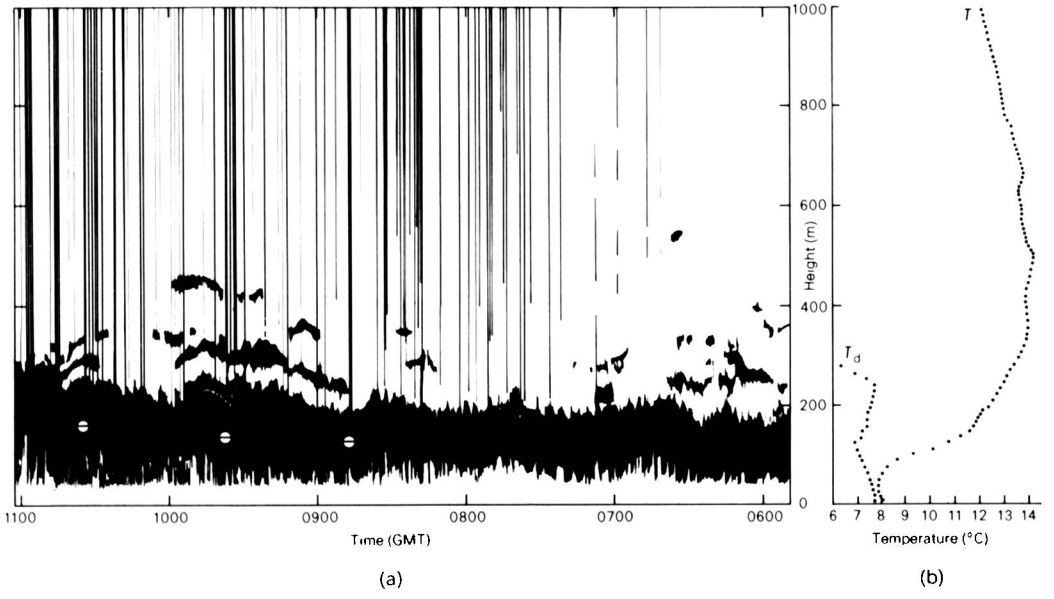

Figure 11. Acoustic sounder record from Bedford (a), 10 November 1983 and a sounding made by a mini-sonde released from Bedford (b) at 0611 GMT for comparison. Fog tops measured by aircraft are indicated by horizontal lines bisecting white circles.

steepest part of the inversion, though more such comparisons are needed to assist interpretation of more complex acoustic records.

A sounding was made at Cardington at 0849 GMT, through the fog shown in Fig. 11(a), using a tethered balloon. Data revealed a pronounced wind shear at the fog top, a typical characteristic of many radiation fogs. In the fog layer the wind was generally north-easterly, 4 m s^{-1}, but just above the fog top was south-easterly, about 9 m s^{-1}.

On some occasions the sounder gives a clear and unambiguous record of inversion layers capping fog, stratus or stratocumulus cloud. One example is given in Fig. 12 where the acoustic record, coupled with data from the standard cloud-base recorder, allowed the cloud height and thickness to be continuously monitored.

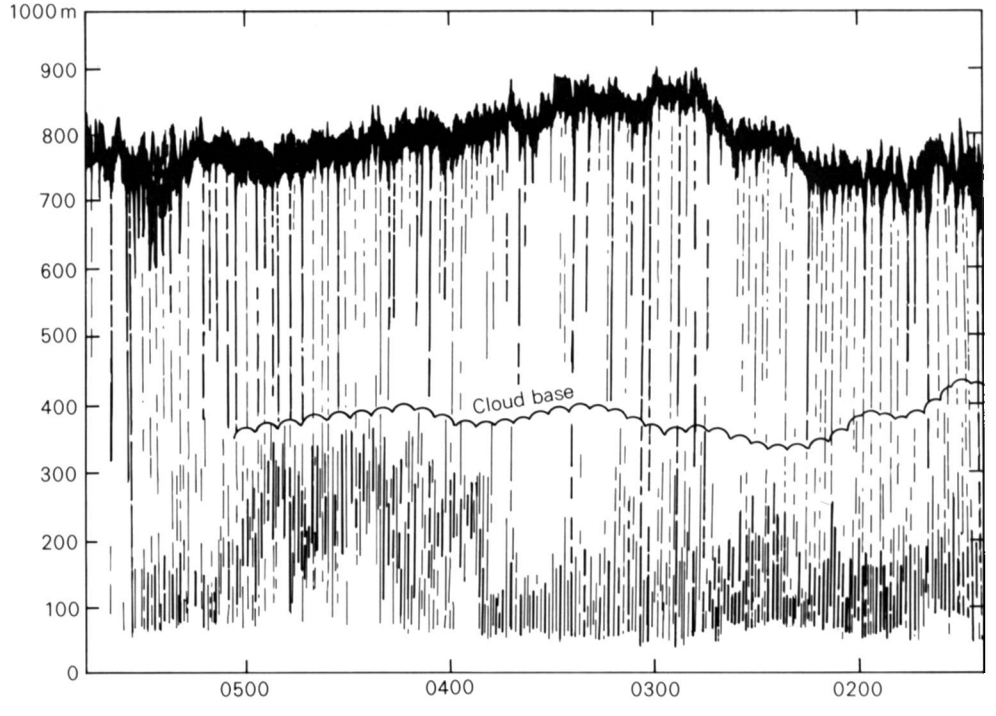

Figure 12. Acoustic sounder record from Bedford, 9 March 1983 monitoring the inversion capping a layer of stratiform cloud. Cloud bases measured by a cloud-base recorder have been entered to indicate the thickness of the cloud.

5. Case studies at Lossiemouth

During the summer of 1983 the mini-sonde system was deployed to Lossiemouth for the study of haar, the sea fog which affects eastern coasts of Scotland and England in the spring and early summer. These studies continued in 1984 when mini-sonde data were supplemented by detailed data gathered offshore by the Hercules aircraft of the Meteorological Research Flight. The results of these experiments will be reported in due course but it is noteworthy that three series of mini-sonde flights were made in conditions when radiation fog formed over the coastal plain after moist sea air had been advected inland during the previous afternoon. In these cases the radiation fogs formed over the airfield with calm or light south-west to west surface winds.

These examples have been analysed in a similar fashion to that of 9–10 November 1983 at Bedford (shown in Fig. 10(d)) and have been included as Figs 10(a), (b) and (c) for comparison with the Bedford example. The reconstructed soundings from Lossiemouth are at 1-hour intervals, rather than at 2-hour intervals, because of the rapidity of development at Lossiemouth.

The radiatively formed fogs at Lossiemouth show very similar characteristics to those listed for Bedford in Section 4(c) and will not be elaborated upon here. It is emphasized, however, that in each of the four examples shown in Fig. 10 the inversion base and fog top rise aloft without significant change of temperature. Rather than the fog top cooling during the night it appears to grow upwards into the cooling layer whilst preserving its temperature. This is evident from the skeletal profiles shown in Fig. 13.

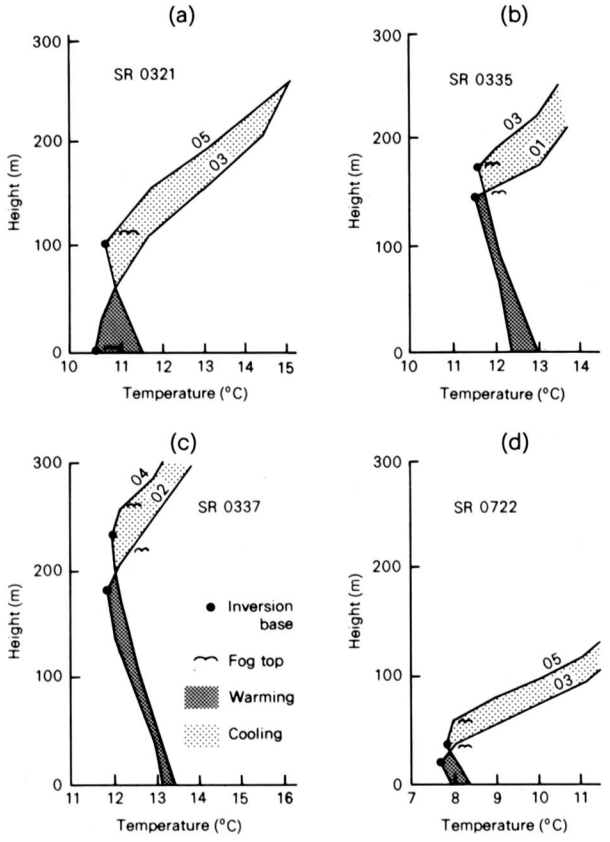

Figure 13. Skeletal profiles of the deepening of radiation fog, illustrating the warming of fog and the growth of its top into the cooling layer at (a) Lossiemouth, 20 June 1983, (b) Lossiemouth, 8 July 1983, (c) Lossiemouth, 11 July 1983 and (d) Bedford, 10 November 1983. SR — sunrise. All times are GMT.

6. Conclusions

The results of the trials to assess the suitability and usefulness of the acoustic sounder, mini-sonde and low-speed anemometer to local forecasters will be circulated elsewhere; here, only conclusions drawn

from the studies of data in fog situations that may be of immediate interest to local forecasters will be noted. These are:

(a) Soundings at Cardington and Bedford show that the top of radiation fog is often 50 m (± 20 m) above the level of the inversion base. The inversion base is on the surface when the sky is visible in fog, but is aloft when the sky is obscured and surface temperature has begun to rise owing to the fog deepening. This confirms earlier studies by Roach *et al.* (1976).

(b) A low-speed anemometer at 2 m can detect the cessation of turbulence at low level which is often coincident with the initial formation of fog *in situ*, or the thickening of an existing shallow fog. The degree of turbulence may be more important than the actual light wind speed. Standard anemometers exposed at a height of 10 m do not detect the changes in the degree of turbulence at the time of fog formation, nor the very light winds associated with non-advective fog formation when the direction of drift may be important. Experiments are now being carried out with the low-speed anemometer mounted at a height of 0.5 m to determine whether the cessation of turbulence can be detected earlier closer to the surface prior to fog formation, and whether there may be some predictive value in such measurements.

(c) Data from the mini-radiosonde system have proved to be invaluable for local fog forecasting by revealing the depth of the moist layer and lapse rate before fog formation and the depth of fog thereafter.

(d) Soundings made by captive balloons at Cardington, and by mini-sondes at Bedford and Lossiemouth, indicate that if radiation fog actually forms at a temperature (T_{AF}) and its temperature subsequently falls to a minimum (T_{MF}) at the time the sky becomes obscured then the temperature of the base of the inversion remains sensibly constant at this value (T_{MF} ± 0.5 °C) as the inversion base rises aloft. After the inversion leaves the surface and the temperature rises to reach, say, T_{HH} at hour HH, then if a saturated adiabatic lapse rate can be assumed between T_{HH} and T_{MF} the height of the base of the inversion may be estimated (see Fig. 14). This relationship appears to apply only during the formation phase whilst fog is still deepening during the night and early morning, and advective effects are minimal. This finding is based on a relatively small number of cases and further studies are required to verify it.

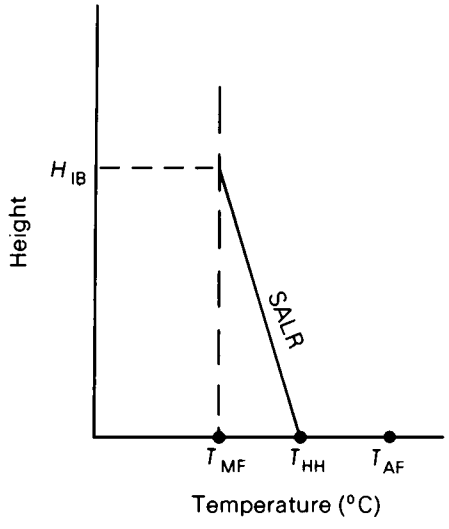

Figure 14. Schematic diagram to estimate height of inversion base, where T_{AF} — temperature at time of actual fog formation, T_{MF} — temperature at time sky became obscured, T_{HH} — temperature at hour HH after sky became obscured, H_{IB} — height of inversion base with fog top possibly 50 m (± 20 m) above. SALR — saturated adiabatic lapse rate.

(e) The acoustic sounder at Bedford has demonstrated its capability of continuously monitoring the height of inversions which cap not only fog layers but those associated with stratus, stratocumulus and haze layers. Fluctuations on long and short time-scales are clearly indicated. However, there are some occasions when the acoustic sounder yields records which are difficult to interpret, or are ambiguous. Further studies with local upper-air temperature soundings are desirable to formulate guidelines for interpretation of the acoustic record.

Acknowledgements

The author wishes to express appreciation to Mr B. A. Cole, the Senior Meteorological Officer at Bedford and his staff for their efforts in using the experimental equipment to gather data during suitable fogs (a task additional to the assessment of the usefulness of the equipment in routine daily forecasting, and also to their normal duties); also to Mr J. M. Malcolm, the Senior Meteorological Officer at Lossiemouth and his staff for similar support. Thanks are also due to the Observational Requirements and Practices, Boundary Layer, and Operational Instrumentation Branches of the Meteorological Office, and to the Meteorological Research Unit at Cardington, for assistance in modifying, siting and maintaining some of the observing systems.

Many helpful discussions have been held with Dr W. T. Roach and the author is grateful for the resulting amendments which have been introduced.

References

Brown, R. and Roach, W. T. 1976 The physics of radiation fog: II — a numerical study. *Q J R Meteorol Soc*, **102**, 335–354.

Caughey, S. J., Dare, W. M. and Crease, B. A. 1978 Acoustic sounding of radiation fog. *Meteorol Mag*, **107**, 103–113.

Findlater, J. 1981 Some characteristics of radiation fog deduced from Balthum data. (Unpublished, copy available in the National Meteorological Library, Bracknell.)

Findlater, J. and Cole, B. A. 1983 Report on the operation of the Sensitron acoustic sounder at Bedford. (Unpublished, copy available in the National Meteorological Library, Bracknell.)

Kraus, H. 1958 Untersuchungen über den nächtlichen Energietransport und Energiehaushalt in der bodennaben Luftschicht bei der Bildung von Strahlungsnebeln. *Ber Dtsch Wetter*, **48**, 7.

Monteith, J. L. 1957 Dew. *Q J R Meteorol Soc*, **83**, 322–341.

Roach, W. T. 1976 On some quasi-periodic oscillations observed during a field investigation of radiation fog. *Q J R Meteorol Soc*, **102**, 355–359.

Roach, W. T., Brown, R., Caughey, S. J., Garland, J. A. and Readings, C. J. 1976 The physics of radiation fog: I — a field study. *Q J R Meteorol Soc*, **102**, 313–333.

Stewart, K. H. 1955 Radiation fog: investigations at Cardington, 1951–54. (Unpublished, copy available in the National Meteorological Library, Bracknell.)

Taylor, G. I. 1917 The formation of fog and mists. *Q J R Meteorol Soc*, **43**, 241–268.

551.501.9:551.508

Instrumentation at Eskdalemuir Observatory

By W. K. Young

(Eskdalemuir Observatory)

Summary

A brief description is given of some of the less commonplace instruments currently at Eskdalemuir Observatory and an indication is presented of the uses made of the instrumental data.

1. Introduction

Eskdalemuir Observatory (Fig. 1), established in 1908, is situated in the south-west of Scotland on the west side of the White Esk valley, which runs north–south. The site is approximately 280 metres (800 feet) above sea level. The region is mountainous by British standards with many peaks in excess of 300 metres. Over the last 20 years the local terrain has been progressively changed from open, exposed, moorland to coniferous forest. A reservoir has also been constructed in the adjacent Black Esk valley.

The site was originally established as a purpose-built geomagnetic observatory. During the 75 years since its opening the staff of Eskdalemuir have carried out a varied program of work which includes among its disciplines seismology, meteorology and atmospheric chemistry. A variety of non-standard instruments have been acquired to support the observational programs over the years. Many of the instruments to be found at Eskdalemuir are of a specialized nature and, in some cases, unique. This

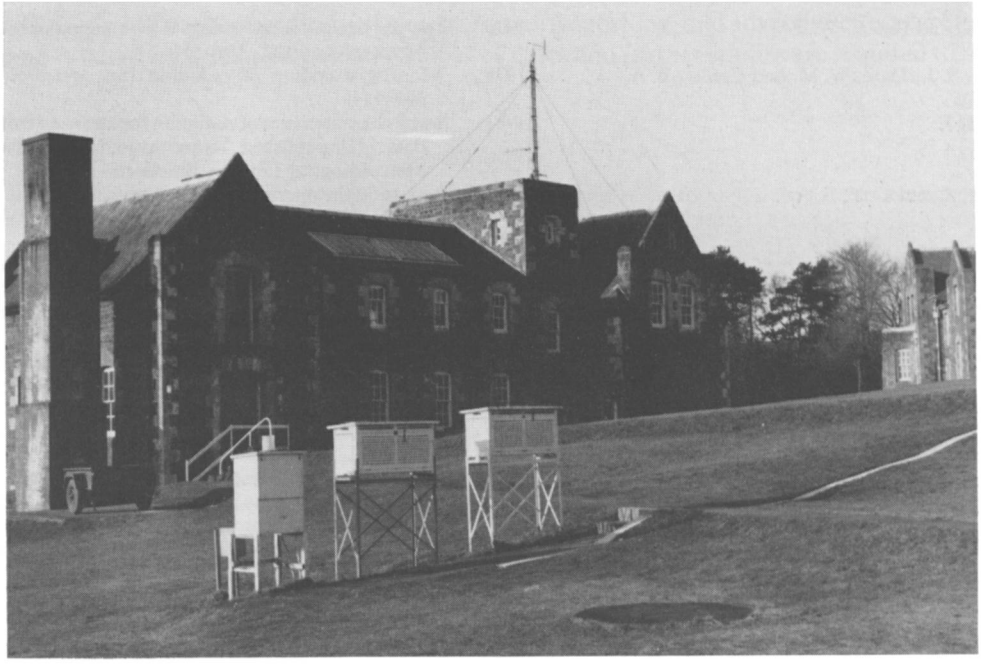

Figure 1. Eskdalemuir Observatory.

paper will concern itself, primarily, with those more unusual devices used for meteorological and environmental monitoring purposes, and the uses to which the data are put.

Not all of the programs have been continuous. Geomagnetism, basic meteorology and seismology have the longest record durations. However, in the case of meteorology, it should be noted that re-siting and changes in the instrumentation have resulted in discontinuities in the long-term records which may not be apparent to the casual user.

2. The current program

The Observatory, at present, contributes to a large variety of programs for both national and international institutions. The British Geological Survey (BGS), who currently have responsibility for the site, maintain both seismological and geomagnetic monitoring on a continuous basis. The meteorological staff are required to carry out an observing program on a 24-hour basis in support of the role of the station as (i) a Principal Land (Synoptic) Station, (ii) a Reference and Principal Climatological Station, (iii) a Principal Radiation Station and (iv) a Regional World Meteorological Organization (WMO) Background Pollution Monitoring Network (BAPMoN) Station. In addition the observers assist BGS in their work by contributing to the daily operation and analysis of both the seismological and geomagnetic records. The pollution monitoring activities are mainly of a supervisory nature and all sample analyses are carried out by those institutions for whom the sampling is done, or their appointed agencies.

Instrumentation which is now in working order consists of a mixture of that needed to support current programs and items of a historical interest which were used in earlier programs. For ease of presentation such instrumentation is grouped below according to the variables it measures rather than the observing programs it supports.

3. Pressure

Apart from the normal precision aneroid and open-scale barometric devices used for synoptic purposes, there are three other pressure measuring instruments working at Eskdalemuir. Two have historical interest and one is in use for a specialized purpose.

The Fortin barometer, introduced in 1928, is still in working condition, though now requiring refurbishment. Occasional checks are made of the readings given by this mercury barometer, though the considerable skill required in setting the mercury level in the bottom chamber leads to an operationally unacceptable variability in the results.

A Dines float barograph (Fig. 2) is also run routinely, mainly for historical reasons. This device consists of a simple mercury barometer with the lower end turned upwards to form an open-topped chamber. Into this is inserted a glass bell float with air trapped between the mercury and the top of the glass dome. Through a pulley system the small changes in level of the mercury caused by variations in the atmospheric pressure are magnified to give a readable trace. Virtually no temperature compensation is required owing to the careful choice of materials employed in the mechanical system. The instrument responds to small pressure fluctuations ($<$0.5 mb/5 min) more effectively than the open-scale recording device in operational use. However, it also suffers, as a consequence of this fast response characteristic, from some wind noise. The chart is changed daily rather than the more usual weekly, enabling the user to see details on a finer time-scale than with the other recorder.

The third pressure measuring instrument is an infra-sonic microbarograph (Fig. 3). This device is designed to detect short-period pressure transients of 1 to 250 microbars amplitude and with a period of

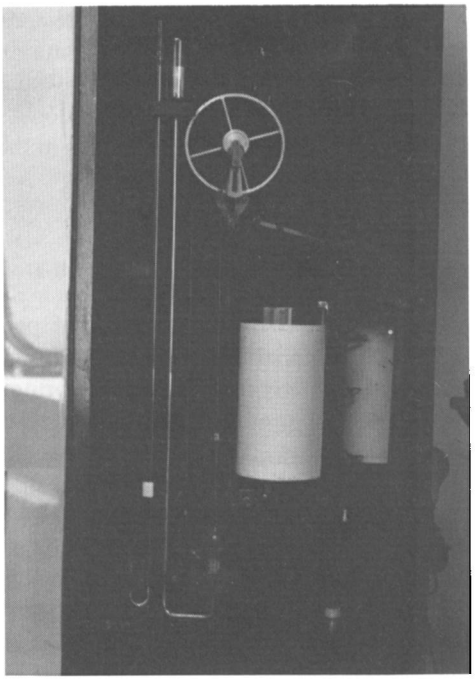

Figure 2. The Dines float barograph.

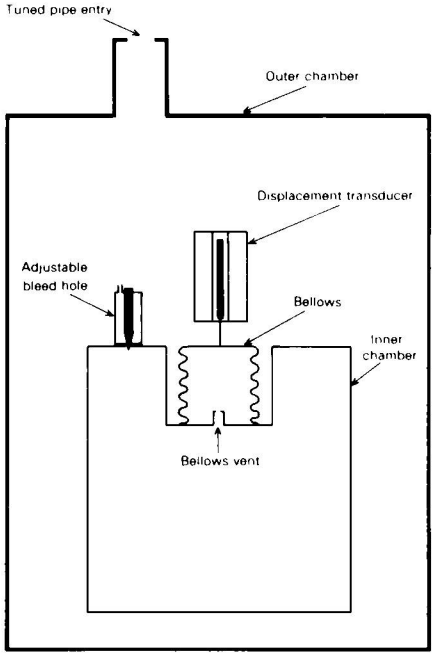

Figure 3. Simplified diagram of the infra-sonic microbarograph.

approximately 1 to 1000 seconds. The absolute value of atmospheric pressure is not measured. Inside an outer, rigid chamber is another smaller and equally rigid cylindrical chamber. At the top of the inner chamber is a small-bore bleed hole which allows the air in the inner chamber to adjust slowly to the familiar scale of pressure changes experienced by synoptic observers. In addition a metal bellows extends downwards from the top of this inner chamber, which is effectively sealed from the atmospheric pressure of the outer cylinder. Atmospheric pressure in the latter is maintained through a tuned pipe. Short-period variations in pressure within the pass-band of the sensor cause the bellows to move a distance proportional to the difference in pressure between the two chambers. This motion is converted to a d.c. voltage and the output from the microbarograph is modified, electronically, to a signal which can be recorded on magnetic tape alongside the output of the BGS seismometers. This enables the seismologist to distinguish between small, real seismological disturbances and those generated by the passage of atmospheric shock waves, and provides an interesting link between what might be viewed as unrelated sciences. A further use for the record, which is also available on sensitized paper, is in the investigation of public complaints about 'sonic bangs'. These acoustic waves produce a high-frequency trace which is very close to the upper limit of response of the sensor. They vary in duration, frequency and number of arrivals according to the distance from the event and the altitude at which it originates. One example of a signal can be seen in Fig. 4. This record shows a combination of the normal background 'microbaroms' — small 5-second tropospheric waves — and illustrates the much faster nature of a 'sonic bang' event.

In the case of a public complaint the authorities occasionally contact the Observatory to determine

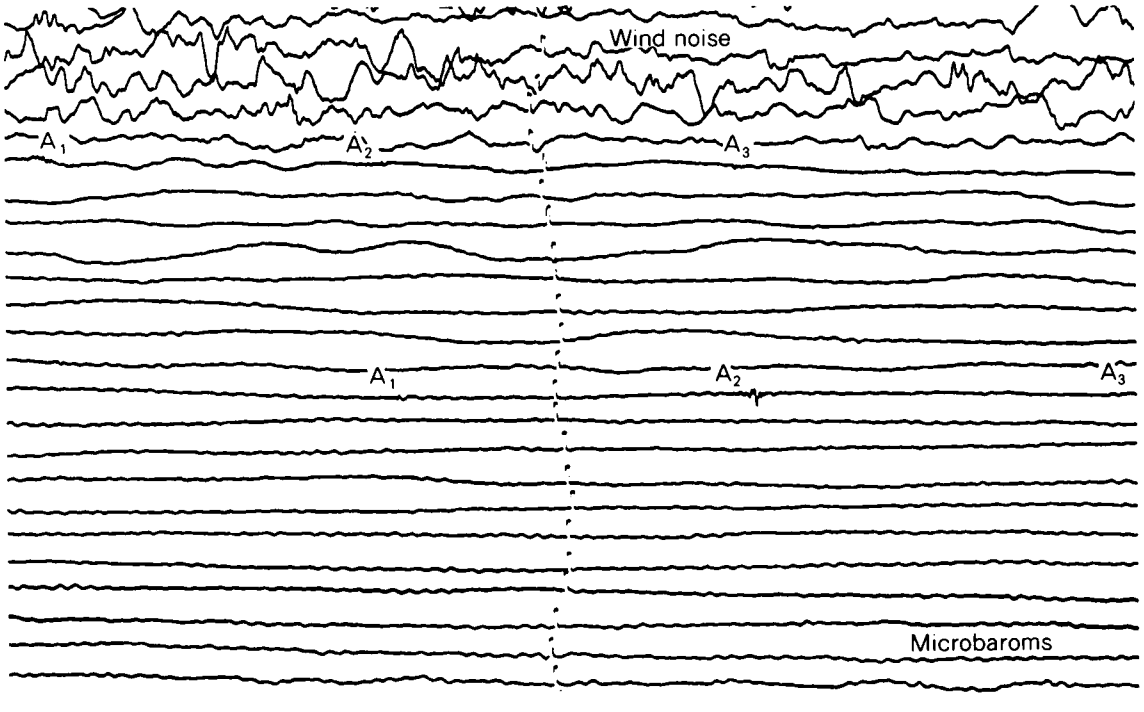

Figure 4. Part of the record produced by the infra-sonic microbarograph. Two 'sonic events' can be seen with triple arrivals A_1–A_3 for each event, which are due to the multi-path nature of the signal.

whether a record is available. If such an event is identifiable on the record, then the time of arrival of the wave can be given. Occasionally it is possible to estimate the distance of the source of the wave providing the event has also registered on some of the remote seismic sensors of the Observatory network. In the instance illustrated the event probably originated some 50–100 km away.

4. Wind

The operational wind sensor is a Mk 4 wind system which feeds data to a DALE (Digital Anemograph Logging Equipment) and has been in use since 1980. The mast is about 300 metres north-west of the main building on slightly sloping ground. Since the introduction of remote reading electrical anemographic equipment to Eskdalemuir in 1965 all wind records have come from this location.

Before the use of electrical sensors the wind system in use was installed on top of the tower in the main building. This consisted of a Dines pressure tube anemograph (PTA) which records direction through direct mechanical coupling from the vane and speed by a Pitot head system connected to a water manometer. The present Dines PTA was installed in 1933. It is principally maintained for historical reasons though it is fully operational and can be brought into service in times of electrical system failure. The effect of oversheltering on the PTA due to adjacent trees and buildings has been described in a letter by McIntosh (1955). This letter should be referred to if any climatological study of wind at Eskdalemuir is intended.

It is worth noting at this point that this is one of the records in which discontinuities are most apparent. There have been four different wind speed recording systems in the 75 years of observing and each has been sufficiently different in sensitivity to cause step changes in the long-term means. The gradual afforestation of the local area coupled with the intermittent lopping of nearby trees has produced a data set which must be treated with caution. It is suspected that the current wind speed measurements are being progressively affected by a plantation on an adjacent ridge. There is, at present, no system whereby a public enquiry to the Meteorological Office about any wind data set is automatically annotated as to deficiencies in, or reservations about, the exposure of the sensor.

5. Precipitation

There are six precipitation gauges currently in use at Eskdalemuir. The main instruments are a 5-inch standard rain-gauge, a 12-inch tilting-siphon recorder (TSR), a 750 mm^2 tipping-bucket rain-gauge (TBR) connected to a magnetic tape event recorder (MTER), and a 5-inch standard rain-gauge in the evaporation tank enclosure. All but the last gauge are in turf wall pits.

The 5-inch gauges give an accumulated total and are read at selected times of the day. The TSR gives a trace which can be used to determine the hourly rainfall, and the data stored on the MTER tape can be read for minute-by-minute rainfall values where rainfall of 0.2 mm gives one pulse or count.

Also installed, in addition to the main gauges, are an open-scale TSR and a Hellman–Fuess gravimetric snow gauge. The open-scale TSR is similar in construction to the normal 24-hour recorder but has a fast-running clock which drives a chart roll lasting 5 days. Minute-by-minute values can be determined more reliably from this record than from the normal TSR owing to its expanded time-scale. The Hellman–Fuess gauge (Fig. 5) is normally installed in a deep pit with a turf wall. This device catches all precipitation in an interchangeable copper bucket through a typical orifice. The lower half of the instrument consists of a dynamic balance with pen plus a chart drive (Fig. 6). The Hellman–Fuess gauge is maintained primarily for historical purposes and is in use every winter. It is the only gauge at the Observatory capable of giving a reasonable indication of rate of snowfall since most other devices used at Eskdalemuir and other meteorological stations are designed to record liquid precipitation only. The

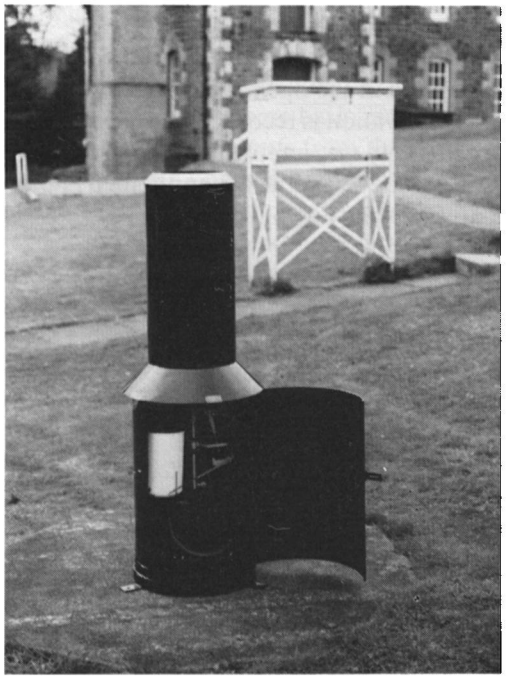

Figure 5. The Hellman–Fuess snow gauge.

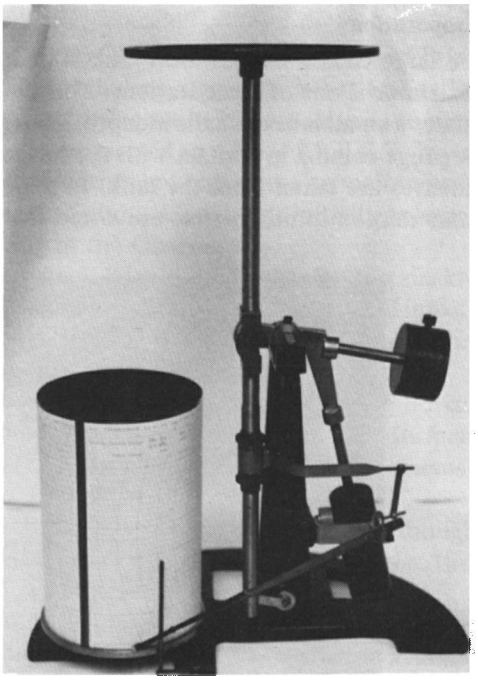

Figure 6. Dynamic balance with pen and chart drive of the Hellman–Fuess snow gauge.

record, however, is not routinely used by the Meteorological Office but this does not detract from its potential value to a researcher. There are three drawbacks to its use: firstly it is prone to wind noise in that gusting moves the bucket causing some blurring of the trace; secondly, the balance system works on knife edges which are delicate and removal of the bucket can cause displacement of the pivots; lastly, the chart gives a 24-hour record of precipitation expressed as millimetres of rainfall up to a maximum of 35 mm and not a snow depth, *per se*. Fig. 7 shows a typical record provided by the snow gauge.

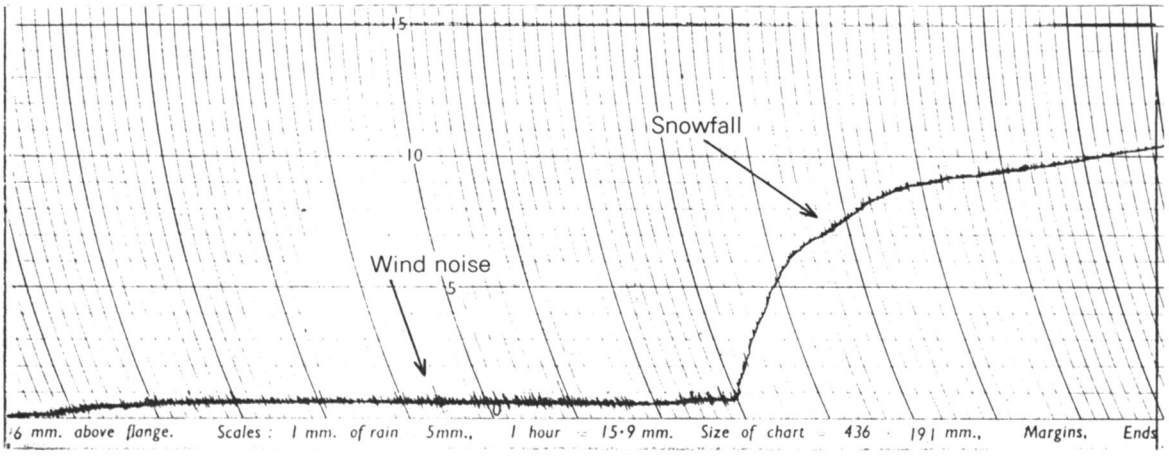

Figure 7. Part of a record produced by the snow gauge.

6. Evaporation

The large British evaporation tank is in use at selected stations throughout the United Kingdom. Eskdalemuir is one of these stations. This device is usually sited in the open and its 6 feet square area simulates a small lake of shallow depth. Water loss due to evaporation is recorded by a rigidly mounted hook gauge coming in contact with the surface of the water. Daily measurements of water loss/gain in millimetres are taken from the tank. In addition, the daily run of wind at 0.5 and 2 metres plus the 24-hour rainfall in millimetres are noted from the site of the tank (Fig. 8).

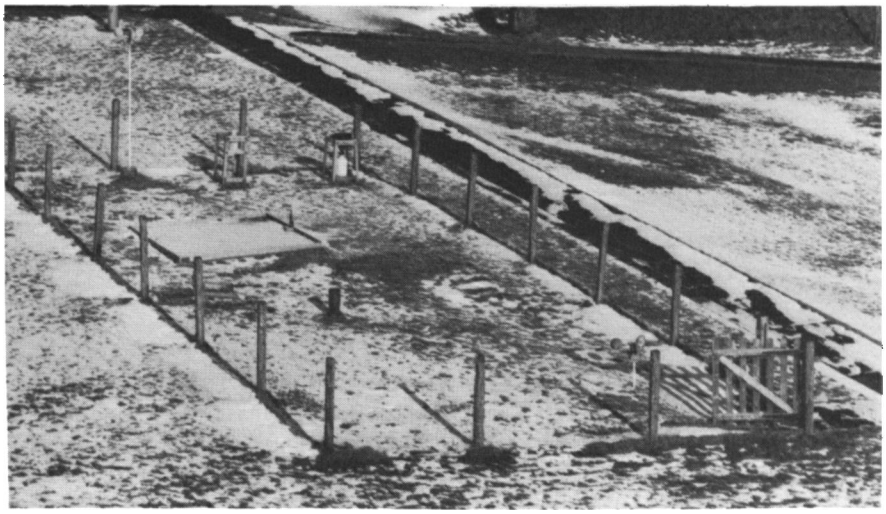

Figure 8. Site of the evaporation tank.

7. Temperature

No unusual instruments are now employed for measurement of temperature though this has not always been the case.

During its history the Observatory has seen several changes to the source of its temperature data. Originally these came from a large photothermograph screen. This was one of the earliest applications of photography in science and consisted of two mercury-in-glass thermometers in which the mercury columns obstructed light focused through their glass capillaries on to photographic paper on a rotating drum. The device was cumbersome and occupied a louvered screen as large as a garden hut. It was possible to read the temperature directly from the thermometers as well as from the recording.

In the 1950s and 1960s temperatures were reported from the thermometer screen situated about 18 metres closer to the main building. Following a short trial in the late 1960s the readings from an aspirated psychrometer, designed at Kew, were substituted for the screen readings in the climatological record. This continued until 1981 when the practice was abandoned in favour of using, once more, the readings from the screen, in order to make Eskdalemuir temperatures compatible with those from the remainder of the UK network.

Soil temperatures at 30 and 100 cm are measured. However, owing to the type of terrain and the generally high water table caused by the adjacent land draining across the measuring site, the soil temperatures at the recommended shallower depths are not recorded. A bare earth patch is not maintained for the same reasons.

8. Sunshine and radiation

Radiation records of one type or another have been kept at this Observatory since 1910. As a Principal Radiation Station, Eskdalemuir records global and diffuse radiation, sunshine hours and radiation balance. In addition to these basic requirements a normal incidence pyrheliometer is used to measure direct radiation. The outputs from the radiation sensors are connected to a Mk 3 MODLE (Meteorological Office Data Logging Equipment). A visible record of instrument output is also maintained on a Kent chart recorder which acts as a back-up in case of logger failure. All data are initially processed at Bracknell in the main computing facility prior to checking at the Observatory.

Both global and diffuse radiation are detected using Kipp's CM5 Moll–Gorczinski-type pyranometers. The Eppley normal incidence pyrheliometer is also a thermopile device fitted into a tube with the sensitive area at its base. The tube is directed so that the image of the solar disc is maintained on the sensing surface by means of a motor-driven equatorial mount.

The radiation balance meter, designed and built at Kew Observatory, consists of two horizontal sensing thermopiles mounted back to back and coated in a durable matt black coating. The surfaces are continually aspirated by a motor-driven fan. Because its surfaces are exposed to the elements it is unreliable in precipitation.

A Campbell–Stokes sunshine recorder has been in use at the Observatory since 1908. Although the siting has been improved in recent years the basic problem of obstructions due to local hills to the east and west cannot be eliminated.

All the data from Eskdalemuir are, after checking and quality-control procedures, stored in the radiation and sunshine archives of the Meteorological Office. From here they are made available to users on request. Applications include climatology, agrometeorology, solar energy feasibility studies, building and engineering design.

9. Atmospheric electricity

Atmospheric electricity measurements were made at Eskdalemuir from 1909 until the end of 1983. These were mainly concerned with the vertical potential gradient. During the late 1970s an attempt was made to introduce air–earth current measurement into the program. This was not successful as the level of precipitation and unreliable nature of the device chosen resulted in the record being too discontinuous to be of any value.

Potential gradient was, in the latter years, measured with a Sigrist PG meter. This device consisted of a remote, electrically isolated probe vertically mounted on a plastic post fixed in concrete flush with the surrounding grass and well away from buildings. At the top of the probe was mounted a radioactive source (americium 241) which prevented accumulation of charge. The sensor was connected to a high impedance amplifier and the output was directly expressed in volts per metre. Calibration was by comparison with a quartz fibre electrometer which had a 1-metre rod sensor of similar design to the probe. Output was fed directly to the MODLE used for radiation data and transferred to the main computer complex at Bracknell. Results of measurements were sent annually to Leningrad where they were sometimes published in a summary produced for WMO.

There are no known users of the data and for this reason the program has been discontinued.

Another related sensor which is still operating at the Observatory is the experimental lightning counter. This device, constructed for BGS to monitor geomagnetic disturbance due to ground strike lightning, consists of a narrow band, fixed gain, VLF receiver tuned to 11 kHz. Any signal at the antenna exceeding a predetermined amplitude threshold triggers a counter. An analogue trace of the activity is also provided. The counter is read daily and the charts are held for examination in cases of extreme

activity. The energy envelope of individual flashes can be visually observed as a wave-form by attaching an oscilloscope to the outlet provided.

10. Pollution

The Observatory grounds are probably the most thoroughly monitored 2 hectares in Britain.

Sampling of radioactive materials is carried out for the Environmental and Medical Sciences Division, Harwell. Two bottles of rain-water are collected, one for measurement of tritium and the other for isotopes. Also a filter for radioactive dust is exchanged each week in a 'hi-volume' sampler. The results of these monitoring programs are published each year by Harwell (Cambray *et al.* 1983).

Several tasks are carried out for Warren Spring Laboratory, Stevenage. These are in support of measurements of:

(a) Smoke in air. This involves changing a filter daily and checking the volume of air sampled.

(b) Solid and gaseous sulphur in air. Both a filter and a special solution are changed daily.

(c) Lead and other heavy metals in air; another filter project, this only needs to be changed once a week.

(d) Acid rain. A bottle is changed on rainy days. These bottles, along with the sulphur samples, are sent weekly to Warren Spring Laboratory.

(e) Suspended particulates (dichotomous sampler). Two magazines of filters, to obtain daily samples of fine and coarse particles, are changed once a month.

Results of most of these activities are available in the publications of the United Kingdom Review Group on Acid Rain (1983), the United Nations Economic Commission for Europe European Monitoring and Evaluation Programme (EMEP) (1984a, 1984b) and Warren Spring Laboratory (1985).

Two further rain-water samples are analysed at the Laboratory of the Government Chemist in London. These samples are slightly different in nature. One is taken from a cabinet with a rain funnel on top. The funnel is continuously open and both dust and rain are collected. The second is taken from an automatic precipitation collector designed and built by the Meteorological Office. This device has an electronic sensor which, when it detects precipitation, opens a lid and allows a funnel to rise up out of the interior to be given a clear exposure. On cessation of precipitation and after a reasonable delay the procedure is reversed.

This latter rainfall sample is one of the three parts of the minimum contribution to WMO BAPMoN expected of a Regional Station. The second part of the BAPMoN program is the measurement of turbidity or atmospheric optical thickness. This is done by monitoring direct solar radiation at four different standard wavelengths using narrow-band filters in a solid-state sunphotometer. Observations are only permissible in clear sky conditions and local weather does not permit very frequent observations! The third part of the minimum contribution is 'hi-volume' sampling of suspended particulate matter. It is intended that suitable equipment will be installed soon.

11. Conclusion

The normal suite of meteorological instruments employed at most Meteorological Office observing stations is, equally, to be found at Eskdalemuir. However, the station has a much greater range of instrumentation and activities.

Whilst use is already made of most of the measurements, it is hoped that this article will bring to the attention of those at present unaware of the facilities offered, the wide scope of the data suite produced by the Observatory.

Acknowledgements

The author wishes to extend his thanks to J. M. Nicholls, Assistant Director (Observational Requirements and Practices) for his encouragement in the preparation of the article, to P. H. Jeffries for his assistance and to the photographic section of the Meteorological Office for their preparation of the photographs.

References

Cambray, R. S., Lewis, G. N. J., Playford, K. and Eakins, J. D. 1983 Radioactive fallout in air and rain: results to end of 1982. Harwell, Atomic Energy Research Establishment. A.E.R.E. R-10859.

EMEP (European Monitoring and Evaluation Programme) 1984a Preliminary data report: April 1982–September 1982. Norwegian Institute for Air Research, Lillestrøm, Norway.

1984b Summary report from the chemical co-ordinating centre for the second phase of EMEP. Norwegian Institute for Air Research, Lillestrøm, Norway.

McIntosh, D. H. 1955 Dines P.T. anemometer. (Unpublished letter, available at Meteorological Office, Edinburgh.)

United Kingdom Review Group on Acid Rain 1983 Acid deposition in the United Kingdom. Stevenage, Warren Spring Laboratory.

Warren Spring Laboratory 1985 UK smoke and sulphur dioxide monitoring networks, summary tables, April 1983–March 1984. Stevenage, Warren Spring Laboratory.

551.507.362.2:551.576.1

Interesting cloud features seen by NOAA-6 3.7 micrometre images

By R. W. Saunders* and D. E. Gray†

(Robert Hooke Institute for Co-operative Atmospheric Research, Clarendon Laboratory, Oxford)

Summary

The appearance of clouds over the British Isles and North Sea at three wavelengths — visible (0.8 micrometres (μm)) and infra-red (3.7 and 11 μm) — is described for 3 July 1984. The daytime 3.7 μm AVHRR (Advanced Very High Resolution Radiometer) images show far more detail over clouds than the other two channels which are normally used for forecasting purposes. A cloud scattering radiative model is used to show the sensitivity of 3.7 μm radiances to water drop size and water/ice phase, and the nearest coincident synoptic chart is given for comparison with the satellite images.

For a trial period from July 1984 NOAA (National Oceanic and Atmospheric Administration, USA) have been disseminating 3.7 μm images over the automatic picture transmissions (APT) from NOAA-6. These daytime 3.7 μm images have shown new features in clouds not seen in the more conventional visible and 11 μm infra-red channels. An example is shown in Fig. 1 where NOAA-6 AVHRR visible 0.8 μm (channel 2), 11 μm (channel 4) and 3.7 μm (channel 3) images over the United Kingdom are shown. The appearance of the 3.7 μm image during the day is complex because it is a mixture of emitted

*Meteorological Office Unit
†Department of Atmospheric Physics

terrestrial and reflected solar radiation. Dark shades represent high radiance and light shades low radiance. One interesting area of clouds marked 'A' is over north-east and central southern England. At visible wavelengths this cloud is not particularly bright, having a lower reflectance than the cloud further out over the North Sea. The 11 μm image shows the cloud-top temperature to be uniform over a large area at about 270 K (derived from the calibrated image) for the clouds over the United Kingdom and the North Sea. The 3.7 μm image, however, shows a significant difference between the cloud over the United Kingdom and north-east coast (marked 'A') and the cloud further out over the North Sea, the former having a much darker appearance corresponding to higher radiance. The cloud area marked 'B' also shows much more structure in the 3.7 μm image than in the other conventional channels where the area appears uniform in reflectance and cloud-top brightness temperature ($\approx$260 K) even after the images were enhanced to show up small changes in radiance.

The large variations in 3.7 μm radiance seen over cloud during the daytime are due to different cloud reflectances at 3.7 μm. This is a different but related effect to that reported by Eyre *et al.* (1984) who make use of the difference between the cloud or fog emissivities at 3.7 μm and 11 μm to detect the presence of fog and low cloud at night. For optically thick clouds the two are related according to the simple expression:

$$r + \epsilon = 1$$

where r is the cloud reflectivity, and ϵ is the cloud emissivity.

To simplify interpretation of the daytime 3.7 μm image the emitted radiation component was subtracted from it by using the 11 μm radiance. Assuming the same surface/cloud emissivity and atmospheric absorption at both wavelengths, a 3.7 μm emitted radiance can be inferred from the 11 μm emitted radiance by applying the Planck function. This emitted 3.7 μm radiance is then subtracted from the observed 3.7 μm radiance leaving the reflected solar radiance at 3.7 μm shown in Fig. 2. Light shades denote high reflected radiance, dark shades low radiance. The cloud layer marked 'A' has a reflectance significantly greater than the cloud over the North Sea. The large variations in reflectance shown in Fig. 2 are certainly real but the assumptions given above are not always valid owing to small differences in emittance at the two wavelengths giving differences in brightness temperature of up to 2.5 K (Eyre *et al.* 1984). Therefore small variations of reflectance in Fig. 2 should be treated with caution.

Cloud reflectances at 3.7 μm have been modelled using a cloud scattering model. This model is based on the matrix operator method of solving the equation of radiative transfer in a scattering medium (e.g. Plass *et al.* 1973, Grant and Hunt 1968). It is azimuth-independent but can be used in the solar infra-red region with the restriction that the sun must be positioned at the zenith. For this case the sun is in fact fairly low (58 degrees from the zenith) so the actual values computed in the model will be different from those observed. However, the relative changes in reflectance as a function of drop size should not be greatly affected by the sun angle. The phase functions for each of the droplet sizes for refractive indices corresponding to both water and ice were calculated using a Mie scattering program. The results were then used as input to the cloud model and first used to calculate the reflection and transmission matrices for a thin initial layer (optical depth $\tau_0 = 2^{-15}$) in which single scattering only is assumed. The matrices for that layer were then combined with those for an identical layer to find the matrices for the layer thickness $2\tau_0$. Continuing with this 'doubling' procedure the reflection matrices were formed for clouds with optical depths $\tau = 0.122, 0.244 \ldots 62.5, 125$ and from them the cloud reflectivities for the satellite zenith angle were selected. The results from the model, shown in Fig. 3, show that the cloud reflectance varies strongly as a function of cloud drop size and thermodynamic phase. These results are in broad agreement with those computed by Arking and Childs (1983) with a solar zenith angle of 60 degrees. Therefore we can infer that the bright clouds in the 3.7 μm image should be made up of mainly small drops whereas the dark clouds (represented by dark shades in Fig. 1(c)) will be made up of larger drops or ice

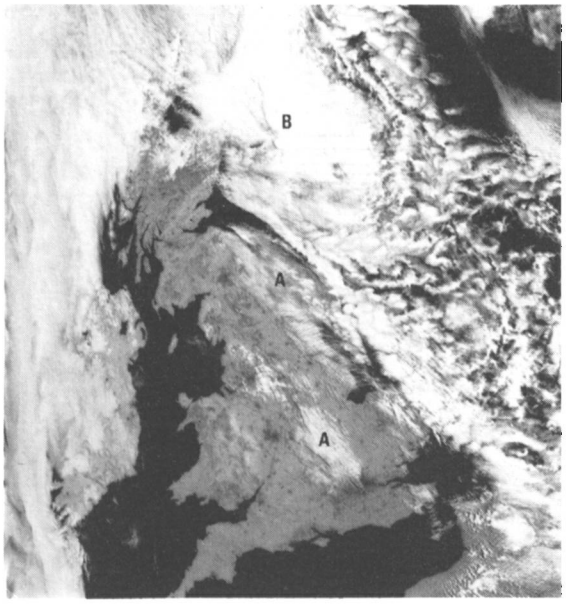

Figure 1(a)

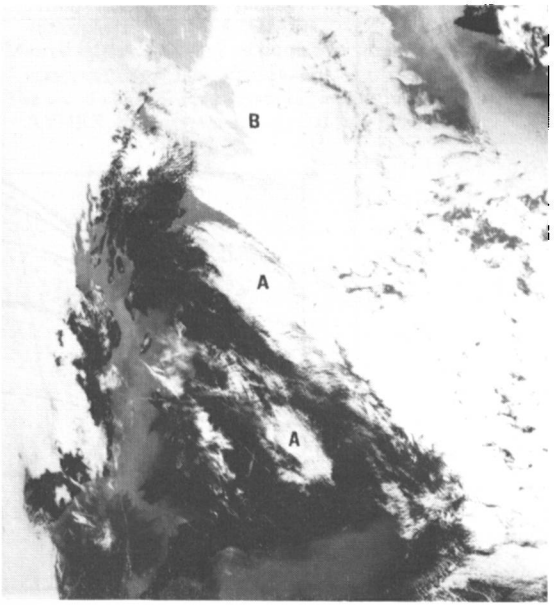

Figure 1(b)

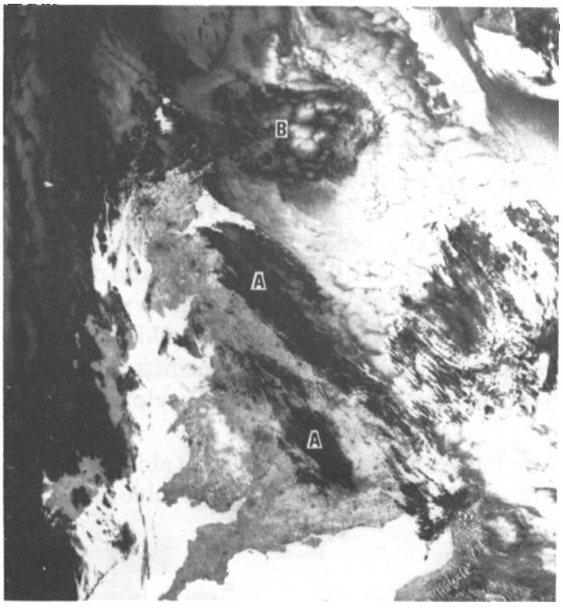

Figure 1(c)

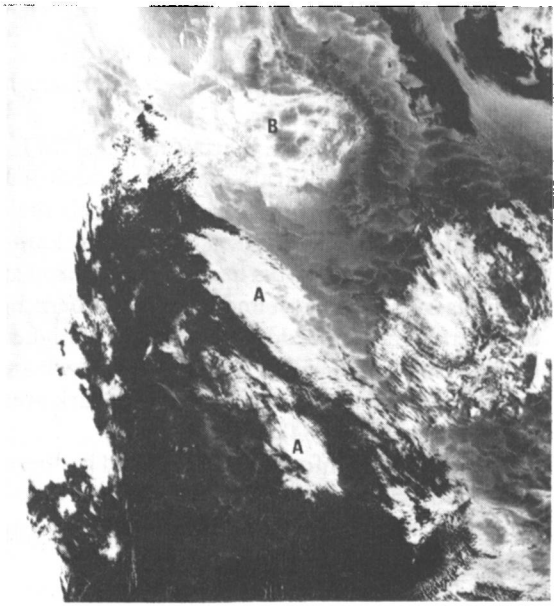

Figure 2

Figure 1. NOAA-6 AVHRR images recorded at 0738 GMT on 3 July 1984 over the United Kingdom and North Sea. The visible image (a) is channel 2 (0.8 μm), the infra-red image (b) is channel 4 (11 μm) and the 3.7 μm image (c) is channel 3. The areas of cloud marked 'A' and 'B' are referred to in the text.

Figure 2. An image constructed from the 3.7 μm and 11 μm images in Fig. 1 of reflected solar radiance at 3.7 μm. Bright areas correspond to high reflectances.

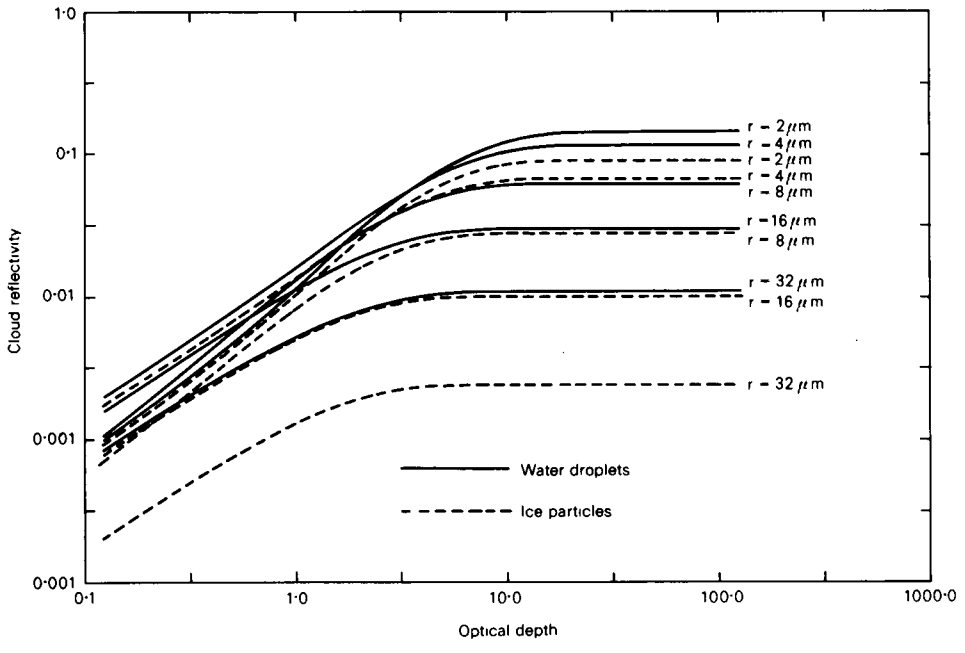

Figure 3. Results from a cloud scattering model where solar zenith angle = 0°, zenith angle of observer = 31.43° and wavelength = 3.7 μm.

particles. The latter are unlikely to be present here given the general appearance of the cloud and the cloud-top temperature.

The surface synoptic chart for 0900 GMT (1 h 22 min after the satellite image was recorded) is reproduced in Fig. 4. Stratocumulus cloud at 3000 ft with lower cumulus is reported along the north-east coast and further south corresponding to the bright cloud in Fig. 2 extending from London to the Midlands. Over the North Sea low stratus cloud with base at 200 ft is reported. This suggests that for this case the North Sea stratus has a different drop size distribution from the stratocumulus and developing cumulus over north-east and central southern England. The cloud area marked 'B' shows up dark areas of low radiance embedded in cloud of a higher radiance as seen in Fig. 2. These could be related to convective activity within the cloud, the dark areas being due to a different drop size distribution in the cloud being convected upwards. These dark areas have also been seen at the tops of developing cumulus cloud by Scorer (1984).

The additional information provided by these 3.7 μm images could be an important aid to forecasters and cloud physicists particularly when the high-resolution AVHRR data become available on a routine basis in real time.

References

Arking, A. and Childs, J. D. 1983 Extraction of cloud cover parameters from multispectral satellite measurements. Report on the fifth conference on atmospheric radiation, October 31–November 4, 1983, Baltimore, Maryland, 258–263.

Eyre, J. R., Brownscombe, J. L. and Allam, R. J. 1984 Detection of fog at night using Advanced Very High Resolution Radiometer (AVHRR) imagery. *Meteorol Mag*, **113**, 266–271.

Grant, I. P. and Hunt, G. E. 1968 Solution of radiative transfer problems in planetary atmospheres. *Icarus*, **9**, 526–534.

Plass, G. N., Kattawar, G. W. and Catchings, Frances E. 1973 Matrix operator theory of radiative transfer. 1: Rayleigh scattering. *Appl Opt*, **12**, 314–329.

Scorer, R. S. 1984 The use of channel 3 photographic images. Report of the UK AVHRR data users meeting, Oxford, 1984, 35.

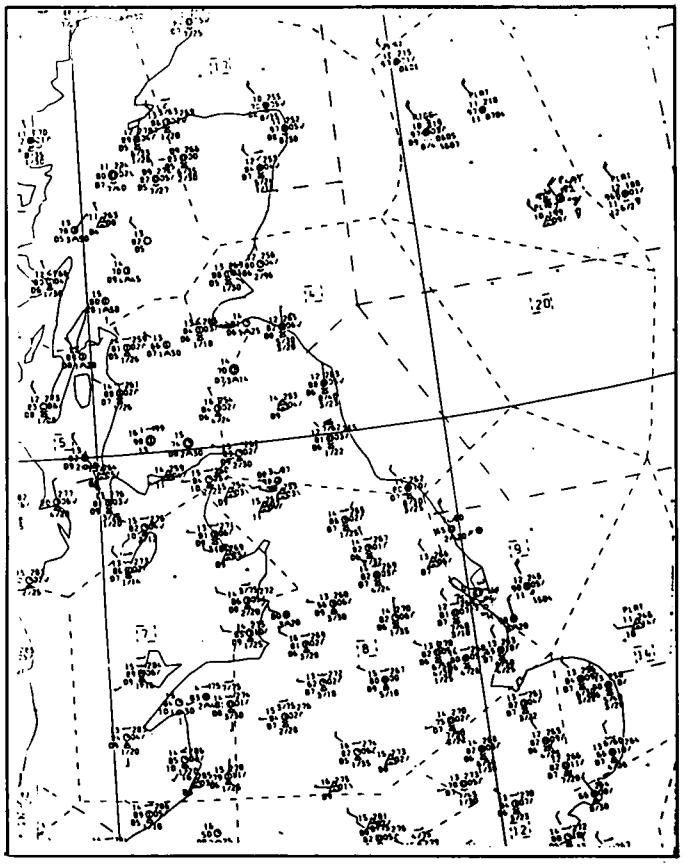

Figure 4. The synoptic chart over part of the United Kingdom and North Sea for 0900 GMT on 3 July 1984.

Awards

L. G. Groves Memorial Prizes and Awards

The presentations of the L. G. Groves Memorial Prizes and Awards for 1983 were made on 21 November 1984 at the Main Building, Ministry of Defence, Whitehall. Air Vice-Marshal L. A. Jones, CB, AFC, FBIM (ACAS(OPS)) presided, and Miss Margaret Groves made the presentations. Miss Groves is the daughter of Leslie Groves, a younger brother of Major Keith Groves in memory of whose son the Prizes and Awards are given each year.

Air Vice-Marshal Jones began the proceedings and conveyed the apologies of Sir Peter Harding, VCAS, for being unable to preside himself owing to other urgent commitments. Air Vice-Marshal Jones gave a brief history of the awards, and offered his congratulations to the winners. Mr Robin Wight, who presented the prizes in 1983, then spoke of how his own contacts in the RAF had told him how valuable a stimulus had been provided by the L. G. Groves Memorial.

The citations were read by Air Commodore T. H. Stonor (Inspector of Flight Safety, RAF), and Miss Groves presented the winners with their prizes and certificates, adding her own personal congratulations.

The 1983 Aircraft Safety Prize was awarded to Sergeant J. Cook, then of the Survival Equipment Section, RAF Gütersloh, Germany (now having left the Service) in recognition of his initiative and inventiveness in designing and producing a modification to the SS10 life-raft. The boarding handles in their present position, i.e. each side of the bow of the life-raft, have been proved to be nearly out of reach of the average aircrew member. This modification removes these handles and replaces them with two strips of running grab handles along both sides of the buoyancy chamber. The modification can be embodied by using current materials and is well within the capacity of all survival equipment sections. It is relatively cheap and simple and greatly improves the survival prospects of all who use the equipment. It has now been accepted for all in-service life-rafts.

The 1983 Meteorology Prize was awarded to Mr C. G. Collier, then of the Radar Research Laboratory at Malvern, Worcs (now Assistant Director (Operational Instrumentation) Meteorological Office), for his work in radar meteorology. Whilst at the Meteorological Office Malvern, between 1976 and 1984, he had been responsible for developing and implementing techniques for the measurement by radar of surface precipitation and for the processing, communication and display of information from a network of radars. This development was based on results from an experimental precipitation radar project, and work at the Royal Signals and Radar Establishment on radar data processing. Mr Collier has extended both of these areas of work to an important degree by bringing them to a state of operational viability. The radar network pictures, which are being made available to a growing number of meteorological officers within minutes of data time, provide the kind of mesoscale detail required by forecasters in generating products for aviation and for other customers needing highly specific forecasts in the 0- to 3-hour time-scale. For instance, while rain itself is not normally a hazard to low-flying aircraft, the associated poor visibility and low clouds are. Although the radar pictures cannot present specific data on these variables, when used in conjunction with conventional observations the extent of hazardous conditions may be inferred. As part of the radar development program Mr Collier has been involved, in collaboration with the water industry, in the North West Weather Radar Project, which demonstrated the operational viability of an unmanned radar system to provide quantitative rainfall data for use in river management and flood prevention schemes. This project has provided the technical basis for a network of radars including one which covers the London area. Mr Collier's ideas are also being taken up within a European context. He has made an outstanding contribution to the scientific and technical development to operational status of a new meteorological observing system.

The Meteorological Observer's Award for 1983 was awarded to Mr A. N. Bentley of the Marine Projects Section, Meteorological Office, for his contribution to the production, installation and maintenance of observing systems capable of providing meteorological data from data-sparse marine areas to guide forecasting for civil and military purposes; noting in particular that his enthusiastic leadership, technical skills and courage in a hostile environment have led to significant progress in the introduction of instrumented buoys and automatic weather stations.

The 1983 Second Memorial Award was awarded jointly to Squadron Leader A. G. Pearce (OC Flying) and Flight Lieutenant M. R. Wistow (SFSO), both of RAF St Athan flight test crew, for their achievement in recommending that the Black and Decker F11 lightweight vacuum cleaner be approved

Sergeant J. Cook, winner of the Aircraft Safety Prize, receives his prize from Miss Margaret Groves.

Mr C. G. Collier, winner of the Meteorology Prize, receives his prize from Miss Margaret Groves.

Mr A. N. Bentley, winner of the Meteorological Observer's Award, is congratulated by Miss Margaret Groves.

Squadron Leader A. G. Pearce (centre) and Flight Lieutenant M. R. Wistow, joint winners of the Second Memorial Award, are congratulated by Miss Margaret Groves.

L. G. Groves Memorial Prize and Award winners with Miss Margaret Groves and Air Vice-Marshal L. A. Jones, left to right: Squadron Leader A. G. Pearce, Flight Lieutenant M. R. Wistow, Sergeant J. Cook, Miss Groves, Air Vice-Marshal Jones, Mr C. G. Collier and Mr A. N. Bentley.

for flight test crews at maintenance units to collect the debris dislodged in aircraft during the trials. The device was tested by the officers in a Jet Provost and a Phantom and the results were most impressive and the debris was easily collected. Later, extension of its use to Flying Training School units is also envisaged. This has proved to be a simple but effective method of removing potentially dangerous cockpit debris such as swarf, dust and metal particles.

Review

Principles of remote sensing, by P. J. Curran. 187 × 245 mm, pp. xi + 282, *illus*. Longman, London, New York, 1985. Price £11.95 (paperback only).

Recently there has been an increasing number of courses available in environmental remote sensing and, as the author states in the preface, this book aims to provide students of these courses with a broad background in the subject. In most respects this book succeeds in this aim, providing a useful introduction to the subject with a wealth of references at the back to allow readers to delve further into their particular areas of interest. The author has written the book in a style that is easy to read and many interesting illustrations (a few in colour) are included. There are very few equations in the text so this book would not be very useful to those readers who want to understand in detail the precise physical mechanisms involved.

The book is essentially divided into three main parts. The first deals with the interaction of electromagnetic radiation with the surface and atmosphere. There is a good section here on defining quantities

and units used and another on the interaction of radiation with vegetation and soil. However, the section on atmospheric effects was covered in one page. A more detailed description of atmospheric absorption and scattering effects would have been useful here, as most satellite remote sensing measurements have to remove these before extracting the parameter of interest. Similarly there is no discussion of the effects of clouds on electromagnetic radiation which should have been included here. The second part deals with the different measurement techniques currently employed for environmental remote sensing. There is a detailed description of aerial photography techniques and the different types of film used, with many illustrations given. Aerial sensors are also discussed with an interesting section on airborne radar. Finally, a good description of satellites used for remote sensing is given by using a logical classification scheme for the different types. There is some confusion over the ERS-1 satellite as there are in fact two (one Japanese and one European). It would have been helpful if the author had stated this at the first mention of ERS-1 in the text. The final part describes various types of image-processing equipment currently available and the many different processing algorithms which can be applied to the data. Analogue image processing is mentioned here but with the advent of low-cost digital image-processing systems most of the text correctly concentrates on discrete (digital) image processing. Topics such as calibration, geometric correction and image enhancement are all covered.

At the back of the book there are some useful appendices containing a list of addresses from which remote sensing data can be obtained, a list of remote sensing journals, a list of acronyms, etc. I am sure that *Principles of remote sensing* will be invaluable to any student on a remote sensing course and worthwhile reading for anybody who would like to find out more about remote sensing without going into too much detail. As the author states at the end of his introduction, the ultimate aim of remote sensing is to obtain, on a routine basis, reliable information to help us manage our fragile planet. This book describes how this goal is now in sight.

R. W. Saunders

Obituary

We regret to record the death on 18 February 1985 of Captain J. H. Jones, Port Meteorological Officer, Bristol Channel Area.

John Holland Jones (Jack to all his friends and colleagues) was born in May 1920 and was due to take retirement only a few months after his untimely demise at the age of 65. He had been appointed Port Meteorological Officer at Cardiff in July 1976 and he elected to continue in the position beyond the optional retirement age of 60.

Jack Jones began his seagoing career as an apprentice indentured to the British Tanker Company in 1937 aboard the *British Engineer* and on obtaining his Second Mate's Certificate in 1941 he was promoted to Third Officer; he then remained with the BP Tanker Company, as it became known, throughout his seagoing career up to 1975 when he retired from the sea as Master of the *British Confidence*. He was promoted to command in 1956 when he became Master of the *British Diligence*.

During his years as Master he sent us a total of 12 meteorological logbooks of which 4 were assessed as Excellent. He received Excellent Awards in 1961, 1970 and 1971.

Highlights of Captain Jones's career included the award of the Coronation Medal and the honour of being selected to lay the Remembrance Sunday wreath at the Cenotaph in Whitehall in November 1973, on behalf of the Merchant Navy and Fishing Fleets.

He was a Warden of the Swansea and South Wales Company of Mariners and a well known and respected member of the local community in his home town of Swansea as well as amongst his many professional contacts in the Cardiff area. He was always the most cheerful and courteous person to talk to, whether it was by telephone with Bracknell or across the table at a conference.

THE METEOROLOGICAL MAGAZINE

No. 1356 July 1985 Vol. 114

CONTENTS

NOTICE

It is requested that all books for review and communications for the Editor be addressed to the Director-General, Meteorological Office, London Road, Bracknell, Berkshire RG12 2SZ and marked 'For Meteorological Magazine'.

The responsibility for facts and opinions expressed in the signed articles and letters published in this magazine rests with their respective authors.

Authors wishing to retain copyright for themselves or for their sponsors should inform the Editor when they submit contributions which will otherwise become UK Crown copyright by right of first publication.

Applications for postal subscriptions should be made to HMSO, PO Box 276, London SW8 5DT.

Complete volumes of 'Meteorological Magazine' beginning with Volume 54 are now available in microfilm form from University Microfilms International, 18 Bedford Row, London WC1R 4EJ, England.

Full-size reprints of Vols 1–75 (1866–1940) are obtainable from Johnson Reprint Co. Ltd, 24–28 Oval Road, London NW1 7DX, England.

Please write to Kraus Microfiche, Rte 100, Millwood, NY 10546, USA, for information concerning microfiche issues.

HMSO Subscription enquiries 01 211 8667.

Printed in England for HMSO and published by
HER MAJESTY'S STATIONERY OFFICE

£2.30 monthly

Annual subscription £27.00 including postage

Dd. 736047 C13 7/85

ISBN 0 11 727561 1
ISSN 0026–1149

THE METEOROLOGICAL MAGAZINE

OPERATIONAL NUMERICAL FORECASTING

Models and Products

HER MAJESTY'S STATIONERY OFFICE

August 1985

Met.O.967 No. 1357 Vol. 114

METEOROLOGICAL OFFICE Met.O.967

THE METEOROLOGICAL MAGAZINE

No. 1357, August 1985, Vol. 114

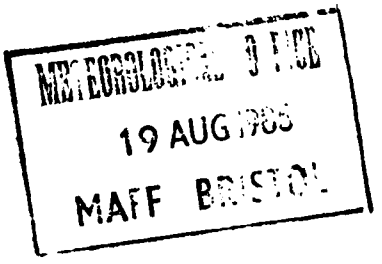

Operational numerical forecasting: models and products

This issue of the *Meteorological Magazine* is devoted to four articles on the Meteorological Office's operational numerical forecasting system. At the core of the system are the 15-level numerical weather prediction models, and these are the subject of the first paper. The second paper deals with the equally important question of the analysis of observations to provide starting conditions for the numerical forecasts. In the third paper attention turns to the dependent oceanographic models, for surface waves and storm surges, which are driven by surface winds and sea-level pressure fields from the atmospheric models. The further processing of results from the models to derive useful output products is the subject of the fourth paper. These products are required both for national purposes and for distribution to other meteorological services in accordance with Bracknell's international roles.

The articles have been prepared by staff in the Central Forecasting Branch of the Meteorological Office, and are intended to provide a survey from an operational viewpoint. The 15-level models and their data assimilation schemes were developed in the Forecasting Research Branch, and the physical parametrizations used in the models were formulated in the Dynamical Climatology and Synoptic Climatology Branches. The reader is referred to the relevant reports prepared in these Research Branches for full details of the various formulations and techniques.

A further four articles, dealing with evaluation and applications of the numerical forecasts, will appear in the next issue of the *Meteorological Magazine*.

The numerical forecasting system described in this issue, built around the 15-level models, has been operational since September 1982. At the time of this publication the system is well established, with a number of earlier problems and shortcomings remedied, and is widely recognized as being highly successful. Nevertheless, further important improvements are currently being researched, and continuing advances in performance may be expected for several years to come.

551.509.313

The 15-level weather prediction model

By A. J. Gadd

(Meteorological Office, Bracknell)

Summary

The 15-level model is introduced in relation to earlier numerical weather prediction models, and the operational roles of both the global and the fine-mesh versions are outlined. Factors involved in the design of the model are discussed. A brief description is given of the main features of the formulation of the model.

1. Introduction

After research investigations during the 1950s and early 1960s, numerical weather prediction has been used operationally in the Meteorological Office since 1965. A 3-level quasigeostrophic model was used on the KDF9 computer until 1972, when a 10-level primitive-equation model in pressure coordinates was introduced on the 360/195 computer. This 10-level model was used in two forms: for the northern hemisphere north of 15°N with a 300 km grid and for a region near the British Isles with a 100 km grid. The 10-level model was used until 1982 and during its lifetime three different integration schemes were used. In 1978 important changes were made in the model's formulation: a more accurate lower boundary condition was introduced and the effects of radiation were included.

In 1982 a 15-level primitive-equation model in sigma coordinates was introduced on the Cyber 205 computer, and this model is the subject of the present paper.

The 15-level model is used operationally in two versions. There is a global version which is required to fulfil the Office's responsibilities in Defence, as a World Area Forecast Centre for civil aviation (Hardman 1985), in support of marine and other commercial services world-wide, and to provide guidance for medium-range forecasting. The horizontal resolution used is the maximum possible for the original configuration of the Cyber 205 computer, with 1.5° spacing of grid points in latitude and 1.875° spacing in longitude. Global forecasts to 6 days ahead are computed twice daily, from 00 GMT and 12 GMT starting conditions, and with results available by 05 GMT and 17 GMT, and, after the necessary further processing (Francis 1985b), are distributed to other countries in Europe and elsewhere.

A second, regional version of the 15-level model has been designed principally to meet the needs of short-range public service forecasting for the United Kingdom (Hunt 1985) and also to support marine services for the European continental shelf and the Mediterranean Sea (Ephraums 1985). For these purposes the predictions of precipitation, surface wind and the positions of fronts are crucially important, and these predictions are known to benefit from a closer spacing of the grid points. This is achieved within the available computing capacity by using a fine mesh of points (with spacing 0.75° by 0.9375°) over a limited area (80°W–40°E, 30°N–80°N). At the lateral boundaries of this region the calculations make use of information provided from integrations on the global grid. Forecasts to 36 hours ahead are computed twice daily, with results available by 03 GMT and 15 GMT, and are distributed internationally for use in most of the nations within the region of coverage. The surface wind forecasts are particularly valuable for input to wave and surge prediction models (Francis 1985a).

The progression of models over the years reflects the scientific advances in numerical weather prediction and the increasing capacity of the computers available. Thus the 15-level model is based on what are currently judged to be the best available treatments of the relevant physics and mathematics, whilst its operational use is made possible by the availability of the powerful Cyber 205 computer.

Along with the progression of modelling techniques there has been an expansion of the area of coverage. This process was completed within the implementation of the global version of the 15-level model. However, as noted above, regional modelling is still important in that it permits a higher horizontal resolution, in a limited area of special interest, for a given computing capacity.

A parallel historical development may be noted in the methods used to provide initial data for the numerical models. The 3-level model required objective analysis of the height field. The 10-level model required objective analysis of the height and humidity fields, but its initial wind values were diagnosed from the height analysis using the balance and omega equations. The 15-level model uses analysis and data assimilation of potential temperature, surface pressure, relative humidity and wind component data derived from observations to obtain initial fields of these variables in sigma coordinates (see the companion paper by Atkins and Woodage 1985). This system has its origins in work carried out as part of the Office's contribution to the Global Weather Experiment in 1979.

The increasing skill of numerical forecasts during the course of this historical development may be seen in sequences of verification statistics (Flood 1985).

2. The design of the 15-level model

The design of the 15-level model was based on research which compared alternative techniques (Cullen *et al.* 1981). During the lifetime of the 10-level model, three different methods for the numerical integration of the primitive equations had been used (Gadd 1978a), each one improving on the efficiency of its predecessor. Changes had also been introduced to improve the accuracy of the finite-difference approximations (Gadd 1978b). It was found that the numerical techniques used in the 10-level model at the end of its development were more efficient than, and equal in accuracy to, the alternatives and so were largely retained. On the other hand the representations of precipitation, convection, boundary-layer turbulence and radiation for the 15-level model were derived from earlier work in the Office on general circulation modelling and climate research (Lyne and Rowntree 1976, Richards 1980, Corby *et al.* 1977). The original formulation of the 15-level model was described in full by Dickinson and Temperton (1984); further improvements are constantly being researched and are introduced operationally as soon as they are sufficiently proven.

At a time when several global modelling centres around the world have changed over to spectral models, some comment is appropriate on the retention of finite-difference methods in the 15-level model. The choice between spectral and finite-difference models is essentially an economic one, there being no intrinsic difference in the quality of result that may be obtained with either approach. In some centres greater accuracy has been obtained in synoptic-scale forecasting with a given computing power by using a spectral model. However, the efficiency and accuracy of the numerical techniques used in the 15-level model are such that it is unlikely that any economic advantage could be obtained using a spectral version. Also important in the context of the Meteorological Office's requirements is that exactly the same finite-difference formulation, indeed the same coding in large measure, can be used in both the global model and the limited area fine-mesh model. Finally, it should be noted that the balance of economic advantage shifts towards finite-difference models when it comes to sub-synoptic features, especially fronts, and this may become more important with the trend to higher and higher resolutions in global models.

3. The grids

In the vertical the sigma (σ) coordinate system is used, where σ is pressure (p) normalized by surface pressure (p_*). Thus the coordinate surfaces follow the shape of the model's orography (grid-scale mean values). The distribution of the 15 levels is shown in Fig. 1. In the mid-troposphere the vertical resolution

is about 100 mb, but near jet-stream levels there is a higher resolution of about 60 mb. A high vertical resolution is provided in the atmospheric boundary layer, with the lowest level approximately 25 m above the surface. The uppermost level is about 25 km above the surface. The 15 levels, at which all the model variables except vertical velocity are calculated, may be regarded as the midpoints (by log σ) of 15 layers of air. The vertical velocity ($\dot{\sigma} = D\sigma/Dt$) is calculated at the layer boundaries. The boundary condition $\dot{\sigma} = 0$ is applied at the earth's surface ($\sigma = 1$) and at the upper boundary of the uppermost layer.

The horizontal grids are defined using spherical polar coordinates ϕ (latitude) and λ (longitude). With grid spacing $\Delta\phi = 1.5°$ and $\Delta\lambda = 1.875°$, the global model has 121 points from pole to pole and 192 points around each latitude circle. The fine-mesh model has a double resolution over its limited area of coverage. In both cases there is a staggering of model variables in the horizontal in an arrangement known as the B-grid and illustrated in Fig. 2. Thus the $121 \times 192 (= 23\,232)$ points of the global grid form the corners of grid boxes. At these corner points the surface pressure (p_*), potential temperature (θ) and humidity mixing ratio (q) are predicted, whilst the geopotential (Φ) and vertical velocity ($\dot{\sigma}$) may be diagnosed. The horizontal velocity components (u, v) are predicted at the centres of the grid boxes. Special procedures are adopted at the poles.

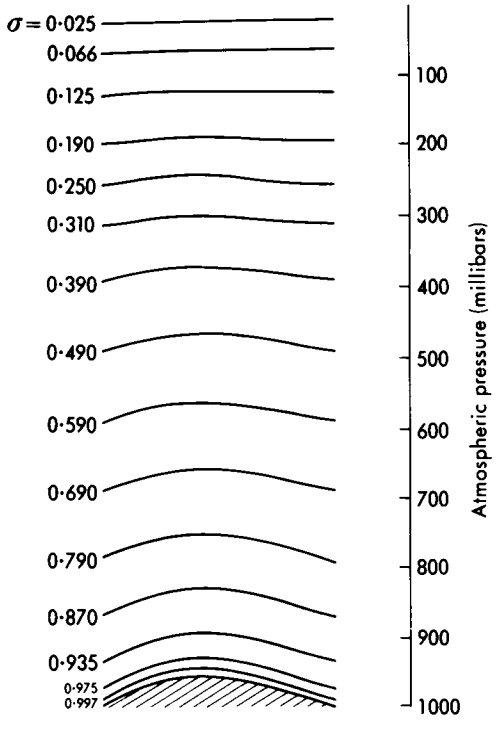

Figure 1. Sigma levels of the 15-level model.

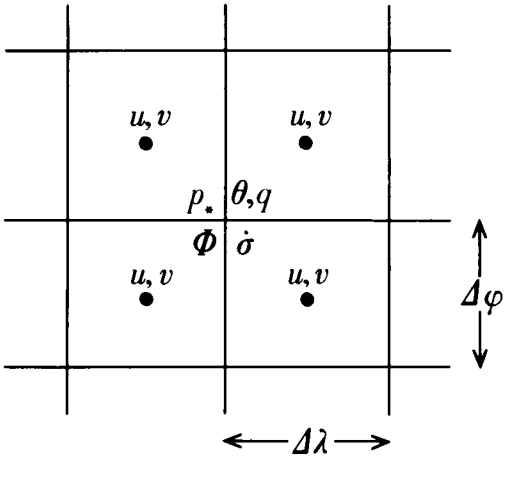

Figure 2. The arrangement of variables on the B-grid.

4. Dynamical and numerical formulation

The primitive equations are used in advective form, and are integrated using the split explicit integration scheme. This includes a modified Lax–Wendroff method for horizontal advection and a forward–backward scheme, with trapezoidal integration of the Coriolis terms, for the gravity–inertia

adjustment stage. The time-step for the integration of the advection terms is three times that for integration of the gravity–inertia terms. The forward–backward scheme includes special features to prevent the spatial lattice separation that can be a problem with the B-grid.

In high latitudes the small east–west separation of the grid points would impose unacceptable restrictions on the time-steps allowed for computational stability if special measures were not taken. Thus stability filtering is applied as necessary in the east–west direction to allow the use of time-steps (15 minutes in the global model and $7\frac{1}{2}$ minutes in the fine-mesh model) governed by the north–south grid spacings. In the global model, Fourier analysis is used around latitude circles and short-wavelength components of the fields are damped using coefficients calculated for each line of latitude and for each forecast, taking account of the maximum wind speed present. Thus the region of filtering extends further towards the equator in a winter hemisphere than in the corresponding summer hemisphere. Where stability filtering is needed in the fine-mesh model, a multipoint filter (25 points) is applied along lines of latitude to provide an approximation to Fourier damping.

5. Parametrizations

As in all modern numerical models of the atmosphere, the parametrization of physical and sub-grid-scale processes is an important aspect of the formulation of the 15-level model. In principle, the parametrizations currently available are used in the same way both in the global and in the fine-mesh versions of the model. However, it is sometimes necessary or desirable to introduce changes first in one version and later in the other.

The current parametrizations are as follows:

(i) *Large-scale precipitation*, including the ice phase and the evaporation of precipitation as it falls.

(ii) *Convection*, producing a redistribution of heat and moisture in the vertical (and convective precipitation where appropriate) and based on parcel theory, modified by entrainment, and detrainment.

(iii) *Surface exchanges and boundary-layer turbulence*, exchanging heat, moisture and momentum among the four lowest model layers and with the surface.

(iv) *Radiation*, including the diurnal cycle of solar radiation, and interactive with temperature and humidity and with cloud inferred from humidity.

(v) *Gravity wave drag*, applied at upper levels, but calculated from low-level wind and static stability and the variance of orographic height within each grid box.

(vi) *Horizontal eddy diffusion*.

(vii) *Vertical eddy diffusion*, at low latitudes only.

The calculations of surface exchanges require values of a number of surface parameters. The distributions of sea-ice and snow cover are specified climatologically. Over open sea the surface contact temperature is analysed every day using ship, buoy and satellite measurements, and is held constant during each forecast. Over land and sea-ice the surface contact temperature is predicted using calculated components of the surface energy balance. Specifications are also required of albedo, soil moisture and effective thermal capacity.

6. Lateral boundary conditions for the fine-mesh model

The advantages available through the higher horizontal resolution of the fine-mesh version of the 15-level model are contingent on an adequate method for updating the lateral boundaries during the course of the forecasts. Theoretical investigation of this problem for the primitive equations has shown

that a mathematically satisfactory method is very difficult to devise. Fortunately a number of pragmatic schemes exist which work adequately well in operational practice, and one of these is used for the 15-level model.

The method that is used involves a complete overspecification of the boundary conditions in that the tendencies of all predicted variables at all boundary points are externally prescribed. These tendencies are derived from values output at hourly intervals from suitable global or hemispheric integrations on the coarser grid and are used to update the fine-mesh boundaries every time-step. An enhanced diffusive damping is used at all grid points within 3 gridlengths of a boundary. Within this boundary zone the coefficients of the non-linear horizontal diffusion formulation are enhanced by a factor of 3 compared with their values in the interior regions.

References

Atkins, M. J. and Woodage, M. J. 1985 Observations and data assimilation. *Meteorol Mag*, **114**, 227–233.

Corby, G. A., Gilchrist, A. and Rowntree, P. R. 1977 United Kingdom Meteorological Office five-level general circulation model. *Methods Comput Phys*, **17**, 67–110.

Cullen, M. J. P., Foreman, S. J., Prince, J. W., Radford, A. M. and Roskilly, D. R. 1981 Forecast intercomparisons of three numerical weather prediction models from the UK Meteorological Office. *Mon Weather Rev*, **109**, 422–452.

Dickinson, A. and Temperton, C. 1984 The operational numerical weather prediction model. (Unpublished, copy available in the National Meteorological Library, Bracknell.)

Ephraums, J. J. 1985 Applications of wave and surge models. *Meteorol Mag*, **114**, 282–291.

Flood, C. R. 1985 Forecast evaluation. *Ibid.*, 254–260.

Francis, P. E. 1985a Sea surface wave and storm surge models. *Ibid.*, 234–241.

1985b Output products of the Bracknell NWP models. *Ibid.*, 242–251.

Gadd, A. J. 1978a A split explicit integration scheme for numerical weather prediction. *Q J R Meteorol Soc*, **104**, 569–582.

1978b A numerical advection scheme with small phase speed errors. *Ibid.*, 583–594.

Hardman, M. E. 1985 The use of 15-level model products by the Central Forecasting Office for forecasting for civil aviation. *Meteorol Mag*, **114**, 273–281.

Hunt, R. D. 1985 The models in action. *Ibid.*, 261–272.

Lyne, W. H. and Rowntree, P. R. 1976 Development of a convective parametrization using GATE data. (Unpublished, copy available in the National Meteorological Library, Bracknell.)

Richards, P. J. R. 1980 The parametrization of boundary layer processes in general circulation models. (Ph.D. thesis, University of Reading.)

551.501:551.509.313

Observations and data assimilation

By Margaret J. Atkins and Margaret J. Woodage

(Meteorological Office, Bracknell)

Summary

Initial fields for the 15-level model are provided by a data assimilation scheme. Conventional and satellite observations of relevant meteorological quantities are processed to provide 'observed' values of model variables. Global analyses are produced at 6-hourly intervals, 00, 06, 12 and 18 GMT, using data valid within 3 hours of each of these times. This is achieved by assimilating the processed observations into the 6-hour forecast from the previous analysis, using univariate optimum interpolation to provide corrections at the model grid points and additional damping to control unwanted high-frequency oscillations. Initial fields for the regional (fine-mesh) model are provided by a fine-mesh assimilation scheme. Analyses are produced at 3-hourly intervals by assimilating observations valid within 1½ hours of the analysis time into the regional model. The fine-mesh assimilation is restarted every 12 hours by interpolation from a global assimilation.

1. Introduction

A necessary condition for a numerical model of the atmosphere to produce a good forecast is that the initial values of the model variables should be well specified. They should properly represent all the features, which can be resolved by the model, present in the atmosphere on a given occasion, and they should not contain imbalances between the variables which would excite spurious oscillations in the subsequent forecast. At the Meteorological Office a data assimilation scheme is used to provide initial conditions for both the global and regional versions of the 15-level model described in the companion paper by Gadd (1985). The scheme has been designed to use as much as possible of all available data, both conventional observations reporting at synoptic hours and satellite and aircraft observations which may report at any time. Before observations can be assimilated into the model they have to undergo quality control and be processed into a suitable form.

2. Observations

Meteorological data consist of measured or derived variables at different levels in the atmosphere, recorded at various times of the day and night. Several different kinds of observation are reported: traditional types are the surface and radiosonde reports which give excellent data coverage at synoptic hours over the land masses and major shipping routes. However, there are some parts of the northern hemisphere and vast areas of the tropics and southern hemisphere where these observations are not available, and it is in such regions that the satellite data have been most beneficial, providing asynoptic observations evenly distributed over the whole globe. Also available, along the major airline routes, are aircraft reports which are particularly useful to the United Kingdom in providing data across the Atlantic.

All observations are transmitted in coded form on the Global Telecommunication System (GTS) and are received at Bracknell by the Telecommunications Branch. From there they are routed to other users (e.g. outstations), as well as being passed to the Meteorological Office IBM computer where they are decoded and stored in the Synoptic Data Bank. At this stage some basic quality control is performed (such as checking reported values against climatological limits and testing radiosonde ascents for internal consistency) and an indicator or 'flag' is set against any datum suspected of being in error. As the observations come in they are monitored by forecasters in the Central Forecasting Office (CFO) who examine the data together with departures from model fields using visual display units. The forecasters

also analyse charts of plotted data at four main levels (surface, 500 mb, 250 mb and 100 mb), and these are considered to be the best available estimate of the state of the atmosphere at the synoptic hours. At this stage forecasters are able to 'intervene', rejecting any data suspected of being erroneous, and inserting 'bogus' or artificial data in areas where observations are sparse and model fields are considered to be poor.

The data assimilation scheme will be described in detail in the second part of this paper, but it is necessary to note here that it requires values of potential temperature (θ), westerly and southerly wind components (u and v), relative humidity (U) and model surface pressure (p_*). All observed data must be presented in the form of these variables in order to be used. Some types of data require only a simple change of variable using a standard formula: examples are the conversion of vector winds to wind components, the conversion of dew-point and temperature to relative humidity, and the conversion of temperature to potential temperature. However, other calculations could be carried out in a variety of ways using different approximations and assumptions, and each method gives a slightly different result. It is very important that the data passed to the model should be as accurate as possible, and that no biases should be introduced. It is equally important that the pre-processing should be carried out efficiently, as any time wasted at this early stage in the operational suite will cause unnecessary delay of the forecast products. A satisfactory balance must be found between the cost incurred and the accuracy attained in choosing methods of pre-processing the data. The methods used for the Meteorological Office 15-level model will now be described.

Surface observations

Surface observations comprise reports from land stations, ships and drifting buoys. These typically provide values of surface temperature, dew-point, wind, and mean-sea-level (msl) pressure. Exceptions to this are drifting buoys, which report msl pressure only, and high-level land stations where the derivation of msl pressure from the (measured) station-level pressure would be unreliable. In this case other variables are reported, such as station-level pressure or the geopotential of a standard pressure level. Surface temperature data are not used in the model, as local anomalies are likely to render them unrepresentative of the atmosphere on the scale of the model grid. For the same reason, surface wind and humidity data are not used over land, although they are used over the sea. The most important data derived from surface observations are values of model-surface pressure (p_*). Where the model orography has the same geopotential as that of the reported pressure (e.g. over the sea), no calculation is necessary as p_* is equal to the reported pressure. However, for most land stations some extrapolation is required, and assumptions must be made about the temperature structure in the layer in order to derive p_*. The best that can be done is to use model values, and ensure that the method adopted is consistent with that used to convert model p_* values to msl pressure for chart output. The calculation is done using the hydrostatic equation integrated assuming a constant lapse rate within the layer. The lapse rate chosen is the ICAO (International Civil Aviation Organization) standard value (6.5 K km^{-1}) and a reference temperature is obtained at the model surface by extrapolating from a level above the model boundary layer (about 800 mb). This method ensures that where msl pressure data are equal to the model output values, no change will be implied in p_* when the data are analysed.

Radiosonde data

Radiosondes provide values of temperature, dew-point and wind at significant levels of the ascent, together with geopotentials of the standard pressure levels. The number of levels reported varies according to the complexity of the atmosphere and the height attained by the sonde balloon, but is typically between 40 and 80. The temperature, wind and humidity data are too numerous to be passed to

the analysis at the reported levels, as the vertical detail could not be resolved by the model. It is therefore necessary to condense each ascent to a representative set of data at levels approximating to those of the model. This is achieved by using all reported values, weighted linearly in log pressure, to calculate mean values of each variable over layers centred on model levels. This has the effect of smoothing out extreme features such as maximum winds and tropopause temperatures which cannot be explicitly resolved by the model. The method is consistent with the assumptions made when output charts of standard-level values are produced, and ensures that geopotential (the main variable used for assessment by forecasters) is accurately represented.

The reported values of standard-level geopotential are not used directly in the model, but for some years statistics have been collected on the differences between observed and analysed 100 mb geopotentials. These are used to identify systematic differences between sondes and to derive appropriate corrections which are given in terms of 100 mb geopotential. In order to use this information in the model, equivalent temperature corrections are derived which are added to the σ-level values passed to the analysis.

Satellite temperature soundings

Temperature soundings are derived from radiance data measured by the polar orbiting satellites. Temperature and humidity mixing ratio are the variables initially derived, but these are converted to thickness (or layer mean virtual temperature) and precipitable water content (PWC) for standard layers, before they are transmitted on the GTS. Since the Meteorological Office model does not analyse these variables, it is necessary to invert the calculations carried out before transmission to reconstruct the original data as accurately as possible. This is done by converting to layer mean temperatures, using the PWC data to make the correction from virtual to true temperatures. The PWC data are not used directly as humidity observations as the errors are rather large, particularly for higher latitudes. For soundings made in cloudy conditions it is not possible to obtain humidity data. The method used to derive thicknesses for transmission in these cases is very complicated and could not be inverted operationally. A simple approximate method is used instead, with a relative humidity of 80% being assumed to carry out the conversion of virtual to true temperature.

Although the soundings transmitted on the GTS provide excellent coverage of temperature data, they are currently available only at spatial intervals of about 500 km (or 250 km in a compressed format) and are received at Bracknell 3 hours or more after the radiance data are recorded. They are valuable for the global coarse-mesh model, but are of limited use for the fine-mesh model which has a resolution of about 75 km and runs operationally 2 hours after data time. For this reason the Satellite Meteorology Branch has developed a system for receiving the radiance data directly from the satellite as it passes over the United Kingdom, and performing the processing locally to provide temperature data directly with a horizontal resolution of about 80 km, typically within 1 hour of being recorded. This processing system is known as HERMES (High-resolution Evaluation of Radiances from Meteorological Satellites) and experiments are being carried out to determine the best way to use these data in the models.

Satellite cloud-track winds

Wind data are derived from observations of movements of clouds at various levels in the atmosphere, recorded by the geostationary satellites which constantly view the same area of the globe. The data are transmitted in the form of a wind with an associated pressure, and can be used directly in the model. There are certain errors inherent in these data, owing mainly to the difficulty in estimating the level of the cloud. However, they provide valuable information in tropical areas where other observations are sparse.

Aircraft reports

Aircraft reports contain values of wind and temperature together with the flight level, position and time of observation. Observations are made every 5° or 10° of longitude along the flight path, and also at certain specified reporting positions. Before the data are used in the model they are checked to eliminate any duplicate or conflicting reports from the same aircraft. Winds and temperatures are passed to the analysis at the pressure level equivalent to the flight level. The conversion of flight level to pressure is carried out using equations based on the ICAO standard atmosphere (see World Meteorological Organization 1966).

Artificial observations

Artificial or 'bogus' observations are generated by forecasters in CFO to change the model fields, generally in areas of sparse data where they may have a better idea of the true state of the atmosphere from continuity, experience, or from data unavailable to the model (e.g. satellite pictures). The bogus observations comprise values of msl pressure, geopotential, wind and humidity at the main analysed levels. The geopotentials must be converted to temperatures, and the method adopted is to use model values to calculate the thickness change over each layer implied by the bogus data. The thickness changes are then converted to temperature increments, which are added to the existing model temperature profile to create a complete bogus ascent. The bogus data are treated by the analysis in the same way as any other conventional observations, but are given a higher weight to encourage the analysis to fit them.

3. Data assimilation

Many of the observations described in the preceding paragraphs may be valid at any time during a 24-hour period. The maximum number of conventional observations are still received for 00 and 12 GMT, this being the time at which most upper-air observations are made. For this reason forecasts still start from an analysis valid at those times. However, significant numbers of both surface and upper-air observations are received for 06 and 18 GMT and reports valid at any time are received from satellites, aircraft and drifting buoys. Data assimilation schemes are designed to make the best use of all this information, in particular, to use information valid at all times of the day to produce the best possible analysis valid at 00 or 12 GMT from which to start a forecast.

At the Meteorological Office, this is achieved by producing a global analysis at 6-hourly intervals, 00, 06, 12 and 18 GMT. All observations valid within 3 hours of each of those times are used to modify a 6-hour forecast starting from the previous analysis. Information from observations valid at all previous times is thus carried forward to the current analysis in a process analogous to the use of continuity charts in subjective analysis. The prognostic variables of the forecast model are potential temperature (θ), westerly and southerly wind components (u, v), humidity mixing ratio (q) and surface pressure (p_*). These are carried on a latitude/longitude grid in the horizontal and 15 levels in the vertical defined in terms of terrain-following sigma coordinates (described in the companion paper by Gadd (1985)). The analysis is performed directly in the model variables (except that U is used rather than q because of advantages for quality control) on a grid identical to that of the forecast model, except that the number of points per latitude circle decreases polewards of 50° to maintain a quasi-uniform spacing. Observations must therefore first be processed (as described in the previous section) to provide data in terms of the analysis variables, but not necessarily at model sigma levels.

Quality control

Univariate, three-dimensional statistical interpolation (sometimes known as optimum interpolation) is used in the analysis to interpolate from the observation points to the grid points. However, before this process is carried out, observations are subjected to quality control making use of the same technique. As a first step the observations are checked against the 6-hour forecast from the previous analysis, and when the difference exceeds a criterion dependent on the characteristic error of both the observations and the forecast, the observation is flagged. In the second step, each observation (including those that have been flagged) is checked by comparing it with a value interpolated from the surrounding unflagged observations, again using statistical interpolation. If the difference exceeds a second criterion, which depends on the characteristic error of the observation and the interpolation error (which may be determined from the method of statistical interpolation), the observation is rejected. Observations which fail the first check may be reinstated if they pass the second check, i.e. observations which differ significantly from the 6-hour forecast field may be retained if they are supported by other observations.

Statistical interpolation

Observations which pass the quality control checks (including those performed within the Synoptic Data Bank and the manual monitoring of the Central Forecasting Office) are used to interpolate values of each of the variables at the analysis grid points. Interpolation is actually carried out in terms of the departure of an observation from the model field to give an increment or correction to the model field at each of the grid points, according to equation (1),

$$\Delta\psi_g = \sum_i w_i \left(\psi_i^{\text{observed}} - \psi_i^{\text{model}}\right), \qquad (1)$$

where ψ_i^{observed} is an observation of one of the variables, θ, u, v, U, p_*,

ψ_i^{model} is the model value of the same variable interpolated to the observation point,

$\Delta\psi_g$ is the correction or observational increment for the variable ψ at the grid point,

and w_i is the weight given to observation ψ_i observed.

The summation is taken over a maximum of seven observations of the given variable surrounding the grid point in three dimensions. The weights w_i are determined by minimizing the interpolation error over a large number of cases. They may then be expressed as a function of the pre-specified characteristic errors of the observations and model field, and the 3-dimensional spatial distribution of the observations around the grid point. The displacement time of the observation from the analysis may be taken into account by modifying the observational error.

Assimilation

In the most common method of applying statistical interpolation, the model field is the 6-hour forecast and the whole of the correction $\Delta\psi_g$ is added to this field to produce the analysis. The technique is usually applied in a more sophisticated form than that described above so that, for example, observations of wind may affect a height analysis, and vice versa, through the geostrophic relationship. However, even when such a sophisticated multivariate scheme is used, the simple correction of a 6-hour forecast by an interpolated increment will excite spurious high-frequency oscillations in a subsequent

forecast. These oscillations are caused by small errors in the analysis which result in imbalances between the mass and wind field and unrealistic values of the divergent component of the wind. They produce a noisy forecast and, more seriously, dissipate much of the information from the observations present in the analysis. The usual technique for overcoming this problem is to apply some kind of initialization. The grid-point values of the model variables are adjusted to satisfy certain mathematical constraints which remove the high-frequency oscillations while at the same time ensuring that the values remain close to the observations. The most popular form used today is non-linear normal mode initialization.

At the Meteorological Office an alternative approach is used. The observations are assimilated into the model during the 6-hour forecast preceding the analysis time. First the interpolation weights w_i are calculated using values of the model forecast error appropriate to a 6-hour forecast. Then at each time-step of the 6-hour forecast preceding the analysis, increments are calculated at each of the grid points from differences between the observations and the current model state using the predetermined weights, by means of equation (1). However, only a small proportion (λ) of these increments is added to the model field. This process is represented in equations (2) to (4). Let one time-step of the model be represented by equation (2)

$$\Psi^*_{t+\Delta t} = \mathrm{M}(\Psi_t), \quad \ldots\ldots\ldots\ldots\ldots\ldots\ldots\ldots\ldots\ldots \quad (2)$$

where Ψ is now a vector representing all the model variables and M is an operator representing one time-step of the model. $\Psi^*_{t+\Delta t}$ is the value of the forecast without assimilating any data. It is then modified by the observations according to equation (3),

$$\Psi_{t+\Delta t} = \Psi^*_{t+\Delta t} + \lambda \Delta\Psi_{t+\Delta t}, \quad \ldots\ldots\ldots\ldots\ldots\ldots\ldots\ldots \quad (3)$$

where $\Delta\Psi_{t+\Delta t}$ is a vector representing increments at the grid points interpolated from the observations for all variables at time $t + \Delta t$. For any variable, ψ, at a grid point

$$\Delta\psi_{t+\Delta t} = \sum_i w_i \left(\psi_i^{\text{observed}} - \psi^*_{i,\,t+\Delta t}\right). \quad \ldots\ldots\ldots\ldots\ldots\ldots\ldots\ldots \quad (4)$$

Equation (4) is the same as equation (1) with a slight change of notation. λ increases linearly from 0 to 0.35 during the 6-hour period, so that only small changes are made to the forecast fields. This process is illustrated schematically in Fig. 1. For humidity, the model field ($\Psi^*_{t+\Delta t}$) is converted from humidity mixing ratio to relative humidity before the increments are calculated. After all variables have been incremented, the resulting field ($\Psi_{t+\Delta t}$) is converted back to humidity mixing ratio. Additional damping is included in the forecast model to control any unwanted oscillations which are generated. Since the interpolation is purely univariate, changes to the surface pressure and temperature fields do not directly affect the winds, and changes to the surface pressure field do not directly affect the temperature structure aloft. To assist the assimilation of the data, additional geostrophic wind increments are calculated from the surface pressure and potential temperature increments, and added to the wind field at each time-step; also, additional potential temperature increments are calculated from the surface pressure increments using the hydrostatic equation and added to the potential temperature field at each time-step.

The 'assimilation cycle' for the global model may be summarized as follows. Observations valid within 3 hours of 0600 GMT are assimilated into the 6-hour forecast starting at 0000 GMT and the resulting field is the 0600 GMT analysis. Observations valid within 3 hours of 1200 GMT are then assimilated into the 6-hour forecast starting from this 0600 GMT analysis. The process continues in a similar way for the remainder of the 24-hour period. In practice the situation is a little more complicated

as forecasts have to be run as early as possible in order to be useful. At present, therefore, the 0000 and 1200 GMT assimilations are actually performed twice, once to start the global model forecast at 0320 or 1520 GMT and once as part of the assimilation cycle at about 1130 or 2330 GMT. This repeat or 'update' assimilation is run as late as possible to allow time for extra data to be received and for CFO to carry out intervention. The update assimilation is followed immediately by the 0600 or 1800 GMT assimilation.

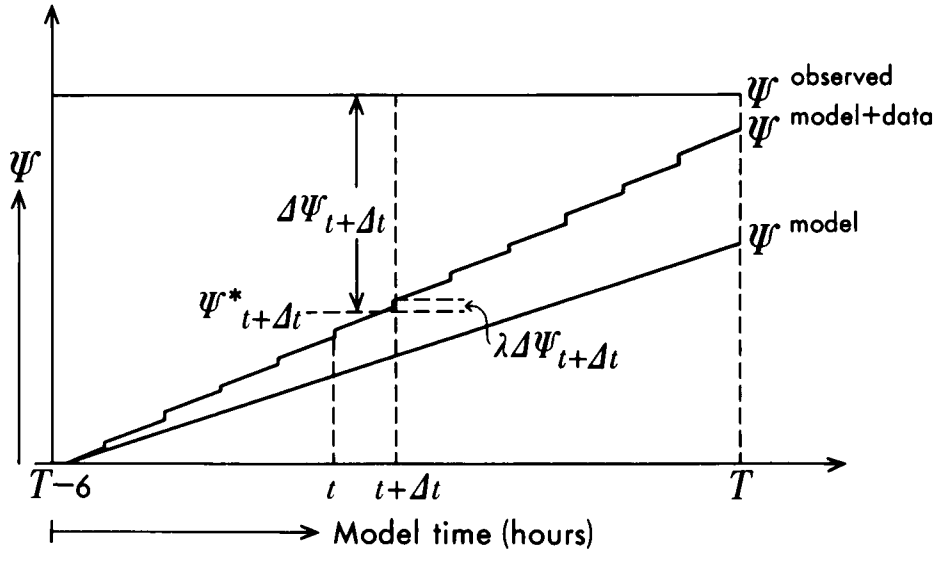

Figure 1. Schematic diagram of data assimilation. The vertical coordinate Ψ represents the state of the model or the atmosphere. The horizontal coordinate is the model time in hours. T is the validity time of the assimilation depicted and T-6 is the time of the previous assimilation. $\Psi^{observed}$ is the state of the atmosphere as determined from observations at time T. Ψ^{model} is the 6-hour forecast from the previous assimilation at time T-6. $\Psi^{model+data}$ is the result of assimilating observations for time T into the 6-hour forecast from T-6. t and $t+\Delta t$ are two successive time-steps of the forecast and $\Psi^*_{t+\Delta t}$, $\Delta\Psi_{t+\Delta t}$ and λ are as defined in the text. Note that $\Psi^{model+data}$ will not equal $\Psi^{observed}$ as allowance is made for errors in the observations.

Fine-mesh assimilation

Initial fields for the regional fine-mesh model are provided by a fine-mesh assimilation. This is based on the same principle as the global assimilation except that the assimilation is performed by the regional model at three-hourly intervals instead of six and, for each assimilation, observations within 1½ hours of the analysis time are used. Global information from observations made at earlier times is incorporated by restarting every 12 hours by interpolation from a global update assimilation, and performing 12 hours of fine-mesh assimilation at 3-hourly intervals to provide an initial field for the fine-mesh model valid at 0000 or 1200 GMT. Lateral boundary conditions for this fine-mesh assimilation are provided by a 12-hour coarse-mesh forecast from the global update assimilation. The fine-mesh assimilation scheme has therefore both a higher spatial and temporal resolution than the global assimilation scheme and this enables more detailed analyses to be made.

References

Gadd, A. J. 1985 The 15-level weather prediction model. *Meteorol Mag*, **114**, 222-226.

World Meteorological Organization 1966 International meteorological tables. Geneva, WMO No. 188 TP. 94.

551.509.313:551.509.58:551.465.75:551.466.3

Sea surface wave and storm surge models

By P. E. Francis

(Meteorological Office, Bracknell)

Summary

Numerical models for use as guidance in oceanographic forecasting have been used in the Meteorological Office for many years. The development of the present state of the art is briefly traced, with reference to the key requirements of forecasting for coastal defences and the North Sea oil industry. The present mode of use, mathematical formulation, and performance characteristics of the operational storm surge and surface wave models are separately discussed. The results of verification exercises illustrate that whereas forecasts of an acceptable accuracy are usually obtained there is still room for model development. Some possible avenues of improvement are discussed, including unification of the two continental shelf models into a single interactive system.

1. Introduction

The operational use of numerical models as an aid in forecasting for marine services has a long history in the Meteorological Office, especially if by the term 'model' we include such mathematical techniques as empirical equations based on statistical models of ocean–atmosphere relationships. Such empirical models were used in the Office for many years before the relatively recent advent of the more sophisticated models which require powerful computing resources in order to solve the basic physical equations.

Following the disastrous coastal flooding of 1953 a Storm Tide Warning Service (STWS) was set up, working closely with the Central Forecasting Office (Synnott 1964). A system of empirical forecasting equations, still in use by the STWS, was first investigated for operational use during the mid 1960s (Keers 1966); before that time much research into the technique had been carried out at the Liverpool Tidal Institute (now Institute of Oceanographic Sciences) and at other oceanographic research centres. These equations, which relate surge residual height (the difference between actual sea level and the astronomical tide) to such meteorological variables as surface pressure and wind speed, were refined during the late 1960s (Keers 1968) and early 1970s (Hunt 1972) by the inclusion of more data and by investigation into methods of representing the non-linear behaviour of the surge in the shallower waters of the southern North Sea. More recently, in 1978, a numerical model that explicitly calculates surge residuals by means of solving the relevant dynamical and physical equations was introduced operationally. This model was also developed by the Institute of Oceanographic Sciences (Flather 1981) and has proved to be of great value to the STWS in their work. The model, its development and basic theory, are described in more detail later in this paper.

The forecasting of surface wave conditions has been a major feature of the services offered by the Office since the development of the North Sea oil industry in the 1970s. Originally, forecasters at London Weather Centre made use of empirical growth curves (World Meteorological Organization 1976) to gain an estimate of likely wave heights, using forecast values of surface wind speed, direction and fetch. Similar methods were also in use to supply the Ship Routeing Service with forecast wave data for the North Atlantic. A numerical model for computing surface waves in deep water was brought into operational use in 1976, followed by a shallow-water version in 1977. Various improvements have been made to these models since that time, leading to the current status of the models which will be described later in this paper.

The output of the dynamical oceanographic models discussed here is used for a wide variety of purposes; these are discussed and illustrated in a paper to appear in the next issue (Ephraums 1985). The

models are run on the CDC Cyber 205 computer, making full use of the vector processing facilities. Results of integrations are then transferred to an IBM front-end system where post-processing is carried out in order to generate data in a form suitable for output purposes.

2. The storm surge model

(a) *General discussion*

A numerical storm surge model has been in operational use at the Meteorological Office since 1978. The model is run as part of the operational forecasting suite, following the high-resolution limited-area atmospheric model, twice a day from September to May. Effectively, forecasts for up to 33 hours ahead are produced since the model products are not available to the forecasters of the STWS until just after 3 hours past the initial data time. The area covered by the model is approximately 11°W to 11°E, 46°N to 63°N, on a latitude–longitude grid with spacing of $\frac{1}{3}° \times \frac{1}{2}°$. The North Sea and near continental shelf are well represented at this resolution, which is slightly coarser than that of the continental shelf wave model. The undisturbed water depth is specified at each grid point.

Surface wind and pressure information is written up every hour during the forecast run of the fine-mesh NWP (numerical weather prediction) model. These data are first of all converted to wind stress and effective hydrostatic pressure respectively, and then linearly interpolated from the $(\frac{3}{4}° \times \frac{15}{16}°)$ grid of the NWP model to that of the surge model. The 'surface' wind field of the NWP model is the wind from the lowest level of the model, located at approximately 25 m above sea level; the implications of using a wind at this level are examined in a later section.

Two runs of the surge model are performed in order to obtain the residual height data. In the first run the tidal predictions for each grid point are calculated using 6 tidal components. These data enable a second run to be made which includes the meteorological effects in addition to the tidal terms. The surge residuals are then obtained by subtracting the results of the purely tidal run from that which includes both tidal and meteorological terms. In this way the tide–surge interaction, which is of greatest importance in shallow water, is included in the calculations.

The initial conditions for a surge model forecast are at present taken from the results of the previous 12-hour forecast. In this way any errors due to a poor wind and pressure forecast are carried over and perpetuated. A method of avoiding such a situation is to introduce a 'hindcast' run, similar to that performed in the surface wave models (see later). Such a system has been tried in the past and proved to be worth while, and there are plans to introduce it for the present storm surge model.

(b) *Mathematical formulation*

The mathematical basis of the model is formed by the depth-integrated equations of motion and continuity. Following the most recent and comprehensive description of the operational model (Procter and Flather 1983), the complete equations are approximated by:

$$\frac{\partial \zeta}{\partial t} + \frac{1}{R\cos\phi}\left\{\frac{\partial}{\partial \lambda}(D\bar{u}) + \frac{\partial}{\partial \phi}(D\bar{v}\cos\phi)\right\} = 0 \quad \ldots\ldots\ldots\ldots\ldots (1)$$

$$\frac{\partial \bar{u}}{\partial t} + \frac{\bar{u}}{R\cos\phi}\frac{\partial \bar{u}}{\partial \lambda} + \frac{\bar{v}}{R}\frac{\partial \bar{u}}{\partial \phi} - f\bar{v} = \frac{g}{R\cos\phi}\frac{\partial}{\partial \lambda}\left[\zeta - \frac{P_a}{\rho g}\right] + \frac{F_s - F_b}{\rho D} \quad \ldots\ldots\ldots\ldots (2)$$

$$\frac{\partial \bar{v}}{\partial t} + \frac{\bar{u}}{R\cos\phi}\frac{\partial \bar{v}}{\partial \lambda} + \frac{\bar{v}}{R}\frac{\partial \bar{v}}{\partial \phi} + f\bar{u} = \frac{g}{R}\frac{\partial}{\partial \phi}\left[\zeta - \frac{P_a}{\rho g}\right] + \frac{G_s - G_b}{\rho D} \quad \ldots\ldots\ldots\ldots (3)$$

where the notation is as follows:

$f = 2\Omega\sin\phi$	the 'Coriolis' parameter;
t, λ, ϕ	time, east-longitude and latitude respectively;
$\bar{u}$, $\bar{v}$,	components of the depth mean current $\boldsymbol{q}$;
ζ	elevation of the sea surface;
h	undisturbed water depth;
$D = h + \zeta$	total water depth;
R, Ω, g, ρ	geophysical constants (earth radius, earth rotation rate, gravity, density of sea water);
P_a	atmospheric pressure at sea level;
F_s, G_s	components of wind stress τ_s on the sea surface;
F_b, G_b	components of stress on the sea bed, τ_b.

The stress on the sea bed is calculated by assuming a quadratic stress law in order to relate the stress to the depth mean current, i.e.

$$\tau_b = -0.0025\ \rho\ \boldsymbol{q}\ |\ \boldsymbol{q}\ | .$$

Similarly the surface stress is computed from the atmospheric wind data by means of the relationship

$$\tau_s = \rho_a\ 10^{-3}\ (0.63 + 0.066\ |\boldsymbol{W}|)\ \boldsymbol{W}\ |\boldsymbol{W}|$$

where ρ_a = the density of air (1.25 kg m^{-3}) and $\boldsymbol{W}$ is the surface wind.

Horizontal boundary conditions are given by assuming zero flow normal to coastlines, and by seeking to prevent artificial reflections from the open boundaries of disturbances generated within the model. The latter effect is achieved by allowing outward propagation as free progressive waves, while ensuring the generation of the tidal constituents at the boundaries. The details of the finite difference schemes adopted for the numerical integrations of equations (1)–(3) may be found in Procter and Flather (1983). By excluding very deep water areas off the continental shelf, the time-step of the integration is allowed to be fixed at 144 seconds.

(c) *Performance characteristics*

During the winter season of 1983/84 the STWS found that in general the model overpredicted positive surge residuals, especially in the southern areas of the North Sea. The data used for verification were taken from reliable tide gauges located at ports around the British coast. Some error statistics for four locations are given in Table I. The tendency for overprediction is shown by the positive mean errors, and also by the larger extreme values of over-forecasts, much larger numerically than the extreme under-forecasts. A small improvement in forecast quality with reduction in forecast period can be seen, but this is really very marginal. A possible explanation of the overestimation seen in these recent verification figures may be found in the direct use of winds taken from the lowest level of the NWP model. Traditionally, winds at 10 m above sea level have been used throughout the development of the surge model, especially in the derivation of the surface wind stress relationship (Smith and Banke 1975). It is thus possible that further modelling of the wind at the output stage, using the thermal structure of the NWP model, in order to generate winds nominally at 10 m above sea level, would be a beneficial development.

3. The surface wave model

(a) *General discussion*

The surface wave model at present run on an operational basis in the Meteorological Office is the result of an evolving series of such models, in use since 1976. Similarly to the surge model, the wave

Table I. *Error statistics of storm surge model residual estimates, winter 1983/84*

Port, and time of issue of forecast before high water		Number of cases	Root-mean-square error	Mean error *metres*	Largest errors overf'cast/underf'cast
Tyne	-12	40	0.20	+0.09	+0.48/-0.19
	-4	33	0.18	+0.04	+0.46/-0.27
Immingham	-12	39	0.23	+0.17	+0.55/-0.11
	-6	33	0.23	+0.13	+0.55/-0.33
Lowestoft	-12	30	0.44	+0.34	+0.89/-0.24
	-6	30	0.33	+0.21	+0.90/-0.33
Sheerness	-12	36	0.38	+0.22	+1.00/-0.33
	-7	24	0.31	+0.22	+0.88/-0.11

models (three versions) are driven by wind fields extracted from the operational NWP models. All models are run twice daily, but throughout the whole year rather than just in the winter season. The three versions in operational use cover different areas on different scales, and are run for different forecast periods (see Table II). The only difference in formulation between these three models is the inclusion of extra shallow-water terms in the continental shelf model. The model integrations are at present carried out on a polar stereographic grid, following the appropriate interpolation of the wind fields from the latitude–longitude grids of the NWP models. The wind input for the wave models is assumed in the basic theory to be at a height of 19.5 m, hence the use of direct lower-level winds from the NWP models is not inappropriate here as it probably is for the surge model.

Table II. *Physical specification of operational wave models in the Meteorological Office*

Model	Resolution at 60°N	Origin and frequency of wind field data	Forecast period	Depth-dependent terms
Northern hemisphere	150 km	Global NWP model, every 1½ hours	3 days	No
Continental shelf	25 km	Fine-mesh NWP model, every ½ hour	36 hours	Yes
Mediterranean	50 km	Fine-mesh NWP model, every ½ hour	36 hours	No

Unlike an NWP model, where there are sufficient observed data to allow an 'analysis' (or starting field) to be calculated for all the different variables, the wave model has to be initialized by means of a 'hindcast'. This is essentially the repeat of the first 12 hours of the previous forecast (run 12 hours ago) but this time using improved wind fields, improved by making use of the intervening analysis runs of the NWP model. There are insufficient measurements of the directional wave spectrum to allow a wave analysis and, additionally, the theoretical mathematical work on which to base such an analysis has yet to be carried out. The hindcast technique yields a series of fields, 12 hours apart, which are the best description of the actual wave fields that can at present be derived. The archive of these fields has many uses; these are discussed in a companion paper (Ephraums 1985).

(b) *Mathematical formulation*

The theoretical basis of the wave model is the representation of the wave field as a spectrum — essentially the variance of the sea surface elevations that are present in a statistically random fashion. The behaviour of individual components of the spectrum can be calculated from known theories, and the more commonly recognized quantities such as wave height and period can be calculated from

moments of the spectrum. A simple example of a directional wave spectrum is shown in Fig. 1. The model at present has 16 equally spaced directions and 14 irregularly distributed frequency values, ranging from 0.04 Hz (25 seconds period) to 0.324 Hz (≈3.1 seconds period). Thus at each model grid point 224 discrete spectral energy density values are stored.

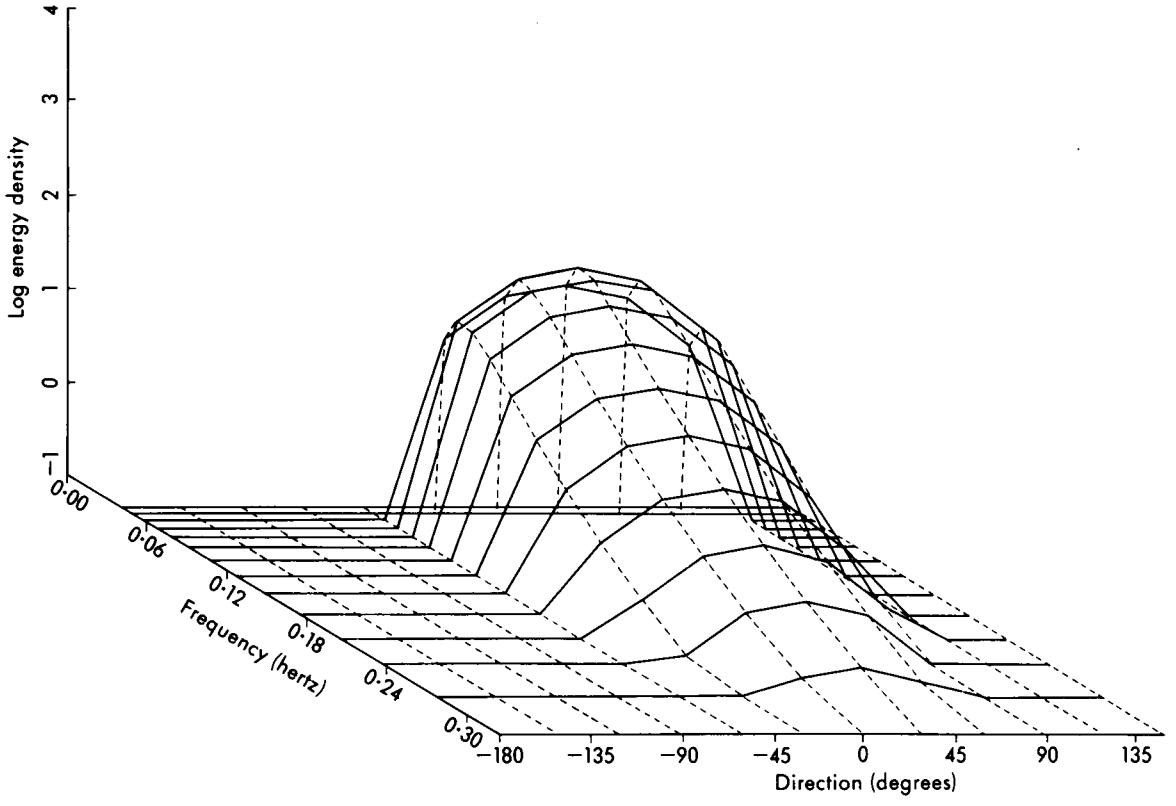

Figure 1. The limiting energy spectrum for a wind of 20 m s^{-1} from 360°.

The variation of these values in time and space is controlled by means of integrating the energy balance equation:

$$\frac{\partial E}{\partial t} + \nabla\cdot(E\boldsymbol{C}_g) + \frac{\partial}{\partial\theta}\left[(\boldsymbol{C}_g\cdot\nabla\theta)E\right] = S_{in} + S_{ds} + S_{nl} \quad .. \; .. \; .. \; .. \; .. \quad (4)$$

(ADVECTION) (REFRACTION) (SOURCE/SINK)

where the following notation is used:

$E(f, \theta, x, t)$ is the energy density in a spectral component with frequency f, travelling in a direction θ, at a location x at time t;

$\boldsymbol{C}_g(f, \theta)$ is the group velocity of the component (a function of depth);

S_{in} represents the energy input from the atmosphere;

S_{ds} represents energy loss; and

S_{nl} represents the internal redistribution of energy due to non-linear interactions.

Full details of the mathematical and physical theories used in the model may be found in a comprehensive paper (Golding 1983). It is sufficient here to outline the processes in a more general way.

The advection, or propagation, term is calculated by means of standard finite difference techniques, with appropriate treatment at coastal and open boundaries in order to prevent reflection. The refraction term is solved by adopting a continuous form of Snell's Law, more familiar in optics, in order to calculate the effects of irregular bottom topography on the component waves. The source and sink terms S_{in}, S_{ds} contain a number of processes which attempt to represent the currently held theories concerning wave growth and decay. In simple terms the growth of sea waves is due to the input of atmospheric energy through boundary-layer transfer processes which are still not completely understood. What is clearly apparent is that growth is inhibited by a limit on wave size and shape, beyond which breaking takes place with an accompanying loss of energy. The growth and decay processes in the model (for deep-water states) are balanced so that the limiting form is attained but not exceeded, and also so that observed growth rates are reproduced. In shallow water an extra dissipation term is introduced to represent the energy loss through frictional effects on the sea bed.

Finally, the non-linear interaction term, S_{nl}, is introduced in order that the eventual spectral shape is close to that observed in physical reality. It is known from an extensive series of measurements that the spectrum of a wind sea (i.e. that portion of the full spectral range within the influence of the local generating wind) is maintained in a recognized shape by means of internal energy transfers from high to low frequency. The calculation of the exact transfer terms is, however, at present beyond the capacity of most computing systems, especially if real-time forecasts are required. Hence we have adopted an empirical approach which assumes a spectral form, the JONSWAP spectrum (Hasselmann *et al.* 1973), and redistributes the wind sea energy, without loss, into that form. The main difficulty with this method is the problem of separating wind sea from swell (i.e. that portion of the spectrum not under the local influence of the wind) in order to generate the spectral shape, but the model results as discussed in the next section confirm that the present empirical scheme is giving an acceptable approximation to a very complex physical process.

(c) *Performance characteristics*

The wave model can be assessed in two distinct ways: firstly by comparison of values of significant wave height (approximately that height assessed by visual estimation, more specifically the mean height of the highest one-third of the waves present) as calculated by the model and as observed and reported from maritime stations; and secondly by means of comparison with measured wave data, for example that from a wave rider buoy or similar device. The first verification technique is performed operationally at Bracknell, where incoming wave data from synoptic reports are routinely compared with model results. Table III shows some error statistics from three representative stations. Ocean Weather Ship 'L' is in deep water, the oil platform Statfjord is near the edge of the continental shelf, depth about 130 m, and the platform K-13 is in the much shallower regions of the southern North Sea, depth about 30 m. Points to note from the figures in the table are:

(i) Errors grow with observed wave height, but not so markedly with forecast period.

(ii) The effects of the extra friction terms in the continental shelf model are apparent in the results for Statfjord where, although the water depth is still appreciable, the coarser-mesh model is yielding higher wave height forecasts throughout all ranges of observed height.

Details of a comparison against data from a wave rider buoy can be found in Fig. 2. The fine-mesh model has given very acceptable forecasts for a location about 500 m offshore in 13 m of water. Such a performance confirms the potential that the model has for many shallow-water applications (Ephraums 1985).

Table III. *Error statistics of significant wave height in operational wave models in the Meteorological Office, 1983 and 1984*

Station	Forecast time	Forecast model	0–3 m N	0–3 m $\bar{X}$	0–3 m σ	3–6 m N	3–6 m $\bar{X}$	3–6 m σ	>6 m N	>6 m $\bar{X}$	>6 m σ
OWS 'L'	00	NH	466	0.1	0.9	633	0.3	1.3	169	0.7	1.6
57°N, 20°W	24		467	0.1	0.9	647	0.3	1.3	178	0.7	1.9
Statfjord	00	NH	586	0.3	0.7	375	0.9	1.0	41	1.2	1.6
61.2°N, 1.8°E	24		598	0.3	0.8	380	0.9	1.2	41	1.2	1.8
	00	CS	580	0.1	0.6	371	0.6	0.8	41	0.7	0.8
	24		587	0.2	0.7	374	0.7	1.1	40	0.8	1.3
K-13	00	CS	1037	0.0	0.3	86	-0.3	0.6	0		
53.2°N, 3.2°E	24		1055	0.2	0.5	87	-0.1	0.8	0		

Wave height ranges are for observations; N = number of cases; $\bar{X}$ = mean error in metres; σ = standard deviation of error in metres; NH = northern hemisphere; CS = continental shelf.

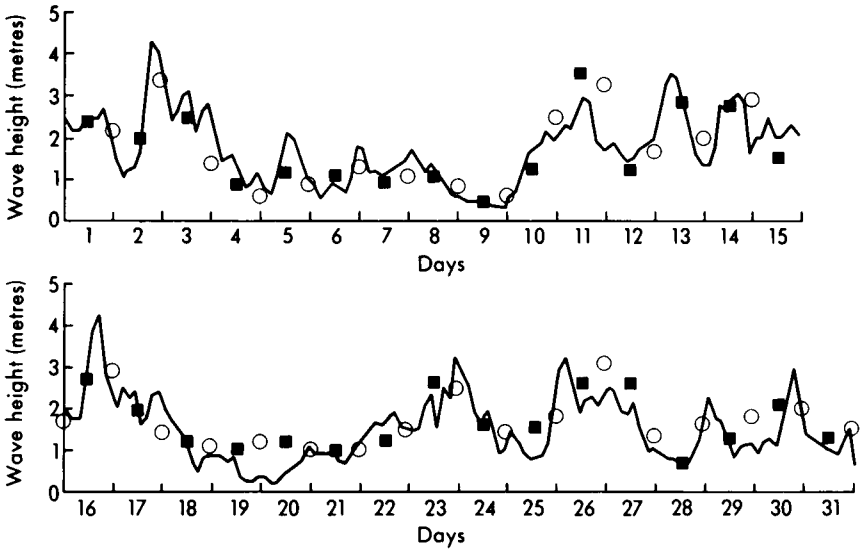

Figure 2. Comparison of wave heights, actual and forecast, for Seaford, January 1984 (by courtesy of Southern Water, and Hydraulics Research, Wallingford).
——— observed wave heights from wave rider buoy
■ ■ ■ 12-hour forecast (for 12 GMT made at 00 GMT)
○ ○ ○ 24-hour forecast (made at 00 GMT the previous night)
Forecasts at location 50.6°N, 0.8°E; Seaford wave rider buoy at 50.76°N, 0.08°E.

4. Future developments

The present situation, in which the storm surge model and the fine-mesh model are run separately, is far from satisfactory since a unified model would add far more to the accuracy of the results than just an increase in operational efficiency. The potential advantages in a unified model are threefold. Firstly, long-wave propagation is strongly influenced by water depth, hence tidal and surge influences on water

depths in areas of shallow mean water level are likely to be significant for wave forecasts. The southern North Sea is a particularly interesting area in this respect. Secondly, it is well known that currents have a marked effect on waves, and it is quite likely that the depth-integrated currents of the surge model could be used to give better wave forecasts in regions of strong tidal currents. Thirdly, the surface stress which drives the surge model is directly linked to the roughness of the sea surface. Thus a knowledge of the state of sea should result in more accurate computations of the stress input for surge modelling.

Both kinds of operational oceanographic model will benefit from the assimilation of measured data on a routine basis. For the surge model the requirement is a balanced set of current and height data; for the wave models a fairly comprehensive description of the directional spectrum is necessary. Such data are at present not readily available and it may be some years before data in large enough amounts, e.g. remotely sensed from satellites, make such an assimilation process viable. In the meantime some research work is necessary in order to solve the mathematical difficulties inherent in the process.

Research work into wave and surge modelling is at present coming to the fore in many European countries, and a joint initiative for co-ordinating further work has recently been inaugurated. The WAM group (WAve Modelling), with members from nearly all the maritime European nations, intends to address itself to the many problems that remain to be solved in order that real-time oceanographic forecasting for a variety of marine applications will achieve even better results than at present.

As part of this program the Meteorological Office is currently performing experiments with a wave model on a latitude–longitude grid, with the intention of providing a full global forecasting capability in 1986. At the same time the new model is to be used as a 'test bed' facility with which to investigate the progress of some of the work in the WAM initiative.

References

Ephraums, J. J. 1985 Applications of wave and surge models. *Meteorol Mag*, **114**, 282–291.

Flather, R. A. 1981 Practical surge prediction using numerical models. *In* Peregrine, D. H. (ed.); Floods due to high winds and tides. London, Academic Press, 21–43.

Golding, B. 1983 A wave prediction system for real-time sea state forecasting. *Q J R Meteorol Soc*, **109**, 393–416.

Hasselman, K., Barnett, T. P., Bouws, E., Carlson, H., Cartwright, D. E., Enke, E., Ewing, J. A., Gienapp, H., Hasselmann, D. E., Kruseman, P., Meerburg, A., Muller, P., Olbers, D. J., Richter, K., Sell, W. and Walden, H. 1973 Measurements of wind-wave growth and swell decay during the Joint North Sea Wave Project (JONSWAP). Hamburg, Deutsches Hydrographisches Institut, *Dtsch Hydrogr Z*, A12.

Hunt, R. D. 1972 North Sea storm surges. *Mar Obs*, **42**, 115–124.

Keers, J. F. 1966 The meteorological conditions leading to storm surges in the North Sea. *Meteorol Mag*, **95**, 261–272.

1968 An empirical investigation of interaction between storm surge and astronomical tide on the east coast of Great Britain. *Dtsch Hydrogr Z*, **21**, 118–125.

Procter, R. and Flather, R. A. 1983 Routine storm surge forecasting using numerical models: procedures and computer programs for use on the CDC CYBER 205 at the British Meteorological Office. Wormley, Institute of Oceanographic Sciences, Report No. 167. (Unpublished.)

Smith, S. D. and Banke, E. G. 1975 Variation of the sea surface drag coefficient with wind speed. *Q J R Meteorol Soc*, **101**, 665–673.

Synnott, J. N. N. 1964 The Storm Tide Warning Service. *Mar Obs*, **34**, 77–83.

World Meteorological Organization 1976 Handbook of wave analysis and forecasting. Geneva, WMO, No. 446.

551.509.313:551.509.5

Output products of the Bracknell numerical weather prediction models

By P. E. Francis

(Meteorological Office, Bracknell)

Summary

The data produced by the numerical weather prediction models are further processed in order that a comprehensive set of output products can be generated operationally. The first step is the generation of an output data set which contains both primary and derived variables, arranged on fields at constant standard pressure levels. The derived variables are those which are not explicitly contained in the forecast model data.

Charts and coded bulletins are then constructed from the output data set, using a variety of formats requested by users, and internationally agreed. Lists are provided of the current charts and code bulletins available. A discussion of back-up arrangements concludes the presentation of output products.

1. Introduction

The numerical weather prediction (NWP) models described in a companion paper (Gadd 1985) yield large amounts of data when run operationally. These data (for different variables, model grid points, model levels, forecast times) are internally arranged and represented in a form that is convenient for the rapid integration of a numerical model. Such a representation is, however, far from convenient for the production of the large quantity of output, in many forms, that is needed to satisfy the requirements of modern meteorological services. In order that a versatile range of output products can be easily generated it is first necessary to rearrange the forecast model data fields into a more suitable format. At the same time it is convenient to generate (by further modelling techniques) those fields which are not explicitly carried in the models, but which are required for operational purposes. These 'derived' fields are listed in Table I, together with the other standard formats for explicitly held variables.

The output variables, held in a comprehensive data set, are then transferred from the Cyber 205 fast vector processor to a conventional 'front-end' processor, currently an IBM 3081. After reformatting, the output data set is available for access by authorized users, as well as being the source of all the operational output data streams. A versatile suite of access routines is available which allow data to be

Table I. *Variables stored in output formats, both basic and derived*

Model variable	Basic output forms	Derived output forms
Wind	Speed and direction on standard pressure levels	Vertical velocity at standard levels. Maximum wind, height, speed, direction. Surface (10 m) wind, speed, direction. Vorticity at standard levels. Clear-air turbulence index (200, 250, 300 mb).
Temperature Surface pressure	Temperatures and heights of standard pressure levels. Mean-sea-level pressure	Tropopause temperature, pressure, height. Height and pressure of freezing level. Surface (1.5 m) temperature. Wet-bulb potential temperature (500, 850 mb).
Humidity	Relative humidity at standard pressure levels $\geqslant$500 mb.	
Precipitation	Dynamic and convective rates and accumulations.	

extracted and then interpolated on to a wide range of latitude–longitude grids, and also on to different map projections, including Polar Stereographic and Mercator. Another advantage of retaining output products on a front-end processor is the ease of communication with other computing systems, and the fact that incoming back-up data from the National Meteorological Center (NMC) in Washington DC, and the medium-range data from the European Centre for Medium Range Weather Forecasts (ECMWF) can be collected and stored in the same output format, ready for presentation in chart form using standard computer software.

2. Output modelling techniques

The first stage in the process of generating output products (Fig. 1) is the construction of a comprehensive data set which consists of the required basic and derived variables, stored on pressure levels. Table I briefly sets out the current contents of the output data set. Not all of the derived fields are generated by both versions of the NWP model (i.e. global and fine-mesh versions), but all of the basic output forms are common to both. Variables directly associated with aviation forecasting (tropopause and maximum wind, for instance) are generated only from global model data.

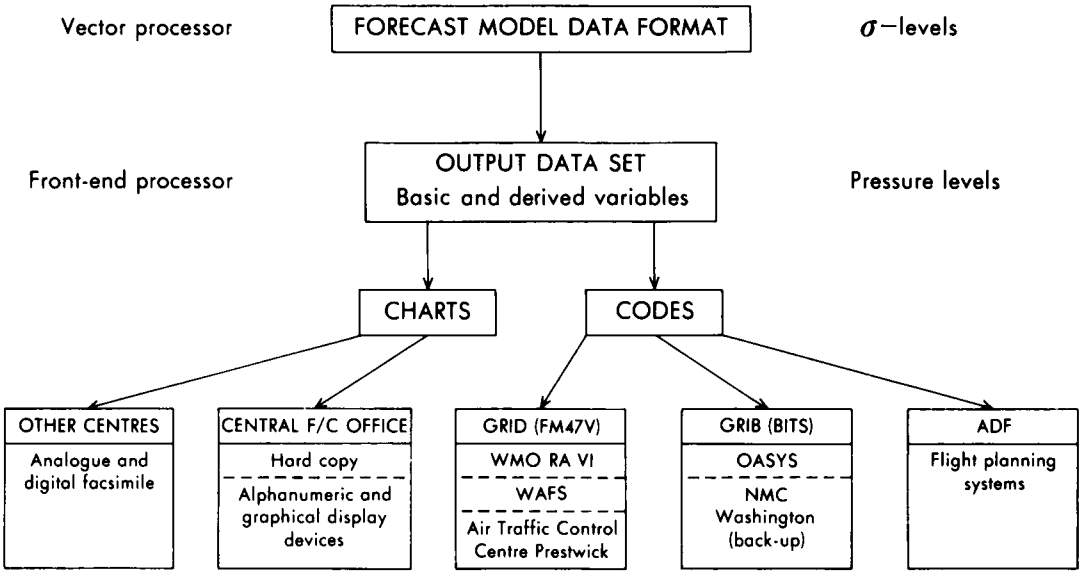

Figure 1. Organization of data set for generating output products.

(a) *Wind modelling*

The initial step in the wind modelling is the calculation of the vertical velocity. This calculation is performed while the horizontal wind components are still on σ-levels, and is carried out in a manner similar to that employed in the forecast model. Divergences at every grid point are calculated for each

model layer and summed from the top downwards. In the same manner, absolute vorticity is also calculated from the horizontal wind components, before interpolation on to pressure levels is carried out. The required interpolation, for both vertical velocity and absolute vorticity, is calculated by assuming that the variables change linearly with the logarithm of pressure, written log (pressure) below.

The next step is to calculate the speed, direction and pressure level of the maximum wind. The wind components are first combined to give a speed and direction, then a search is made for the σ-level that contains the maximum value of wind speed. The maximum of the implied continuous profile may then be assumed to lie within one model layer on either side of the designated σ-level. A cubic spline function is fitted to the wind speed values outside of the boundary layer, and by means of straightforward but detailed calculus and algebra it is possible to calculate both the profile maximum value and its level. An enhancement of the maximum value is not at present thought to be necessary since the improved definition of jet streams in the present model gives acceptable results in most situations. The direction of the maximum wind is found by means of interpolation in log (pressure) once the level has been determined.

Consistent with the vertical interpolation used for other wind parameters, wind speed and direction on standard levels are determined by assuming a linear variation with log (pressure) of the u, v components between the σ-levels. The maximum wind information is used as an extra level in order to give consistency in that region. Standard levels that fall below model orography are assigned the wind speed and direction of the lowest σ-level.

Another derived 'wind' parameter is the clear-air turbulence (CAT) index, which is calculated using the formulation established for the previous NWP model (Dutton 1980). Work on updating the formulation, using data from the new NWP model related to aircraft reports of CAT, is now under way, and should lead to improvements in the definition of this very important aviation index.

Finally in this section on wind modelling, we turn to the problem of calculating a surface wind defined as the wind at 10 m above the ground or sea surface. For many forecasting applications such a wind parameter is an essential element and it is important that realistic values are derived. The technique used during the output modelling calculations is consistent with that employed in the forecast model for representing boundary-layer effects. An integral part of the system is the calculation of a boundary-layer Richardson number, taken to be a function of wind, temperature and humidity values at the surface and lowest σ-levels. This Richardson number then determines the profiles used to evaluate both surface wind and temperature over land and over sea. The profiles vary with the implied stability in the boundary layer, and contain the implicit contributions of surface roughness length and drag coefficient. The direction of the surface wind is taken to be that of the wind in the lowest σ-level.

(b) *Temperature modelling*

The first stage in the process of calculating the heights and temperatures of standard levels is to convert the potential temperatures on σ-levels, used in the forecast model, into the associated temperature values. Then the thickness between σ-levels can be calculated using the σ-level virtual temperatures. In this way the effects of humidity on the thicknesses are included. The heights of the σ-levels can then be derived by summation of thicknesses from the lowest level upward. The temperature at each standard pressure level is calculated firstly by locating it between two σ-levels, and then by assuming a constant temperature lapse rate between those levels. The height at each standard pressure level is calculated by assuming a constant virtual temperature for the layer between the pressure level and the lower (in height) of the two reference σ-levels.

For pressure levels below the model orography it is necessary to adopt a pragmatic approach in order to obtain acceptable temperature and height values. The associated calculation of pressure at mean sea

level is performed in a consistent manner. Height values below orography are primarily required so that realistic contour charts can be produced for the forecaster. Such charts require to be smooth, and to appear as if the intruding orographic feature was not present. Accordingly it is acceptable to extrapolate from a 'free atmosphere' level in order to obtain the temperature for a subterranean standard level, thus avoiding the effects of the boundary layer. The extrapolation uses a standard lapse rate of 0.0065 K m^{-1}. The height at the subterranean standard level is obtained by subtracting the thickness of the layer between the lowest σ-level and the standard pressure level concerned, again calculated using the assumption of a constant virtual temperature throughout the layer. The pressure at mean sea level is given by an equivalent calculation using the orographic height and an extrapolated temperature profile as above. For zero orography the pressure at mean sea level is of course equal to the surface pressure.

The next task is to locate the tropopause and assign a consistent temperature and height. The essence of the method employed to do this is the assumption that the tropopause should be associated with a layer mean lapse rate of less than 0.002 K m^{-1}, at a height above that of surface inversions and other low-level temperature features. Layer mean lapse rates are therefore calculated, from the σ-level data, and a search is carried out (above 500 mb) for the relevant critical lapse rate. Having found the first layer for which the *mean* lapse rate is less than the critical value it is a straightforward algebraic task to calculate the exact σ-level for which the lapse rate equals 0.002 K m^{-1}, assuming a linear variation in the lapse rate between the mid-points of adjacent layers. Following further algebraic manipulation the temperature of the tropopause can be determined, and then in the same manner as described earlier the height can be calculated.

Three other temperature-dependent variables are also derived. The freezing level is located by searching upward through the σ-level data for the first value of temperature less than 273 K. The freezing level height is then calculated by assuming a constant lapse rate through the appropriate model layer. The technique for modelling surface parameters was outlined earlier in the discussion of wind variables. By this method a temperature at 1.5 m is modelled and made available for output. Finally, values of wet-bulb potential temperature are calculated by an iterative technique after the necessary temperature and humidity information has been transferred on to pressure levels.

(c) *Humidity and rainfall*

The forecast model produces values of humidity mixing ratio on σ-levels whereas for output purposes relative humidity on pressure levels is required. The first step in the transformation process is the calculation of saturation mixing ratio, performed by using a look-up table for saturation vapour pressure with reference to the σ-level temperature. The look-up table assumes saturation with respect to water for temperatures greater than −5 °C, and with respect to ice for temperatures less than −10 °C. For intermediate values the table has an interpolated entry between the two saturation states. The information is then at hand to be able to first calculate saturation mixing ratio and then relative humidity. Interpolation to pressure surfaces is again achieved by assuming a linear variation in log (pressure).

Rainfall information in the models is available as the result of both convective and dynamic processes, the basic parameter being an instantaneous rate. By accumulating the rates at each time step and multiplying by the appropriate constant it is also possible to derive values for dynamic and convective accumulations over a period. This calculation is performed in the forecast model. Enhancement of the grid-point convective values in order to represent possible convective activity in a fraction of a grid square is at present performed empirically; but the use of relevant information from the convective parametrization in the forecast model may lead to a more satisfactory procedure for such enhancement.

3. Chart output

The conventional presentation of most forecast products is by means of a chart, either containing isopleths of the required field or having numerical values printed on a regular grid. Chart products form a very important part of the output stream from the numerical models run at Bracknell. Including all kinds of charts, and those required for back-up purposes, nearly 1000 are produced in a 24-hour cycle. Not all of these are transmitted by facsimile broadcasts of course. Nearly half of them are for back-up purposes, i.e. for use if a later forecast run fails. Many are for use in the Central Forecasting Office and are not designed for wider dissemination. About 100 charts are prepared for facsimile broadcast in a 24-hour period, including a substantial number of hand-drawn products. These latter charts are prepared by forecasters at Bracknell, using forecast model products as a guide, along with other information such as satellite pictures and later observations. The final chart represents a 'man–machine mix', that is, a synthesis of computer speed and efficiency with human experience and intuition. Both hard-copy and visual display unit presentations are available to the forecaster at Bracknell (Fig. 1) for the preparation of hand-drawn products.

Three chart examples are shown in Fig. 2, and other examples are to be found in companion papers. The computer-drawn charts are produced on a Calcomp 1581 device, using a software package which extracts data from the comprehensive output data set (described earlier), and prepares it for either line drawing or grid plotting on a versatile range of chart areas and projections. Tables II and III summarize the charts currently available on facsimile broadcasts. The more acceptable modern method of disseminating forecast data is by means of coded broadcasts using higher speeds, which enable a wider range of data to be transmitted. This system will be discussed in the next section.

4. Coded output

(a) *Bracknell's dual role*

The Meteorological Office at Bracknell has a dual function as far as the dissemination of coded forecast data is concerned. As a Regional Meteorological Centre (RMC) for Region VI of the World Meteorological Organization (WMO), Bracknell makes available numerical analysis and forecast data covering Europe and the North Atlantic to other national meteorological centres. Acting as a World Area Forecast Centre (WAFC) of the World Area Forecast System (WAFS), initiated by the International Civil Aviation Organization (ICAO), Bracknell provides data with a global coverage, both directly to airlines and also to regional centres of the WAFS. The provision of these data requires the use of agreed code forms, so that rapid transmissions from centre to centre are achieved without confusion or ambiguity of meaning.

(b) *The code formats*

The rapid progress in telecommunication techniques, leading to high-speed lines and computer-to-computer connections, has resulted in a parallel development in the use of codes for transmitting numerical forecast data from one centre to another (Fig. 1). The most widely used code form is WMO GRID code (FM 47-V) which was devised for use on low-speed lines, using a character-based format, with relatively high overheads associated with possible output on line-printer devices. The majority of coded bulletins from Bracknell are in this format, and will remain so for the forseeable future; however, more efficient forms have been devised (see below) which should prove attractive enough for a major change in emphasis over the next five years. GRID code forms the mainstay of the network between national weather centres in Region VI.

The data required for flight planning purposes by airlines have traditionally been supplied in Aviation

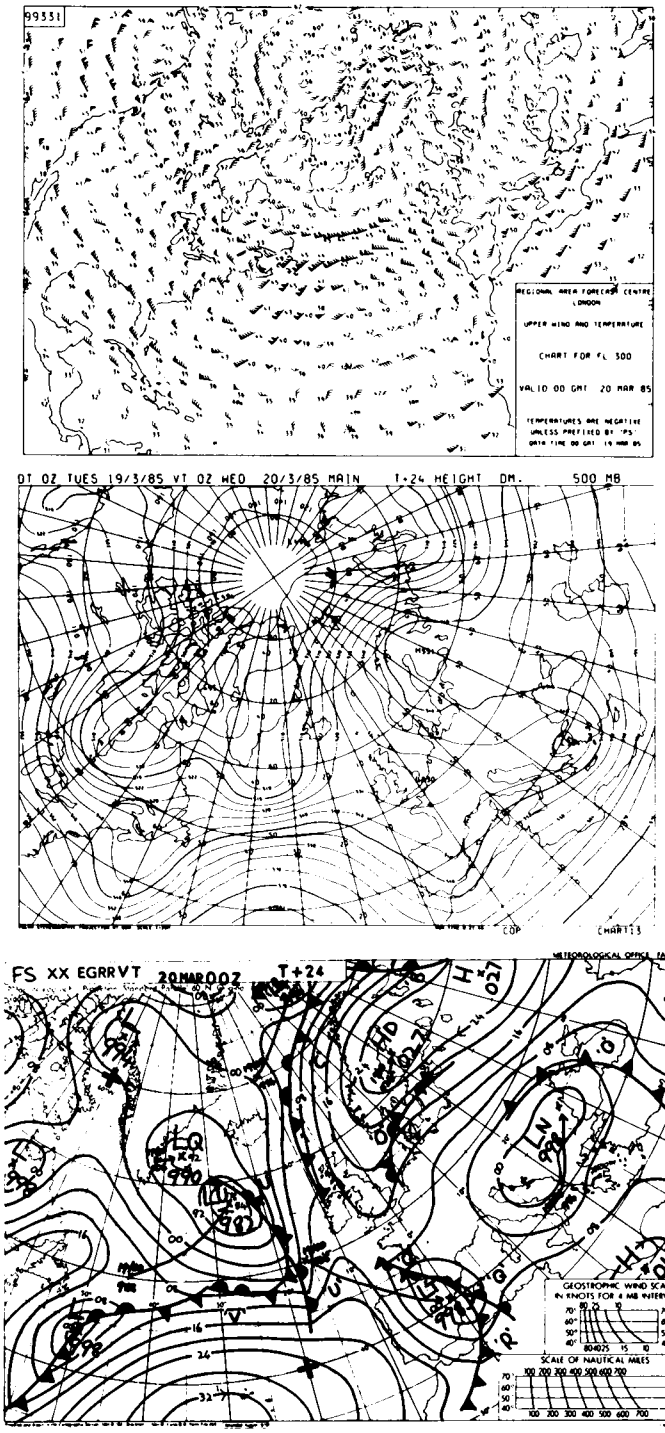

Figure 2. Examples of forecast charts.

Table II. *List of available chart products using Analogue Facsimile transmissions*

In the following tables all the computer-produced charts are based on data from the global numerical weather prediction model. Most of the subjectively drawn charts (M) are also largely based on the products of the same model or its derivatives.

(a) *Analysis products*

Field identifier	Reference time (GMT) and area of coverage (see Table III) 00	06	12	18	Method of production (Machine contours — C, Manual input — M)
Surface pressure, with front and centres	F D	F	F	F	M M
850, 700, 500, 300, 200 and 100 mb contours, and 500–1000 mb thickness	A		A		C
500 mb contours	D				M
500 mb contours and 500–1000 mb thickness	H		H		C
Sea surface temperature	M				M
Sea ice			E		M
State of sea	G		G		M

(b) *Forecast products*

	Data time	Validity time (hours after data time) and area of coverage (see Table III) 18	24	48	72	96	120	Method of production (Machine contours — C, Grid data — G, Manual input — M)
Surface pressure, with fronts and centres	00		F	C	C			M
	06		F					M
	12		F	C	C	C	C	M
	18		F					M
850, 700, 500, 300, 200 and 100 mb contours	00		A					C
	12		A					C
500–1000 mb thickness	00		A					C
	12		A					C
Winds and temperatures (DDFFFTT) at 850, 700, 500, 400, 300, 250 and 200 mb	00	K	K					G
	12	K	K					G
Winds and temperatures (DDFFFTT) at 500, 300, 250 and 200 mb	00	B	B					G
	12	B	B					G
Significant weather (jets, tropopause, CAT, etc.)	00	B						M
	06	B						M
	12	B						M
	18	B						M
State of sea (wave height, direction)	00		G					M
	12		G					M

Table III. *Bracknell (Regional Meteorological Centre) — list of chart areas. The projection used for all of these charts is Polar Stereographic.*

Code letter	Area				Scale in millionths
A	(48°N, 145°W)	(32°N, 68°E)	(18°N, 12°E)	(28°N, 71°W)	1:20
B	(28°N, 145°W)	(24°N, 54°E)	(09°N, 05°W)	(02°N, 84°W)	1:20
C	(42°N, 90°W)	(66°N, 90°E)	(30°N, 20°E)	(20°N, 40°W)	1:30
D	(29°N, 155°W)	(28°N, 63°E)	(08°N, 06°W)	(08°N, 85°W)	1:30
E	(57°N, 96°W)	(71°N, 71°E)	(46°N, 14°E)	(38°N, 48°W)	1:10
F	(69°N, 111°W)	(37°N, 50°E)	(19°N, 10°E)	(34°N, 55°W)	1:20
G	(42°N, 112°W)	(60°N, 32°E)	(28°N, 10°W)	(21°N, 74°W)	1:20
H	(80°N, 05°W)	(44°N, 32°E)	(28°N, 05°W)	(43°N, 41°W)	1:20
K	(53°N, 50°W)	(53°N, 65°E)	(26°N, 34°E)	(26°N, 18°W)	1:17
L	(31°N, 20°W)	(23°N, 150°E)	(06°S, 102°E)	(05°S, 33°E)	1:36
M	(67°N, 37°W)	(70°N, 18°E)	(47°N, 07°E)	(45°N, 19°W)	1:5

Digital Forecast (ADF) code. ADF was designed for a specific purpose and thus differs from GRID code (and its successors) in that the data are arranged in columns rather than in horizontal fields. The code uses a 'packed-decimal' format, i.e. more efficient than GRID code, but is still character based and thus carries a large overhead penalty. Bracknell currently provides forecast data in this code form to British Airways, Scandinavian Airlines System, and the Société Internationale de Télécommunications Aéronautiques.

In order to exchange the very large amounts of data required for the operation of the WAFS it was necessary for a much more efficient code form to be devised. As an interim measure Bracknell and the National Meteorological Center in Washington developed a bit-orientated code form, H code, which was implemented between the two centres in 1984. Subsequently WMO extended and developed the concept; a more widely agreed bit-orientated code, GRIB (GRIdded Binary), was ready for use at Bracknell from 1 January 1985, and the complete switch-over from H code took place in April 1985. This bit-orientated code has been designed for use on fully automated computer-to-computer systems and is compatible with the more efficient telecommunication protocols required for transmission on high-speed lines. The supply of data from Bracknell to automated systems (OASYS) at London Weather Centre and Heathrow Airport is an example of this computer-to-computer facility. The major part of the Bracknell coded products list is now available in GRIB code.

(c) *Products available in code*

Table IV contains a concise summary of the products that are currently available in coded form from Bracknell. Three distinct classes of product are identified: those taken from the fine-mesh NWP model, primarily for use in WMO Region VI; regional products from the global coarse-mesh NWP model, again for use in Region VI and extending into the medium range; and global products from the coarse-mesh model, formulated primarily for use in the WAFS but also available for supply to other interested users. Details of the elements contained in the bulletins, areas covered, bulletin resolution and forecast times are all to be found in Table IV.

The most recent additions to this list of products are the very-high-resolution ($1\frac{1}{4}° \times 1\frac{1}{4}°$, every 3 hours) bulletins taken from fine-mesh NWP model data. The Royal Netherlands Meteorological Institute requested such data for input to a scheme being developed for forecasting of maritime weather and state of sea conditions along the Dutch coast. Other recent requests for data, which have been met by bulletins from the extensive range available at Bracknell, came from Zimbabwe, Mauritius, Hong Kong and the Seychelles.

Table IV. *List of available forecast fields from Bracknell.*

Forecast runs are made from both 00 and 12 GMT data time. Bulletins are coded in WMO GRID (FM 47-V). Details of bulletin headings and contents can be supplied on request, including details of GRIB-code bulletins.

	Regional fine-mesh products	Regional coarse-mesh products	Global coarse-mesh products
Elements	Surface pressure, surface wind (10 m), accumulated precipitation. Heights, winds and temperatures for 850 and 500 mb.	Surface pressure, surface wind (10 m). Heights, winds and temperatures at 850, 700, 500, 400, 300, 250, 200, 150, 100 mb.	Surface pressure, surface wind (10 m), 500 mb height. Maximum wind and tropopause. Winds and temperatures at 850, 700, 500, 400, 300, 250, 200, 150, 100 mb.
Areas	The 3 areas all span 32½°N to 75°N. The longitudes covered are 70°W to 35°W (area W or 255), 35°W to 0° (area X or 256), 0° to 35°E (area Y or 257).	There are 5 areas. Four span 25°N to 75°N; the longitudes are 90°W to 45°W (area Z or 205), 45°W to 0° (area N or 206), 0° to 45°E (area O or 207), 45°E to 90°E (area P or 208). The fifth area (area I or 201) covers 75°N to 90°N and 90°W to 90°E.	There are 16 areas. In each hemisphere there are two polar areas covering latitudes 70° to 80° and 80° to 90° and 4 mid-latitude areas spanning 20° to 70° in quadrants. A further 4 areas spanning 20°N to 20°S cover the tropical belt.
Resolution	The data are normally supplied on a latitude–longitude grid at 2½° resolution. 1¼° resolution is available if required for fields of surface pressure, wind and precipitation.	The data are supplied on a latitude–longitude grid with a 2½° resolution. For the polar area (area 201), the resolution is 2½° latitude by 10° longitude.	The mid-latitude areas are at a resolution of 2½° latitude by 5° longitude; the tropical belt is at 5° latitude by 5° longitude. In the polar regions there is reduced longitudinal resolution.
Forecast times	Fields are available at 6-hour intervals from the analysis (T+0) to a forecast time of T+36. Fields of surface pressure, wind and precipitation are available at 3-hour intervals on the finer grid.	Fields are available at the following forecast times: T+0, T+6, T+12, T+18, T+24, T+30, T+36, T+42, T+48, T+60, and T+72. In addition, surface pressure and 500 mb height are available at T+96 and T+120.	Fields are available at 6-hour intervals from the analysis (T+0) to a forecast time of T+48. In addition surface pressure and 500 mb height are available at T+60, T+72, T+96, and T+120.

5. Back-up arrangements

Although modern computing systems are very reliable and have operational performance figures that approach 100% it is still inevitable that occasions will arise when the computing facilities at Bracknell, especially the Cyber 205 used for running the numerical models, are non-operational. At such times there is a need for reliable back-up arrangements, so that both chart and coded products can be supplied to the user without noticeable interruption. A computer outage of less than 12 hours is covered by ensuring that forecast data (in required formats) are routinely prepared for a period of 12 hours beyond that normally required. By storing the data on the front-end processing system it is then possible to supply operational users on the basis of a 12-hour-old forecast run without the users becoming aware of it.

To ensure coverage beyond 12 hours there is a mutual exchange of global forecast data between Bracknell and Washington, using GRIB code as a medium. Data from Washington arrive at Bracknell too late to be used operationally in real time, but after decoding and storage in a compatible output data set they can be used to give an almost complete range of products, although again from a 12-hour-old forecast run.

The obvious omissions from the product list when operating in a back-up mode are those from the fine-mesh NWP model. Although in the recent past it has proved possible to run versions of the previous Bracknell NWP model on the front-end processors, this is now considered to be increasingly unsatisfactory and other sources of high-resolution forecast data are required. It is possible that other members of Revion VI will be able to supply such data for back-up purposes.

References

Dutton, M. J. O. 1980 Probability forecasts of clear-air turbulence based on numerical model output. *Meteorol Mag*, **109**, 293–310.

Gadd, A. J. 1985 The 15-level weather prediction model. *Meteorol Mag*, **114**, 222–226.

THE METEOROLOGICAL MAGAZINE

No. 1357 August 1985 Vol. 114

CONTENTS

NOTICE

It is requested that all books for review and communications for the Editor be addressed to the Director-General, Meteorological Office, London Road, Bracknell, Berkshire RG12 2SZ and marked 'For Meteorological Magazine'.

The responsibility for facts and opinions expressed in the signed articles and letters published in this magazine rests with their respective authors.

Authors wishing to retain copyright for themselves or for their sponsors should inform the Editor when they submit contributions which will otherwise become UK Crown copyright by right of first publication.

Applications for postal subscriptions should be made to HMSO, PO Box 276, London SW8 5DT.

Complete volumes of 'Meteorological Magazine' beginning with Volume 54 are now available in microfilm form from University Microfilms International, 18 Bedford Row, London WC1R 4EJ, England.

Full-size reprints of Vols 1–75 (1866–1940) are obtainable from Johnson Reprint Co. Ltd, 24–28 Oval Road, London NW1 7DX, England.

Please write to Kraus Microfiche, Rte 100, Millwood, NY 10546, USA, for information concerning microfiche issues.

HMSO Subscription enquiries 01 211 8667.

Printed in England for HMSO and published by
HER MAJESTY'S STATIONERY OFFICE

£2.30 monthly

Dd. 738362 C14 8/85

Annual subscription £27.00 including postage

ISBN 0 11 727562 X
ISSN 0026–1149

THE METEOROLOGICAL MAGAZINE

OPERATIONAL NUMERICAL FORECASTING

Evaluation and Applications

HER MAJESTY'S STATIONERY OFFICE

September 1985

Met.O.967 No. 1358 Vol. 114

METEOROLOGICAL OFFICE Met.O.967

THE METEOROLOGICAL MAGAZINE

No. 1358, September 1985, Vol. 114

Operational numerical forecasting: evaluation and applications

This issue of the *Meteorological Magazine* is devoted to four articles on the evaluation of results from the Meteorological Office's operational numerical prediction models and on applications of the numerical models to forecasting and other services. These articles form a sequel to those on the numerical forecasting system itself which appeared in the previous issue of the *Meteorological Magazine*.

The first article deals with the evaluation of forecasts and demonstrates the improving performance of numerical prediction over the years as well as some characteristics of the errors that remain. The second article shows how the improved numerical guidance is used in a 'man–machine mix' approach to public service forecasting of surface weather in the Central Forecasting Office at Bracknell. Upper-air forecasts for civil aviation, which are the subject of the third article, are very largely based on the direct use of numerical products, though the human forecaster plays an important role in the preparation of significant-weather charts. In the final article attention turns to the application of numerical forecasts of sea surface waves and storm surges to a wide range of marine services.

551.509.5

Forecast evaluation

By C. R. Flood

(Assistant Director (Public Services), Meteorological Office, Bracknell)

Summary

This paper shows results of a number of evaluation statistics produced routinely by the Meteorological Office to monitor the forecasts. Changes in the forecast skill over a period of 20 years or more are examined. The impact and performance of the operational numerical models currently run at Bracknell are discussed, but no attempt is made to compare the results with those from models run at other major centres.

Introduction

Although it is difficult to produce consistent and meaningful evaluations of weather forecasts, there are excellent reasons for attempting to do so. The professional customers, the public and the meteorologists all need to know the capabilities and limitations of weather forecasting since these may well influence decisions taken. On a different level, those involved in producing forecasts need to be able to assess the effects of possible changes to their forecast system (changes to the observing network or to the numerical model, for example).

Problem of evaluation

Evaluation is by no means straightforward even for the numerical forecast fields which are conveniently stored on the computer for analysis. The main difficulty is what to use as the truth. One possibility is to use observations. This is attractive in many ways but there is a danger of biasing the statistics to the areas where observations are concentrated and there is the problem of how to deal with erroneous observations. Some form of quality control is needed to exclude the rogues, which can otherwise have a significant effect (for example on a root-mean-square error), but where should the line be drawn? In addition, long-term statistics may be influenced by changes in the quality of the observations, irrespective of whether the forecasts are thereby improved.

An alternative is to use the numerical analyses as truth. Here the question marks lie over the character of the analysis and there is the danger of a self-fulfilling prophecy. In areas where there are few or no data, the analysis must inevitably rely heavily on the 6- or 12-hour forecast from the previous run of the model. More subtly, such matters as the smoothness of the analysis and the extent to which the observations are fitted by the analysis can affect the figures produced even if the forecast is unchanged.

It can be seen that comparisons may be misleading unless figures are produced in an identical fashion. Nevertheless, when used with care, the forecast evaluation statistics have proved to be generally reliable over the years and extremely useful. For example, a few weeks' figures can on occasion lead to the detection of an unwanted side effect from a change to the numerical forecast suite.

Long-term improvements

One aspect of evaluation is to be able to monitor progress over the years. This can be seen most readily from the numerical model forecast results. Fig. 1 shows the root-mean-square height error of the 500 mb 48-hour forecasts for the area shown in Fig. 2 for each year since 1967. The different symbols

represent the different models in operation, from the limited-area 3-level model (Bull 1966) to the 300 km resolution 10-level hemispheric model (Burridge and Gadd 1977) and the current 150 km resolution 15-level global model. Changes during the lifetime of a model (of varying significance) are not shown.

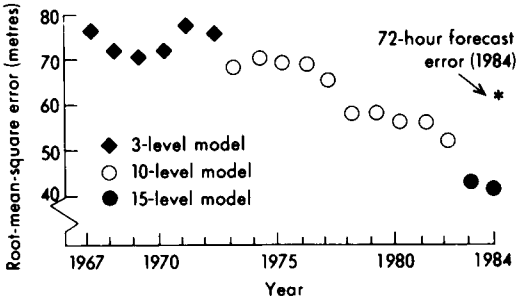

Figure 1. 500 mb height errors for 48-hour forecasts, verified using analyses. (Note that 1972 and 1982 were transition years.)

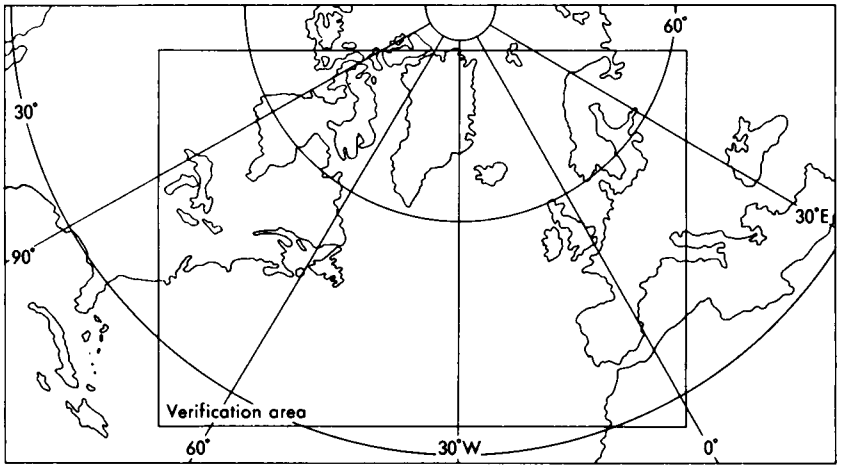

Figure 2. Map showing verification area (inset).

Even the 3-level model in the late 1960s showed distinct skill. This can be judged by comparing the root-mean-square (r.m.s.) error of 70–80 metres with the 'persistence error' of about 110 metres (the error which would have been obtained if the 48-hour forecast was simply one of no change from the initial conditions). The improvement in the figures since then is marked and it is interesting to note the current accuracy of the 72-hour forecast, shown by an asterisk on Fig. 1. The value of 62 metres is lower than for any of the 48-hour forecasts before 1978. Similarly the 1976 value of 42 metres for the 24-hour forecast was slightly higher than that for the 1984 48-hour forecast. This improvement in forecasting skill by 1 day out of 2 or 3 within 6 years or so is quite striking and is borne out by a wide range of evaluation statistics. Another example is shown in Fig. 3 which shows the increase in the 1000 mb height change correlation coefficient, i.e. the correlation between the height change from the initial conditions predicted to occur and that actually taking place. This is over the same area (Europe, the Atlantic and part of North America) and there is a separate line for each forecast period.

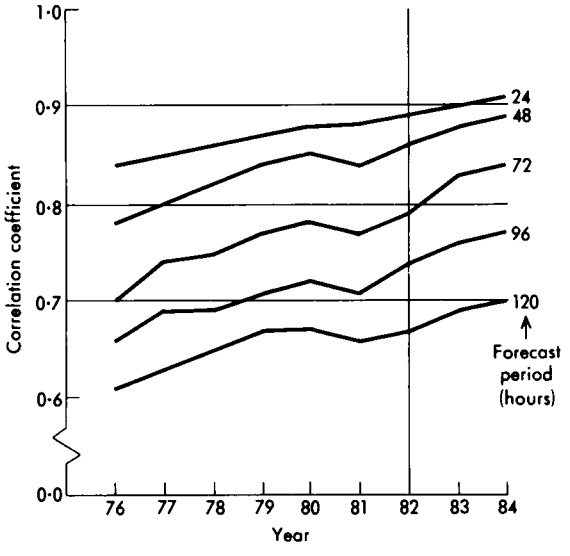

Figure 3. 1000 mb height change correlations for different forecast periods.

Long-term comparisons of a different kind may be made by considering the forecast errors of the position of fronts on 24-hour surface prognoses. In an internal paper by B. C. V. Oddie figures are quoted for each year from 1951 to 1960; these vary somewhat but 110 nautical miles (n mile) is a mean figure. In a similar exercise carried out in the winter of 1983/84, the figure was about 50 n mile, with 84% of cases showing errors less than 100 n mile. This is a substantial improvement. Although the forecast frontal positions continue to be produced subjectively, the positions inferred from the numerical model products now play a major part. The 850 mb wet-bulb potential temperature field is considered the most useful tool and is regarded as very good guidance by the forecasters (Woodroffe 1984).

A contribution to the improvement in all these evaluation figures comes from changes in the observation network (for example the introduction and subsequent improvement of the satellite soundings in the late 1970s) and from a better understanding of the atmosphere. However, the primary influence has been the considerable advances in numerical modelling. Alongside the research effort, the developments in computer technology have been a necessary ingredient. The much faster computers have allowed the use of finer horizontal and vertical resolutions and a more realistic representation of the physical and dynamical processes. The current global model with about a third of a million grid points produces forecasts quicker than the 3-level model did with fewer than six thousand grid points.

Impact on forecasting

In the case of upper-air forecasts, the numerical products have reached the stage where it is difficult for the forecaster to add very much, at least in terms of forecasting upper winds and temperatures. A study in 1983 showed that when the forecaster made changes to the 12-hour 'spot wind' forecasts for civil aviation (which he attempted for less than 10% of the values), only 51% were for the better. The forecaster had some success with amending the 18-hour numerical forecasts; the corresponding figure was 70%, but this was with the advantage of later data (i.e. the subjective forecast was really only for 12 hours ahead). Although delineation of the significant weather areas remains in the forecaster's domain, most upper-air forecasts for civil aviation are now pure numerical products.

For forecasts of surface weather which are of prime interest to many users, not least the general public, the forecaster has an important contribution to make. While the improvement in forecasting surface fronts has been noted above, this does not always translate into better weather forecasts. After all, even if the forecaster is presented with a perfect surface prognosis, there is still scope for error in terms of the surface weather. For example, in a thundery situation it is difficult to assess even 24 hours ahead the amount of activity, how widespread it will be and so on. Dramatic differences can take place with quite subtle changes in air mass characteristics or air movement, quite apart from the problem of the large variations which occur over small distances in this type of situation.

Although attempted, subjective evaluations of weather forecasts have proved to be rather unreliable. With one method a whole series of forecasts was re-marked several years later; although the same guidelines were used it was apparent that standards had changed meanwhile, perhaps as a result of different expectations of what could be achieved. An objective statistic which bears on the question is shown in Fig. 4. These are the results of a simple question posed to the Senior Forecaster each afternoon: will it rain in the London area (more precisely at either of two specific rain-gauges) between 0600 and 1800 tomorrow? While there is a certain chance element, especially in a showery regime, the marking system has the merit of objectivity and statistics are available back to 1962. Setting aside 1970 (a difficult year?) the general improvement probably results from improved numerical model guidance. In this case the effect of the 'man–machine' mix in forecasting can be seen; the M (74% for 1984) represents the value if the model guidance had been followed literally. The difference from the 83% actually achieved would not be so apparent in other parameters, e.g. surface pressure or wind, and it should also be said that the model was modified in May to reduce the overforecasting of small amounts of rain. The model figure for May to December 1984 is 77%, which is very comparable with the Senior Forecasters' scores using the 10-level model.

A more dramatic improvement can be seen in the longer term-forecasts (2–5 days ahead). Fig. 5 gives an indication of how the forecasts deteriorate as the forecast period lengthens. As with Fig. 1 this uses the r.m.s. 500 mb height error (but again other parameters show the same effect). The errors of a 'persistence forecast' are included as a yardstick. Comparison of the 1974 and 1984 values shows that for the longer-period forecasts there is a gain of about 2 days, i.e. the 1984 5-day forecast is only marginally worse than the 1974 72-hour forecast. This very much bears out the experience of the forecasters. Of

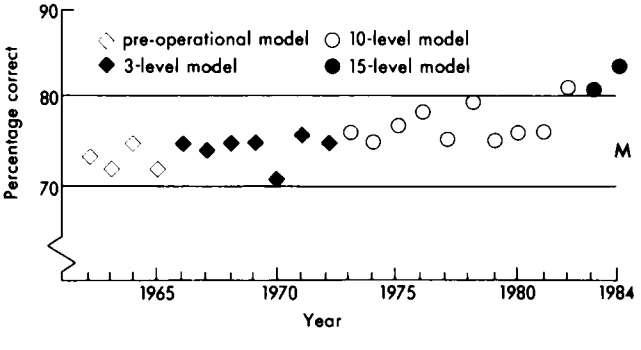

Figure 4. Percentage of correct London precipitation forecasts for the next day. Forecasts produced subjectively; symbol indicates model guidance available. M indicates score directly from the fine-mesh model in 1984.

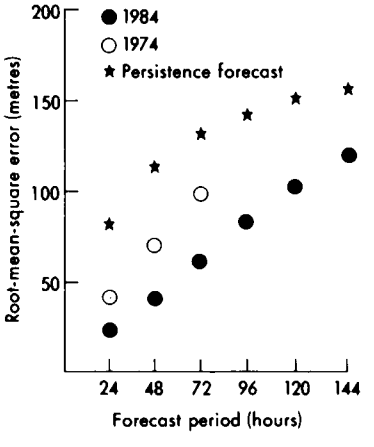

Figure 5. 500 mb height errors for forecasts of different periods (verified using analyses).

course, it depends considerably on what is required by the user (some requirements are very exacting), but there is now good and justifiable confidence in the evolution of the forecast out to day 3 in a way which was not apparent 10 years ago. The 5-day forecasts too have considerable merit, though clearly they need to be used more cautiously. The forecast of the character of the weather is sufficiently good and detailed to be useful to farmers in planning the week's work. The same is true for the offshore industry and in certain situations it is possible to forecast a 'weather window' of several days with winds remaining below a critical threshold, as has been demonstrated in practice during the towing out of some of the very large oil rigs.

15-level model performance

The statistics in this section largely relate to 1984 and indicate how the errors vary in space and time.

Fig. 6 shows the way the temperature and wind errors vary in the vertical. For wind these are r.m.s. vector errors, i.e. taking into account direction as well as speed errors. The figures relate to the same area as in Fig. 2 but are based on comparisons with observations; r.m.s. errors against analyses are generally a little lower, though there is fair agreement between the two. The wind errors peak noticeably at the main jet-stream levels around 250 mb. Temperatures behave similarly though with a less pronounced maximum. The aviation community is a major user of upper-air forecast information. Improvements of forecast accuracy here have a direct bearing on fuel savings resulting from better flight planning. Fig. 7 shows the change over the last 5 years for the winds and temperatures at 200 mb, again verified against

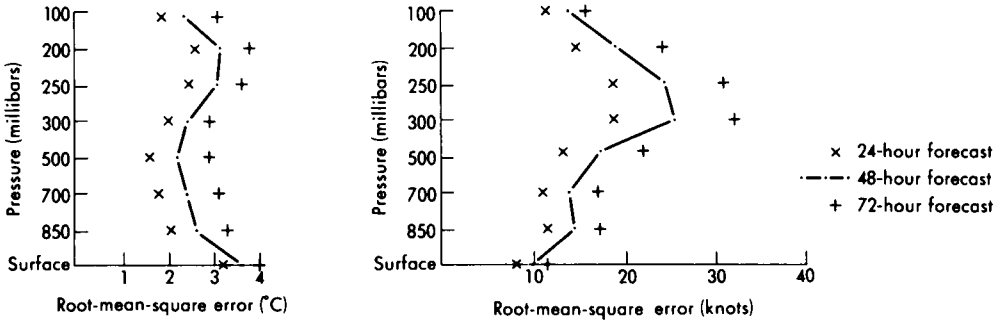

Figure 6. Temperature and wind errors (verified using observations), 1984.

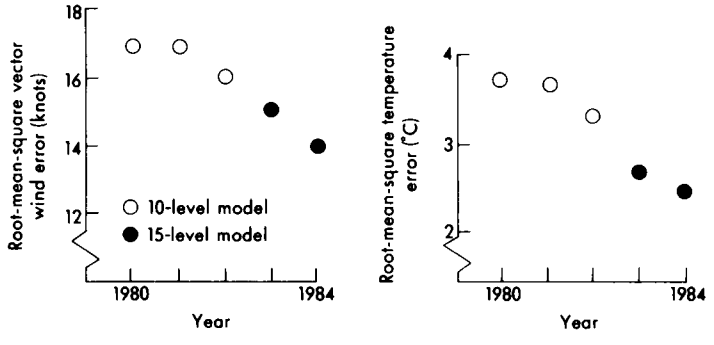

Figure 7. 200 mb wind and temperature errors for 24-hour forecasts (model changed September 1982).

observations. Although 1984 was the best year on record the improvement is maintained into 1985 with r.m.s. errors reduced by a further 1–2 knots in each of the first 3 months of the year compared with the corresponding months in 1984.

Returning to Fig. 6 and looking at the surface, it can be seen that the winds are generally very good. Of course the particular location is important and in the stormy mid-Atlantic r.m.s. vector wind errors at the surface are just over 10 knots for 24-hour forecasts and about 13 knots for 48-hour forecasts. The importance of the wind direction in the vector error can be judged by comparing these with the corresponding r.m.s. wind speed errors of 6 knots at 24 hours and 8 knots at 48 hours for the same stations. The surface winds are used extensively in forecasting for shipping and the offshore industries. They are also the vital input to the numerical wave models, the accuracy of which is quoted elsewhere (Francis 1985). The considerable variations of surface temperature are not so well captured by the model and r.m.s. errors are about 3 °C at 24 hours. Model changes to the radiation scheme and the boundary-layer physics are expected to lead to improvements. A contributory factor is also the significant mean errors, especially for stations whose heights differ from the somewhat smoothed topography in the model.

So far, for convenience, the evaluation statistics have all related to the same area. Fig. 8 shows the latitudinal variation of the errors. These are very much related to the natural variability of the atmosphere and the surface-pressure and 500 mb height errors show a distinct minimum in tropical regions. The smaller atmospheric variability is reflected in much lower errors from a persistence forecast; at 24 hours these vary from 7.2 mb for 30–90°N, 2.1 mb for 30°N–30°S to 8.1 mb for 30–90°S.

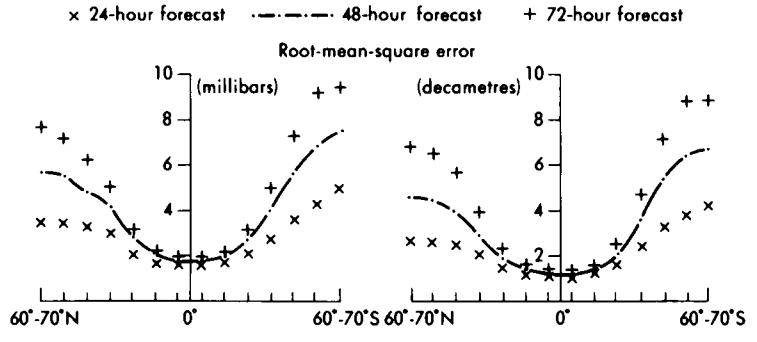

Figure 8. Surface pressure and 500 mb height errors by 10° latitude bands, 1984.

Considered as a percentage of the persistence error, numerical forecasts in tropical areas are poorer than those in higher latitudes; other parameters of more relevance to forecasting in the tropics, e.g. the 850 mb wind, show the same effect. It is interesting to compare the two hemispheres. The persistence errors (measured over a year to avoid seasonal effects) are similar, though a little larger in the southern hemisphere. The observing network, on which the forecasts are based, is much sparser in the southern hemisphere. However, comparing the forecasts in mid-latitudes there is roughly only a 12–24 hours difference in forecast skill. Thus the southern hemisphere 2-day forecast error is smaller than the northern hemisphere 3-day forecast error. Linking this with the conclusion from Fig. 1 it is not unreasonable to suggest that the southern hemisphere forecasts are as good as those in the northern hemisphere were in the late 1970s.

Variations through the year are shown in Fig. 9. Bearing in mind this is for the area in Fig. 2 (mostly north of 30°N) the surface-pressure error changes are not unexpected, reflecting the quieter summertime

conditions. The difference between January and December (both 1984) is a little unreal as a significant model change in December reduced errors by about 0.5 mb at 24 hours and about 1 mb at 72 hours judging from 1985 results. There is much less annual variation in the upper-wind errors and there is some evidence of the rather random month-to-month variability, perhaps dependent on the synoptic situation. The relatively flat curve is a little surprising with the strong jet streams in winter; however, the jets are also more coherent and are generally below 200 mb in the area concerned.

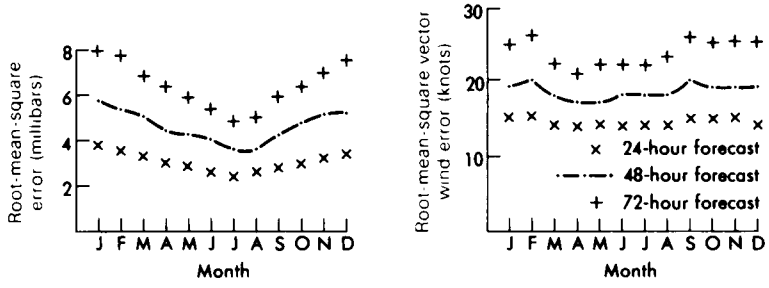

Figure 9. Surface pressure and 200 mb wind errors month by month in 1984.

Conclusions

It is clear that numerical forecasts have improved markedly since their operational inception in the mid-1960s and have become a major tool in forecasting for all but the shortest forecast periods, up to 6 hours. For the bulk of upper-air forecasting the numerical products are such that they can be issued directly with little reference to the forecaster. For surface weather forecasts, the 'man–machine mix' continues to be very important. Even so, much greater reliance is now placed on the model products and the improved standard of forecasting, particularly for parameters which are well related to the synoptic pattern (e.g. surface wind and frontal rainfall), is apparent. There is clearly scope for further improvement — but the signs are healthy and the positive trend in forecasting is expected to continue.

References

Bull, G. A. 1966 Three-parameter atmospheric model used for numerical weather prediction. (Unpublished, copy available in the National Meteorological Library, Bracknell.)

Burridge, D. M. and Gadd, A. J. 1977 The Meteorological Office operational 10-level numerical weather prediction model (December 1975). *Sci Pap, Meteorol Off*, No. 34.

Francis, P. E. 1985 Sea surface wave and storm surge models. *Meteorol Mag*, **114**, 234–241.

Woodroffe, A. 1984 Short-range weather forecasting — a current assessment. *Weather*, **39**, 298–310.

551.509.313

The models in action

By R. D. Hunt

(London Weather Centre)

Summary

A number of examples of fine-mesh and global model forecasts are shown, covering a wide range of weather situations. The results demonstrate the very good guidance which is given by the models to the forecasters in the Central Forecasting Office.

Introduction

Other papers in this issue describe the latest weather forecasting models developed by the Meteorological Office and the form in which the output from these models reaches the forecasters. This article gives an indication of how useful the models have been in providing assistance to the forecasters in both the short range (up to 24 hours ahead) and the medium term (up to 6 days ahead) by looking at examples of recent model forecasts in different weather situations.

The Central Forecasting Office (CFO) in Bracknell is responsible for producing forecasts in the form of charts and descriptive texts which are used by the forecasting offices in the United Kingdom as guidance for the preparation of detailed forecasts to the public, the media and many weather-dependent industries. Together with this national role, Bracknell also has a wider, international responsibility. As a Regional Meteorological Centre, Bracknell sends analyses and forecasts produced by CFO to other Meteorological Centres in Europe, while as one of the two World Area Forecast Centres, Bracknell provides forecasts to civil aviation for use in many parts of the world. CFO is therefore a major forecasting centre and it is vital that the products issued are of the highest possible standard. Since the autumn of 1982, the 15-level fine-mesh and global models have been available operationally and the output from the computer in the form of various forecast charts has been of great benefit to the forecasters.

The main fine-mesh model output consists of forecast charts at 6-hourly intervals up to 36 hours ahead; the charts are of surface pressure, rainfall and various other parameters needed to assist with the forecasting of frontal positions, surface temperature, the likelihood of showers and many other features of the weather. The output from the global model consists of a smaller range of products at 12-hourly intervals but going forward to 6 days ahead. Some examples of both are given below.

Example 1: 15 October 1983

Fig. 1 shows the analysis for midday on 14 October 1983. Most of the United Kingdom lay in a showery south-westerly airstream; parts of the east in particular were quite sunny. In the Atlantic a depression was about 600 miles west of Scotland with associated fronts moving eastwards towards Britain. The forecast for midday on 15 October produced by the fine-mesh model, based on data from midday on the 14th and available to the CFO forecasters during the afternoon of that day, is shown in Fig. 2. (It should be noted that the actual frontal positions as such are not predicted by the model but output is produced, such as the 850 mb wet-bulb potential temperature field, from which positions of fronts can be inferred.) The analysis for midday on the 15th is shown in Fig. 3 taken from London Weather Centre's *Daily Weather Summary*.

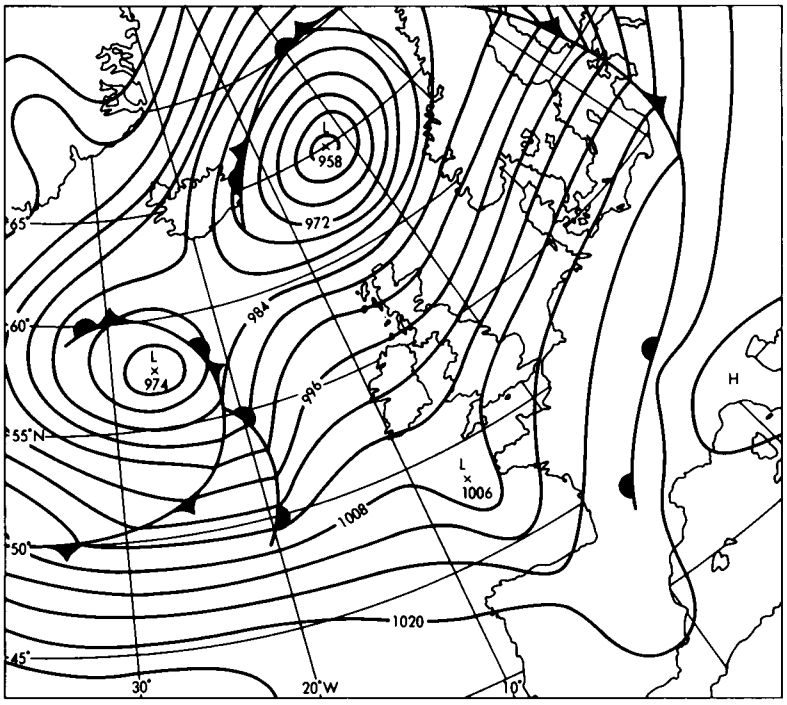

Figure 1. Analysis for 12 GMT on 14 October 1983.

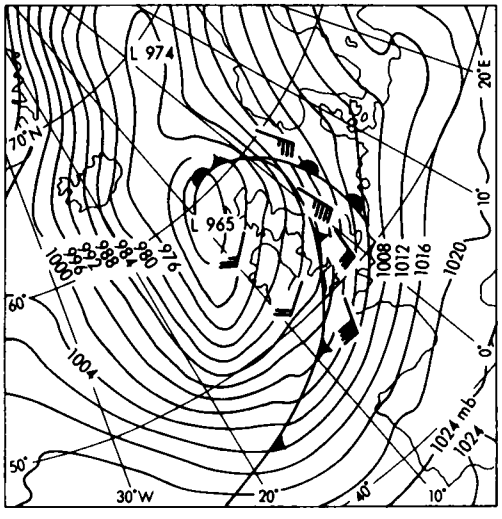

Figure 2. Forecast for 12 GMT on 15 October 1983, produced by the fine-mesh model and based on data from 12 GMT on the 14th.

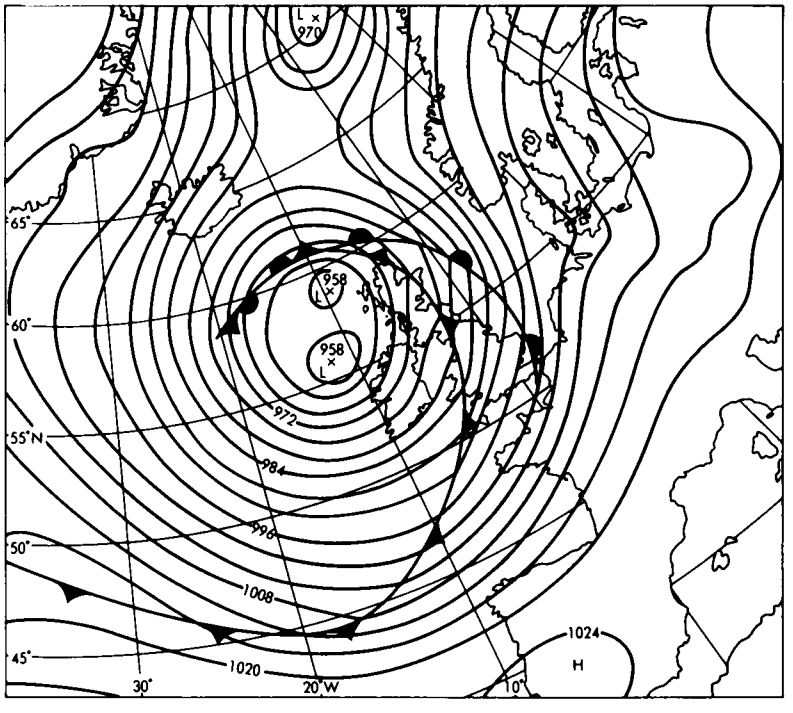

Figure 3. Analysis for 12 GMT on 15 October 1983.

The basic forecast pattern is clearly very good, although there are some differences between the forecast and the analysis. The positions of the fronts over the United Kingdom show good agreement although the forecast cold front is a little too far advanced, particularly in the North. Fig. 2 shows that the main depression near north-west Scotland was forecast to have only one centre of depth 965 mb whereas in reality there were two centres each about 7 mb deeper. Also the forecast has marked troughing in the isobars to the south-west of the main centre which Fig. 3 shows to be exaggerated.

The closeness of the isobars on the forecast chart indicates the model's prediction of winds of severe gale force in many places, but especially ahead of the cold front with a noticeable decrease in wind strength behind it. Fine-mesh surface wind forecasts at some locations are shown on the forecast chart. Fig. 3 shows that these important general features were correct; gusts of over 60 kn were reported widely during the day with a gust of 80 kn on the Isle of Wight. After the cold front passed the winds did decrease markedly, which is also evident from Fig. 3.

Looking at some other products, it can be seen that Fig. 4 shows the expected rainfall pattern at the verifying time. In this diagram, the circles represent dynamic rain of a continuous nature with the size of the circle being proportional to the intensity of the rain, while the convective rain, or showers, is represented by 'V's, again with appropriate size variation. This figure shows a large area of rain, quite heavy in places, associated with the cold front, and showers coming into Ireland and much of Scotland behind it. Smaller amounts of rain are associated with the warm front and the warm air. Fig. 5 shows where the rain was actually occurring at the time. Essentially the agreement is very good although there are some differences, the most notable being the spread of heavy rain across southern counties of England which actually occurred well ahead of the cold front. Rainfall totals predicted by the fine-mesh

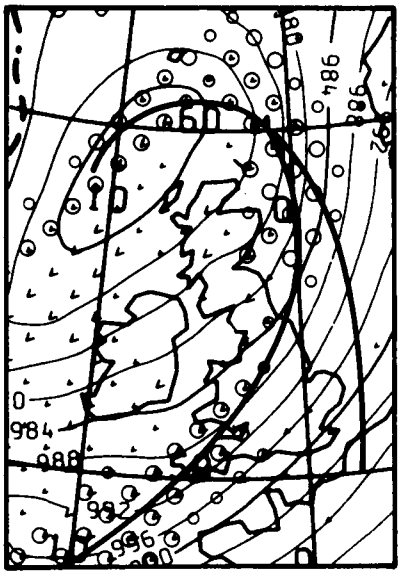

Figure 4. Expected rainfall at the verifying time of 12 GMT on 15 October 1983. Data time is 12 GMT on the 14th.

model for 15 October were widely in excess of 10 mm and over 20 mm in parts of the south and south-west; these totals were well representative of what actually occurred (although the rainfall distribution on that day showed large local variations due to topography which are inevitably smoothed out somewhat by the 75 km horizontal resolution of the model).

The forecast for 15 October then, based on the fine-mesh products from the previous day, successfully predicted widespread severe gales with heavy rain moving from west to east across the United Kingdom, followed by showers.

Example 2: 22 January 1984

Fig. 6 shows the analysis for 00 GMT on 21 January with a cold south-easterly airstream over most parts of Britain and with a depression well to the west moving north-eastwards. Figs 7 and 8 show the 18-hour and 30-hour fine-mesh forecasts from that time. The depression was expected to move northwards to the west of the United Kingdom, the associated frontal system bringing precipitation and strong winds across many parts overnight. These figures also include the 'snow probability lines' from the model based on the 1000–850 mb thickness field, indicating 20%, 50% and 80% probabilities that any precipitation falling will be snow. These probabilities require considerable interpretation, the chance of snow increasing not only on higher ground but also as the precipitation becomes heavier and more continuous. On this occasion the model was suggesting that much of the frontal precipitation would be sleet or snow at first with only south-west Wales and south-west England being outside the 20% line at 18 GMT on 21 January and much of the precipitation in the north falling within the 50%

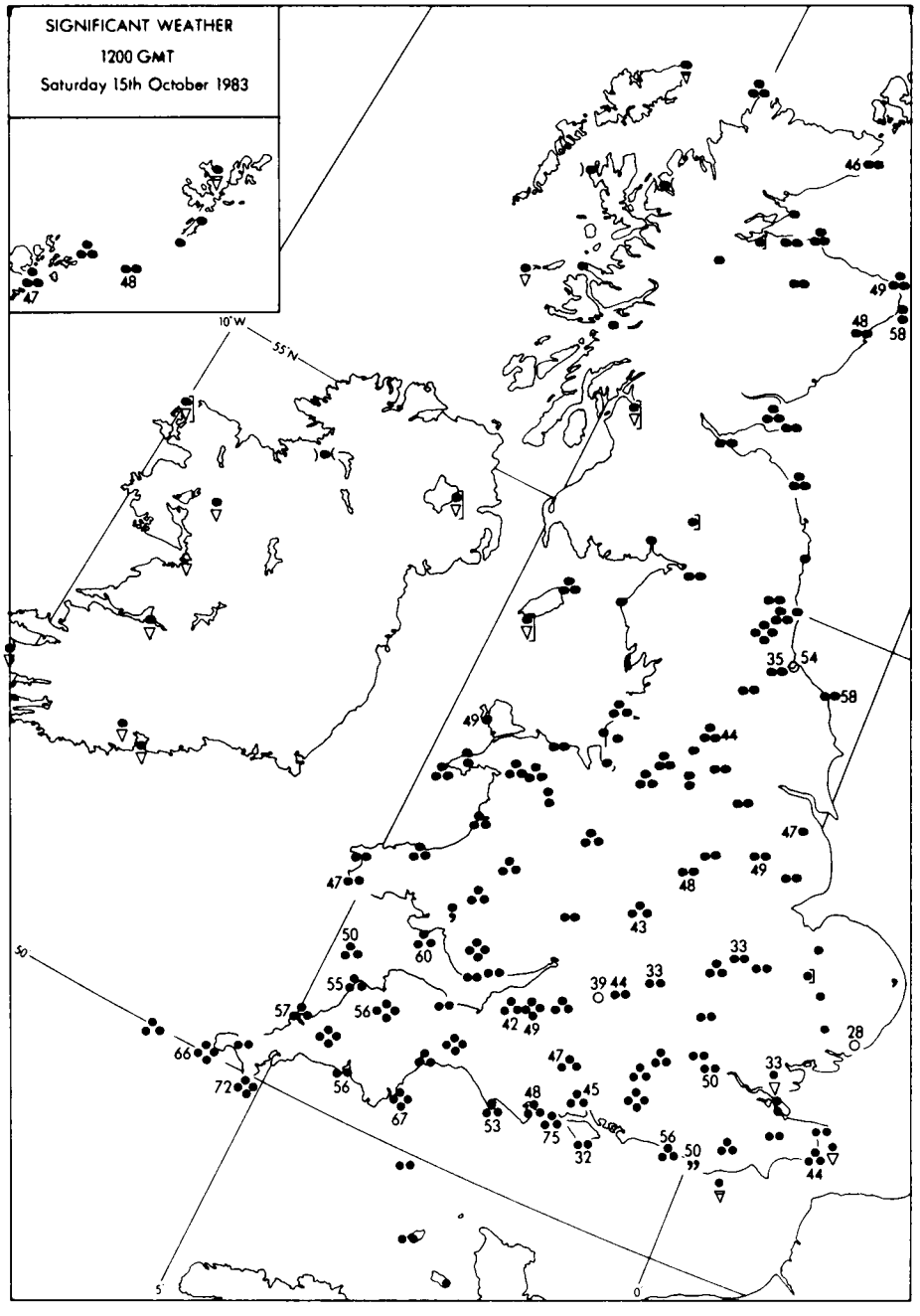

Figure 5. Actual distribution of rain at 12 GMT on 15 October 1983, the verification time of the forecast chart shown in Fig. 4. The figures on the chart are maximum gusts (kn).

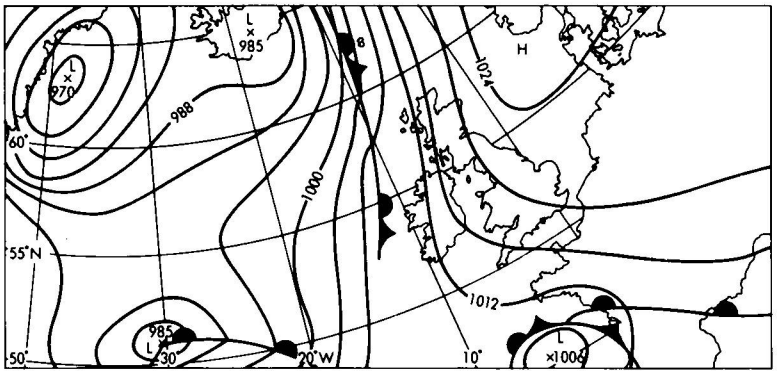

Figure 6. Analysis for 00 GMT on 21 January 1984.

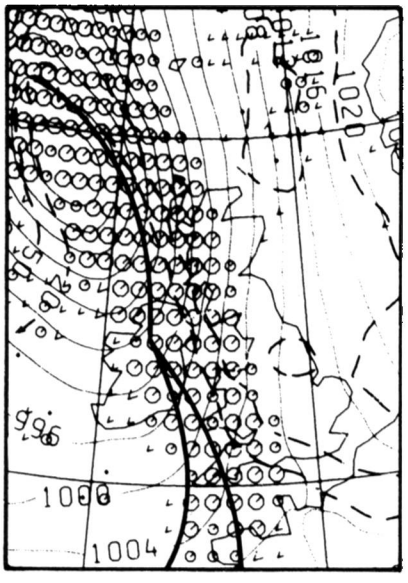

Figure 7. 18-hour fine-mesh forecast from 00 GMT on 21 January 1984.

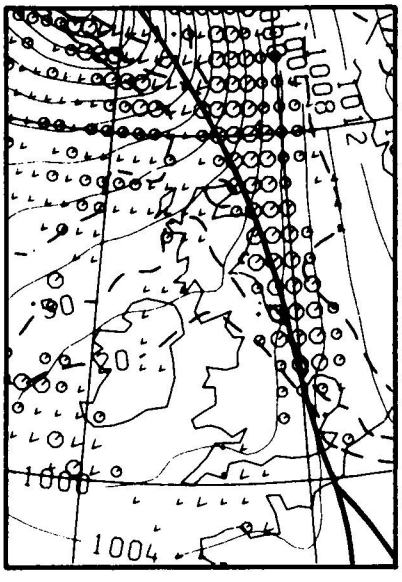

Figure 8. 30-hour fine-mesh forecast from 00 GMT on 21 January 1984.

line. During the night, however, the model was warming up the low-level air in central and south-western areas and the retreat eastwards of the 20% line suggested that the sleet or snow would turn to rain before dying out.

Fig. 9 shows the analysis at 06 GMT on 22 January, corresponding to the forecast shown in Fig. 8. The front is somewhat further west than the model had implied and the area experiencing precipitation was consequently slightly misplaced. However, precipitation fell as sleet or snow in many areas and with accompanying strong winds, considerable drifting of snow had taken place in the east and north leading to considerable disruption of transport. In more southern counties early snow had turned to rain while in some western areas the precipitation had died out to be followed by showers, wintry in the north-west, much along the lines of the fine-mesh forecast. The model forecast gave very good guidance in a critical situation of great importance to the public and sections of industry.

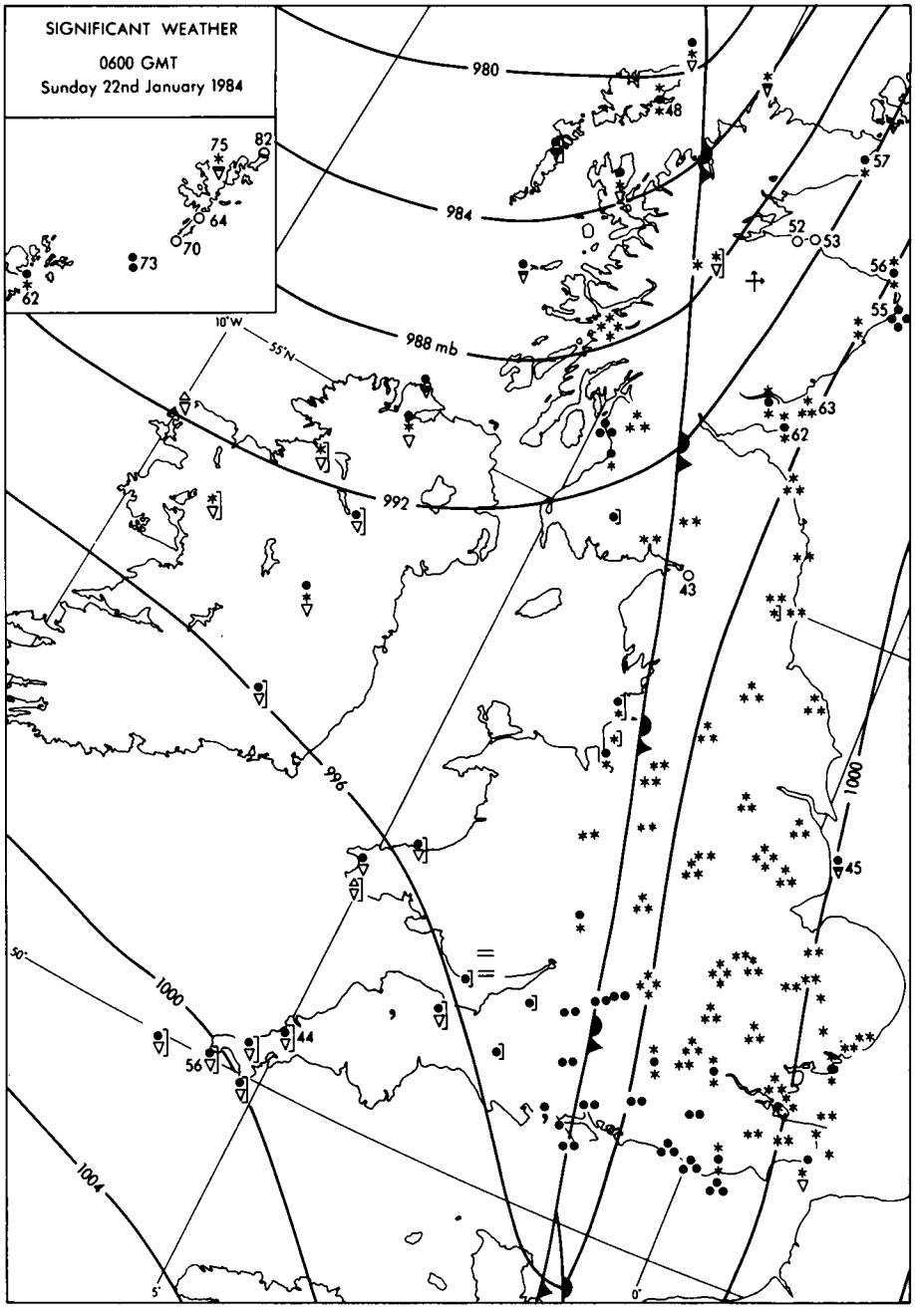

Figure 9. Analysis for 06 GMT on 22 January 1984, the verification time of the forecast shown in Fig. 8. The figures are maximum gusts (kn).

Example 3: 17 June 1984

At midnight on 16 June 1984 an anticyclone was centred over Northern Ireland and covered most of the United Kingdom, with a weak warm front having just crossed Scotland moving into the North Sea. The analysis is shown in Fig. 10. The fine-mesh forecast run at that time, however, showed that, despite the high surface pressure, showers were expected to develop in central and northern areas on the 16th and in the south-east on the 17th. The 36-hour forecast verifying at 12 GMT on 17 June is shown in Fig. 11. As well as indicating the approach of another warm front towards north-western areas, it also shows a number of shower symbols over England, particularly in the south-eastern quarter, with some large symbols indicating heavy showers. With high daytime temperatures in a summer month, forecasters interpreted this as a likelihood of thunderstorms, taking into account the other model output relating to atmospheric stability.

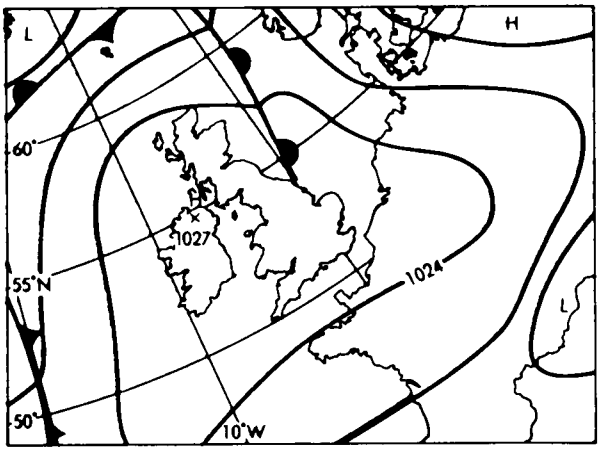

Figure 10. Analysis for 00 GMT on 16 June 1984.

By midday on the 17th scattered thunderstorms were developing over south-east England and by 18 GMT widespread storms were occurring in an area very similar to that shown by the model forecast for 6 hours earlier. Fig. 12 shows the distribution of thunderstorms between 12 and 18 GMT; some very large rainfall totals were reported, up to 60 mm locally, with some flooding and several lightning casualties. Once more there were errors in detail in the fine-mesh forecast. The model had developed the showers too early and produced some showers over northern England shown in Fig. 11 which failed to materialize. Also the light rain in Ireland ahead of the warm front is a little too far advanced. Nevertheless, the model had again given good guidance of the most significant weather event in the forecast period.

Global model example 1: 12 GMT on 18 May 1984

On 19 May 1984 a depression was forming over north Africa which developed as it moved northwards across Italy and central Europe during the following 2 days. It then developed a rather complex structure with one part turning westwards towards the United Kingdom and another section moving east and filling. The analysis for 12 GMT on 22 May is shown in Fig. 13; the centre of the depression was close to London with the associated warm front having crossed England from the east bringing rainfall in excess of 20 mm to many central and southern parts of the country. The low-pressure area subsequently turned

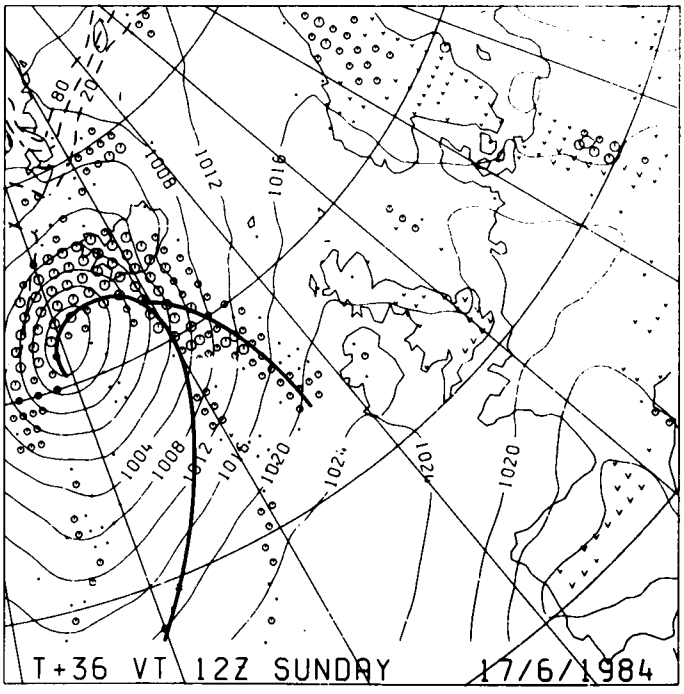

Figure 11. 36-hour forecast verifying at 12 GMT on 17 June 1984.

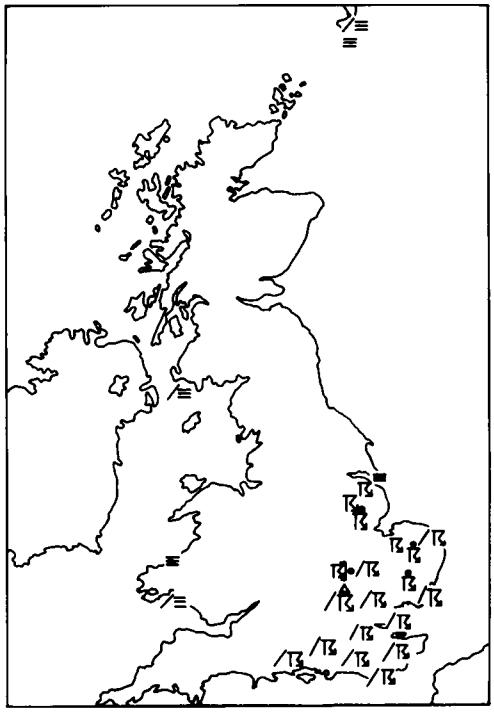

Figure 12. Significant weather at 18 GMT on 17 June 1984. Solidus denotes weather in previous 6 hours.

south-westwards towards Biscay. The track of the depression and the amount of rain associated with it made this a very unusual and particularly difficult situation to forecast.

Fig. 14 is the 96-hour forecast run at 12 GMT on 18 May and verifying at 12 GMT on 22 May. The global model had correctly predicted the development of the depression over north Africa, its track across Europe and its approach towards the British Isles from the east. In fact the forecast centre was rather too deep and its position a little too far to the north-east. Nevertheless, the forecast was considered to be remarkably accurate, particularly if the unusual nature of the development is borne in mind. Incidentally, the fine-mesh forecast runs from 21 May (not shown) were very successful in predicting the timing, areal distribution and quantity of rain on the following day.

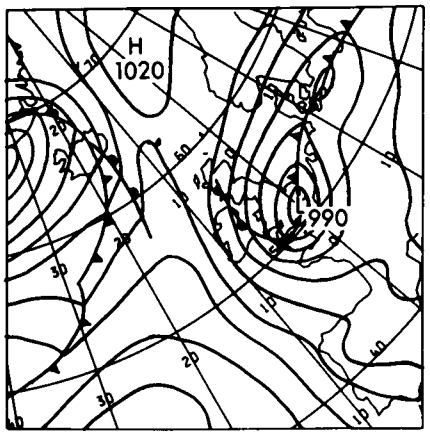

Figure 13. Analysis for 12 GMT on 22 May 1984.

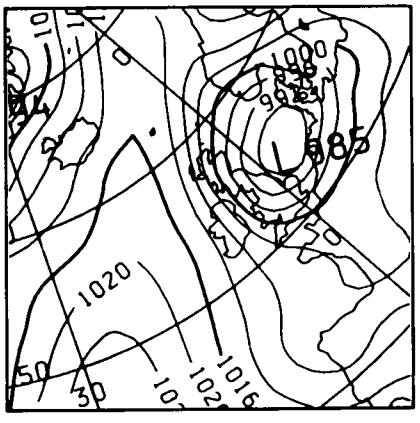

Figure 14. 96-hour forecast run at 12 GMT on 18 May and verifying at 12 GMT on 22 May 1984.

Global model example 2: 12 GMT on 30 August 1984

One of the most important aspects of forecasting several days ahead is to be able to predict significant changes in weather type. It is vital for forecasters to give as much advance notice as possible of, say, a change from dry, settled weather to changeable, wet weather or from warm to cold conditions. One such change of type occurred on 4 September 1984 when a prolonged spell of dry, warm weather over the southern half of England and Wales with mainly southerly winds gave way to a much cooler, northerly airstream, following the passage of an area of low pressure across northern England. Maximum temperatures over much of England and Wales were up to 9 °C lower than on the previous day giving the coolest day generally there since the end of June.

Fig. 15 gives the analysis for 12 GMT on 4 September showing the depression which brought about the change in weather approaching Denmark. The 5-day forecast verifying at that time, run at 12 GMT on 30 August is shown in Fig. 16. The general agreement is good, with the model showing the much cooler airstream established over the British Isles behind the cold front then over France. The position of the model's cold front, inferred from the 850 mb wet-bulb potential temperature field, is spectacularly accurate for 120 hours ahead. There are differences between the forecast and the verifying analysis of course. The model had taken the depression responsible for the change in weather across Scotland to southern Norway, the track being somewhat further north than was actually the case. The ridge of high pressure in the Atlantic had built more than the model had predicted allowing a stronger northerly gradient to be established over the United Kingdom. But these are essentially differences in detail which

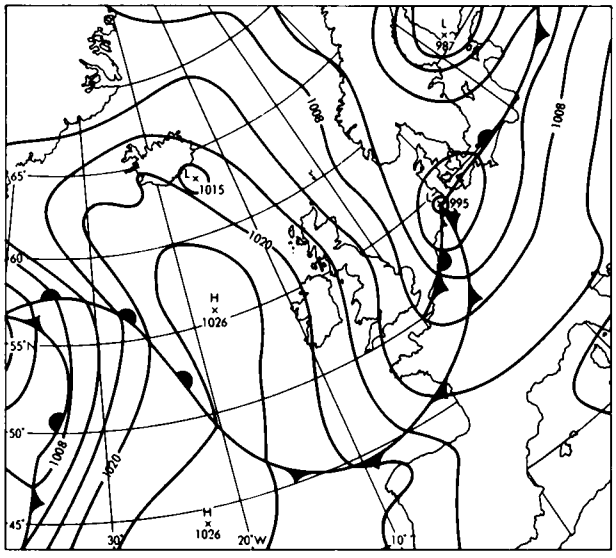

Figure 15. Analysis for 12 GMT on 4 September 1984.

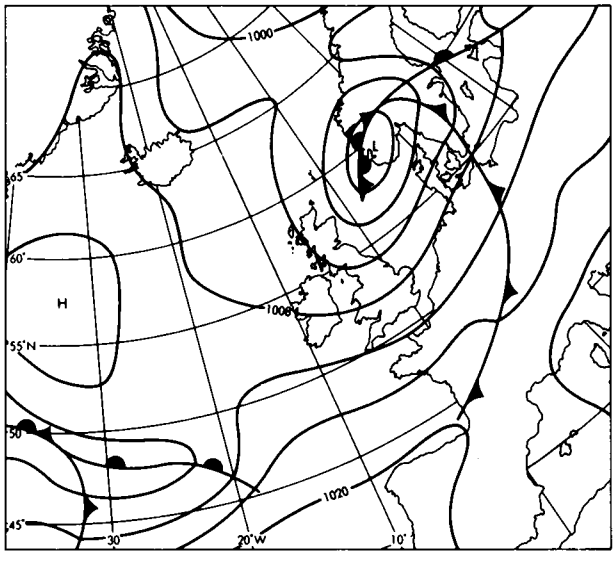

Figure 16. 5-day forecast run at 12 GMT on 30 August and verifying at 12 GMT on 4 September 1984.

can only be expected in a forecast for 5 days ahead. On this occasion it was the change in basic weather type which was by far the most significant aspect of the forecast and in this respect the forecast was very good. Using it as guidance, the medium-range forecasters in CFO were able to predict 5 days ahead the end of the long summery spell of weather over southern Britain.

Interpretation of forecasts

An assessment of the performance of the Meteorological Office's weather prediction models in general terms is given elsewhere in this issue. The examples given here demonstrate how effective they have been in some difficult and important situations. In the light of these the temptation might be to underestimate the role of the human forecaster in CFO or elsewhere. This would be a mistake, as there is little doubt that his contribution is still vital. Firstly, the success of a particular forecast depends crucially on the model's analysis. Forecasters must thoroughly investigate as much of the data received at Bracknell as possible, including satellite pictures, to ensure that the analysis is as accurate as possible. They must also assess the effect any shortcomings in the analysis may have on the subsequent forecast. Secondly, the forecaster is able to adjust the model forecast using his knowledge of the model formulation, his experience of model behaviour and in the light of actual developments. This is often important when considering forecast rainfall patterns, but also applies more generally, for example in the development of a small-scale but intense depression.

Lastly, the model forecast requires considerable interpretation. Even with a very good sequence of surface-pressure charts, skill and judgement are required to forecast the many aspects of weather which are of importance to customers. For example, forecasts of maximum and minimum temperatures, the possibility of frost, the amount of cloud and the likelihood of fog are essential. Some of the model output is of indirect assistance to the forecasters in these respects (e.g. the 1000–850 mb thickness charts are a useful aid to surface temperature forecasting), but sometimes contradictory factors need to be taken into account. Even those aspects such as rainfall amount and distribution which form part of the direct output from the models require careful interpretation. Limitations in the vertical resolution can lead to incorrect predictions of convective rainfall for instance; the forecasters need to judge when this is likely to be the case.

Nevertheless, the latest weather forecast models in operational use in the Meteorological Office have proved to be an invaluable aid to the forecasters, and the increasing confidence the customers have shown to possess in the forecast products stems largely from the improved accuracy of these tools not only for the British Isles, to which all of the examples apply, but over the whole world.

551.509.313:551.509.58:629.7

The use of 15-level model products in the Central Forecasting Office for forecasts for civil aviation

By M. E. Hardman

(Meteorological Office, Bracknell)

Summary

The use of the 15-level global prediction model as a basis for Bracknell's role in the World Area Forecast System for civil aviation is described. Some further developments are mentioned which are expected to lead to further increases in the accuracy of the forecasts and the effectiveness of the service.

1. Introduction

A number of features of the design of the 15-level model, when compared with its predecessor the 10-level model, enable it to provide an improved representation of the atmosphere near those levels of most importance for modern commercial airliner operations. These include greater horizontal and vertical resolution, improved output modelling of tropopause and maximum-wind data, and the use of winds and temperatures as primary model variables.

In recognition of these features and the capability of global coverage from the model, Bracknell was designated by the International Civil Aviation Organization as one of two World Area Forecast Centres (WAFCs) within the framework of the new World Area Forecast System (WAFS) for civil aviation. The role of the World Centres in Bracknell and Washington is to provide numerical forecasts of winds and temperatures (primarily in coded bulletins of grid-point values) with a global coverage. These are distributed to a network of Regional Area Forecast Centres (RAFCs) with responsibility for providing planning information and flight documentation for the user airlines. The Central Forecasting Office (CFO) assumed the role of an RAFC, one of three in Europe, on 1 February 1984.

This paper describes the products available from WAFC Bracknell and their use, with other model data, by RAFC Bracknell.

2. World Area Forecast Centre products

Using a data cut-off time of T+3 hours 20 minutes, global forecast fields of grid-point values of wind and temperature at standard flight levels from FL 050 (850 mb) to FL 530 (100 mb) and for verification times T+12, 18, 24, and 30 are transmitted using WMO GRID code (FM 47–V) typically commencing at T+4 hours 30 minutes. The GRID resolution for bulletins, (compared to a model grid of $1\frac{1}{2}°$ latitude by $1\frac{7}{8}°$ longitude) is $2\frac{1}{2}°$ latitude by 5° longitude between 20° and 70° north or south and 5° by 5° in the tropical belt. A lower resolution is used over polar regions. Additional bulletins containing maximum winds and tropopause data are also transmitted. Back-up for the data, to cover a failure or delay of the subsequent forecast run, is provided by bulletins for T+36, 42 and 48. In the event of unavailability of the global model for two consecutive runs, grid-point data from WAFC Washington, using a data time 12 hours earlier, are transmitted. Full details are given by Francis (1985).

3. CFO as a Regional Area Forecast Centre

Regional Centres are tasked with the processing of WAFC products to provide flight documentation. Charts are required for transmission by facsimile to users. In the United Kingdom these are made available through the CAMFAX circuits which serve the larger aerodromes throughout the country. They are sent by landline to a number of international centres including Paris and Frankfurt — the other European RAFCs — and are also broadcast by radio facsimile (GFE).

Charts may be divided into two categories: (a) those constructed directly from the model products and depicting wind and temperature at standard flight levels (Fig. 1); and (b) those constructed by a combination of subjective methods and data from the model such as significant-weather charts (Fig. 2). Figs 1 and 2 also show the primary area of responsibility of RAFC London (Bracknell), the so-called 'NAT' area, extending from the Persian Gulf to the west coast of North America. Both charts are transmitted at A2 size to users — a scale of approximately 1:36 million. Output (a) also includes charts covering the 'MID' area from Europe to south-east Asia, the 'AFI' area covering routes to Africa and South America, and on a larger scale a 'EUR' chart covering Europe and the Mediterranean. Charts are issued on a 6-hourly sequence of verification times, normally at 18 and 24 hours from the corresponding model data times. Transmission sequences commence at 5½ and 11 hours respectively for charts (a). Corresponding significant-weather charts are available to users by T+9 and T+15 hours.

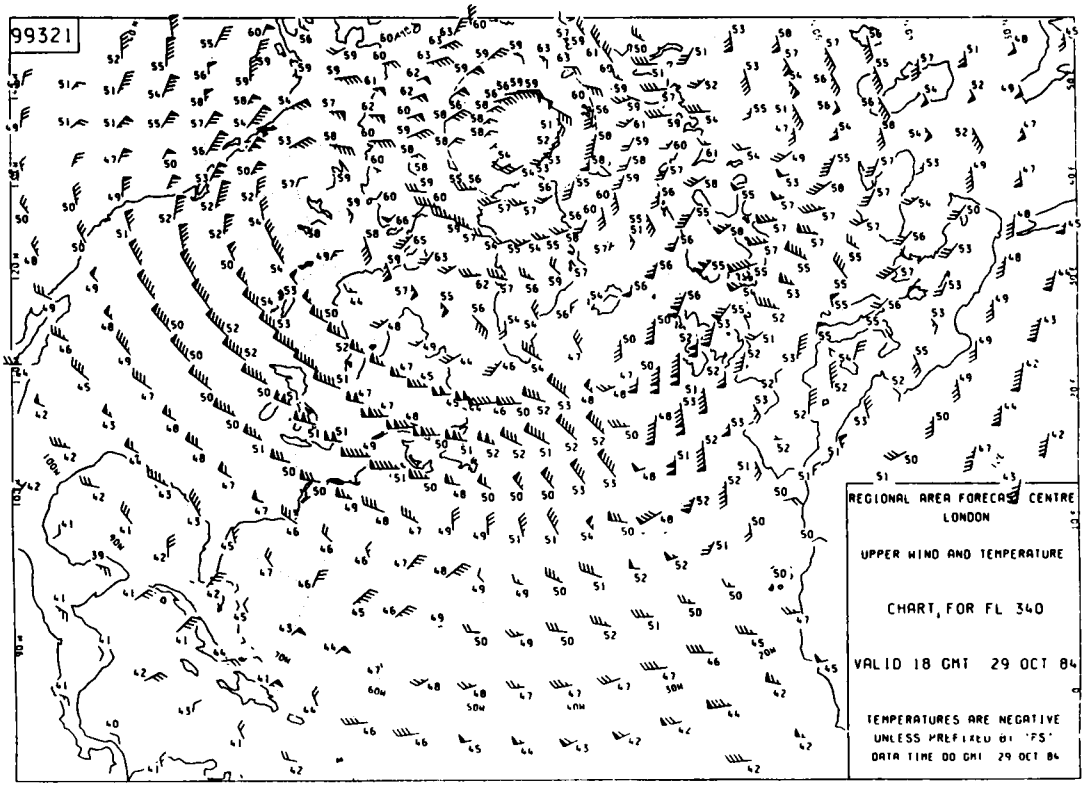

Figure 1. Flight documentation chart of winds and temperatures at flight level 340 (250 mb), 'NAT' area 18-hour forecast from data time 00 GMT on 29 October 1984, as issued by Central Forecasting Office (Regional Area Forecast Centre, London).

4. Construction of significant-weather charts

For the purposes of WAFS the atmosphere is divided vertically into 3 regions, i.e. surface to 10 000 feet (700 mb), 10 000 to 25 000 feet (400 mb) and 25 000 to 45 000 feet (150 mb). Routine significant-weather output for the NAT area from CFO covers only the high-level region. On this chart (Fig. 2) are depicted tropopause heights, the height, strength and position of jet-stream axes, areas of moderate or severe clear-air turbulence (CAT), and areas of significant weather, e.g. widespread thunderstorm activity and associated icing and turbulence. Where such features are associated with frontal zones or surface-pressure centres these are also indicated.

On request, for specified routes, a low- or middle-level chart is also provided. The construction of the NAT chart is a collaborative effort. Preliminary significant-weather charts for overlapping segments of the eastern half of the NAT area are exchanged between the three European RAFCs. CFO has responsibility for the completed eastern half which is then exchanged at a 1:25 million scale with a chart from RAFC Washington covering the western half. These are then merged into the final issue which is photo-reduced to the required A3 size (1:36 million) and distributed as flight documentation. A careful balance has to be struck to ensure consistency between segments and with the corresponding wind and temperature charts.

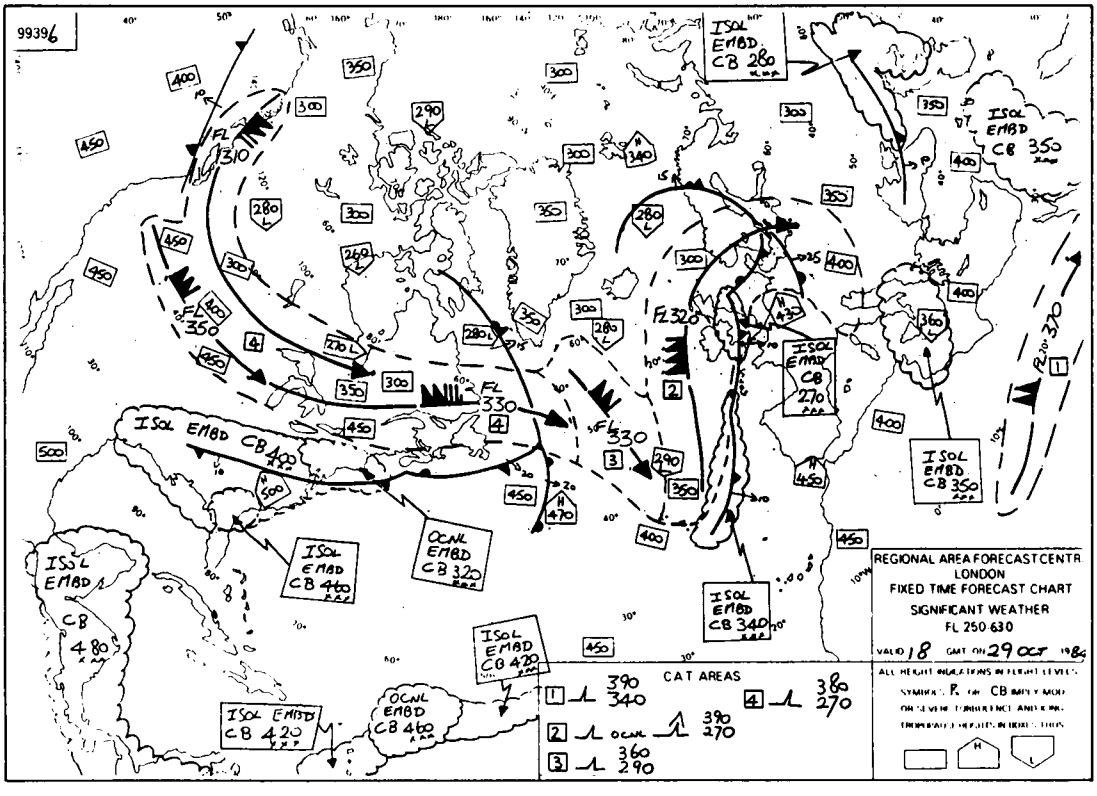

Figure 2. Flight documentation chart of 'significant weather' for flight levels between 250 and 630 (400 to 70 mb). Time and area are as for Fig. 1.

Numerical fields of significant-weather parameters are available as guidance (Fig. 3):

(a) maximum wind speed
(b) maximum wind level
(c) tropopause height,

} — derived by curve fitting to the data at the 15 model levels

and

(d) probability of clear-air turbulence — based on statistical and physical relationships between model variables and CAT.

In addition, forecast vertical temperature profiles available on a visual display unit give an indication of deep convection. To this model information the forecaster adds a considerable amount of subjective experience both of the relationship between the synoptic features and significant-weather parameters and of the model's ability to handle these features in different situations. Later observations, both from pilot balloons and aircraft, together with satellite imagery, are also useful.

5. Model accuracy

Elsewhere in this issue is an historical account of the accuracy of forecasts from the Meteorological Office operational models. This shows the marked improvement as a result of the introduction of the current global model. The recent performance of this model in forecasting winds at the levels of commercial airline operations is illustrated in more detail in Fig. 4. This shows analysed and 24-hour forecast values of mean wind-speed error (a) and root-mean-square (r.m.s.) vector wind errors (b) at 250 mb, as verified against observations over an area covering Europe, the North Atlantic and eastern parts of North America. Monthly values are plotted from August 1983 to December 1984. The r.m.s. 24-hour forecast values show only a small seasonal variation, highest in early winter, between 16 and 20 kn, and r.m.s. analysis values show a slight growth from 7 kn to a peak of about 10 kn in October 1984. A small underestimate of generally less than 2 kn is seen in the mean errors at this level.

All winds at 250 mb are taken into account in these figures giving a general indication of the accuracy of wind forecasts for civil aviation. A more selective approach is required to assess the ability of the model to predict such features as the position and strength of jet streams, and their associated horizontal and vertical shears which are important for the forecasting of CAT. One such approach is to verify model forecasts of maximum wind speed against radiosonde observations. A severe test is to select only cases where the observed value is greater than 90 kn (Fig. 5). It is seen that there is a considerably larger mean error, with these stronger winds underestimated by between 12 kn in winter and 25 kn in summer for 24-hour forecasts (Fig. 5(a)). The explanation lies partly in the statistical treatment since winds greater than 90 kn comprise a much smaller fraction of the population in summer than in winter. Subjective examination of maxima depicted on model output (e.g. Fig. 3(a)), however, confirms that part of the variation is real. Indeed, while forecasters in CFO had reported jet maxima 'well handled' by the model during its first winter (1982/83), as summer 1983 approached an increasing number of seriously underestimated maxima were observed in model output, leading to the setting up of a subjective investigation to study the problem. This showed that for all jets over a 6-week period in July and August 1983 the mean bias in the model's 24-hour forecast of jet strength was −19.5 kn, in broad agreement with the results in Fig. 5(a), when compared to subjectively analysed jet cores. Positional errors were ignored. Subjectively amended 24-hour forecasts issued by CFO reduced this bias to 5.6 kn. While such improvements are possible with jet cores, investigations have shown that subjective amendment of general wind forecasts is more difficult.

A breakdown of the mean speed error against jet orientation showed that the largest values occurred with flow from due north or south. Jets with an easterly component were also less well handled, though

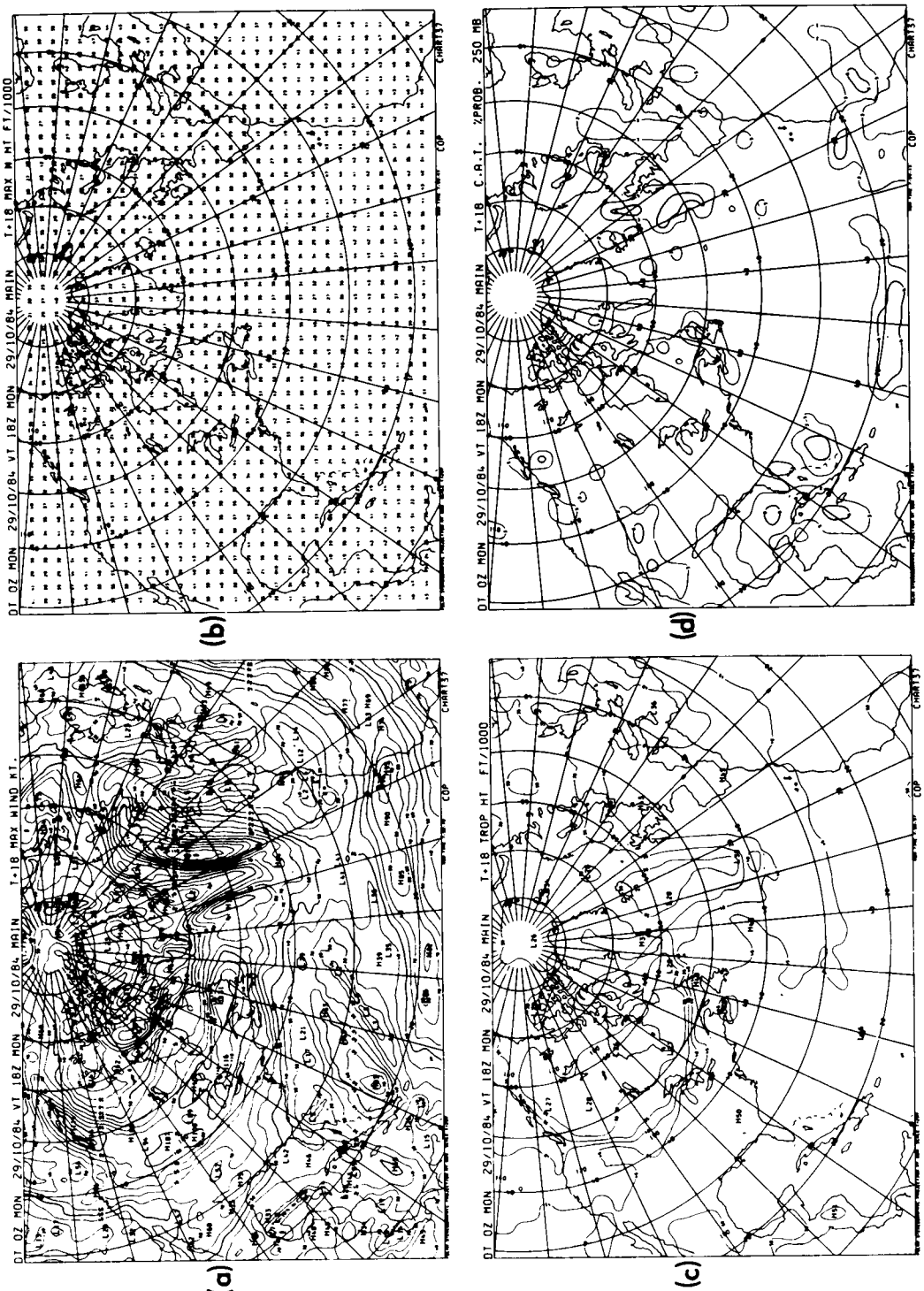

Figure 3. Model output charts from the global model. These are 18-hour forecasts from the same data time as Figs 1 and 2. (a) Maximum wind speed. (b) Maximum wind level (ft × 1000). (c) Tropopause level (ft × 1000). (d) Probability (%) of moderate or severe clear-air turbulence at 250 mb.

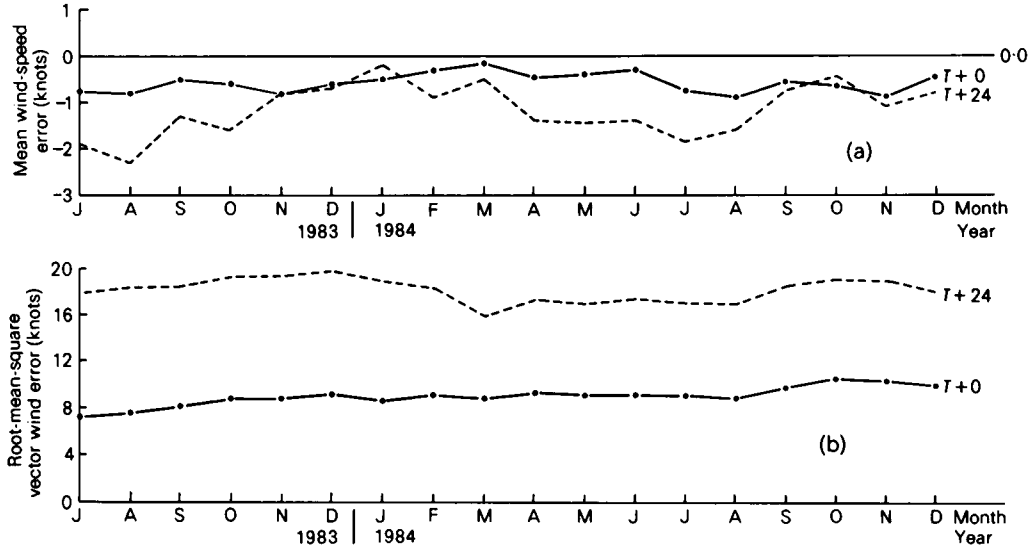

Figure 4. Errors in global model wind analyses and 24-hour forecasts at 250 mb by months from July 1983 to December 1984, as verified against radiosonde observations, for an area covering Europe, the North Atlantic and the easternmost parts of North America. (a) Mean wind-speed error. (b) Root-mean-square vector wind error.

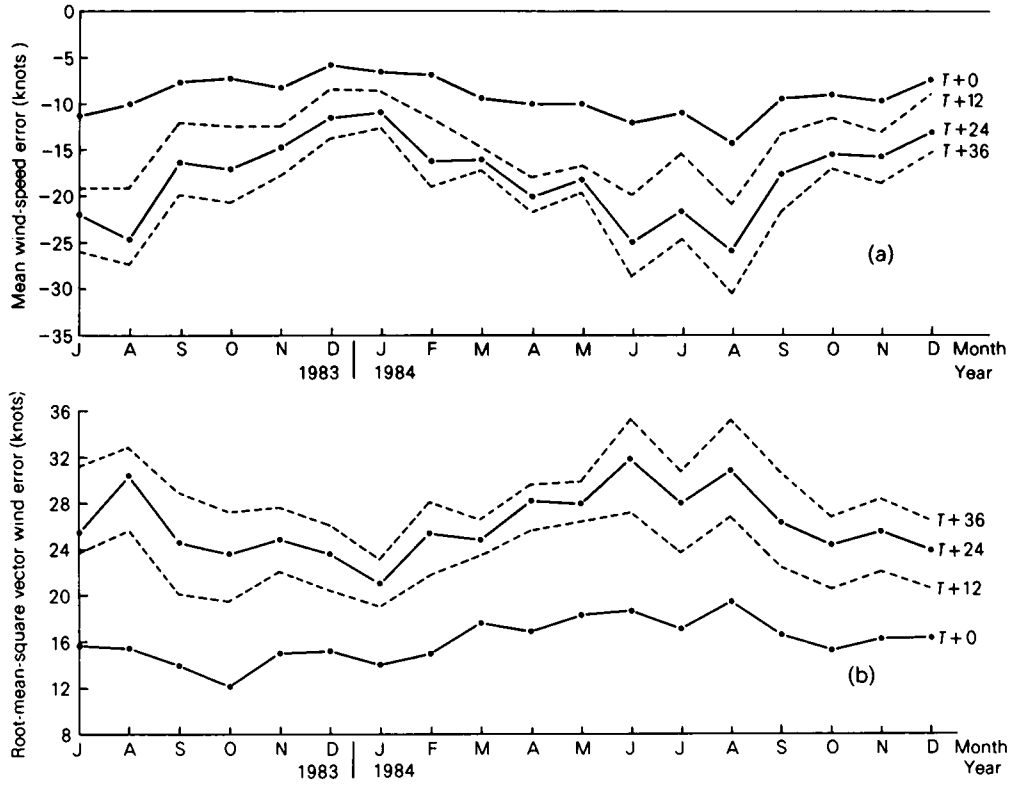

Figure 5. As Fig. 4 but for model maximum wind data verified only when observed value was greater than 90 kn. (a) Mean wind-speed error. (b) Root-mean-square vector wind error.

relatively few in number. However, recent modifications to the model designed to improve the handling of blocked and meridional synoptic patterns with which many of these jets are associated shows encouraging signs of success with January 1985 verifications of upper winds the lowest yet.

6. A 6-hourly forecast cycle?

Data assimilation in the global model is currently carried out on a 6-hourly cycle while forecasts are run only from the main upper-air observation times of 00 and 12 GMT. The large amount of asynoptic data within 3 hours of 06 and 18 GMT (e.g. aircraft reports and satellite temperature soundings) suggests that it might be profitable to make use of a 6-hourly cycle of forecast runs so that, for example, the 24-hour aviation forecasts from 00 and 12 GMT could be replaced by more accurate 18-hour forecasts from 06 and 18 GMT. This was tested during December 1983 when extra runs were made at 18 GMT and comparison of forecasts, both subjective and objective, carried out. The results have been discussed in detail by Hardman and Day (1984). In summary, while 12-hour forecasts from 00 GMT were clearly better than 24-hour forecasts from 12 GMT, the expectation that perhaps half of this improvement might be demonstrated with 18-hour forecasts from 18 GMT was not realized. Fig. 6 shows r.m.s. mean errors for wind and temperature data verified against radiosonde observations. A similar picture was gained in subjective comparisons of model forecast jet maxima (i.e. ignoring position errors) where, on balance, the 24-hour forecasts were marginally but not significantly superior. The reasons for this lack of improvement are not clear but probably relate to the differing ratios of data types and their assimilation using the current analysis system. It may well be that revised methods of assimilation could change the situation in the future.

7. Flight planning data

Aviation data are also supplied directly from the numerical model to the airlines in grid-point form using aviation digital code — a vertically stacked format. Full details are given in the paper by Francis (1985). Recipients include British Airways, Scandinavian Airlines System, Japan Air Lines, and SITA (Société Internationale de Télécommunications Aéronautiques) which represents a substantial group of airlines. These data are supplied on direct computer-to-computer links with no subjective input or formal amendment procedure.

8. The role of the Principal Forecasting Office at London (Heathrow) Airport

While CFO at Bracknell has assumed the role of an RAFC under the new system, Heathrow remains the Principal Forecasting Office in the network of UK civil aviation stations, with primary responsibilities for flights in and around the United Kingdom. Using data in grid-point form, directly transmitted to its OASYS computer, Heathrow provides a comprehensive service at national level for civil and general aviation. It is not the purpose of this article to describe in detail these activities. Examples cited below give brief indications of more specialized uses of 15-level model output. A primary task is the production of significant-weather and grid-point ('spot') wind and temperature charts for an area covering the United Kingdom, North Sea and near continent. The 'spot wind' chart is produced by subjective modification of direct computer output (Fig. 7) which provides considerable detail at lower levels. In contrast to higher-level forecast output using pressure altitudes, flight rules require information on this chart to be computed relative to a mean-sea-level datum. While freezing-level data may also be numerically produced, it has proved more effective to add this subjectively. Beneficial subjective amendment of winds at low level takes advantage of more recent surface observations.

Wind and temperature forecasts for Concorde operations are also based directly on NAT area model output, in this case for 150 and 100 mb. Before the advent of the 15-level model, the temperature forecasts for Concorde had been derived largely subjectively as significant model errors were found at these levels. The extension of model levels to around 30 mb provides a greatly improved product from the 15-level model (Atkins 1983) and it has proved possible to extend use of direct model output to the levels at which Concorde operates.

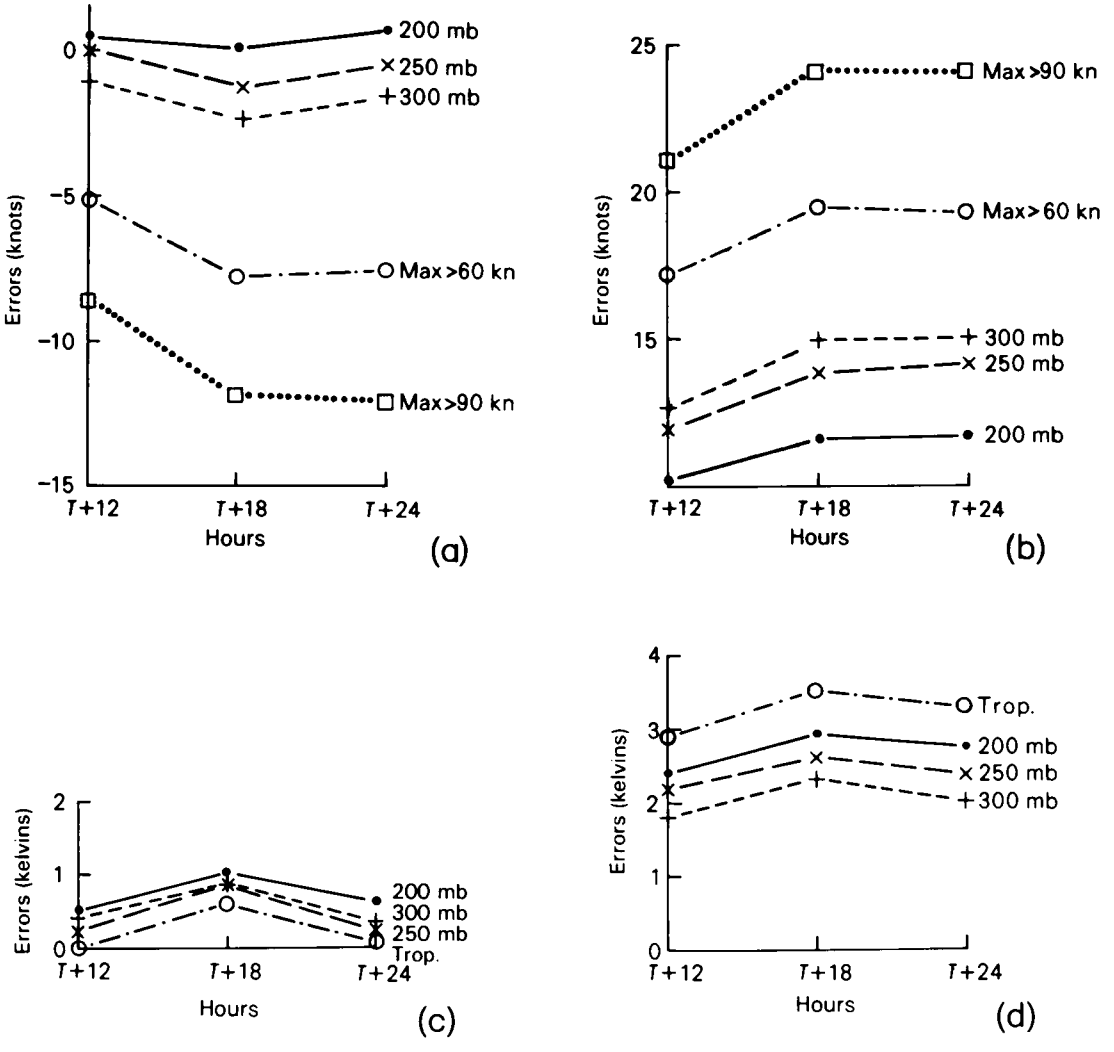

Figure 6. Assessment of forecasts based on 18 GMT data time, December 1983, as verified against radiosondes. (a) Mean wind-speed errors, including maximum-wind forecasts. (b) Root-mean-square wind-speed errors, including maximum-wind forecasts. (c) Mean temperature errors, including tropopause. (d) Root-mean-square temperature errors, including tropopause.

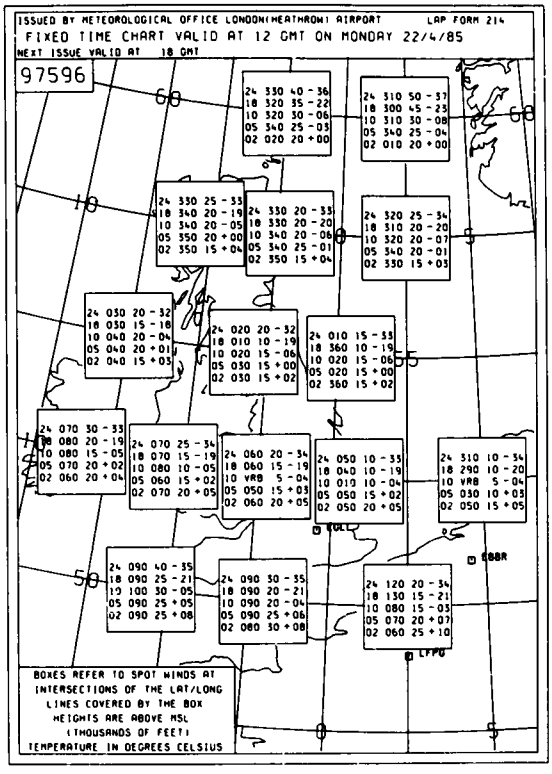

DT 00Z 22/4/85 T+12

Figure 7. Spot-winds chart as produced numerically. Temperatures and winds are represented at heights of 2000, 5000, 10 000, 18 000 and 24 000 feet above mean sea level.

Acknowledgement

The assistance of Mr B. A. Hall in the analysis of data from the Jet Stream investigation is acknowledged.

References

Atkins, N. J. 1983 Concorde forecasts and the new 15-level model. *Meteorol Mag*, **112**, 261–265.

Francis, P. E. 1985 Output products of the Bracknell numerical weather prediction models. *Meteorol Mag*, **114**, 242–251.

Hardman, M. E. and Day, A. P. 1984 A comparison of forecasts run from 18Z data times with those run from 12Z data. (Unpublished, copy available in the National Meteorological Library, Bracknell.)

551.509.58:551.465.75: 551.466.3

Applications of wave and surge models

By J. J. Ephraums

(Meteorological Office, Bracknell)

Summary

Applications of numerical sea surface models range from the routeing of cargo vessels across the North Pacific to predicting flooding by waves and surges along the east coast of England. In the former case, model output is one of the many tools available to the forecaster, whereas in the latter it is possible to send numerical output directly from the computer to the customer for rapid and reliable warnings. In this paper the operational applications and distribution of wave and surge model forecasts are briefly described. Of almost equal importance is the archive of wave model hindcast data which provides vital information to outside customers when measured data are unavailable in their area of interest. There are also many occasions when it is cost effective to hindcast historical storm events using reconstructed wind fields, and on some occasions the model may be judiciously used with idealized wind fields to simulate extreme wave conditions.

1. Applications using real-time operational data

(a) *Introduction*

Some of the operational characteristics of the wave and surge models have already been outlined in the companion paper by Francis (1985); in Table I are the details of the products at present available from the Meteorological Office computer system, COSMOS. The way in which the various real-time recipients of wave and surge model forecasts make use of these products is described below.

Table I. *Operational products from wave and surge models*

Model	Run time *minutes*	Output time GMT	Forecast quantities available	Output format
Fine-mesh wave model	4¼	0230 1430	Wind speed/direction Total wave height/period	Charts Grid code
Mediterranean wave model	2¼	0240 1440	Wind sea height/period Swell height/period/direction	Tables
Coarse-mesh wave model	4¾	0430 1630	(Wave spectra)	
Surge model	1¾	0240 1440	Tidal residuals (Currents)	Tables

Notes: Output quantities shown in brackets could be provided but are not produced operationally at the time of writing. The model run times include the hindcast run required for the forecast starting state.

(b) *Offshore industry forecasts*

Forecasts for the offshore industry in the North Sea are produced by a specialized team of forecasters at London Weather Centre (LWC). Because of the sensitive nature of most operations and the differing requirements of each customer it is necessary to provide a tailored service of forecasts with the option of direct and immediate contact between the operators and the forecast bench in rapidly changing weather.

The need for accurate wind and wave forecasts is paramount in all routine and one-off operations. As

winds and waves increase it may become necessary to curtail drilling and to disconnect the riser pipe through which oil is pumped to production platforms. These processes take several hours to complete, and in the oil business every hour of idle time is costly. There are now guidelines for the evacuation of crews from accommodation platforms in extreme storms — early and accurate warning is essential to avoid disaster or unnecessary effort. In less severe weather there is a hidden danger when large barges are being used to transport and lift large loads to and from platforms. The presence of low-amplitude swell at the resonant frequency of the barge can cause pronounced oscillations which would be more than inconvenient in the middle of a lifting operation! Many of these towing and construction jobs have to be planned well in advance, so here it is the forecast of a wave and weather window of strictly defined limits which is required.

Although forecasts of visibility, precipitation and temperature, for instance, are all required by the offshore industry, the most important operating parameters are wind speed and wave activity.

Some numerical model data are transmitted to LWC via GRID code but the most popular format is a selection of high-resolution charts showing forecast fields of winds or waves. These are now transmitted from Bracknell in digital form to the Outstation Automation System (OASYS) computer where charts can be plotted locally, thus saving almost half-an-hour over the old analogue transmissions of facsimile charts. The wave charts cover the North Sea and coastal waters surrounding the British Isles (see Fig. 1), and are provided in contours of total sea or spot values of swell height and period.

Because the wave model analysis incorporates no measured wave data it is important that the forecaster is aware of the potential errors in the numerical product even at this stage, and this is possible to achieve by comparison with reports. However, these data themselves are subject to errors and

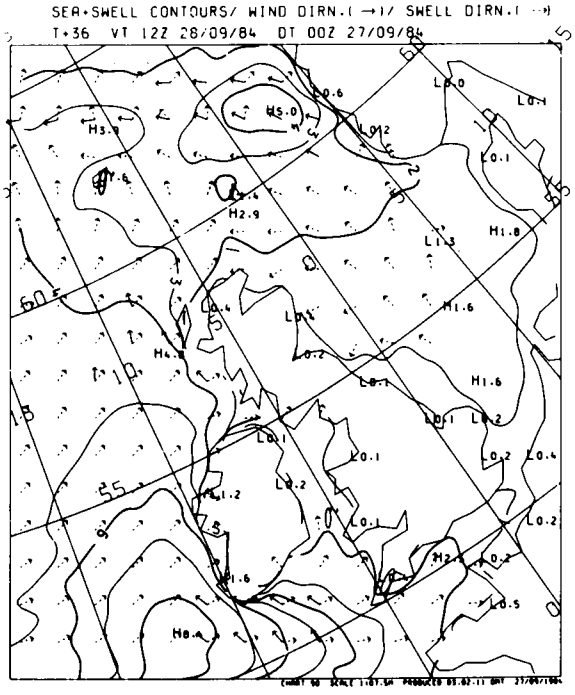

Figure 1. An example of the fine-mesh wave forecast charts received by London Weather Centre.

subjective bias, and their spatial distribution does not immediately favour a subjective analysis. In the forecast there may be errors in the forecast winds which the forecaster can anticipate; in these circumstances it may be necessary to perform a graphical wave forecast by hand to estimate the error in the model prediction.

The forecasters have built up a good knowledge of the present wave prediction model and are able to take into consideration all these problems to produce a forecast blended by a man–machine mix which surpasses the accuracy of either the man or the machine alone (Morris 1981). The accuracy of these tailored forecasts, together with the personal contact available through the Weather Centre or on location, places LWC in the premier position for forecasts to the offshore industry.

One forecast which we hope will never be required entails the supply of forecast surface winds to oil companies for use with the oil spill dispersion program SLIKFORKAST developed by the Continental Shelf Institute in Norway for predicting the drift and spread of oil slicks. These winds are extracted from the fine-mesh numerical weather prediction (NWP) model in the event of such as emergency, and sent to subscribers in the affected areas.

(c) Shipping forecasts

Forecasts for shipping take the form of general broadcasts via the media or dedicated routeing advice through the Meteorological Office Ship Routeing Service (Metroute) based in the Central Forecasting Office (CFO) (Mackie 1982). As the WMO Regional Meteorological Centre, CFO has the responsibility for transmitting wave analyses and forecasts for the north-eastern Atlantic area in the form of radio-facsimile charts. These are produced in CFO by forecasters who rely greatly on the output from the coarse-mesh wave model since real-time wave data from the open oceans are nearly all in the form of visual observations of sparse distribution.

As is the case at LWC the production of wave forecast charts for users is based on the combined talents of the model and the forecaster. The model is able to produce an excellent basic forecast to which the forecaster is able to add extra detail and information based on his assessment of the NWP model forecast winds and the actual wave conditions at the time. Fig. 2 shows an example of the wave model output available to forecasters from which the transmitted chart shown below it was produced.

These forecast charts are handed to the Ship Routeing bench whose job it is to select the most favourable route for individual ships given the predicted conditions of the sea. Although the calculation of least-time routes has traditionally been by manual techniques, there is now a numerical program being tested which uses the wave model forecasts directly to arrive at a detailed route; again this facility is designed to produce speedy and reliable guidance to the forecasters who will modify the product to the best advantage.

Note that although wave forecasts for the Atlantic are produced by CFO forecasters for Metroute there are no specific forecast charts compiled manually for the North Pacific. In this case the Ship Routeing bench must use the unmodified wave model predictions for this area, but nevertheless the model is found to be reliable and accurate.

The numerical surge prediction model has applications in shipping and navigation, through its ability to forecast negative surges at ports. Warnings of particularly low tides due to this effect are sent by the Storm Tide Warning Service (STWS) to Port Meteorological Offices and to the Navy's Radio Navigational Warnings Unit for relaying to coastal radio stations which broadcast to shipping.

(d) *Flood warning forecasts*

Much of the British coastline in winter is under threat of flooding owing to storm tides or high waves, and this is especially so in the low-lying regions of the east coast of England. The most notable storm

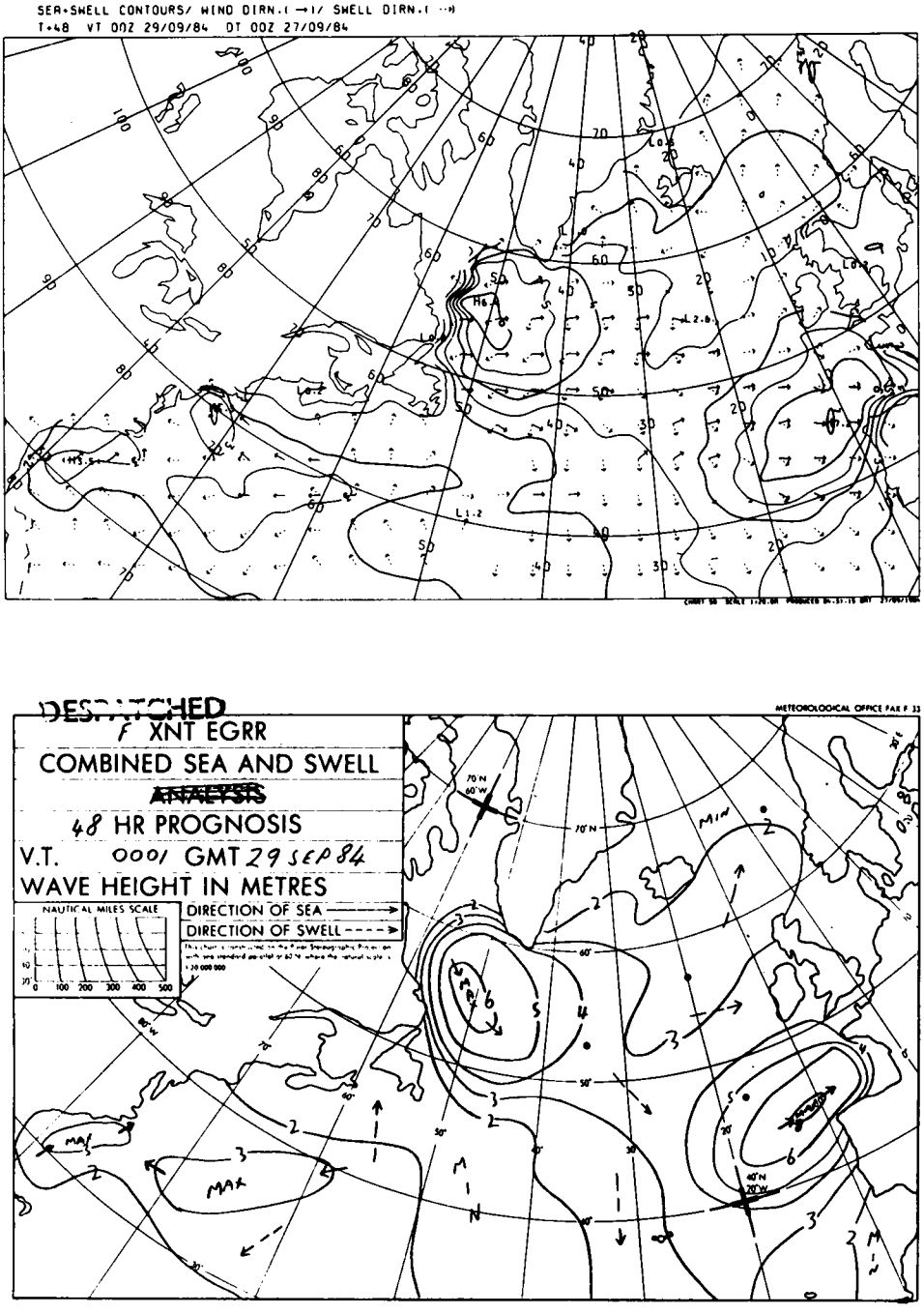

Figure 2. The production of North Atlantic wave forecast charts. The upper chart shows the model guidance and the lower chart is the forecaster's final product. Note that he has enhanced the high waves in the Biscay area.

surge in recent times was the disastrous flood on the night of 31 January 1953 when 300 people drowned and London experienced its last major flood (Grieve 1959). On 13 February 1979, with no imminent large tides and no severe weather present, Portland Isle was severely damaged by exceptionally high swell waves originating from an Atlantic storm several days earlier (Draper and Bownass 1983). Both these events prompted the formation of separate services to warn of such occurrences. In the first case, numerical models were not available for guidance until 1978, but in the second there was already an operational model in use which could be used immediately for warnings of such events after it had been shown that the model was capable of predicting the arrival of distant swell as well as local wind-sea (Golding 1981).

For the prediction of storm surges the STWS uses output from the storm surge prediction model presented in the format of a table of hourly residuals for specific ports (Fig. 3 (upper)). They also have at their command instantaneous readings from the tide recorders situated at 11 ports, empirical prediction techniques using a microcomputer, and up-to-the-minute guidance from CFO.

The model is relied on for prompt and detailed guidance for many locations, but since it lacks the inclusion of measured tidal data it is also necessary for the STWS staff to use the empirical equations

STORM SURGE FORECAST. RESIDUAL ELEVATIONS IN METRES. DATA STARTS AT 0 HRS GMT 27/ 9/1984

GMT	1687 NLYN	1513 ILFR	1471 AVON	1467 MILF	1380 FISH	1293 BARM	1248 HOLY	1207 HILB	1119 HEYS	1074 WORK	1608 PMTH	1604 PLND	1645 PLYM	1610 NWHN	1524 DVER
0	.02	.02	.03	.04	.04	.06	.06	.05	.06	.05	.01	.02	.02	.01	.01
100	.01	.05L	.01	.05L	.04	.06	.06	.06	.06	.06	.01	.01L	.01L	.01	.01H
200	.01	.03	.01	.04	.04	.03	.06	.05	.06	.07	.01	.01	.02	.01	.00
300	-.01	.02	.02L	.05	.05L	.05	.06	.05	.06	.08	.01	.02	.01	.00	-.01
400	.02	.04	.03	.04	.06	.07	.08	.06	.07	.09	.01	.01	-.01	.00	-.02
500	.04	.02	.03	.06	.08	.08L	.10L	.08	.08	.09	.01	-.01	.03	.00	-.03
600	.05H	.07	.03	.09	.09	.10	.10	.09	.10	.10	-.01L	.01	.04	-.01L	-.04
700	.04	.10H	.05	.12H	.11	.12	.12	.11L	.11L	.11L	-.02	.02	.03H	-.02	-.03
800	.05	.12	.09	.12	.13	.12	.13	.11	.12	.13	.01	.03H	.04	-.02	-.03L
900	.06	.11	.13H	.12	.12H	.14H	.14	.12	.13	.14	-.02	.03	.04	-.02	-.04
1000	.06	.09	.13	.12	.14	.15	.15	.12	.14	.16	-.01	.04	.06	-.02	-.04
1100	.09	.11	.11	.14	.14	.15	.17H	.14	.15	.16	.01H	.05	.07	-.01	-.04
1200	.09L	.13	.09	.14	.15	.18	.18	.15H	.16H	.18	.01	.06	.08	-.01	-.05

FOR TRANSMISSION TO SOUTHERN WATER AUTHORITY VIA MET.O.5 PAGE 1

INITIAL DATA TIME 0Z 27/ 9/84

LOCATION 50.6N 0.8E

HOURS AFTER DATA TIME	WIND SPEED KTS	WIND DIRECTION DEG(FROM)	TOTAL WAVES HEIGHT M	TOTAL WAVES PERIOD SECS	WIND SEA HEIGHT M	WIND SEA PERIOD SECS	SWELL HEIGHT M	SWELL PERIOD SECS	SWELL DIRECTION DEG(FROM)
0.0	4.7	159.	0.5	4.9	0.0	0.0	0.5	4.9	244.
3.0	8.5	198.	0.5	4.3	0.0	0.0	0.5	4.3	234.
6.0	7.9	189.	0.5	4.0	0.4	3.2	0.4	5.8	252.
9.0	5.4	189.	0.4	5.2	0.0	0.0	0.4	5.2	249.
12.0	5.6	185.	0.5	5.1	0.0	0.0	0.5	5.1	245.
15.0	13.3	187.	0.8	3.9	0.6	3.2	0.5	5.6	242.
18.0	11.9	177.	0.9	4.0	0.7	3.6	0.5	7.1	256.
21.0	11.6	182.	0.9	4.1	0.7	3.6	0.5	6.9	256.
24.0	12.7	193.	1.0	4.2	0.8	3.7	0.5	6.9	255.
27.0	11.2	185.	0.9	4.1	0.8	3.7	0.5	7.2	250.
30.0	9.5	174.	1.0	4.3	0.7	3.5	0.7	6.4	237.
33.0	8.4	181.	1.0	4.6	0.6	3.3	0.8	5.9	239.
36.0	13.1	175.	1.1	4.5	0.8	3.7	0.7	7.5	250.

Figure 3. Forecasts for flood warning. The upper print-out shows hourly forecast data from the surge model reference port points. High (H) and low (L) water times are marked for convenience. The lower print-out shows 3-hourly forecast data from the fine-mesh wave model for a point in the Channel.

developed during the years before models were generally available. These equations are based on the behaviour of some 200 historical surges, the most common of which travel southwards along the eastern coast, growing or decaying according to the local winds. Their strength is in the use of real-time measured tidal data from northern ports, and the ease with which they can be recomputed with updated wind forecasts during rapidly changing situations when the model may contain timing errors. The forecasters also consider physical processes not included in the model, in particular the effect known as set-up which is the raising of the water level at a beach subjected to large breaking waves. This mechanism can sometimes account for an extra metre in the recorded level. More details of the work of the STWS can be found in Townsend (1981).

Warnings of storm surges are sent to the police authorities in the affected areas who are then responsible for alerting the local flood organization and issuing public warnings. A special arrangement exists with the controllers of the Thames Barrier who receive advice on whether water levels in the Thames estuary will require the barrier to be raised. They also have access to unmodified surge model data, and fine-mesh NWP model wind and pressure forecasts via a computer-to-computer link so that they can run their own limited-area surge model which is being currently developed.

The warnings of wave-induced flooding are distributed by another means since it is believed that the fine-mesh wave model is capable of predicting with accuracy the near-shore values of waves and swell without the requirement for manual intervention. Tables of 3-hourly wind, wave and swell forecasts up to T+36 are printed out by the computer for selected locations and these are sent immediately by document-facsimile (DOCFAX) to subscribers, notably water authorities on the east, south and north-west coasts (see Fig. 3(b) for example). Although the fine-mesh wave model is a shallow-water model it was not designed for use in coastal regions where small-scale processes such as tides and local refraction can dominate . It is therefore surprising and encouraging that verification of the model against measured data in several coastal positions has revealed an impressive accuracy in the magnitude and timing of high-wave events (Francis 1985). The importance of good timing is crucial since the relative occurrence of high waves and tide may dictate whether flooding occurs or not.

2. Applications using archived operational data

(a) *Introduction*

Diagnoses of state of sea produced every 12 hours by the operational wave-model hindcast cycle have been archived operationally since 1977 (see Table II) and will be kept permanently both for internal use in verification and development work and for access by external customers. Some of the applications of this archive are described below.

Table II. *Details of the Meteorological Office wave model archive*

Period	Data time GMT	Models	Archive form
Dec. 1977–Sept. 1982	00, 12	Fine-mesh	Grid-point wave spectra
		Coarse-mesh	Grid-point wave spectra
Feb. 1983–present date	00, 12	Fine-mesh	Grid-point wave spectra
		Mediterranean	Grid-point wave heights, etc.
		Coarse-mesh	Grid-point wave heights, etc.

Notes: The integrated quantities of wave height etc. can be derived from the wave spectra by the archive extraction programs. The archive prior to September 1982 comprises the lower-resolution models run from the 10-level models on the IBM computer at that time.

(b) *Wave energy research*

In the late 1970s and until fairly recently there was an enormous interest in the potential use of wave power as an alternative energy source. During this time the requirements for reliable wave data around the British coast proved the necessity of maintaining a permanent archive of wave-model hindcast fields for use when measured data were absent from the sites of investigation.

In 1981 a detailed joint study by the Meteorological Office, the Institute of Oceanographic Sciences and the Hydraulics Research Station compared the performances of the Meteorological Office wave model and the NORSWAM wave model against measured data during March 1980 (Ewing *et al.* 1981). It was found that both models (which used identical forcing winds and boundary conditions supplied by the Meteorological Office) produced accurate hindcasts of wave height and power, thus justifying their use to estimate wave power levels for design purposes. Winter (1980) found that the archive data from the Meteorological Office model agreed with measured wave data from Ocean Weather Ship 'I' to give an agreement of mean wave power levels to within 6%. He then proceeded to use the model archive, on the basis of this verification, to estimate the mean power levels for various locations round the west and north of the British Isles. Mollison (1980, 1982) performed a similar exercise and found that the wave model archive could be confidently used to map the wave power resource off the Irish coast.

The success of the wave model in providing an accurate climatology of wave power lies in its strength at modelling the frequently occurring medium-height waves which contribute most to the mean wave power. Errors in the frequently occurring but insignificant low waves, and the infrequent large waves, do not have an impact on this quantity.

(c) *Design studies*

The fine-mesh wave model archive data base covering the continental shelf over a period of 7 years is often the only alternative to conventional data bases of measured or observed data when trying to construct a wave climatology. Reliable measurements of waves have been made at only a handful of locations, and even then for a limited time-span which is usually less than that required to extract useful information. For many customers there is insufficient time to start wave measuring programs when the results are required immediately for the design or development of a new or existing platform at a given location. As well as being a complete source of data in itself the model archive is frequently used to fill in missing data gaps when wave recorders have been out of operation.

The ability of the model to reproduce the wave climate at a given site has been shown by Houghton (1984) who verified some early wave-model data against measurements and found little bias in the mean errors of wave height. It is therefore possible to use wave-model archive data for determining some climatological wave values on which to base design criteria for offshore structures.

(d) *Environmental studies*

In a similar manner the wave-model archive has been used as a substitute for measured data in environmental studies and, in particular, near-shore data from the model have been used in projects to calculate coastal erosion and beach sediment transport rates.

(e) *First-order verification of remote-sensing data*

With the rapid proliferation of remote-sensing devices and projects there is a growing need for ground-truth data against which to validate the various devices, whether they are ground or satellite based. At the University of Birmingham there is a group developing a ground-based radar which is capable of measuring the ocean-wave spectra over an area of several hundreds of square kilometres.

As well as deploying waverider buoys they have used archived wave spectra and wind data from the fine-mesh model as a first-order approximation on which to base their verification.

Satellite-based measuring devices, such as synthetic-aperture radars, altimeters and scatterometers, require the same information for verification. By the nature of their operation it is necessary to have reference data available for a very large area so that results from each separate pass can be used. A mission of the Space Shuttle in October 1984 deployed synthetic-aperture radar to image the sea surface, and several ground tracks covered the southern waters of the British Isles. The Meteorological Office contributed archived model wave and wind data to a joint wave measuring program co-ordinated by the Institute of Oceanographic Sciences.

Active participation in remote-sensing experiments such as these is becoming more important if we are to fully realize the benefits of state of sea measurements which will be produced in real time by such vehicles as the European Space Agency Earth Resource Satellite (ERS-1) which is due to be launched in 1989.

(f) *Insurance enquiries*

Another occasional use of the wave-model archive is in instances of loss or damage to ships or their cargo caused by severe waves. In some cases the insurance enquiry may request an independent estimate of sea conditions to uphold a claim by the insured party. In the absence of neighbouring ships against which to corroborate reports it has been necessary in the past to refer to archive data from the Meteorological Office wave model.

3. Applications using non-operational models

(a) *Introduction*

The powerful computational facilities of the Meteorological Office are ideally suited to running non-operational wave models for hindcasts or experiments. There is usually no shortage of synoptic data from which wind fields may be derived. Wave models may be run with these winds to produce a reasonable alternative to traditional forms of measured or observed wave data which are in scarce supply. Some of the uses of non-operational models are mentioned below.

(b) *Hindcast studies*

There are many requirements for high-quality wave data which require a data time-span greater than that covered by the model archive. A case in point is the derivation of 50-year return values of maximum waves or, more generally, the qualification of wave climate severity. For these applications it has been necessary in the past to use the model to hindcast waves for specific historical extreme storm events using reconstructed wind fields.

A good example of this type of project is a hindcast of 17 North Sea storms by the Meteorological Office wave model which was commissioned by the United Kingdom Offshore Operators' Association and completed in 1980. The wind fields for these storms were painstakingly re-created by hand from synoptic charts (Harding and Binding 1978) and used as input to the wave model in order to see how effective it would be at simulating the maximum wave conditions in past severe storms. One of the problems in this sort of study is how to judge the model's performance — the very fact that the exercise was required stemmed from the shortage of reliable measured data!

Such hindcast studies are useful for our own needs in research and development of the model formulation. Recent work has been done to look at the model's accuracy in shallow water using two storms from November 1981 for which the winds could be re-created and good measured spectral data

could be obtained. As an extra source of information we exchanged the wind data with the Royal Netherlands Meteorological Institute and the Max-Planck Institute in Hamburg so that they could run their models in parallel for comparison (Bouws *et al.* 1985).

Similar hindcast experiments using the storm surge prediction model based on grid areas of different resolutions have been performed by the Institute of Oceanographic Sciences who are responsible for its scientific development (Flather 1981).

(c) *Artificial idealized experiments*

One advantage that wave prediction models have over atmospheric models is that they are dependent on the input of forcing fields and not completely dependent on the initial state. Operationally this is of course a nuisance — there is a constant need for better and more detailed wind fields, and considerable uncertainty in the validity of the starting analysis. When it comes to examining the model physics, however, this is a welcome property for much information can be gained by discarding the complicated varying structure of synoptic wind fields and adopting idealized wind patterns instead. Models can be retained on their geographical grids, reduced to one-dimensional arrays for fetch-limited studies or even pared to a single point.

In the first case, for which there has been a commercial application, the fine-mesh model was used to estimate the maximum possible wave height at locations in the North Sea by specifying values of constant wind from different directions. The advantage of this technique is its simplicity and cheapness in providing spatial variations in extreme waves due to geographical and sea-bottom effects only. The disadvantage is that it is not so easy to relate the artificial results to real-life storms and their probability of occurrence.

The more idealized cases involving simple grids have been much used by wave modellers to compare their scientific assumptions in the parametrization of the poorly understood processes. The SWAMP experiment was the first such large-scale use of this idea. Ten wave models were run under identical simple wind geometries to highlight the different physical mechanisms (Allender *et al.* 1982, 1984). The same concept was employed for shallow-water wave models to specifically isolate the depth dependency in each (Bouws *et al.* 1984). In all cases it has been found that the differences of behaviour of each model are much more apparent than in their results from real situations.

4. Conclusions

It has been shown how operational wave and surge model data can be used, both in real-time forecasting and in applications using the operational archive of hindcasts. These models can also be run with non-operational wind fields to produce reconstructions of historical events or to simulate extreme situations. In all cases the model is a reliable substitute for measured wave data which is in very poor supply, and it provides detailed forecasts which would be unobtainable through traditional manual prediction techniques within the tight schedule of a forecaster's timetable.

There is no doubt that wave and surge models now form an integral part of the forecast and consultancy service provided by the Meteorological Office.

References

Allender, J. H., Barnett, T. P., Bertotti, L., Bruinsma, J., Cardone, V. J., Cavaleri, L., Ephraums, J. J., Golding, B. W., Greenwood, A., Guddal, J., Gunther, H., Hasselmann, K., Hasselmann, S., Joseph, P., Kawai, S., Long, R. B., Lybanon, M., Maeland, E., Rosenthal, W., Toba, Y., Uji, T. and de Voogt, W. J. P. 1982 Sea Wave Modelling Project (SWAMP). An intercomparison study of wind-wave prediction models. Part 2 — A compilation of results. De Bilt, Royal Netherlands Meteorological Institute, Publication No. 161.

1984 Sea Wave Modelling Project (SWAMP). An intercomparison study of wind-wave prediction models. Part 1 — Principal results and conclusions. Proceedings of IUCRM Symposium on Wave Dynamics and Radio Probing of the Ocean Surface, Miami. Plenum Press.

Bouws, E., Ephraums, J. J., Ewing, J. A., Francis, P. E., Gunther, H., Janssen, P. A. E. M., Komen, G. J., Rosenthal, W. and de Voogt, W. J. P. 1985 A shallow water intercomparison of wave models. *Q J R Meteorol Soc.* (In press.)

Draper, L. and Bownass, T. M. 1983 Wave devastation behind Chesil Beach. *Weather*, **38**, 346–352.

Ewing, J. A., Ephraums, J. J., Golding, B. W. and Worthington, B. A. 1981 Comparisons of the Meteorological Office and NORSWAM wave models with measured wave data collected during March 1980. Wormley, Institute of Oceanographic Sciences, Report No. 127. (Unpublished, copy available in National Meteorological Library, Bracknell.)

Flather, R. A. 1981 Practical surge prediction using numerical models. *In* Peregrine, D. H. (ed.); Floods due to high winds and tides. London, Academic Press, 21–43.

Francis, P. E. 1985 Output products of the Bracknell numerical weather prediction models. *Meteorol Mag*, **114**, 242–251.

Golding, B. W. 1981 The meteorological input to surge and wave prediction. *In* Peregrine, D. H. (ed); Floods due to high winds and tides. London, Academic Press, 9–20.

Grieve, H. 1959 The Great Tide: the story of the great flood disaster in Essex 1953. Essex County Council.

Harding, J. and Binding, A. A. 1978 The specification of wind and pressure fields over the North Sea and some areas of the North Atlantic during 42 gales from the period 1966 to 1976. Wormley, Institute of Oceanographic Sciences, Report No. 55. (Unpublished, copy available in the National Meteorological Library, Bracknell.)

Houghton, I. 1984 A long time-series verification of hindcasts from the Meteorological Office wave model archive. *Meteorol Mag*, **113**, 317–329.

Mackie, G. V. 1982 The Meteorological Office Ship Routeing Service. *Meteorol Mag*, **111**, 218–224.

Mollison, D. 1980 The prediction of device performance. *In* Count, B. (ed.); Power from sea waves. London, Academic Press, 135–168.

1982 Ireland's wave power resource. Report for National Board for Science and Technology, Dublin.

Morris, R. M. 1981 The accuracy of London Weather Centre forecasts of surface wind and total wave heights and their comparison with computer products. *Meteorol Mag*, **110**, 133–143.

Townsend, J. 1981 Storm surges and their forecasting. *In* Peregrine, D. H. (ed.); Floods due to high winds and tides. London, Academic Press, 1–7.

Winter, A. J. B. 1980 The UK wave energy resource. *Nature*, **287**, 826–829.

THE METEOROLOGICAL MAGAZINE

No. 1358 September 1985 Vol. 114

CONTENTS

NOTICE

It is requested that all books for review and communications for the Editor be addressed to the Director-General, Meteorological Office, London Road, Bracknell, Berkshire RG12 2SZ and marked 'For Meteorological Magazine'.

The responsibility for facts and opinions expressed in the signed articles and letters published in this magazine rests with their respective authors.

Authors wishing to retain copyright for themselves or for their sponsors should inform the Editor when they submit contributions which will otherwise become UK Crown copyright by right of first publication.

Applications for postal subscriptions should be made to HMSO, PO Box 276, London SW8 5DT.

Complete volumes of 'Meteorological Magazine' beginning with Volume 54 are now available in microfilm form from University Microfilms International, 18 Bedford Row, London WC1R 4EJ, England.

Full-size reprints of Vols 1–75 (1866–1940) are obtainable from Johnson Reprint Co. Ltd, 24–28 Oval Road, London NW1 7DX, England.

Please write to Kraus Microfiche, Rte 100, Millwood, NY 10546, USA, for information concerning microfiche issues.

HMSO Subscription enquiries 01 211 8667.

Printed in England for HMSO and published by
HER MAJESTY'S STATIONERY OFFICE

£2.30 monthly

Dd. 738362 C14 9/85

Annual subscription £27.00 including postage

ISBN 0 11 727563 8
ISSN 0026–1149

THE METEOROLOGICAL MAGAZINE

HER MAJESTY'S
STATIONERY
OFFICE

October 1985

Met.O.967 No. 1359 Vol. 114

METEOROLOGICAL OFFICE Met.O.967

THE METEOROLOGICAL MAGAZINE

No. 1359, October 1985, Vol. 114

551.509.58:551.515.4:551.515.8:551.577.12

Conceptual models of precipitation systems

By K. A. Browning

(Deputy Director (Physical Research) Meteorological Office, Bracknell)

Summary

Imagery from radars and satellites is one of the main ingredients of nowcasting. When used to provide very detailed forecasts of precipitation for a few hours ahead, the imagery needs to be interpreted carefully in terms of synoptic and mesoscale phenomena and their mechanisms. This paper gives an overview of some conceptual models that are useful for this purpose. The models represent a variety of systems associated with mid-latitude cyclones and also mesoscale convective systems in the tropics and mid-latitudes. Specific phenomena discussed are:

(i) warm conveyor belts, including those with rearward and forward sloping ascent in ana and kata cold frontal situations respectively;

(ii) cold conveyor belts ahead of warm fronts;

(iii) narrow rainbands associated with line convection at the boundary of a pre-cold frontal low-level jet;

(iv) wide mesoscale rainbands associated with mid-tropospheric convection;

(v) squall lines in the tropics and mid-latitudes;

(vi) non-squall mesoscale convective systems in the tropics and mid-latitudes;

(vii) sub-synoptic-scale comma clouds associated with cold air vortices; and

(vii) polar trough conveyor belts and instant occlusions.

1. Introduction

Nowcasting, i.e. the generation of detailed site-specific forecasts for a few hours ahead, is a particularly challenging task in the presence of precipitation-producing weather systems. This is partly because of the difficulty in observing these systems adequately owing to the large amount of mesoscale and convective sub-structure they contain. It is also because of the difficulty in predicting how these complex patterns will evolve even in the very short term.

Direct, *in situ* measurements by themselves do not offer an adequate means of observing on the mesoscale. Satellite-based measurements and ground-based radar observations, on the other hand, do provide a good opportunity for describing many of the fine-scale features, especially the cloud and precipitation patterns. Mesoscale temperature information is not so easily obtained because, for example, of the problem of retrieving satellite soundings when the field of view is contaminated by cloud and precipitation. It is, however, possible to make useful inferences about the fields of airflow (and to a

limited extent the location of temperature gradients) from the form and movement of these same cloud and precipitation patterns although this calls for some subjective interpretation of the patterns.

Subjective interpretation is even more necessary in the generation of very-short-range forecasts. It is well known that simple objective extrapolation by itself is of only limited value for forecasting precipitation and that, in order to obtain an indication of probable areas of development and decay, it is necessary to be able to infer where the areas of potential instability and slantwise ascent are likely to be. Numerical models can provide guidance about the broader-scale features but subjective interpretation is still needed to unravel the complexity of the mesoscale.

Until recently a major factor impairing the forecasters' ability to exploit satellite and radar imagery has been the inadequacy of the systems for displaying and manipulating the data. Forecasters are, however, beginning to be provided with modern display systems — sometimes with facilities for action replay, image reprojection and enhancement and, in a few cases, superimposed model products. The primary impediment to using these data effectively is now the forecaster's limited ability to make sense of the cloud and precipitation patterns in terms of the dynamical factors that are producing them. There is thus a clear need for more training of forecasters in the meteorological interpretation of the imagery. As part of this training the forecaster needs to be provided with a better conceptual framework within which to interpret the imagery. In short, he needs a set of conceptual models of precipitation systems. These same conceptual models can be expected to be helpful in interpreting not only the imagery but also numerical model guidance in terms of surface weather, especially where the forecaster is able to display sequences of satellite and radar imagery superimposed on the model predictions for corresponding times.

The purpose of this article is to present some examples of conceptual models that are thought to be helpful in the interpretation of imagery. The scope of the article is limited to mesoscale precipitation systems and their larger-scale context. Both frontal systems and convective systems are discussed. The emphasis is mainly, but not entirely, on mid-latitude systems. Individual thunderstorms are not considered. Terrain effects, though important, are also excluded.

2. Conveyor belt models applicable to mid-latitude frontal systems

The frontal models of the Norwegian school have dominated our ideas of frontal structure for over half a century. Forecasters still struggle to interpret mesoscale details of mid-latitude precipitation systems within the context of the simple archetypes of the warm, cold and occluded front. These models are at best inadequate and at worst misleading and an overdependence on them has tended to bring frontal analysis into disrepute. But the task of improving on the existing models is not an easy one. Thus in this paper we can present only a few faltering steps towards a new conceptual approach in frontal analysis.

The first requirement for analysing the mesoscale features of cloud and precipitation in frontal systems is to have a synoptic-scale framework that is able to reconcile the observations in a natural (i.e. system-centred) way. A concept that has been found useful is based on the idea of the 'conveyor belt', the essence of which is that it identifies the major cloud and precipitation-producing flows in a system-relative frame of reference.

2.1 *The warm conveyor belt*

The dominant mechanism in frontal systems is baroclinic slantwise ascent and Fig. 1, from Green *et al.* (1966), shows a simplified depiction of the corresponding large-scale pattern of flow in a major trough–ridge system. The key feature is the elongated band of cloud that forms along the boundary of a major confluence zone at the leading edge of the trough. In a frame of reference moving with the

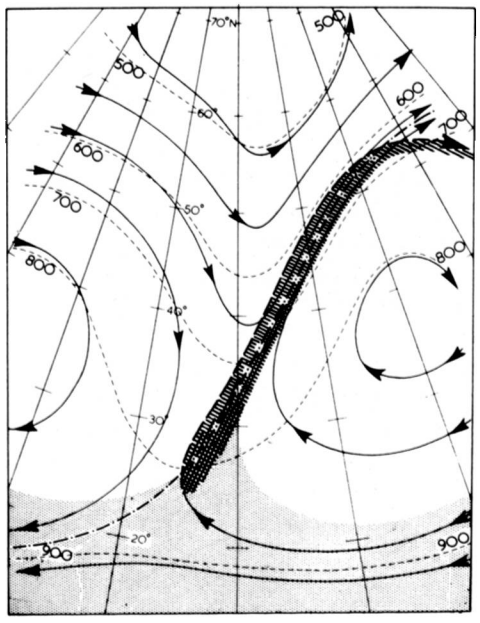

Figure 1. Schematic representation of relative flow in a major trough of large-scale slantwise convection over an ocean on a surface of constant potential temperature, θ, (about 30 °C). The isobars (mb) on the surface are shown by dashed lines. The cold frontal zone, in which the narrowing of the separation between two isobars indicates a steepening of the isentropic surface, contains a (dot-dashed) line of confluence between two principal airstreams. The stippled zone in the south shows where trajectories of the mean flow lie within the layer of small-scale convection in the boundary layer in which θ, and even more so wet-bulb potential temperature, θ_w, increases along the flow. The air is unsaturated in most areas except for the hatched area which marks a band of clouds rising above the isentropic surface. This is the region of strong south to south-westerly flow which we refer to as the warm conveyor belt. The clouds in the warm conveyor belt first form in low latitudes, where they are liable to develop into more or less deep convective clouds (in the region shown by cross-hatching); they appear subsequently as middle-level layer clouds, and eventually as ice clouds (baroclinic cirrus) in the high troposphere of middle latitudes (where they lie near and to the right of the axis of the upper-tropospheric jet stream). These clouds evaporate after the flow at their level has turned to become north-westerly and the airstream begins to subside (from Green *et al.* 1966).

trough–ridge system, warm air is seen to be drawn into the cloud belt from the convective boundary layer in low latitudes; it rises into the middle troposphere as it travels within the cloud belt and eventually produces a deck of upper tropospheric cirrus which decays ahead of the frontal system. Following Harrold (1973) we refer to the narrow airstream as the warm conveyor belt because of its role in conveying large quantities of heat (and also moisture and westerly momentum) polewards and upwards. The region of cirrus cloud associated with it is referred to by Weldon (1979) as baroclinic zone cirrus.

The warm conveyor belt has been found to be a useful concept for accounting for frontal systems not only in north-west Europe where the idea was first evolved but also in the USA (Carlson 1980) and Australia (Ryan and Wilson 1985). Cahir *et al.* (1985) have carried out a composite analysis of a large number of warm conveyor belts and show that, in these high-speed flows of warm moist air, the relative wind jet stream is situated within and closely parallel to the typically sharp left-hand cloud edge. An example of a well-defined cloud belt associated with a long warm conveyor belt is given in Fig. 2. Warm conveyor belts vary greatly in length and certainly are not always as long as in Figs 1 and 2.

Air in the warm conveyor belt flows along the length of the cold front, part of it often being in the form of a low-level jet within the boundary layer just ahead of the surface cold front (Browning and Pardoe 1973). The warmest air of all, having originated farthest south, is usually to be found immediately ahead

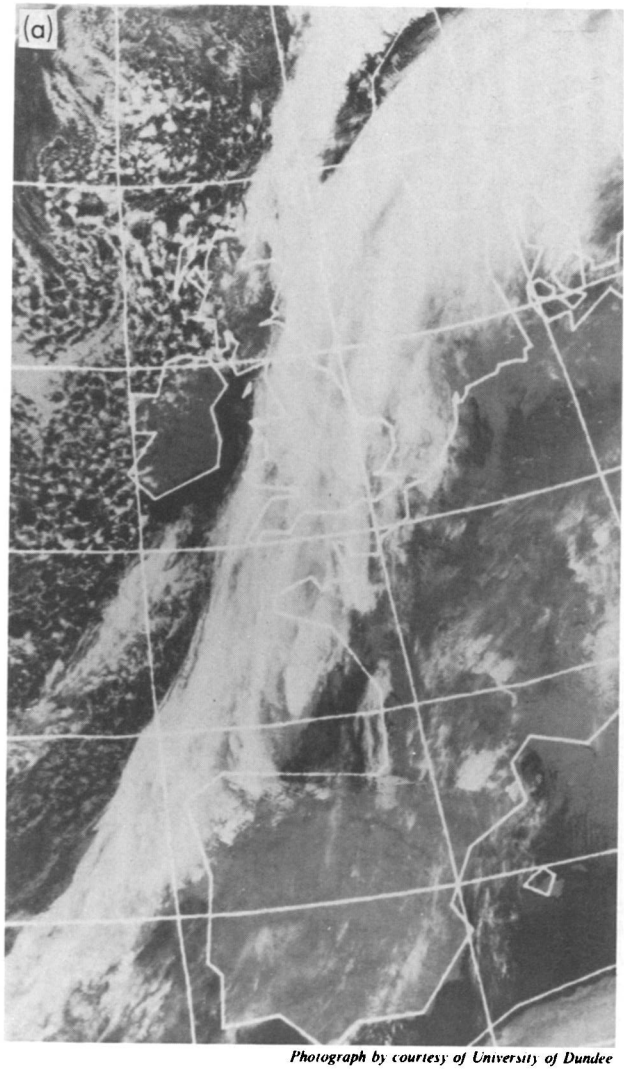

Photograph by courtesy of University of Dundee

Figure 2(a). Infra-red photograph from a NOAA satellite at 0317 GMT on 13 January 1983 showing an elongated belt of cloud associated with a major warm conveyor belt.

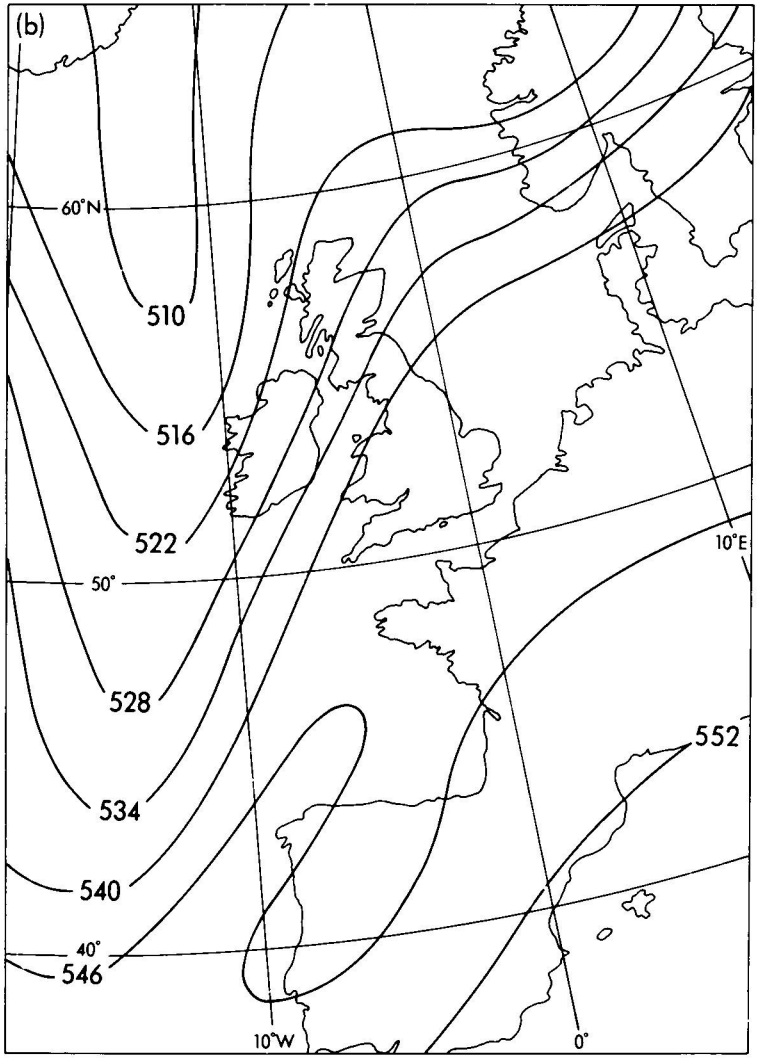

Figure 2(b). 1000–500 mb thickness (dagpm) analysis for 0000 GMT on 13 January 1983 showing the major trough–ridge system with which the warm conveyor belt was associated.

of the surface cold front. The associated negative horizontal temperature gradient ahead of the cold front in the warm conveyor belt accounts, through the thermal wind relationship, for the decrease in wind speed above the low-level jet.

Although the main component of motion within the warm conveyor belt is parallel to the cold front, the relatively small and mainly ageostrophic component perpendicular to the front has an important bearing on the frontal structure. It is useful to distinguish two contrasting situations:

(i) A 'rearward sloping ascent' configuration in which the air in the warm conveyor belt has a component of motion rearwards relative to the movement of the cold front and in which the slantwise ascent occurs in the vicinity of and above the cold frontal zone (Fig. 3).

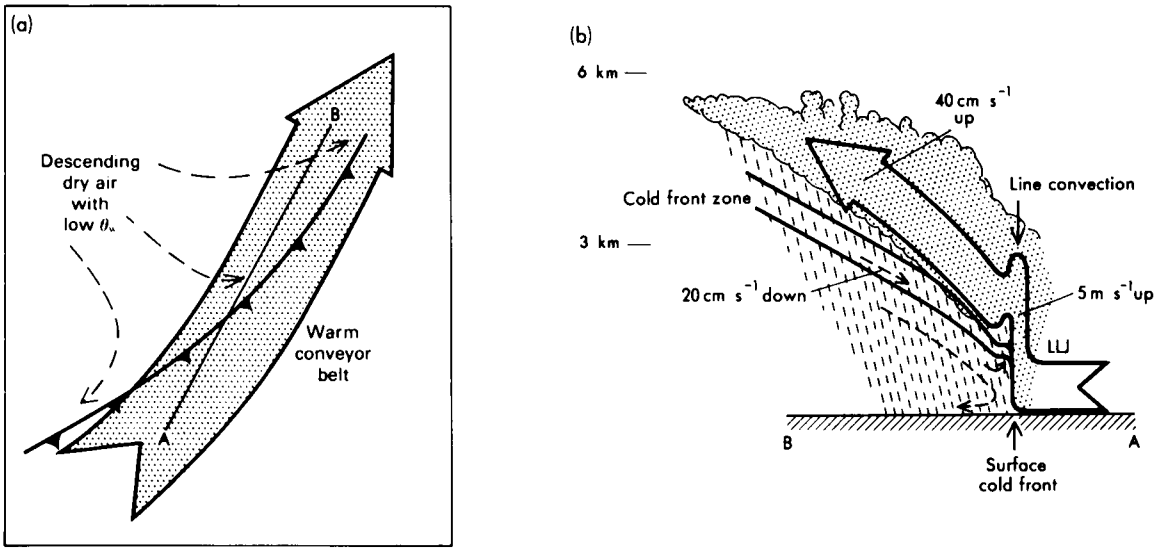

Figure 3. Schematic portrayal of airflow at a classical ana cold front showing the warm conveyor belt (bold arrow) undergoing rearward sloping ascent above the cold frontal zone with the cold air (dashed lines) descending beneath it: (a) plan view, (b) vertical section along AB in (a) (LLJ marks axis of low-level jet). Flows are shown relative to the moving frontal system.

(ii) A 'forward sloping ascent' configuration in which the air in and above the warm conveyor belt has a component of motion forwards relative to the movement of the cold front, with its main region of slantwise ascent occurring farther downwind in regions of warm frontal baroclinicity (Fig. 4).

Transitions between rearward and forward sloping ascent can occur; the transition may occur both in time and in space (along the length of a cold front).

2.2 *The warm conveyor belt with rearward sloping ascent*

The rearward sloping ascent configuration (Fig. 3), in which some or all of the warm conveyor belt air rises with a component rearwards above an advancing wedge of cold air, corresponds to the classical ana cold frontal situation (Sansom 1951). In the United Kingdom this configuration is not as common as the situation of forward sloping ascent described in section 2.3. In contrast to situations of forward sloping ascent, the surface cold front in cases of rearward sloping ascent tends to be sharp. The warm air in the boundary layer ahead of the surface cold front is lifted abruptly at up to several metres per second within a narrow strip adjacent to the surface cold front. This is a region of intense cyclonic shear (10^{-2} s^{-1}) on the western boundary of the pre-cold frontal low-level jet and the vertical air velocity is consistent with the expected Ekman layer convergence. Release of latent heat in the presence of friction has been shown to

be an important factor contributing to the strength of both the low-level jet and the cyclonic shear (Hsie *et al.* 1984).

The air rises only 2–3 km during its abrupt ascent at the surface cold front. It undergoes further ascent in slantwise fashion, at a few tens of centimetres per second, above the wedge of cold air (Browning and Harrold 1970). These two regions of ascent produce two distinct patterns of precipitation:

(i) A narrow band of very heavy rain at the surface cold front.

(ii) A broad belt of light-to-moderate rain extending behind and often to some extent ahead of the surface cold front.

These features are discussed further in section 3.

2.3 *The warm conveyor belt with forward sloping ascent*

The forward sloping ascent configuration, shown in Fig. 4, corresponds to a kata cold front situation for which the main ascent occurs ahead of the surface cold front and recently descended air with low wet-bulb potential temperature (θ_w) overruns the warm conveyor belt in the middle troposphere (Miles 1962). This leads to the generation of potential instability which is realized as convection once the general flow has been lifted sufficiently. This convection sometimes occurs as deep convection from the surface (section 4.1) but more usually in the United Kingdom it occurs as shallow middle-level convection. Eventually the cloudy warm conveyor belt flow turns anticyclonically (i.e. to the right) as it overtakes and ascends over the cold air ahead of the surface warm front. The convex-poleward

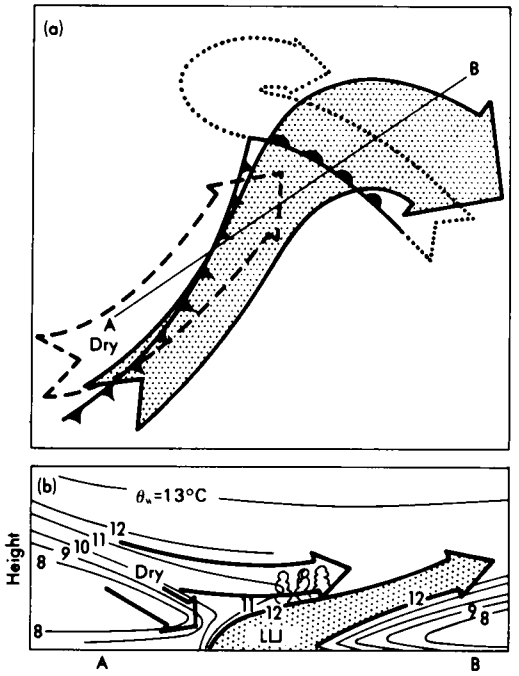

Figure 4. Schematic portrayal of airflow in a mid-latitude cyclone in which the warm conveyor belt (bold arrow with stippled shading) is undergoing forward sloping ascent ahead of a kata cold front before rising above a flow of cold air ahead of the warm front (dotted arrow, referred to in section 2.4 as the cold conveyor belt). Cold middle-tropospheric air with low θ_w (dashed arrow) is shown overrunning the cold front and generating potential instability in the upper portion of the warm conveyor belt: (a) plan view, (b) vertical section along AB in (a) (LLJ marks axis of low-level jet). Flows are shown relative to the moving frontal system.

boundary to this flow where it ascends and turns to the right is often clearly detectable in satellite visible imagery from the shadow the upper cloud casts on the lower cloud layer.

The leading edge of the overrunning dry, low θ_w air advancing ahead of the surface cold front often appears as a well-defined upper cold front (UU in Fig. 5). Ahead of the upper cold front the depth of the warm moist air increases abruptly in association with an organized band of convection. This gives a wide band of moderate-to-heavy rain, often at the trailing edge of a region of rather lighter warm frontal precipitation much of which may evaporate before reaching the ground. The passage of the upper cold front is followed by a shallow moist zone with scattered outbreaks of weakly convective rain and drizzle perhaps with some outbreaks of deeper convection close to the cyclone centre. Because of the separate existence of the upper cold front ahead of the surface cold front, this is referred to as a split front model (Browning and Monk 1982). Split cold fronts are very common in the United Kingdom. There is much

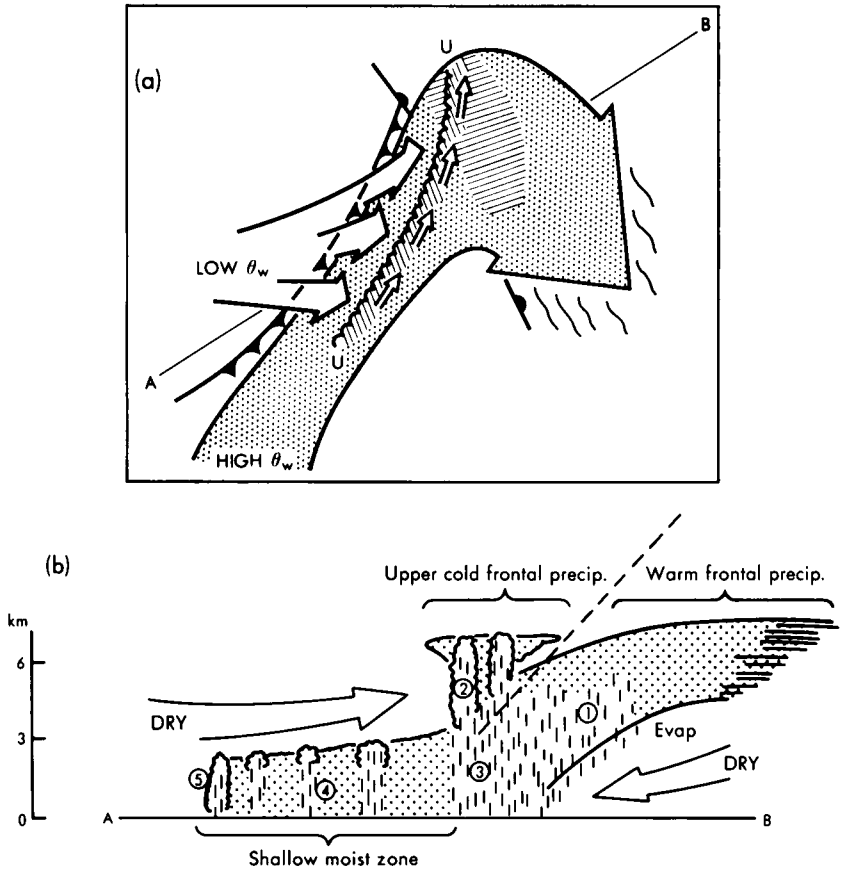

Figure 5. Schematic portrayal of the same situation as in Fig. 4, i.e. with the warm conveyor belt undergoing forward sloping ascent, but drawing attention to the split front characteristic and the overall precipitation distribution: (a) plan view, (b) vertical section along AB in (a). In (a) UU represents the upper cold front. The hatched shading along UU and ahead of the warm front represents precipitation associated with the upper cold front and warm front respectively. Numbers in (b) represent precipitation type as follows: 1, warm frontal precipitation; 2, convective precipitation-generating cells associated with the upper cold front; 3, precipitation from the upper cold frontal convection descending through an area of warm advection; 4, shallow moist zone between the upper and surface cold fronts characterized by warm advection and scattered outbreaks of mainly light rain and drizzle; 5, shallow precipitation at the surface cold front itself (after Browning and Monk 1982).

confusion in their analysis when forecasters attempt to apply the simple classical frontal model. To avoid this confusion the traditional cold frontal symbolism should be reserved for the surface cold front and the upper cold front should be identified differently, perhaps by a scalloped line as in Fig. 5(a). More often than not the two fronts are better defined in the humidity (and θ_w) fields than in the temperature field, in which case they are better regarded as 'humidity fronts'.

2.4 *The cold conveyor belt*

The warm conveyor belt has been identified as the dominant cloud- and precipitation-producing flow in mid-latitude systems. A secondary cloud-producing flow is the cold conveyor belt (dotted arrow in Fig. 4) which originates in the anticyclonic low-level flow to the north-east of a cyclone (Carlson 1980, Ludlam 1980). Relative to the advancing cyclone, air in the cold conveyor belt travels westwards just ahead of the surface warm front beneath the warm conveyor belt. At first this air subsides and is very dry. Precipitation from the warm conveyor belt evaporates on falling into it. As it travels westwards towards the cyclone centre this air begins to ascend, reaching into the middle troposphere near the apex of the warm sector. Air on the cyclonically sheared edge of the cold conveyor belt, near the surface warm front, experiences enhanced ascent due to frictional convergence. If and when the cold conveyor belt emerges beneath the western edge of the warm conveyor belt, it may ascend anticyclonically and merge with the warm conveyor belt as sketched in Fig. 4; alternatively it may descend cyclonically around the cyclone centre. The area of cloud associated with the emerging cold conveyor belt constitutes the head of a large-scale comma cloud system.

3. Classification of mesoscale rainbands in mid-latitude frontal systems

The main cloud and precipitation-producing airstreams have been described in section 2 in terms of system-relative flows called conveyor belts. To a first approximation the rain areas are aligned along these flows. Often the flows are parallel to surface fronts and the belts of precipitation take on a similar orientation. At other times a conveyor belt may be oriented across a surface front. This happens, for example, in association with an upper cold front where it overruns the surface warm front. In such a case the belt of precipitation will be oriented parallel to the upper cold front instead of the underlying warm front.

Precipitation is seldom uniform across a conveyor belt. Convective and mesoscale circulations develop which modify the distribution of precipitation and lead to quite complex patterns even in the absence of terrain-induced effects. The convection leads to a tendency for the precipitation to concentrate in small-scale cells. The mesoscale circulations are of two kinds. One of them leads to groups of convective cells forming in clusters, giving rise to so-called mesoscale precipitation areas tens of kilometres across. The other, discussed more fully below, leads to banded precipitation features. Sometimes the rainbands are rather uniform along their length; more often they consist of aligned mesoscale precipitation areas. Some rainbands are perhaps no more than mesoscale precipitation areas roughly and perhaps fortuitously aligned along the axis of a conveyor belt. Other rainbands are clearly the result of more nearly two-dimensional mesoscale circulations. Considerable attention has been paid to the nature of mesoscale rainbands and many categories have been identified. Broadly speaking, however, there are two principal categories: narrow rainbands and wide rainbands. Examples of these two types are shown in Figs 6 and 7.

3.1 *Narrow rainbands*

Narrow rainbands are largely boundary-layer phenomena. Although narrow bands of light rain and drizzle, probably generated by helical vortex circulations, can be generated within warm sectors, the

Figure 6(a). Radar display showing a narrow cold frontal rainband over England. Pink and red, heavy rain mostly associated with the narrow rainband; blue, light and moderate rain. Resolution is 5 km × 5 km.

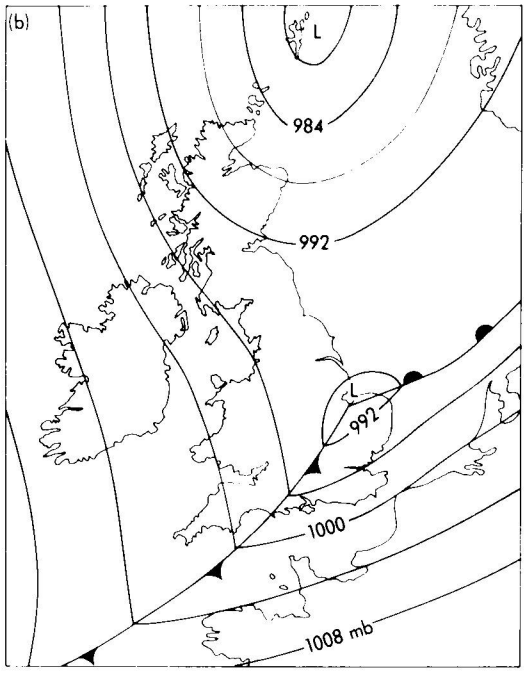

Figure 6(b). Surface analysis corresponding to Fig. 6(a).

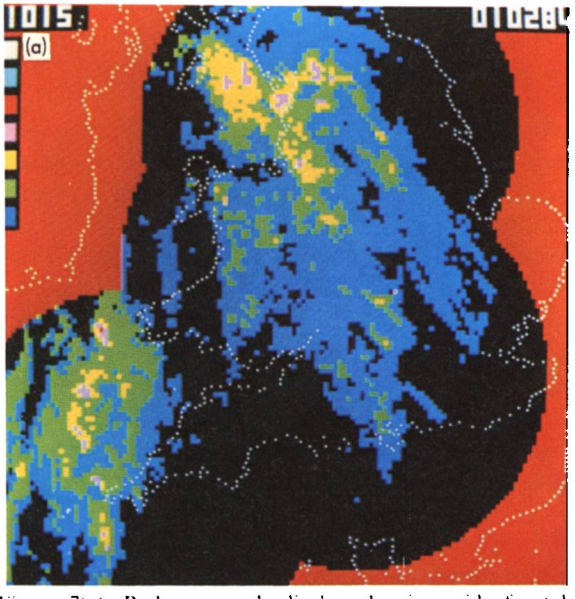

Figure 7(a). Radar network display showing wide frontal rainbands. Those over northern and central England are associated with a warm front. Those in the south-western approaches are associated with a cold front. The ill-defined ragged nature of these bands is typical of wide rainbands. Some (not all) of the complexity is due to orographic effects. Pink and yellow, heavy rain; green, moderate rain; blue, light rain.

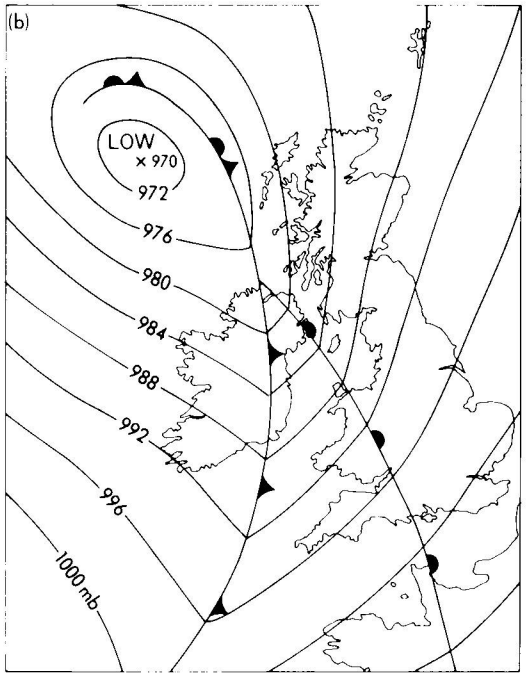

Figure 7(b). Surface analysis corresponding to Fig. 7(a).

most significant narrow bands are those that occur in the cold seasons at the sharp surface cold frontal discontinuity in the situations of rearward sloping ascent described in section 2.2. In the region immediately ahead of the front the boundary layer can be 2–3 km deep, capped by a stable layer. The narrow rainbands that occur here are aligned along the length of the surface front and, even though they are seldom more than 3 km deep and the same in width, they frequently produce a burst of very heavy rain and sometimes small hail.

The band of almost vertical convection that gives rise to a narrow cold frontal rainband is referred to as line convection (Browning and Harrold 1970). The line convection occurs immediately in advance of the cold air, the leading edge of which has the properties of a density current (Carbone 1982). Its passage is associated with a characteristic temperature drop and pressure kick. The boundary layer ahead of the front is neutrally stratified with respect to saturated ascent and the density current has the effect of generating convection which is forced rather than free. Line convection can on occasion extend as an unbroken line for 100 km but, more usually, it is broken into series of line elements each of the order of 10 km long. This is associated with a horizontal shearing instability on the strongly sheared edge of the low-level jet that occurs ahead of the front (cf. section 2.2). The resulting rainfall pattern is as shown in Fig. 8 (Hobbs and Biswas 1979, James and Browning 1979).

The narrow rainbands associated with the line convection tend to occur towards the leading edge of the belt of stratiform cloud associated with the slantwise convection. Sometimes they occur right at the leading edge, in which case they may be detectable in the satellite imagery. More often the shallow cumulonimbus associated with the line convection is embedded deep within the main mass of stratiform cloud (Fig. 8); it is then not evident in the satellite imagery (Fig. 9(a)) although it can be seen clearly by radar (Fig. 9(b)).

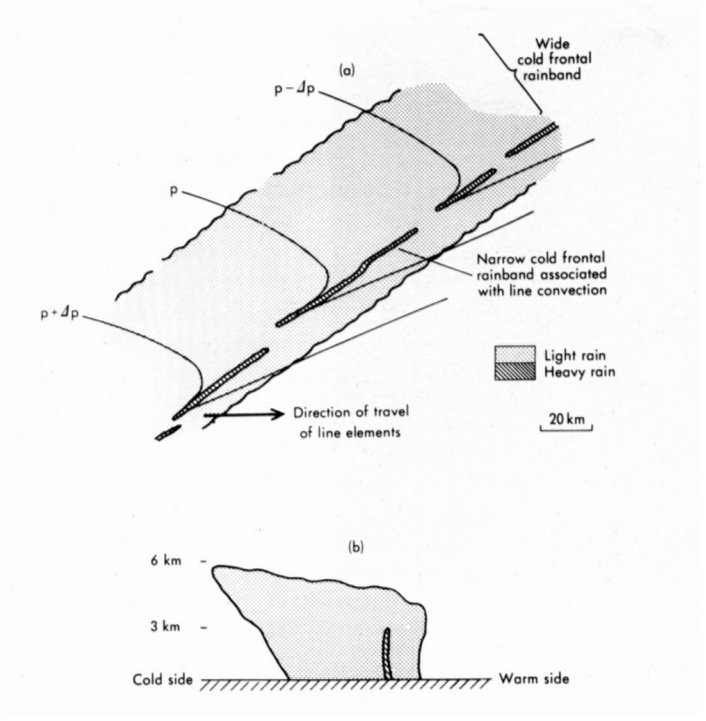

Figure 8. Schematic depiction of the pattern of precipitation and pressure (p) at a sharp cold front: (a) plan view; (b) vertical section normal to the front.

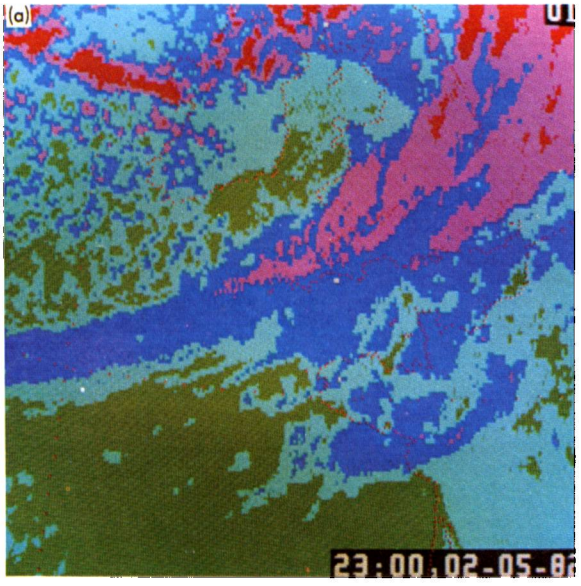

Figure 9(a). False colour infra-red satellite image from Meteosat showing a cold frontal cloud band oriented SW–NE across England and Wales. Red and pink, high cloud; dark blue, medium cloud; pale blue, low cloud and cold land; green, sea and warm land.

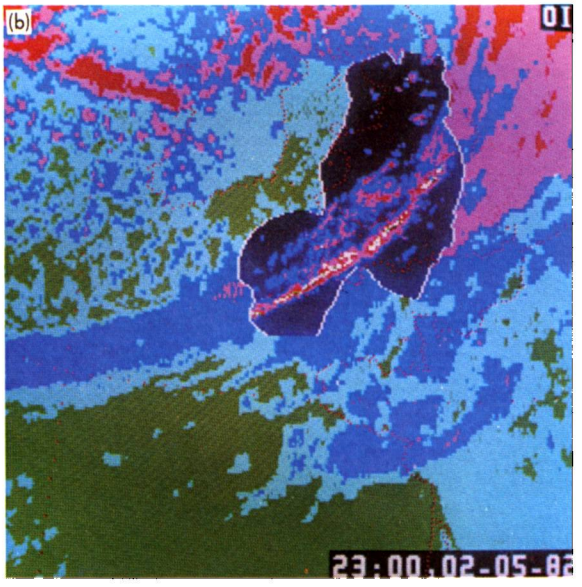

Figure 9(b). Same as Fig. 9(a) but with data from a network of four radars embedded within it on the same scale and projection where white represents very heavy rain; red, heavy rain; pink, moderate rain; blue, light rain; and black, no rain.

Narrow rainbands are associated with sharp cold fronts but such fronts are not uniformly sharp. The sharpest transitions of pressure, wind, temperature and humidity occur at the line elements of the narrow rainband. In the gaps between line elements there is a more gradual transition as shown by Fig. 10. When such a gap passes over a surface reporting station it can give the misleading impression that the surface front is of the diffuse kind normally associated with kata cold fronts (cf. section 2.3).

3.2 *Wide rainbands*

The broad zone of generally light-to-moderate rain associated with the slantwise ascent of the conveyor belt often contains organized bands of moderate-to-heavy rain several tens of kilometres wide (Fig. 7(a)). These are associated with mesoscale circulations within the warm conveyor belt about an axis parallel to the relative mean flow. There are several theories to account for them but one of the most promising is that they are associated with conditional symmetric instability (Bennetts and Hoskins 1979).

Types of wide rainbands are listed in Table I. The deep convective rainbands referred to in the table are of two kinds. Those occurring in the warm sector are sometimes associated with squall lines (see section 4.1). The post-frontal rainbands correspond to the cold air comma clouds which are discussed in section 5.1. However, the most common type of wide rainband within major frontal systems in the United Kingdom is the upper-level (U-type) rainband. Although U-type bands may occupy different positions within a frontal system (Fig. 11), they nevertheless all have rather similar dynamical characteristics and can conveniently be considered as one dynamical type. The characteristics of U-type rainbands may be summarized as follows:

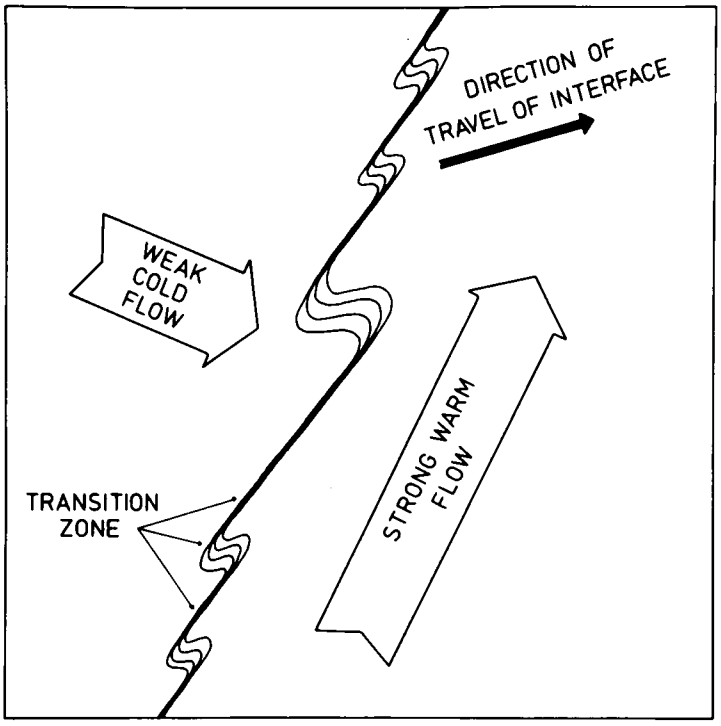

Figure 10. Schematic depiction of the transition zone at a sharp surface cold front. Line convection elements, with intense low-level convergence, strong updraughts and heavy precipitation, occur in the regions with a sharp transition zone. The regions where the temperature gradient is more gradual correspond to gaps between the line convection elements. The broad arrows, representing the flow at low levels on either side of the interface, are drawn relative to the ground (from James and Browning 1979).

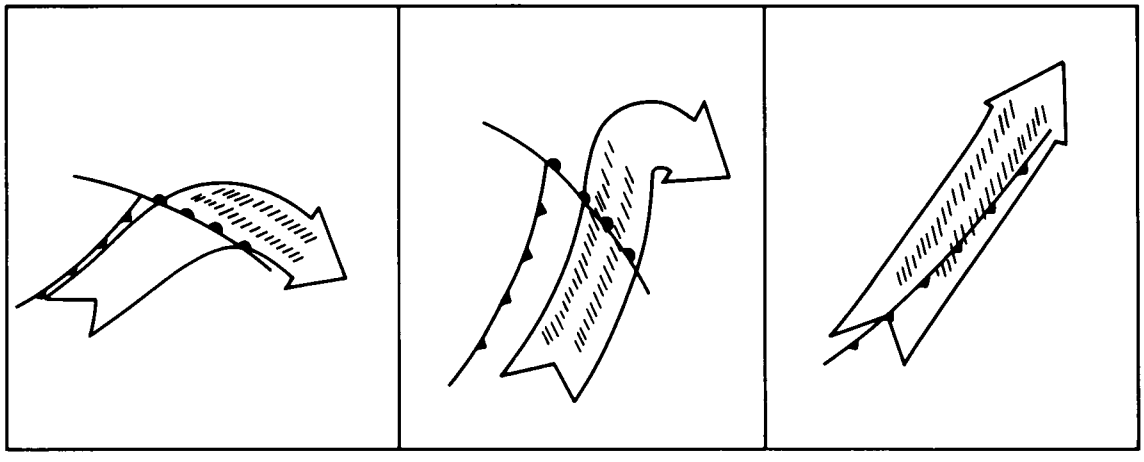

Figure 11. Idealized representation of three types of configuration of U-type wide rainbands (hatched shading) in relation to the warm conveyor belt flow (broad arrows): (a) and (b) forward sloping ascent situations with warm frontal and pre-frontal cold surge rainbands, respectively, (c) rearward sloping ascent with cold frontal rainbands. Narrow rainband elements occur in the boundary layer along the surface cold front coexisting with the wide rainbands in (c).

Table I. *Types of wide mesoscale rainbands*

Broad classification	Detailed classification (after Hobbs 1978)	Frontal archetype with which associated	Location and orientation	Some published examples
Upper- (or mid-) tropospheric convective rainbands (U-type)	Warm frontal rainband	Forward sloping ascent	Parallel to the warm front and either on or ahead of it	Browning and Harrold 1969, Herzegh and Hobbs 1978a, Heymsfield 1979
	Pre-frontal cold surge rainband	Forward sloping ascent	Parallel to and just ahead of an overrunning upper cold front	Kreitzberg 1964, Kreitzberg and Brown 1970, Browning *et al.* 1973
	Cold frontal rainband	Rearward sloping ascent	Parallel to and either behind or straddling an active surface cold front	Browning and Harrold 1970, Hobbs *et al.* 1978
Deep convective rainbands	Warm sector rainband	Either?	Ahead of and parallel to the surface cold front	Nozumi and Arakawa 1968, Herzegh and Hobbs 1978b
	Post-frontal rainband	Either?	Behind the main frontal system and parallel to the cold front	Houze *et al.* 1976

(i) They are associated with the ascending parts of the warm conveyor belt where its top reaches into the middle troposphere.

(ii) They contain upper- or middle-level convective cells, often in clusters, which are generated within a shallow layer of potential instability where air with low θ_w overruns the warm conveyor belt. The underlying air is generally statically stable, occasionally markedly so at some levels.

(iii) They are 50 km wide (within a factor of 2) and typically a few hundred kilometres long, with an orientation parallel to the baroclinicity at their level. (The baroclinicity in the lower troposphere is often much stronger and may be oriented differently.)

The structure and evolution of U-type rainbands have been described by Kreitzberg and Brown (1970). They use the term 'leafed hyper-baroclinic structures' to describe the wrinkling of the surfaces of constant θ_w in the warm conveyor belt above a frontal zone caused by the mesoscale circulations. Each major wrinkle, or warm tongue, in the conveyor belt gives rise to a separate U-type rainband. The wrinkles locally enhance the potential instability and promote the upper- or mid-tropospheric convective generating cells.

4. Mesoscale convective systems

4.1 *Mid-latitude squall lines*

The shallow cold frontal line convection discussed in section 3.1 is characterized by a sudden wind shift. However, although the low-level winds ahead of such cold fronts are invariably strong, the sharp

veer which occurs at the passage of the line convection is, more often than not, accompanied by a drop in wind speed. The most vigorous squalls, therefore, do not occur in situations of line convection; nor in general do they occur in the situations that promote line convection, i.e. when the warm conveyor belt air undergoes rearward sloping ascent behind the surface cold front as described in section 2.2. Instead, major squall lines in middle latitudes occur in association with lines of deep convective cells which break out within warm sectors, often 200–300 km ahead of the surface cold front, in the kind of synoptic situation described in section 2.3. This is the situation in which, relative to the large-scale frontal system, the warm conveyor belt air undergoes forward sloping ascent ahead of the surface cold front and is overrun by dry, recently descended air with low θ_w in the middle troposphere. In the United Kingdom this synoptic situation usually gives rise to an upper cold front characterized by middle-level convection as in the split front model in Fig. 5. However, when the value of θ_w near the ground is high, as often happens in the United States Midwest in the spring storm season, deep convection may occur from the surface. This can lead to vigorous convective cells with strong squalls at the surface forming along or just behind the line corresponding to UU in Fig. 5(a).

A cross-section through a squall line system, from Newton and Newton (1959), is shown in Fig. 12.

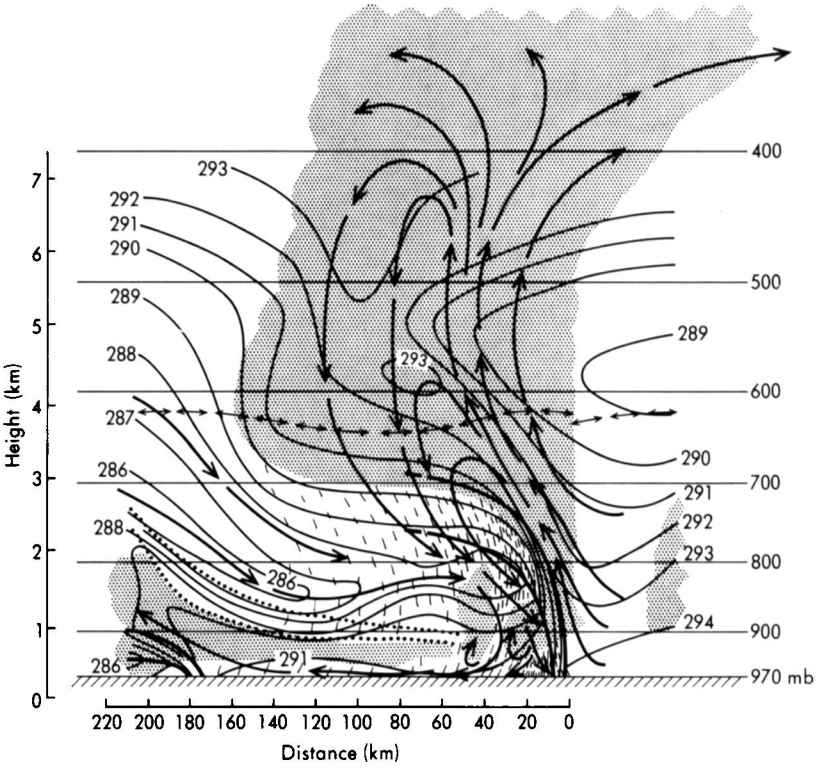

Figure 12. Vertical section through a squall line obtained from a sequence of radiosondes (from Newton and Newton 1959). Distance scale calculated from the speed of advance of the system. Heavy lines are boundaries of stable layers, the cold front being far to the left of the squall-line system. Dots indicate a stable layer in the squall sector with shallow clouds beneath and relatively dry sinking air above. Thin lines are isopleths of θ_w (K). Double-headed arrows represent the melting level. Stippled shading represents cloud. 'Raindrops' below cloud base suggest precipitation intensities. Arrows showing overall circulation are schematic.

The system, travelling from left to right in the figure, has an organized circulation in the direct solenoidal sense. The moist air of high θ_w at low levels ahead of the storm ascends steeply through the conditionally unstable air mass. In the case shown here, in which the squall line was propagating faster than the cold frontal system, much of the updraught air tends to be left behind the storm as a trailing anvil. In other systems the anvil may advance mainly ahead of the storm. In either event the flow in the anvil usually also has a strong component into the plane of Fig. 12. Precipitation falling from the updraught evaporates into dry air that enters the storm circulation at middle levels. Evaporative chilling causes this air to sink by virtue of its increased density. The cold squall-sector air formed in this manner spreads out within an elongated mesohigh pressure region beneath the line of storms. In so doing, the leading edge of the cold air forms a density current or pseudo cold front which triggers renewed convection there and controls the rate of propagation of the squall line as a whole.

Mid-latitude squall lines tend to be segmented into clusters of thunderstorms with overall dimensions 30–100 km (Fankhauser 1964, Pedgley 1962). Just as individual thunderstorms often consist of a number of updraught cells with new ones forming on the right hand side and old ones dissipating on the left, so too in squall lines the clusters form on the right (southern) end and, after a lifetime of about 5 hours, dissipate at the left end.

4.2 *Tropical squall lines*

Tropical squall lines have an organization similar in many ways to that of mid-latitude squall lines except that, being embedded in an easterly flow, they travel towards the west rather than the east: see the conceptual model in Fig. 13. In both cases the squall lines tend to travel by a combination of cell translation and discrete propagation. New updraught cells in the tropical systems form systematically on the leading edge (left side of Fig. 13) triggered by a density current outflow (gust front) at the surface which in the tropical squall lines travels westwards faster than the winds at any level. These cells grow to become the main cells of the squall line before eventually decaying at the rear. Air having a low θ_w, originating from middle levels at the front of the storm feeds negatively buoyant downdraughts within these cells. On reaching the surface some of the downdraught air spreads forward to produce the gust front and some of it is left behind as an extensive wake of cool stable air in the boundary layer. The

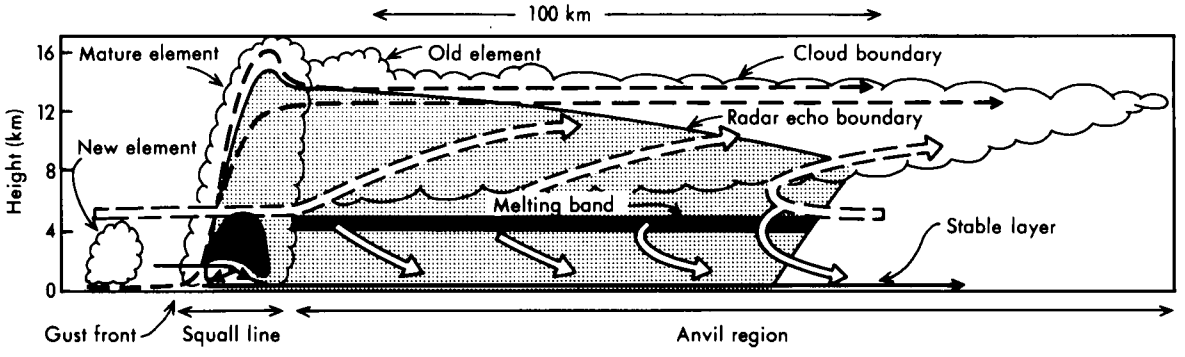

Figure 13. Schematic depiction of a typical cross-section through a tropical squall system. Dashed and continuous streamlines, respectively, show convective-scale updraughts and downdraughts associated with the mature squall-line elements, and also their inflows and outflows. Wide dashed and solid arrows, respectively, show mesoscale updraught and downdraught circulations. Dark shading shows strong radar echoes in the melting layer and in the heavy precipitation zone of the mature squall line element. Light shading shows weaker radar echoes. The scalloped line indicates the visible cloud boundary (from Houze and Hobbs 1982).

trailing anvil region aloft has a predominantly stratiform nature. The continued generation of light precipitation aloft in this region implies a zone of mesoscale ascent in the upper troposphere. There is a corresponding zone of mesoscale descent in the lower troposphere.

4.3 *Tropical non-squall convective systems*

The visible satellite photograph in Fig. 14 shows tropical cloud systems ranging from fields of scattered small cumulus to mesoscale cloud clusters. One of the clusters produced a squall line, which

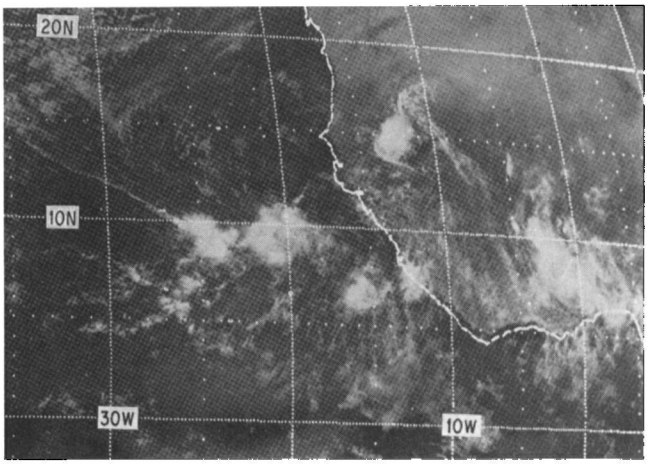

Figure 14. Visible image from the SMS-1 geostationary satellite showing tropical cloud systems ranging from fields of small cumulus to large cloud clusters. The latter are evident from their large cirrus shields at 9°N 24°W, 9°N 21°W, 7°N 16°W, 8°N 12°W and 14°N 13°W. The last of these was a squall cluster with an arc cloud line on its leading (south-west) side (from Houze and Hobbs 1982).

can be seen as a cloud arc on the south-western boundary of the cluster. All the other clusters lacked squall line characteristics. Non-squall cloud clusters are by far the commonest form of mesoscale system in the tropics.

The model of a non-squall cloud cluster in Fig. 15 shows three of the four stages of the life cycle identified by Leary and Houze (1979). The four stages are:

(i) Formative stage: scattered convective cells triggered by some initial mesoscale convergence at low levels (Fig. 15(a)).

(ii) Intensifying stage: further convective cells form while existing cells grow and merge, leading to a large continuous area in which the convective cells are interconnected by stratiform precipitation of moderate intensity falling from a spreading anvil deck.

(iii) Mature stage: a mixture of convective and stratiform precipitation as before but with the area of stratiform precipitation becoming extensive and containing mesoscale updraughts and downdraughts (Fig. 15(b)).

(iv) Dissipating stage: rate of formation of new convective cells diminishes but the area of stratiform upper cloud persisting for some time with light rain or virga (Fig. 15(c)).

Altogether the four stages last about a day, the convective circulations dominating in the early stages and the mesoscale circulations dominating in the later stages.

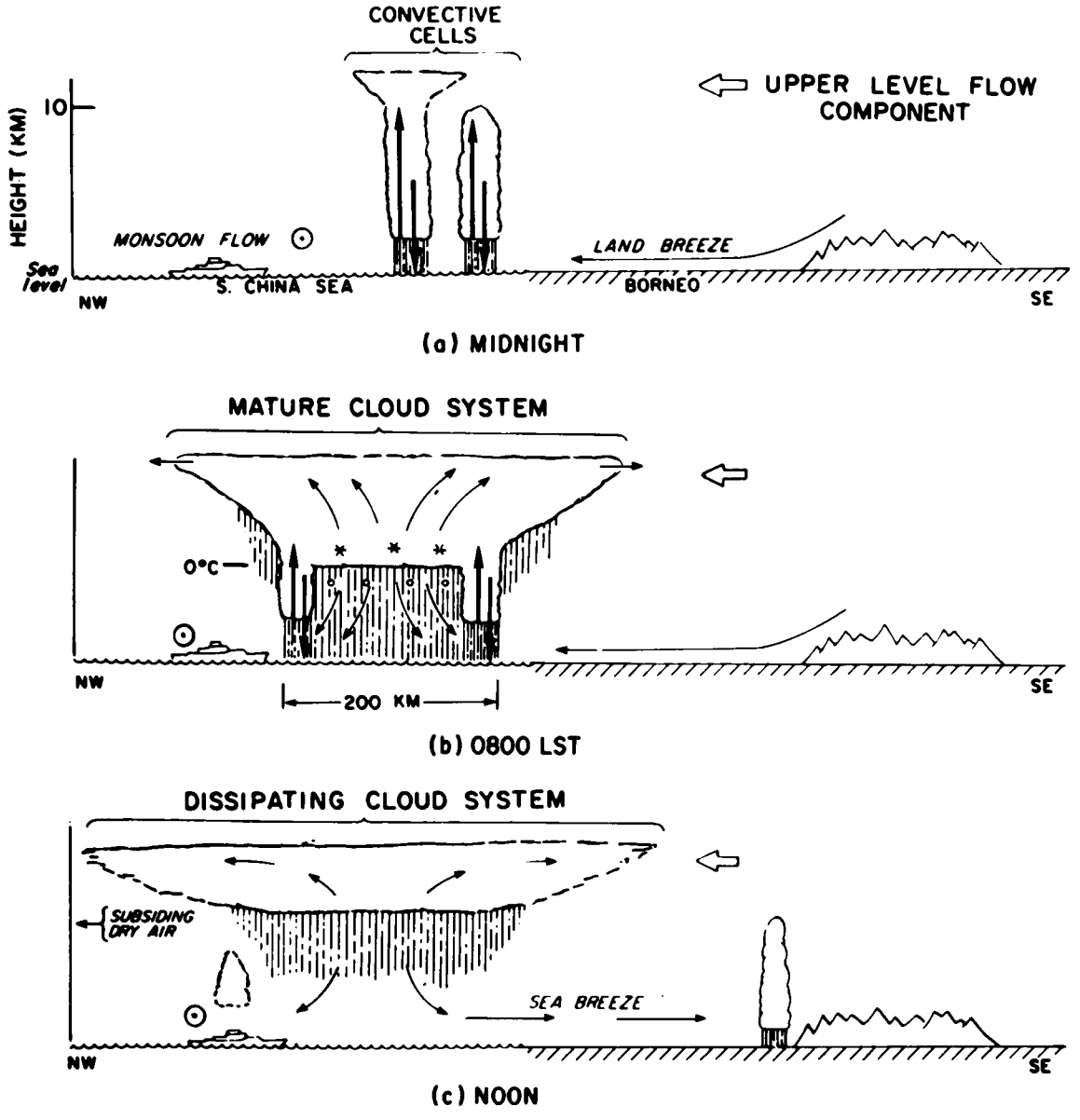

Figure 15. Schematic depiction of the development of a diurnally generated non-squall tropical cloud cluster off the coast of Borneo. Various arrows indicate airflow. The circumscribed dot indicates north-easterly monsoon flow out of the page. The wide open arrow indicates the component of the typical east-south-easterly upper-level flow in the plane of the cross-section. Heavy vertical arrows in (a) and (b) indicate cumulus-scale updraughts and downdraughts. Thin arrows in (b) and (c) show a mesoscale updraught developing in a mid- to upper-level stratiform cloud with a mesoscale downdraught in the rain below the middle-level base of the stratiform cloud. Asterisks and small circles indicate ice above the 0 °C level melting to form raindrops below this level (from Houze *et al.* 1981).

4.4 *Mesoscale convective systems in mid-latitudes*

Systems resembling tropical cloud clusters also occur in mid-latitudes where they are referred to as mesoscale convective complexes (Maddox 1980) or mesoscale convective systems. The above life cycle model of Leary and Houze applies to them as well. Their distinctive visual feature is the rather symmetrical upper-level cloud shield generated by the combined anvil outflows from the constituent thunderstorm cells. The top of the cloud shield is high, cold, and sharp edged, and it shows up prominently in satellite imagery (Fig. 16(a)). Table II shows the criteria used by Maddox to identify mesoscale convective complexes in infra-red satellite pictures. The Table gives an indication of the large area of many of these systems; however, the particular criteria are unduly restrictive since there are many smaller systems that appear to have structures and mechanisms similar to those ascribed to mesoscale convective complexes (Zipser 1982).

Fig. 16(b) shows the precipitation distribution that was associated with the distinctive cloud pattern in Fig. 16(a). A mesoscale region of fairly uniform, essentially stratiform, rain is seen to have developed beneath the cirrus shield downwind (to the north-west) of the active convection. In such situations thunder may be widespread throughout the areas of both convective and stratiform rain and the whole area may be characterized by a mesohigh produced by evaporative cooling.

Although mesoscale convective systems are dominated by sub-synoptic-scale circulations their development is nevertheless influenced by synoptic-scale forcing. The system portrayed in Fig. 16 formed in a locally intensified baroclinic zone on the flank of a cold pool and it was fed by an airflow with high θ_w (W_1W_2 in Fig. 17) which originated at low levels just ahead of a surface cold front. The

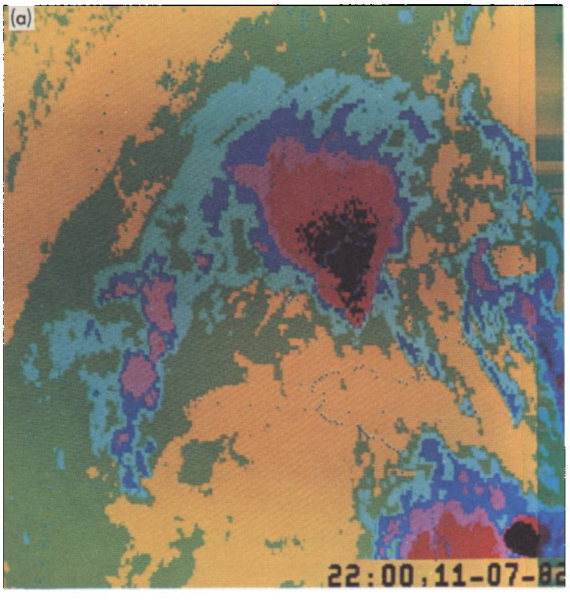

Figure 16(a). False colour infra-red satellite image from Meteosat showing a mesoscale convective system over south-west England. Area of coverage is 1280 km × 1280 km. Black ≤ -52 °C; red ≤ -43 °C; pink ≤ -35 °C; dark blue ≤ -27 °C; pale blue ≤ -16 °C; green ≤ -5 °C; yellow > -5 °C.

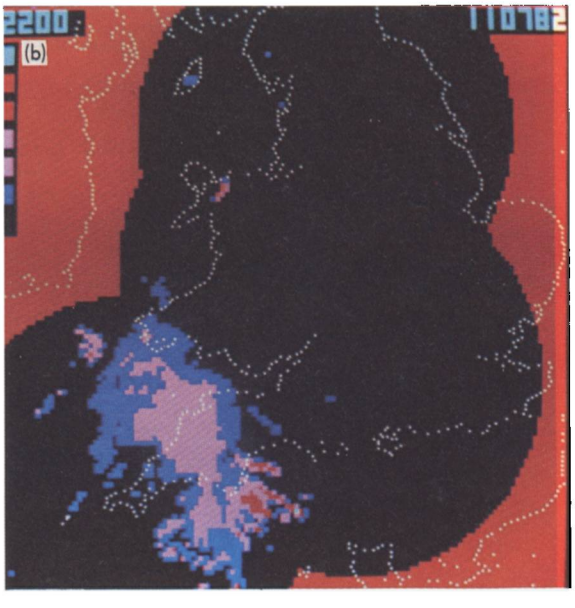

Figure 16(b). Rainfall echo distribution, at time corresponding to Fig. 16(a), as given by the UK weather radar network. Red ≥ 16 mm h^{-1}; mauve ≥ 4 mm h^{-1}; blue ≥ 1 mm h^{-1}.

Table II. *Criteria used to identify mid-latitude mesoscale convective complexes in infra-red satellite data (from Maddox 1980)*

	Physical characteristics
Size	(a) Cloud shield with continuously low infra-red temperatures $\leqslant -32$ °C must have an area $\geqslant 100\,000$ km^2
	(b) Interior cold cloud region with temperature $\leqslant -52$ °C must have an area $\geqslant 50\,000$ km^2
Initiation	Size definition (a) and (b) are first satisfied
Duration	Size definitions (a) and (b) must be met for a period $\geqslant 6$ h
Maximum extent	Contiguous cold cloud shield (infra-red temperature $\leqslant -32$ °C) reaches maximum size
Shape	Minor axis/major axis $\geqslant 0.7$ at time of maximum extent
Termination	Size definitions (a) and (b) no longer satisfied

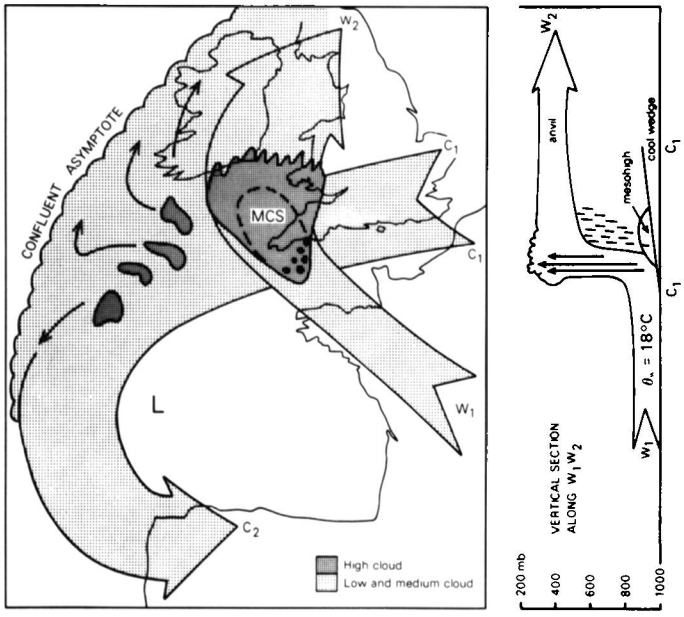

Figure 17. Schematic model of the mature mesoscale convective system (MCS) portrayed in Fig. 16 (from Browning and Hill 1984). Key to plan view (left): heavy stippled shading, high cirrus shield; dashed lines within MCS, boundary of surface rain and mesohigh; blobs in south-east of MCS, convective cores; arrow W_1W_2, air with high θ_w entering MCS below 800 mb and leaving in upper troposphere; arrow C_1C_2, cool air circulating around cold pool; small arrows, diffluent flow of mid-tropospheric cloudy air approaching the confluent asymptote. Key to vertical section (right): arrow W_1W_2, same as arrow in plan section; vertical arrows, representation of convective cores; dashed shading, mesoscale downdraught; dome shape, rain-chilled mesohigh dome; wedge shape, wedge of cool surface easterlies associated with arrow C_1C_2 in plan view.

configuration of this flow resembles that of the warm conveyor belt in Fig. 4 except that instead of ascending gradually as in most frontal systems the slantwise ascent is seen to have been short-circuited within the convective updraughts of the mesoscale convective system. This happened where the airflow with high θ_w encountered, and began to ride over, a wedge of cold air (C_1C_2) corresponding to the cold conveyor belt of the model in Fig. 4.

5. Other mid-latitude systems

5.1 *Sub-synoptic-scale comma clouds associated with cold air vortices*

The distinction between frontal, i.e. baroclinic, and convective phenomena tends to be blurred in reality. Thus we have shown that frontal rainbands usually take on a convective character. Likewise some phenomena often classified as essentially convective can take on frontal characteristics. Nowhere is this dual character more evident than with the comma-shaped cloud and precipitation systems associated with cold pools within polar air streams. Such systems are generally of sub-synoptic scale, being spaced at intervals of the order of 1000 km when they occur in multiple form. They develop most often over the oceans in winter, originating in regions of low-level heating and enhanced convection and acquiring the comma-shaped cloud pattern as they mature.

Sub-synoptic-scale comma cloud systems occur in association with baroclinicity throughout some or all of the depth of the troposphere, and at the same time conditional instability through a substantial depth. A wide spectrum of situations can occur but in all of them the two forms of instability coexist. At one end of the spectrum are the polar lows that form in very cold northerly outbreaks over warm oceans (e.g. off the Norwegian coast) in which convection is vigorous and a CISK (Conditional Instability of the Second Kind) mechanism appears to be the more important driving force (Rasmussen 1983). At the other end of the spectrum are those comma clouds in which baroclinic slantwise ascent is the primary driving force. This seems to be the case for the short-wave polar troughs commonly encountered in the westerly flows behind major cold fronts approaching the north-west of Europe and the USA (Reed 1979, Locatelli *et al.* 1982). An example of a comma cloud associated with a polar trough is shown in Fig. 18.

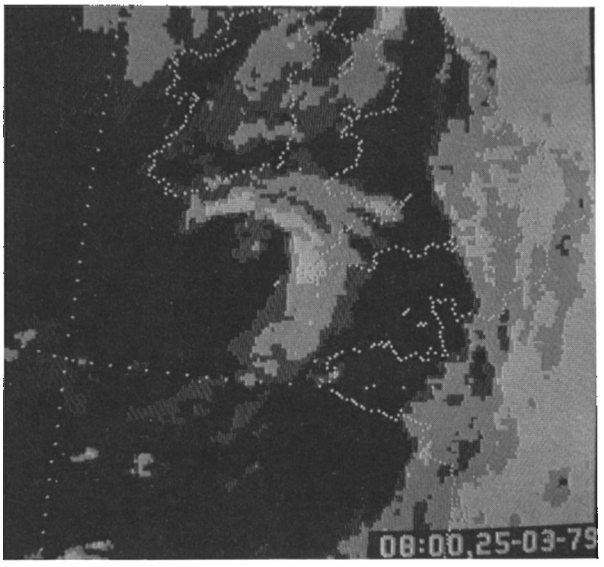

Figure 18. Infra-red satellite image from Meteosat showing a small, cold air comma cloud over south-west England. Pale grey, high cloud; medium grey, medium cloud; dark grey, low cloud.

The axis of the trough is situated along the trailing edge of the comma cloud. The sub-synoptic-scale flow responsible for the comma cloud is like a diminutive version of the warm conveyor belt discussed in section 2.1. The comma cloud zone is characterized by convective precipitation and also by a distinct low-level jet as in the case of the synoptic-scale warm conveyor belt ahead of a cold front. Fox (1982) has shown that this is true even for very small polar air systems.

Sub-synoptic-scale comma cloud systems usually develop near the leading edge of a cold pool behind a major frontal system (Fig. 19). According to Matsumoto *et al.* (1982) the cloud penetrates through the upper boundary of the cold dome and reaches the level of the tropopause, which is low in such regions. When cloud from the preceding frontal system gets carried around the back of the cold pool, to give what synopticians refer to as a back-bent occlusion, comma clouds may develop from elements of this cloud as they travel around the southern flank of the cold pool (Fig. 20).

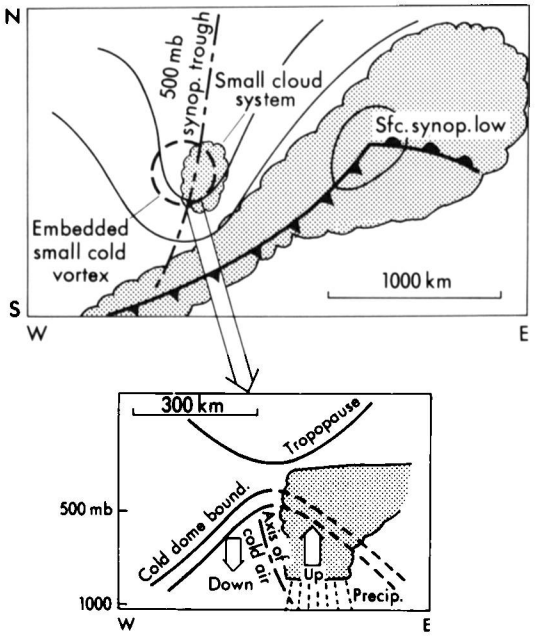

Figure 19. Schematic representation of a sub-synoptic-scale cold vortex (from Matsumoto *et al.* 1982).

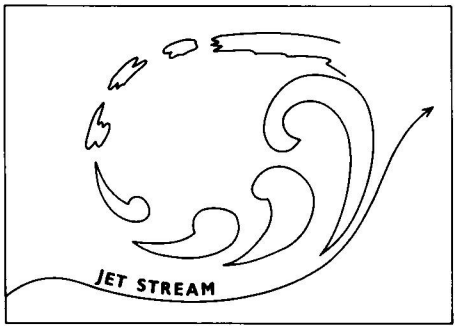

Figure 20. Schematic representation of successive stages in the life cycle of a sub-synoptic-scale comma cloud as it travels around a cold pool behind an upper-level jet stream (from Zick 1983).

5.2 *The polar trough conveyer belt and instant occlusion*

An instant occlusion is the name given to the lambda-shaped cloud pattern produced when a cloud band associated with a polar trough interacts with a cloud band associated with the polar front (Zillman and Price 1972, Reed 1979, Thepenier and Cruette 1981, Weldon 1975). Fig. 21 shows an example of a variant of the instant occlusion referred to as a pseudo occlusion. Fig. 21(a) shows an early stage in its

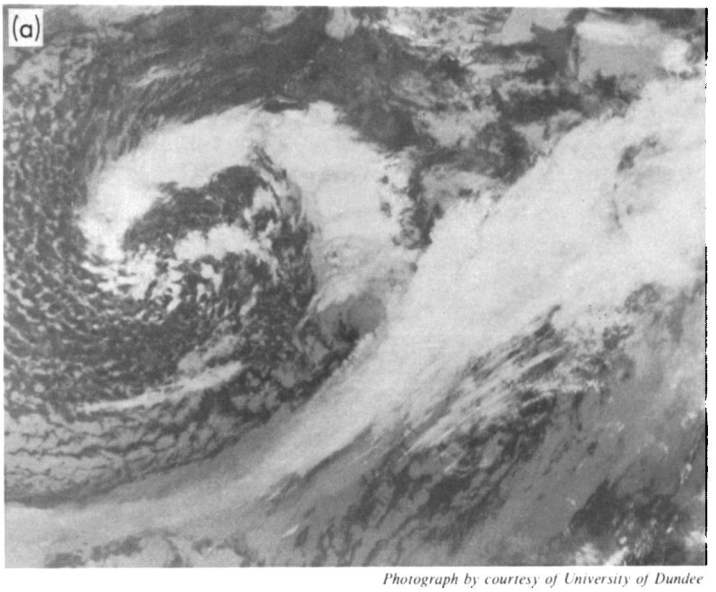

Photograph by courtesy of University of Dundee

Figure 21(a). Infra-red photograph from a NOAA satellite at 0817 GMT on 9 September 1983 showing a convective cloud band (associated with a polar trough conveyor belt) wrapped around the leading edge of a cold pool and situated in close proximity to a stratiform cloud band (associated with a polar front conveyor belt).

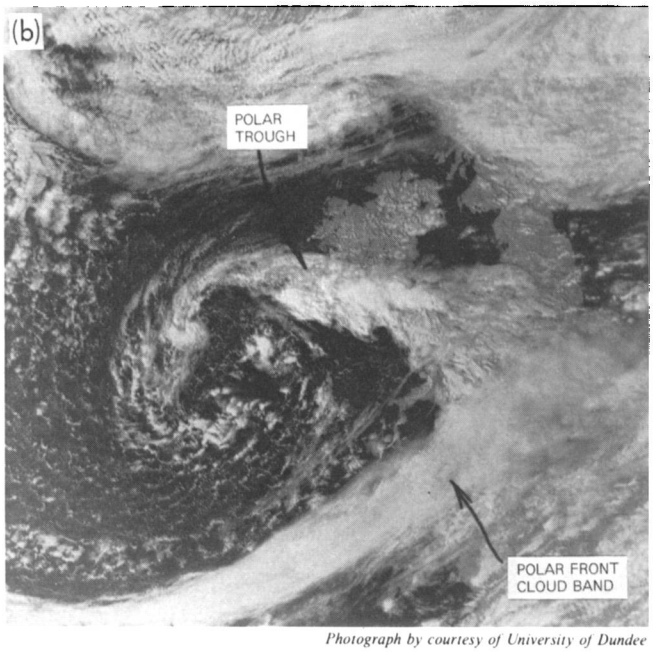

Photograph by courtesy of University of Dundee

Figure 21(b). Same as Fig. 21(a) but taken at 1502 GMT and showing the two cloud bands merged to form a lambda-shaped pattern.

development just before the two cloud bands merge to produce the characteristic lambda pattern shown in Fig. 21(b). This process is interpreted by Browning and Hill (1985) in terms of a dual conveyor belt configuration, with two small conveyor belt flows intersecting at right angles as shown in Fig. 22. The

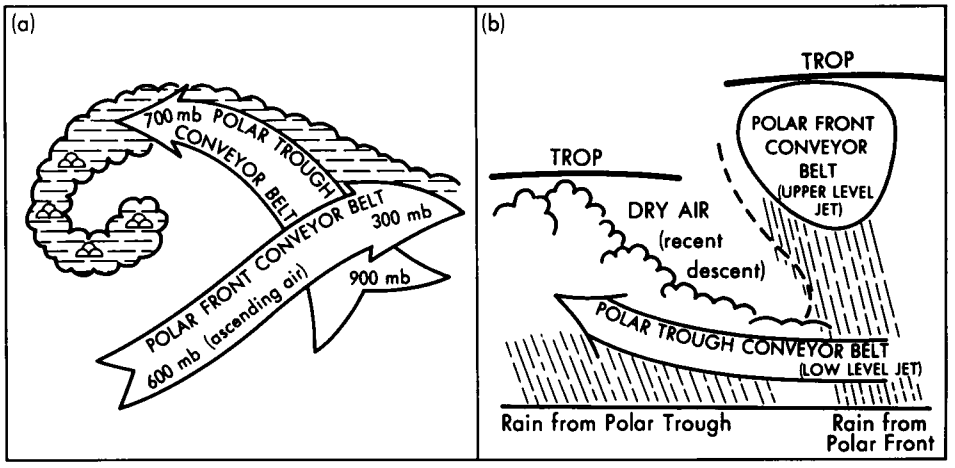

Figure 22. Schematic model of the cloud system in Fig. 21(b) showing intersecting polar trough conveyor belt and polar front conveyor belt: (a) plan view, (b) vertical section along axis of polar trough (from Browning and Hill 1985).

feature labelled 'polar front conveyor belt' corresponds to a warm conveyor belt ascending as an upper tropospheric jet streak. The polar trough conveyor belt corresponds to a low-level jet with an associated cloud band extending above it on the poleward side of the polar front. This low-level jet is situated beneath the left exit of the upper jet streak and may be part of an ageostrophic circulation forced by the latter (Uccellini and Johnson 1979). Although having a disposition similar to the cold conveyor belt in Fig. 4, the polar trough conveyor belt is in fact characterized by a local maximum in θ_w, the air being drawn polewards at low altitudes as it were from the tip of an ill-defined warm sector. Far from being associated with a classical occlusion process, the air within the polar trough conveyor belt has its greatest positive anomaly of temperature and humidity in the lowest kilometre or two. Cooler, drier air circulating around the low centre overruns the polar trough conveyor belt leading to outbreaks of convective precipitation within it.

The instant or pseudo occlusion can be thought of as part of a spectrum of types (Figs 23 and 24) in which the form of the disturbance depends on the position of the short wave trough or vorticity maximum with respect to the polar front (Zillman and Price 1972). The simple comma cloud development represented in Fig. 23(a) shows the short wave trough and associated vorticity maximum occurring well within the cold air and not interacting significantly with the main polar front (Fig. 24(a)). By contrast when the vorticity maximum is at the latitude of the polar front (Fig. 23(c)), a frontal wave forms in which the main warm conveyor belt associated with the polar front gets involved in the circulation and dominates the cloud pattern (Fig. 24(c)). In the intermediate situation of the instant or pseudo occlusion (Figs 23(b) and 24(b)) there are two distinct cloud belts, associated with the polar trough and the polar front.

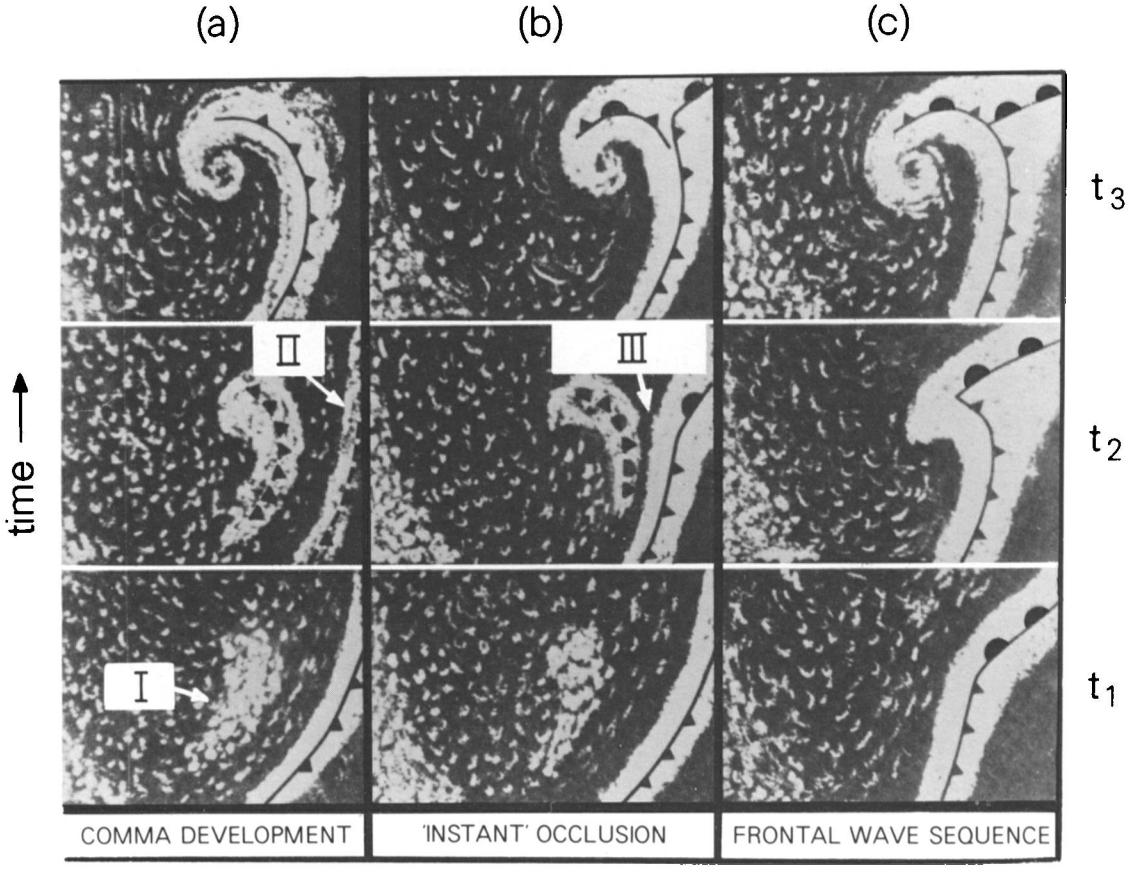

Figure 23. Schematic depiction of three basic sequences of vortex development evident in satellite imagery: (a) development of a comma cloud entirely within the cold air, (b) development of an instant occlusion, (c) development of a frontal wave. The Figure (adapted from Zillman and Price 1972) was derived from observations over the Southern Ocean but it is printed vertically inverted so as to apply to the northern hemisphere. Frontal symbols indicate one scheme for representing the various evolution sequences using the tools of conventional frontal analysis. I, II and III, respectively, indicate a region of enhanced convection, a decaying cloud band and a convective cloud band merging with a frontal cloud band.

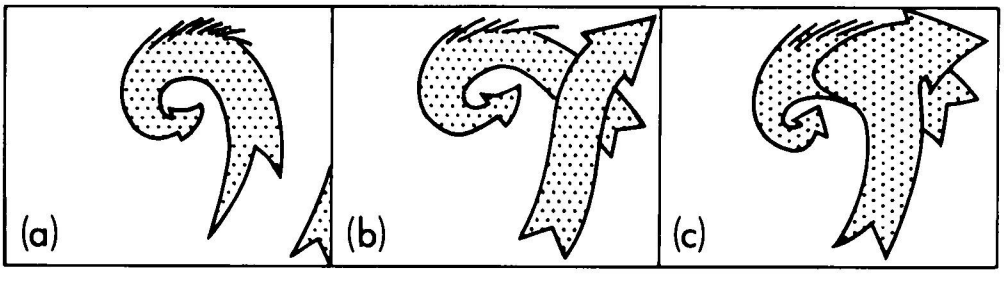

Figure 24. Schematic depiction of the conveyor belt flows associated with the cloud patterns at time t_1 in Figs 23(a), (b) and (c).

6. Concluding remarks

One of the benefits of conceptual models of the kind described in this article is that they provide a framework for the interpretation of imagery from satellite and radar. Although such imagery has been available for many years, there remains considerable scope for improving the extent to which forecasters are able to exploit it. Therefore, with the practising forecaster in mind, it is planned to begin a series of articles in the *Meteorological Magazine* which will give various examples of the use and interpretation of imagery in weather analysis and forecasting. The first in this series, on the use of imagery to identify a particularly persistent form of mesoscale shower band set up by land–sea boundaries will be published shortly (Browning *et al.* 1985).

References

Bennetts, D. A. and Hoskins, B. J. 1979 Conditional symmetric instability — a possible explanation for frontal rainbands. *Q J R Meteorol Soc*, **105**, 945–962.

Browning, K. A. and Harrold, T. W. 1969 Air motion and precipitation growth in a wave depression. *Q J R Meteorol Soc*, **95**, 288–309.

1970 Air motion and precipitation growth at a cold front. *Q J R Meteorol Soc*, **96**, 369–389.

Browning, K. A. and Hill, F. F. 1984 Structure and evolution of a mesoscale convective system near the British Isles. *Q J R Meteorol Soc*, **110**, 897–913.

1985 Mesoscale analysis of a polar trough interacting with a polar front. *Q J R Meteorol Soc*, **111**, 445–462.

Browning, K. A. and Monk, G. A. 1982 A simple model for the synoptic analysis of cold fronts. *Q J R Meteorol Soc*, **108**, 435–452.

Browning, K. A. and Pardoe, C. W. 1973 Structure of low-level jet streams ahead of mid-latitude cold fronts. *Q J R Meteorol Soc*, **99**, 619–638.

Browning, K. A., Eccleston, A. J. and Monk, G. A. 1985 The use of satellite and radar imagery to identify persistent shower bands downwind of the North Channel. *Meteorol Mag*, **114**, 325–331.

Browning, K. A., Hardman, M. E., Harrold, T. W. and Pardoe, C. W. 1973 The structure of rainbands within a mid-latitude depression. *Q J R Meteorol Soc*, **99**, 215–231.

Cahir, J. J., Forbes, G. S., Lottes, W. D. and Staskiewicz, T. (1985) Structural aspects of the warm conveyor belt. (Submitted to *Mon Weather Rev.*)

Carbone, R. E. 1982 A severe frontal rainband. Part I: Stormwide hydrodynamic structure. *J Atmos Sci*, **39**, 258–279.

Carlson, T. N. 1980 Airflow through midlatitude cyclones and the comma cloud pattern. *Mon Weather Rev*, **108**, 1498–1509.

Fankhauser, J. C. 1964 On the motion and predictability of convective systems as related to the upper winds in a case of small turning of wind with height. Report No. 21, National Severe Storms Project, Kansas City, Mo. US Dept of Commerce.

Fox, A. D. 1982 Vertical structure and dynamics of mesoscale wave disturbance (MWD) inferred from GOES satellite imagery and ground truth data. 9th Conference weather forecasting & analysis, Seattle, Wash., 152–159. Am Meteorol Soc, Boston, Mass.

Green, J. S. A., Ludlam, F. H. and McIlveen, J. F. R. 1966 Isentropic relative-flow analysis and the parcel theory. *Q J R Meteorol Soc*, **92**, 210–219.

Harrold, T. W. 1973 Mechanisms influencing the distribution of precipitation within baroclinic disturbances. *Q J R Meteorol Soc*, **99**, 232–251.

Herzegh, P. H. and Hobbs, P. V. 1978a Air motions and precipitation growth in a mesoscale precipitation band associated with a warm front. 18th Conference on radar meteorology, Atlanta, Georgia, 28–31 March 1978. Am Meteorol Soc, Boston, Mass.

Herzegh, P. H. and Hobbs, P. V.	1978b	Generating cells and precipitation growth in mesoscale rainbands. Conference on cloud physics and atmospheric electricity, Issaquah, Wash., 31 July–4 August 1978. Am Meteorol Soc, Boston, Mass.
Heymsfield, G. M.	1979	Doppler radar study of a warm frontal region. *J Atmos Sci*, **36**, 2093–2107.
Hobbs, P. V.	1978	Organization and structure of clouds and precipitation on the mesoscale and microscale in cyclonic storms. *Rev Geophys Space Phys*, **16**, 741–755.
Hobbs, P. V. and Biswas, K. R.	1979	The cellular structure of narrow cold-frontal rainbands. *Q J R Meteorol Soc*, **105**, 723–727.
Hobbs, P. V., Locatelli, J. D., Matejka, T. J. and Houze, R. A., Jr.	1978	Air motions, mesoscale structure and cloud microphysics associated with a cold front. Conference on cloud physics and atmospheric electricity, Issaquah, Wash., 31 July–4 August 1978. Am Meteorol Soc, Boston, Mass.
Houze, R. A., Jr. and Hobbs, P. V.	1982	Organization and structure of precipitating cloud systems. Advances in Geophysics, **24**, 225–315. New York, Academic Press.
Houze, R. A., Jr., Geotis, S. G., Marks, F. D., Jr. and West, A. K.	1981	Winter monsoon convection in the vicinity of North Borneo. Part I: Structure and time variation of the clouds and precipitation. *Mon Weather Rev*, **109**, 1595–1614.
Houze, R. A., Jr., Hobbs, P. V., Biswas K. R. and Davis, W. M.	1976	Mesoscale rainbands in extratropical cyclones. *Mon Weather Rev*, **104**, 868–878.
Hsie, E-Y., Anthes, R. A. and Keyser, D.	1984	Numerical simulation of frontogenesis in a moist atmosphere. *J Atmos Sci*, **41**, 2581–2594.
James, P. K. and Browning, K. A.	1979	Mesoscale structure of line convection at surface cold fronts. *Q J R Meteorol Soc*, **105**, 371–382.
Kreitzberg, C. W.	1964	The structure of occlusions as determined from serial ascents and vertically-directed radar. Research report AFCRL-64-26, Air Force Cambridge Research Laboratories, Bedford, Mass.
Kreitzberg, C. W. and Brown, H. A.	1970	Mesoscale weather systems within an occlusion. *J Appl Meteorol*, **9**, 417–432.
Leary, C. A. and Houze, R. A., Jr.	1979	The structure and evolution of convection in a tropical cloud cluster. *J Atmos Sci*, **36**, 437–457.
Locatelli, J. D., Hobbs, P. V. and Werth, J. A.	1982	Mesoscale structure of vortices in polar air streams. *Mon Weather Rev*, **110**, 1417–1433.
Ludlam, F. H.	1980	Clouds and storms. Pennsylvania State University Press.
Maddox, R. A.	1980	Mesoscale convective complexes. *Bull Am Meteorol Soc*, **61**, 1374–1387.
Matsumoto, S., Ninomiya, K., Hasegawa, R. and Miki, Y.	1982	The structure and the role of a subsynoptic-scale cold vortex on the heavy precipitation. *J Meteorol Soc Japan*, **60**, 339–354.
Miles, M. K.	1962	Wind, temperature and humidity distribution at some cold fronts over SE England. *Q J R Meteorol Soc*, **88**, 286–300.
Newton, C. W. and Newton, Harriet R.	1959	Dynamical interactions between large convective clouds and environment with vertical shear. *J Meteorol*, **16**, 483–496.
Nozumi, Y. and Arakawa, H.	1968	Prefrontal rain bands located in the warm sector of subtropical cyclones over the ocean. *J Geophys Res*, **73**, 487–492.
Pedgley, D. E.	1962	A meso-synoptic analysis of the thunderstorms on 28 August 1958. *Geophys Mem*, **14**, No. 106, Meteorological Office, HMSO.
Rasmussen, E.	1983	A review of meso-scale disturbances in cold air masses. *In* Lilly, D. K. and Gal-Chen, T. (eds), Mesoscale meteorology — theories, observations and models. Dordrecht, D. Reidel.
Reed, R. J.	1979	Cyclogenesis in polar air streams. *Mon Weather Rev*, **107**, 38–52.
Ryan, B. F. and Wilson, K. J.	1985	The Australian summertime cool change. Part III: Subsynoptic and mesoscale model. *Mon Weather Rev*, **113**, 224–240.
Sansom, H. W.	1951	A study of cold fronts over the British Isles. *Q J R Meteorol Soc*, **77**, 96–120.

Thepenier, Rose-May and Cruette, Denise	1981	Formation of cloud bands associated with the American subtropical jet stream and their interaction with midlatitude synoptic disturbances reaching Europe. *Mon Weather Rev*, **109**, 2209–2220.
Uccellini, L. W. and Johnson, D. R.	1979	The coupling of upper and lower tropospheric jet streaks and implications for the development of severe convective storms. *Mon Weather Rev*, **107**, 682–703.
Weldon, R. B.	1975	The structure and evolution of winter storms. Satellite training course notes. (Unpublished lecture notes, Applications Division, National Environmental Satellite Services, NOAA, US Dept of Commerce.)
	1979	Cloud patterns and the upper air wind field. Satellite training course notes. Scott AFB, Ill., Air Weather Service AWS/TR-79/003.
Zick, C.	1983	Method and results of an analysis of comma cloud developments by means of vorticity fields from upper tropospheric satellite wind data. *Meteorol Runsch*, **36**, 69–84.
Zillman, J. W. and Price, P. G.	1972	On the thermal structure of mature Southern Ocean cyclones. *Australian Meteorol Mag*, **20**, 34–48.
Zipser, E. J.	1982	Use of a conceptual model of the life-cycle of mesoscale convective systems to improve very-short-range forecasts. *In* Browning, K. A. (ed.), Nowcasting. London, Academic Press.

Reviews

Weather (second edition), by Louis J. Battan. 150 mm × 227 mm, pp. vii + 135, *illus.* Prentice-Hall Inc., Englewood Cliffs, New Jersey, 1985. Price £17.15.

This is a popular exposition of his subject which no meteorologist would blush to give to his non-meteorological friends. To any objection that it should more appropriately have been entitled 'Meteorology' rather than 'Weather' the author has deftly countered by giving his own definition of weather as being 'the state of the atmosphere and its variations over relatively short periods — from minutes to months'. Months? Well, that goes some way towards justifying the contents of the chapter on 'climatology' and, to be fair, there is plenty of weather in this slim book which presents, for scientifically literate readers, an informed and up-to-date account of many sides of meteorology.

It is recognizably the same book as the original edition of 1974, but there are some major differences. New material has been introduced in a number of places and there has been some rearrangement of sections of the original text. This has resulted, in particular, in a new chapter entitled 'weather analysis and forecasting' at the expense of the old one on 'applications' of meteorology. The new chapter includes some modern topics, such as numerical weather prediction and nowcasting, which sound impressive, but in fact the bulk of the text is of familiar air-mass and frontal depression concepts. The general standard of this and the two chapters which lead up to it ('air motions' and 'general circulation of the atmosphere') is sixth form A-level physics. It is a pity that neither here nor anywhere else in the book is the nature of meteorological observational data touched upon. Instead the subject is built up on a basis of idealized conceptual models and such statements as 'huge masses of observational information... are fed into computers that analyse... the state of the atmosphere...' can only leave an impression which is at best unreal or, more likely, quite false.

The book is relatively strong on the physical aspects of weather phenomena. There are chapters on 'the nature of the earth's atmosphere', 'clouds', 'rain, snow and hail' and, essential for the American public, 'severe storms'. Topics which appear for the first time in this edition are acid precipitation, freons, downbursts and microbursts. And in the chapter on 'climatology' there is now a mention of El Niño, the Southern Oscillation and the importance of the temperature of the sea surface. The brief mention of such currently important topics does not mean that they are in any sense treated fully or adequately. This is a book with limited space allowing only a quick sketch of a very broad subject.

It is, however, a brave and largely successful attempt to present an up-to-date sketch. Inevitably, however successful it may be in general, there are some questionable details. For instance, within a few lines of describing supercooled droplets, is the statement '. . . below 0 °C, most clouds are composed of ice crystals'. And in the main diagram displaying the ten main cloud genera is a sketch of stratus with a higher cloud base than the neighbouring cumulus. Even so, this is a welcome update of a good little book. The new edition is well produced, with many clear diagrams and pictures, though British readers will regret that there are not more from this side of the Atlantic.

Shall we, in fact give this book unblushingly to our friends? Unfortunately, I doubt it — not at the advertised price!

P. G. Wickham

Looking at weather, by Ingrid Holford. 145 mm × 208 mm, pp. 48, *illus.* Weather Publications, Brockenhurst, 1985. Price £1.95.

This book is an attempt by the author to produce, for the layman, an introductory guide to the weather and the mechanisms which go into its making.

It is a slim paperback, divided into 15 chapters which range from temperature and wind, through precipitation, cloud and fog, to radiation, depressions and anticyclones, and pressure belts of the world, with a final chapter on meteorological instruments. With such a diverse range of topics it is not surprising to find that each topic is only touched on briefly. For the layman this is probably enough to whet his appetite.

Throughout the book Ingrid Holford tries to relate weather principles to the domestic environment. For instance, she likens the amount of water vapour in the atmosphere to the 'variable number of guests in an hotel'; and this is typical of the level of the text. The descriptions of certain meteorological phenomena whilst never being totally incorrect could have perhaps had more thought put into them. The statement on page 32 that 'anticyclones are so called because they are different from depressions' or on page 38 that 'convection clouds are called cumulus because they accumulate upwards in thermals' both fall into this category.

A criticism of this book is that the sketches (which I assume are by the author) are of a very poor standard and add nothing to the understanding of the topic under consideration. These, I am sure, could have been greatly improved. Also throughout the book there are references to feet, miles, inches and other 'imperial units' whereas for school use the metric equivalents would have been more useful.

This book provides a very brief introduction to the weather and its workings. It may be useful in schools; however, it would have to be supplemented by further reading.

H. Wilson

Atmospheric electrodynamics, by Hans Volland. 160 mm × 235 mm, pp. ix + 205, *illus.* Springer-Verlag, Berlin, Heidelberg, New York, Tokyo, 1984. Price DM 98.00, US $35.70.

Atmospheric electrodynamics is the eleventh in a series of geophysical monographs dealing with a variety of topics, including geomagnetic micropulsations, geomagnetically trapped charged particles, geochemistry of the moon and planets, optical aurora, coronal expansion and the solar wind, non-linear phenomena in the ionosphere, and plasma instabilities. Written by a distinguished meteorologist, it brings together two subjects which are usually treated separately: 'low-frequency electromagnetic fields of lower-atmospheric origin and those of upper-atmospheric origin. The first, known as geoelectricity, deals with thunderstorm phenomena and related problems..., (the) second subject... with ionospheric and magnetospheric electric fields and currents'.

The first main section of the book summarizes what is known about the ion composition of the atmosphere, which renders the atmosphere electrically conducting, particularly at the upper levels. Thunderstorms and related phenomena are discussed in the second section, which includes accounts of thunderstorm electrification, lightning, sferics and electromagnetic pulses generated by nuclear explosions. The third section deals with dynamo action associated with tidally induced motions in the ionosphere, one manifestation of which are rapid small amplitude fluctuations in the magnetic field observed at the surface of the earth. Finally, an account is given of the interaction of the solar wind with the magnetosphere, the study of which has benefited enormously from many new observations from spacecraft and rapid advances in magnetohydrodynamic theory.

Throughout the book the author stresses the interconnections between the various areas of geophysics involved, at a level accessible to anyone with a basic knowledge of electrodynamics, but without attempting to provide a comprehensive treatment. The material will appeal to those meteorologists who, despite the exigencies of their immediate responsibilities, still find time to satisfy their curiosity about important activities in neighbouring areas of geophysics, and have access to a library which can afford to purchase expensive monographs.

R. Hide

Books received

The listing of books under this heading does not preclude a review in the Meteorological Magazine at a later date.

The climatic scene, edited by M. J. Tooley and G. M. Sheail (London, Boston, Sydney, George Allen and Unwin, 1985. £23.00) is a volume of essays compiled in honour of Gordon Manley, a major and distinctive twentieth-century figure in climatology. The range and scope of the topics covered reflect the eclectic interests of Manley, whose orientation was always towards the importance of climate and its impact on mankind. The state of the art of climatic change is considered at different scales by the contributors: from instrumental records on a local scale from Durham and Manchester to discussions on the regional and continental scale. Methodological problems relating to climatic change are treated and the effects of climate and climatic change on plant distribution, disease vectors and agricultural pests are also considered.

Global change, edited by T. F. Malone and J. G. Roederer (Cambridge University Press, 1985. £35.00) comprehensively explores the interaction between the physical and living world by examining the Earth, its environs and life in the biosphere as a single system. It is a synthesis of the symposium of the same title, sponsored by the International Council of Scientific Unions in September 1984, and addresses the possibility of an interdisciplinary approach to understanding our planet's subtle, and often synergistic, physical, chemical and biological processes.

Handbook of applied meteorology, edited by David D. Houghton (New York, Chichester, Brisbane, Toronto, Singapore, John Wiley and Sons Ltd, 1985. £98.25) is the first comprehensive and authoritative reference on applied aspects of climate and weather for meteorologists and other professionals in fields where atmospheric conditions play a significant role. For technicians and professionals outside the meteorological profession it serves as a ready source of useful data and technical knowledge on all aspects of meteorology essential in engineering and scientific applications. The book also surveys recent advances — particularly in measurement techniques and data sources — never before available in published form.

Chemistry of atmospheres, by Richard P. Wayne (Oxford, Clarendon Press, 1985. £30,00, £14.50 (paperback)) links atmospheric chemistry with the traditional natural sciences to allow the reader to place in context advances and problems in atmospheric science. Its presentation makes it intelligible to scientists of any discipline. Many of the ideas are familiar to chemists and physicists, and teaching them serves a useful function by showing a practical application of fundamental physical chemistry.

Changes in global climate, edited by K. Ya. Kondrat'ev (Rotterdam, A. A. Balkema, 1985. £22.00, US $29.50) is a study of the effects of radiation and other factors during the present century. Possible variations in the solar constant, gaseous composition and aerosol content of the atmosphere have been discussed in detail. The author has examined the properties of atmospheric aerosol and its possible effect on climate and also studied the effect of anthropogenic factors on the ozone layer and their influence on the influx of radiant heat in the stratosphere.

World-wide weather, edited by K. Takahashi (Rotterdam, A. A. Balkema, 1985. £17.50) is divided into three parts. Part I deals with global meteorological phenomena, Part II describes meteorological characteristics of specific locations and Part III discusses the relationship of meteorology with our lives. The main aim of the book is to introduce to the general reader the various global meteorological phenomena which are of current interest.

Air pollution by photochemical oxidants, edited by Robert Guderian (Berlin, Heidelberg, New York, Tokyo, Springer-Verlag, 1985. DM 158.00) introduces air chemistry related to photochemical oxidant formation, including modelling and transport, and after treatment of the physicochemical properties of photochemical oxidants and precursor substances, the current analytical techniques for their determination are presented and strategies for reduction of ambient concentrations are discussed. The book treats the effects of the two most important phytotoxic components of photochemical oxidants, ozone and PAN, both individually and in combination with other air pollutants, on the ecosystem, and on autonomous or conditioned plant resistance, with methods for recognizing, determining and judging these effects. Air quality criteria for vegetation protection are developed from the dose-effect relationships.

Recent advances in planetary meteorology, edited by Garry E. Hunt (Cambridge, London, New York, New Rochelle, Melbourne, Sydney, Cambridge University Press, 1985. £20.00, US $39.50) is a collection of papers presented at the Seymour Hess Memorial Symposium at the IUGG General Assembly, Hamburg, in August 1983. Topics covered include: the photochemical processes involved in the formation of clouds on Venus, Jupiter, Saturn and Uranus; the meteorology of Mars, Jupiter and Saturn; and energy conversion processes in the outer planets. The final paper in the book discusses the major observational results and theoretical problems of planetary atmospheres and relates them to important problems of geophysical fluid dynamics.

New views on an old planet: continental drift and the history of the earth, by Tjeerd H. van Andel (Cambridge, London, New York, New Rochelle, Melbourne, Sydney, Cambridge University Press, 1985. £15.00, US $19.95) is a book intended for the general reader. Ancient climates, ice ages, continental drift, the evolution of life, and the ways in which these processes interact, are discussed in a style which provides an easy introduction to the earth sciences.

Award

We are pleased to note that the thirtieth International Meteorological Organization Prize has been awarded to Sir Arthur Davies, KBE, Secretary-General Emeritus of the World Meteorological Organization (WMO).

Dr D. A. Davies (as he was for most of his career) joined the Meteorological Office in 1936 after graduating from the University of Wales with first-class honours in mathematics and physics. In 1949 he was appointed Director of the East African Meteorological Department and, following the formation of WMO in 1951, was elected President of RA I, the Regional Association for African states. In 1955 he was appointed Secretary-General of WMO by the Second Congress in succession to the first incumbent, Dr G. Swoboda, and served in this capacity until he retired in December 1979. During his term of office WMO grew from a membership of 83 states and territories to one of 143, there were large political changes over the whole world, and great scientific and technological advances. Sir Arthur Davies's contribution to co-ordinating all the international co-operative endeavour which is so essential to modern operational meteorology has been very great, and he was particularly helpful to many new emergent meteorological services during their formative years.

He was awarded the United Nations Peace Medal in 1979, and the following year was made a Knight Commander of the British Empire.

Obituary

We regret to record the death of Mike Farley, Scientific Officer, of the Central Forecasting Branch (Met O 2) on 2 March 1985.

Mike Farley joined the Office as a Scientific Assistant in 1958, working on the quality control of rainfall observations in M.O.3b. In 1961 he was posted to Upavon where, with the exception of a two-year detachment to El Adem, he worked until 1971. Four years at Fairford were followed by promotion to Scientific Officer and a posting to the Data Processing Branch (Met O 12) in 1975.

Mike will be remembered particularly for his enthusiastic contribution to the teamwork in the computer installation of Met O 12, which encompassed the need to produce operational output by strict deadlines and at the same time to provide objective guidance to others working under the pressures of the computer room. In April 1984 he was posted to Met O 2b where he quickly commanded the respect of his colleagues for his hard work.

Mike's outside interests included golf and football. He was also a very active and highly respected member of the Meteorological Office Branch Council of the Institution of Professional Civil Servants, to which he was first elected in 1973. He held several posts, including that of Vice-Chairman, and in 1982 he was elected to the National Science Group Executive Committee. He always presented direct, honest and objective opinions, and listened intently to other points of view. His approach to problems was admired equally by both management and trade unionists.

THE METEOROLOGICAL MAGAZINE

No. 1359 October 1985 Vol. 114

CONTENTS

NOTICE

It is requested that all books for review and communications for the Editor be addressed to the Director-General, Meteorological Office, London Road, Bracknell, Berkshire RG12 2SZ and marked 'For Meteorological Magazine'.

The responsibility for facts and opinions expressed in the signed articles and letters published in this magazine rests with their respective authors.

Authors wishing to retain copyright for themselves or for their sponsors should inform the Editor when they submit contributions which will otherwise become UK Crown copyright by right of first publication.

Applications for postal subscriptions should be made to HMSO, PO Box 276, London SW8 5DT.

Complete volumes of 'Meteorological Magazine' beginning with Volume 54 are now available in microfilm form from University Microfilms International, 18 Bedford Row, London WC1R 4EJ, England.

Full-size reprints of Vols 1–75 (1866–1940) are obtainable from Johnson Reprint Co. Ltd, 24–28 Oval Road, London NW1 7DX, England.

Please write to Kraus Microfiche, Rte 100, Millwood, NY 10546, USA, for information concerning microfiche issues.

HMSO Subscription enquiries 01 211 8667.

Printed in England for HMSO and published by
HER MAJESTY'S STATIONERY OFFICE

£2.30 monthly

Dd. 736047 C15 10/85

Annual subscription £27.00 including postage

ISBN 0 11 727564 6
ISSN 0026–1149

THE METEOROLOGICAL MAGAZINE

HER MAJESTY'S
STATIONERY
OFFICE

November 1985

Met.O.967 No. 1360 Vol. 114

METEOROLOGICAL OFFICE Met.O.967

THE METEOROLOGICAL MAGAZINE

No. 1360, November 1985, Vol. 114

551.501.81:551.507.362.2:551.515.4(261.27)

The use of satellite and radar imagery to identify persistent shower bands downwind of the North Channel*

By K. A. Browning†, A. J. Eccleston‡ and G. A. Monk§

(Meteorological Office Radar Research Laboratory, Royal Signals and Radar Establishment, Malvern)

Summary

Organized bands of showers downwind of the North Channel often occur during cold north-westerly or northerly outbreaks in autumn and winter. Examples are given which show the value of satellite and radar imagery in identifying such bands and in tracking individual showers over periods of several hours.

1. Introduction

A band of convective showers can often be observed during unstable north-westerly or northerly outbreaks, extending downwind of the stretch of sea between Scotland and Northern Ireland known as the North Channel. The bands, which occur mainly in autumn and winter, are often hundreds of kilometres long. Sometimes they are isolated, and frequently they persist for many hours. They can lead to notable local weather anomalies. Places only 20 km apart can experience persistently different weather conditions when such a band remains stationary. Thus on one such occasion we have observed small hail accumulating in drifts near Manchester and on other occasions sustained snowfalls have occurred over the Preseli Mountains in south-west Wales at times when most other areas had none. Although the bands can take different orientations, one of the commonest is such as to cause showers to reach the Midlands by way of the Cheshire Gap.

The occurrence of significant shower activity downwind of the North Channel in unstable conditions is well known. Evidence of this can be found in *Aerodrome weather diagrams and characteristics*

*No. 1 in the series *The use and interpretation of satellite and radar imagery in weather forecasting.*

†Now Deputy Director (Physical Research) Meteorological Office, Bracknell.

‡Now at the Computer Department, 73 Church St, Malvern.

§Now at Meteorological Office, Bracknell.

(Meteorological Office)* for airfields at Blackpool, Manchester, Shawbury and Brawdy. In particular, the characteristics for Blackpool state that 'most showers, except those associated with troughs, occur in unstable north-westerly airstreams which reach Blackpool via the North Channel'. Farther away at Brawdy in south-west Wales no specific mention is made of the North Channel, but instability in airstreams coming from the general direction of the North Channel is clearly important since it is stated that 'frequent showers can occur from the north in autumn and winter by day and night' and, although thunderstorms occur on average only 9 days per year, these occur 'mostly in northerly airstreams in winter'. Despite the local experience accumulated at these stations, however, the well-defined and persistent nature of these shower bands did not become really obvious until the advent of frequent imagery from satellites and radars. In fact the shower bands are often quite narrow and composed of sequences of individual convective cells and so they are not well described by the conventional surface observational network alone.

2. The nature of North Channel shower bands

Infra-red satellite photographs for five cases of shower bands originating from the North Channel are shown in Figs 1(a), 2(a), 3(a), 4(a) and 5(a). The corresponding surface analyses are given in Figs 1(b), 2(b), 3(b), 4(b) and 5(b). The characteristics of these and other cases we have studied may be summarized as follows:

(i) The shower bands occur in situations of strong north-westerly or northerly polar airstreams with convective instability from the surface to typically 700–600 mb. Maximum temperature excesses assuming parcel theory are about 2 °C.

(ii) The bands may be well defined and isolated, particularly at night. However, during the day in the more strongly unstable conditions, showers are likely to be more widely distributed, especially over hills.

(iii) The bands consist of successions of fast-moving convective showers each of which produces a short heavy burst of precipitation as it passes over a given location. Averaged over a 1-hour period a typical rainfall amount near the axis of a band would be about 1 mm.

(iv) Suitable synoptic patterns can be persistent with showers following almost identical tracks downwind of the North Channel for many hours. Accumulations of precipitation will then be confined to a narrow swath, with a half-width of perhaps a few tens of kilometres.

(v) The shower cells travel at the speed of the wind over a well-mixed layer between 900 and 700 mb. Their direction of travel tends to be close to (actually a few degrees to the right of) the corresponding wind direction.

(vi) Individual shower cells are long lived and can be tracked for a period of 4 to 5 hours as they travel downwind from the region between the North Channel and the Isle of Man.

(vii) With a north-westerly wind the showers can penetrate inland over the Midlands to give a band up to 400 km long. They can survive passage over the southern end of the Pennines but tend to die out if they cross the Pennines farther north where the hills are higher. With a northerly wind showers originating near the North Channel tend to travel down the Irish Sea, only occasionally encountering land. The resulting shower bands can be twice as long as those forming with a north-westerly wind.

*Meteorological Office; *Aerodrome weather diagrams and characteristics*. (Unpublished, copy available in the National Meteorological Library, Bracknell.)

Figures 1–5. (a) NOAA satellite infra-red photographs (*by courtesy of University of Dundee*) showing a band of shower clouds extending downwind of the North Channel and (b) corresponding surface analyses (mb). Times and dates are as shown.

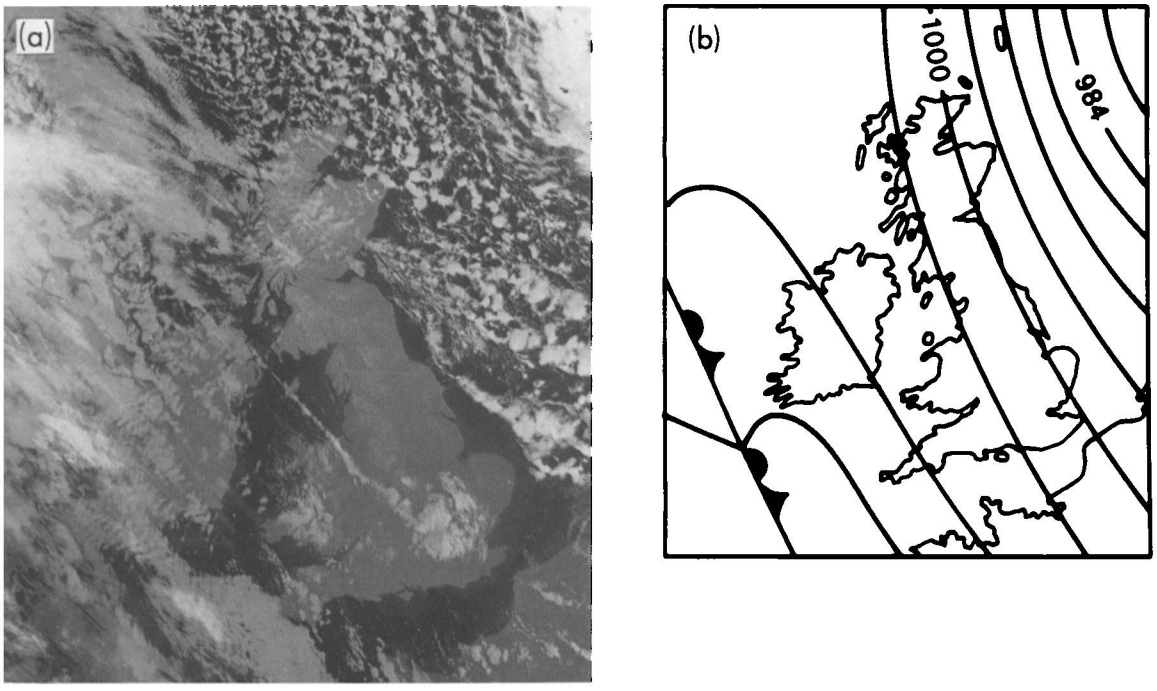

Figure 1. (a) 1903 GMT on 15 January 1981, (b) 1800 GMT on same date.

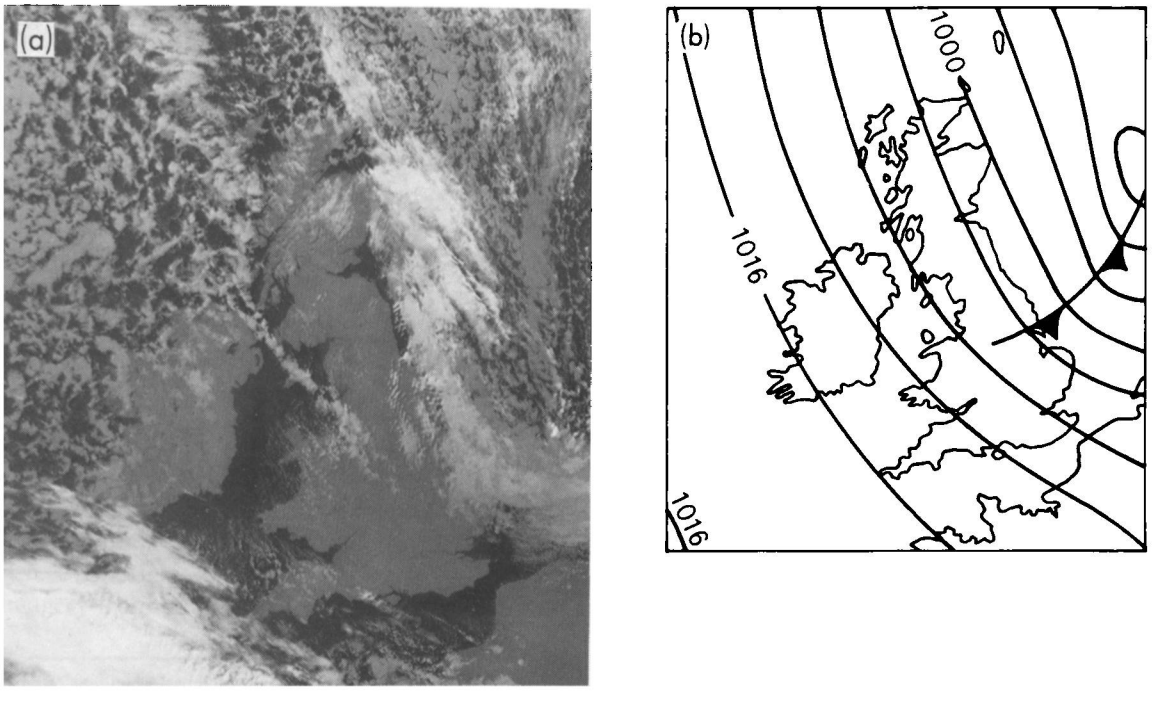

Figure 2. (a) 0301 GMT on 13 October 1981, (b) 0000 GMT on same date.

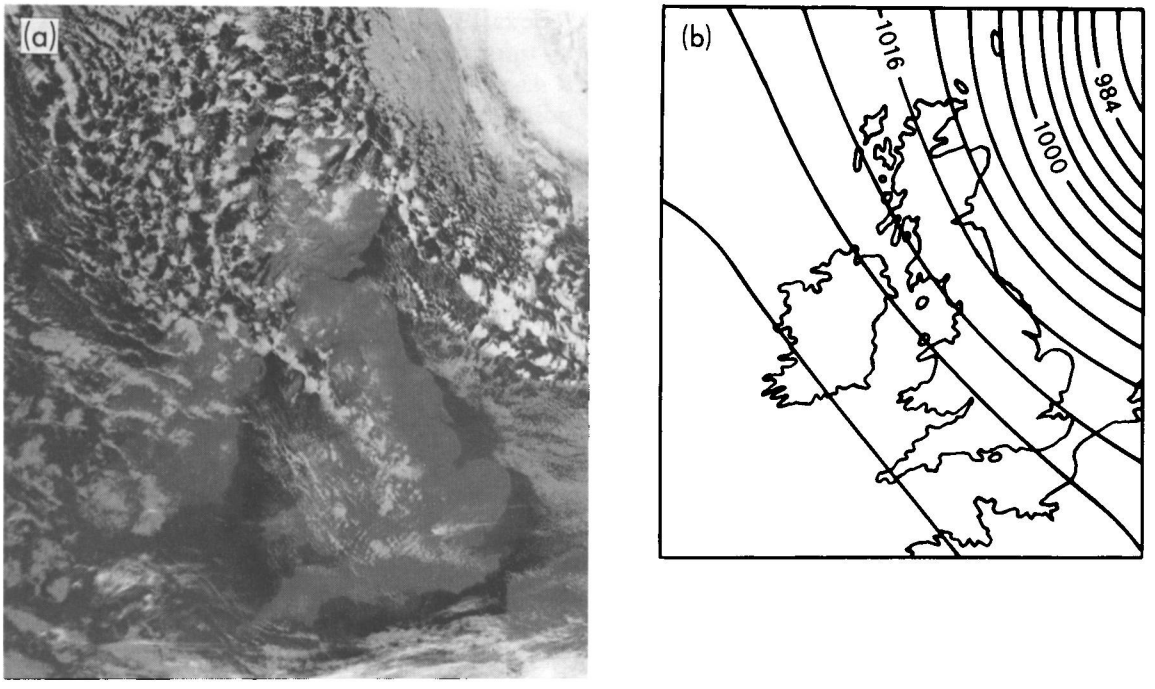

Figure 3. (a) 1314 GMT on 24 November 1981, (b) 1200 GMT on same date.

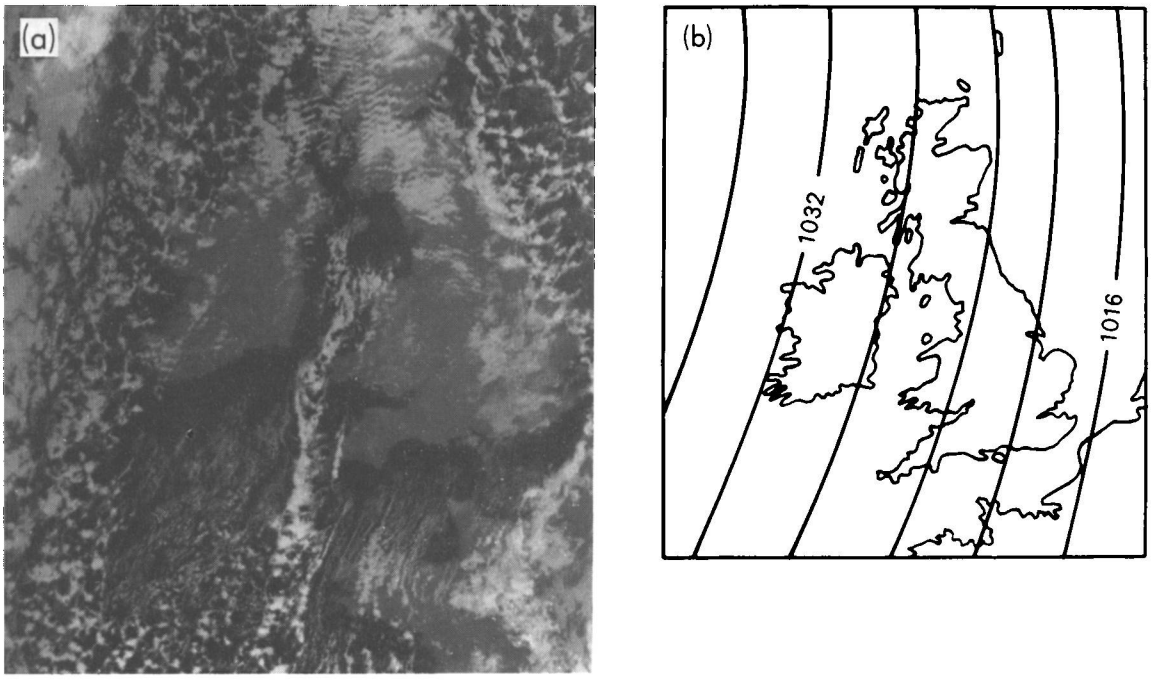

Figure 4. (a) 1430 GMT on 19 December 1979, (b) 1200 GMT on same date.

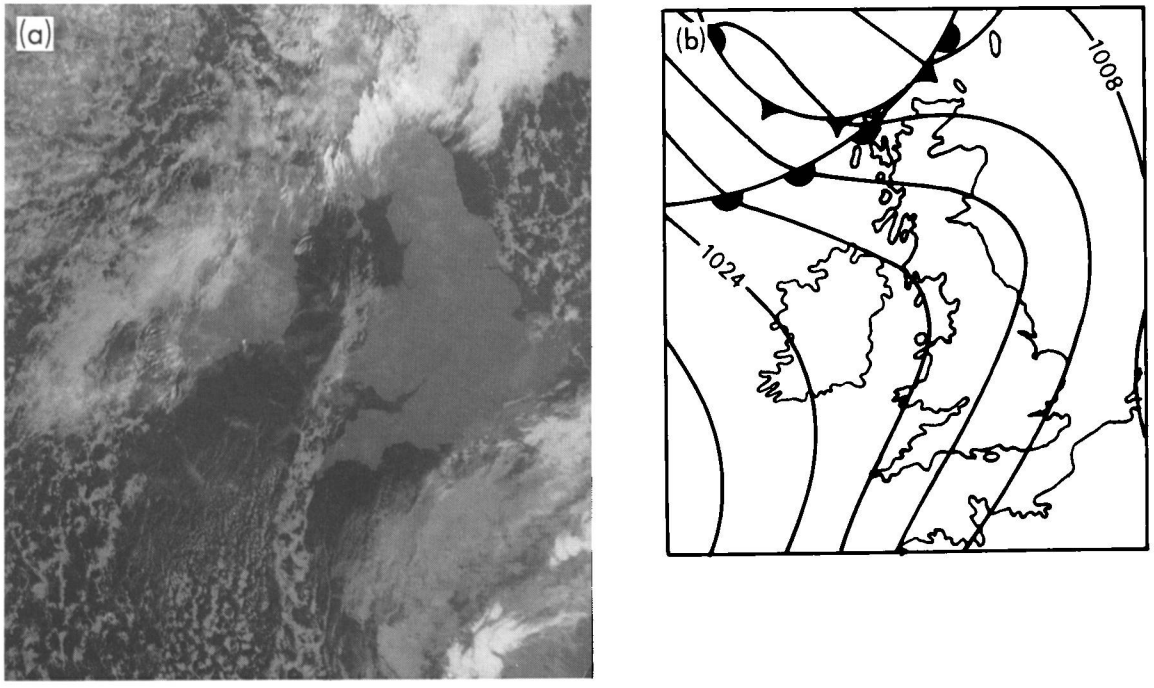

Figure 5. (a) 0928 GMT on 26 November 1980, (b) 0600 GMT on same date.

(viii) Most of the well-defined shower bands observed so far have occurred during the autumn and winter when the sea surface temperature was high compared with the surface temperature over land.

3. Mode of generation of North Channel shower bands

In each of the examples shown in Figs 1 to 5, it appears that the North Channel led to a mesoscale region of ascent, tens of kilometres wide and extending some hundreds of kilometres downwind, within which convection was preferentially maintained. There are two principal ways in which this kind of mesoscale circulation might arise:

(i) the convection might be generated from scratch in the North Channel gap, as seems to be the case in Fig. 1(a), owing to differential heating and frictional effects between land and sea; or

(ii) the North Channel might merely allow pre-existing convective activity to pass through it, albeit with a change in organization from open cells to a longitudinal line of shower cells, as appears to be the case in Figs 2(a) and 3(a).

In some cases both these mechanisms seem to be at work. Fig. 6(a) shows a North Channel shower band during a winter-time north-westerly outbreak as detected by the weather radar network, with the corresponding surface analysis in Fig. 6(b). The radar network does not yet extend far enough upwind to detect the origin of the showers. However, the shower clouds have been tracked using the half-hourly imagery from the European weather satellite, Meteosat.* The tracks of four of the individual shower

*Image sequences from Meteosat can be displayed on a television monitor in the same format as the weather radar network pictures. Although radar network pictures are being received at an increasing number of forecast outstations, the only outstation receiving the Meteosat imagery in this format at present is RAF Lyneham.

551.506.3(423):551.582.2:551.524.36

Exeter temperatures: monthly means from 1840 to 1984

By R. F. M. Hay

(Burnham Market, Norfolk)

Summary

A table of monthly mean temperatures representative of the vicinity of Exeter has been derived for the period from 1840 to 1984. From 1840 to 1879 the long daily record kept at the Devon and Exeter Institution (DEI) in Exeter was the most valuable source, supplemented until 1853 by the Heberden record (also for Exeter), and, from 1865 onwards, by a number of stations — Sidmouth, Cullompton, Killerton and others. From 1880 until 1941 the DEI record appears to be homogeneous and almost unbroken; while the record from Exeter Airport, which was started in 1942, continues unbroken up to the present time. A few short breaks in the DEI record, mainly during 1937 to 1939, were filled using the appropriate data from stations nearby at Cullompton and Killerton.

Introduction

In two papers Manley (1953, 1974) has derived monthly mean temperatures (MMTs) for central England for 1659 to 1973. Following his suggestion made a few years ago that the derivation of a homogeneous record of temperature for south-west England would be valuable, a table is presented here of MMTs for Exeter for 1840 to 1984. The choice of Exeter was suggested by Professor Manley since extensive temperature records were already known to be available from stations in Exeter and its vicinity, while details of these records were kindly provided by him personally to the present writer on several occasions (Transactions n.d., Glaisher n.d., Heberden n.d., Shapter 1862).

Derivation of the record

No problems were encountered in the period going back from the present (1984) as far as 1899. The Exeter Airport series goes back to 1942; before this date the long record kept in Exeter under the auspices of the Devon and Exeter Institution (DEI) provides the main source of data back as far as 1840 and earlier (Devon and Exeter Institution n.d.). Daily values of maximum and minimum temperatures are available for Exeter DEI throughout this period, and for other stations included in Table I for shorter periods. All monthly means were obtained initially as means of daily values of ½ (maximum + minimum); subsequently corrections as described in the text here were applied to obtain as

Table I. *Corrections used for derivation of Exeter monthly temperatures*

Station	Distance from Exeter (DEI) *miles*	Height *feet*	Height *metres*	Temperature correction *degrees Celsius*
Tiverton	12.5	230	70	0.1
Cullompton	11.5	202	62	0.1
Sidmouth (Sidmount)	12.5	30	9	0.1
Whimple	8	160	49	0.0
Killerton	7	159	48	0.0
Exeter (DEI)	0	155	47	0.0
Brampford Speke	4	140	43	0.0
Exeter (Devon and Exeter Hospital)	0.5	112	34	-0.1
Exeter Airport	5	100	30	-0.1

homogeneous a series as possible. For the period from 1942 back to 1840 it is understood that the maximum and minimum thermometers were exposed out of doors near the north-east corner of a small building facing a garden on the north side of the DEI building. Fuller details are given at the end of Table II. Exeter Cathedral and its close are situated nearby to the south of the Institution. Reference to a publication (Sharp 1946) that includes maps of the city boundaries for several dates shows that, whereas the city appears to have more than doubled in area between 1740 and 1840, the increase in area between 1840 and 1919 was quite small. In the 20 years up to 1940 the area of Exeter more than doubled again, and some further increase has presumably taken place since then. The maps also show that the growth of Exeter has been mainly to the east and less extensively to the south-west of the medieval city surrounding the cathedral and its close, which are situated on relatively high ground. These facts suggest that the effect of urbanization upon the Exeter temperature record, during the period covered here, should probably have been less than upon the corresponding temperature records kept at places such as Greenwich, Kew or Oxford (Chandler 1964, Knox-Shaw and Balk 1932).

There was one gap in this period, for 1937 to 1939 inclusive, when records were not available for any station in Exeter itself. After scrutiny of the *Monthly weather report* (Meteorological Office 1937, 1938,

Table II. *Details of principal stations used for analysis of Exeter temperatures*

Exeter Airport (Meteorological Office), 50° 44'N, 03° 25'W, height 100 ft amsl

Period used	1942 until the present
Observing practices	World Meteorological Organization standard practices
Times of observation	Standard procedures
Max. and min. observed	Standard procedures
Exposure	Good. Open country nearby although some building has taken place adjacent to the enclosure in recent years.
Thermometers	Standard

Exeter, Devon and Exeter Institution, 50° 43'N, 03° 32'W, height 155 ft amsl

Period used	1840 to 1941
Observing practices	Not known
Times of observation	Around 0930 (clock time)
Max. and min. observed	Around 0930 (clock time)
Exposure	The thermometers were exposed about 5 ft above ground level on the north-facing side of a vertical wooden frame* which was fixed near to the corner formed at the meeting of the north and east walls of a small house. It is understood that this position of the thermometers has been unchanged throughout the period. In this position the thermometers were completely sheltered from direct sunshine at all times of the year. Before about 1950 a small garden and an orchard existed to the north of the site, but after that date some new buildings were erected where the orchard had been, leaving only a small garden. There is a rather high (13–14 ft) wall of red sandstone, running north-north-east to south-south-west about 6 ft east of the former thermometer frame, which was built (probably) around 1500. The site has, therefore, always been somewhat obstructed for easterly and southerly winds but until about 1950 the exposure was tolerably good for westerly and northerly winds.
Thermometers	According to staff of the DEI Library, at least between about 1940, or earlier, and 1975, the thermometers used were standard ones made by Negretti and Zambra and were bought from a 'good shop in Exeter'. It appears that no corrections were applied. No records remain regarding thermometers used during earlier periods. It can be reasonably assumed that some members of the DEI, physicians, geophysicists, etc., were concerned to maintain as good standards of observation as were possible at the time.

*The vertical wooden frame was about 15 inches high by 12 inches broad, and was surrounded by a thin wooden edge some 4 inches wide all around (horizontal at top and bottom, vertical at the sides). It was probably stained many years ago, but was not painted and had no louvers at any time.

1939), and some comparisons with other years, it was found that monthly temperatures for Exeter for this period could be represented satisfactorily by taking the mean of Cullompton and Killerton and hence these values have been utilized for Exeter for 1937 to 1939.

Table I shows distances from Exeter DEI and heights of all stations in the vicinity that have been utilized in deriving this series. Initially all monthly temperatures were corrected to the height of the DEI (155 ft above mean sea level (amsl)) as shown here. However, in the tables presented in the Appendix the whole series from 1840 to 1984 has been corrected to the height of Exeter Airport (100 ft amsl) to enable direct comparisons to be made with readings in the future.

Between 1881 and 1898 the record for Cullompton appears to have been accepted for publication by Transactions of the Devon Association (Transactions n.d.), with the exception of 1887, in preference to the Exeter DEI record.

For 1887 a record is also available for the Devon and Exeter Hospital. However, a comparison made between the respective monthly mean values and ranges (maximum – minimum) for Exeter DEI and Exeter Hospital for 1887 suggested that the DEI values were the more reliable and consistent, so these values were adopted and Exeter DEI is retained for 1887, while Cullompton is used from 1881 to 1886 and 1888 to 1898 for the series in the Appendix.

A comparison made of the difference between monthly mean maxima and monthly mean minima found in July at Exeter DEI and Cullompton, for the 11 years that are available at each station between 1870 and 1894, showed a good agreement (Exeter DEI 8.8 °C, Cullompton 9.3 °C). This suggests Cullompton readings can be used with confidence for periods when values for Exeter are not available, or were not published by Transactions of the Devon and Exeter Association.

Before 1881 the derived series depends mainly upon the DEI record with some support from other stations in various years mainly as shown in Table III.

Table III. *Supporting stations also used for analysis of Exeter temperatures*

Station	Latitude	Longitude	Periods used here
Devon and Exeter Hospital	50° 43'N	03° 32'W	—
Brampford Speke	50° 47'N	03° 32'W	1878–79
Killerton	50° 48'N	03° 27'W	1936–39
Whimple	50° 46'N	03° 21'W	—
Tiverton	50° 54'N	03° 28'W	1876–78
Cullompton	50° 52'N	03° 23'W	1881–98, 1936–39
Sidmouth (Sidmount)	50° 41'N	03° 14'W	1865–72, 1875–79
Truro	50° 16'N	05° 02'W	1840–44
Falmouth	50° 08'W	05° 04'W	1840–44
Scilly	49° 55'N	06° 19'W	1840–44
Oxford	51° 46'N	01° 16'W	See text

Details of site, exposure and instruments for Oxford are given in Knox-Shaw and Balk (1932). Details for remaining stations above are not available.

Inspection of the DEI monthly data showed too high maxima in spring and summer and similarly low minima in autumn and winter before 1881 when compared with those of later years. This discrepancy has been largely removed by the following simple procedure. For a long period before 1879 the sole observations available for comparison with Exeter are those made at Sidmouth, which are complete for 12 of the years between 1865 and 1879. Information available regarding the sites at both places, and scrutiny of the two records, suggested that thermometers at the more urban site at Exeter were reading rather too high in summer months and a little too low in winter months respectively.

The modern values for the corrections of monthly means of Exeter temperatures to those of Sidmouth for each month January to December are readily obtained from the respective monthly means for 1941 to 1970. These values of Exeter minus Sidmouth in °C have been called 'correction A' and represent a correction to be applied to Exeter to obtain Sidmouth values of MMT on account of geographical and climatological factors (see Table IV, column 1).

Values for the corrections of monthly means (Exeter minus Sidmouth) were similarly obtained for January to December using the 12 years of complete observations available at both stations between 1865 and 1879. These values were denoted by 'correction B' (see Table IV, column 2).

Table IV. *Monthly mean temperature differences (°C)*

Month	Exeter Airport minus Sidmouth (uncorrected) 1941–70 averages (correction A)	Exeter (DEI) minus Sidmouth (uncorrected) 1865–72, 1876–79 averages (correction B)	Temperature differences due to exposure	
			Unsmoothed (correction C)	Smoothed (correction C)
Jan.	-0.3	-0.3	0.0	0.0
Feb.	-0.4	0.0	-0.4	-0.2
Mar.	0.1	0.2	-0.1	-0.3
Apr.	0.2	0.8	-0.6	-0.6
May	0.2	1.2	-1.0	-1.0
June	0.3	1.7	-1.4	-1.2
July	0.3	1.2	-0.9	-1.1
Aug.	0.1	1.1	-1.0	-0.8
Sept.	-0.2	0.2	-0.4	-0.5
Oct.	-0.5	-0.1	-0.4	-0.3
Nov.	-0.5	-0.4	-0.1	-0.1
Dec.	-0.4	-0.7	0.3	0.1
Year	-0.1	0.4	-0.5	-0.5

Correction A minus correction B is defined as correction C, and represents the correction to be applied to Exeter DEI on account of the urban site and exposure.

On the reasonable assumption that the differences of differences in temperature due to climatological and geographical factors between Exeter and Sidmouth were very small as between 1941 to 1970 and 1865 to 1879, it follows that the monthly values of 'correction A minus correction B' give approximately the differences between instrumental errors (and site errors) at the two places, since the climatological and geographical differences have been largely eliminated. If we can assume that instrumental errors were broadly the same at both stations, it follows that 'correction A minus correction B' broadly represents the differences between the urban site at Exeter and the better, more rural and coastal, site at Sidmouth. This difference will be denoted by 'correction C' from now on. Using this argument the Exeter values before 1879 have all been corrected back to 1840 by the appropriate (smoothed) monthly values of 'correction C' in each instance (see Table IV, column 4). These corrections in column 4 have then been applied to the values given in the DEI record from 1879 back to 1840 to derive the results given for these years in the finalized series of Exeter MMTs set out in the Appendix. Some indication that this correction goes far to eliminate errors in the exposure at Exeter DEI is provided by a statistical comparison made between the differences of the decadal means of May minus March and August minus October MMTs at Exeter DEI, as between earlier decades when the results have been 'corrected' as

suggested by Table IV and the similar differences during recent decades. The differences between the effects of overexposure to daytime sunshine and night-time radiation under clear skies should be nearly at a maximum as between March and May and again August to October. But a comparison of these differences between decadal means during the overall periods from 1901 to 1980 and 1851 to 1900 by means of the 'Student's' *t*-test shows no evidence that these decadal MMT differences are significantly different in magnitude as between 1851 to 1900 and 1901 to 1980.

Further evidence that the monthly corrections given under the heading 'correction C' in Table IV are satisfactory was provided by a comparison made between values of Exeter DEI (with corrections applied as in Table IV) with MMTs derived as the mean of Bradford Speke, Sidmouth and Tiverton for the period from 1876 to 1879 when these data were available. In only 4 of these 48 months was the difference between Exeter DEI and the mean of Bradford Speke, Sidmouth and Tiverton greater than 0.6 °C and the largest individual difference was 0.8 °C.

When it was subsequently found that the DEI record had overlapped for more than 20 years after temperature observations were started at Exeter Airport, it became possible to make a comparison between the two records. This is shown here as Table V.

Table V. *Differences (rounded down) between means of monthly means (°C), Exeter DEI minus Exeter Airport for the period 1943–64*

	Jan.	Feb.	Mar.	Apr.	May	June	July	Aug.	Sept.	Oct.	Nov.	Dec.
Differences of monthly means as above 'M'	0.0	0.2	0.4	0.8	1.2	1.2	1.2	0.9	0.7	0.4	0.1	-0.1
Correction C* (see Table IV, col. 4)	0.0	0.2	0.3	0.6	1.0	1.2	1.1	0.8	0.5	0.3	0.1	-0.1
M-C	0.0	0.0	0.1	0.2	0.2	0.0	0.1	0.1	0.2	0.1	0.1	0.0

*Correction C is here expressed as the difference Exeter DEI minus Sidmouth for comparability with 'M' in Table V.

Monthly values of correction C are also shown in Table V together with the differences between the two comparisons. These results afford confidence in the accuracy of the corrections C based on differences between Sidmouth and Exeter DEI which were derived and used at a much earlier stage of the work (see Table IV). In the course of revising the data in the Appendix, the corrections C have thus been applied to all periods between 1840 and 1941 when Exeter DEI was unsupported by data from another station (see Table I).

Before 1865, when Sidmouth temperatures begin, there were no other temperature records available in the region. Some reliance was therefore put on the Oxford record (Knox-Shaw and Balk 1932). Oxford monthly temperatures were 'corrected' for normal climatological temperature differences by subtracting the respective MMTs for the period 1941 to 1970 from each other and assuming, as above, that the same 'climatological difference' in temperature prevailed in the mid-19th century as during 1941 to 1970. (This assumption seems justifiable when, as here, it is made for the purposes of comparison and not for any systematic adjustment of actual monthly means.) From these Oxford temperatures, corrected to Exeter values for climatological factors, values of Exeter DEI minus 'Oxford corrected' were derived for the period 1840 to 1864. It was found that for 1840 to 1844 the differences were much

larger than for subsequent years. For 1844 to 1864 the mean monthly differences (°C) Exeter DEI minus 'Oxford corrected' were as follows:

Jan.	-0.3	July	0.1
Feb.	0.0	Aug.	0.1
Mar.	-0.1	Sept.	0.4
Apr.	0.4	Oct.	0.1
May	0.3	Nov.	0.2
June	-0.3	Dec.	-0.1

The small value of these differences is considered satisfactory.

For the years from 1840 to 1844 short records of MMTs were available for one or more stations simultaneously selected from Truro, Falmouth and Scilly (Royal Cornwall Polytechnic Society n.d.). Use was also made of Oxford temperatures as these five stations (including Exeter) lie roughly aligned along the great circle through Scilly and Oxford. Climatological 'corrections' were applied (as previously for Oxford using averages for 1941 to 1970) to each station to 'correct' it to the Exeter location and the residual differences Exeter DEI minus Scilly, etc., corrected, were obtained. The results were set out in a table (not given here), and after careful scrutiny, all the means derived for Exeter DEI (after correction C was applied) were found to be in satisfactory agreement with the differences from the supporting stations. These early results for Exeter DEI are therefore included in the Appendix with reasonable confidence in their accuracy.

References

Chandler, T. J. 1964 North-wall and Stevenson screen temperatures at Kew Observatory. *Q J R Meteorol Soc*, **90**, 332–333.

Devon and Exeter Institution n.d. Meteorological observations kept daily in observation books at the Devon and Exeter Institution in Exeter, 1840–1975 and a few earlier years.

Glaisher, J. n.d. Meteorology of England, 1851–1862. London, Eyre and Spottiswoode for HMSO.

Heberden, T. n.d. Weather record of the Rev. Thomas Heberden, 1785–1855. (Original manuscript available in the Devon Record Office, Central Library, Exeter.)

Knox-Shaw, H. and Balk, J. 1932 Radcliffe observations, **55**.

Manley, G. 1953 The mean temperature of central England, 1698 to 1952. *QJR Meteorol Soc*, **79**, 242–261.

1974 Central England temperatures: monthly means 1659 to 1973. *QJR Meteorol Soc*, **100**, 389–405.

Meteorological Office 1937 Monthly weather report.

1938 Monthly weather report.

1939 Monthly weather report.

Royal Cornwall Polytechnic Society n.d. Meteorological observations for Scilly, Falmouth, Truro. 7th Annual Report, 1839 *et seq.*

Shapter, T. 1862 The climate of the south of Devon, 2nd edition. London, John Churchill.

Sharp, T. 1946 Exeter Phoenix. London, Architectural Press.

Transactions n.d. Devon Association, 1862 to 1871, volumes 1 to 4, then yearly volumes 1872 to 1941.

Appendix

Table A.I. *Monthly mean and yearly temperatures (°C) for Exeter, 1840–1984, together with extreme values for each month and year of occurrence*

	Jan.	Feb.	Mar.	Apr.	May	June	July	Aug.	Sept.	Oct.	Nov.	Dec.	Year
1839	—	—	—	—	—	—	—	—	—	—	—	5.7	
1840	6.0	4.2	4.3	9.8	12.7	14.4	14.8	17.0	12.5	9.4	7.8	2.4	9.6
1841	3.4	2.4	7.7	8.3	13.0	13.4	14.6	15.3	14.5	10.0	6.9	6.2	9.6
1842	2.7	5.3	7.3	7.9	11.5	16.7	15.7	17.7	14.2	8.3	7.5	9.1	10.3
1843	6.8	3.2	6.8	9.5	10.8	13.0	15.8	16.4	16.3	10.2	7.5	8.4	10.4
1844	5.9	4.0	6.1	10.4	11.3	15.5	15.2	13.7	14.2	10.3	8.0	2.5	9.8
1845	5.2	2.6	3.0	8.8	10.4	14.4	14.4	13.5	12.4	10.5	8.4	6.4	9.2
1846	7.6	7.5	7.0	8.9	11.7	17.1	16.1	17.0	15.0	10.4	8.4	2.7	10.8
1847	4.8	4.3	5.9	7.5	11.5	13.8	17.0	15.7	12.9	11.7	9.0	6.7	10.1
1848	2.9	6.9	6.7	8.9	13.3	13.4	15.5	14.5	13.2	10.4	7.3	7.4	10.0
1849	6.1	6.4	6.3	7.0	11.9	13.9	15.3	15.9	13.6	11.4	8.2	4.9	10.1
1850	2.0	7.9	4.9	9.7	9.8	14.6	15.5	15.0	13.0	8.4	8.8	6.4	9.7
1851	7.4	5.5	6.9	7.9	10.4	13.9	14.9	16.0	12.4	11.3	4.2	5.4	9.7
1852	5.9	4.7	5.2	7.5	10.9	12.7	17.9	15.7	13.0	8.6	9.0	8.6	10.0
1853	5.7	1.3	4.3	8.7	11.4	14.2	15.5	15.2	13.0	10.6	6.9	2.7	9.1
1854	5.2	4.9	7.0	9.3	9.9	12.4	14.9	15.2	14.3	9.9	5.7	6.4	9.6
1855	2.8	-0.4	4.1	7.6	9.3	12.9	15.9	15.9	14.0	10.3	6.0	4.8	8.6
1856	4.9	6.5	4.9	8.3	9.7	13.9	16.1	16.9	12.9	11.5	6.8	6.2	9.9
1857	3.9	5.8	5.5	7.8	10.8	14.6	16.4	17.0	14.9	11.2	7.4	8.0	10.3
1858	4.7	3.7	5.9	8.8	10.8	15.8	14.8	15.7	15.4	10.3	5.1	6.7	9.8
1859	6.2	6.4	7.8	8.5	11.6	14.9	18.0	16.2	13.8	11.2	7.2	3.5	10.4
1860	5.6	2.9	6.5	7.0	12.2	12.0	14.9	14.3	11.8	10.7	6.2	3.2	8.9
1861	2.5	6.0	6.5	7.8	11.5	14.3	13.8	15.8	13.2	11.5	4.8	4.8	9.4
1862	5.3	5.5	6.4	10.0	11.6	12.4	14.1	15.0	13.9	12.0	5.4	7.8	10.0
1863	5.4	6.5	6.9	10.3	11.9	12.0	16.6	15.7	12.8	10.6	8.8	7.7	10.4
1864	3.9	3.2	6.3	9.4	12.4	13.8	16.0	15.0	14.0	10.0	6.2	3.9	9.5
1865	2.9	4.0	3.8	11.3	12.3	15.9	16.3	14.9	16.3	10.9	8.0	6.5	10.3
1866	6.9	5.3	5.7	9.0	9.7	14.9	15.9	15.1	13.0	11.2	8.9	7.9	10.3
1867	2.7	8.0	3.8	10.1	10.9	13.9	15.2	16.0	13.7	10.6	5.8	4.3	9.6
1868	4.7	6.8	7.8	9.5	12.8	15.2	18.7	17.3	14.5	9.7	6.5	8.6	11.0
1869	7.3	8.3	4.5	10.2	10.3	13.3	16.1	15.9	14.2	11.0	7.5	4.0	10.2
1870	4.7	3.4	5.4	9.0	11.3	14.9	17.4	16.0	13.9	10.6	6.2	1.7	9.5
1871	2.2	7.2	7.5	9.9	11.2	13.0	15.0	17.2	13.2	11.7	5.1	4.0	9.8
1872	6.4	8.0	7.8	8.5	9.8	13.7	16.4	15.7	14.0	9.0	8.0	6.9	10.4
1873	6.4	3.0	6.3	8.5	10.8	14.4	15.7	16.1	12.3	9.7	7.7	5.6	9.7
1874	6.6	6.1	7.8	10.2	11.1	14.4	17.1	15.5	13.7	11.2	8.3	2.9	10.4
1875	8.0	3.4	6.1	7.8	12.2	14.0	14.6	16.4	15.7	10.2	6.9	5.0	10.0
1876	4.2	6.7	5.5	8.5	9.7	14.2	17.9	16.7	13.9	11.8	6.5	7.5	10.3
1877	7.0	7.7	6.2	7.9	9.4	15.3	15.0	15.7	12.0	10.5	8.3	5.9	10.1
1878	5.9	6.4	6.7	9.2	12.0	14.8	17.0	16.5	13.9	10.9	4.8	1.9	10.0
1879	1.5	5.1	5.7	5.8	9.3	13.0	14.2	15.0	13.2	10.6	4.9	1.9	8.4
1880	1.8	7.0	7.8	8.9	12.2	14.8	16.7	16.6	15.4	8.2	6.7	7.3	10.3
1881	-0.6	4.5	6.7	8.7	12.4	13.6	16.9	14.7	12.9	8.1	9.6	5.1	9.4
1882	5.8	6.4	7.9	9.1	11.7	13.0	15.1	15.4	11.8	10.0	6.9	5.3	9.9
1883	6.2	6.4	3.3	8.3	10.8	14.1	14.5	15.5	14.0	10.4	6.8	5.3	9.6
1884	7.1	6.1	6.8	6.9	11.6	14.4	15.9	16.5	15.1	9.9	6.4	5.5	10.2
1885	4.3	7.0	5.3	7.5	9.4	14.6	16.5	14.5	12.8	8.5	7.5	3.9	9.3
1886	2.8	2.0	5.0	8.7	11.3	14.4	16.4	16.3	14.3	12.0	7.1	3.3	9.5
1887	3.9	4.5	4.0	6.6	10.4	15.6	17.5	16.6	12.3	7.6	5.3	4.4	9.1
1888	3.6	2.2	4.4	7.1	11.1	13.9	14.6	14.6	12.8	8.9	8.8	5.7	9.0
1889	4.0	4.4	5.6	7.9	12.9	15.7	15.5	14.6	13.4	8.8	8.1	3.6	9.5
1890	6.7	4.1	6.7	8.3	12.3	14.4	15.0	15.0	14.6	10.7	6.6	0.2	9.6

	Jan.	Feb.	Mar.	Apr.	May	June	July	Aug.	Sept.	Oct.	Nov.	Dec.	Year
1891	2.0	4.5	4.7	7.0	9.9	15.0	14.8	14.5	14.4	9.8	6.1	5.9	9.0
1892	3.2	4.5	3.7	8.9	11.9	13.7	15.3	15.9	12.9	7.6	7.4	3.9	9.1
1893	3.9	6.1	8.0	11.6	13.7	16.0	16.8	17.2	13.4	10.1	6.2	5.3	10.7
1894	4.1	6.2	7.3	10.1	10.0	14.8	15.7	15.4	12.6	10.6	8.4	6.4	10.1
1895	1.4	-1.3	6.4	9.4	13.0	15.4	15.8	15.4	16.0	7.9	9.0	5.5	9.5
1896	5.3	5.0	8.3	10.1	13.4	16.4	16.9	15.4	14.1	7.9	4.1	4.8	10.1
1897	2.7	8.0	8.1	8.8	11.5	16.1	17.6	16.2	12.9	11.4	8.3	6.1	10.6
1898	7.0	5.6	4.9	9.0	11.6	14.6	16.4	17.2	15.5	12.0	7.9	8.1	10.8
1899	6.1	6.2	6.0	8.8	10.7	15.2	17.3	18.0	14.7	10.4	9.2	4.2	10.6
1900	6.3	4.7	4.0	8.8	10.8	14.9	17.4	15.0	14.0	11.0	7.8	7.4	10.2
1901	4.6	3.7	4.6	8.6	12.3	14.0	17.8	15.8	14.5	10.1	5.4	4.4	9.7
1902	5.9	2.5	7.6	8.2	9.9	13.6	15.6	15.8	13.5	10.6	8.9	5.9	9.8
1903	6.2	7.8	8.1	7.8	11.5	13.2	15.7	15.3	14.0	11.8	7.9	4.8	10.3
1904	5.5	4.8	5.4	9.6	11.5	14.0	16.4	15.7	13.5	11.1	6.8	6.8	10.1
1905	5.1	6.5	7.9	9.0	11.5	15.0	17.6	14.9	13.3	8.5	5.3	6.4	10.1
1906	6.8	4.2	6.3	7.9	11.5	14.4	16.3	17.2	14.4	11.1	7.9	5.2	10.3
1907	5.3	3.6	7.0	8.1	11.3	13.3	15.1	15.6	14.4	10.5	8.6	6.6	9.9
1908	4.4	6.7	5.1	7.5	12.9	14.8	16.3	15.6	13.4	12.4	8.9	6.4	10.4
1909	4.8	4.0	4.9	9.3	11.4	12.7	15.5	16.5	13.3	11.5	5.9	4.7	9.5
1910	5.2	6.5	6.9	8.2	11.7	14.6	14.8	16.0	13.9	11.6	5.6	7.5	10.2
1911	4.4	6.2	6.7	8.7	13.4	15.0	18.6	18.5	13.6	11.0	6.8	7.8	10.9
1912	5.3	6.7	8.5	9.8	12.8	14.0	16.2	13.5	12.2	8.7	7.6	8.4	10.3
1913	6.4	5.6	7.2	8.7	11.9	14.1	15.8	16.3	14.5	11.7	9.3	6.0	10.6
1914	4.7	7.4	7.5	10.3	11.4	14.9	16.2	16.4	13.5	10.9	7.1	5.6	10.5
1915	5.3	5.1	6.1	9.2	12.0	14.4	14.8	15.9	13.1	10.2	3.9	7.3	9.8
1916	8.4	4.7	3.6	8.8	12.0	11.8	16.0	16.9	14.1	12.1	6.9	3.0	9.9
1917	2.3	2.6	4.8	6.6	12.5	14.9	16.1	15.7	14.5	8.8	9.4	3.3	9.3
1918	5.2	7.7	6.7	7.8	12.9	14.1	16.3	16.4	13.3	10.2	7.4	8.6	10.5
1919	4.1	4.1	5.5	8.2	13.2	14.4	15.1	17.2	13.7	8.1	4.3	7.1	9.6
1920	6.4	7.2	7.4	9.4	12.3	14.6	14.6	13.9	13.9	11.5	7.8	5.6	10.4
1921	9.0	5.6	8.0	8.9	12.2	16.1	19.7	16.5	15.8	13.7	7.9	7.9	11.8
1922	5.7	6.2	5.7	6.8	14.0	15.0	14.3	14.6	13.2	8.9	6.7	6.8	9.8
1923	6.5	7.7	7.7	8.8	10.5	13.5	17.6	15.9	13.3	11.0	4.3	6.1	10.2
1924	6.5	4.0	5.2	8.3	11.7	12.3	15.2	14.9	13.9	11.0	7.7	7.8	9.9
1925	6.6	6.3	6.1	8.5	11.3	16.0	17.2	16.4	12.5	11.6	4.7	5.2	10.2
1926	6.3	8.3	7.6	9.6	11.0	13.6	17.6	17.6	16.2	9.7	7.3	5.5	10.9
1927	6.0	6.1	8.6	8.9	13.0	13.3	16.5	16.0	13.5	11.2	7.6	4.5	10.4
1928	6.9	7.5	7.1	9.0	12.0	13.7	16.9	15.6	13.4	11.5	9.2	5.7	10.7
1929	2.9	2.5	6.6	7.8	11.4	13.6	16.2	15.6	16.1	10.5	7.8	6.9	9.8
1930	6.4	3.2	6.4	8.9	11.7	15.9	15.6	16.0	14.7	11.9	7.6	6.2	10.4
1931	4.9	5.0	4.9	8.5	11.5	14.8	15.5	15.1	12.8	10.5	9.1	7.0	10.0
1932	8.4	5.2	6.2	7.9	10.9	14.6	16.1	18.1	14.8	9.7	8.1	6.8	10.6
1933	3.7	5.6	8.4	9.2	13.3	15.0	17.4	17.9	16.1	11.2	6.8	2.0	10.5
1934	5.7	3.8	6.3	8.7	12.2	15.9	18.4	15.4	15.9	11.7	7.8	9.5	10.9
1935	6.3	7.2	6.2	9.1	12.3	14.7	17.9	16.7	12.9	10.9	7.4	5.4	10.6
1936	5.9	4.6	7.9	7.1	11.6	14.7	15.3	16.4	15.1	10.5	7.2	6.9	10.3
1937	6.2	7.0	5.2	10.7	12.6	15.0	16.4	16.9	14.0	10.7	5.7	3.8	10.4
1938	6.7	5.5	9.3	8.4	10.9	14.8	15.6	16.4	14.1	11.5	9.7	5.2	10.7
1939	5.7	6.4	7.5	9.4	12.7	15.5	15.6	17.0	14.6	9.3	9.9	3.7	10.6
1940	0.9	5.2	7.1	9.7	13.4	16.5	15.3	16.7	14.2	10.9	8.3	5.3	10.3
1941	3.0	5.2	7.2	7.7	12.7	15.3	17.1	15.4	14.9	11.7	8.2	7.0	10.5
1942	3.3	1.4	6.7	9.9	11.1	14.1	15.6	15.9	14.1	11.2	5.5	8.3	9.7
1943	7.0	6.6	7.1	10.9	12.1	14.3	15.8	16.1	13.1	10.9	7.4	4.7	10.5
1944	7.6	4.4	5.8	9.9	11.4	14.4	16.3	17.7	13.3	9.7	7.8	4.8	10.3
1945	1.4	8.1	7.6	10.4	12.4	14.4	15.8	16.2	14.9	12.5	8.1	6.9	10.7

	Jan.	Feb.	Mar.	Apr.	May	June	July	Aug.	Sept.	Oct.	Nov.	Dec.	Year
1946	4.5	7.4	5.8	9.7	11.3	12.9	16.0	14.9	14.2	11.2	9.4	3.5	10.1
1947	3.6	-0.4	5.7	9.1	12.1	14.5	16.5	18.7	14.6	10.9	8.9	6.4	10.0
1948	6.7	5.6	8.7	9.2	12.1	14.1	15.9	15.2	14.4	10.9	9.7	7.1	10.8
1949	6.5	6.3	8.2	10.1	11.1	15.4	17.8	17.2	16.4	12.6	7.8	6.8	11.3
1950	5.3	7.1	8.3	8.5	11.8	16.1	16.1	15.5	13.9	10.6	7.1	2.6	10.2
1951	5.8	5.0	5.6	7.6	10.1	13.8	16.7	14.9	14.4	10.5	9.6	7.3	10.1
1952	4.4	4.3	7.6	9.5	12.9	14.5	17.3	16.6	11.6	10.5	5.7	5.1	10.0
1953	4.2	4.9	6.2	8.6	12.5	14.5	16.3	16.4	14.2	10.6	9.6	8.4	10.5
1954	4.3	4.5	7.2	8.2	11.3	13.7	14.5	15.1	13.7	12.9	8.2	7.9	10.1
1955	4.8	2.6	3.6	9.5	10.3	14.5	18.1	18.2	14.4	10.1	7.6	7.9	10.1
1956	5.3	0.2	7.1	7.4	11.9	14.2	16.7	14.3	14.9	10.6	7.1	7.5	9.8
1957	6.2	6.8	10.1	9.6	11.2	15.7	17.1	16.1	14.1	11.6	6.7	5.5	10.9
1958	4.6	7.2	5.0	7.7	11.3	13.7	15.9	16.3	15.4	11.8	7.5	5.7	10.2
1959	4.1	5.4	7.8	9.6	12.6	15.2	17.1	17.0	15.3	13.1	8.2	7.5	11.1
1960	5.5	5.3	7.6	9.4	12.8	15.9	15.7	15.4	13.7	11.0	8.7	4.7	10.5
1961	5.5	8.3	8.1	10.9	11.5	14.9	16.0	16.0	15.4	11.4	7.3	4.3	10.8
1962	6.1	5.7	3.8	8.5	10.4	13.7	15.4	15.0	13.1	11.3	6.3	4.0	9.4
1963	-2.4	1.1	6.9	9.3	10.9	15.5	15.3	15.2	13.9	12.1	9.7	3.5	9.3
1964	4.6	5.5	5.9	9.0	13.1	14.6	16.7	15.9	14.9	9.9	8.8	5.1	10.3
1965	4.8	3.7	6.4	8.9	11.5	14.5	14.8	15.5	12.4	12.0	6.4	6.5	9.8
1966	4.7	7.9	7.5	8.9	11.5	15.5	15.7	15.7	14.9	11.1	6.0	7.5	10.6
1967	5.7	6.5	7.7	8.9	10.8	14.9	16.5	15.9	14.5	11.9	6.5	5.8	10.4
1968	6.5	3.2	7.0	7.7	10.5	15.1	15.6	16.1	14.5	13.5	8.1	5.3	10.3
1969	7.1	2.3	5.6	8.9	11.3	14.4	16.7	16.1	14.5	13.3	6.7	4.7	10.1
1970	5.7	5.0	5.1	7.9	12.7	16.4	15.9	16.1	14.8	11.3	9.5	4.9	10.4
1971	6.1	5.4	5.9	8.2	11.8	13.2	17.5	16.6	15.3	12.4	6.7	7.6	10.6
1972	5.1	5.9	7.5	9.2	10.5	11.5	16.1	15.5	12.1	11.3	7.1	7.7	9.9
1973	5.5	5.5	6.3	7.9	11.7	14.7	15.5	17.1	15.1	10.1	8.1	6.3	10.3
1974	7.5	6.7	6.5	8.6	10.9	14.1	15.9	15.3	12.4	8.7	8.3	9.1	10.3
1975	7.9	6.4	5.8	8.8	11.1	15.1	17.9	18.4	13.7	11.1	7.8	5.6	10.8
1976	7.0	5.4	5.9	8.3	11.9	17.3	18.5	17.9	14.1	11.3	7.7	3.5	10.7
1977	4.3	7.0	8.1	8.2	11.3	12.9	16.7	15.9	13.6	12.6	7.3	7.7	10.5
1978	5.1	3.9	7.4	7.3	11.9	14.0	15.3	15.5	14.5	12.9	9.5	6.4	10.3
1979	1.3	2.9	6.1	8.6	9.9	14.0	16.9	15.2	13.9	12.3	8.3	7.2	9.7
1980	3.2	7.7	6.0	9.3	11.6	13.9	14.8	16.4	15.4	10.1	7.4	6.8	10.2
1981	6.3	4.3	9.3	8.7	11.5	14.1	16.5	17.1	14.8	9.6	9.1	3.7	10.4
1982	5.1	6.7	6.9	9.3	11.6	15.6	16.9	16.2	15.2	11.1	9.3	5.9	10.8
1983	7.9	3.4	7.6	7.4	10.5	15.2	19.9	18.1	14.9	11.3	8.8	6.9	11.0
1984	5.6	5.3	5.5	8.7	10.7	15.7	16.9	17.7	14.5	12.2	8.7	6.5	10.7

Extreme values for each month and year of occurrence

	Jan.	Feb.	Mar.	Apr.	May	June	July	Aug.	Sept.	Oct.	Nov.	Dec.	Year
Highest	9.0	8.3	10.1	11.6	14.0	17.3	19.9	18.7	16.4	13.7	9.9	9.5	11.8
	1921	1869 1926 1961	1957	1893	1922	1976	1983	1947	1949	1921	1939	1934	1921
Lowest	-2.4	-1.3	3.0	5.8	9.3	11.5	13.8	13.5	11.6	7.6	3.9	0.2	8.4
	1963	1895	1845	1879	1855 1879	1972	1861	1845 1912	1952	1887 1892	1915	1890	1879
Overall means 1841-1980	5.0	5.2	6.4	8.7	11.5	14.4	16.1	16.0	14.0	10.7	7.4	5.8	10.1

Table A.II. *Decadal monthly mean temperatures (°C) for Exeter, 1841–1984*

Years	Jan.	Feb.	Mar.	Apr.	May	June	July	Aug.	Sept.	Oct.	Nov.	Dec.	Year
1841–50	4.7	5.1	6.2	8.7	11.5	14.6	15.5	15.5	13.9	10.2	8.0	6.1	10.0
1851–60	5.2	4.1	5.8	8.1	10.7	13.7	15.9	15.8	13.5	10.6	6.5	5.5	9.6
1861–70	4.6	5.7	5.7	9.7	11.5	14.1	16.0	15.7	13.9	10.8	6.8	5.7	10.0
1871–80	5.0	6.1	6.7	8.5	10.8	14.2	16.0	16.1	13.7	10.4	6.7	4.9	9.9
1881–90	4.4	4.8	5.6	7.9	11.4	14.4	15.8	15.4	13.4	9.5	7.3	4.2	9.5
1891–1900	4.2	4.9	6.1	9.3	11.7	15.2	16.4	16.0	14.1	9.9	7.4	5.8	10.1
1901–10	5.4	5.0	6.4	8.4	11.5	14.0	16.1	15.8	13.8	10.9	7.1	5.9	10.0
1911–20	5.3	5.7	6.4	8.7	12.4	14.2	16.0	16.1	13.6	10.3	7.1	6.3	10.2
1921–30	6.3	5.7	6.9	8.5	11.9	14.3	16.7	15.9	14.3	11.1	7.1	6.3	10.4
1931–40	5.4	5.5	6.9	8.9	12.1	15.1	16.3	16.7	14.5	10.7	8.0	5.6	10.5
1941–50	4.9	5.2	7.1	9.5	11.8	14.5	16.3	16.3	14.4	11.2	8.0	5.8	10.4
1951–60	4.9	4.6	6.8	8.7	11.7	14.6	16.5	16.0	14.2	11.3	7.9	6.7	10.3
1961–70	4.8	4.9	6.4	8.9	11.4	14.9	15.9	15.7	14.3	11.8	7.5	5.2	10.1
1971–80	5.3	5.7	6.5	8.4	11.3	14.1	16.5	16.4	14.0	11.3	7.8	6.8	10.3
1981–84 (4 years)	6.2	4.9	7.3	8.5	11.1	15.1	17.5	17.3	14.9	11.1	9.0	5.7	10.7
Overall means 1841–1980	5.0	5.2	6.4	8.7	11.5	14.4	16.1	16.0	14.0	10.7	7.4	5.8	10.1

Table A.III. *Seasonal mean temperatures (°C) for Exeter, 1840–1984*

	Winter	Spring	Summer	Autumn		Winter	Spring	Summer	Autumn
1840	5.3	8.9	15.4	9.9					
1841	2.7	9.7	14.4	10.5	1871	3.7	9.5	15.1	10.0
1842	4.7	8.9	16.7	10.0	1872	6.1	8.7	15.3	10.3
1843	6.4	9.0	15.1	11.3	1873	5.4	8.5	15.4	9.9
1844	6.1	9.3	14.8	10.8	1874	6.1	9.7	15.7	11.1
1845	3.4	7.4	14.1	10.4	1875	4.8	8.7	15.0	10.9
1846	7.2	9.2	16.7	11.3	1876	5.3	7.9	16.3	10.7
1847	3.9	8.3	15.5	11.2	1877	7.4	7.8	15.3	10.3
1848	5.5	9.6	14.5	10.3	1878	6.1	9.3	16.1	9.9
1849	6.6	8.4	15.0	11.1	1879	2.8	6.9	14.1	9.6
1850	4.9	8.1	15.0	10.1	1880	3.6	9.6	16.0	10.1
1851	6.4	8.4	14.9	9.3	1881	3.7	9.3	15.1	10.2
1852	5.3	7.9	15.4	10.2	1882	5.8	9.6	14.5	9.6
1853	5.2	8.1	15.0	10.2	1883	6.0	7.5	14.7	10.4
1854	4.3	8.7	14.2	10.0	1884	6.2	8.4	15.6	10.5
1855	2.9	7.0	14.9	10.1	1885	5.6	7.4	15.2	9.6
1856	5.4	7.6	15.6	10.4	1886	2.9	8.3	15.7	11.1
1857	5.3	8.0	16.0	11.2	1887	3.9	7.0	16.6	8.4
1858	5.5	8.5	15.4	10.3	1888	3.4	7.5	14.4	10.2
1859	6.4	9.3	16.4	10.7	1889	4.7	8.8	15.3	10.1
1860	4.0	8.6	13.7	9.6	1890	4.8	9.1	14.8	10.6
1861	3.9	8.6	14.6	9.8	1891	2.2	7.2	14.8	10.1
1862	5.2	9.3	13.8	10.4	1892	4.5	8.2	15.0	9.3
1863	6.6	9.7	14.8	10.7	1893	4.6	11.1	16.7	9.9
1864	4.9	9.4	14.9	10.1	1894	5.2	9.1	15.3	10.5
1865	3.6	9.1	15.7	11.7	1895	2.2	9.6	15.5	11.0
1866	6.2	8.1	15.3	11.0	1896	5.3	10.6	16.2	8.7
1867	6.2	8.3	15.0	10.0	1897	5.2	9.5	16.6	10.9
1868	5.3	10.0	17.1	10.2	1898	6.2	8.5	16.1	11.8
1869	8.1	8.3	15.1	10.9	1899	6.8	8.5	16.8	11.4
1870	4.0	8.6	16.1	10.2	1900	5.1	7.9	15.8	10.9

	Winter	Spring	Summer	Autumn
1901	5.2	8.5	15.9	10.0
1902	4.3	8.6	15.0	11.0
1903	6.6	9.1	14.7	11.2
1904	5.0	8.8	15.4	10.5
1905	6.1	9.5	15.8	9.0
1906	5.8	8.6	16.0	11.1
1907	4.7	8.8	14.7	11.2
1908	5.9	8.5	15.6	11.6
1909	5.1	8.5	14.9	10.2
1910	5.5	8.9	15.1	10.4
1911	6.0	9.6	17.4	10.5
1912	6.6	10.4	14.6	9.5
1913	6.8	9.3	15.4	11.8
1914	6.0	9.7	15.8	10.5
1915	5.3	9.1	15.0	9.1
1916	6.8	8.1	14.9	11.0
1917	2.6	8.0	15.6	10.9
1918	5.4	9.1	15.6	10.3
1919	5.6	9.0	15.6	8.7
1920	6.9	9.7	14.4	11.1
1921	6.7	9.7	17.4	12.5
1922	6.6	8.8	14.6	9.6
1923	7.0	9.0	15.7	9.5
1924	5.5	8.4	14.1	10.9
1925	6.9	8.6	16.5	9.6
1926	6.6	9.4	16.3	11.1
1927	5.9	10.2	15.3	10.8
1928	6.3	9.4	15.4	11.4
1929	3.7	8.6	15.1	11.5
1930	5.5	9.0	15.8	11.4
1931	5.4	8.3	15.1	10.8
1932	6.9	8.3	16.3	10.9
1933	5.4	10.3	16.8	11.4
1934	3.8	9.1	16.6	11.8
1935	7.7	9.2	16.4	10.4
1936	5.3	8.9	15.5	10.9
1937	6.7	9.5	16.1	10.1
1938	5.3	9.5	15.6	11.8
1939	5.8	9.9	16.0	11.3
1940	3.3	10.1	16.2	11.1
1941	4.5	9.2	15.9	11.6
1942	3.9	9.2	15.2	10.3
1943	7.3	10.0	15.3	10.5
1944	5.6	9.0	16.1	10.3
1945	4.8	10.1	15.5	11.8
1946	6.3	8.9	14.6	11.6
1947	2.2	9.0	16.6	11.5
1948	6.2	10.0	15.1	11.7
1949	6.6	9.8	16.8	12.3
1950	6.4	9.5	15.9	10.5
1951	4.5	7.8	15.1	11.5
1952	5.3	10.0	16.1	9.3
1953	4.7	9.1	15.7	11.5
1954	5.7	8.9	14.4	11.6
1955	5.1	7.8	16.9	10.7
1956	4.5	8.8	15.1	10.9
1957	6.8	10.3	16.3	10.8
1958	5.8	8.0	15.3	11.6
1959	5.1	10.0	16.4	12.2
1960	6.1	9.9	15.7	11.1
1961	6.2	10.2	15.6	11.4
1962	5.4	7.6	14.7	10.2
1963	0.9	9.0	15.3	11.9
1964	4.5	9.3	15.7	11.2
1965	4.5	8.9	14.9	10.3
1966	6.4	9.3	15.6	10.7
1967	6.6	9.1	15.8	11.0
1968	5.2	8.4	15.6	12.0
1969	4.9	8.6	15.7	11.5
1970	5.1	8.6	16.1	11.9
1971	5.5	8.6	15.8	11.5
1972	6.2	9.1	14.4	10.2
1973	6.2	8.6	15.8	11.1
1974	6.8	8.7	15.1	9.8
1975	7.8	8.6	17.1	10.9
1976	6.0	8.7	17.9	11.0
1977	4.9	9.2	15.2	11.2
1978	5.6	8.9	14.9	12.3
1979	3.5	8.2	15.4	11.5
1980	6.0	9.0	15.0	11.0
1981	5.8	9.8	15.9	11.2
1982	5.2	9.3	16.2	11.9
1983	5.7	8.5	17.7	11.7
1984	5.9	8.3	16.8	11.8

Table A.IV. *Decadal seasonal mean temperatures (°C) for Exeter, 1841–1984*

Years	Winter	Spring	Summer	Autumn
1841–50	5.1	8.8	15.2	10.7
1851–60	5.1	8.2	15.1	10.2
1861–70	5.4	8.9	15.2	10.5
1871–80	5.1	8.7	15.4	10.3
1881–90	4.7	8.3	15.2	10.1
1891–1900	4.7	9.0	15.9	10.5
1901–10	5.4	8.8	15.3	10.6
1911–20	5.8	9.2	15.4	10.3
1921–30	6.1	9.1	15.6	10.8
1931–40	5.6	9.3	16.1	11.1
1941–50	5.4	9.5	15.7	11.2
1951–60	5.4	9.1	15.7	11.1
1961–70	5.0	8.9	15.5	11.2
1971–80	5.9	8.8	15.7	11.1
1981–84 (4 years)	5.7	9.0	16.7	11.7
Overall means 1841–1980	5.3	8.9	15.5	10.7

551.5(09):551.501.9(468.2)

The history of the Meteorological Office at Gibraltar

By D. Hyde*

Summary

The Meteorological Office at Gibraltar was opened in November 1935. To celebrate its 50th anniversary an account is given of meteorological observing and forecasting work at Gibraltar over the last two centuries, with more detailed attention being given to the activities of Meteorological Office staff since 1935. Most of these were concerned with aviation, but more general public service work has been increasing in recent years.

Introduction

One of the earliest events to concentrate the minds of Gibraltar's citizens on the weather occurred on 31 January 1776 when 50 people were killed in a great deluge of unrecorded intensity. The siege of Gibraltar commenced in 1779 and a climatological account (Drinkwater 1905) refers to 'heavy rains, high winds and most tremendous thunder, with dreadful vivid lightning'. In 1790 the Royal Engineers introduced their 'pluviometer' to commence a virtually continuous record of rainfall over nearly 200 years. In 1862 responsibility for weather records was handed over to the Colonial Government who assigned the rather grand title of Government Observatory to a stone hut at South Bastion where observations were made. As instrumentation on the Rock evolved, rain-gauges and anemometers became rather like wandering minstrels jostled by the populace at large as space became a valuable commodity. Even the police became involved in making observations. In 1923 one officer struggling

*Formerly of the Main Meteorological Office, Royal Air Force Gibraltar.

with a strange instrument at a remote site reported 'it is impossible to see the vane of the anemometer at 9.0 p.m. owing to the darkness'. In 1929 the South Bastion station moved to Alameda Gardens in the charge of the head gardener (one Harry Bently) and his two deputies. No doubt they were relieved to see a direction dial fitted to the anemometer a year later, thus avoiding the police officer's dilemma. Hurst (1959) provides an excellent review of early observations together with a map of meteorological stations at Gibraltar.

In the early part of this century aviation was starting to emerge as a force to be reckoned with. Soon after the Wright brothers made their first flight, the Balloon Section of the Royal Engineers sampled Gibraltar in 1904–5 but it is suspected that wind and weather proved too much for them. The racecourse was used to operate military aircraft on a small scale during the First World War and a few seaplanes were also used. Forthcoming dependence on meteorological services was revealed in some of the remarks of pilots at that time — 'dropping 600 feet in one act' near the Rock did not impress them.

In 1931 Gibraltar Airways Limited was formed to provide a service to Tangier. This first attempt proved abortive but it did set the scene for years of discussion on Gibraltar's airfield of the future. It was in 1935 that the Meteorological Office interest in the ancient fortress came to fruition with the arrival of British staff.

1935 to 1955

In 1935 the observing site was moved from Alameda Gardens (just south of the city) to Windmill Hill near the southern extremity of the Rock. The new office occupied a commanding position at about 400 feet above sea level overlooking the Strait. Naval ratings supervised by Air Ministry meteorologists got the office established and began the new sequence of observations. In 1938 the Air Ministry formally took over the station using locally employed staff in the observer role. At about that time General Ironside took over as Governor and started to press for facilities to make the Rock viable as a base for air operations. The outbreak of war in 1939 meant rapid expansion at Windmill Hill with 24-hour observing and forecasting services. External communications became very difficult with cable exchanges with London replacing earlier radio messages. By the early 1940s it was obvious that something had to be done to provide close meteorological support to the joint military staffs and the aircrews. Early in 1942 the forecast service was moved to New Camp (the flying boat base); from there the forecasters served both the newly formed Combined HQ and RAF North Front by motorcycle and side-car. In the meantime the provision of a runway at North Front, between the Rock and nearby Spain (see Figs 1 and 2) was going ahead, ably pushed and prodded by the Governor, Lord Gort. Later in 1942 the Combined HQ together with the forecast section moved into secure accommodation in the centre of the Rock. The external exchange of meteorological information was going more smoothly by using encyphered radio messages. On 2 November 1942 the first meteorological reconnaissance Hudson aircraft took off from the new runway. All this activity culminated in Operation Torch, the allied landings at Algiers, Oran and Casablanca. A third Meteorological Office had to be opened at North Front during the build-up and it became Gibraltar's Main Meteorological Office north of the runway in the post-war years.

Although Gibraltar's weather was regarded as relatively reliable, the aircrews quickly found out that it was not a factor to be trifled with (Dyer 1976). Heavy rain flooded the runway during a vital stage of Operation Torch. In October 1942 five Hudson aircraft of 233 Squadron circled above the fog-bound runway for three hours — one aircraft was forced to ditch but the remaining four landed safely. During the 1946/47 winter, the author witnessed an extraordinary landing by an American transport aircraft. In a south-westerly gale with heavy rain, the pilot elected to make his approach to runway 27 from the north over La Linea thus avoiding the severe turbulence in the lee of the Rock. On arrival over the

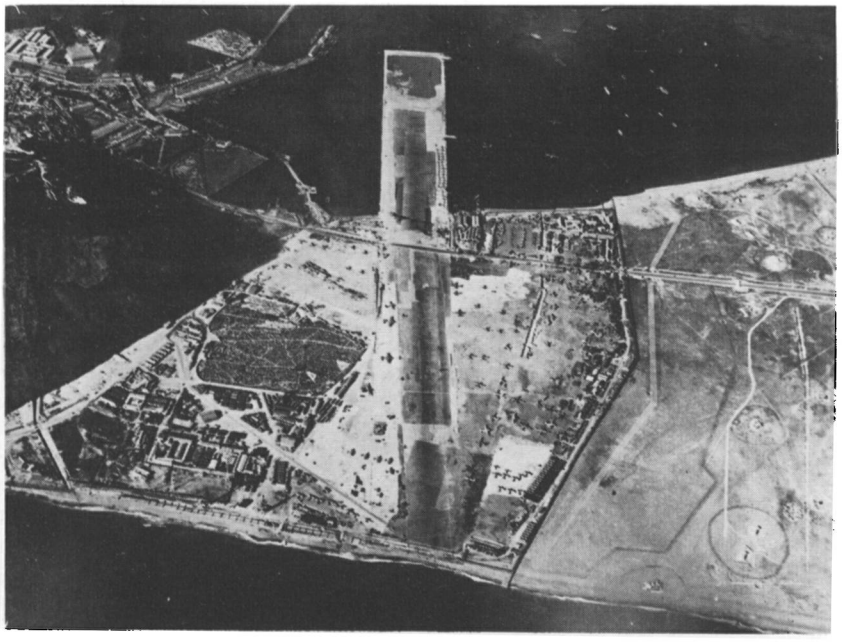

Figure 1. Royal Air Force, North Front, Gibraltar February 1943; looking westwards.

Figure 2. Royal Air Force, Gibraltar today; looking eastwards, Main Meteorological Office in Control Tower — middle distance left of runway.

runway with the Rock dead ahead he executed a steeply banked turn to starboard a few feet above the surface and landed safely — a superb feat of airmanship.

The military activity gave impetus to solving the problem of providing adequate data for the forecasters to work with. Using Halifax aircraft 520 Squadron made regular daily meteorological reconnaissance flights (code-named Nocturnal) from 1944 to 1951. Gladiator aircraft carried out vertical temperature soundings in 1943 and 1944 but the program was later replaced by the radiosonde unit formed by the author in 1946 (Fig. 3). The unit was housed in temporary accommodation north of the runway some distance from the North Front Meteorological Office. Surface observations based on adequate exposure and a wide range of instruments commenced at North Front in 1944 and the Windmill Hill station was closed in 1948. Apart from minor changes, notably in radiosonde, the years of upheaval ended in 1955 when the Main Meteorological Office moved into the new air traffic control building.

1955 to 1985

In a more stable operational environment, and with the winding down of military requirements, the Office was able to use part of its resources to tackle some of the meteorological problems arising from Gibraltar's unique location and orography (see Fig. 4). A concerted effort was made in the 1960s and 1970s to evaluate turbulence in the vicinity of the Rock, potentially the worst problem in the light of earlier wartime experience (Briggs 1963, Barnham and Spavins 1965, Cook 1976). For this purpose the Meteorological Office and the Royal Air Force secured the co-operation of the Royal Aircraft Establishment and the Building Research Advisory Service. Using in-flight observations and wind-tunnel data it was possible to correlate turbulence patterns and intensities with measured surface winds at North Front. A related problem was the forecasting of surface wind not only for turbulence but for a wider selection of elements. The orography of the Strait area imposed either westerlies or easterlies with a few (significant) variations. The weather associated with each regime was surprisingly different and effective forecasting of surface wind opened the door to success in other fields. McKay (1977) developed useful relationships between low-level winds and the pressure difference between Alicante and Casablanca which had been used subjectively in earlier years. In the 1980s the main effort in local investigations has been directed towards numerical products, especially the evaluation and verification of fine-mesh pressure and rainfall forecasts which are received at Gibraltar in the form of grid-point values.

When the Meteorological Office became centred on North Front in 1955 civilian staff had replaced service radio operators in a new cell dedicated entirely to reception of meteorological data on four channels with a further channel for transmission. In 1974 the RAF again took over the meteorological communications role. Since then channels were provided on the Defence communication network and in the 1980s most data are received by teleprinter direct from the automated telecommunication centre at Bracknell. There have been some changes in weather observing and monitoring as well. In 1963 the main instrument enclosure at North Front was removed from the immediate vicinity of the Main Meteorological Office to a site on British Lines Road adjacent to the border fence and near the present radiosonde unit. The standard recording anemometer at the Main Meteorological Office was supplemented by installations at both ends of the runway in addition to one at Rock Gun (near the Rock top at 390 metres, overlooking the runway). In 1972 automatic picture transmission equipment was added and is currently awaiting replacement by a more advanced station. At the radiosonde unit technical enhancement continued, the main highlights being the replacement of the old Army gun-laying radar with Cossor equipment in 1973 and the introduction of the Grawsonde in 1979 to replace the earlier Meteorological Office system.

Figure 3. One of the first radiosonde launches from Gibraltar, June 1946; author — middle distance centre, Halifax meteorological reconnaissance aircraft — middle distance right.

Photograph by courtesy of NASA Johnson Spaceflight Center

Figure 4. Satellite photograph showing location and orography of Gibraltar.

It is to be expected that this article reveals preoccupation with aviation matters but this is not to say that other customers have been neglected in satisfying the general thirst of the Gibraltarians for meteorological information. Radio and television broadcasts for the general public were developed steadily with special attention being given to the large sailing community. A mini-studio was installed by the British Forces Broadcasting Service in 1979 to enable the forecasters to make personal radio presentations either live or on tape. The Gibraltar Broadcasting Corporation provided both radio and television outlets. It is perhaps not generally appreciated that the audience included many thousands of English-speaking people on the Costa del Sol. More specialist services were provided to the Army, Navy, Property Services Agency, local government and the private sector. Even a local hotelier received a special warning service to help protect his guests from the vagaries of the weather. Fig. 5 shows the hotel in question with damage to water catchments above it caused by powerful lifting forces associated with lee turbulence. On the debit side, there is no doubt that smugglers took heed of meteorological advice to their advantage — the tables were turned on more than one occasion when the prosecution secured convictions in court using meteorological evidence in support. Oceanographers have always shown a great deal of interest in the seas around Gibraltar. In 1982 an international field experiment named 'Donde Va' examined the many aspects of sea water behaviour in the Strait and the Alboran Sea. Although the United Kingdom did not participate directly, the Main Meteorological Office was able to give useful support which was much appreciated. Local climatological services developed apace. Monthly and annual statistics were given a wide circulation within Gibraltar and usually received suitable attention in the media.

Meteorological observers, amateur and professional, are a dedicated breed the world over. None of the achievements in the long history of meteorology at Gibraltar would have been possible without a similar response from those who pioneered in the early days and the locally employed staff who have

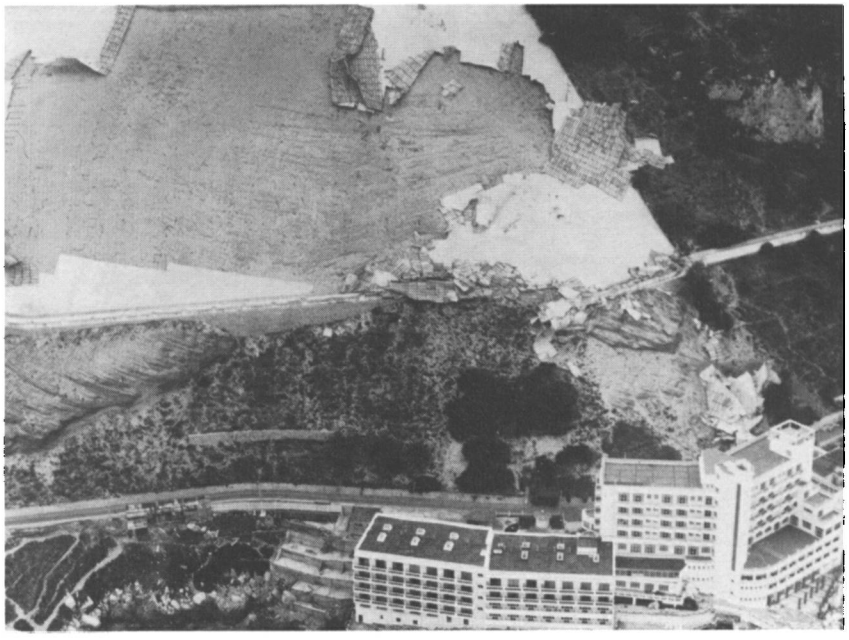

Figure 5. Damage to east-facing water catchments at Gibraltar, March 1975.

carried on ever since. Initially the forecasters faced an almost impossible task in times of crisis but local investigations have slowly eroded the areas of uncertainty. Unlike the Meteorological Office at home, Main Meteorological Office Gibraltar is unlikely to reap the benefits of advanced communications and computer technology (but see Briggs 1963) in the near future — with the probable exception of better satellite imagery. Nevertheless there is every reason to predict a promising future, one hopes in the dawn of a new era of good relations with nearby Spain.

References

Briggs, J.	1963	Airflow around a model of the Rock of Gibraltar. *Meteorol Off Sci Pap* No. 18.
Barnham, J. and Spavins, C. S.	1965	Gusts on the approach at Gibraltar Airfield. RAE Technical Report No. 65099.
Cook, N. J.	1976	Aircraft flightpaths at RAF Gibraltar. Building Research Advisory Service Report of special investigation No. 3072. London, Department of the Environment.
Drinkwater, J.	1905	A history of the Siege of Gibraltar (1779–1783). Spilsbury.
Dyer, P. C.	1976	Flying from the Rock. The story of aviation at Gibraltar (1901–1945). (Unpublished RAF document, copy available in the RAF Library, Gibraltar.)
Hurst, G. W.	1959	A brief history of meteorology in Gibraltar. *Weather*, **14**, 41–46.
McKay, W.	1977	Surface and low level winds at Gibraltar in relation to surface pressure differences between Casablanca and Alicante. (Unpublished note, copy available in the Main Meteorological Office Library, Gibraltar.)

551.593.653

Noctilucent clouds over western Europe during 1984

By D. M. Gavine

(Leith Nautical College, Edinburgh)

Table I summarizes the noctilucent cloud (NLC) reports received by the Aurora Section of the British Astronomical Association (BAA) during 1984, from observers in Great Britain, Belgium, Denmark and Finland.

Times (UT) in the second column are of sightings, not necessarily the durations, of displays. Maximum elevations and, where possible, limiting azimuths are included. Coordinates of the observing stations are given to the nearest half-degree.

No routine hourly sky reports were received from British meteorological stations. All known 'negative' nights (i.e. clear sky but with no visible NLC) are based on the reports of regular, experienced observers in Great Britain (G), Belgium (B) and Finland (F). Positive reports were received from 16 British amateurs and 5 meteorological stations, Mr van Loo (Itegem, Belgium), Mr Olesen and Mr Persson (Denmark), and the highly organized team of 16 observers throughout Finland co-ordinated by Mr V. Mäkelä, whose excellent report forms the bulk of this summary. In Finland 31

positive NLC sightings were made between 2/3 May and 24/25 August, of which only one was seen in June; but only 11 were made in Britain which, despite a dry summer, experienced a great deal of night tropospheric cloud, especially in the north. Many of our regular observers, including the staff at Sumburgh, saw nothing over the entire season. Seven NLC were observed in Denmark, one in Belgium. A positive NLC sighting on 10/11 August by Mr Frydman at Wembley and Meteorological Office staff at Bedford, and four by Finnish observers in the second half of August, suggest a careful watch beyond the expected 'season' (Simmons and McIntosh 1983).*

Dr M. Gadsden (Aberdeen) carried out polarimetric work on the brilliant display of June 28/29 but cloud cover rendered parallactic photography by fixed-bracket cameras unsuccessful.

Thanks are due to all observers, amateur and professional, for their efforts, to Mr N. M. Bone, Director of the Aurora Section, Junior Astronomical Society, for helpful collaboration, and to Drs Gadsden and McIntosh for their advice and encouragement. The BAA Aurora Section carries out routine observation of aurora and noctilucent cloud to provide data for possible future research and its activities are almost entirely in the hands of amateurs. We would like to see a network of voluntary observers spread widely throughout north-west Europe, as was organized by James Paton during the International Geophysical Year. Information on the Section and observing instructions may be obtained from the Director, Mr R. J. Livesey, 46 Paidmyre Crescent, Newton Mearns, Glasgow G77 5AQ.

Table I. *Displays of noctilucent clouds over western Europe during 1984*

Date — night of	Times UT	Notes	Station position (to nearest 0.5 degree)	Time UT	Max elev.	Limiting azimuths
					degrees	
30 Apr/ 1 May		No NLC (F)				
1/2 May		No NLC (F)				
2/3	1915–2130	At Vaasa, poorly defined band. No NLC at Helsinki and Toivala.	63°N 21.5°E	2105–2130	15	355–030
3/4		No NLC (F)				
5/6 to 11/12		No NLC (F)				
12/13	1940–2250	Suspect small patch of bands and veil at Lapua, but no NLC seen by 8 other Finnish stations.	63°N 23°E	2145 2155–2210	50 90	350–045 180–000
13/14 to 5/6 June		No NLC (F)				
6/7 June	2145–2300	Bluish faint bands at Helsinki. No NLC (G).	60°N 25°E 61°N 29°E	2230–2300 2145–2200	15 No NLC	340–010
7/8		No NLC (G)				
8/9		No NLC (F, G)				
9/10	2256–0210	Weak parallel bands at Edinburgh and Morpeth, photographed at Petworth. No NLC (B, F).	56°N 03°W	2256 2304 2308 2315 2330	40 45? 22 13? 22	320–040 –025 –030 345–005
			55°N 01.5°W	2300 2315 2330 2345 0000 0045	30 40 48 37 No NLC 15	300–008 320–030 317–020 332–017 005–020

*Simmons, D. A. R. and McIntosh, D. H.; An analysis of noctilucent cloud over western Europe during the period 1966 to 1982, *Meteorol Mag*, **112**, 1983, 289–298.

Date — night of	Times UT	Notes	Station position (to nearest 0.5 degree)	Time UT	Max elev.	Limiting azimuths
					degrees	
9/10 (contd)			51°N 00.5°W	0145	3	
				0200	4	020–045
10/11	2150–2300	Medium-bright bands at Morpeth. No NLC (F).	55°N 01.5°W	2150	7	290–300
				2200	8	292–351
				2215	11?	Faint veil
				2230	No NLC	
11/12		No NLC (F)				
13/14		No NLC (G)				
14/15		No NLC (F, G)				
15/16 to 24/25		No NLC (F); also 15/16, 21/22 no NLC (B); no NLC (G) on 18/19, 23/24. Suspect band at Herstmonceux 22/23, 0120.				
27/28	2150–2324	Greenish NLC at Rönne.	55°N 14.5°E	2150–2324		NE
28/29	2115–0250	Brilliant display visible as far S as Yorkshire, and in Denmark. Intense gold-blue area in NE, strong waves parallel to horizon, fainter waves and bands N. From 0115 large-scale irregularities and whirl structure. Display illuminated rapidly from low in NE to high in N from 0130. Veil, bands and waves in tropospheric cloud at Rönne.	57°N 02°W	2210	No NLC	
				2230	30	000–030
				2255	20	000–045
				0145	Zenith and SE	
			56.5°N 03°W	2300	10	045–090
				2315	15	000–090
				2330	20	000–090
			56°N 03°W	2345	NLC in cloud	
				0000	9	027–065
				0015	11	012–070
				0030	11	000–070
				0045	12	012–074
				0100	11	–080
				0115	13	006–080
				0130	30	–070
				0145	40	356–072
				0200	42	
				0215	NLC visible	
			55°N 01.5°W	2300	Bands visible	
				2315	16	342–023
				2330	11	340–025
				2345	9	340–018
				0000	7	342–070
				0015	6	345–080
				0030	11	350–082
				0045	12	353–095
				0100	20	356–095
				0115	22	355–095
				0130	32	344–083
				0145	38	340–065
				0200	20	340–070
				0215	Traces	
				0230	No NLC	
			55°N 14.5°E	2115	30	315–045
				2200	Cloud	
			54.5°N 01°W	2330	8	Cloud
			54°N 01°W	2240	7	345–015
				2345	8	340–080
				0000	8	340–080
				0100	7	350–070
				0200	15	350–060
				0250	No NLC	
29/30	2200–0230	Extensive but fairly weak display of bands, slight wave structure, becoming lower in altitude. Visible as far S as Exeter.	56°N 03°W	2325	15?	Cloud
				2350	11?	–005
				0017	10?	330–030
				0030	NLC in cloud	
			55°N 01.5°W	2220	40	000
				2250	17	330–030
				2305	17	340–010
				2315	18	335–005
				2320	6	317–000
				2330	5	304–000
				0015	4	000–017
				0030	4	036–062
				0045	5	000–060

Date — night of	Times UT	Notes	Station position (to nearest 0.5 degree)	Time UT	Max elev.	Limiting azimuths
					degrees	
29/30 (contd)			54.5°N 03.5°W	0030	15	310–010
			52.5°N 00.5°E	2215	30	320–015
				2300	30	Cloud
				2315	Cloud	
			52°N 02°W	2200	35	320–000
				2250	25	315–010
			50.5°N 03.5°W	0200	4	010–
				0218	6	010–
				0228	8	
				0230	No NLC	
30 June/ 1 July	2150–2240	Very small faint veil at Turku. No NLC (B, G).	60.5°N 22.5°E	2150–2240	65	290
1/2 July		No NLC (F)				
2/3	2150–2210	Faint, poorly defined bands, central Finland. No NLC (G).	60.5°N 22.5°E	2150–2210	30	005–040
3/4	2140–2300	Faint blue-white veil and bands, S Finland. No NLC (G).	60.5°N 22.5°E	2215–2300	90	
			60°N 25°E	2140	35	300–000
4/5	2100–2325	Bands over W coast of Finland, veil to S. Waves over Helsinki. Veil suspected at Cockermouth despite moon. (a) Mr Parviainen, (b) Mr Frydman.	60.5°N 22.5°E	2200–2300	45	300–050
			60°N 25°E(a)	2100	Cloud	
				2125	25	000
				2140	60	315–095
				2200	100	315–090
				2215	70	330–180
				2230	40	330–045
			60°N 25°E(b)	2151	30	290–015
				2220	50	300–010
				2230	30	300–010
				2245	20	320–000
				2300	Cloud	
			54.5°N 03.5°W	2250–2325	25	350–040
5/6	2100–0050	Well-defined bands along Finnish–Soviet border, moving NE to SW. NLC visible in cloud at Morpeth.	63°N 27.5°E	No NLC		
			62.5°N 27°E	2210	18	080–140
				2220	24	095–150
				2235	20	110–170
				2245	18	130–170
				2255	18	145–180
			61°N 29°E	2215–2245	100	040–050
			60.5°N 22.5°E	0000–2215	No NLC	
			60°N 25°E	2150	11	Trace NW?
				2215	20	290–055
				2240	NLC in cloud NW	
			55°N 01.5°W	2320	26	350–060
				0020	35	In cloud
				0035	28	–038
				0050	Cloud	
6/7	2100–2343	Bands NNE–SSW with waves and whirls over central Finland. Faint bands at Itegem.	62.5°N 27°E	2220	145	
				2230	145	Cloud
			62°N 25°E	2145–2245	40	010–050
			60.5°N 22.5°E	2100	No NLC	
				2140	16	030–080
				2200	16	030–075
				2215	15	030–080
				2230	13	030–080
			60°N 25°E	2152	70	330–080
				2215	60?	340–015
				2222	20	330–015
				2240	20	340–015
				2300	20	310–015?
				2315	40	300–015
				2330	62	275–005
				2343	60	280–000
			51°N 04.5°E	2144	23	312–010
7/8	2120–2248	Bands and ripples low in NW. Blue-green, eastward drift, at Birkerød. No NLC (F).	56°N 12.5°E	2120		315
				2143	Low	
				2248	No NLC	

Date — night of	Times UT	Notes	Station position (to nearest 0.5 degree)	Time UT	Max elev.	Limiting azimuths
					degrees	
8/9	2045–0003	Faint bands and ripples at Helsinki, in tropospheric cloud. At Rönne, bands with rapid changes in whirl structure from 2223, westward drift. NLC seen in Sweden — no details. No NLC (B).	62°N 25°E	2200–2245	No NLC	
			60°N 25°E	2222	20	In cirrus
				2245	20	340–010
				2305	30	330–010
				2335	50	285–005
				2345–0003	NLC?	
			55°N 14.5°E	2045	13	045
				2130	13	045
				2210	10	340–020
				2223	10	
				2320	NLC	
9/10	2100–0000	Veil and bands over Gulf of Bothnia and Sweden. Brilliant bands and billows up to 30° drifting W at Rönne. Mr Olesen photographed panorama of display. (a) Mr Manner, (b) Mr Frydman.	61°N 29°E	No NLC		
			60.5°N 22.5°E	2100	No NLC	
				2150	NLC	305
				2200	20	300–350
				2215	30	290–030
				2230	35	270–005
			60°N 25°E(a)	2200–2300	15	270–340
			60°N 25°E(b)	2143	10	240–315
				2209	18	265–315
				2221	16	260–335
				2230	15	260–345
				2245	18	257–355
				2300	18	258–342
				2315	22	260–002
				2330	27	260–000
				2345	14	290–345
				0000	12	295
			55°N 14.5°E	2110	30	340–045
				2130	30	315–135
				2145	30	315–135
				2230	13	315–135
				2320	10	
10/11		No NLC (F)				
11/12		No NLC (F)				
12/13	2105–2300	Veil and bands over SW Finland, Gulf of Bothnia and central Sweden. Thin bands seen at Morpeth and S Shields. No NLC (B).	63°N 27.5°E	No NLC		
			60.5°N 22.5°E	2105	30	015–045
				2200	90	280–120
				2215	110	250–130
				2230	105	250–090
			60°N 25°E	2238	28	350–080
				2240	35	350–015
				2300	Cloud	
			55°N 01.5°W (Morpeth)	2155–2200	40	260–000
				2300	No NLC	
			(S Shields)	2234	25	340
13/14		No NLC (B). Possible trace of NLC at Helsinki 2230–2240, no NLC at Imatra.				
15/16		No NLC (F, B)				
16/17		No NLC (F)				
17/18	2212–0005	Very faint NLC trace at Helsinki, faint band at Edinburgh.	60°N 25°E	2212	No NLC	
				2308	13	345
				2313	Cloud	
			56°N 03°W	2345	11	020–060
				0000	14	050–060
				0005	Cloud	
18/19	2200–2355	Weak bands, gradually brightening, at Alrö. No NLC (F).	56°N 10°E	2200	5	000
				2300	10	
				2355	NLC	
19/20		No NLC (F)				
21/22		No NLC (F)				

Date — night of	Times UT	Notes	Station position (to nearest 0.5 degree)	Time UT	Max elev.	Limiting azimuths
					degrees	
22/23	2130–2300	Poorly defined bands over E Finnish border. No NLC (G).	62.5°N 27°E	2130	No NLC	
				2205	10	010–070
				2230	15	040–085
				2245–2300	16	050–080
23/24	2045–2250	Bands and waves observed in a cloudy sky in E Finland. Mr Frydman (Helsinki) describes intense 'corkscrew' form 2237, NLC in NW sky. Faint NLC in cloud Alrö, no NLC (G).	63°N 23°E	No NLC		
			62.5°N 27°E	2220	24	050–100
				0145–0150	50	070–120
			61°N 29°E	No NLC? cirrus		
			60°N 25°E	2103	NLC suspected	
				2130	30	270–000
				2150	Cloud	
				2210	NLC in cloud	
				2228		355–015
				2237	30	
				2245	Cloud	
			56°N 10°E	2145	NLC in cloud	
24/25	2015–2247	Bands over USSR–Finnish border. No NLC (G).	63°N 27.5°E	2015–2100	No NLC	
			62.5°N 27°E	2130	No NLC	
				2205	56	000–058
				2215	56	000–058
				2225	66	038–068
				2235	66	042–062
				2242	66	066–122
25/26		No NLC (F, B, G)				
26/27	2045–2130	Veil over W Bothnia, observed from Turku. No NLC (G).	60.5°N 22.5°E	2045	NLC present	
				2100	18	315–000
				2130	8	315–010
27/28	2045–2250	Bands over USSR E of Finland. (a) Mr Koistinen, (b) Mr Heikkinen, (c) Mr Nousiainen, (d) Mr Pekkola.	62.5°N 29.5°E	2030–2130	No NLC	
			62.5°N 27°E(a)	2111	11	046–070
				2140	19	038–068
				2157	15	040–080
			62.5°N 27°E(b)	2112	10	040–070
				2218–2240	12	010–080
			62.5°N 27°E(c)	2120	12	040–070
				2215–2230	12	040–095
			62.5°N 27°E(d)	2140	13	045–085
				2210	10	040–095
				2225	9	030–095
				2245	9	050–085
28/29	2045–0015	Bright and extensive display covering almost all Finland. All forms visible, bands and waves aligned mainly NNE–SSW and ENE–WSW. Most observers in patchy tropospheric cloud ((a), (b), (c), (d) as before).	66°N 24.5°E	2215–2231	45	036–090
			63°N 23°E	2040	20	040–080
			62.5°N 27°E(a)	2313	100	250–090
				2340–0000	30	010–100 (In cloud)
			62.5°N 27°E(b)	2100	14	350–060
				2150–2200	20	025–080? (In cloud)
			62.5°N 27°E(c)	2100–2130	28	320–065
			62.5°N 27°E(d)	2115	26	010–070
				2145	40	030–080
				2318	100	260–090
				2340	30	000–130
				0005	28	090–170
29/30	2015–0315	Extensive display over most of Finland, long bands, waves, large whirls over Vaasa. Waves aligned NNW–SSE. Bands visible in Carlisle and Bedford ((b), (c), (d) as before).	63°N 21.5°E	2210–2240	80	275–080
			63°N 23°E	2100–2130	90	260–330
			62.5°N 27°E(b)	2140	100	300–040
				2225	14	350–065
			62.5°N 27°E(c), (d)	2150	100	300–040
				2225	14	350–065
			61°N 29°E	2015	60	270–000
			60.5°N 22.5°E	2025	20	020
				2045	50	320–070
				2100	55	315–070
				2115	40	330–040
				2130	28	300–050
				2145	25	335–045
				2200	20	330–045

Date — night of	Times UT	Notes	Station position (to nearest 0.5 degree)	Time UT	Max elev.	Limiting azimuths
					degrees	
29/30 (contd)			55°N 03°W	0300–0315	30	045
			53°N 00.5°W	0250	10	000–030
30/31		No NLC (F)				
31 July/ 1 Aug	2000–2240	Poorly defined areas in N and central Finland not seen S of 62°N. All forms seen in N, bands and veil farther S. Possible drift SE. No NLC (G).	63°N 27.5°E	2130–2220	12	000–060
			63°N 23°E	2140–2200	50	030–040
			62.5°N 27°E	2135	No NLC	
				2150	8	010–070
				2200	8	010–060
			62°N 25°E	2040–2245	15	015–030
1/2 Aug	2000–2315	Small areas of veil, waves and whirls in central Finland? Most observers negative, one suspects aurora — fast drift of forms.	63°N 23°E	2150	10	030–040
			63°N 27.5°E	2100–2115	40	330–040
			62.5°N 27°E	2205	46	320–355 Aurora?
2/3	2030–2230	Bright display, all forms with long bands, over N Finland and Sweden. In tropospheric cloud gaps ((b), (c) as before).	63°N 27.5°E(b)	2100	20	330–060
				2130	18	000–065
			63°N 27.5°E(c)	2100	20	320–060
				2150	18	340–040
			62.5°N 27°E	2150	12	340–050
			(Kutunjarvi)	2213	16	005–035
				2225	16	340–070
			62.5°N 27°E	2125	14	350–010
			(Rautalampi)	2130	16	340–050
				2220	12	345–050
			62°N 25°E	2030–2100	20	020–060
3/4	2000–2230	Veil, bands and whirls over N central Finland.	63°N 27.5°E (Kuopio)	2115–2140	45	300–025
			63°N 27.5°E (Toivala)	2300	No NLC	
			62.5°N 29.5°E	2000–2200	40	315–012
4/5	2000–2300	Large bright NLC area over N Finland and Sweden, all forms, mainly E–W bands. Bands seen in Campbeltown and Paisley.	63°N 21.5°E	2155	20	310–000
				2250	10	315–010
			63°N 27.5°E	2035	45	270–020
				2045–2115	30	270–030
			63°N 23°E	2100–2120	40	340–030
			62.5°N 29.5°E	2000–2300	Bands	
			62.5°N 27°E	2032	32	300–024
				2110	25	300–010
			61°N 29°E	2045	25	310–010
				2115	20	310–010
			60.5°N 22.5°E	2000–2050	No NLC	
			56°N 04.5°W	2130–2145	10	045
			55.5°N 05.5°W	2210	12	355–015
5/6 to 8/9		No NLC (F)				
9/10	2215–2300	Bluish veil and bands over Lapland.	66°N 24.5°E	2215–2300	45	350–085
10/11	2000–0402	Long bands, waves and whirls over Gulf of Bothnia. Thin bands and ripples seen at Bedford and photographed near London.	62°N 25°E	2030–2100	40	315–040
				2130	25	320–030
				2215–2300	20	340–010
			53°N 00.5°W	0245	4	000–050
				0310	9	000
				0330	Low NLC	
			51.5°N 00°	0323	10	350–020
				0334	9	340–020
				0345	8	345–010
				0354	5	355
				0402	No NLC	
11/12 to 13/14		No NLC (F)				
15/16		No NLC (F)				
16/17	2120–2130	Veil and bands over extreme N of Scandinavia.	63°N 21.5°E	2120–2130	5	350–015

Date — night of	Times UT	Notes	Station position (to nearest 0.5 degree)	Time UT	Max elev.	Limiting azimuths
						degrees
17/18	1830–2225	Poorly defined patches of veil over Lapland and central Finland.	63°N 23°E	2200–2225	50	120–140
			63°N 21.5°E	2035–2050	5	355–010
			61°N 29°E	No NLC		
18/19	1900–2130	Veil, E Bothnia.	62°N 25°E	1930–2130	15	000–025
			61°N 29°E	No NLC		
20/21		No NLC (F)				
22/23		No NLC (F)				
23/24		No NLC (F)				
24/25	1900–0030	Poorly defined veil over Lapland.	66°N 24.5°E	2230–2315	4	000–015
			63°N 23°E	No NLC		
			62°N 25°E	1900–0030	10	320–010
25/26		No NLC (F)				
26/27		No NLC (F)				
28/29		No NLC (F)				
31 Aug/ 1 Sept		No NLC (F)				

Photographs

9/10 June	0145–0200	Petworth	D. Strachan
27/28	2314–16, 2324	Rönne	J. O. Olesen
28/29	2330–0155	Aberdeen	M. Gadsden
	0000	Aviemore	D. McConnell
	2300, 0020	Dundee	G. Young
	0000–0143	Edinburgh (Joppa)	D. Gavine
	0050–0140	Edinburgh	J. Shepherd
	2322–0148	Morpeth	A. McBeath
8/9 July	2223, 2232	Rönne	J. O. Olesen
9/10	2135–2240	Rönne	J. O. Olesen
18/19	2355	Alrö	J. O. Olesen
10/11 Aug	0329–0332	Wembley	D. Frydman

551.5:06(a):556.02

HOMS — The World Meteorological Organization Commission for Hydrology Operational Multipurpose Sub-programme

By B. R. May

(Meteorological Office, Bracknell)

One of the World Meteorological Organization's (WMO's) major programmes of work is the Hydrology and Water Resources Programme (HWRP) which, in these days of increasing flood demand, drought and flood hazard, assumes a particular importance. The developing countries are most likely to be affected by water resource problems, whereas at least some experience of tackling these problems resides in the developed countries so that some means of promoting the international exchange of hydrological and hydrometeorological techniques is required.

The WMO Commission for Hydrology which supports the HWRP through its Operational Hydrology Programme decided that an effective way of promoting this exchange of technical experience would be through the Hydrological Operational Multipurpose Sub-programme (HOMS). HOMS has involved the preparation of a reference manual giving brief but comprehensive descriptions of a large number of items (called 'components') of practical interest to hydrologists and hydrometeorologists. These components are subdivided into 12 broad sections:

A policy, planning and organization,
B network design,
C instruments and equipment,
D remote sensing,
E methods of observation,
F data transmission,
G data storage, retrieval and dissemination,
H primary data processing,
I secondary data processing,
J hydrological models for forecasting and design,
K analysis of data for planning, design and operation of water resource systems, and
X mathematical and statistical computation.

Within each of these sections there are further subject subdivisions. For example, within section I these are: general water quality, sediment transport data, precipitation data, evaporation (general), evaporation (computation from meteorological measurements), snow data, ground water, and river discharge data.

The individual components consist of, for instance, descriptions of instruments and their use, advice on networks of instruments and the design of data sets, recommendations for observing standards, and computer programs to meet a wide range of data-processing and modelling requirements.

There are now over 330 HOMS components summarized in the reference manual. Each summary is arranged to a uniform format with information under these headings: purpose and objectives, description, input, output, operational requirements and restrictions, form of presentation, operational experience, originator and technical support, availability, and conditions on use.

The components are largely independent but some, usually from different sections, are designed to be used together to perform a logical progression of operations — these are arranged in sequences of which there are now 11 specified in the manual. For instance a particular sequence entitled 'Catchment potential evaporation using synoptic data' contains six individual components, the first of which deals

Within GARP and the GWE considerable emphasis was given to tropical meteorology, and papers presented at the conference showed how this had borne fruit in improved understanding of tropical weather systems. Some improvement has also been achieved in predictive capabilities in the tropics, but more experience is needed in the application of global model results to tropical forecasting and, if possible, in the use of tropical fine-mesh models. Given the special features of tropical weather systems, coupled with the difficulties in establishing adequate computing and telecommunication facilities in many regions, the tangible benefits of the GWE to date are effective mainly in the technologically more advanced parts of the world. One of the major challenges which follows from the success of the GWE is to maintain a steady progress towards an enhanced WWW — known within WMO as WWW 2000 — which by the end of the century will permit further substantial progress in forecasting skill, with demonstrable benefits in all parts of the world.

551.58:69:019.941

An international seminar on building climatology

By M. J. Prior

(Meteorological Office, Bracknell)

The National Swedish Institute for Building Research (SIB) hosted a seminar from 28 to 31 May 1985 for the working commission of the International Council for Building Research Studies and Documentation responsible for building climatology (CIB-W71). Seventeen delegates from meteorological services, building research institutes and university departments attended, representing the four Nordic countries, the United Kingdom, Austria, Italy and Israel.

The seminar opened with a visit to the SIB laboratories at Gävle, where a 28-metre wind-tunnel, a mobile laboratory for microclimate studies and a computer-controlled thermal mannikin (for studies of the effects of the environments of buildings upon their occupants) were examined with interest.

The main part of the seminar was held in the 'think-tank' atmosphere of an 18th century manor house at Österbybruk. Energy conservation, test reference years, human comfort, standards for presenting climatic data and the use of microcomputers for manipulating data were among the topics covered during presentations of the work of the delegates, which were followed by a business session of W71. It was resolved that links with the relevant groups within the World Meteorological Organization (WMO) and the International Federation for Housing and Planning should be strengthened so that, for example, at least one representative of each group is present at the various meetings of these groups. The revision of the 1972 CIB/WMO report 15 — *Survey of meteorological information for architecture and building* — and arrangements for future symposia and working commission meetings were also discussed.

On the last day a visit was made to the Swedish housing exhibition at Upplands Väsby near Stockholm, where new housing designs and rehabilitation work by a housing association on 30-year old apartment blocks were seen. A common feature was the use of extensive glazing for conservatories and shared courtyards for energy conservation and amenity reasons.

The SIB is to be congratulated for arranging such an interesting and stimulating three days.

Notes and news

Mr P. Goldsmith

Mr P. Goldsmith, Director of Research in the Meteorological Office, has been granted special leave from 13 August 1985 to take up the appointment of Director of Earth Observations and Microgravity at the European Space Agency.

Mr Goldsmith's post in the Meteorological Office has been filled by Mr A. Gilchrist, previously Deputy Director (Dynamical Research).

Reviews

Nuclear winter, by Mark A. Harwell. 150 mm × 235 mm, pp. xxi + 179, *illus.* Springer-Verlag, Berlin, Heidelberg, New York, Tokyo, 1984. Price DM 54.00.

This book is concerned with an evaluation of the long-term impact of nuclear warfare on man and his environment. The short-term effects (which include blast damage, heat radiation and nuclear radiation) have been known about since the first nuclear weapon was exploded in July 1945. Concern as to longer-term effects focused first on radioactive fall-out and, in the 1970s, on possible destruction of the ozone layer (with subsequent enhancement of biologically damaging ultraviolet radiation at the surface) by the oxides of nitrogen injected into the stratosphere in the fireballs of the high-yield weapons then being developed. More recent research suggests that ozone reductions would be smaller, in part because there has been a trend towards smaller warheads. However, the possibility that mass fires would liberate large amounts of highly absorbing smoke, which would prevent solar radiation from reaching the surface and thus lead to a 'nuclear winter', has received a great deal of attention (and considerable publicity) in the last three years. It is in this area that the present book places much (but by no means all) of its emphasis.

The spectre of nuclear winter was first raised in 1982 in an article by Crutzen and Birks in a special issue of the journal *Ambio*, published by the Swedish Academy of Sciences, which was devoted to the environmental effects of nuclear war. This created a great deal of interest in the United States, where several groups began research projects and various committees were set up to produce reports. The first results were presented at a Conference on the Long-Term Biological Consequences of Nuclear War, which took place in Washington in late 1983. A paper by Turco and others (later published in *Science* and often known as TTAPS after the initials of its five authors) developed a range of war scenarios and through a chain of calculations (which they stressed were subject to great uncertainties) arrived at mean atmospheric smoke and dust loadings as a function of time. The climatic response was assessed using a one-dimensional radiative–convective model. The TTAPS results were used as input to a study of the environmental consequences by a team of biologists. Harwell's book began life as a technical support document for this part of the meeting.

This is both a complex and an emotive subject, so it is important that the uncertainties in the predictions are understood. A major fault in this book is that the TTAPS results are accepted virtually without qualification and the impression is given that firm projections are being made. It is worth summarizing here the chain of events which is supposed to lead to nuclear winter in order to bring out these uncertainties.

It is widely believed that a limited nuclear war is very unlikely and that there would be rapid escalation to a large-scale exchange, though this depends on assumptions which (one hopes) cannot be checked fully. Likely targets include military (bases, command centres, missile silos, etc.), strategic (industrial, communications and transport centres) and civilian (large cities). There is a wide range of possible

scenarios for the number and nature of the targets and for the size of the warhead used on each. The thermal pulse from a nuclear explosion can ignite combustible materials over a wide area, so that extensive city, industrial and forest fires would be expected, depending on many factors such as the nature of the target and the ambient weather. In such fires, some fraction of the burning material would create smoke and a proportion of this would be elemental carbon. The smoke particles would initially be expected to be much smaller than 0.1 μm, but would grow by coagulation and would ultimately be removed by gravitational settling and by incorporation into precipitation. The exact size, shape, physical and chemical composition of the aerosol from a large fire are very uncertain. Central to the nuclear winter hypothesis is that sufficient carbonaceous aerosol would remain in the crucial size range around 0.1 μm radius to alter radically the radiation balance. Such an aerosol has unusual optical properties; it strongly absorbs solar radiation but is too small to have an appreciable influence on long-wave radiation. If sufficient quantities were lofted, one would therefore expect strong atmospheric heating while at the same time the surface would cool. Merging of smoke plumes and spreading by the winds is supposed to lead to most of the northern hemisphere being covered by smoke, with land surface temperatures up to several tens of degrees Celsius below normal for several weeks. This projection depends on an enormous extrapolation of current knowledge. The aerosol would have to run the gauntlet of scavenging by precipitation, which may be very important as large fires often lead to cumulonimbus clouds. At Hiroshima, for example, such a cloud formed and 'black rain' fell.

By varying the assumptions one can predict any response from surface warming to a cooling so severe that some authors have even raised the possibility that the next ice age would be initiated. Atmospheric scientists expecting to find a discussion of these uncertainties will be disappointed by this book. Nevertheless, it is worth reading if only to see what biologists get up to when presented with such possibilities and to enjoy some of the pretentious conclusions on the jacket cover and in the foreword and summary of consequences. For what should be a more careful review of the current status of this subject I recommend the report of the SCOPE-ENUWAR project, due to be published this September.

It is easy to pour scorn on the projections of a nuclear winter, but the uncertainties will only be reduced if scientists are prepared to spend time studying them. As with many other environmental issues, by focusing attention on areas of atmospheric science which are poorly understood, research may be stimulated which has wider application and thus enriches the science. However, even if these projections were shown to be incorrect, nuclear war would still be an appalling prospect. It is a terrible indictment of our age that such weapons are considered necessary as the ultimate deterrent, or to provide the ultimate solution, in the resolution of conflicts between nations.

A. Slingo

Recent advances in planetary meteorology, edited by Garry E. Hunt. 178 mm × 252 mm, pp. xiv + 161, *illus.* Cambridge University Press, Cambridge, London, New York, New Rochelle, Melbourne, Sydney, 1985. Price £20.00, US $39.50.

Recent spacecraft missions and other improved observational techniques have, over several years, led to the collection of a body of data concerning the structure, composition and dynamics of planetary atmospheres. These observations present the meteorologist with a challenge and an opportunity to test ideas developed by analysing data from our own atmosphere which, although extensive in coverage, are obtained under a limited range of conditions. This book contains a selection of reviews of several aspects of planetary meteorology which will be of interest to many. The seven contributions were originally prepared as keynote lectures at sessions of an International Union of Geodesy and Geophysics meeting on planetary meteorology held in Hamburg in 1983. The session was dedicated to the memory of

Seymour Hess whose contributions to this field of meteorology and to the success of the Viking missions to Mars are well known.

The seven papers fall into three groups. The first two papers are concerned with aspects of the chemical composition and chemical evolution of the atmospheres of Venus, Jupiter, Saturn and Uranus. The next two papers are concerned with particular aspects of the local atmospheric conditions or 'weather' on Mars, and the final three papers address aspects of the dynamical structure of the atmospheres of Jupiter and Saturn and the way in which planetary atmospheres provide tests of theories developed for explaining the observed circulation of the Earth's atmosphere.

In the first paper Prinn describes the chemistry of the atmosphere of Venus emphasizing the reactions involving the radiatively important sulphur compounds. The complex chemistry is presented in a way which may be followed by the non-specialist. The chemical reactions can be classified by three time-scales but, although these are clearly distinguished, a more quantitative assessment of the rate-determining steps in complex systems of reactions would have been useful. A minor deficiency of this paper is the lack of figure captions although the diagrams are described in the text.

The chemistry of the outer planets is described by Atreya and Romani who provide a comprehensive review of the many reactions which are important at the temperatures and pressures experienced on these planets. Unfortunately the rather brief discussion of the observations of the chemical structure of the atmospheres makes it difficult to critically evaluate the different reactions. The calculation of the cloud structure and the effects of the formation of solution droplets are clearly presented and the results showing the clouds expected at different heights are particularly interesting.

Leovy *et al.* describe the meteorological data obtained from the Viking 'landers' on Mars and it is this and subsequent papers that many meteorologists will find of most interest; despite the relative lack of observations compared with the observing systems with which we are more familiar, much has been deduced concerning the Martian 'weather'. Although conditions are relatively settled in summer (the landers were at subtropical and mid-latitudes) with alternating upslope and downslope winds, the winters are more disturbed and fall into two groups. The importance of dust in the atmosphere is stressed and the observations show that baroclinic activity is suppressed when major global dust storms occur. The circulations associated with baroclinic waves produce limited dust storms which are confined to the lower layers of the atmosphere. It is suggested that the differences between those years in which global dust storms occur and those in which they do not, represent the differences between two pseudo-equilibrium states between which transitions may be triggered by small random fluctuations.

Martian dust storms are discussed in more detail by James, making use of the Viking orbiter data. The similarities and differences between dust storms on Earth and Mars are clearly described and the relevance of particle size and air density demonstrated. The relationship between the different climatic types and the small-scale processes leading to dust raising is also described. Both this paper and the preceding one are largely descriptive and, although presenting a considerable body of information, are very readable.

Hunt *et al.* provide a comprehensive description of the atmospheres of Jupiter and Saturn using data from many sources. Theoretical explanations of the observations are presented although the discussion is largely qualitative. The importance of the internal energy source for these circulations, which implies that the incoming and outgoing radiative fluxes need not balance, is demonstrated. Naturally, in the discussion of Jupiter's atmosphere, theories of the Great Red Spot receive attention and the current ideas concerning soliton and baroclinic theories are briefly but adequately described. It is perhaps a reflection on our understanding of atmospheric dynamics that such gross and long-lived features are still not fully understood.

The conversion between different forms of energy is important in determining the forms of atmospheric circulations as well as in maintaining features such as the Great Red Spot against

dissipation. Conversion processes are discussed in general terms by Gierasch and Conrath who draw attention to the energy sources which are important in some planetary atmospheres if not in the Earth's atmosphere. While the terrestrial meteorologist is only concerned with changes of phase involving water, latent heating or cooling during phase changes involving silicon and magnesium compounds is significant at the high temperatures deep in some planetary atmospheres.

A brief concluding paper by Leovy and Hunt presents observations of planetary circulations and indicates how these may be used to extend theories of the Earth's atmosphere. While some of the material summarizes that in earlier papers, attention is drawn to the theoretical ideas and to areas where no adequate explanations exist.

These invited papers are clearly written and will be understood by a non-specialist readership; a uniform standard has been achieved despite the number of contributing authors. The material presented is both up to date and comprehensive. The text (typescript) and figures are clear and there is little duplication between the papers. While the general reader will probably be content to accept the material as presented, extensive additional references are provided and the short subject index should enable the book to be used for reference. The book, although short, will serve to bring the reader up to date in this rapidly developing field and should help encourage some to see the circulation of the atmosphere of the Earth as but one example of an atmospheric circulation.

P. R. Jonas

New views on an old planet: continental drift and the history of the earth, by Tjeerd H. van Andel. 182 mm × 258 mm, pp. xii + 324, *illus.* Cambridge University Press, Cambridge, London, New York, New Rochelle, Melbourne, Sydney, 1985. Price £15.00, US $19.95.

Professor van Andel is a geologist at Stanford University and a member of the Royal Netherlands Academy of Sciences. He is also a skilful writer of lucid and elegant English prose who has produced an excellent introductory book designed for anyone who has an interest in the history of the earth but no prior knowledge of geology. The book arose from an undergraduate course at Stanford, taught mainly to students who did not intend to become geologists, and contains no mathematics. Anyone, therefore, with an interest in modern scientific advances can read it with profit and enjoyment, an enjoyment enhanced by the quotations introducing each major section which are culled from a wide range of scientific and imaginative literature and the illustrations that accompany them which come from 18th and 19th century scientific books.

This book covers basic geological principles and how we may read the record of the rocks; past and present climates; continental drift and plate tectonics; oceanic circulations and the ice ages; the dawn of life and its development and evolution; and the various crises and catastrophes for which there is evidence including the Permian marine collapse and the great Cretaceous extinction of the dinosaurs. Professor van Andel refers to all the main hypotheses and theories put forward to account for climatic change (the main topic of professional interest to meteorologists in the book) and explains the fundamental ideas behind them. He also points out the difficulties and anomalies in the evidence which none of the theories as yet fully account for; his sober appraisal of our knowledge (certainly increasing) and our ignorance (still very great) is a salutary corrective to many more sensational accounts.

There is a useful glossary of technical terms at the end, but there is at least one omission; few non-geologists know that the sea nymph Tethys gave her name to the Mesozoic sea that stretched across the mid-Atlantic and the Mediterranean out into the Indian Ocean.

R. P. W. Lewis

No. 1360 November 1985 Vol. 114

CONTENTS

NOTICE

It is requested that all books for review and communications for the Editor be addressed to the Director-General, Meteorological Office, London Road, Bracknell, Berkshire RG12 2SZ and marked 'For Meteorological Magazine'.

The responsibility for facts and opinions expressed in the signed articles and letters published in this magazine rests with their respective authors.

Authors wishing to retain copyright for themselves or for their sponsors should inform the Editor when they submit contributions which will otherwise become UK Crown copyright by right of first publication.

Applications for postal subscriptions should be made to HMSO, PO Box 276, London SW8 5DT.

Complete volumes of 'Meteorological Magazine' beginning with Volume 54 are now available in microfilm form from University Microfilms International, 18 Bedford Row, London WC1R 4EJ, England.

Full-size reprints of Vols 1–75 (1866–1940) are obtainable from Johnson Reprint Co. Ltd, 24–28 Oval Road, London NW1 7DX, England.

Please write to Kraus Microfiche, Rte 100, Millwood, NY 10546, USA, for information concerning microfiche issues.

HMSO Subscription enquiries 01 211 8667.

Printed in England for HMSO and published by
HER MAJESTY'S STATIONERY OFFICE

£2.30 monthly

Annual subscription £27.00 including postage

Dd. 736047 C15 11/85

ISBN 0 11 727565 4
ISSN 0026–1149

THE METEOROLOGICAL MAGAZINE

HER MAJESTY'S
STATIONERY
OFFICE

December 1985

Met.O.967 No. 1361 Vol. 114

THE METEOROLOGICAL MAGAZINE

No. 1361, December 1985, Vol. 114

551.501.45:551.578.4(495):551.547.5:551.524.77

Air mass characteristics above Athens during snowfall

By N. G. Prezerakos

(National Meteorological Service, Greece)

Summary

A description is given of the structure of the atmosphere above Athens during periods of snowfall, based on surface and upper-air observations at the Hellinikon meteorological station for the period 1956–73. Mean tephigrams are plotted, and mean vector winds at all standard levels calculated. The variation of mean temperature and geopotential for standard levels is studied from two days before the beginning of a snowy period to one day after the end of the period, and also the covariation of temperature and geopotential at 500 and 850 hPa. The performance of various snow predictors defined by previous researchers (mainly British) is checked against the results, proving that they are generally successful in the Athens region.

1. Introduction

This paper is the third to discuss snowfall in Athens, and it deals mainly with the air mass structure above Athens during snowfall. The first paper (Prezerakos and Angouridakis 1979) considered basic characteristics of snowfall in Athens, and the second (Prezerakos and Angouridakis 1984) studied the synoptic evolution of atmospheric circulation systems causing those snowfalls.

Brief reviews of previous papers which dealt with snowfall in Greece (and specifically in Athens) were provided in the earlier papers. Although these two papers describe the data and method used and they give the statistical characteristics of the meteorological elements under consideration, there is a need for some of this material to be briefly repeated here for the sake of continuity.

2. Data and method used

To study the structure of the atmosphere above Athens during snowfall, the surface and upper-air observations at the Hellinikon meteorological station (World Meteorological Organization No. 16716) were used. Hellinikon is about 15 km south of the centre of Athens and about 300 metres from the coastline, at an elevation of 10 m.

Comparison of the snowfall dates at Hellinikon with other stations in the Athens region led to the conclusion that when it snowed at Hellinikon, it also snowed in the city of Athens. Thus 'snow-days' at the Hellinikon meteorological station can be considered as 'snow-days' in Athens.

Dates of snow-days in Athens, selected in the 1956–73 period according to the definition below, are again used for the sake of continuity with the two previous papers. A 'snow-day' in Athens is said to occur when at least one of the eight synoptic observations daily at Hellinikon reports snow in the present weather (ww 70 to 79) or past weather code (W = 7), independently of whether the snow remains lying on the ground or whether it melts.

From the dates found it was realized that occurrences could be divided into groups of one, two and three successive days. Examination of the daily meteorological bulletins for the days selected showed that during the first day ('F-day') of a group of successive snow-days in Athens, the synoptic situation was typical and could be classified into two types, A and B (Prezerakos and Angouridakis 1979, 1984). *Type A* is associated with a surface anticyclone over western Europe with its centre over the Alps, whereas *type B* is associated with a surface anticyclone which extends over central Europe with its centre over south-western Russia.

To study the structure of the atmosphere above Athens during snowfall, mean soundings at 0000 GMT have been calculated and plotted on tephigrams for each synoptic type A and B separately and for the days F–2, F–1, F, and for E-day, where E-day (or END day) is the day immediately following a group of sucessive snow days. Graphs have also been prepared showing the variation of mean temperature and mean geopotential at the 850, 700, 500, 300 and 200 hPa* isobaric surfaces, for both synoptic types A and B, together with mean sea level (MSL) pressure variation for days F–2, F–1, F and E. Other graphs have also been drawn to present the covariation of geopotential and temperature at standard isobaric levels on day F at 0000 GMT. Finally a mean tephigram for Hellinikon closest to the time of snowfall in Athens (independently of the synoptic situation) has been plotted and analysed. Scatter diagrams have been prepared showing the relationship between temperature and geopotential at 850 and 500 hPa levels.

3. Mean structure of the atmosphere above Athens during snowfall

There were 40 snow-days during the period considered; 15 occurrences were attributable to type A and 8 to type B, some pressure systems causing two or three snow-days (Prezerakos and Angouridakis 1984). The mean structure of the atmosphere and particularly of the troposphere for the groups of days F–2, F–1, F and E is presented schematically in Figs 1 to 8 for types A and B separately and together.

3.1 *Type A situations*

Fig. 1(a) shows the mean structure of the atmosphere on day F–2 (that is, two days before snow in Athens) with a synoptic situation of type A. The air mass is relatively moist since the dew-point depression is less than 6 K in the lower layers from the surface up to 750 hPa. The air mass is also relatively cold and conditionally stable so that it does not appear as even a pseudo-latent type of instability. Examination of the wet-bulb curve (dotted line) shows that the wet-bulb potential temperature (θ_w) increases with height. Thus the relation $\partial\theta_w/\partial z > 0$ is valid for every layer of the atmosphere, and so the atmosphere is also potentially stable. The variation of wind direction with height shows some cold advection in the lower layers from the surface up to about 650 hPa, whereas above 650 hPa the advection does not appear with a constant sign.

On day F–1 (Fig. 1(b)) the situation remains almost unchanged with a slight increase in humidity and consequent decrease in potential stability. The cold advection in the lower levels is maintained.

On day F (Fig. 2(a)) the absolute humidity of the lowest part of the troposphere up to 650 hPa has decreased but the relative humidity has increased (since the temperature has decreased). The dew-point depression shows that the cloud amount is probably more than 6 oktas in the layer from lifting condensation level up to 650 hPa (Meteorological Office 1975). The air mass stability remains unchanged and the variation of wind direction with height shows a little warm advection from the surface up to 900 hPa, whereas from 900 hPa up to 600 hPa the advection becomes cold. Above 600 hPa there is no distinct thermal advection. The height of the tropopause has also lowered during these three days.

* The hectopascal (hPa) is now the preferred unit of atmospheric pressure; it is numerically equal to the millibar (mb). Both units will continue to be used in *Meteorological Magazine* at present, the choice being left to individual authors.

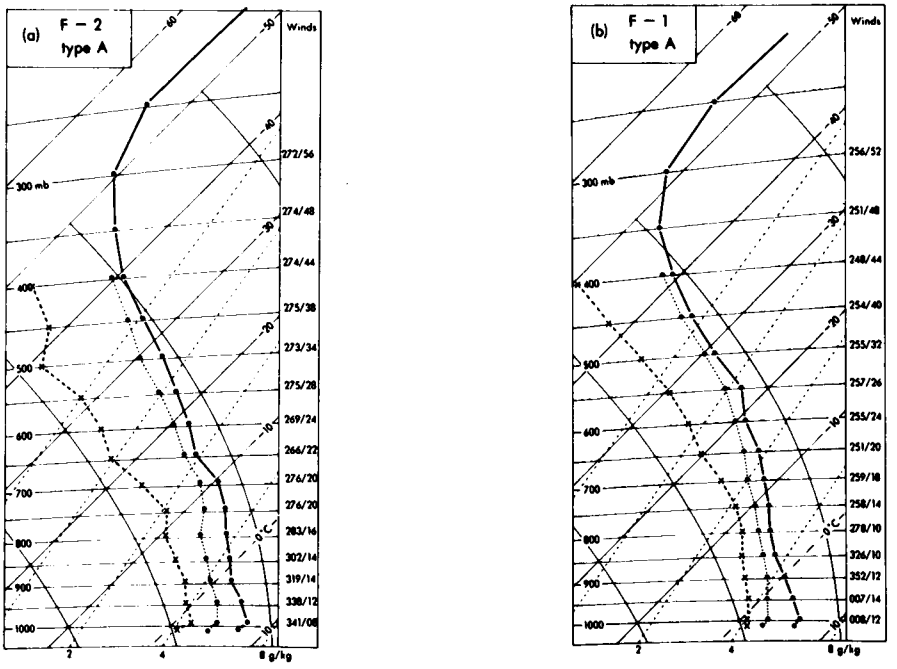

Figure 1. Mean sounding for Hellinikon for type A synoptic pattern at 0000 GMT on day F–2 (a) and F–1 (b). The continuous line is air temperature, the dotted line wet-bulb temperature and the dashed line dew-point temperature. Direction (degrees) and speed (kn) of the vector mean wind are given for standard levels.

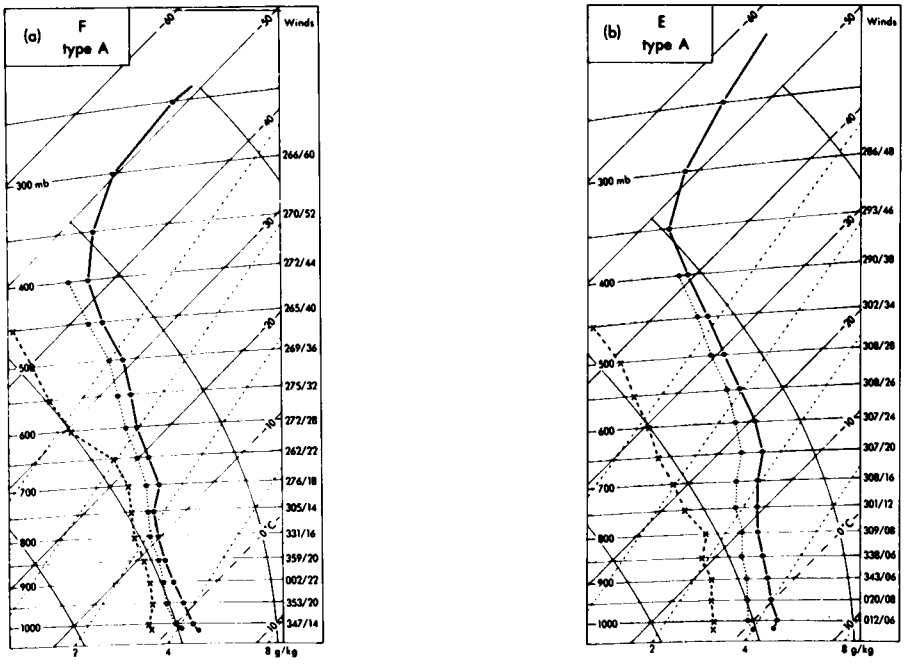

Figure 2. As for Fig. 1 but for day F and E.

The atmospheric structure above Athens on day F (Fig. 2(a)) indicates that the clouds would be basically stratocumulus and nimbostratus, while the cause of the air mass lifting must be dynamical (vorticity advection, convergence) or forced lifting. This is shown more clearly in the evolution of the pressure systems which cause snowfall in Athens (discussed in Prezerakos and Angouridakis 1984).

On day E (Fig. 2(b)), the relative humidity (and therefore the absolute humidity) has decreased, whereas the stability of the atmosphere has increased. The surface winds have veered to north-easterly while the cold advection in the lower part of the atmosphere is unchanged.

3.2 *Type B situations*

Fig. 3(a) shows the mean structure of the atmosphere above Athens two days before snowfall, with a synoptic situation of type B. The structure is stable, with the greatest stability in the layer nearest the ground. The variation of wind direction with height shows cold advection in the layer from the surface up to 650 hPa; there is no clearly-defined thermal advection at higher levels.

On the following day (F–1), Fig. 3(b), the humidity increases in the same way as that of the corresponding day of type A, but only up to 750 hPa; cloudiness in the lower layers is, therefore, increased. The cloud must consist of stratocumulus owing to the general stability of the air mass. Winds have become more northerly; their variation with height clearly shows cold advection in most of the troposphere.

Fig. 4(a) shows that on day F in type B situations the structure of the atmosphere is slightly unstable in the layer from the surface up to 850 hPa (and particularly so up to 950 hPa). This is due to the warming of the air passing above the sea coming from regions which lie to the north-east of Athens. Because of this warming the planetary boundary layer becomes unstable. The structure of the atmosphere above 850 hPa is stable both conditionally and potentially. The winds are north-easterly up to 800 hPa and north-westerly above that. Their variation with height shows some cold advection above 750 hPa.

On day E, Fig. 4(b), the relative humidity decreases and the structure of the atmosphere becomes stable even in the lowest part of the boundary layer (owing to the cold ground). The winds become north-easterly up to 650 hPa, backing slightly with height, showing that some cold advection is still present.

3.3 *Mean ascents during snowfall*

The mean ascent of upper-air observations at Hellinikon nearest to the time of snowfall occurrence (independently of the type of synoptic situation) is shown in Fig. 5.

This plotted tephigram is the most representative of the structure of the atmosphere during snowfall. The diagram is based on the average of 39 soundings (40 snow-days during the period 1956–73, less one missing sounding). The basic characteristics of the tephigram also reflect the stable stratification, the cold air mass ($T_{850} = -7.5$ °C, $T_{500} = -31.5$ °C) and the increased moisture in the lower layers. The latter fact implies a considerable amount of stratiform clouds, and specifically that the cloudiness in the layer from 950 hPa up to almost 800 hPa is 8 oktas because the dew-point depression is less than 2 K (Air Weather Office 1959, Meteorological Office 1975).

The winds are mainly from the north. They are the vector means of both types A and B but the winds of the type A synoptic situation are north-westerly in the lower levels of the troposphere during snowfall, whereas the winds of the type B synoptic situation are north-easterly, producing a rather complicated resultant. Thus north-westerly winds occur near the surface, north-easterly winds are found above them and finally north-westerly winds return again in the region above 750 hPa.

4. The variation of temperature and geopotential of standard isobaric surfaces from day F–2 to E

The variation of surface temperature and that of the standard isobaric levels was examined from day F–2 to E. The data considered were 0000 GMT radiosonde observations, and inevitably there were cases

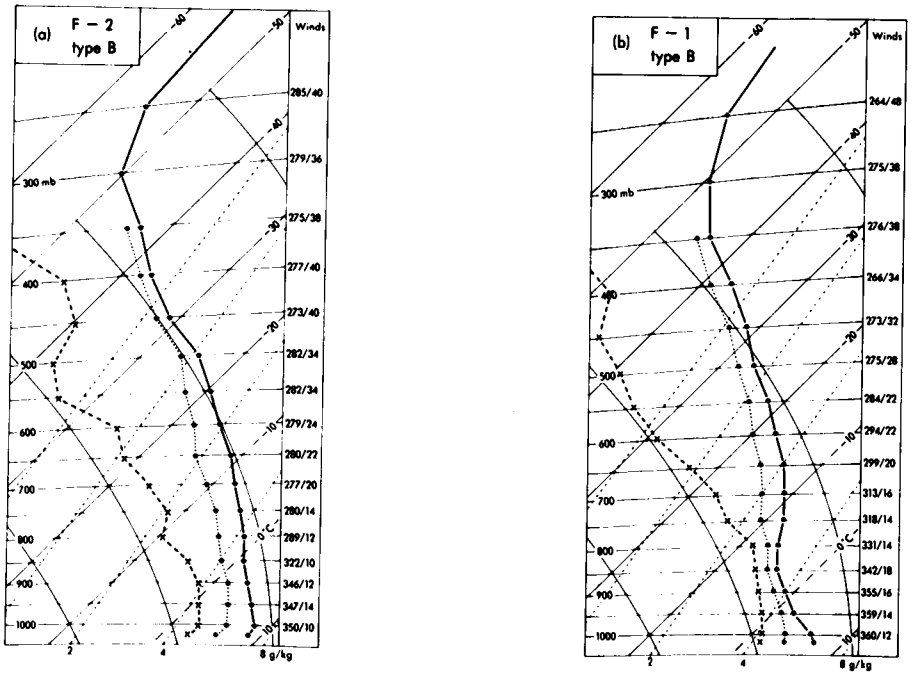

Figure 3. As for Fig. 1 but for type B synoptic pattern.

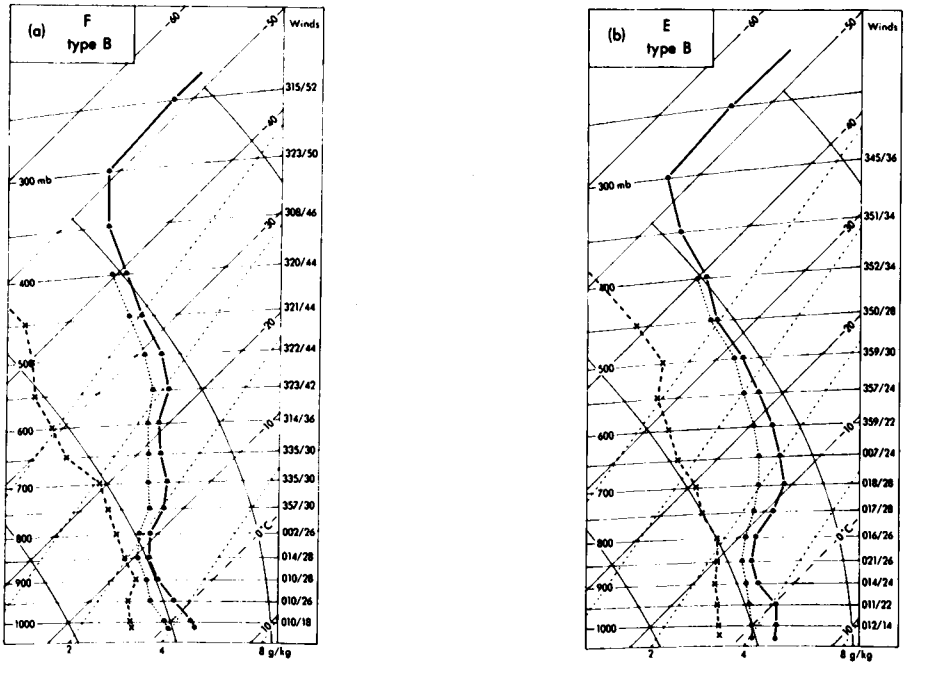

Figure 4. As for Fig. 2 but for type B synoptic pattern.

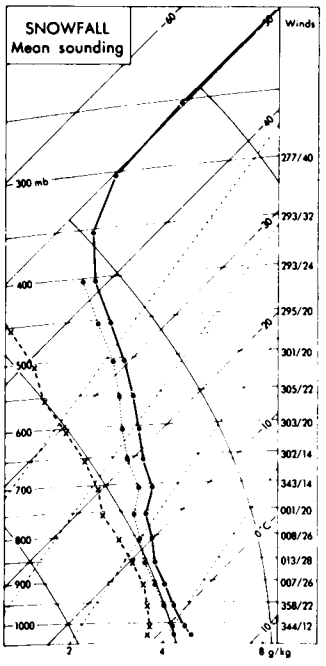

Figure 5. Mean tephigram for Hellinikon for the upper-air sounding nearest to the time of snowfall (independently of synoptic pattern). Direction (degrees) and speed (kn) of the vector mean wind are given for standard levels.

where the radiosonde launch was more than 12 hours from the time of snowfall. This departure was, on average, five hours for synoptic type A and nine hours for type B on day F (Prezerakos and Angouridakis 1979).

Day F was, on average, the coldest day at all levels up to 500 hPa, whereas it appeared slightly warmer at the 300 and 200 hPa levels (Fig. 6, and Table I). Day F–1 was the coldest day at 300 and 200 hPa because the tropopause lay beneath the 300 hPa level. Also worthy of attention is the fact that type A temperatures appear generally to be colder than type B and only at 850 hPa on day F–1, day F and E does the latter appear to be colder than the corresponding day of type A. At 300 hPa day E of type B appears to be colder than the corresponding day of type A, whereas both types on day F have almost the same temperature. Day F of both types also appeared to have the same temperature at 200 hPa. The values of the mean temperature by day and by type given in Fig. 6 have been a significant help in forecasting snowfall in Athens.

In Fig. 7 and Table II the variation of barometric pressure at station level and the variation of the geopotential of the standard isobaric surfaces of both types A and B from day F–2 to day E are shown. From this it is clear that the barometric pressure at station level reaches its minimum value on day F–1 and that the pressure values of type A are less than the corresponding values of type B. It is also apparent that the variation in pressure under type B from day F–2 to day F–1 is negligible, whilst its increase from day F–1 to day F is significant, as in type A. These data suggest that snowfall in type A synoptic situations occurs when some perturbation, which causes the pressure to fall in the Athens area, has passed, whereas snowfall of type B is due to strengthening of the anticyclonic circulation (which increases the barometric pressure) and the mass uplifting is of the forced type. Such cases arise when an anticyclonic ridge extends towards Greece from the north.

The 850 hPa geopotential under type B appears unchanged from day F–1 to day F, whereas at all other levels the geopotential falls to a minimum value on day F.

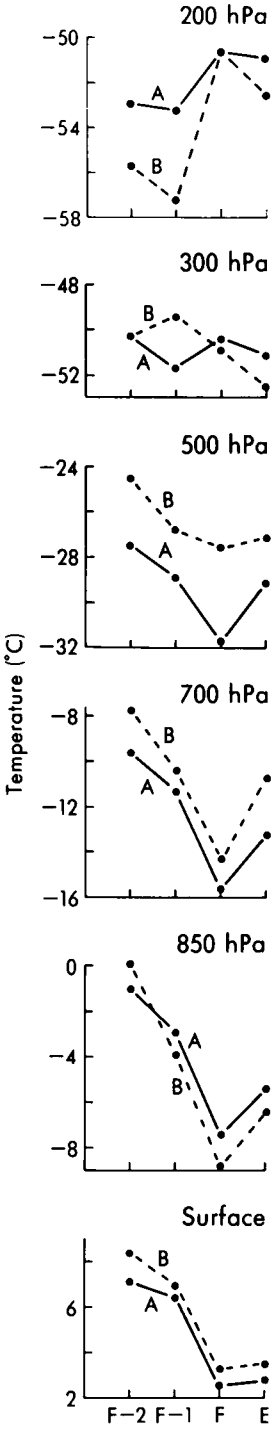

Figure 6 (*left*). Mean temperature for the surface and standard isobaric levels for type A and B synoptic patterns from day F−2 to E.

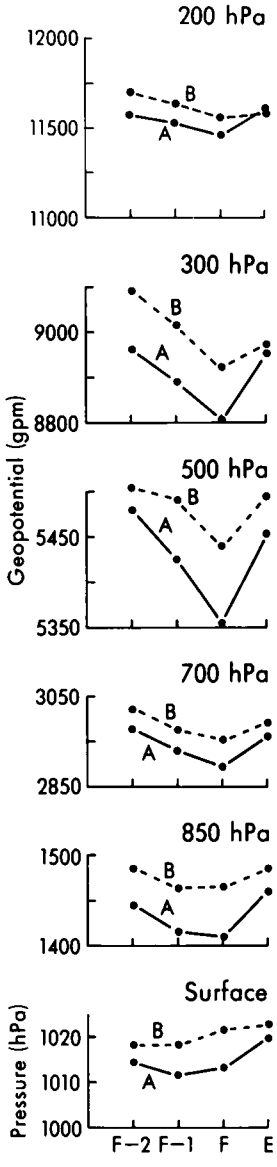

Figure 7. Variation of geopotential of standard isobaric surfaces and surface pressure for type A and B synoptic patterns from day F−2 to E.

Table I. *Mean temperatures (°C) and standard deviations (SD, in K) at standard isobaric surfaces and at the surface for days F–2 to E at Hellinikon near Athens (see text for further details). These values are presented graphically in Fig. 6*

	Day			
	F–2	F–1	F	E
200 hPa				
Mean — type A	−53.1	−53.2	−50.6	−51.0
— type B	−55.7	−57.2	−50.6	−52.6
SD — type A	4.8	4.7	4.2	6.8
— type B	5.5	5.5	2.6	3.3
300 hPa				
Mean — type A	−50.3	−51.7	−50.4	−51.1
— type B	−50.2	−49.4	−50.9	−52.5
SD — type A	2.9	2.5	3.3	2.0
— type B	4.4	2.8	2.4	3.6
500 hPa				
Mean — type A	−27.5	−28.9	−31.7	−29.1
— type B	−24.5	−26.8	−27.5	−27.1
SD — type A	4.9	4.9	3.3	5.4
— type B	2.9	3.8	4.1	2.8
700 hPa				
Mean — type A	−9.6	−11.3	−15.5	−13.2
— type B	−7.7	−10.4	−14.3	−10.7
SD — type A	5.4	3.0	2.0	5.5
— type B	4.1	3.7	3.2	3.4
850 hPa				
Mean — type A	−1.0	−2.9	−7.2	−5.4
— type B	0.9	−3.9	−8.8	−6.4
SD — type A	5.7	3.6	1.8	5.6
— type B	4.8	4.2	2.5	2.1
Surface				
Mean — type A	7.1	6.4	2.4	2.6
— type B	8.4	7.0	3.3	3.6
SD — type A	4.1	3.2	1.4	3.4
— type B	3.0	3.0	2.1	2.9

The average geopotentials of the isobaric surfaces and the values of the barometric pressure at station level of type A synoptic situations were less than those of type B. These facts support the above hypothesis, namely that snowfall of type A is due to perturbations causing positive advection of vorticity towards the Athens region, while snowfall of type B is caused basically by the forced uplifting of the very cold air above orographic obstacles. This cold air is directed towards the Athens region by a north-easterly wind associated with the elongated ridge of high pressure.

Table II. *Mean and standard deviation geopotentials (gpm) for standard isobaric surfaces and mean and standard deviation of surface pressure (hPa) for days F–2 to E at Hellinikon near Athens (see text for further details). These values are presented graphically in Fig. 7*

	Day			
	F-2	F-1	F	E
200 hPa geopotential				
Mean — type A	11 583	11 518	11 460	11 597
— type B	11 694	11 642	11 557	11 592
SD — type A	109	83	82	106
— type B	102	144	122	107
300 hPa geopotential				
Mean — type A	8 961	8 889	8 805	8 954
— type B	9 095	9 016	8 924	8 976
SD — type A	146	129	111	166
— type B	110	126	79	86
500 hPa geopotential				
Mean — type A	5 482	5 427	5 355	5 453
— type B	5 506	5 490	5 441	5 499
SD — type A	99	82	73	108
— type B	78	83	50	49
700 hPa geopotential				
Mean — type A	2 974	2 931	2 898	2 962
— type B	3 021	2 978	2 953	2 992
SD — type A	58	52	56	61
— type B	53	58	29	32
850 hPa geopotential				
Mean — type A	1 448	1 416	1 410	1 462
— type B	1 485	1 464	1 467	1 487
SD — type A	36	44	54	52
— type B	41	58	35	33
Surface pressure				
Mean — type A	1 014.5	1 011.5	1 013.7	1 019.5
— type B	1 018.3	1 018.1	1 021.6	1 022.7
SD — type A	3.9	5.4	6.8	7.7
— type B	6.1	8.1	5.4	4.1

5. Covariation of temperature and geopotential of the 850 and 500 hPa isobaric surfaces on snow-days

Forecasters' experience suggests that knowledge of the temperature and geopotential at 850 and 500 hPa and their covariation when it is snowing in Athens are a significant help in forecasting snowfall. For these reasons an attempt has been made to correlate the 0000 GMT geopotential and temperature at 850 and 500 hPa on day F for each synoptic type situation separately. This correlation has been done graphically because there are few cases (15 snow-days of type A with 14 available 0000 GMT upper-air observations, and 8 of type B with 7 available 0000 GMT observations), they are very easy to plot and

the regression curve can be easily drawn (Meteorological Office 1975). Linear correlation equations have been derived only for the (39) observations nearest in time to the snowfall, independently of synoptic type.

5.1 *850 hPa*

The values of 850 hPa temperature and geopotential on day F at 0000 GMT are illustrated in Fig. 8(a) for synoptic type A, and Fig. 8(b) for type B. Temperatures ranged from -5.5 °C to -11.5 °C for type A and from -7 °C to -13 °C for type B, i.e. in both cases there was a range of 6 K. The geopotential values for type A ranged from 1330 gpm to 1485 gpm (a range of 155 gpm) and from 1390 gpm to 1505 gpm (a range of 115 gpm) for type B. It is clear from Table III that north-westerly winds dominate in type A and north to north-easterly in type B. The type B air mass at 850 hPa appears to have higher relative humidity (Table III) because it has been advected by north-easterly winds passing over the Black Sea and the Aegean Sea thus picking up moisture. The type A air mass is advected by north-westerly winds passing over land (central Europe). Figs 8(a) and 8(b) also show that on snow-days in Athens the 850 hPa geopotential usually increases with decreasing temperature. Finally Figs 8(a) and 8(b) show that snow is unlikely in Athens unless the 850 hPa temperature is below -5.5 °C and the associated geopotential less than 1505 gpm.

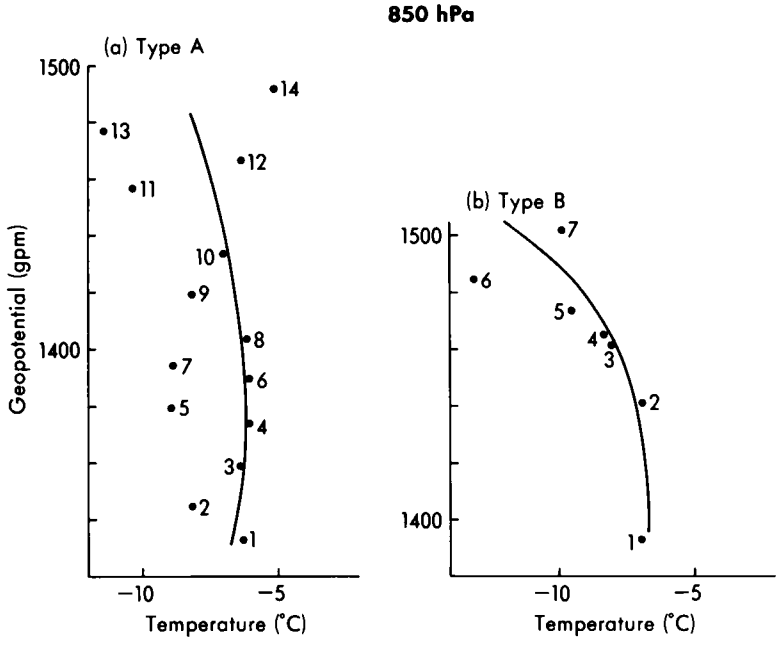

Figure 8. Scatter plot of temperature and geopotential of the 850 hPa surface for (a) synoptic type A and (b) synoptic type B on day F, at 0000 GMT. The numbered points refer to the values in Table III.

Table III. *Wind direction (degrees) and speed (m s^{-1}) and humidity (%) for the numbered points on the scatterplot of 850 hPa temperature against geopotential (Figs 8(a), 8(b)). The points are numbered consecutively from the lower axis and do not necessarily correspond to similarly-numbered points in Tables IV or V or Figs 9 and 10*

Fig. 8(a) (Type A)

Point No.	Wind direction	speed	Humidity
1	350	08	75
2	040	09	77
3	340	10	80
4	330	04	85
5	350	12	90
6	290	08	57
7	350	19	99
8	040	15	99
9	350	08	95
10	290	04	87
11	350	11	90
12	310	09	89
13	350	18	81
14	330	08	95

Fig. 8(b) (Type B)

Point No.	Wind direction	speed	Humidity
1	020	18	87
2	020	15	87
3	350	15	86
4	020	16	92
5	350	12	81
6	020	12	90
7	020	22	98

5.2 *500 hPa*

Figs 9(a) and 9(b) show the correlation of geopotential and temperature at the 500 hPa isobaric surface. In these figures temperature usually increases with geopotential as do most isobaric surfaces (Angouridakis 1977), but in the lower part of the type A curve (Fig. 9(a)) the variation is reversed. Furthermore it can be seen that days with snow in Athens are characterized by temperatures at 500 hPa in the range from -24 °C to -35.5 °C and geopotentials ranging from 5270 gpm to 5510 gpm; westerly winds predominate in synoptic type A and north-westerly winds in type B (Table IV). Relative humidity appears to be higher in type A than in type B. This seems to be due to the dynamical large-scale upward velocity resulting in adiabatic cooling which occurs on snow-days in Athens with type A synoptic situations, whilst the upward velocities are forced and limited to the lower levels with type B synoptic situations (Prezerakos and Angouridakis 1984). Type B, as mentioned above, appears to be warmer than type A at 500 hPa with a temperature range from -35 °C to -24 °C and a geopotential range from 5380 gpm to 5510 gpm.

5.3 *All snow-days*

The general argument in the discussion of Figs 8 and 9 is based on a rather small sample which may limit the validity of the derived conclusions. Therefore, Figs 10(a) and 10(b) have been drawn based on the data for all snow-days (40 days with 39 upper-air observations available). The temperature and geopotential values used in Figs 10(a) and 10(b) are more representative of the snowfall time than those used in Figs 8 and 9.

Figs 10(a) and 10(b) are more interesting because they provide, to a good approximation, the true relation between temperature and geopotential at the 850 hPa and 500 hPa isobaric surfaces during snowfall in Athens. On these figures are shown two kinds of regression lines, the continuous one drawn empirically by hand and the pecked one which has been derived mathematically.

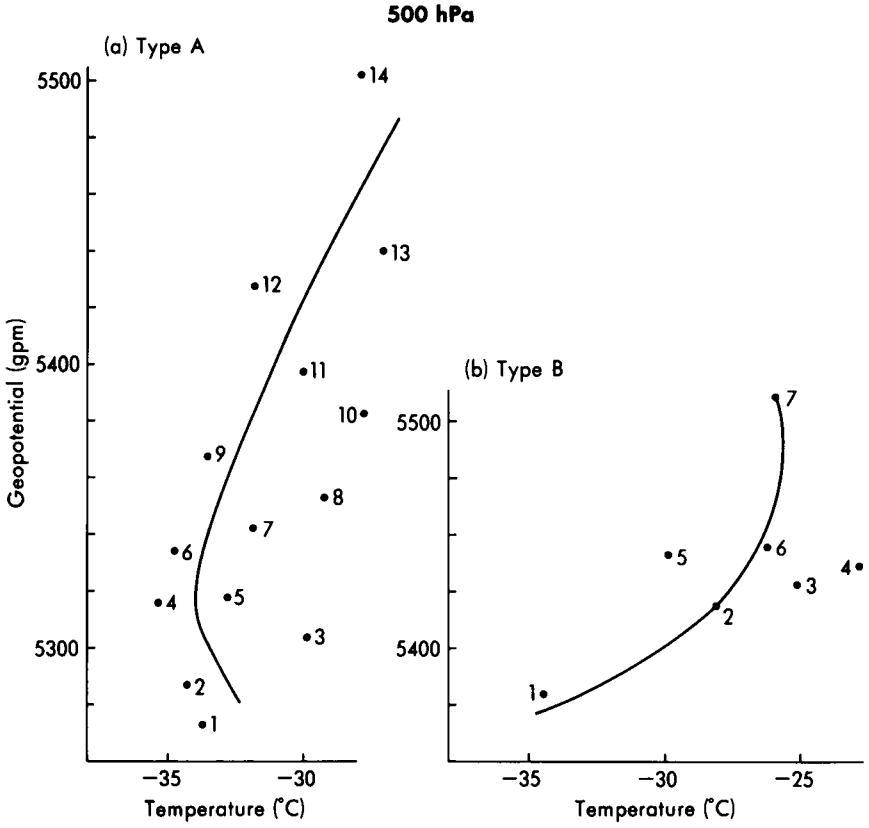

Figure 9. As for Fig. 8 but for the 500 hPa surface, the numbered points referring to Table IV.

Table IV. *Wind direction (degrees) and speed (m s^{-1}) and humidity (%) for the numbered points on the scatterplot of 500 hPa temperature against geopotential (Figs 9(a), 9(b)). The points are numbered consecutively from the lower axis and do not necessarily correspond to similarly-numbered points in Tables III or V or Figs 8 and 10*

Fig. 9(a) (Type A)

Point No.	Wind direction	Wind speed	Humidity
1	220	22	67
2	220	14	78
3	260	36	36
4	240	11	34
5	240	20	43
6	020	13	61
7	020	20	40
8	260	30	55
9	260	14	56
10	330	45	19
11	260	35	36
12	270	25	27
13	260	22	19
14	260	39	48

Fig. 9(b) (Type B)

Point No.	Wind direction	Wind speed	Humidity
1	290	25	56
2	320	30	33
3	040	30	20
4	330	41	18
5	290	22	42
6	310	31	19
7	020	28	40

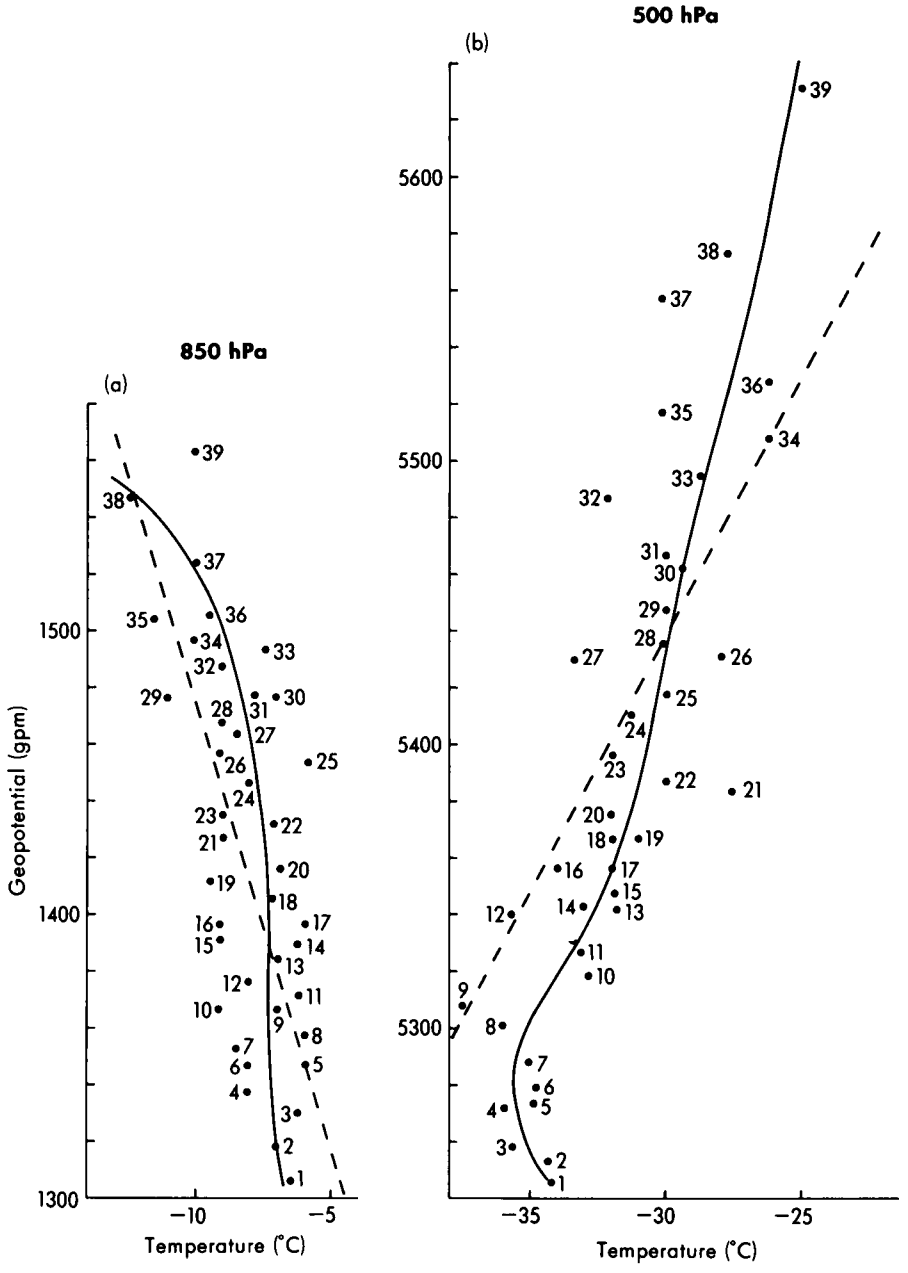

Figure 10. Regression lines of temperature and geopotential of (a) the 850 hPa surface and (b) the 500 hPa surface for both synoptic types A and B together for upper-air observations closest to the time of snowfall. The pecked line is the regression line derived mathematically, the continuous line is the regression line drawn empirically. The numbered points refer to Table V.

At 850 hPa (Fig. 10(a)) temperatures range from −6 °C to −12 °C. The mean temperature is −7.7 °C with standard deviation 3.2 K. The mean vector wind (Table V) is north-easterly, speed 14 m s^{-1} (about 28 kn) and the mean relative humidity 83%, implying 7–8 oktas cloud at this level. There is a considerable range in geopotential (250 gpm, from 1310 gpm to 1560 gpm). Furthermore it is important to mention that, while the temperature and geopotential vary in the same sense (Austin 1953, Angouridakis 1977), the curves of Fig. 10(a) and especially their upper parts show an inverse correlation, i.e. the temperature decreases as the geopotential increases. This is explained by the fact that the 850 hPa isobaric surface is influenced by the cold mass of the anticyclonic ridge which accompanied snowfall. In other words the 850 hPa geopotential in this case presents the same correlation with the MSL pressure as shown (Holton 1973), i.e. cold advection results in an increase in surface barometric pressure.

Table V. *Wind direction (degrees) and speed (m s^{-1}) and humidity (%) for the numbered points on the scatterplot of 850 hPa and 500 hPa temperature against geopotential (Figs 10(a), 10(b)). Identically-numbered points do not necessarily relate to the same ascent*

Fig. 10(a) (850 hPa)				*Fig. 10(b) (500 hPa)*			
Point No.	Wind direction	Wind speed	Humidity	Point No.	Wind direction	Wind speed	Humidity
1	020	27	72	1	040	04	73
2	360	10	81	2	350	25	60
3	350	08	81	3	360	30	50
4	360	15	83	4	260	10	46
5	020	13	83	5	350	25	48
6	030	09	84	6	220	22	67
7	020	12	77	7	350	20	60
8	020	14	83	8	200	21	79
9	020	15	85	9	340	40	55
10	350	12	87	10	240	02	43
11	150	04	91	11	290	20	45
12	020	20	90	12	350	38	45
13	020	19	85	13	040	05	43
14	040	21	85	14	300	08	52
15	350	19	99	15	300	10	40
16	010	15	85	16	260	12	68
17	030	15	90	17	280	10	40
18	340	22	80	18	290	10	55
19	350	16	70	19	240	15	79
20	340	20	70	20	020	09	32
21	350	17	75	21	330	45	19
22	350	24	69	22	300	10	60
23	340	22	70	23	040	05	40
24	020	15	84	24	260	13	77
25	200	03	81	25	260	30	45
26	030	14	86	26	290	38	19
27	020	10	92	27	080	29	21
28	020	10	85	28	040	10	45
29	020	15	82	29	260	20	45
30	020	16	83	30	350	16	41
31	040	15	81	31	330	40	30
32	020	18	85	32	260	30	30
33	020	15	82	33	330	23	19
34	360	19	84	34	260	30	30
35	350	17	87	35	330	10	30
36	110	05	91	36	330	10	35
37	020	23	80	37	330	10	40
38	350	12	91	38	330	22	19
39	020	15	96	39	110	04	36

The empirical regression line of 500 hPa geopotential with temperature (continuous line in Fig. 10(b)) is almost straight (with the exception of its lowest part) indicating that 500 hPa temperature and geopotential are linearly correlated during snowfall in Athens. However, in the area of the lower geopotentials there are four observations in which the trend is in the opposite direction. The mean temperature is -31.1 °C and the mean relative humidity 45%. The range of temperature is from -25 °C to -36 °C, whilst the range of the 500 hPa geopotential is from 5250 gpm to 5680 gpm. The 500 hPa mean vector wind (Table V), as mentioned above, is north-westerly (301°) at 10 m s^{-1}.

In Figs 10(a) and 10(b) the pecked lines are the calculated regression lines which show the linear correlation between geopotentials (H, gpm) and temperatures (T, °C). The equations of these lines are:

$$H = 21.98T + 6088.10$$

at 500 hPa with correlation coefficient $R_{500} = 0.77$ and standard error of estimation = 59.28, and

$$H = -27.86T + 1198.19$$

at 850 hPa with correlation coefficient $R_{850} = -0.70$ and standard error of estimation = 47.87. Thus conclusions drawn from the empirical regression lines are also supported by the mathematical regression line since there are no significant differences between them with the exception of the inverse relationship shown at the bottom of Fig. 10(b) which is ignored by the calculated equation. However, the F-test (Brooks and Carruthers 1953) shows that both correlation coefficients are significant at 0.01 level of significance.

6. Comparison of the results with some snow predictors

Various meteorologists have attempted to contribute to the improvement of snow forecasting by devising indices. Most of these are a combination of various meteorological parameters of the free atmosphere and the boundary layer. For this study a check of the performance of these indices, using upper-air data very close to the time of snowfall, has proved very useful. (Only the snow predictors and meteorological parameters which can be used easily and quickly in a forecasting office are considered in this context.)

The interest in the verification of the various snow predictors comes from the fact that the upper-air data used in this study differed from the time of snowfall occurrence at Hellinikon by an average of only one hour (Figs 10(a) and 10(b)). A similar study has been made by Lioki-Livada-Tselepidaki (1979) but most of the upper-air data used differed by up to 12 hours from the time of snowfall. Furthermore, snow-days in Athens in that study were even considered to include days on which it snowed only at Tatoi (a meteorological station located north of Athens, close to Parnitha Mountain, at an elevation of 237 m).

Many research meteorologists have dealt with the relation between snowfall and the 1000–500 hPa thickness (Murray 1952, Boyden 1964, Lamb 1955, Smith 1970, Lioki-Livada-Tselepidaki 1979). In this paper it has been found that the mean thickness value at Hellinikon for snow-days in Athens, and for the radiosonde observations nearest in time to the snowfall occurrence, is 5230 gpm with a standard deviation of 47 gpm (ranging from 5379 gpm to 5189 gpm). These results are in agreement with other researchers' results: Murray (1952) found values which ranged from 5160 gpm to 5230 gpm, but he also found cases with values as high as 5420 gpm. Lamb (1955) found a mean value of 5280 gpm (with a standard deviation 45 gpm) but some of his values reached 5440 gpm. Boyden (1964) found a mean value of 5260 gpm. The above researchers used British data from different stations, which may have caused small differences. It could be concluded that the results of the present research are essentially in agreement with the above-mentioned researches, since they do not show deviations much greater than those referred to.

The comparison of the results of this paper with those in Lioki-Livada-Tselepidaki's thesis (who found values in the range 5150 gpm to 5510 gpm, with a mean value of 5291 gpm) confirms what was

expected, namely lower thickness values (because the upper-air observations are those nearest to the time of snowfall). Otherwise the results are in agreement with those of Lamb (1955), who found that the mean 1000–500 hPa thickness at coastal sites is, at the time of snowfall, about 60 gpm less than the corresponding value coming from other regions. (This is because the surface air at coastal stations will, in most cases, have been warmed by advection over a much warmer sea; the mean 1000–500 hPa temperature (i.e. thickness) thus needs to be considerably lower than it does at inland stations for the surface air to remain cold enough for snow to reach the ground.)

A more important factor than the 1000–500 hPa thickness is the 1000–850 hPa thickness, because this has a greater influence on whether the snow will reach the ground. Boyden (1964) found that the 1000–850 hPa thickness on snow-days ranged from 1280 to 1300 gpm; furthermore, he calculated a 50% probability of snow if the 1000–850 hPa thickness was less than 1295 gpm. Similarly, Lioki-Livada-Tselepidaki (1979) found that 1000–850 hPa thickness values of 1260–1350 gpm (with a mean value of 1300 gpm) occurred on snow-days, while Sahsamanoglou and Makrogiannis (1978), working on data from northern Greece, found a mean 1000–850 hPa thickness value of 1310 gpm, with a minimum value of 1280 gpm and a maximum of 1350 gpm.

In this research a mean 1000–850 hPa thickness of 1282 gpm (with a standard deviation of 34 gpm and a range from 1263 to 1309 gpm) was found. These values appear less than those found by Lioki-Livada-Tselepidaki (1979) for the same reasons as mentioned above. They are also less than the values derived by Sahsamanoglou and Makrogiannis (1978) using surface observations covering the whole of northern Greece, often some hours away from the 1200 GMT radiosonde ascent at Thessaloniki/Mikra (WMO No. 16622). In the present case, surface and upper-air data are from the same station and are almost simultaneous.

It is commonly accepted that the freezing level plays the most important role in determining whether the precipitation that reaches the earth's surface will be snow, sleet or rain. Lowndes *et al.* (1974) found that the probability of precipitation falling as snow is greater than 50% when the freezing level is 38 to 41 hPa above the earth's surface, and that this probability rose to 90% when the freezing level was within ± 4 hPa of the surface. In this work the freezing level averaged 980 hPa, some 38.6 hPa above the surface (since the mean barometric pressure at station level at the time of radiosonde release was 1018.6 hPa Prezerakos and Angouridakis (1979)). This value is in agreement with the results of Lowndes *et al.* (1974) wherein an index I_w (defined as surface pressure minus pressure at wet-bulb freezing level) was introduced to define the precipitation type. It was found that when $I_w \leqslant 10$ hPa the probability of the precipitation falling as snow was 50%, but when $I_w \leqslant 0$ rain or sleet never occurred. In this work the mean value of I_w was found to be 8.6 hPa (standard deviation 1.4 hPa), a fact which suggests that the index could be used in deciding whether the precipitation will be snow or not.

Another index which seems very useful in determining likely precipitation type was proposed by Booth (1973). His conclusion was that when the sum of the surface temperature T and dew-point T_d is $\leqslant 1$ °C precipitation was always snow. Here care is needed in the application of the index, for it does not in itself help forecast precipitation but only helps in the determination of precipitation *type* (the likelihood or otherwise of precipitation being forecast by other methods; obviously there will be cases when the sum $T + T_d \ll 1$ °C, under clear skies for example). In all cases of snow in Athens the sum $T + T_d$ appeared to be less than 1 °C, with a mean value of −0.6 °C.

Another useful meteorological parameter in determining precipitation type is θ_w at the 850 hPa level (Bradbury 1977) and/or the wet-bulb temperature T_w. Bradbury found that when θ_w at 850 hPa was less than 3 °C then the probability that precipitation will fall as snow was 60% or more. Lioki-Livada-Tselepidaki (1979) found that values of θ_w at 850 hPa ranged between −4 °C and +10 °C, with a mean value of +2.4 °C; in this work the mean value of θ_w at 850 hPa was +0.5 °C (with values ranging between −6 °C and +3 °C). The average wet-bulb temperature at 850 hPa was found to be −9 °C in this research,

Met.O.967

THE METEOROLOGICAL MAGAZINE

1985 *Volume 114*

INDEX

Published for the Meteorological Office by Her Majesty's Stationery Office

whereas Lioki-Livada-Tselepidaki found values ranging between −13.3 °C and +8 °C. These latter boundary values, compared with the results obtained by Booth (1973) and during the current investigation, indicate an extension of the 850 hPa wet-bulb temperatures to the positive end point. One final point arising from the observations used in this work is that they show the lower part of the troposphere to be much colder than was shown by Lioki-Livada-Tselepidaki's corresponding values.

7. Conclusions

The main conclusions derived from this study are briefly as follows:

(i) There were 23 synoptic systems associated in the snowfall in Athens in the period under consideration (1956–73) — fifteen cases belong to type A, and eight cases to type B. Thus the number of F days are 15 for type A and 8 for type B, whereas the total number of snow-days is 40.

(ii) The atmospheric structure above Athens during F–2, F–1, F and E days has been found to be potentially stable ($\partial\theta_w/\partial z > 0$). However, for type A on F day the stability decreases in the lower levels and the relative humidity increases, the same also happens for the type B and even on E day the layer from surface up to 850 hPa appears to be potentially unstable.

(iii) The characteristics of the atmospheric structure during snowfall are:

(a) stable stratification

(b) cold air mass (mean temperature at 850 hPa −7.5 °C, mean temperature at 500 hPa −31.5 °C)

(c) increased relative humidity ($T - T_d < 3$ K in the layer from 950 up to 800 hPa)

(d) northerly winds from 950 to 750 hPa, backing higher up, to north-westerly. At the surface type A is characterized by north-westerly winds, and type B by north-easterly winds.

(iv) Temperature values derived from Hellinikon 0000 GMT upper-air observations showed that temperature decreases from F–1 day to F day and increases on END day at all standard levels. The warmest day at 200 hPa is F day. Also type A appears to be colder than type B at almost all standard levels and warmer on F–1, F, E days at 850 hPa level.

(v) The standard isobaric surface geopotentials decrease from day F–2 to F and they increase on E day apart from the geopotential of 200 hPa isobaric surface which continues decreasing on the E day.

(vi) Various indices defining the precipitation types which have been introduced over a long period of meteorological practice have been compared with the results of this research. Characteristic values of various meteorological parameters associated with these indices for snowfall time are:

(a) mean value of 1000–500 hPa thickness = 5230 gpm with a standard deviation 47 gpm

(b) mean value of 1000–850 hPa thickness = 1282 gpm with standard deviation 34 gpm

(c) mean distance of the freezing level from the ground = 38.6 hPa

(d) mean value of index I_w = 8.6 hPa with a standard deviation 1.4 hPa

(e) $T + T_d \leqslant 1$ °C on average

(f) $\theta_{w850} = 0.5$ °C on average

(g) $T_{w850} = -9$ °C on average.

These values when compared to the corresponding values found by other researchers showed that the lower part of the troposphere was much colder than the observations used by previous researchers had shown.

References

Air Weather Office 1959 *Modern Weather Techniques II*, 147, Illinois, USA.

Angouridakis, V. E. 1977 Covariation of atmospheric pressure at MSL and certain parameters of the 500 mb and 300 mb mandatory levels, in the area of Attica-Greece. *Meteorologika*, **65**, 1–24.

Austin, J. M.	1953	Sea-level pressure patterns associated with 500 mb contour patterns. *MIT Technical Report No. 14*, Cambridge, Massachusetts.
Booth, B. J.	1973	A simplified snow predictor. *Meteorol Mag*, **102**, 332–4.
Boyden, C. J.	1964	A comparison of snow predictors. *Meteorol Mag*, **93**, 353–65.
Bradbury, T. A. M.	1977	The use of wet-bulb potential temperature charts. *Meteorol Mag*, **106**, 233–51.
Brooks, C. E. P. and Carruthers, N.	1953	Handbook of statistical methods in meteorology. HMSO, London, 412.
Holton, J. R.	1973	An introduction to dynamical meteorology. Academic Press, London and New York, 319.
Lamb, H. H.	1955	Two-way relationship between the snow or ice limit and 1000–500 mb thicknesses in the overlying atmosphere. *Q J R Meteorol Soc*, **81**, 172–189.
Lioki-Livada-Tselepidaki, H.	1979	*Snowfall in Greece*. University of Athens Ph.D. thesis (in Greek).
Lowndes, C. A. S., Beynon, A. and Hawson, C. L.	1974	An assessment of the usefulness of some snow predictors. *Meteorol Mag*, **102**, 341–58.
Meteorological Office	1975	Handbook of weather forecasting, Chapters 19 and 23. Bracknell, UK.
Murray, R. A.	1952	Rain and snow in relation to the 1000–700 mb and 1000–500 mb thicknesses and the freezing level. *Meteorol Mag*, **81**, 5–8.
Prezerakos, N. G. and Angouridakis, V. E.	1979	Characteristics of snowfalls in Athens. *Bull Hellenic Meteorol Soc*, **5**, 12–32 (in Greek).
	1984	Synoptic consideration of snowfall in Athens. *J Climatol*, **4**, 269–85.
Sahsamanoglou, C. S. and Makrogiannis, T. J.	1978	The precipitation type in north Greece in relation to the values of suitable indices. *Bull Hellenic Meteorol Soc*, **2**, 11–20 (in Greek).
Smith, M. F.	1970	Winter precipitation over East Anglia. *Meteorol Mag*, **90**, 20–27.

551.577.37(423.4)

An analysis of extreme rainfalls observed in Jersey

By A. P. Butler
(Imperial College, London*)
Jennifer D. Grundy
(Jersey Meteorological Department)
and B. R. May
(Meteorological Office, Bracknell)

Summary

A depth–duration–frequency analysis of extreme rainfalls observed on the island of Jersey has been made using the methods described in the Natural Environment Research Council's *Flood Studies Report*, Volume II. Results of a comparison of the Jersey observations and the Flood Studies model (which was based on rainfall observations on the mainland of the United Kingdom) are given. It is concluded that for most practical purposes the Flood Studies model is applicable to extreme rainfalls on Jersey.

1. Introduction

On 31 May 1983 a violent shower occurring between 20 and 21 GMT produced an hourly rainfall total of 43.3 mm at Jersey Airport, with a 09 to 09 GMT total of 52.2 mm at the nearby St Peter's Rectory. Serious flooding resulted in the west of the island with consequent insurance claims and questions regarding the effectiveness of drainage systems and practices. On the basis of records dating from the last century both the Jersey Meteorological Department and the news media described this event as a rare occurrence. However, less than a week later, another thunderstorm approached the island from the south-west in an unstable airstream across France. Again, flooding occurred but this time the worst-affected area was in the north-west of the island, although some unfortunate farmers and householders suffered damage to their properties on both occasions. Soon after midnight on 5 June the rain-gauge at the airport recorded 28 mm in less than an hour and other daily gauges recorded higher totals (such as the 53.3 mm at an unofficial site at St John's Rectory).

Although surprising, and of considerable concern to enquirers who suffered damage or loss, this repetition of events is understandable to the meteorological statistician with a clear idea of the 'return period' concept. However, these two storms did highlight the need to produce extreme rainfall data for design or planning purposes for Jersey and it was decided to study the application of Volume II of the *Flood Studies Report* (Natural Environment Research Council 1975b), hereinafter referred to as the FSR, to the island. The FSR provides design rainfall estimates for the United Kingdom† based on plentiful and comprehensive precipitation data. Applicability of the findings of the report to Jersey could not be assumed without investigation, since the proximity of Jersey to France means that the island often receives heavy rainfalls in spring and summer originating from thundery activities over Brittany and Normandy where temperatures can be much higher than those recorded over southern England. The precipitation regime of Jersey might thus differ sufficiently from that of coastal areas of southern England to invalidate the FSR approach.

After discussions between the Jersey Meteorological Department and the Agriculture and Hydrometeorology Branch of the Meteorological Office at Bracknell, it was decided to carry out a co-operative study of Jersey rainfall data to assess whether rainfall regimes were sufficiently alike to those

* Formerly of the Meteorological Office, Bracknell.

† The United Kingdom comprises England, Wales, Scotland and Northern Ireland, but not the Channel Islands or the Isle of Man.

in the United Kingdom to apply the FSR methods, and to produce estimates of extreme-event occurrence. These are of potential interest not only to climatologists but also more practically to engineers, farmers and insurance companies, and those individuals who have to cope with flooding on a local scale. It was intended that the benefits of a statistical extreme-value analysis, using records of considerable length, would be shared by both the organizations.

2. The data and their extraction

The climate of Jersey, located as shown in Fig. 1, has been described by Blench (1967) who points out that the major factor influencing rainfall is the occurrence of moist westerly winds from the Atlantic Ocean. Average monthly rainfall amounts are fairly constant throughout the year but the average annual rainfall (AAR) is greater in the north of the island where the higher ground is situated (see Fig. 2). The island is also subject to heavy rainfalls from convective storms which form over France and move northwards.

Long rainfall records are available from a number of sites on Jersey. The rain-gauge sites, types of data and record lengths are given in Table I.

For each month the maximum rainfalls for the following durations were extracted from the records: 1, 2, 4, 6 and 12 hours from Jersey Airport and St Louis Observatory, 1 and 2 days from all sites; 3, 4, 8 and 25 days from Millbrook Reservoir.

Durations of from 1 to 12 hours start on integral GMT hours ('clock hours'), days start at 09 GMT and all durations are allotted to the month in which they start. The analysis involves the series of maximum rainfall amounts (for a specified duration) in each year, or in a particular month or season of that year, and these are referred to as the annual, monthly and seasonal maxima respectively (as in the FSR).

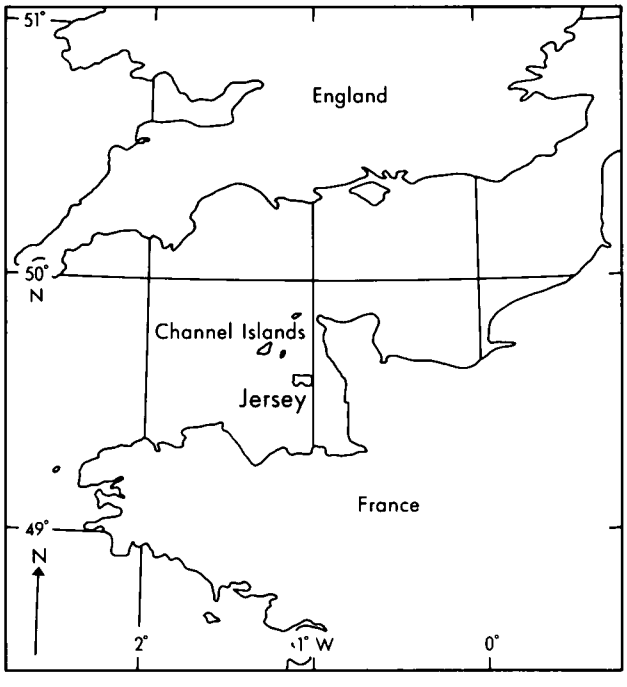

Figure 1. Location of Jersey in relation to England and France.

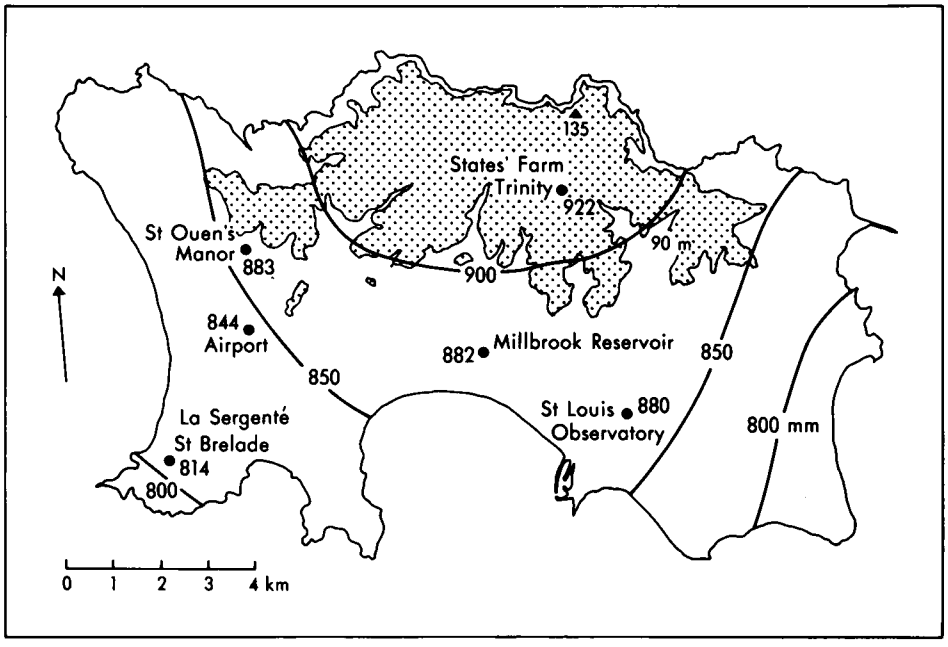

Figure 2. Location of rain-gauges on Jersey with average annual rainfalls in millimetres (1941–70 averages). Dotted area indicates ground over 90 m above mean sea level.

Table I. *Rainfall records for Jersey. The sites referred to are shown in Fig. 2*

Site	Universal Transverse Mercator (UTM) grid ref. Zone 30U WV (554)	Altitude *metres*	Daily (D) or hourly (H) values	Period of record
Jersey Airport	583513	84	H and D	1951–82
St Louis Observatory	662493	54	H	1940–43, 1947–82
			D	1894–1920, 1925–83
St Brelade	566486	58	D	1917–41, 1948–83
St Ouen's Manor	583530	79	D	1917–34, 1948–74
Trinity	650540	104	D	1936–41, 1948–83
Millbrook Reservoir	632507	16	D	1912–82

3. Analysis of extreme-value data

A good introduction to the use of statistics of extremes in meteorology is provided by Tabony (1983); only an outline is given here.

Consider a series of observations of the maximum values of some variable occurring in equal time intervals arranged in ascending order 1 to n, for instance, the maximum 1-hour rainfalls in each year R_1 to R_n. With the mth value R_m we need to associate a probability F that it will not be exceeded in any year. The median value of this probability can be estimated by Chegodayev's formula (see FSR):

$$F = (m - 0.31)/(n + 0.38). \quad (1)$$

The probability of R_m being exceeded is $1 - F$ and the average duration in years between exceedances is

$$T = 1/(1 - F) \quad (2)$$

where T is the return period. For instance, if $n = 10$ and $m = 5$, $F = 0.452$ and $T = 1.82$ (years) for the associated value R_5. F is also called the 'plotting position' and the plotting positions given by equation (1) were used in the analysis in the FSR.

Annual, monthly and seasonal maxima of rainfall amounts for specified durations are frequently used in extreme-value analysis because they are usually readily retrievable from convenient data sets. However, their use overestimates the return period of exceedance for a specified amount and the effect is important, especially for return periods of less than 5 years. This arises because in some years the second (or third etc.) largest rainfall, which is ignored in the annual maximum series, can be greater than the maximum for another year which is included in the series. As a consequence a more accurate estimate of the return period can be obtained by selecting and ordering all exceedances of the specified amount into the 'partial duration' series. Fortunately a return period T_E from the partial duration series can be related to its corresponding T_M in the annual maximum series by the formula (Langbein 1949)

$$T_E = 1/\{\ln T_M - \ln(T_M - 1)\}$$

so that the convenience of the analysis of maxima in fixed intervals can be retained. For $T_M \geqslant 5$ years, $T_E \approx T_M - 0.5$ years and the rainfalls corresponding to the two periods are usually negligibly different.

For a particular duration, to estimate the rainfall amount for a specified T, interpolation within or extrapolation beyond the T values for each member of an ordered series given by equations (1) and (2) is required. The theory of extreme values indicates that the ordered maxima can be related to the 'reduced variate' $y = -\ln\{\ln(1/F)\}$.

As an example, Fig. 3 shows the annual maximum rainfall of 1-hour duration at Jersey Airport (32 points) plotted against y_M, where $y_M = -\ln\{\ln(1/F_M)\}$, and $F_M = (T_M - 1)/T_M$, on linear scales. The values lie on a fairly smooth curve with an indication, mainly from the two uppermost points, of a slope increasing with y_M. Denoting the general extreme-value variable by x, a curve of the form

$$x = x_0 + (\alpha/k)\{1 - \exp(-ky_M)\} \quad (3)$$

can be fitted to the extreme values where α is the scaling factor and k is the slope curvature factor. The slope $dx/dy_M = \alpha \exp(-ky_M)$ so that for small k, $dx/dy_M \approx \alpha$ while for the straight-line case $k = 0$, $dx/dy_M = \alpha$ and hence $x = x_0 + \alpha y_M$. For T less than 10 years, maximum rainfalls as in Fig. 3 can usually be represented by a line of small or zero k.

Results in this paper are quoted for standard return periods of $T_1 = 0.5$, 1 and 2 years and T_E or $T_M = 5$, 10, 20 and 50 years. With the record lengths available, rainfalls for T up to 50 years can be estimated well because they are covered by the range of individual T values given by equations (1) and (2); beyond 50 years extrapolation of the extreme-value distribution is involved with increasing uncertainty. For Millbrook Reservoir with its longer record of 71 years, the upper limit of T can be increased to 100 years.

From individual maxima plotted as in Fig. 3 reliable observed values for the standard return periods are calculated using one of three methods:

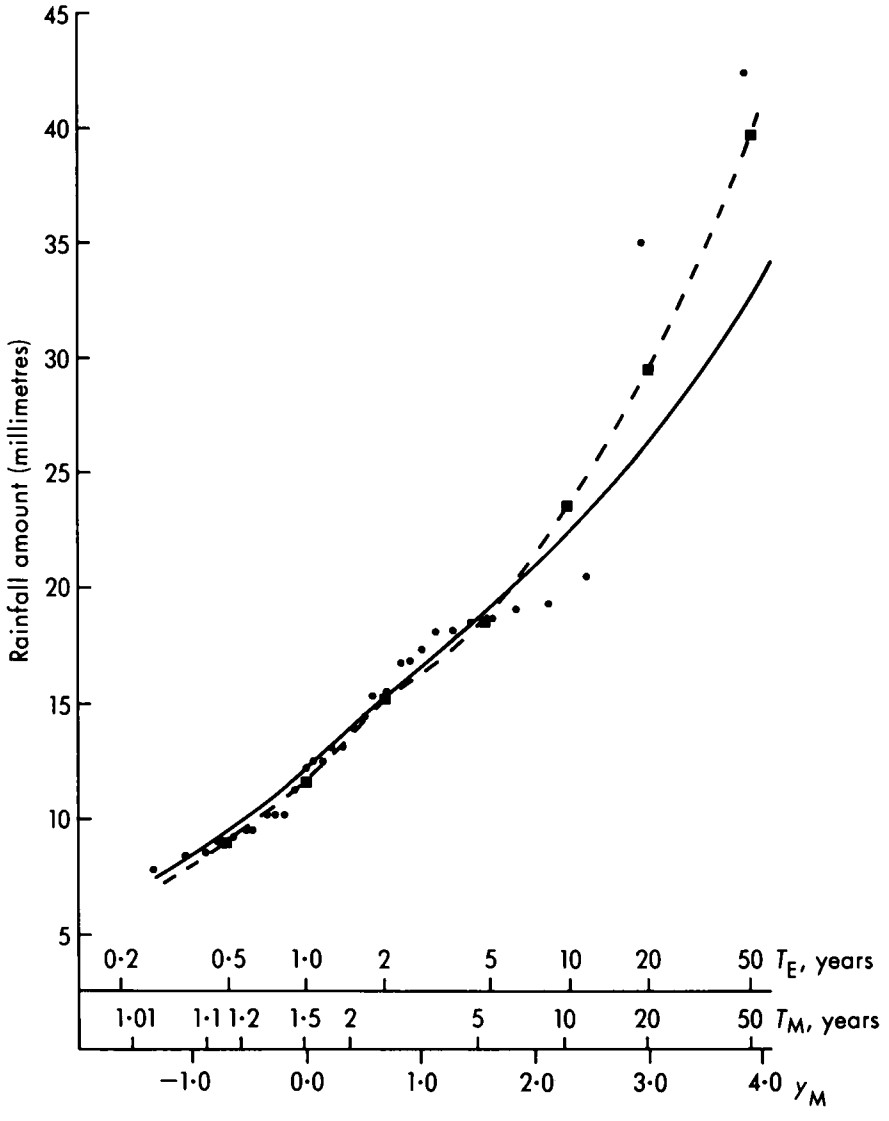

Figure 3. Analysis of annual maximum 1-hour rainfalls at Jersey Airport (32 years).
● observed annual maximum 1-hour rainfalls
■--■ adopted observed values for standard return periods
—— FSR model

(i) *For T_1 = 0.5 and 1 year (2M and 1M values)*

Jenkinson (1975) showed that if a set of maxima in ascending order was divided by quartiles then the geometric mean of the values below the lower quartile is a good estimate of the twice-yearly rainfall (denoted by 2M), i.e. for $T_1 = 0.5$ years, and the geometric mean of the values lying between the lower quartile and the median gives the 1M value (T_1 = 1 year).

(ii) *For T_E = 2 years (M2 value)*

The geometric mean of the values in the interquartile range is a good estimate of the value for $T_M = 2$ years which is equivalent to $T_E = 1.44$ years. The value for $T_E = 2$ years is calculated by adding to the $T_M = 2$-year value a correction of $+0.325\alpha$. The factor 0.325 is the difference between the values of y_M for $T_E = 2$ years (or $T_M = 2.54$ years) i.e. $y_M = 0.692$ and for $T_M = 2$ years i.e. $y_M = 0.367$; strictly this factor applies only to linear extreme-value distributions but in practice the error in the correction is negligible.

(iii) *For $T_M \geqslant 5$ years (M5, M10, M20, M50, M100)*

Curves of the form of equation (3) are fitted to the values over the whole range of y_M using the maximum likelihood technique (Jenkinson 1969). Interpolated values appropriate to the standard return periods taken from the curves are regarded as the best estimates based on these observations.

4. Errors of 2M, 1M ... estimates

For a linear distribution of extreme values an estimate of the standard error (S.E.) of a point on the line is given by the FSR (Natural Environment Research Council 1975a):

$$\text{S.E.} = (\alpha/n^{1/2})(1.11 + 0.52y_M + 0.16y_M^2)^{1/2}$$

where n is the number of observations in the sample. This expression is also adopted here where the distribution of extreme values is close to being linear.

5. The Flood Studies model

In the early 1970s a large number of rainfall records for sites in the United Kingdom were analysed by the Meteorological Office as a part of the background work for the FSR. It was later shown that the depth–duration–frequency relationship for all locations could be represented by a simple computer-based model described by Keers and Wescott (1977). To estimate the rainfall amount for a particular duration (in the range 5 minutes to 25 days) and return period (greater than 0.5 year) the model requires four input parameters to be specified. These are:

(i) 60-minute M5 rainfall;
(ii) 2-day M5 rainfall;
(iii) 25-day M5 rainfall; and
(iv) average annual rainfall.

The 60-minute M5 rainfall (which is not constrained to start on a clock hour) has been found to be greater than the 'constrained' clock-hour value by a factor of 1.15.

The first step in the application of this model is to estimate (essentially by interpolation within the above values) the M5 value for the duration of interest. This does not necessarily require all the input items (i) to (iv) above to be specified — for instance, to estimate the 1-day M5 rainfall requires only items (i) and (ii) to be known. The second step is to calculate the value for the required T_M from the M5 value from step 1. For $T_M \geqslant 5$ years the relationship

$$M_T = M5 \cdot \exp\{c(y_M - 1.5)\}$$

is used, in which c is a constant which depends upon the M5 value, and y_M is the reduced variate corresponding to T_M. For $T_E = 0.5$, 1 or 2 years the corresponding 2M, 1M and M2 values are available as a tabulated percentage of the M5 value, for different ranges of M5.

6. Results

(i) *General*

Comparisons have been made between rainfalls for various durations from 1 hour to 25 days and return periods from 0.5 to 100 years as determined from the Jersey observations (denoted by O) and those from the FSR model (F) as calculated by the Keers and Wescott computerized method.

As an example, the results for annual maximum 1-hour rainfalls at Jersey Airport are tabulated against return period in Table II. Differences ($O - F$) are given in millimetres, as percentage relative difference ($\{(O - F)/F\} \times 100\%$) and as a fraction of the estimated S.E.

Table II. *Comparison of Jersey Airport and FSR rainfalls of 1-hour duration*

Return period	Observed rainfall (O) and S.E.	FSR rainfall (F)	$(O-F)$	$(O-F)/F$	$(O-F)$/S.E.
years	*millimetres*	*millimetres*	*millimetres*	*per cent*	
0.5	9.0 (0.8)	9.5	-0.5	-5.3	-0.63
1	11.8 (0.8)	12.1	-0.3	-2.5	-0.38
2	15.3 (1.0)	15.3	0.0	0.0	0.00
5	18.6 (1.4)	18.9	-0.3	-1.6	-0.21
10	23.6 (1.8)	22.4	1.2	5.3	0.67
20	29.7 (2.2)	26.4	3.3	12.5	1.49
50	39.8 (2.7)	32.6	7.2	22.1	2.67

The observed and FSR rainfalls in Table II are also shown in Fig. 3 described previously. It can be seen that the estimated observed values for the standard return periods obtained using the methods described in section 3 are a good representation of the basic values over the range $T = 0.5$ to 10 years and particularly for $T \leqslant 5$ years. For $T \leqslant 10$ years the relative difference is less than 6% and the difference relative to the S.E. is in the range -0.7 to +0.7. For $T > 10$ years larger differences appear which are discussed below.

(ii) *Annual maxima*

In Fig. 4 are plotted the percentage relative differences for durations of 1, 4 and 12 hours for Jersey Airport and St Louis Observatory for the range of return periods. For $y = 5$ years the differences are small or zero (because of the method of application of the FSR); for $T < 5$ years they vary systematically from negative values for 1 hour to positive values for 12 hours for both sites, but all differences are within 10%. For $T > 5$ years the differences again vary systematically and in the same way for both sites but this time are positive for 1 hour and negative for 12 hours duration. This indicates that Jersey experiences larger rainfalls of short duration and smaller rainfalls of longer duration than the United Kingdom for the rarer events. These rainfalls are associated with summer thunderstorms ahead of upper troughs west of France, and with cold fronts weakening and becoming quasi-stationary near the Channel Islands. Nevertheless, the FSR model fits these sub-daily rainfall observations within -20% to + 30% for T up to 50 years.

Fig. 5 shows results in the same style for 1-day duration rainfalls from all the six sites. For $T < 5$ years the differences tend to be positive but are less than 11%, while for $T = 50$ years the errors are larger, ranging between ±15%. There is no obvious relationship between sites with differences of the same sign and so these ranges of differences can be regarded as being typical for a selection of sites randomly situated over this island.

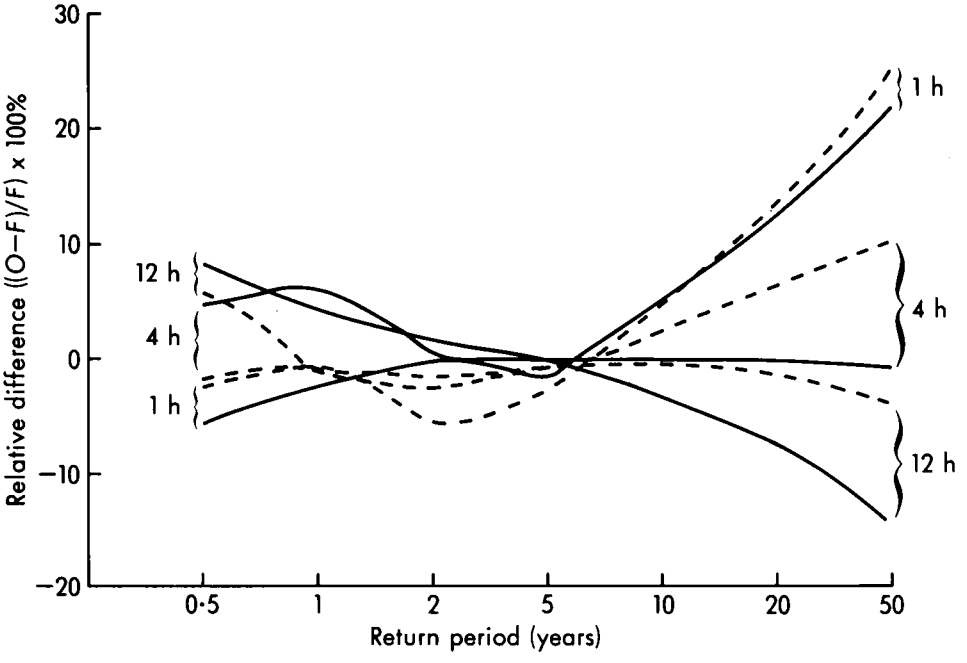

Figure 4. Variation of percentage relative differences (observed – FSR) for sub-daily duration rainfalls at Jersey Airport (——) and St Louis Observatory (- - -).

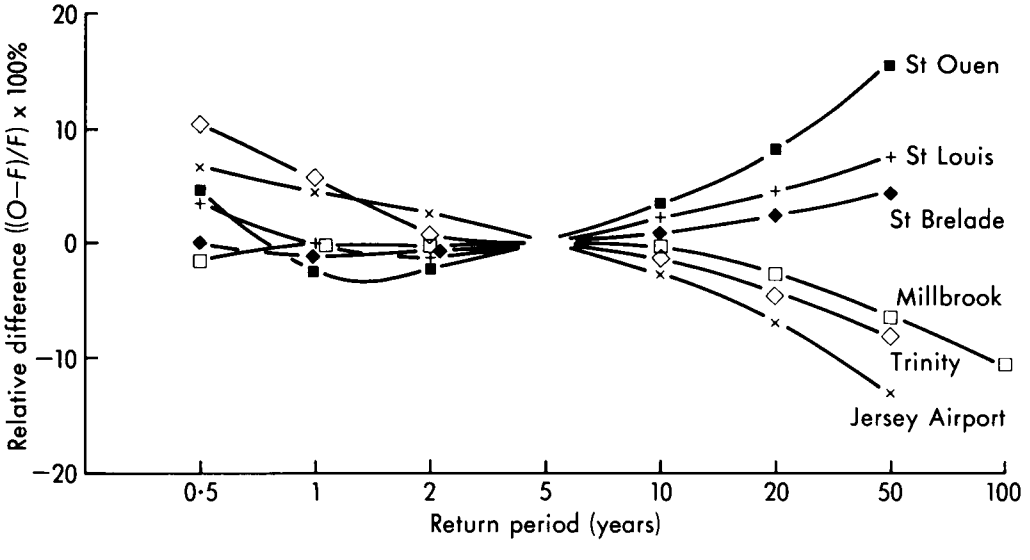

Figure 5. Variation of percentage relative difference (observed – FSR) for 1-day duration rainfalls.

Results for 2-, 4-, 8- and 25-day durations for Millbrook Reservoir are shown in Fig. 6. The differences here are mainly negative, increasingly so for the larger T, but even so for the whole range $0.5 \leqslant T \leqslant 100$ years the differences are all smaller than 16%. From the similarity of the 1-day duration (Fig. 5) and the 2-day to 25-day duration (Fig. 6) curves for Millbrook it is suggested that the 2-day to 25-day duration curves for the other sites will show approximately the same spread about their 1-day duration curves.

The largest individual difference relative to the S.E. is for St Louis Observatory, 1-hour duration, $T = 50$ years, at +3.3; otherwise the differences are usually in the range ±2.0 S.E.

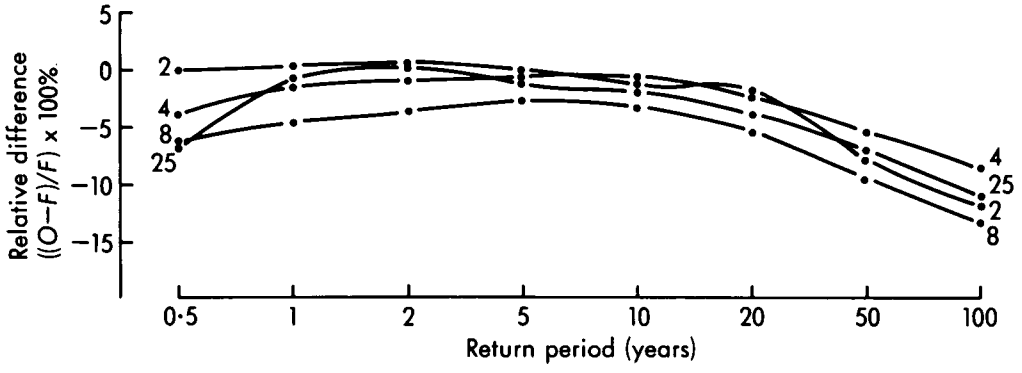

Figure 6. Variation of percentage relative difference (observed - FSR) for 2- to 25-day duration rainfalls at Millbrook Reservoir.

(iii) *Monthly and seasonal maxima*

Results of depth–duration–frequency analyses of annual maxima have been described, but for some purposes similar analyses of rainfalls in particular months or seasons need to be considered. Such analyses of the Jersey data proceeded exactly as for annual maxima except that the maximum rainfalls extracted were for each month and season (winter — November to April, summer — May to October, to agree with the FSR).

In the FSR the variations of M5 for monthly and seasonal maxima are expressed as a percentage of the M5 for annual maxima, for durations from 1-hour to 25 days and for a range of average annual rainfalls; the Jersey results are presented here in a similar way. The variation of percentage with month from the FSR model (AAR range 800–1000 mm) is shown in Fig. 7 in comparison with the percentages from the Jersey data for durations of 1 hour, 1 day and 25 days only for clarity. For each duration the form of the curves from the two sources is very similar but there are small differences of up to 16%, mainly in February and March, and October to December. Differences are also apparent, but to a lesser extent, in the seasonal results also shown in Fig. 7.

In general then it appears that the FSR model of the depth–duration–frequency relationship applies well to the Jersey extreme rainfalls within the percentage relative differences indicated, but adjustments based on Figs 3–7 can be applied if required.

7. Representative depth–duration–frequency curves for Jersey

(i) *Annual maxima*

The differences quoted in section 6 indicate the extent to which the FSR model can represent depth-duration-frequency relationships for both United Kingdom and Jersey extreme rainfalls, for specified input parameters (i) to (iv) in section 5. They are not necessarily representative of the errors of predicted

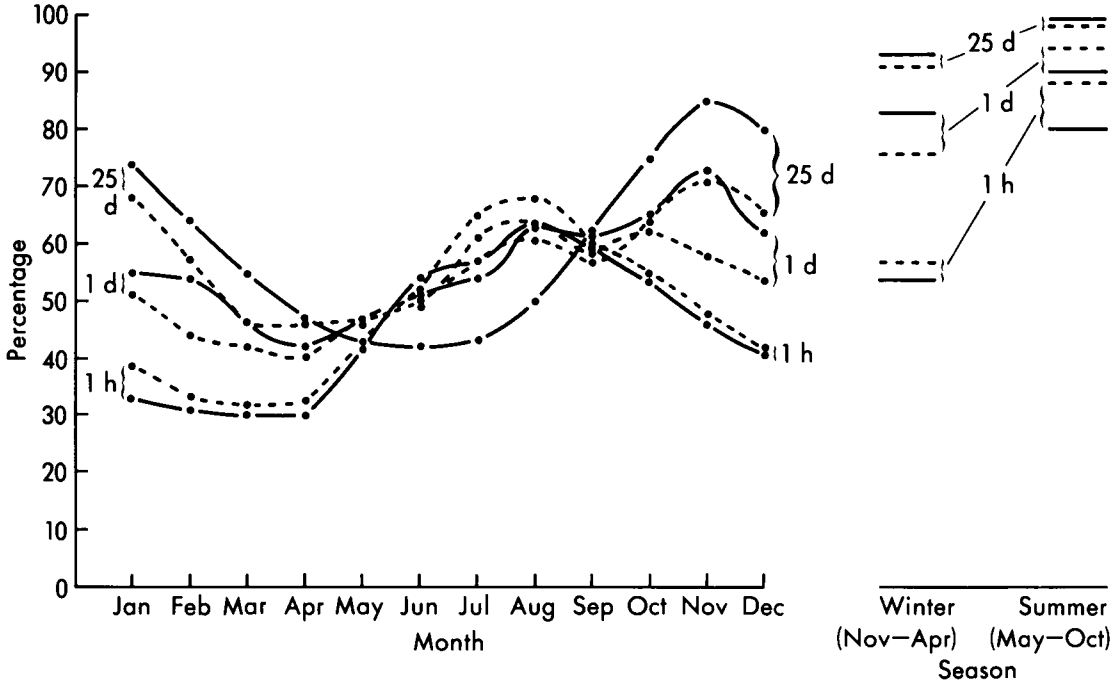

Figure 7. Comparison of variations of M5 for Jersey (——) and FSR (- - -) for monthly and seasonal maxima as a percentage of M5 for annual maxima of 1-hour, 1-day and 25-day durations.

extreme rainfalls or return periods for an ungauged location, which are dependent upon the accuracy with which the input parameters can be estimated. The available values of these parameters are given in Table III.

Table III. *Values of FSR model input parameters for Jersey sites*

Location	M5 rainfalls 60-minute	2-day	25-day	Average annual rainfalls 1941–70 averages
			millimetres	
Jersey Airport	21.4	48.7	—	844
St Louis Observatory	21.3	53.9	—	880
Trinity	—	55.3	—	922
St Ouen's Manor	—	50.1	—	883
St Brelade	—	50.6	—	814
Millbrook Reservoir	—	55.8	196.6	882

From the entries in Table III it can be seen that there are no large variations of the M5 values of 60-minute, 2-day or the AAR over this small area. We can therefore adopt the following representative set of values for Jersey:

60-minute M5	21.9 mm
2-day M5	52.4 mm
25-day M5	200.0 mm
AAR	880.0 mm

— which differ by no more than 7% from the individual values in Table III (in the FSR model an x% change in an M5 value for a specified duration changes the M5 value for a similar duration by about the

same amount). These representative values have been used with the FSR model to produce the depth–duration–frequency curves (also known as design rainfall curves) in Fig. 8 generally applicable to all locations on the island. Although the record lengths only cover the range of T up to 50–100 years the curves in Fig. 8 have been extended to $T = 1000$ years for guidance.

(ii) *Seasonal maxima*

From the observed percentage curves in Fig. 7 (and for other intermediate durations) and the M5 values in Fig. 8 the generally applicable curves for monthly and seasonal M5 rainfalls for Jersey have been constructed and are shown in Fig. 9. The curves for duration of less than 60 minutes were derived solely from the methods in the FSR as no sub-hourly rainfalls for Jersey sites were extracted from the records. The curves show well the contrary seasonal changes in short- and long-duration M5 rainfalls

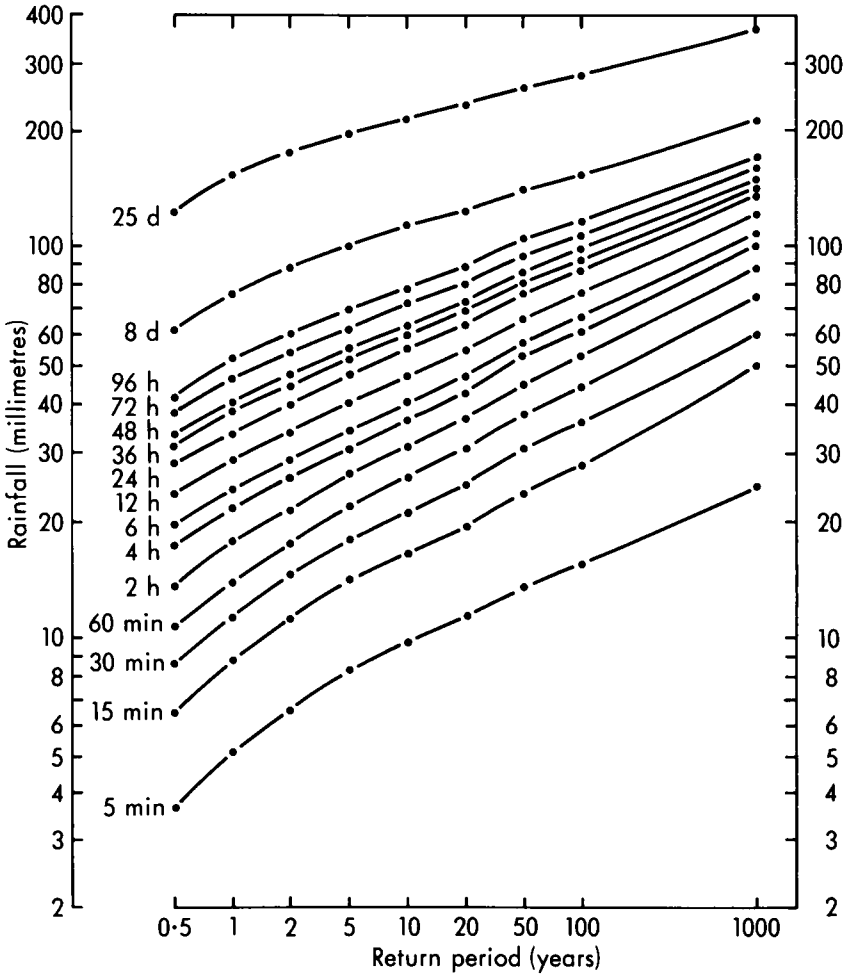

Figure 8. Depth-duration-frequency relationship for Jersey.

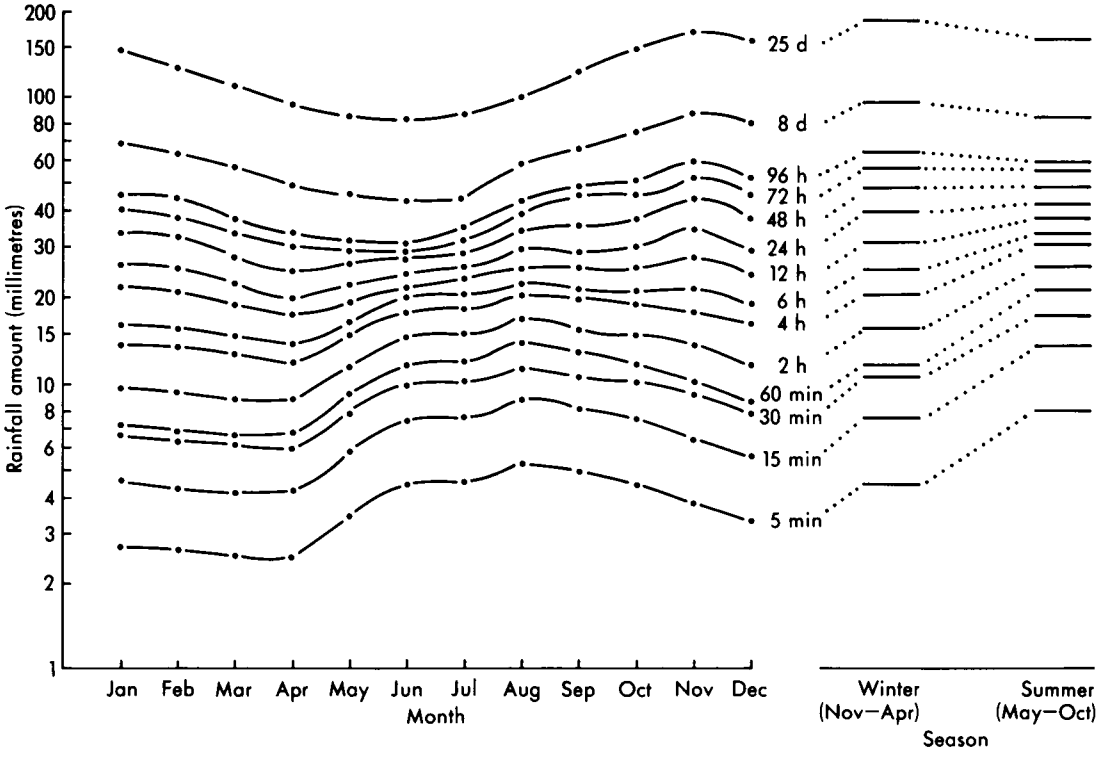

Figure 9. Monthly and seasonal variation of M5 rainfalls for Jersey.

with rainfalls of duration less than 60 minutes being much smaller in winter than in summer (owing to the influence of summer convective storms), and 1-day rainfalls being larger in winter than in summer owing to the greater influence of prolonged rainfalls from winter depressions.

8. Conclusions

Extreme rainfalls for durations from 1 hour to 25 days from six sites on Jersey with records from 32 to 71 years have been analysed. The rainfalls for return periods from 0.5 to 50 years are usually within ±15% of the amounts inferred from the *Flood Studies Report* model, for model input parameters (M5 values of the 60-minute, 2-day and 25-day duration rainfalls and the annual average rainfall) observed at gauged sites. Further errors of up to ±7% can result from errors in estimating the input parameters from ungauged sites.

It is concluded that for most practical purposes the FSR model is applicable to extreme rainfalls in Jersey and the neighbouring Channel Islands.

References

Blench, B. J. R.	1967	An outline of the climate of Jersey. *Weather*, **22**, 134–139.
Jenkinson, A. F.	1969	Statistics of extremes. *In* Estimation of maximum floods. Geneva, WMO, *Tech Note* No. 98, Chapter 5.
	1975	Extreme value analysis in meteorology. Boston, Massachusetts, American Meteorological Society. Fourth Conference on Probability and Statistics in Atmospheric Science, 83–89.
Keers, J. F. and Wescott, P.	1977	A computer-based model for design rainfall in the United Kingdom. London, *Sci Pap, Meteorol Off*, No. 36.
Langbein, W. B.	1949	Annual floods and the partial duration flood series. Washington, *Trans Am Geophys Union*, **30**, 879–881.
Natural Environment Research Council	1975a	Flood Studies Report. Volume I (Hydrological studies).
	1975b	Flood Studies Report. Volume II (Meteorological studies).
Tabony, R. C.	1983	Extreme value analysis in meteorology. *Meteorol Mag*, **112**, 77–98.

Notes and news

Pressure to change

The use of hectopascals (hPa) in the paper by Dr Prezerakos published in this issue has recalled to us the following short poem by Mr Ernest Gold CB, DSO, OBE, FRS published over the initials E.G. in *Symons's Meteorological Magazine* for December 1919 (Vol. 54, p. 136). The occasion was the decision by a majority vote of the Congress of Directors of Independent Meteorological Services, held in Paris, to adopt the millibar as the unit of atmospheric pressure in preference to the millimetre of mercury. (Mr Gold, Deputy Director of the Office during and immediately after the Second World War, played an outstanding role in organizing international meteorological co-operation.)

The Directors of Science in Congress assembled,
Agreed that in future no discord should mar
The values of pressure so often dissembled
By units derived from a platinum bar.
The inch and the metre and gravity trembled,
As into the Congress there tripped lightly skipping
An innocent damsel who'd just 'scaped a whipping;
Her name in plain English was Miss Milly Barr.
Dear Milly Barr
Bjerknesian star;
A thousand of you
Shall be ever our cue,
As our standard of pressure wherever we are.

We look forward to receiving a similar poetic salute to Hecto(r) Pascal.

Books received

The listing of books under this heading does not preclude a review in the Meteorological Magazine at a later date.

Atmospheric ozone, edited by C. S. Zerefos and A. Ghazi (Dordrecht, Boston, Lancaster, D. Reidel Publishing Company, 1985. £69.95) contains progress papers in atmospheric ozone research which were presented at the Quadrennial Ozone Symposium held in Halkidiki, Greece, from 3 to 7 September 1985. The papers are grouped into nine chapters corresponding to the nine sessions of the symposium, the titles of which are as follows: chemical–radiative–dynamical model calculations, ozone–climate interaction, observations of relevant trace constituents and their budgets, analysis of ozone observations, recent developments in observational techniques, interaction of ozone and circulation, laboratory measurements of absorption cross-sections and of chemical rate constants, radiation topics relevant to atmospheric ozone, and non-urban tropospheric ozone.

The global climate, edited by John T. Houghton (Cambridge University Press, 1984; first paperback edition 1985. £11.95) is a paperback edition of this volume issued in hardback last year. The aim of the book is to introduce scientists and students working in climate research or related fields to the global climate problem, and the complex processes and interactions which play a part in climatic change. The text is centred around the World Climate Research Programme, whose aims are to determine, firstly, to what extent changes in climate can be predicted, and secondly the extent of man's influence on climate.

Climatic hazards in Scotland, edited by S. John Harrison (Norwich, Geo Books, 1985. £8.00) covers the proceedings of the joint Royal Scottish Geographical Society and Royal Meteorological Society symposium held at the University of Stirling in June 1984. The Scottish experience of excess weather conditions is reported. Extremes in rainfall and resultant flooding conditions, and windthrow damage in the uplands, are discussed. Also dealt with is the general influence of climatic extremes, with regard to insurance aspects and research, and also as regards the city of Glasgow.

THE METEOROLOGICAL MAGAZINE

No. 1361 December 1985 Vol. 114

CONTENTS

Printed in England for HMSO and published by
HER MAJESTY'S STATIONERY OFFICE

£2.30 monthly

Dd. 738362 C14 12/85

Annual subscription £27.00 including postage

ISBN 0 11 727566 2
ISSN 0026–1149